

2017

Quaternary River Erosion, Provenance, and Climate Variability in the NW Himalaya and Vietnam

Tara Nicole Jonell

Louisiana State University and Agricultural and Mechanical College

Follow this and additional works at: https://digitalcommons.lsu.edu/gradschool_dissertations



Part of the [Earth Sciences Commons](#)

Recommended Citation

Jonell, Tara Nicole, "Quaternary River Erosion, Provenance, and Climate Variability in the NW Himalaya and Vietnam" (2017). *LSU Doctoral Dissertations*. 4423.

https://digitalcommons.lsu.edu/gradschool_dissertations/4423

This Dissertation is brought to you for free and open access by the Graduate School at LSU Digital Commons. It has been accepted for inclusion in LSU Doctoral Dissertations by an authorized graduate school editor of LSU Digital Commons. For more information, please contact gradetd@lsu.edu.

QUATERNARY RIVER EROSION, PROVENANCE, AND CLIMATE VARIABILITY IN
THE NW HIMALAYA AND VIETNAM

A Dissertation

Submitted to the Graduate Faculty of the
Louisiana State University and
Agricultural and Mechanical College
in partial fulfillment of the
requirements for the degree of
Doctor of Philosophy

in

The Department of Geology and Geophysics

by
Tara Nicole Jonell
B.S., Kent State University 2010
M.S., New Mexico State University, 2012
May 2017

ACKNOWLEDGMENTS

There are so many people for which I am thankful. Words can barely express the gratitude I have for my advisor, Dr. Peter D. Clift, who has countlessly provided humor and outstanding support throughout this project. I cannot imagine completing this research without his untiring guidance both in the lab and outside in the field. I also wish to thank my advisory committee for their invaluable insight and patience: Dr. Barbara Dutrow, Dr. Sophie Warny, and Dr. Robert Rohli.

This work would not have been possible without financial support from the Charles T. McCord Jr. chair in petroleum geology at Louisiana State University. Further financial assistance was provided by a Geological Society of America Student Research Grant, the Farouk El-Baz Student Research Award, and scholarships awarded by Louisiana State University and the New Orleans and Shreveport geological societies.

My co-authors cannot be recognized enough for sharing their wisdom and expertise: Dr. Andrew Carter, Dr. Philipp Böning, Dr. Lewis A. Owen, Dr. Jean-Luc Schwenniger, Dr. Long V. Hoang, Dr. Hella Wittmann, Dr. Katharina Pahnke, Dr. Tammy Rittenour, Tina Hoang, and Dr. Madhav Musari. Many thanks to Jan Blöthe, Henry Munack, Jason Dortch, and Eduardo Garzanti for their astute advice on geomorphometric analysis and sediment provenance.

Without the logistical genius of Fida Hussein Mittoo, Afzal and Efu Mittoo, Tashi, and all of Rockland Tourism, little would have been accomplished in Ladakh and Zaskar. Through the power of lemon tea, lime pickle, fresh *chulli*, Godfather5000, and chocolate, peaks were reached and basins explored. I am very grateful for the unwavering generosity provided by Dr. Arun Ahluwalia at Panjab University while in India, and Dr.

Long V. Hoang at the Hanoi University of Mining and Geology in Vietnam.

I would like to thank all of the department administrative and laboratory staff, especially Heather Lee, Rick Young, Michael Strain, and Wanda Leblanc. To my past and present Louisiana State University students, cohorts, and lab mates: you are all weird and wonderful and gave me such flack and friendship that I will constantly cherish.

And lastly, to my family: I blame all of you for introducing me to the wild, fascinating universe and for challenging me to become a better explorer and scientist. Without your unyielding support, I would not be here.

PREFACE

The chapters in this dissertation are written in a format for publication in peer-reviewed academic journals. Each of the main chapters contains a separate abstract, introduction, methods, results, and discussion, so that each chapter can be considered independently. All cited references are compiled together under one heading after the conclusion for continuity between chapters. An introduction is provided for the reader to outline the overall objectives and themes of this project, and a final summary to underscore the larger findings and implications of this work.

TABLE OF CONTENTS

ACKNOWLEDGMENTS.....	ii
PREFACE.....	iv
LIST OF FIGURES.....	viii
LIST OF TABLES.....	xv
ABSTRACT.....	xvi
CHAPTER 1. INTRODUCTION.....	1
1.1 Objectives and Themes.....	1
1.2 Organization.....	2
CHAPTER 2. CLIMATIC AND GLACIAL IMPACT ON EROSION PATTERNS AND SEDIMENT PROVENANCE IN THE HIMALAYAN RAIN SHADOW, ZANSKAR RIVER, NW INDIA.....	4
2.1 Abstract.....	4
2.2 Introduction.....	5
2.3 Background.....	7
2.3.1 Climatic and Geographic Setting.....	7
2.3.2 Geologic Setting.....	11
2.4 Methods.....	14
2.4.1 Basin Morphology.....	15
2.4.2 Bulk Sediment Petrography.....	17
2.4.3 Major and Trace Element Geochemistry.....	18
2.4.4 Isotope Geochemistry.....	18
2.4.5 Detrital U-Pb Zircon Geochronology.....	24
2.5 Results.....	28
2.5.1 Basin Morphology.....	28
2.5.2 Bulk Sediment Petrography.....	30
2.5.3 Major and Trace Element Geochemistry.....	31
2.5.4 Isotope Geochemistry.....	33
2.5.5 Detrital U-Pb Zircon Geochronology.....	35
2.6 Discussion.....	37
2.6.1 Downstream Provenance Evolution.....	37
2.6.2 Controls on Erosion.....	46
2.7. Conclusions.....	50
CHAPTER 3. QUANTIFYING EPISODIC EROSION AND TRANSIENT STORAGE ON THE WESTERN MARGIN OF THE TIBETAN PLATEAU, UPPER INDUS RIVER.....	52
3.1 Abstract.....	52
3.2 Introduction.....	53

3.3 Background.....	55
3.3.1 Sediment Buffering in the Indus River.....	55
3.3.2 Zaskar River Climate and Geology.....	59
3.4 Methods.....	62
3.4.1 Field Observations and Sampling.....	63
3.4.2 Sediment Petrography.....	63
3.4.3 Detrital U-Pb Zircon Geochronology.....	67
3.4.4 Optically Stimulated Luminescence Dating.....	72
3.4.5 Basin Morphology and Sediment Volumes.....	75
3.5 Results.....	81
3.5.1 Bulk Sediment Petrography.....	81
3.5.2 Detrital U-Pb Zircon Geochronology.....	81
3.5.3 Optically Stimulated Luminescence Dating.....	82
3.5.4 Basin Morphology and Sediment Volumes.....	83
3.6 Discussion.....	84
3.6.1 Provenance and Spatial Patterns of Erosion.....	84
3.6.2 Fluvial Infilling and Incision.....	96
3.6.3 Drivers of Quaternary Sedimentation.....	98
3.6.4 Quaternary Buffering and Sediment Recycling.....	101
3.7 Conclusions.....	104

CHAPTER 4. CONTROLS ON EROSION PATTERNS AND SEDIMENT TRANSPORT IN A MONSOONAL, TECTONICALLY QUIESCENT DRAINAGE, SONG GIANH, CENTRAL

VIETNAM.....	107
4.1 Abstract.....	107
4.2 Introduction.....	108
4.3 Geological Setting.....	109
4.4 Methods.....	112
4.4.1 Topographic Analysis.....	114
4.4.2 Major and Trace Element Geochemistry.....	117
4.4.3 Isotope Geochemistry.....	119
4.4.4 Detrital Zircon U-Pb Geochronology.....	123
4.4.5 Detrital Apatite Fission Track Geochronology.....	126
4.4.6 <i>In situ</i> ¹⁰ Be Cosmogenic Nuclide Data.....	127
4.4.7 Optically Stimulated Luminescence Dating.....	128
4.5 Results.....	133
4.5.1 Topographic Analysis.....	133
4.5.2 Major and Trace Element Geochemistry.....	134
4.5.3 Isotope Geochemistry.....	135
4.5.4 Detrital U-Pb Zircon Geochronology.....	137
4.5.5 Detrital Apatite Fission Track Geochronology.....	140
4.5.6 <i>In situ</i> ¹⁰ Be Cosmogenic Nuclides.....	140
4.5.7 Optically Stimulated Luminescence Dating.....	140
4.6 Discussion.....	141
4.6.1 Chemical Weathering.....	141

4.6.2 Sediment Provenance.....	143
4.6.3 Fluvial Disequilibrium.....	149
4.6.4 Exhumation History.....	153
4.6.5 Controls on Erosion Patterns.....	155
4.6.6 Terracing.....	156
4.7 Conclusions.....	158
CHAPTER 5. SUMMARY AND CONCLUSIONS.....	160
REFERENCES.....	163
APPENDIX A. CONSENT FOR CHAPTER 2.....	191
APPENDIX B. U-Pb ZIRCON AGES OF ZANSKAR RIVER SEDIMENTS.....	192
APPENDIX C. U-Pb ZIRCON AGES OF ZANSKAR RIVER TERRACE SEDIMENTS.....	240
APPENDIX D. CONSENT FOR CHAPTER 4.....	250
APPENDIX E. U-Pb ZIRCON AGES OF SONG GIANH SEDIMENTS.....	251
APPENDIX F. APATITE FISSION TRACK AGES OF SONG GIANH SEDIMENTS.....	290
VITA.....	291

LIST OF FIGURES

Figure 2.1. Digital elevation model (DEM) maps of South Asia, the Himalaya, and Zaskar River basin. (A) Shuttle Radar Topography Mission 90 m (SRTM90) map of South Asia depicting the Indus River (gray lines) and all Himalayan river drainage outlines above 500 m (black lines). Gray overlay shows location of Figure 2.4; (B) SRTM DEM and hillshade of all Himalayan drainage basins with location of the Zaskar River basin (Fig. 2.1C) outlined in black; (C) Topographic map of the Zaskar River basin with sample numbers and locations. Glacial extent from Global Land Ice Measurements from Space (GLIMS) Version 1 data (Shrestha et al., 2014). Drainage basin polygons provided freely online by Bodo Bookhagen. Sample locations noted with white dots and village locations with black squares. Numbers in circles are after Table 2.1. Dashed gray line indicates extent of internally drained Tso Kar basin. Village names abbreviated as: C = Chilling; HN = Hanumil; PG = Pang; PM = Padum; PS = Pishu; and SR = Sarchu	8
Figure 2.2. Swath profiles for topography and rainfall across the Himalayan front and into the Himalayan rain shadow. Values for profiles were extracted from a 50 km by 280 km transect shown in Fig. 2.1A. Solid lines indicate mean values with shaded regions signifying $\pm 2\sigma$	11
Figure 2.3. Simplified geologic map of the Zaskar River basin after Fuchs (1987) with additions from Zaskar Shear Zone from Dèzes et al. (1999), southern Zaskar (Lahul) from Steck et al. (1993) and Tso Kar area (Epard and Steck, 2008). N-T = Nyimaling-Tso Morari gneiss dome.	12
Figure 2.4. Parameter maps for evaluating morphology and erosion in the Zaskar River basin. (A) TRMM mean annual rainfall distribution map illustrating the precipitation gradient from west to east. Rainfall map was created using the 1998–2009 TRMM time series for mean annual rainfall; (B) Mean slope for the Zaskar River basin calculated using a 1-km radius circular moving window; (C) Local 5-km relief expressed as the difference between maximum and minimum elevation in a given area of a 5-km radius circular moving window; (D) Normalized channel steepness index (k_{sn}) calculated using TopoToolbox 2.0 (Schwanghart and Scherler, 2014). Subcatchments within the Zaskar River basin are outlined in gray in Figs. 2.2 A-C.	29
Figure 2.5. Longitudinal profiles for tributaries of the Zaskar River. (A) Raw channel profiles were smoothed using a 2 km radius moving average window to remove elevation spikes. Black dashed lines mark trunk river tributaries; light gray dotted lines mark minor tributaries to Tsarap River catchment. Arrows indicate published locations of recessional moraines (Burbank and Fort, 1985; Damm, 2006; Mitchell et al., 1999; Owen and Benn, 2005); (B) Mean normalized channel steepness index (k_{sn}) values plotted every 2 km along river longitudinal profiles for all main streams. Values were extracted using MATLAB code adapted from TopoToolbox 2.0 (Schwanghart and Scherler, 2014). Abbreviations for streams are: K = Khurna; M = Markha; O = Oma Chu; S = Stod; T = Tsarap; TC = Tsarap Chu; TZ = Toze Lungpa; and Y = Yunam.	30

Figure 2.6. Bulk petrographic compositions of Zanskar sediments. (A) Bulk compositions classified by Q (quartz), F (feldspathic), and L (lithic) framework grains following the Gazzi-Dickinson method of point counting (Ingersoll et al., 1984) and classified after Garzanti and Vezzoli (2003). Gray lines indicate data corrections for Source Rock Density (SRD; Vermeesch et al., 2016). Open diamonds are petrographic data from the lower Zanskar Gorge, where Z = Zanskar-Indus confluence and M = Markha River (Blöthe et al., 2014); (B) Bulk composition of Zanskar sediments plotted onto the (garnet + kyanite + sillimanite) – pyroxene – (zircon + tourmaline + rutile + amphibole + epidote) ternary diagram. Fields for Greater Himalaya “Formation I” kyanite- and fibrolite-bearing gneiss, Tethyan and Lesser Himalaya drawn after Garzanti et al. (2007). Samples are numbered after Table 2.1.32

Figure 2.7. Bulk major element geochemistry of Zanskar River sediments plotted on the ternary $\text{Al}_2\text{O}_3\text{-CaO+Na}_2\text{O-K}_2\text{O}$ diagram (Fedo et al., 1995) with Chemical Index of Alteration (CIA) values (Nesbitt et al., 1980). Mineral abbreviations are as follows: bt = biotite; chl = chlorite; gb = gibbsite; il = illite; kao = kaolinite; ksp = potassium feldspar; m = muscovite; pl = plagioclase; sm = smectite. Samples for average Archean upper crust (gray square), average granodiorite (open square), average granite (open diamond), and average A-type granite (gray diamond) are shown (Anderson and Bender, 1989; Condie, 1993; Winter, 2010). Line indicates typical weathering evolution path for bedrock unaffected by K-metasomatism (Fedo et al., 1995). Samples are numbered after Table 2.1.33

Figure 2.8. Crossplot of ϵ_{Nd} and $^{87}\text{Sr}/^{86}\text{Sr}$ compositions for Zanskar River sediments compared to other bedrock data from the Panjal Traps (Shellnutt et al., 2012; Shellnutt et al., 2014), the Greater and Lesser Himalaya (Ahmad et al., 2000; Deniel et al., 1987; Inger and Harris, 1993; Parrish and Hodges, 1996), Transhimalaya (Rolland et al., 2002), and additional Tethyan Himalaya (diamonds) and Greater Himalaya (squares; Richards et al., 2005) from the Sutlej River. Samples are numbered after Table 2.1.34

Figure 2.9. Diagram showing the progressive downstream variation in bulk sediment. (A) $^{87}\text{Sr}/^{86}\text{Sr}$ and (B) ϵ_{Nd} compositions for the Zanskar River. Error bars are smaller than symbol size for propagated Sr and ϵ_{Nd} errors. Samples are numbered after Table 2.1.35

Figure 2.10. KDE diagrams of U-Pb zircon ages from Zanskar River sediments.36

Figure 2.11. Schematic diagram illustrating detrital framework grain and detrital zircon populations of Zanskar sands. Q = quartz; F = feldspars; Lc = lithic carbonate; Lsm = other sedimentary and low-rank metasedimentary; Lm = medium- to high-rank metamorphic; and Lv = volcanic and metavolcanic. Rank of metamorphic grains and Metamorphic Index (0–500; Garzanti and Vezzoli, 2003). Concentrations of Zr >> 300 ppm may indicate hydraulic sorting and enrichment of sample in dense phases. Black line denotes trunk Zanskar River, with gray lines for tributaries. Samples are numbered after Table 2.1.40

Figure 2.12. Multidimensional scaling (MDS) plots showing the Kolmogorov-Smirnov distances between Zaskar River sediments and selected bedrock. (A) Classical MDS plot of bulk major element geochemistry data; (B) Nonmetric MDS plot of SRD-corrected bulk petrographic data; (C) Nonmetric MDS of Zaskar River detrital zircon U-Pb ages; and (D) Nonmetric MDS of selected Himalaya bedrock and Zaskar River detrital zircon U-Pb ages. Regional Himalayan U-Pb zircon data are same as Figure 2.13. Samples are numbered after Table 2.1. Data were plotted using R code ‘provenance’ written by Vermeesch et al. (2016). Solid lines indicate closest neighbor and dashed lines near neighbors in similarity calculations. Bedrock abbreviations in Fig. 2.12D mostly follow depositional ages: pЄ-Є = Proterozoic to Cambrian; D-O = Devonian to Ordovician; M-P = Mississippian to Permian; T-J = Triassic to Jurassic; LK = lower Cretaceous; uK-Pg = upper Cretaceous to Paleogene; and ZGH = Zaskar Greater Himalayan bedrock (Horton and Leech, 2013).42

Figure 2.13. KDE diagrams for selected bedrock U-Pb data for the Zaskar River Basin. Selected samples are from the Indus and Tar Groups (Henderson et al., 2010; Wu et al., 2007), Zaskar region Greater Himalaya (Horton and Leech, 2013), Panjal Traps (Shellnutt et al., 2011), and Cambro-Ordovician granites in Zaskar and the NW Himalaya (Cawood et al., 2007; Girard and Bussy, 1999; Kwatra et al., 1999; Miller et al., 2001; Pognante et al., 1990). Selected bedrock ages for southern Tethyan Himalaya, Greater Himalaya, and correlative strata from the eastern and central Himalaya were plotted (in gray) according to depositional age and compiled into composite KDE diagrams (Clift et al., 2014; DeCelles et al., 2000; Gehrels et al., 2011; Hu et al., 2015; Hu et al., 2012; McQuarrie et al., 2008; Myrow et al., 2010; Myrow et al., 2003).....44

Figure 3.1. Setting of the Zaskar River and Tso Kar basins. (A) Location of Indus River (gray) and Zaskar River basin (black outline; Figure 3.1B); (B) Topographic map river drainage and sample locations outside of the Padum Basin. Dashed boxes indicate location of Figures 3.4–3.5 and 3.9; (C) Oblique hillshade view to the southwest over the Padum Basin showing major tributaries (white), sample locations (stars), and Figure 3.3 cross-section locations (black lines). Topographic data were derived from Shuttle Radar Topography Mission 30-m grid data (SRTM30). Abbreviations are: HN = Hanumil; K = Karsha; KK = Karakoram; PM = Padum; PO = Pidmo; PS = Pishu; R = Rinam; ZG = Zangla; and ZZ = Zozar.56

Figure 3.2. Simplified geologic map of the Zaskar River basin after Fuchs (1987) with additions from Dèzes et al. (1999), southern Zaskar (Lahul) from (Steck et al., 1993) and Tso Kar area (Epard and Steck, 2008). Sample locations denoted by stars. Modified after Jonell et al. (in press).60

Figure 3.3. Schematic cross-sectional profiles (A–G) of river terraces in the Padum Basin. Profile locations indicated in Figure 3.1C. Diamonds indicate locations of OSL samples.64

Figure 3.4. Geomorphologic map of western Zaskar and Padum Basin. (A) Quaternary deposits of Padum Basin and Stod River valley; (B) Quaternary deposits of Padum Basin

on trunk Zanskar River (blue lines). Boxes indicate locations of Figs. 3.4C-E; (C) Quaternary deposits at Pishu village; (D) Quaternary deposits at Pidmo village; (E) Quaternary deposits at Hanumil. Reported ages from this study and literature: (a) Saha et al. (2015); (b) Sharma et al. (2016); and (c) Taylor and Mitchell (2000).65

Figure 3.5. Geomorphologic map of eastern Zanskar and Sarchu Basin of upper Tsarap River (blue lines). Reported ages from this study and literature: (a) Saha et al. (2015); (b) Sharma et al. (2016); and (c) Taylor and Mitchell (2000).67

Figure 3.6. Bulk petrographic compositions of modern river and terrace sediments from Zanskar. Compositions are classified by Q(quartz), F(feldspathic), and L(lithic) framework grains following the Gazzi-Dickinson method of point counting (Ingersoll et al., 1984) and classified after Garzanti and Vezzoli (2003). Gray lines indicate data corrections for Source Rock Density (SRD; Vermeesch et al., 2016). Fields for Greater Himalaya and Tethyan Himalaya are after Garzanti et al. (2007). Diamonds indicate trunk Zanskar River samples from Blöthe et al. (2014). Sample numbers follow Table 3.1.70

Figure 3.7. Kernel density estimation (KDE) diagrams of detrital zircon U-Pb ages from Zanskar River terrace sediments with age interval ranges illustrated in pie diagrams.73

Figure 3.8. Stacked river profiles of all Zanskar River tributaries. (A) Longitudinal river profiles with stacked slope ($<35^\circ$) and elevation values orthogonal to 2-km-wide swath profiles (marked with *). Swath profiles in narrow gorges used 1-km wide swaths (Markha, Khurna, Oma, Kurgiakh, and Tsarap Chu). Lower slope values ($<10^\circ$, blue) are layered above higher slope values. Profile colors and numbers are in reference to (B) for clarity. To best illustrate Rupshu Plateau valley-fills from Munack et al. (2016), the Toze Lungpa and Zara River profiles overlap. Gray shaded regions indicate large valley-fills within the Zanskar River basin from this study. Stored volumes reported in Table 3.4 are indicated next to each valley-fill. (B) Layout of Zanskar River tributaries with longitudinal profile numbers. RP = Rupshu Plateau (includes the More Plain). Confluence marked by “M” notes end of Rupshu Plateau.78

Figure 3.9. Pleistocene Rupshu Plateau valley-fills (pink) of the More Plain and upper Tsarap River tributaries, the Toze Lungpa, Sumkhel Lungpa, and Zara River (blue lines). Tso Kar maximum extent (shaded blue) after Wünnemann et al. (2010). Proposed paleo-Toze Lungpa drainage (dashed blue) and reported ~135 ka age for More Plain terrace (Munack et al., 2016).84

Figure 3.10. Bulk petrography downstream mixing schematic of framework grains from modern river tributary sediments (Jonell et al., in press) and selected terrace sediments. Q = quartz; F = feldspars; Lc = lithic carbonate; Lsm = other sedimentary and low-rank metasedimentary; Lm = medium- to high-rank metamorphic; and Lv = volcanic and metavolcanic. Rank of metamorphic grains and Metamorphic Index (0–500; Garzanti and Vezzoli, 2003). Black line denotes trunk Zanskar River, with gray lines for tributaries. Samples are labelled and numbered after Table 3.1.86

Figure 3.11. Multidimensional scaling (MDS) plots showing the Kolmogorov-Smirnov distances between modern Zaskar River sediments, river terrace sediments, and local bedrock. Number labels follow Table 3.1. (A) Nonmetric MDS plot of Source Rock Density(SRD)-corrected bulk petrographic data; (B) Nonmetric MDS plot of all Zaskar River detrital zircon U-Pb ages; (C) Zaskar River terrace sediments compared with modern Zaskar River sediments and compiled regional Himalayan bedrock U-Pb zircon age from Figure 3.12. Solid lines indicate closest neighbor and dashed lines nearest next neighbors. Data plotted using R ‘provenance’ package by Vermeesch et al. (2016). Bedrock abbreviations mostly follow depositional ages: pC-C = Proterozoic to Cambrian; D-O = Devonian to Ordovician; M-P = Mississippian to Permian; T-J = Triassic to Jurassic; LK = lower Cretaceous; uK-Pg = upper Cretaceous to Paleogene; and ZGH = Zaskar Greater Himalayan bedrock (Horton and Leech, 2013).88

Figure 3.12. KDE diagrams for detrital U-Pb zircon ages for all modern and Quaternary Zaskar River Basin sediments. Color bars indicate age peaks associated with Mississippian-Permian (245–380 Ma) magmatism, Cambro-Ordovician (440–550 Ma) magmatism, and a strong age peak (750–850 Ma) reported in modern Zaskar River sediments (Jonell et al., in press). Labels according to Table 3.1.90

Figure 3.13. KDE diagrams for detrital U-Pb zircon ages from the Zaskar River Basin and selected Himalayan bedrock. Selected samples are from the Indus and Tar Groups (Henderson et al., 2010; Wu et al., 2007), Zaskar region Greater Himalaya (Horton and Leech, 2013), Panjal Traps (Shellnutt et al., 2011), and Cambro-Ordovician granites in Zaskar and the NW Himalaya (Cawood et al., 2007; Girard and Bussy, 1999; Kwatra et al., 1999; Miller et al., 2001; Pognante et al., 1990). Selected bedrock ages for southern Tethyan Himalaya, Greater Himalaya, and correlative strata from the eastern and central Himalaya were plotted (in gray) according to depositional age and compiled into composite KDE diagrams (Clift et al., 2014; DeCelles et al., 2000; Gehrels et al., 2011; Hu et al., 2015; Hu et al., 2012; McQuarrie et al., 2008; Myrow et al., 2010; Myrow et al., 2003). Color bars indicate age peaks associated with Mississippian-Permian (245–380 Ma) magmatism, Cambro-Ordovician (440–550 Ma) magmatism, and a strong age peak (750–850 Ma) reported in modern Zaskar River sediments from references reported above. Labels according to Table 3.1. Figure adapted from Jonell et al. (in press).92

Figure 4.1. Study location in reference to southeast Asia. (A) Regional geographic map of southeast Asia outlining Song Gianh basin (black polygon) and political border of Vietnam (gray line), AR = Annamite Range, CH = Central Highlands, H = Hainan, KM = Kontum Massif, KP = Khorat Plateau, RR = Red River, and SH-Y = Song Hong-Yinggehai Basin; (B) Shaded topographic map derived from void-filled SRTM90 v.4.1 digital elevation model (DEM) grid data with delineated stream network (black line)..110

Figure 4.2. Geological map of the Song Gianh basin showing the simplified geology overlain with the modern drainage network. Map is redrawn from Fromaget et al. (1971). Sample colors follow Figure 4.1.113

Figure 4.3. Annual rainfall, local mean slope, and local relief maps for the Song Gianh basin. (A) Annual rainfall values derived from TRMM 3B42 data from 1998–2009 at $0.25^\circ \times 0.25^\circ$ resolution (Bookhagen and Burbank, 2006); (B) Average mean local slope calculated from DEM for Song Gianh basin. Black lines and open circles denote stream network and sample locations, respectively; (C) Mean local relief map, expressed as maximum elevation difference, using a moving ~ 5 km radius moving window.116

Figure 4.4. Longitudinal river profiles for the main stream and major tributaries of the Song Gianh with sample locations. Black stars mark modern sediment and white stars for terrace samples; black and white stars denote location with dual sampling. Dashed lines mark minor tributaries along the main stream. Colors follow Figure 4.1. Note the large knickpoint as a result of karst terrain and a perched alluvial basin at ~ 185 m above modern river level on the Song Nan. Also present are smaller perched alluvial basins and corresponding knickpoints in the upper reaches and lower Song Nan at ~ 50 m above modern river level.118

Figure 4.5. Plot of Chemical Index of Alteration (CIA) versus silica content of the samples considered in this study. SiO_2 is used as a proxy for the quartz sand content. Fields showing fine grained material from the Pearl, Mekong, and Red Rivers (gray crosses) are from Liu et al. (2007). Red River fine grained and sandy sediments analyzed by Clift et al. (2008) are gray circles. Lack of SiO_2 data precludes plotting Song Gianh terraces here.135

Figure 4.6. Downstream evolution in CIA within the Song Gianh basin. Note the general decrease in CIA downstream and that the terrace sediments are generally lower in CIA compared to the modern river at that location. Terrace samples are from the mainstream, except for those labeled ST that are from the Song Trac. Ages in parentheses are OSL ages. Sample colors follow Figure 4.1.136

Figure 4.7. Cross plot of Sr versus Nd isotope compositions for the Song Gianh compared with river sediments measured from the Red, Mekong and Pearl Rivers by Liu et al. (2007) and Clift et al. (2008). Basement samples from central and northern Vietnam are from Hoa et al. (2008), Lan et al. (2003) and Nagy et al. (2000). Central Highland volcanic rocks are compiled from various sources from Hoang et al. (1996). Sample colors follow Figure 4.1.137

Figure 4.8. Plots showing the downstream evolution in (A) Sr and (B) ϵ_{Nd} isotope compositions within the Song Gianh. Note that the mainstream stabilizes in composition in its middle reaches and does not seem much affected by flow from either of the northern tributaries. Error bars smaller than symbol size for Sr in Fig. 4.8A and propagated error for ϵ_{Nd} in Fig. 4.8B are gray brackets. Sample colors follow Figure 4.1.....138

Figure 4.9. KDE plots of U-Pb zircon dates from Song Gianh sediments, compared with bed rock data from the Kontum Massif from Nagy et al. (2001) and the Khorat

Plateau from Carter and Moss (1999) and Carter and Bristow (2003), and the Vietnamese Central Highlands from Carter et al. (2001).139

Figure 4.10. (A) Radial plot of apatite fission track data from the Song Trac tributary showing an approximately single population clustered around a central age of 54 Ma. (B) A KDE plot of the apatite fission track data.141

Figure 4.11. Multidimensional scaling (MDS) plot showing the Kolmogorov-Smirnov distances between sample zircon age spectra, following the method of Vermeesch (2013). Sample colors follow Figure 4.1.146

Figure 4.12. Plots showing downstream variation in specific age populations (A-E) within the mainstream (black dots linked by a solid line) and major tributaries showing how addition of sediment from the tributaries acts (or not) to influencing the bulk composition downstream of the confluence.148

LIST OF TABLES

Table 2.1 Sample locations for Zaskar River sediments.....	16
Table 2.2 Bulk petrography of Zaskar River sediments.....	19
Table 2.3 Major and trace element geochemistry of Zaskar River sediments.....	21
Table 2.4 Nd and Sr isotope geochemistry of Zaskar River sediments.....	25
Table 3.1 Sample locations for modern and terrace Zaskar River sediments.....	68
Table 3.2 Bulk petrography of Zaskar River terrace sediments.....	69
Table 3.3 OSL sample results for Zaskar River sediments.....	76
Table 3.4 Stored sediment volumes for Zaskar River and Tso Kar basins.....	80
Table 3.5 Zaskar River sediment yield estimates.....	103
Table 4.1 Sample locations for Song Gianh sediments.....	115
Table 4.2 Major and trace element geochemistry of Song Gianh sediments.....	120
Table 4.3 Nd and Sr isotope geochemistry of Song Gianh sediments.....	124
Table 4.4 Cosmogenic nuclide data for Song Gianh sediments.....	129
Table 4.5 OSL sample results for Song Gianh sediments.....	131

ABSTRACT

The influence of Quaternary climate variation on sediment generation, storage, and transport in two mountainous Asian river basin was examined in the largest tributary to the upper Indus River in the Himalayan rain shadow, the Zaskar River basin (~15,000 km²), and the smaller, subtropical Song Gianh basin (<3,500 km²) of central Vietnam.

Spatial patterns of erosion in the Zaskar River Basin were established to quantify the dominant controls on Quaternary sedimentation in the Himalayan rain shadow on the edge of the Tibetan Plateau. Glacial erosion and precipitation along the High Himalaya together dominate sediment production and transport in the Zaskar River basin, in contrast to the monsoon-dominated frontal Himalaya and the arid plateau interior.

Alluvial terrace document major phases of fluvial aggradation correlating with strong phases of monsoon and westerlies-derived precipitation during the Late Pleistocene (25–32 ka) and mid-Holocene (~6–8 ka), as similarly observed in the frontal Himalaya.

Valley-fills in the Zaskar River Basin emphasize a long history of climate-modulated sediment buffering in the rain shadow. Results here indicate that only a modest proportion of stored volumes (40% of total) are exported to the trunk Indus River during the Holocene. The work further underscores that sediment buffering outside of low floodplain regions can be volumetrically significant to the total sediment flux.

This work next explores the strongly monsoonal Song Gianh Basin of central Vietnam to better constrain how climate-driven erosional signals are transported and transformed downstream. Spatial patterns of erosion and dating of river terraces indicate that strong monsoonal rainfall drives modern sediment generation in the steep, upper reaches of the Song Gianh especially during the early Holocene (7.4–8.5 ka). Apparent

contrast between sediment provenance proxies and younger terracing (medieval and 18–19th century) instead reflect high sediment flux related to agricultural disruption rather than in response to Holocene climatic change. Human-induced erosion inundates modern Song Gianh river sediment compositions with old, weathered soils. This implies that modern offshore sediment signals delivered by larger rivers may be strongly modified by human activities and so must be considered judiciously when used as analogs for the geologic record.

CHAPTER 1. INTRODUCTION

1.1 Objectives and Themes

The Himalayan-Tibetan orogen has become a definitive natural laboratory for investigating interactions between solid Earth and earth surface processes because of its ongoing tectonic deformation, high elevation and relief, the highest concentration of glaciers outside polar latitudes, dramatic precipitation gradients, and extensive river drainages routing sediment to some of the largest submarine delta and fan systems in the world (Milliman and Meade, 1983; Dyurgerov and Meier, 2005). The geographic intersection of these features provides unparalleled opportunity for reconciling sedimentary histories and tectonic-climate-erosion feedbacks in landscapes over a range of spatial and temporal scales. Chapters 2 and 3 investigate links between Quaternary climate variability and erosion in the NW Himalaya.

This fruitful intersection between strong tectonic-climatic drivers and erosion in the Himalaya, however, is a double-edged sword. Unravelling an isolated response (i.e., erosion) to a forcing mechanism (i.e., summer monsoon) in active orogens and in large river systems with prolonged transport is problematic. A sedimentary signal of erosion deposited in the offshore is the many-fold, combined response to the perturbation(s) producing the signal in the source region, and all of the transport processes influencing that signal as it is routed from source to sink (Armitage et al., 2011). Episodic storage and release of sediments during transport, or sediment buffering, is one such process recognized to distort signals of erosion at least over 10^3 – 10^5 yr timescales (Jerolmack and Paola, 2010). Buffering makes constructing records for tectonic and/or climate from sedimentary deposits especially challenging. To isolate the impact of climatic signals and

eliminate the potential influence of sediment buffering and tectonism, a small, tectonically quiescent monsoonal river system with little/no floodplain in Vietnam is investigated in Chapter 4.

Quantifying and understanding the processes involved in buffering is one of the prime motivators for this dissertation. Each main chapter touches on sediment buffering but Chapter 3 explores this process in detail through river terracing in the NW Himalaya. Alluvial river terraces as landforms are unequivocal evidence for sediment buffering. Directly controlled by upstream sediment supply and run off, alluvial terraces record episodic river aggradation and incision, such that they offer a particularly promising archive for connecting geomorphic responses (i.e., sediment storage) to changes in tectonics, climatic, and/or drainage geometries through time. The utility of river terraces as landscape archives is also explored throughout this work.

1.2 Organization

The main chapters of this dissertation are arranged in a format that is characteristic for publication in peer-reviewed journals. The main chapters are already published or submitted for review. As each chapter was formatted with the intent to stand independently, some of the information may appear repetitive but is included here for clarity and continuity.

Much of this dissertation focuses on the relationship between Quaternary climate change and surface processes in two mountainous river systems in South and Southeast Asia, the Zaskar River of the NW Indian Himalaya and Song Gianh of central Vietnam. Chapter 2 first presents evidence for climatic controls on modern erosion in the Himalayan rain shadow by investigating the Zaskar River basin. Understanding how the modern climate-erosion relationship established in Chapter 2 may have varied spatially in

the past is further explored in Chapter 3. Quaternary volumetric sediment budgets are included and regional implications for erosion on the Tibetan Plateau margins are also discussed. Chapter 4 presents a separate but complementary study from the much smaller, but very monsoonal Song Gianh to understand how erosion, topography, and climate are linked outside the Himalaya. This chapter continues with the overall climate-erosion theme and expands to include anthropogenic influence on erosion and landscape evolution. And lastly, Chapter 5 briefly summarizes the broader impacts of these studies on the current state of knowledge regarding climate change and surface process linkages.

CHAPTER 2. CLIMATIC AND GLACIAL IMPACT ON EROSION PATTERNS AND SEDIMENT PROVENANCE IN THE HIMALAYAN RAIN SHADOW, ZANSKAR RIVER, NW INDIA

2.1 Abstract

Erosion is a key step in the destruction and recycling of the continental crust yet its primary drivers continue to be debated. The relative balance between climatic and solid Earth forces in determining erosion patterns and rates, and in turn orogenic architecture, is unresolved. The monsoon-dominated frontal Himalaya is a classic example of how surface processes may drive focused denudation and potentially control structural evolution. We investigate whether there is a clear relationship between climate and erosion in the drier Himalayan rain shadow on the periphery of the Tibetan Plateau where a coupled climate-erosion relationship is less clear. We present a new integrated dataset combining bulk petrography, geomorphometric analysis, detrital U-Pb zircon geochronology, and bulk Nd and Sr isotope geochemistry from modern river sediments that provides constraints on spatial patterns of sediment production and transport in the Zaskar River. Zaskar River sands are dominated by Greater Himalayan detritus sourced from the glaciated Stod River catchment that represents only 13% of the total basin area. Prevalent zircon peaks from the Cambro-Ordovician (440–500 Ma) and Mississippian-Permian (245–380 Ma) indicate more abundant pre-Himalayan granitoids in the northwest Indian Himalaya than in the central and eastern Himalaya. Erosion from the widely-exposed Tethyan Himalaya, however, appears modest. Spatial patterns of

This chapter previously appeared as: Jonell, T.N., Carter, A., Böning P., Pahnke, K. and Clift, P.D., 2016, Climatic and glacial impact on erosion patterns and sediment provenance in the Himalayan rain shadow, Zaskar River, NW India: Geological Society of America Bulletin, doi:10.1130/B31573. It is reprinted by permission of the Geological Society of America.

erosion do not correlate with highest channel steepness. Our data demonstrate that Zaskar differs from the monsoon-soaked frontal Himalaya and the arid, extremely slow-eroding Tibetan orogenic interior in that focused erosion and sediment production are driven by glaciers. Subsequent remobilization of glacially-derived sediments is likely controlled by monsoonal rainfall and we suggest sediment reworking plays an important role. These data support a strong climatic control on modern orogenic erosion in the Himalayan rain shadow on the periphery of the Tibetan Plateau.

2.2 Introduction

The destruction of orogenic systems is governed by the distribution and pace of tectonically driven rock uplift and surface processes. Solid Earth and climatic forces together facilitate denudation that in turn regulates the flux and composition of sediments recycled through rivers to the oceans. How these forces and their resultant erosion shape orogens is debated. Many studies argue for strongly linked climate-precipitation and focused erosion (e.g., Beaumont et al., 2001; Hodges et al., 2004; Thiede et al., 2004; Clift et al., 2008; Kirby and Ouimet, 2011) while others favor a decisive solid Earth control (Burbank et al., 2003; Wallis et al., 2016). Constraining the roles of these processes is crucial in quantifying how sedimentation may reflect tectonic and climatic conditions. Sedimentary records often provide the only means to reconstruct and compare exhumation and paleoenvironmental histories from long denuded mountain belts in relative continuity over geologic time.

The dramatic topographic and climatic gradients of the Himalaya-Tibetan orogen provide unparalleled opportunity to assess the interdependency between tectonics, climate, and surface processes. Intense summer monsoonal rainfall on the southern flank

of the Himalaya produces extreme erosion, steep topographic relief (Bookhagen et al., 2005a; Bookhagen and Burbank, 2006; Gabet et al., 2008), and some of the highest riverine fluxes of sediment to the ocean (Milliman and Meade, 1983). Erosion in river basins across the wet, frontal Himalaya, like the Marsyandi (e.g., (Attal and Lavé, 2006; Garzanti et al., 2007), Sutlej (Bookhagen and Burbank, 2006), and Alaknanda Rivers (Srivastava et al., 2008) tightly correlate with the spatial distribution and intensity of monsoon precipitation (Fig. 2.1). Moreover, focused erosion on the Himalayan front has been proposed to control the distribution of deep exhumation and tectonic strain (e.g., (Beaumont et al., 2000; Thiede et al., 2004).

How erosion is facilitated by climatic processes is less clear farther north in the Himalayan rain shadow, where high topography impedes northward advection of monsoonal moisture onto the Tibetan Plateau. Arid regions north of the Indus River in Ladakh and the Karakorum show exhumation rates scale with tectonically generated topography and glacial cover rather than with precipitation as found along the Himalayan front (Dortch et al., 2011b; Munack et al., 2014; Wallis et al., 2016). Despite this apparent lack of correlation between precipitation and erosion, some observations suggest the Himalayan rain shadow may be especially sensitive to climatic perturbations. Intense summer rainstorms have resulted in modern day examples of extreme erosion (i.e., Hobley et al., 2012) and suggest that volumetrically large sediment signals (>60% total flux) can be produced by only a few events (Bookhagen et al., 2005a; Wulf et al., 2010; Wulf et al., 2012). Yet whether these climatic events are geologically important is questioned by cosmogenic nuclides from river sediments analyzed by Munack et al. (2014) that indicate consistent rates of erosion both before and after the intensive climatic

events of the summer 2010 in Ladakh.

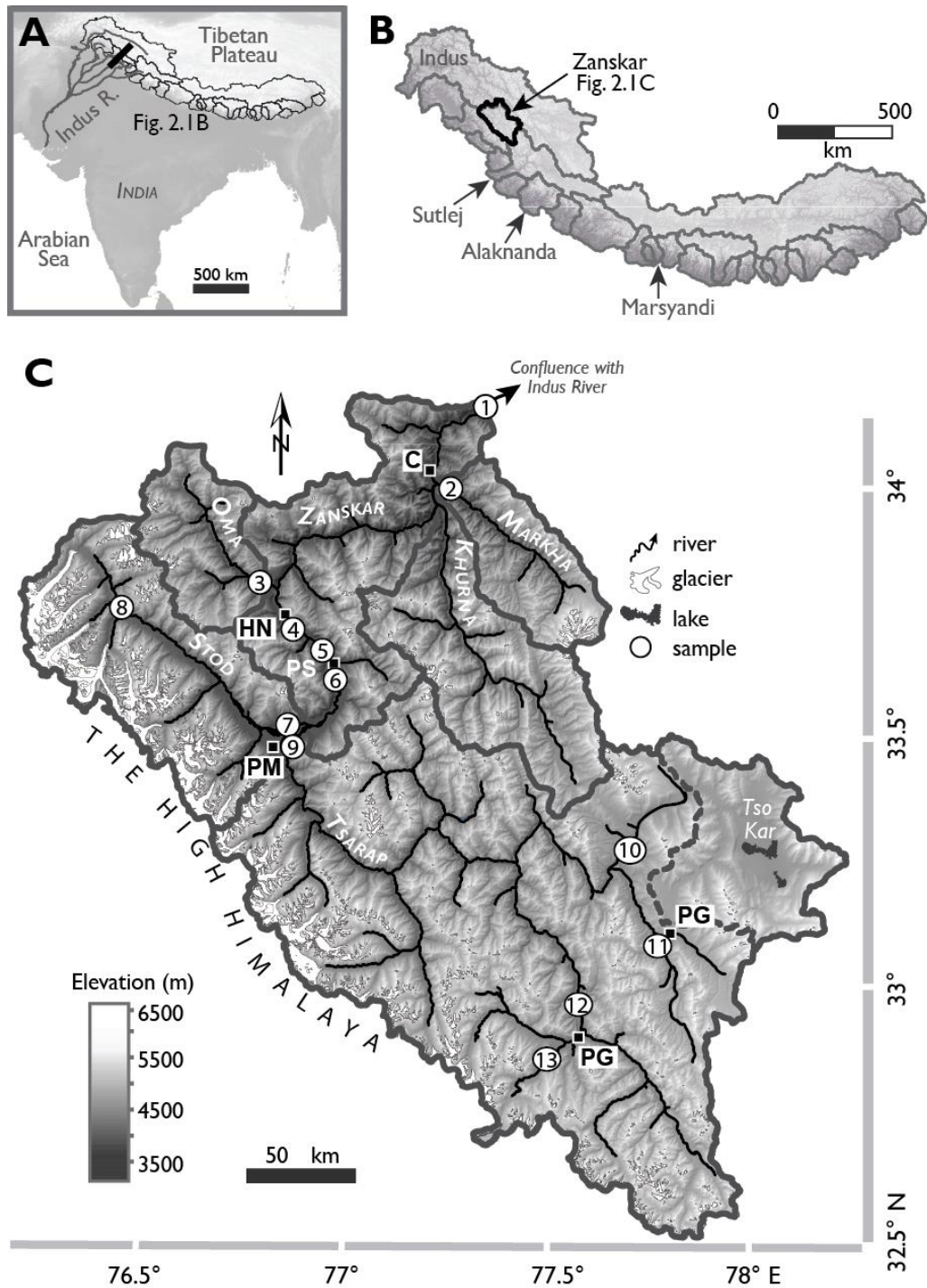
Here we examine whether precipitation, glaciation, or rock uplift dominate in controlling modern erosion on the western margin of the Tibetan Plateau in the Zaskar River basin. This river is ideally situated for evaluating coupling between climate and erosion because it is the largest river basin in the Himalayan rain shadow draining the High Himalaya towards the north, directly into the trunk Indus River. Our investigation sets out to quantify sediment provenance in the Zaskar River basin to establish the modern spatial distribution of erosion, or the “erosion patterns”. We further explore whether climate modulates sediment production and transport in the rain shadow as it does in the frontal ranges, or if present-day erosion instead reflects strong, underlying tectonic control.

2.3 Background

2.3.1 Climatic and Geographic Setting

The Zaskar River basin lies directly north of the Himalayan topographic divide on the southern edge of the Tibetan Plateau and occupies a modern drainage area of 14,939 km² (Fig. 2.1). All material sourced from the Zaskar River basin transmits to the Indus River, the main river system routing water and sediment from the western Himalaya into the Arabian Sea for roughly the last ~45 m.y. (Clift et al., 2001). The broader Zaskar River basin can be subdivided into five catchments of the main tributaries: the Tsarap, Stod, Khurna, Markha, and Oma Rivers (Fig. 2.1C). Glaciers occupy 8% of the Zaskar River basin, with some glacial tongues extending as low as ~4100 m (Taylor and Mitchell, 2000; Owen, 2011). Recessional and terminal moraines are preserved throughout Zaskar. Although glaciers were not much more widespread

Figure 2.1. Digital elevation model (DEM) maps of South Asia, the Himalaya, and Zaskar River basin. (A) Shuttle Radar Topography Mission 90 m (SRTM90) map of South Asia depicting the Indus River (gray lines) and all Himalayan river drainage outlines above 500 m (black lines). Gray overlay shows location of Figure 2.4; (B) SRTM DEM and hillshade of all Himalayan drainage basins with location of the Zaskar River basin (Fig. 2.1C) outlined in black; (C) Topographic map of the Zaskar River basin with sample numbers and locations. Glacial extent from Global Land Ice Measurements from Space (GLIMS) Version 1 data (Shrestha et al., 2014). Drainage basin polygons provided freely online by Bodo Bookhagen. Sample locations noted with white dots and village locations with black squares. Numbers in circles are after Table 2.1. Dashed gray line indicates extent of internally drained Tso Kar basin. Village names abbreviated as: C = Chilling; HN = Hanumil; PG = Pang; PM = Padum; PS = Pishu; and SR = Sarchu.



at the Last Glacial Maximum (~20 ka), older glaciations were quite extensive (Owen et al., 2005; Dortch et al., 2011; Hedrick et al., 2011; Dortch et al., 2013). One terminal moraine dated to ~78 ka extended as low as ~3400 m to create the Padum Basin, which is

a key confluence within the Zaskar catchment (Taylor and Mitchell, 2000; Owen et al., 2002).

Precipitation is delivered by the Summer Monsoon and Winter Western Disturbances (Westerlies) as rainfall in the summer (Jun–Aug) and snowfall in the winter, respectively (Benn and Owen, 1998). Dramatic attenuation of monsoonal precipitation across the topographic barrier of the High Himalaya produces a rain shadow to the north in the orogenic interior (Fig. 2.2). Likewise, a gradient is observed for Westerly-derived precipitation that decreases considerably to the southeast across this region (Leipe et al., 2014). Sutlej River basin weather station and hydrologic modelling data imply that 30–50% of the total annual precipitation to upper Indus River tributaries is received as winter snowfall, and contributes as much as ~66% of the total yearly discharge as snow or glacial meltwater (Bookhagen and Burbank, 2010; Burbank et al., 2012).

Modern erosion rates in the frontal Himalaya are tightly coupled with monsoonal rainfall and discharge (e.g., Goodbred, 2003; Gabet et al., 2008; Bookhagen and Burbank, 2010). Overall annual sediment fluxes from arid rain shadow regions, like the drier upper drainages of the Indus, Sutlej, and Marsyandi River basins (Fig. 2.1B), are lower because of lower runoff. In the upper Marsyandi and Sutlej Rivers, highest suspended sediment yields occur during late summer when temperatures are highest suggests that subglacial drainage channels provide the initial flux, with progressively rather than at the onset of monsoon season (Burbank et al., 2012; Wulf et al., 2012). This increasing contributions from hillslopes and river channels as summer monsoon rainfall arrives (e.g., Bookhagen and Burbank, 2010). Despite lower annual precipitation, high

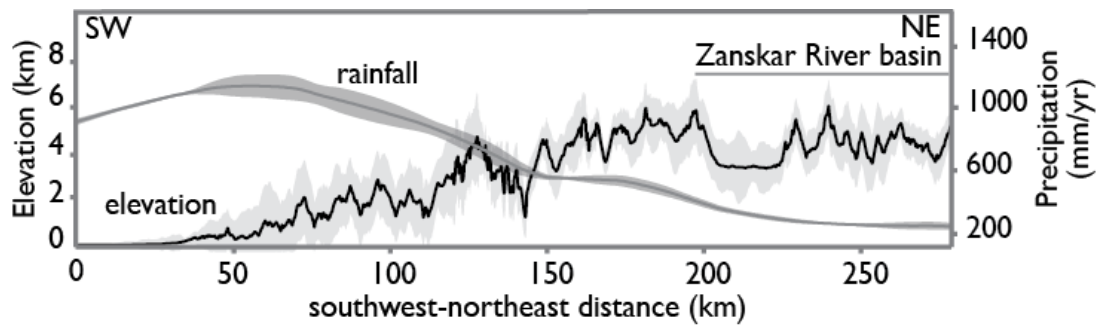


Figure 2.2. Swath profiles for topography and rainfall across the Himalayan front and into the Himalayan rain shadow. Values for profiles were extracted from a 50 km by 280 km transect shown in Fig. 2.1A. Solid lines indicate mean values with shaded regions signifying $\pm 2\sigma$.

intensity monsoonal rainstorms can produce extreme erosion and, in only a few events, produce 30–50% of the total annual sediment flux in semi-arid to arid regions (Wulf et al., 2010; Wulf et al., 2012). These observations suggest, that at least under modern day climatic conditions, regions directly adjacent to the present rainfall maxima in the rain shadow could potentially produce disproportionate sediment signals during such events (Bookhagen, 2010).

2.3.2 Geologic Setting

Basement rocks exposed in Zaskar can be divided into three lithotectonic groups: (1) the Tethyan Sedimentary Sequence, or Tethyan Himalaya; (2) the High Himalayan Crystalline Sequence, or Greater Himalaya; and (3) the Indus Suture Zone (Fig. 2.3). Exposures of these groups are structurally controlled by orogen parallel structures related to SW-verging thrust nappes and the Zaskar Shear Zone (ZSZ) (Dèzes et al., 1999). The ZSZ represents a ~150 km long strand of the South Tibetan Detachment (Herren, 1987), the major tectonic boundary that separates the Greater and Tethyan Himalaya in this part of the orogen (Burchfiel and Royden, 1985; Clark et al., 2004).

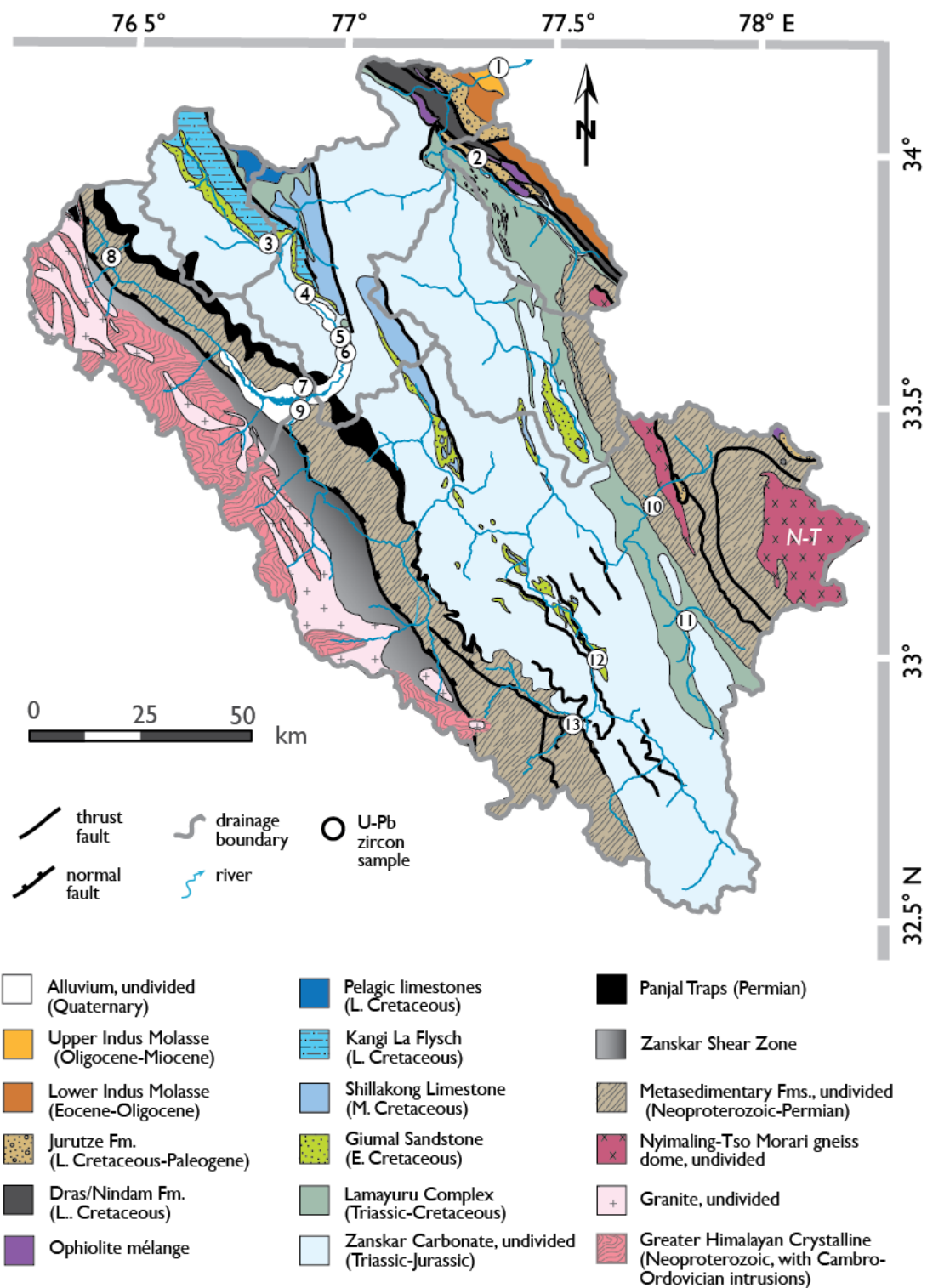


Figure 2.3. Simplified geologic map of the Zaskar River basin after Fuchs (1987) with additions from Zaskar Shear Zone from Dèzes et al. (1999), southern Zaskar (Lahul) from Steck et al. (1993), and Tso Kar area (Epard and Steck, 2008). N-T = Nymaling-Tso Morari gneiss dome.

The Tethyan Himalaya is a package of Neoproterozoic to early Paleocene sandstones, limestones, dolostones, and shales classically considered to have been deposited as a passive margin sequence on the northern margin of Greater India (Gaetani et al., 1983; Gaetani et al., 1986; Garzanti et al., 1986; Green et al., 2008). Tethyan Himalayan rocks are very low- to low-grade metasedimentary rocks, although parallel to the ZSZ and Nyimaling-Tso Moriri gneiss dome Neoproterozoic-Ordovician formations locally reach lower amphibolite facies (e.g., Gaetani et al., 1986; Fuchs, 1987; Steck et al., 1993; Dèzes et al., 1999).

Paleozoic magmatism produced two igneous suites observed in the Zaskar region: (1) Pan-African Cambro-Ordovician granitic plutons and (2) Mississippian-Permian granitic plutons associated with Panjal Traps flood basalts. U-Pb zircon ages constrain Pan-African (or Bhimphedian) Orogeny plutonism from ~435 to ~483 Ma (Pognante et al., 1990; Noble and Searle, 1995; Girard and Bussy, 1999; Godin, 2001; Cawood et al., 2007; Horton and Leech, 2013). Later Gondwanan rifting produced isolated granitic plutons dating 268–305 Ma (Spring et al., 1993; Noble et al., 2001; Horton and Leech, 2013) as well as Panjal Traps flood basalts at ~289 Ma (Singh et al., 1976; Shellnutt et al., 2011; Shellnutt et al., 2014).

Structurally below the Tethyan Himalaya and forming the core of the High Himalaya in Zaskar are the exhumed high-grade equivalents of the Neoproterozoic-Ordovician Tethyan Himalaya and late Paleozoic granitic intrusions, collectively referred to as the Greater Himalaya (Honegger et al., 1982; Pognante and Lombardo, 1989; Pognante et al., 1990; Searle et al., 1992; Dèzes et al., 1999; Walker et al., 2001; Schlup et al., 2003; Schlup et al., 2011; Horton and Leech, 2013). The Greater Himalaya in

Zaskar consists of amphibolite to lower granulite facies Neoproterozoic-early Cambrian paragneiss and metapelite (Herren, 1987), Cambro-Ordovician orthogneiss (Frank et al., 1977; Mehta, 1977; Stutz and Thöni, 1987; Pognante et al., 1990; Noble and Searle, 1995; Walker et al., 1999; Horton et al., 2015), and Mississippian-Permian orthogneiss (Honegger et al., 1982; Spring et al., 1993; Noble et al., 2001; Horton and Leech, 2013).

Rapid exhumation of the Greater Himalaya between the Main Central Thrust (MCT) and ZSZ from 26 Ma (Robyr et al., 2006) to ~17 Ma (Leloup et al., 2010) induced partial melting and injection of leucogranitic melts into the Greater and lower Tethyan Himalayan series (Noble and Searle, 1995; Dèzes et al., 1999; Robyr et al., 2006). Exhumation of Greater Himalayan material continued until ~16 Ma in the south of Zaskar to ~8 Ma around the Nyimaling-Tso Morari gneiss dome (Schlup et al., 2003; Schlup et al., 2011). No significant neotectonic activity in the Zaskar region is observed (Jade et al., 2010).

Sedimentation related to the collision of Greater India and Eurasia is documented in the third lithotectonic group, the Indus Suture Zone (e.g., Searle, 1983; Searle et al., 1990). Thrust slices of ophiolitic *mélange*, Indus Molasse sandstones, and Cretaceous-Eocene forearc basin strata are exposed near the Zaskar-Indus confluence (Searle et al., 1990; Pedersen et al., 2001; Clift et al., 2002; Henderson et al., 2010).

2.4 Methods

We use several complementary methods to constrain the provenance of modern sediment in the Zaskar River and understand how bulk sediment compositions evolve downstream before reaching the Indus River confluence. Sediment samples from the Zaskar River and its major tributaries were collected from 2012 to 2014 during

monsoon seasons from active channel beds and point bars (Table 2.1). We preferentially sampled very fine- to medium sand ($>63\ \mu\text{m}$) because this size fraction is commonly targeted for single-grain mineral provenance techniques that often limit evaluation of finer grain sizes owing to analytical spot size. By only targeting the bedload we cannot consider how suspended load contributes to provenance and this introduces biases to our analyses (Garzanti et al., 2009; Garzanti et al., 2011). However, we argue that our selected size fraction can be considered representative of the bulk zircon provenance (Yang et al., 2012) and provide important initial constraints on patterns of erosion in the Zaskar River basin.

2.4.1 Basin Morphology

We evaluated basin-wide and river channel morphology by extracting topographic parameters and longitudinal river profile data from digital elevation models. Topographic parameters were generated from the void-filled Shuttle Radar Topography Mission (SRTM) V4 90-m digital elevation model (Jarvis et al., 2008) provided by the Consultative Group on International Agricultural Research (<http://srtm.csi.cgiar.org>) and post-processed with an iterative fill routine (Whipple et al., 2007). Slope values were calculated using a 1 km-radius circular moving window. Local relief, expressed as maximum elevation difference, was calculated using a 5 km-radius circular moving window. Mean annual rainfall values were generated from the 1998–2009 Tropical Rainfall Measuring Mission (TRMM) 2B31 and 2B42 data products for the Himalaya (Bookhagen and Burbank, 2010). Extent of modern glaciers in the Zaskar River basin were derived from the Global Land Ice Measurements from Space (GLIMS) Version 1 data (Shrestha et al., 2014).

Table 2.1. Sample locations for Zaskar River sediments.

ID	Sample	Location	Lat (°N)	Long (°E)	Elevation (m)
1	8081203	Zaskar-Indus	34.162	77.326	3129
2	14072807	Markha	33.992	77.241	3311
3	12072207	Oma Chu	33.792	76.829	3420
4	13071402	Hanumil	33.716	76.877	3407
5	12072401	Pishu	33.682	76.941	3411
6	13071201	Pishu	33.635	76.983	3433
7	12072504	Lower Stod	33.518	76.911	3520
8	13071703	Upper Stod	33.817	76.432	4027
9	12072507	Lower Tsarap	33.461	76.883	3540
10	14080401	Zara	33.342	77.713	4454
11	13072301	Toze Lungpa	33.124	77.774	4496
12	13072302	Gata	33.008	77.594	4185
13	14080609	Yunam	32.885	77.533	4328

Longitudinal river profiles were generated from digital elevation model (DEM) data and smoothed every 2 km to remove elevation spikes. Under topographic steady-state, local channel slopes (S) follow a simple power-law scaling relationship with upstream drainage area (A):

$$k_s = \frac{S}{A^{-\theta}} \quad (2.1)$$

where k_s is the channel steepness index and θ is the concavity index (Hack, 1957; Flint, 1974). Channel steepness is often dependent on uplift rate but other pertinent factors, such as rock strength, precipitation, sediment flux, channel width, and channel hydraulic geometry, commonly influence this relationship (e.g., Sklar and Dietrich, 1998; Lavé and Avouac, 2001; Roe et al., 2002; Tucker and Whipple, 2002; Whipple and Tucker, 2002; Craddock et al., 2007). Discrimination of abrupt breaks in channel steepness can help identify factors perturbing model channel morphologies. Application of this index to longitudinal river profiles has become a powerful quantitative tool for extracting

information about the relationship between regional tectonics, topography and erosion in fluvial systems (e.g., Kirby and Whipple, 2001; Whipple and Tucker, 2002; DiBiase et al., 2010).

In this study we applied a fixed reference concavity, $\theta_{\text{ref}} = 0.45$, to facilitate comparison of data between river basins (Wobus et al., 2006) and generate a normalized channel steepness index, k_{sn} . Following a methodology similar to Ouimet et al. (2009), we used the freely available MatLab and ArcMap scripts (<http://www.geomorphotools.org>) to generate k_{sn} values every 2 km for all major tributaries draining $>100 \text{ km}^2$.

2.4.2 Bulk Sediment Petrography

Bulk, unsieved sediments were counted in thin sections with at least 200 points following the Gazzi-Dickinson method (Ingersoll et al., 1984) with lithic fragments classified after Garzanti and Vezzoli (2003) by noting the composition and metamorphic rank of rock fragments (MI Index). Thin sections were stained with alizarin red-S to distinguish calcite from dolomite. Sands were classified according to the relative proportion of quartz, feldspar, and lithic material in each sample exceeding 10%. Hydrodynamic processes can produce significant variability in the composition of sediments with identical provenance (Gazzi et al., 1973; Frihy et al., 1995; Garzanti et al., 2009). We can correct for this environmental bias and limit intrasample variability by applying a “Source Rock Density” (SRD) correction to our petrographic data (Garzanti and Andò, 2007a; Vermeesch et al., 2016). The relative abundance of mineral phases is adjusted according to their densities for each sample and corrected to a suitable SRD value appropriate for provenance type and erosion level (Garzanti and Andò, 2007b, a).

Data were corrected with an SRD of 2.71 g/cm³. Bulk petrographic data are reported in Table 2.2.

2.4.3 Major and Trace Element Geochemistry

Samples were analyzed for major and trace elements to provide a base characterization of the composition and the degree of chemical alteration. Carbonate was not removed prior to total digestion. All samples were freeze-dried and ground before mixing 600 mg of sample with 3600 mg of lithium tetraborate (LiB₄O₇; Spectromelt). Samples were pre-oxidized at 500°C with NH₄NO₃ and fused to glass beads. Samples were analyzed by X-Ray Fluorescence for Si, Al, Ti, Fe, Na, Ca, K, P, and Rb using a Philips PW 2400 X-ray spectrometer at the Institut für Chemie und Biologie des Meeres (ICBM) at the Carl von Ossietzky Universität, Oldenburg, Germany. Measurements on the XRF were followed after Böning et al. (2009). To assure accuracy and precision, several in-house standards and the certified standard of GSD-12 were analyzed, and results were better than 3%. Data are presented in Table 2.3.

2.4.4 Isotope Geochemistry

All sediments were analyzed for Sr and Nd isotopes as these isotopic systems can provide complementary insight on chemical weathering and provenance in sedimentary systems. Sr isotopic compositions are largely a function of the age and composition of silicate bedrock but chemical weathering is known to elevate ⁸⁷Sr/⁸⁶Sr values (Derry and France-Lanord, 1996). However, when provenance can be constrained by a system unaffected by transport or diagenetic processes, such as the largely immobile Sm- Nd system (Goldstein et al., 1984), the paired Rb-Sr and Sm-Nd isotopic systems make a powerful provenance proxy for siliciclastic sediments that has a proven track record in

Table 2 2. Bulk petrography of Zaskar River sediments.

ID	Sample	Location	Framework grains						Mica		Dense minerals									
			Q	F	Lc	Lsm	Lm	Lv	Mu	B	ZTR	Ep	Gt	Ky	Sil	A	Px	Ap	&	
1	8081203	Zaskar-Indus	28	10	6	119	10	18	0	0	0	0	0	0	156	0	0	3	1	
2	14072807	Markha	19	6	58	82	0	13	13	3	2	1	0	0	153	0	0	0	1	
3	12072201	Oma Chu	53	48	5	45	12	1	1	1	1	0	0	6	63	5	1	6	6	
4	13071402	Hanumil	36	39	44	28	11	10	2	2	1	0	0	3	93	4	0	16	2	
5	12072401	Pishu	58	56	15	19	18	6	0	1	2	0	0	3	58	3	1	5	4	
6	13071201	Pishu	73	64	2	21	21	3	1	2	2	0	0	3	47	0	1	4	2	
7	12072504	Lower Stod	12	26	32	60	16	17	6	0	1	0	0	2	125	4	4	6	3	
8	13071703	Upper Stod	27	51	31	48	4	4	1	7	4	1	0	3	87	2	0	11	4	
9	12072507	Lower Tsarap	39	36	0	6	71	0	4	4	1	2	0	1	77	0	1	16	2	
10	14080401	Zara	2	2	11	65	0	0	5	0	1	0	0	0	182	0	0	1	0	
					13															
11	13072301	Toze Lungpa	9	3	7	38	0	0	3	1	2	0	0	0	175	0	0	3	1	
12	13072302	Gata	19	12	5	59	79	0	2	4	0	0	0	0	143	0	0	0	3	
13	14080609	Yunam	23	31	10	59	34	4	3	3	0	0	0	2	107	2	0	6	2	

Table 2.2 (continued). Bulk petrography of Zaskar River sediments.

ID	Sample	Classification*	Dominant Lithology
1	8081203	quartzo-feldspatholithic	(meta)carbonaticlastic
2	14072807	quartzolithic	sedimentalclastic
3	12072201	quartzolithic	carbonaticlastic
4	13071402	feldspatho-quartzolithic	carbonaticlastic
5	12072401	feldspatho-quartzolithic	carbonaticlastic
6	13071201	feldspatho-quartzolithic lithic-	(meta)carbonaticlastic
7	12072504	feldspathoquartzose	metamorphiclastic
8	13071703	feldspatholithic	(meta)carbonaticlastic
9	12072507	quartzo-feldspatholithic	carbonaticlastic
10	14080401	feldspatho-quartzolithic	metamorphiclastic
11	13072301	lithic	carbonaticlastic
12	13072302	lithic	carbonaticlastic
13	14080609	quartzolithic	metamorphiclastic

Note:

* Classified according to relative proportion of quartz, feldspar, and lithic material exceeding 10% of QFL total.

the NW Himalaya (e.g., Clift et al., 2002). The bulk silicate sediment fraction was analyzed for most samples, but a few samples only allowed analysis of the <300 μm fraction.

Samples were first leached using buffered acetic acid to remove any carbonate-bound Sr prior to total digestion. Mn-Fe oxides containing authigenic Sr, and potentially any material bearing authigenic Nd, were removed with a leach of 25% (v/v) acetic acid and 0.02 M hydroxylamine hydrochloride (HH). All Sr and Nd signatures measured are therefore assumed to originate from the silicate fraction, perhaps with minor fractions of dolomite. Leached sediments were digested in closed PTFE-vessels following the procedure described in Böning et al. (2004). Briefly, organic matter was oxidized from all samples by treatment with concentrated HNO_3 overnight. Subsequently, HF and HClO_4

Table 2.3. Major and trace element geochemistry of Zaskar River sediments.

ID	Sample	Location	SiO ₂	TiO ₂	Al ₂ O ₃	Fe ₂ O ₃	MnO	MgO	CaO	Na ₂ O	K ₂ O	P ₂ O ₅
1	8081203	Zaskar-Indus	46.87	0.41	8.57	3.13	0.05	2.03	19.79	1.30	1.69	0.12
2	14072807	Markha	46.16	0.43	7.43	4.33	0.07	2.38	20.46	0.94	1.11	0.14
3	12072207	Oma Chu	43.04	0.70	7.52	4.77	0.04	2.81	20.57	0.60	1.48	0.14
4	13071402	Hanumil	61.78	0.63	9.60	3.43	0.17	1.56	11.44	1.82	1.62	0.39
5	12072401	Pishu	58.89	0.39	9.49	2.72	0.05	1.61	12.49	1.79	2.03	0.14
6	13071201	Pishu										
7	12072504	Lower Stod	71.57	0.43	12.14	2.77	0.09	1.12	3.85	2.41	2.60	0.21
8	13071703	Upper Stod	46.37	0.56	8.19	3.99	0.06	3.40	19.48	1.38	1.26	0.12
9	12072507	Lower Tsarap	59.69	0.31	8.76	2.28	0.08	1.31	13.34	1.84	1.78	0.13
10	14080401	Zara	76.97	0.64	10.64	3.91	0.07	1.31	0.83	1.78	2.25	0.14
11	13072301	Toze Lungpa	26.23	0.30	6.54	3.65	0.04	2.10	32.97	0.52	0.81	0.08
12	13072302	Gata	31.42	0.37	4.42	2.26	0.03	2.80	32.05	0.44	0.94	0.09
13	14080609	Yunam	74.47	0.45	6.64	3.13	0.08	1.88	5.33	0.44	1.95	0.12

Table 2.3 (continued). Major and trace element geochemistry of Zaskar River sediments.

ID	Sample	Location	As	Ba	Ce	Co	Cr	Cu	Ga	Mo	Ni	Nb	Pb	Rb	Sr	Th	Y	V	U	Zn	Zr
1	8081203	Zaskar-Indus	8	313	75	8	59	16	11	0	30	11	20	70	612	11	20	51	5	39	153
2	14072807	Markha	12	173	55	15	263	22	10	1	83	10	16	50	794	11	25	62	3	52	197
3	12072207	Oma Chu	15	222	79	10	103	17	11	1	42	17	12	50	442	10	19	90	3	61	233
4	13071402	Hanumil	14	419	278	8	33	9	11	0	7	21	23	57	349	38	69	48	10	31	703
5	12072401	Pishu	5	442	73	7	37	8	10	0	17	12	25	82	343	14	21	46	9	32	170
6	13071201	Pishu																			
7	12072504	Lower Stod	5	691	154	8	32	8	13	0	12	15	31	92	358	19	36	42	6	32	289
8	13071703	Upper Stod	5	262	59	10	70	17	9	2	31	11	12	48	365	13	22	85	1	31	216
9	12072507	Lower Tsarap	6	293	51	6	23	10	10	0	11	7	23	71	280	11	29	34	7	25	191
10	14080401	Zara	10	300	46	12	43	12	13	0	21	14	17	113	72	14	26	57	7	41	194
11	13072301	Toze Lungpa	3	115	39	10	43	13	10	1	23	9	10	43	838	11	18	57	-2	40	101
12	13072302	Gata	9	130	46	7	27	7	5	1	11	10	8	37	611	11	18	44	0	19	276
13	14080609	Yunam	12	315	57	8	31	10	8	1	16	11	10	78	80	10	18	45	2	19	211

were added and the vessels were heated for 12 h at 180°C. After digestion, solutions were evaporated on a heated metal block (180°C) and residues were redissolved, fumed three times with 6N HCl, and dissolved finally in 1N HNO₃. All acids were of ultrapure quality. To isolate rare earth elements (REEs) and Sr, the remaining solutions were put through two-step column chemistry using Eichrom TRU-Spec resin. Nd was separated from interfering REEs using Eichrom LN-Spec resin with 0.23–0.25 N HCl as eluant. The fraction containing Rb and Sr was loaded on Eichrom Sr-Spec columns using HNO₃, Rb was washed out with HNO₃, and Sr was eluted with Milli-Q water.

Isotopic compositions of Nd and Sr were analyzed using a Thermo Neptune Plus Multicollector ICP-MS at the ICBM in Oldenburg. Samples for Nd were analyzed using the Nd standard JNdi-1. The ¹⁴³Nd/¹⁴⁴Nd values of all samples were corrected for internal mass fractionation using ¹⁴⁶Nd/¹⁴⁴Nd = 0.7219 and normalized to the reported JNdi-1 value of ¹⁴³Nd/¹⁴⁴Nd = 0.51215 (Tanaka et al., 2000). Internal mass fractionation for Nd was corrected for using ¹⁴⁶Nd/¹⁴⁴Nd = 0.7219. Nd isotopic compositions are expressed in ε_{Nd} notation:

$$\epsilon_{\text{Nd}} = \left[\frac{\left(\frac{^{143}\text{Nd}}{^{144}\text{Nd}} \right)_{\text{sample}}}{\left(\frac{^{143}\text{Nd}}{^{144}\text{Nd}} \right)_{\text{CHUR}}} - 1 \right] * 10^4 \quad (2.2)$$

(¹⁴³Nd/¹⁴⁴Nd)_{CHUR} is the Chondritic Uniform Reservoir with a value of 0.512638 (Jacobsen and Wasserburg, 1980). The external reproducibility is calculated for each session separately using the analyses of JNdi-1 and was generally better than ±0.000015 or ± 0.3 ε_{Nd} units (2σ). The BCR-2 standard (n = 4) had an ε_{Nd} value of 0.1 (± 0.3, 2σ) and was well within the reported ε_{Nd} value of 0.0 ± 0.2 (Raczek et al., 2003). The procedural blank was ≤ 30 pg Nd.

Samples for Sr were analyzed using standard-sample bracketing techniques using NBS987 and normalized to the reported value of 0.710248 (Thirlwall, 1991). Mass fractionation for Sr was corrected using $^{86}\text{Sr}/^{88}\text{Sr} = 0.1194$. Contents of Kr, Rb, and Ba were monitored and found to be negligible. The external reproducibility is calculated using the analyses of NBS987 and was generally better than 80 ppm (2σ). The BCR-2 standard ($n = 4$) had a $^{87}\text{Sr}/^{86}\text{Sr}$ ratio of 0.70502 ± 0.00004 (2σ) and was within the reported $^{87}\text{Sr}/^{86}\text{Sr}$ ratio of 0.70496 ± 0.00002 (Raczek et al., 2003). The procedural blanks were negligible throughout. Results are reported in Table 2.4.

2.4.5 Detrital U-Pb Zircon Geochronology

Detrital zircon U-Pb dating has an established history of resolving questions on sediment provenance within Himalayan river systems (e.g., Amidon et al., 2005; Alizai et al., 2011) and in other drainage basins in Asia (e.g., He et al., 2013; Robinson et al., 2014). Zircon is a common mineral and is chemically and mechanically resistant to erosion, such that several cycles of erosion and sedimentation do not significantly alter U and Pb compositions (Gehrels, 2014). In this study we target the 63–250 μm size fraction because this range can effectively yield the same distribution of all significant age populations present in the bulk zircon population (Yang et al., 2012).

The use of U-Pb zircon dating for the Zaskar River is especially appropriate because there are a significant number of existing U-Pb zircon bedrock analyses from Himalaya bedrock. Although lithostratigraphic units in the western Himalaya have zircon populations that overlap, strong preferential occurrence of certain age groups can aid in identifying regions of sediment yield (e.g., Clift et al., 2004; Bernet et al., 2006; Wu et al., 2007; Gehrels et al., 2011; White et al., 2011; Shellnutt et al., 2014). Samples were

Table 2.4. Nd and Sr isotope geochemistry of Zaskar River sediments.

ID	Sample	Location	Size fraction	normalized $^{143}\text{Nd}/^{144}\text{Nd}^{\S}$	internal error $^{143}\text{Nd}/^{144}\text{Nd}$ (2 σ)	ϵ_{Nd}	external error (2 σ SD)	external error (ϵ_{Nd} , 2 σ SD)	propagated error (2 σ) $^{\&}$
1	8081203	Zaskar-Indus	<300um	0.511877	0.000010	-14.8	0.000008	0.16	0.25
2	14072807	Markha	bulk	0.511983	0.000004	-12.8	0.000010	0.21	0.21
3	12072207	Oma Chu	<300um	0.512125	0.000009	-10.0	0.000007	0.14	0.23
4	13071402	Hanumil	bulk	0.511891	0.000006	-14.6	0.000010	0.21	0.23
5	12072401	Pishu	<300um	0.511842	0.000005	-15.5	0.000011	0.22	0.24
7	12072504	Lower Stod	<300um	0.511897	0.000004	-14.5	0.000008	0.16	0.17
8	13071703	Upper Stod	bulk	0.511985	0.000008	-12.7	0.000010	0.21	0.25
9	12072507	Lower Tsarap	<300um	0.511939	0.000009	-13.6	0.000008	0.16	0.23
10	14080401	Zara	bulk	0.511835	0.000003	-15.7	0.000010	0.21	0.21
11	13072301	Toze Lungpa	bulk	0.511852	0.000006	-15.3	0.000010	0.21	0.23
12	13072302	Gata	bulk	0.511745	0.000012	-17.4	0.000010	0.21	0.30
13	14080609	Yunam	bulk	0.511753	0.000006	-17.3	0.000010	0.21	0.23

Notes:

\S measured $^{143}\text{Nd}/^{144}\text{Nd}$ ratios were normalized to the JNdi-1 value of 0.512115 (Tanaka et al., 2000).

ϵ measured $^{87}\text{Sr}/^{86}\text{Sr}$ ratios were normalized to the NBS987 value of 0.710248 (Thirlwall, 1991).

$\&$ reported error, determined as $\sqrt{\{(\text{internal error})^2 + (\text{external error})^2\}}$

Table 2.4 (continued). Nd and Sr isotope geochemistry of Zaskar River sediments.

ID	Sample	Location	normalized $^{87}\text{Sr}/^{86}\text{Sr}^{\epsilon}$	internal error (2σ SD)	external error (2σ SD)	propagated error (2σ) ^{&}
1	8081203	Zaskar-Indus	0.722856	0.00001	0.000025	0.000027
2	14072807	Markha	0.715952	0.00003	0.000021	0.000036
3	12072207	Oma Chu	0.715388	0.00002	0.000025	0.000030
4	13071402	Hanumil	0.725956	0.00001	0.000021	0.000025
5	12072401	Pishu	0.729091	0.00001	0.000030	0.000033
7	12072504	Lower Stod	0.723722	0.00001	0.000025	0.000027
8	13071703	Upper Stod	0.723463	0.00001	0.000021	0.000022
9	12072507	Lower Tsarap	0.752802	0.00002	0.000025	0.000029
10	14080401	Zara	0.755070	0.00002	0.000021	0.000028
11	13072301	Toze Lungpa	0.722722	0.00001	0.000021	0.000023
12	13072302	Gata	0.713990	0.00001	0.000021	0.000026
13	14080609	Yunam	0.749729	0.00003	0.000021	0.000039

Notes:

[§] measured $^{143}\text{Nd}/^{144}\text{Nd}$ ratios were normalized to the JNdi-1 value of 0.512115 (Tanaka et al., 2000).

^ε measured $^{87}\text{Sr}/^{86}\text{Sr}$ ratios were normalized to the NBS987 value of 0.710248 (Thirlwall, 1991).

[&] reported error, determined as $\sqrt{\{(\text{internal error})^2 + (\text{external error})^2\}}$

separated for zircon using standard magnetic and heavy liquid techniques. A rare-earth element hand magnet was passed several times over the sample to remove extremely magnetic material and sieved again to 63–250 μm before magnetic separation. All samples were pre-treated using hydrogen peroxide, acetic acid, and oxalic acid to remove organic material, carbonate, and Fe-oxides, respectively. Zircons were mounted in epoxy, polished, and imaged by reflected light and cathodoluminescence.

U-Th-Pb isotopic compositions were determined at the London Geochronology Centre facilities at University College London using a New Wave 193 nm aperture-imaged frequency-quintupled laser ablation system, coupled to an Agilent 7700 quadrupole-based ICP–MS. An energy density of $\sim 2.5 \text{ J/cm}^2$ and a repetition rate of 10 Hz were used during laser operation. Laser spot diameter was $\sim 30 \mu\text{m}$ with sampling depth of $\sim 5 \mu\text{m}$. Sample-standard bracketing by measurement of external zircon standard PLESOVIC (Sláma et al., 2008) and NIST 612 silicate glass (Pearce et al., 1997) were used to correct for instrumental mass bias and depth-dependent intra-element fractionation of Pb, Th and U. Temora (Black et al., 2003) and 91500 (Wiedenbeck et al., 2004) were used as secondary zircon age standards. Over 100 grains were analyzed for each sample to provide a statistically robust dataset for lithologically diverse units (Vermeesch, 2004). Age data were filtered using a $\pm 15\%$ discordance cut-off. For grains with ages less than 1000 Ma, the $^{206}\text{Pb}/^{238}\text{U}$ ratio was used and the $^{207}\text{Pb}/^{206}\text{Pb}$ ratio for grains older than 1000 Ma. All measurements were processed using GLITTER 4.4 data reduction software (Griffin et al., 2008). Time-resolved signals recording isotopic ratios with depth in each crystal enabled filtering to remove signatures owing to overgrowth boundaries, inclusions and/or fractures. Individual U-Pb ages are reported at 1σ .

Kernel density estimations (KDE) provide robust age distributions and are presented in the text for visual analysis of age population distributions and abundance. Traditional probability density functions may smooth older age populations that inherently have a greater age error than younger populations at 1σ , therefore KDEs are favored in this study to prevent this bias (Vermeesch, 2012). Multidimensional scaling (MDS) was performed using R.info Version 3.1.1 programming codes modified after Vermeesch (2013) to quantitatively compare zircon spectra.

2.5 Results

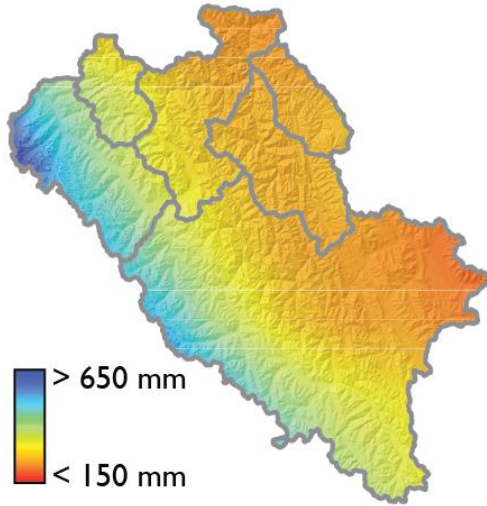
2.5.1 Basin Morphology

A large-scale rainfall gradient exists across Zaskar from the southwest to the northeast (Fig. 2.2 and 2.4A), with highest mean annual rainfall (>400 mm/yr) values observed in the northwest inside the Stod River catchment. Lowest values (<150 mm/yr) occur around Tso Kar (Fig. 2.1C). Steepest slopes are in the Stod and Khurna catchments, as well as the Zaskar Gorge, (Fig. 2.4B), that correspondingly also indicate regions of highest local relief (Fig. 2.4C).

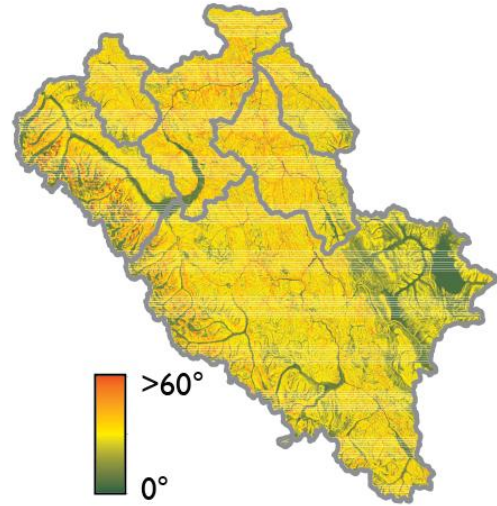
Zaskar channel profile geometries (Fig. 2.5) indicate strong glacial modification. Remnants of multiple recessional moraines exist in the lower Tsarap River, the overdeepened Stod and Khurna Rivers, and the steep, headwater Tsarap tributaries. The broad, alluviated Padum Basin ends with a terminal moraine at Hanumil (Fig. 2.1C). The Zaskar Gorge can be characterized in general as a large knickzone. Reworking of a recessional moraine results in a small knickzone in the lower Tsarap River, although the knickzone is likely enhanced in part by a remaining artifact in the DEM data.

Normalized channel steepness values (Fig. 2.4D) correspond to several locations

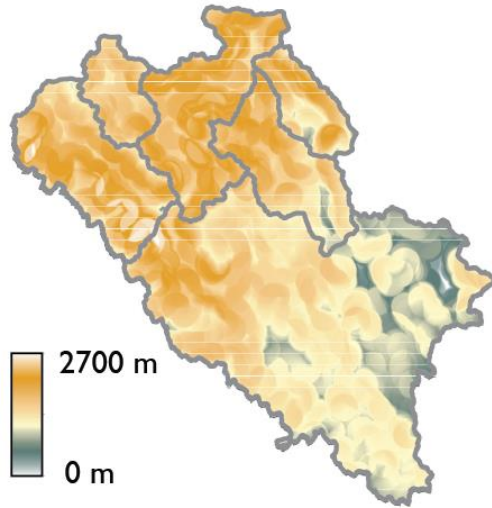
A. Mean annual rainfall



B. Slope



C. Local 5-km relief



D. Normalized channel steepness (k_{sn})

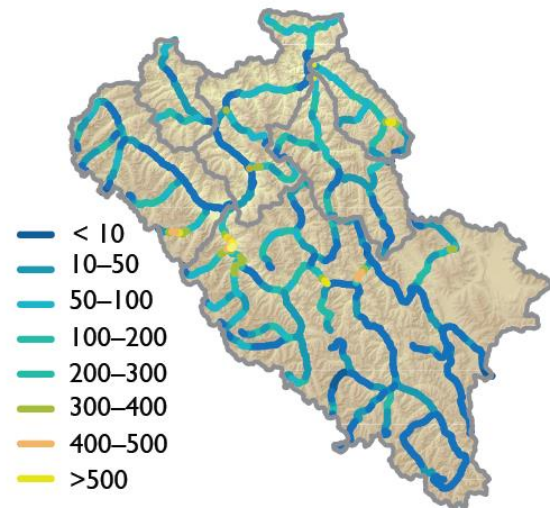


Figure 2.4. Parameter maps for evaluating morphology and erosion in the Zanskar River basin. (A) TRMM mean annual rainfall distribution map illustrating the precipitation gradient from west to east. Rainfall map was created using the 1998–2009 TRMM time series for mean annual rainfall; (B) Mean slope for the Zanskar River basin calculated using a 1-km radius circular moving window; (C) Local 5-km relief expressed as the difference between maximum and minimum elevation in a given area of a 5-km radius circular moving window; (D) Normalized channel steepness index (k_{sn}) calculated using TopoToolbox 2.0 (Schwanghart and Scherler, 2014). Subcatchments within the Zanskar River basin are outlined in gray.

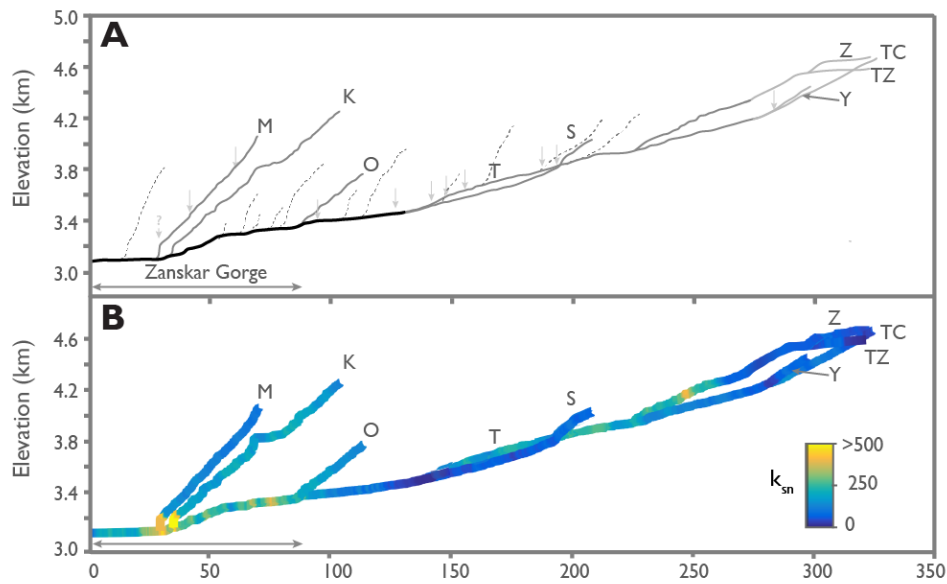


Figure 2.5. Longitudinal profiles for tributaries of the Zanskar River. (A) Raw channel profiles were smoothed using a 2 km radius moving average window to remove elevation spikes. Black dashed lines mark trunk river tributaries; light gray dotted lines mark minor tributaries to Tsarap River catchment. Arrows indicate published locations of recessional moraines (Burbank and Fort, 1985; Mitchell et al., 1999; Owen and Benn, 2005; Damm, 2006); (B) Mean normalized channel steepness index (k_{sn}) values plotted every 2 km along river longitudinal profiles for all main streams. Values were extracted using MATLAB code adapted from TopoToolbox 2.0 (Schwanghart and Scherler, 2014). Abbreviations for streams are: K = Khurna; M = Markha; O = Oma Chu; S = Stod;; T = Tsarap; TC = Tsarap Chu; TZ = Toze Lungpa; and Y = Yunam.

for recessional moraines in small, headwater tributaries, and in the lower Tsarap, Khurna and Markha Rivers (Fig. 2.5). The highest k_{sn} values (>500) occur in the upper Zanskar Gorge and in short segments in the middle reaches of the Tsarap River containing bedrock gorges. We do not include k_{sn} values for the presently endorheic Tso Kar basin (Fig. 2.4D) but do include other morphometric parameters for this region for reference.

2.5.2 Bulk Sediment Petrography

The Zanskar River transports an incredible diversity of sands that range from lithic carbonaticlastic to feldspatho-quartzolitic metamorphiclastic compositions (Table 2.2). Framework petrography indicates abundant quartz, feldspar, low rank

metacarbonate, high-rank fibrolite-bearing metafelsite fragments, with minor chert, epidote-bearing metabasite, and serpentinized ultramafic rock fragments. Abundant mineral grains include calcite and dolomite spar, mica, sillimanite, green amphibole, and ultrastable minerals such as zircon, blue-green tourmaline, rutile, and titanite. Minor kyanite, garnet, staurolite, and brown amphibole are noted. Most sands contain moderate amounts of mica and/or dense minerals but most carbonaticlastic sands are poor in both micaceous and dense phases.

Zanskar River sediments roughly divide into two petrographic groups (Fig. 2.6). Samples containing slightly more lithic fragments, predominantly more carbonate and lesser volcanic fragments, fall within rocks of Tethyan Himalayan affinity (Fig. 2.6A). Samples that are slightly more quartzofeldspathic lie closer to rocks with Greater Himalayan affinity. Similarly, samples with higher grade metamorphic minerals fall nearer rocks of known Greater Himalayan affinity (Fig. 2.6B).

2.5.3 Major and Trace Element Geochemistry

Major element geochemistry can be effective in assessing the intensity of chemical weathering. The “Chemical Index of Alteration” proxy expressed as:

$$CIA = \left[\frac{Al_2O_3}{(Al_2O_3 + Na_2O + K_2O + CaO^*)} \right] * 100 \quad (2.3)$$

can be used to compare the relative leaching of labile elements (K, Na, silicate-only Ca) to residual, immobile Al during feldspar weathering (Nesbitt et al., 1980). CIA values range from 50 to 100 with higher values indicating stronger chemical weathering. A correction is made to CIA values if excess CaO is present in carbonates and phosphates by assuming a reasonable Ca/Na ratio for the silicate material and correcting for CaO in phosphate (Singh et al., 2005).

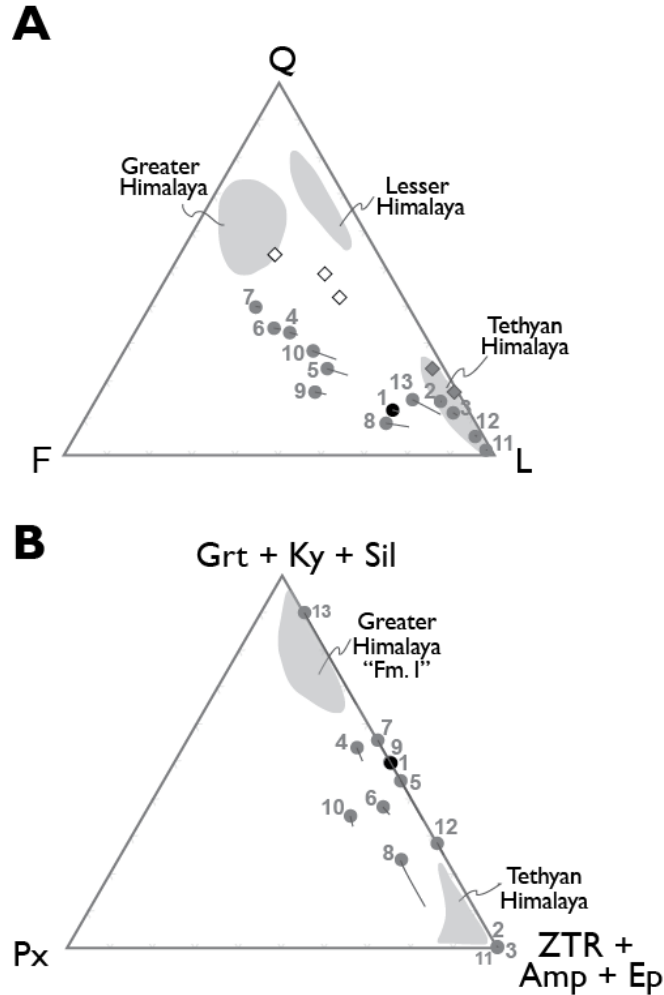


Figure 2.6. Bulk petrographic compositions of Zaskar sediments. (A) Bulk compositions classified by Q (quartz), F (feldspathic), and L (lithic) framework grains following the Gazzi-Dickinson method of point counting (Ingersoll et al., 1984) and classified after Garzanti and Vezzoli (2003). Gray lines indicate data corrections for Source Rock Density (SRD; Vermeesch et al., 2016). Open diamonds are petrographic data from the lower Zaskar Gorge, where Z = Zaskar-Indus confluence and M = Markha River (Blöthe et al., 2014); (B) Bulk composition of Zaskar sediments plotted onto the (garnet + kyanite + sillimanite) – pyroxene – (zircon + tourmaline + rutile + amphibole + epidote) ternary diagram. Fields for Greater Himalaya “Formation I” kyanite- and fibrolite-bearing gneiss, Tethyan and Lesser Himalaya drawn after Garzanti et al. (2007). Samples are numbered after Table 2.1.

Zaskar River sediments (Table 2.3; Fig. 2.7) span low to moderate CIA values (52–71). In general, higher CIA values occur in upstream tributaries and lower values, indicating less intense weathering, occur in the lower Tsarap (ID #9) and Stod (ID #7, #8)

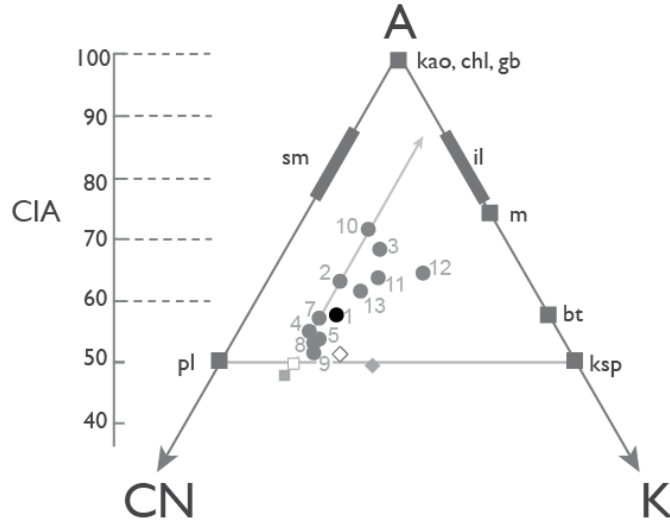


Figure 2.7. Bulk major element geochemistry of Zanskar River sediments plotted on the ternary Al_2O_3 - $\text{CaO}+\text{Na}_2\text{O}$ - K_2O diagram (Fedo et al., 1995) with Chemical Index of Alteration (CIA) values (Nesbitt et al., 1980). Mineral abbreviations are as follows: bt = biotite; chl = chlorite; gb = gibbsite; il = illite; kao = kaolinite; ksp = potassium feldspar; m = muscovite; pl = plagioclase; sm = smectite. Samples for average Archean upper crust (gray square), average granodiorite (open square), average granite (open diamond), and average A-type granite (gray diamond) are shown (Anderson and Bender, 1989; Condie, 1993; Winter, 2010). Line indicates typical weathering evolution path for bedrock unaffected by K-metasomatism (Fedo et al., 1995). Samples are numbered after Table 2.1.

Rivers, and Padum Basin sediment samples of Pishu (#5) and Hanumil (ID #4). CIA values are poorly correlated to SiO_2 , with slight negative correlation as silica contents increase.

2.5.4 Isotope Geochemistry

Variations in Sr and Nd isotopes for Zanskar River sediments and regional bedrock source terranes are plotted in Figure 8. Isotopic compositions for decarbonated Zanskar River sediments display a range in ϵ_{Nd} values from -10 to -17.4 and a wide range of $^{87}\text{Sr}/^{86}\text{Sr}$ isotope values from 0.713990 to 0.755070. No coherent correlation exists between the isotopic systems.

The widest variation in $^{87}\text{Sr}/^{86}\text{Sr}$ values occurs in the upstream Tsarap River

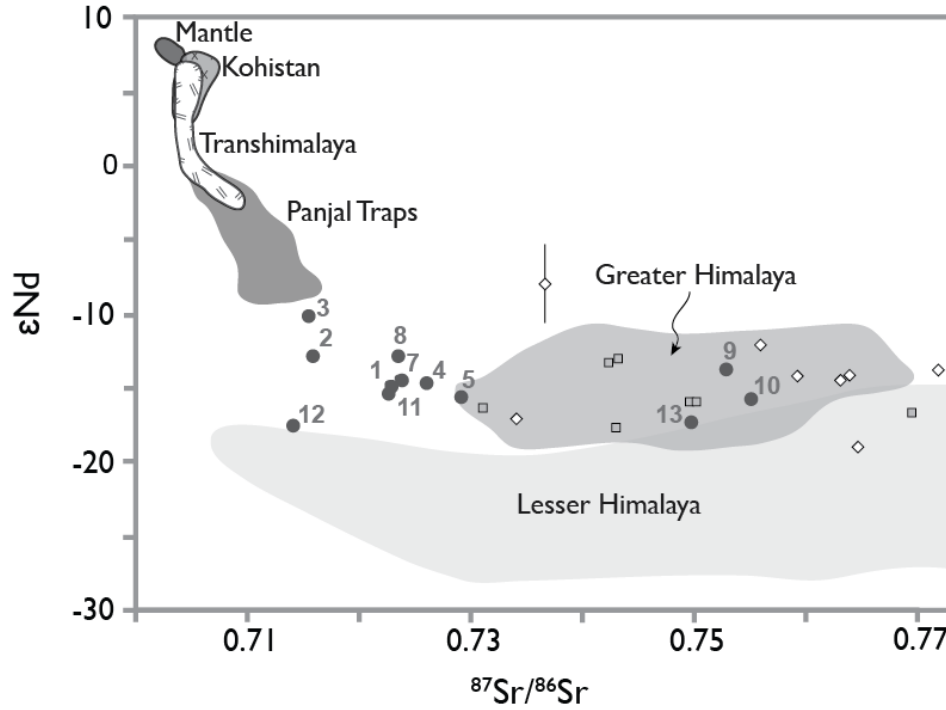


Figure 2.8. Crossplot of ϵ_{Nd} and $^{87}\text{Sr}/^{86}\text{Sr}$ compositions for Zaskar River sediments compared to other bedrock data from the Panjal Traps (Shellnutt et al., 2012; Shellnutt et al., 2014), the Greater and Lesser Himalaya (Deniel et al., 1987; Inger and Harris, 1993; Parrish and Hodges, 1996; Ahmad et al., 2000), Transhimalaya (Rolland et al., 2002), and additional Tethyan Himalaya (diamonds) and Greater Himalaya (squares; Richards et al., 2005) from the Sutlej River. Samples are numbered after Table 2.1.

tributaries (Fig. 2.9). The Zara (ID #10), lower Tsarap (ID #9), and Yunam (ID #13)

River samples display the greatest enrichment, and Gata (ID #12) one of the least enriched. The Stod River (ID #7, #8) sediments remain remarkably consistent with a $^{87}\text{Sr}/^{86}\text{Sr}$ value of ~ 0.723 . After the confluence with the Stod River, $^{87}\text{Sr}/^{86}\text{Sr}$ values become only slightly less enriched down the Zaskar River as the Oma (ID #3) and Markha (ID #2) Rivers join the trunk river.

The Stod River, in contrast to the Sr isotopes, demonstrates a shift to more negative ϵ_{Nd} values downstream (Fig. 2.9). Similar ϵ_{Nd} values are seen at Yunam (ID #13) and Gata (ID #11), as well as at Toze Lungpa (ID #11) and Zara (ID #10). Curiously, the

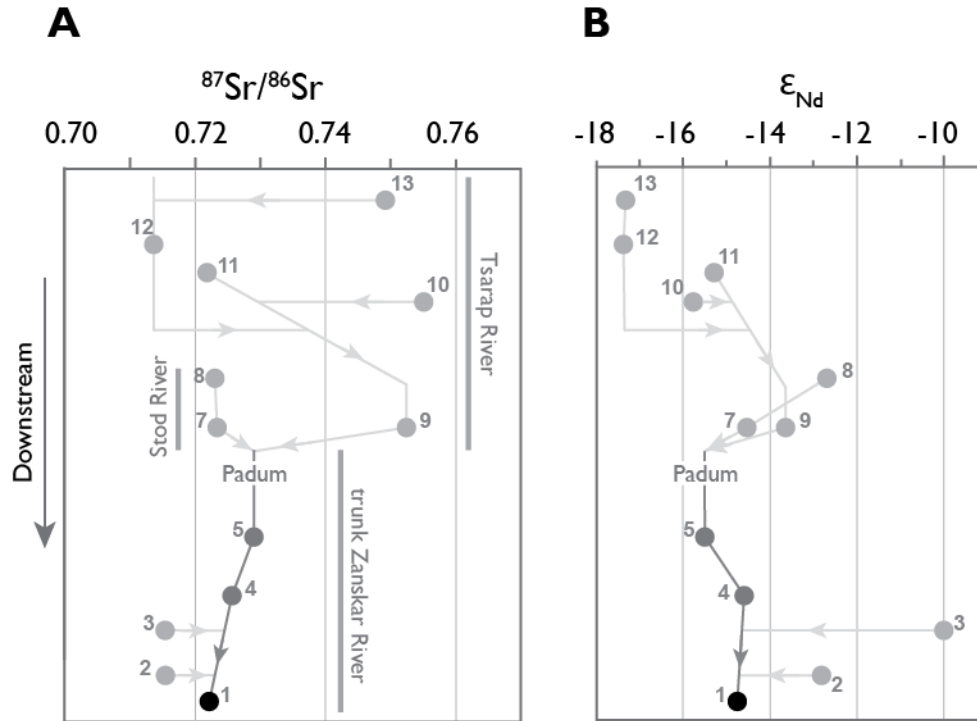


Figure 2.9. Diagram showing the progressive downstream variation in bulk sediment. (A) $^{87}\text{Sr}/^{86}\text{Sr}$ and (B) ϵ_{Nd} compositions for the Zanskar River. Error bars are smaller than symbol size for propagated Sr and ϵ_{Nd} errors. Samples are numbered after Table 2.1.

trunk sample at Pishu (ID #5) demonstrates a more negative ϵ_{Nd} value than either the lower Stod (ID #7) or Tsarap (ID# 9) Rivers after they join. Downstream of Pishu (ID#5), the trunk river values do not vary even downstream of the more positive Markha (ID #2) and Oma (ID #3) River confluences.

2.5.5 Detrital U-Pb Zircon Geochronology

All dated Zanskar River samples are presented as kernel density estimate (KDE) diagrams following Vermeesch (2004) in Figure 10. All Zanskar age analyses are presented in Appendix B. Most samples contain one or more peak populations at 245–380 Ma, 440–500 Ma, 500–600 Ma, and 750–850 Ma. Some samples have a composite peak from 750–1250 Ma comprised of smaller subsidiary peaks at ~900 Ma, ~1000 Ma

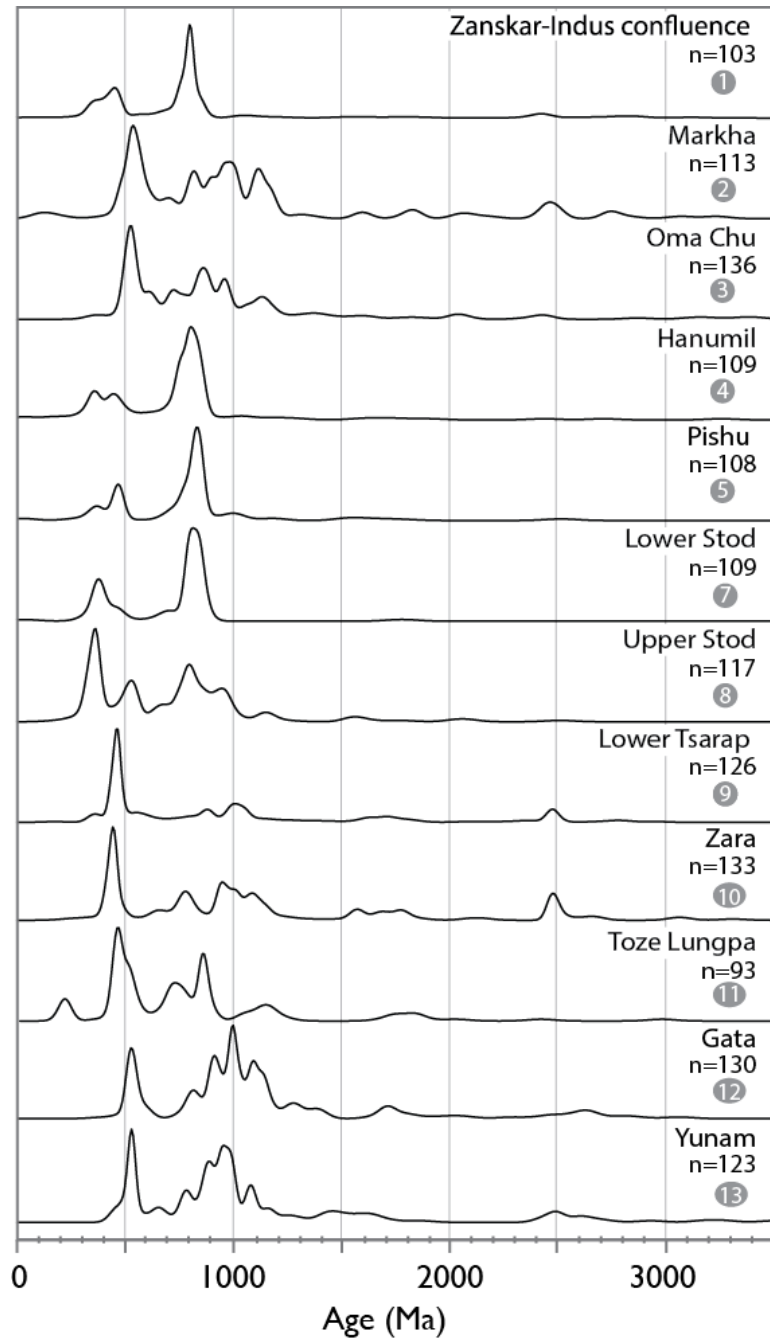


Figure 2.10. KDE diagrams of U-Pb zircon ages from Zanskar River sediments.

and ~1100 Ma. Paleoproterozoic and Archean peaks are found from 1600–1900 Ma and at ~2500 Ma, with very few ages at ~3200 Ma and ~3400 Ma.

Lower Stod (ID #7), Pishu (ID #5), Hanumil (ID #4), and Zanskar-Indus (ID #1)

confluence samples display similar age spectra to one another, with very prominent peaks at 750–850 Ma, and with two smaller peaks at ~350 Ma and ~450 Ma. Tsarap tributary samples populate a second group that also display the prominent ~450 Ma peak but contain older ages clustered at ~530 Ma, the broad 750–1250 Ma peak and an older, less populous peak from 1600–1900 Ma. The Zara (ID #10), Lower Tsarap (ID #9), Markha (ID #2), and to a lesser extent Yunam (ID #13), samples contain peaks at ~2500 Ma.

Zircons less than 300 Ma were uncommon in most samples but some tributaries yielded Mesozoic and Cenozoic ages. Pishu (ID #5), Hanumil (ID#4) and the Zaskar-Indus confluence (ID #1) yield zircon with ages clustered at ~260 Ma. Toze Lungpa (ID #11) was the only sample that yielded five zircon with a latest Triassic-earliest Jurassic mean age of 209 ± 6 Ma. The Markha River yielded two late Cretaceous ages, one at 130.5 ± 3.4 Ma and 97.2 ± 2.8 Ma. One late Paleocene age at 57.7 ± 1.1 Ma was yielded from the Zaskar-Indus confluence. Three samples (Lower Stod, Hanumil, Pishu) contained Oligocene and Miocene grains with ages ranging from 18–32 Ma.

2.6 Discussion

2.6.1 Downstream Provenance Evolution

Little variability in Sr and Nd isotopic compositions is observed in the trunk river downstream of Padum. The Zaskar-Indus (ID #1) confluence sample is most comparable to the Lower Stod River (ID #7; Fig. 2.9). Even so, Sr values decrease and Nd values increase slightly downstream of Padum suggesting minor addition of sediment from smaller (<100 km²) Zaskar Gorge tributaries (Fig. 2.5). This sediment must be isotopically similar to the Oma (ID #3) and Markha (ID #2) Rivers because of the observed decrease in $^{87}\text{Sr}/^{86}\text{Sr}$ values and increase in ϵ_{Nd} . Nonetheless, contribution from

the Oma River is negligible as the trunk river does not change its ϵ_{Nd} value downstream of this confluence.

Much of the geochemical variability in Zanskar River sediments occurs upstream of Padum before the confluence of the Lower Stod (ID #7) and Tsarap (ID #9) Rivers. $^{87}Sr/^{86}Sr$ values from the Upper (ID #8) and Lower Stod are within error of each other, but the Upper Stod is marked by a more positive ϵ_{Nd} value. The downstream decrease in ϵ_{Nd} values along the Stod River likely results from contribution of felsic, less radiogenic crystalline Greater Himalaya ($\epsilon_{Nd} = -15.2 \pm 2.2$; Robinson et al., 2001). Sediment from Panjal Traps basalts ($\epsilon_{Nd} = -8$ – 0 ; Shellnutt et al., 2014) added into the Upper Stod can account for the more positive ϵ_{Nd} values seen.

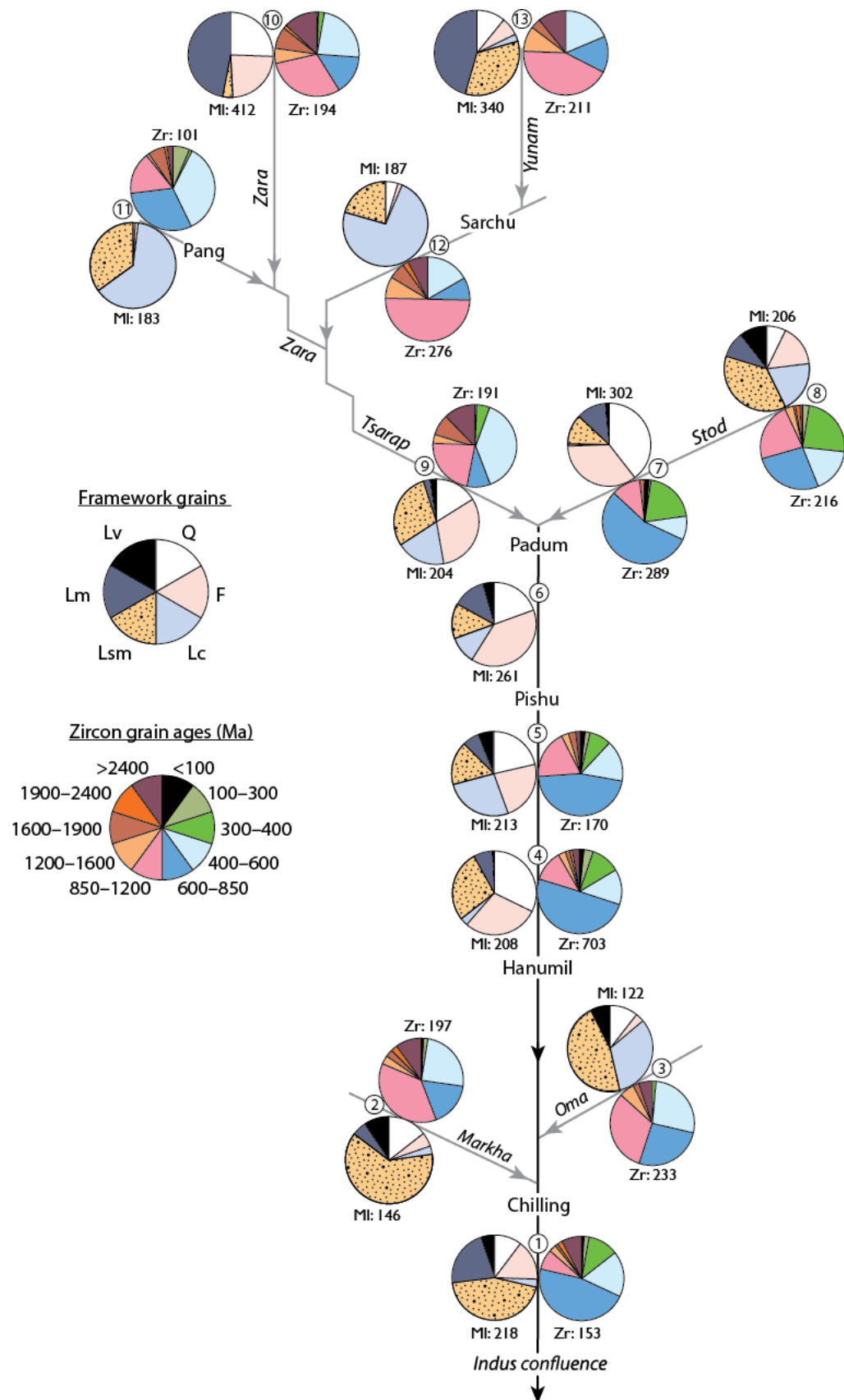
The Tsarap River drains almost all lithologies exposed in the Zanskar River basin and this in part rationalizes the wide variability observed in Tsarap catchment isotope compositions (Lower Tsarap (ID #9), Toze Lungpa (ID #11), Zara (ID #10), and Yunam (ID #13)). We conclude that the Lower Tsarap sample is not representative of a Tsarap catchment-averaged composition. This is because the ϵ_{Nd} value observed at Pishu (ID #5; $\epsilon_{Nd} = -15.5$) after mixing of the Lower Stod (ID #7; $\epsilon_{Nd} = -14.5$) requires that the net contribution from the Tsarap be more negative than -15.5 (consistent with measurements in the upper Tsarap), in contrast to the measured Lower Tsarap sample (ID #9; $\epsilon_{Nd} = -13.6$). This raises the possibility that the Lower Tsarap sample is locally derived. Alternatively, this sample could represent a transient pulse of sediment in the Tsarap derived from enhanced erosion sourced from similar bedrock and/or sediments further upstream, perhaps linked to older, large volume mass movements triggered by climatic events (e.g., cloud bursts; Hobley et al., 2012).

Bulk petrography and detrital zircon analyses suggest two models for sediment mixing downstream (Fig. 2.11). Framework grains indicate a continued, progressive compositional evolution of sediments downstream, with marginally greater contribution of sediment from the Stod River (ID #7, #8) than other tributaries. In contrast, detrital zircon grains demonstrate an overwhelming dominance of material sourced from the Stod River and little variation in zircon populations downstream of Padum. MDS analysis of detrital zircon samples clearly segregates sediments into two groups, whereas bulk petrography and major element compositions form slightly less discrete groups (Figs. 2.12A-C). Selected source bedrock U-Pb age data are plotted for comparison in Figures 2.12D and 2.13.

Below the Tsarap (ID #9) and Stod (ID #7) River confluence at Padum, each detrital zircon sample on the trunk river contains 600–850 Ma grains as the majority population (Fig. 2.11). A small increase in >2400 Ma ages at the Zaskar-Indus (ID #1) confluence, however, does suggest minor contribution from the Markha River (ID #2). Bulk petrography also argues for an additional contribution from the Markha and Oma (ID #3) Rivers, and likely other small Zaskar Gorge tributaries. After exiting the gorge in the lower reaches, river sediments contain more Tethyan sedimentary and low-grade metasedimentary lithics than below Hanumil (ID #4) at the gorge entrance.

Lithic grains of trunk river samples above the gorge display closest similarity to the Lower Tsarap (ID #9) River (Figs. 2.11 and 2.12). Pishu (ID #5, #6) and Hanumil (ID #4) samples contain abundant Tethyan Himalayan metapelitic and carbonate fragments, with very few high-grade, coarsely crystalline Greater Himalayan gneiss and calc-gneiss fragments. Although these trunk river samples do not contain a lot of high-grade lithic

Figure 2.11. Schematic diagram illustrating detrital framework grain and detrital zircon populations of Zanskar sands. Q = quartz; F = feldspars; Lc = lithic carbonate; Lsm = other sedimentary and low-rank metasedimentary; Lm = medium- to high-rank metamorphic; and Lv = volcanic and metavolcanic. Rank of metamorphic grains and Metamorphic Index (0–500; Garzanti and Vezzoli, 2003). Concentrations of Zr \gg 300 ppm may indicate hydraulic sorting and enrichment of sample in dense phases. Black line denotes trunk Zanskar River, with gray lines for tributaries. Samples are numbered after Table 2.1.



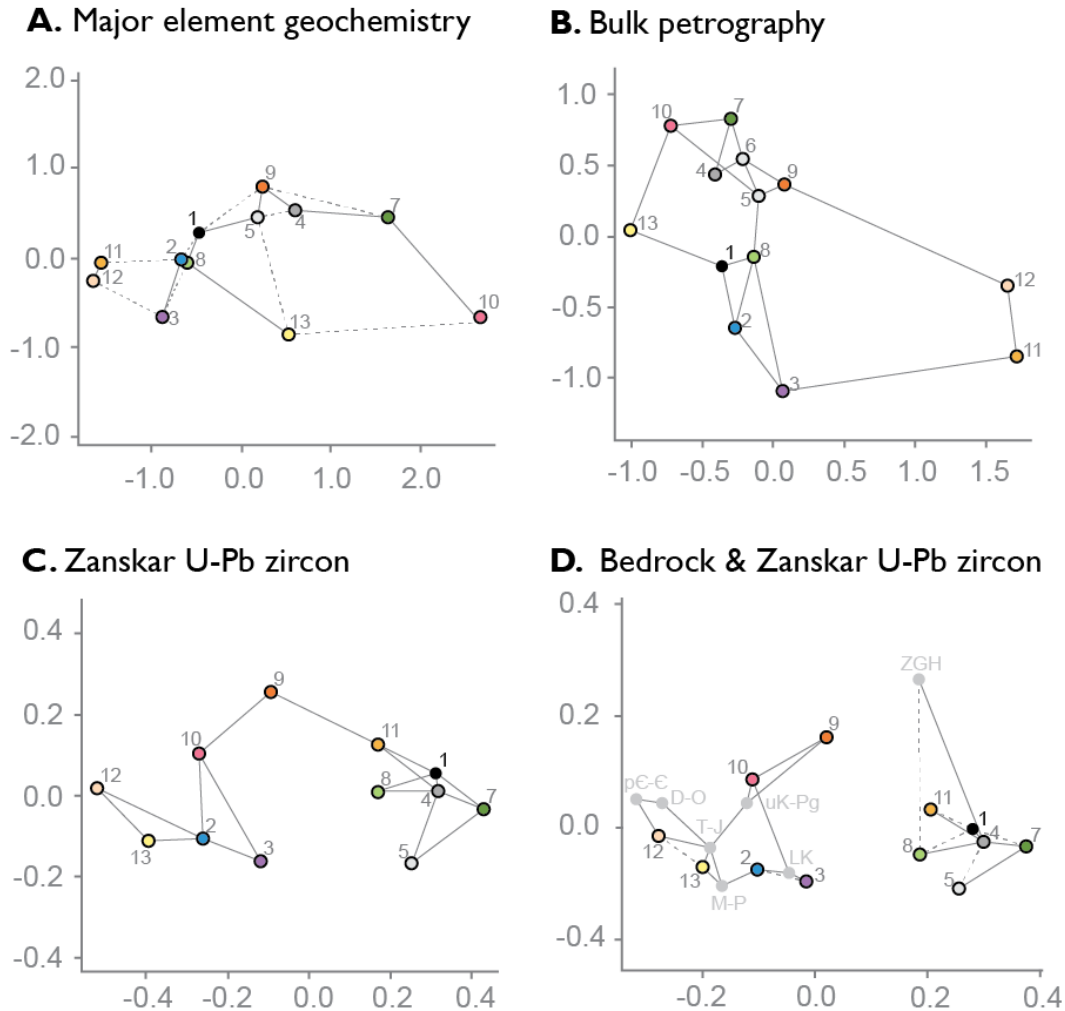
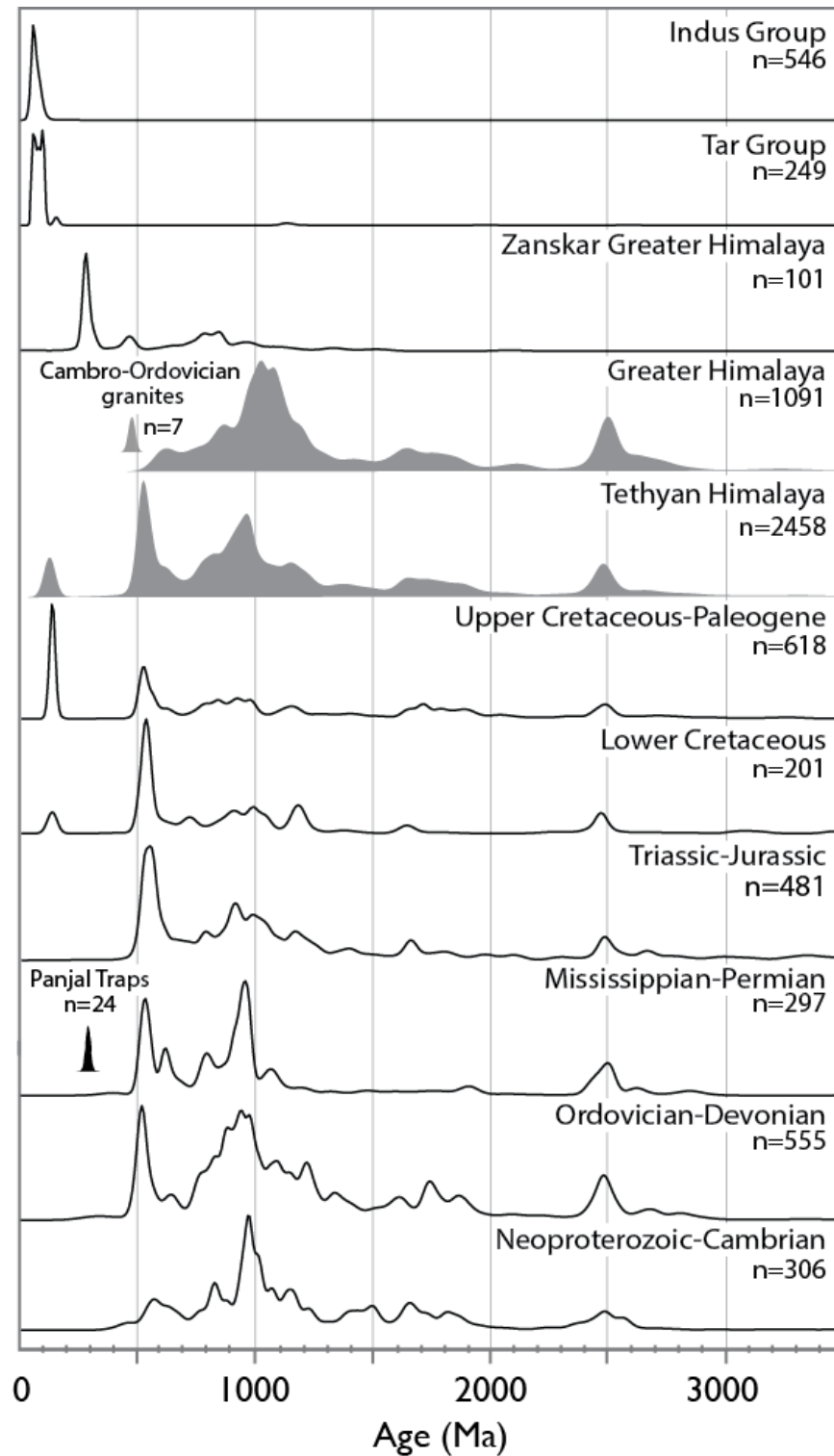


Figure 2.12. Multidimensional scaling (MDS) plots showing the Kolmogorov-Smirnov distances between Zanskar River sediments and selected bedrock. (A) Classical MDS plot of bulk major element geochemistry data; (B) Nonmetric MDS plot of SRD-corrected bulk petrographic data; (C) Nonmetric MDS of Zanskar River detrital zircon U-Pb ages; and (D) Nonmetric MDS of selected Himalaya bedrock and Zanskar River detrital zircon U-Pb ages. Regional Himalayan U-Pb zircon data are same as Figure 2.13. Samples are numbered after Table 2.1. Data were plotted using R code ‘provenance’ written by Vermeesch et al. (2016). Solid lines indicate closest neighbor and dashed lines near neighbors in similarity calculations. Bedrock abbreviations in Fig. 2.12D mostly follow depositional ages: pC-C = Proterozoic to Cambrian; D-O = Devonian to Ordovician; M-P = Mississippian to Permian; T-J = Triassic to Jurassic; LK = lower Cretaceous; uK-Pg = upper Cretaceous to Paleogene; and ZGH = Zanskar Greater Himalayan bedrock (Horton and Leech, 2013).

fragments, the abundance of quartz, feldspar and fibrolite still indicate strong contribution of Greater Himalayan material. This sediment is likely sourced in part from the Cambro-Ordovician and Mississippian-Permian granitic gneisses exposed as part of the Greater Himalaya along the ZSZ, rather than from the Zara River (Fig. 2.3). The abundance of quartzofeldspathic, micaceous, and schistose metamorphiclastic detritus in the Zara (ID #10) sample might suggest an overspill connection existed between Tso Kar and the Zaskar River, as proposed by Demske et al. (2009) and Wünnemann et al. (2010). Our provenance data from the Zara River neither support nor preclude sediment supply to the Zaskar River via an overspill connection (e.g., Munack et al., 2016). Potential parent bedrock sources to the Zara River are exposed immediately northeast, outside the Tso Kar basin, as well as along strike into that basin and further southeast to Tso Morari. Furthermore, we suggest the Zara River does not contribute much Nyimaling-Tso Morari gneiss dome material to trunk river samples because none is found in bulk sediments lower in the Tsarap River (Fig. 2.11). Similarly, the Yunam River (ID #13) carries abundant Greater Himalayan metamorphic material but is simply diluted by the Tethyan Himalayan sedimentary fragments sourced from other tributaries downstream.

Detrital zircon populations with central ages at ~350 Ma, ~450 Ma, and ~530 Ma (Fig. 2.10) support previous findings for abundant Cambro-Ordovician and Mississippian-Permian granites found in the Greater Himalaya in Zaskar and elsewhere in the northwest Himalaya (Fig. 2.13; Honegger et al., 1982; Spring et al., 1993; Horton and Leech, 2013). Detrital zircon ages clustered at ~260 Ma could be sourced from Panjal Traps but are younger than the reported ages (~289 Ma) northeast of Zaskar

Figure 2.13. KDE diagrams for selected bedrock U-Pb data for the Zaskar River Basin. Selected samples are from the Indus and Tar Groups (Wu et al., 2007; Henderson et al., 2010), Zaskar region Greater Himalaya (Horton and Leech, 2013), Panjal Traps (Shellnutt et al., 2011), and Cambro-Ordovician granites in Zaskar and the NW Himalaya (Pognante et al., 1990; Girard and Bussy, 1999; Kwatra et al., 1999; Miller et al., 2001; Cawood et al., 2007). Selected bedrock ages for southern Tethyan Himalaya, Greater Himalaya, and correlative strata from the eastern and central Himalaya were plotted (in gray) according to depositional age and compiled into composite KDE diagrams (DeCelles et al., 2000; Myrow et al., 2003; McQuarrie et al., 2008; Myrow et al., 2010; Gehrels et al., 2011; Hu et al., 2012; Clift et al., 2014; Hu et al., 2015).



(Singh et al., 1976; Shellnutt et al., 2014). Permian granites are not recognized in Greater Himalaya units from the eastern and central Himalaya (Gehrels et al., 2011). The relative

lack or presence of such prominent age peaks between the central/eastern and northwest Himalaya encourages future caution when using detrital zircon compilations to correlate strata across the orogen when such heterogeneities exists (Fig. 2.13).

Heavy mineral fertility likely plays a role in the apparent contrast observed between bulk petrography and detrital zircon analyses. For example, detrital zircon ages at Yunam (ID #13) appear to be transmitted downstream to Gata (ID #11; Figs. 2.9 and 2.11), consistent with a stable ϵ_{Nd} value over that stretch of river. However, the bulk petrography and Sr isotope values change markedly between these two samples, requiring significant sediment dilution. This discrepancy requires that either the material being added has the same zircon and Nd-bearing phases but different bulk lithologic composition, or that the sediment contributed from tributaries between Yunam and Gata (ID #11) is lacking in those phases. We favor the latter as being more likely.

2.6.2 Controls on Erosion

While our dataset cannot quantify sediment yields, we here provide the first initial constraints on sediment provenance and the relative contributions of sources downstream in the Zaskar River. The data presented above yield a clear image of the Stod River being a significant source of sediment to the Zaskar. This influence is moderated by downstream sediment contributions from tributaries and minor, side valley tributaries. We argue that the bulk of sediment production in the Zaskar River is driven by strong glacial erosion in the Stod River valley and lesser hillslope erosion across the catchment. We favor glacial erosion as the primary process controlling erosion because westernmost Zaskar and Stod River hillslopes and valleys have been strongly modified by glaciation for at least the last 78 k.y. (Taylor and Mitchell, 2000) and continue to be conditioned by

active alpine glaciers. Glaciers comprise ~28% of the modern Stod River basin versus 7-8% of the modern Tsarap and overall Zaskar River basins. Spatial patterns of erosion in Zaskar may not correlate significantly with convexities in river profiles caused by lithologic changes or high channel steepness (Figs. 2.2 and 2.5). Instead, the highest yields come from the Stod River catchment that contains a broad, overdeepened and alluviated U-shaped valley, steep hillslopes housing north-facing glaciers, low to moderate k_{sn} values, and convexities along the river profile reflecting earlier glaciation.

Hillslope processes acting at high elevation in semi-arid regions cannot be ruled out as significant producers of sediment. Soil creep, gussification, granulation, and salt weathering are known to generate sediment along the Indus River valley but are likely less influential than (peri-) glacial and fluvial processes in driving bedrock erosion and evacuating sediment in paraglacial environments (Hales and Roering, 2007; Scherler, 2014; Blöthe et al., 2015; Dietsch et al., 2015). Hillslope processes operate at slower rates and the material that is produced is not readily mobilized. Erosion in drier, unglaciated catchments in Zaskar is likely strongly driven by slow hillslope processes but unlikely operating at comparable rates or volumes as glaciated catchments.

Bookhagen et al. (2005a) indicate that mass wasting is fundamental in driving increased sediment flux and shaping landscapes in the dry Himalayan interior. Debris flows and deep-seated landslides are facilitated when intense summer rainfall destabilizes poorly vegetated hillslopes. Over the Holocene, mass wasting events correlate well with periods of enhanced monsoonal rainfall in steep rain shadow reaches (Bookhagen et al., 2005b; Dortch et al., 2009). Our findings do not support rainfall-modulated landsliding as a primary control on modern erosion in the Zaskar River. The few mass wasting deposits

identified in the basin neither correlate with modern erosion patterns nor major knickzones.

Seasonal summer monsoonal precipitation, however, may provide a first-order control on sediment transport. We propose that glacial erosion drives production of unconsolidated sediments that are then later reworked during high-intensity monsoon events in the modern Zaskar River basin. Snow and glacial meltwater cause heightened discharge and suspended sediment flux in the dry Himalaya during the early summer (Anderson et al., 2004; Burbank et al., 2012), but later monsoonal storm events more effectively drive sediment transport. The magnitude of glacial sediment production and/or flux of reworked sediment from the Stod River catchment is great enough that significant dilution of this signal does not occur downstream, even after addition of mobilized hillslope sediments. This is in contrast to what has been observed in the frontal Himalaya where glacial sediment production is masked by much stronger monsoonal erosion (Godard et al., 2012). Erosion in Zaskar also contrasts to that seen in the unglaciated basins along the Indus valley that receive $<115 \text{ mm} \cdot \text{yr}^{-1}$ precipitation and have extremely slow integrated rates of erosion (Dortch et al., 2011b; Munack et al., 2014; Dietsch et al., 2015). We argue that sediment production and transport in the Zaskar River basin are modulated by the same primary drivers of erosion (i.e., glaciers and monsoon rainfall), but that these operate at different relative magnitudes compared to the frontal Himalaya, as well as the more slowly denuding regions along the Indus valley.

Our study of modern erosion patterns in the Zaskar River naturally solicits comparisons between contemporary and Quaternary erosive conditions. While modern sediments in semi-arid to arid Ladakh and Zaskar may in part be mobilized during high

intensity storm events (e.g., Hobley et al., 2012; Stolle et al., 2015), it cannot be assumed that these conditions held true in the past. Stronger Holocene monsoon phases at 8–10 ka and 30–35 ka brought enhanced precipitation onto Tibetan Plateau margins that promoted greater vegetative cover (Shi et al., 2001; Herzsuh, 2006; Demske et al., 2009; Wünnemann et al., 2010). Increased slope stability as a result of more vegetation could reduce the erosive capability of high-intensity storm perturbations and potentially reduce erosional response (e.g., Beaumont et al., 2000). Under prolonged enhanced monsoonal conditions, it is unlikely storm events had equivalent impacts over the region, and if these events had similar recurrence, transience, and magnitude. In light of the devastating debris flows in 2010 and 2015 in Ladakh, more work is needed to understand the nature of these high intensity events and their erosional impact.

Next, our work begs the question whether the material yielded from the Stod River is eroded from bedrock or primarily reworked from glacial moraines. We cannot definitively untangle the relative contribution of reworked glacial material at least with our dataset, however, based on the present observation of abundant incised glaciofluvial terraces we prefer the idea that large-scale recycling of material generated during the Last Glacial Maximum is the primary source of sediment to the Stod River. Furthermore we recognize that longer term glacial and monsoonal phases dictating sediment generation and reworking might be disrupted by shorter duration, perhaps stochastic, climatic perturbations. However, the generally cohesive trends in our provenance data would indicate that the modern signal is not dominated by these events.

Significant dissection of Pleistocene valley-fills in the upper Tsarap catchment

highlights a long history of sediment reworking into the paleo-Zaskar River (Munack et al., 2016). Although our data here do not indicate a strong contemporary contribution from these deposits to the modern Zaskar River, to what extent the provenance signal may have been distorted as a result of such recycling in the past remains open to investigation. This combined understanding of erosion in Zaskar further emphasizes that sediment buffering over millennial to even multi-millennial timescales is likely an important process controlling sediment routing in the Himalayan rain shadow and the overall transfer of climate-erosion signals downstream.

2.7 Conclusions

We applied a suite of geochemical and geochronological techniques to establish spatial patterns of erosion in a rain shadow river system. Our findings demonstrate that modern sediment provenance in Zaskar is driven by focused glacial erosion and monsoonal rainfall along the Greater Himalaya and Zaskar Shear Zone. The Stod River catchment, representing only 13% of the total area of the Zaskar River basin, dominates in delivering sediment to the modern drainage. The distribution of erosion in Zaskar is not directly controlled by monsoonal rainfall as is the case in the frontal Himalaya, but rather the precipitation gradient promotes a concentration of permanent, north-facing glaciers that efficiently scour the High Himalaya. The Zaskar differs from its wetter neighbors to the south in being less controlled by mass wasting but also differs from drier, formerly glaciated catchments further north in having enough precipitation to regularly mobilize the sediment produced by glaciation. Dry, low relief, unglaciated regions of Zaskar contribute minimally to the total modern sediment flux. We suggest that increased flux from these arid regions may only be significant when extreme

monsoon storms, or even prolonged, intense Holocene monsoon phases, mobilize sediments from unvegetated hillslopes.

Our data are broadly consistent with the glacially-dominated sediment production model of Blöthe et al. (2014), but here our analyses the potential importance of monsoon precipitation in remobilizing sediment and allowing its transportation into the main Indus River system. While the majority of sediment may be fluxed during deglacial and post-glacial times, we argue that it monsoon may control sediment transport rather than deglaciation itself (c.f., (Blöthe et al., 2014). This appears to be true at least in the present day in this transitional setting between the wet frontal Himalaya and the arid orogenic interior of the Tibetan Plateau. In the absence of tectonic forcing in Zaskar, our results support climatic control on erosion in the Himalaya. If surface processes dominate over million year timescales then these would shape orogenic architecture in the way favored by critical wedge and channel flow extrusion models (Beaumont et al., 2001; Robinson et al., 2006).

CHAPTER 3. QUANTIFYING EPISODIC EROSION AND TRANSIENT STORAGE ON THE WESTERN MARGIN OF THE TIBETAN PLATEAU, UPPER INDUS RIVER

3.1 Abstract

Transient storage and recycling of large valley-fills, or sediment buffering, is a fundamental but poorly quantified process that may significantly bias estimates of fluvial sediment budgets and compositions preserved in marine archives used vitally for paleoclimatic and tectonic reconstructions. Optically stimulated luminescence dating, sediment petrography, detrital U-Pb zircon geochronology, and morphometric analysis quantify sediment buffering in the upper Indus River in the NW Himalaya over timescales 10^3 - 10^5 yrs. This study defines the timing, provenance, and volumes of Late Quaternary valley-fills and infers the dominant controls on their formation and release. Fluvial aggradation is associated with enhanced precipitation over strong phases of the summer monsoon and winter westerlies during the Late Pleistocene 25–32 ka and by the mid-Holocene (~6–8 ka), followed by incision as the monsoon weakened. Focused glacial erosion and precipitation along the High Himalaya together control sediment export to the trunk Indus River, in contrast with both the monsoon-dominated frontal Himalaya and the extremely arid Transhimalayan orogenic interior. Volumetrically large but isolated valley-fills in the orogenic interior may only be liberated during significantly wet climatic intervals. It is primarily those basins on the plateau margin that produce and mobilize much of the total sediment exported from the Himalayan rain shadow. Climate, and in particular precipitation, plays a more pivotal role governing Himalayan rain shadow sediment storage and transport than previously recognized.

3.2 Introduction

Deep marine sediments represent the final erosional record delivered by river systems to the ocean. These sediments are a consequence of an integration of material from multiple source regions, transfer through floodplains, and modification by surface processes. As sediments are routed from their mountain sources to the final depocenter, transient storage and recycling, or sediment buffering, modulate erosional signals such that any propagated signal of erosion can be dampened, shredded, or erased altogether (e.g., Castelltort and Van Den Driessche, 2003; Jerolmack and Paola, 2010; Armitage et al., 2011). The potential for significant buffering calls into question the utility of using marine sedimentary archives for long-term reconstructions of orogenic erosion and paleoclimate at high resolution. Large uncertainties remain in the understanding of how buffering attenuates erosional signals and over what timescales this process may be significant in source-to-sink transport systems (Goodbred, 2003; Clift, 2006; Allen, 2008; Armitage et al., 2011; Simpson and Castelltort, 2012).

Sediment budgets that have attempted to characterize buffering in large river systems have principally focused on quantifying storage and reworking of deposits in extensive, foreland basin floodplains (Allison et al., 1998; Métiévier and Gaudemer, 1999; Castelltort and Van Den Driessche, 2003). Only recently in the Himalayan Indus and Ganges-Brahmaputra headwaters has the capacity for substantial buffering in mountain source regions been recognized (Blöthe and Korup, 2013; Clift and Giosan, 2014). Across the Himalaya, wide (>5 km), glacially-scoured, and over-deepened intermontane river basins provide exceptional accommodation space for stored sediments (Owen et al., 2006; Korup et al., 2010; Bolch et al., 2012; Blöthe and Korup, 2013) and thick alluvial

river terrace sequences document considerable storage and release of sediment over the Quaternary (Bookhagen et al., 2005a; Srivastava et al., 2008; Blöthe et al., 2014; Scherler et al., 2015; Dey et al., 2016; Munack et al., 2016).

While buffering may be taking place it is unclear what processes control the storage and release of material from these valleys. Tectonic forcing can be significant over longer geologic timescales ($>10^6$ yr), but in this study the role played by climate in modulating storage and release of sediment is examined. In particular, this study focuses on the relative importance of glaciation and precipitation provided by the Asian summer monsoon and winter mid-latitude westerlies in the NW Himalaya. Although the mechanisms for storage and release of sediment have been investigated in the monsoonal, south-facing front of the Himalaya (e.g., Bookhagen et al., 2005a), it is less clear what processes influence sediment production and transport on the edge of the Tibetan Plateau in the Himalayan rain shadow preserving dramatic, large volume valleys-fills (Blöthe and Korup, 2013; Hedrick et al., in press).

Here, alluvial terraces are targeted in the Zaskar River Basin, the largest tributary ($\sim 15,000$ km²) discharging to the upper Indus River, to evaluate the effects of transient storage and recycling on modern and Quaternary Indus sediments. Through optically stimulated luminescence (OSL) dating, sediment petrography, and detrital U-Pb zircon analysis, the ages and sources of valley-fill sediments are defined to establish spatial patterns of erosion since ~ 35 ka. Estimates for volumes of stored valley-fill sediments are made from field observations and morphometric analysis. These findings are compared with regional budgets to provide a more concrete understanding on how, and over what timescales, climatic phases may influence sediment flux to the trunk

Indus through recycling of Quaternary valley-fills from the Himalayan rain shadow.

3.3 Background

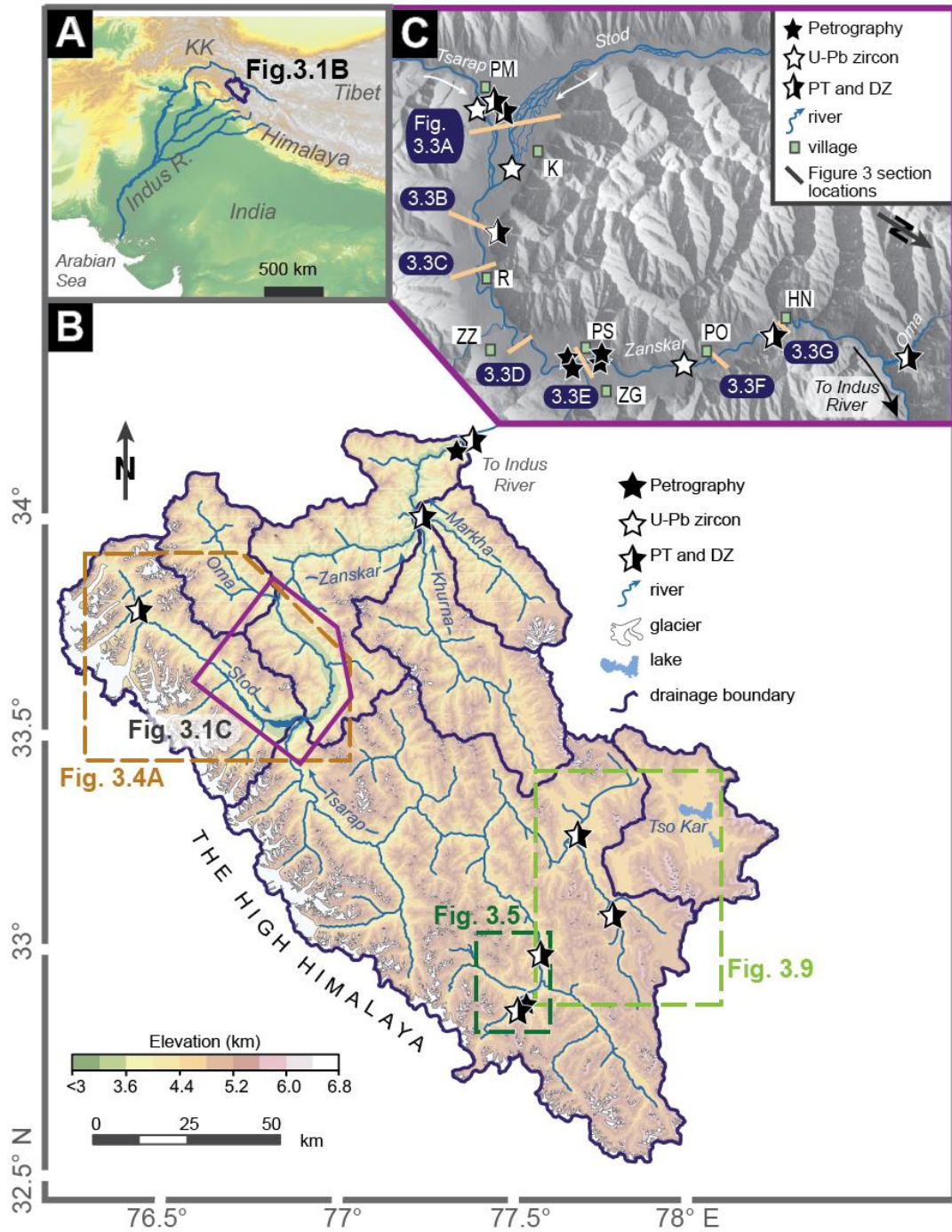
3.3.1 Sediment Buffering in the Indus River

The Indus River system has routed water and sediment from the western Himalaya and Tibetan Plateau to the Arabian Sea for at least the last ~45 Ma (Clift et al., 2001). Four major Indus tributaries drain the Himalayan foreland basin, with the upper trunk of the Indus River cutting up through the northwest Himalaya and Karakoram onto the Tibetan Plateau (Fig. 3.1).

Erosion and sediment transport in the frontal Himalaya are presently strongly controlled by the distribution of Asian summer monsoon precipitation (Galy and France-Lanord, 2001; Gabet et al., 2008). Records from speleothems (Fleitmann et al., 2003), marine cores (Prins et al., 2000; Gupta et al., 2003; Staubwasser and Weiss, 2006), Central Asian paleolake sediments (Fang, 1991; Gasse et al., 1991; Gasse et al., 1996; Shi et al., 2001), and pollen records (Herzschuh, 2006) indicate strong Quaternary summer monsoon phases at ~34–44 ka and after the last glacial maximum (LGM; ~20 ka) to the mid-Holocene (~5 ka) across south and central Asia.

Variation in summer monsoon intensity has crucially controlled the volumes and compositions of sediments delivered to the Indus delta and submarine fan, especially in the last ~20 ka. Clear changes in provenance synchronous with monsoon strengthening and enhanced erosion along the frontal Himalaya from 14 to 9 ka are recorded in Indus delta sediments (Clift et al., 2008a). Mid-late Holocene downcutting of the Indus River into the alluvial plain has since significantly reworked sediments into the delta (Giosan et al., 2012). Until pre-industrial damming of the Indus River, reworked deposits dominated

Figure 3.1. Setting of the Zaskar River and Tso Kar basins. (A) Location of Indus River (gray) and Zaskar River basin (black outline; Figure 3.1B); (B) Topographic map river drainage and sample locations outside of the Padum Basin. Dashed boxes indicate location of Figures 3.4–3.5 and 3.9; (C) Oblique hillshade view to the southwest over the Padum Basin showing major tributaries (white), sample locations (stars), and Figure 3.3 cross-section locations (black lines). Topographic data were derived from Shuttle Radar Topography Mission 30-m grid data (SRTM30). Abbreviations are: HN = Hanumil; K = Karsha; KK = Karakoram; PM = Padum; PO = Pidmo; PS = Pishu; R = Rinam; ZG = Zangla; and ZZ = Zozar.



changes in upstream erosion and sediment provenance were strongly diluted (Clift and Giosan, 2014). Such observations underscored the necessity for further quantification of buffering in controlling the river sediment load volumes and compositions.

Dissected valley-fills can be recognized even in the mountainous headwaters of

the Indus River system across the Karakoram and Transhimalaya. While some occur within steep bedrock gorges as a result of landslide and glacial damming (Hewitt, 1998, 2002; Dortch et al., 2010; Korup et al., 2010), infilled alpine topography accommodates extensive alluvial sediments elsewhere in the northwest Himalaya. The thickness (~150–300-m thick) and longevity (~122–530 k.y.) of some preserved remnants attest to major cycles of Indus River aggradation and incision in the past (Blöthe et al., 2014; Munack et al., 2016). These deposits confirm long residence times and substantial reworking of sediments from the Indus headwater regions for at least the last two glacial cycles. Older moraine deposits (>385 ka; Owen et al., 2006; Blöthe et al., 2014) and abundant dammed lacustrine sediments, together with preserved terraces >400 m above modern river level (Pant et al., 2005; Phartiyal et al., 2005), further testify to a long (>10⁶ yr) history of sediment storage and residence in the upper Indus River basin.

Critically, how reworking of Himalayan valley-fill deposits contributes to Quaternary Indus River sediment flux remains largely unresolved. Volumetric estimates suggest reworking of valley-fills may easily dominate over contributions from fresh bedrock erosion since the Pleistocene (Blöthe and Korup, 2013; Munack et al., 2016). Provenance studies do not support substantial recycling from Pleistocene terraces into the modern river bedload (Blöthe et al., 2014; Jonell et al., in press) but do not preclude that recycling may have played a stronger role in the past under different climatic conditions. While initial attempts to quantify buffering indicated that rain shadow valley-fills were not a dominant source in the Indus basin, these prior budgets were based on a number of assumptions that require further ground-truthing to establish their significance over wider areas of the Himalaya and over 10³–10⁵ time scales (Clift and Giosan, 2014).

3.3.2 Zaskar River Climate and Geology

This study investigates the Zaskar River located in the Ladakh region of the Transhimalaya (Fig. 3.1). The modern Zaskar River basin can be divided into five subbasins from the main tributaries: the Tsarap, Stod, Khurna, Markha, and Oma. Adjacent to the Zaskar River basin is the internally-drained Tso Kar basin (with an area of 1042 km²). Lying north of the orographic barrier of the High Himalaya on the periphery of the Tibetan Plateau, the Zaskar is characterized alternately by narrow bedrock gorges with rugged topography and peaks >6000 m elevation, and by broad (3–6 km), glacially-modified river valleys ranging from ~3000 to 4500 m above sea level (asl). Much of Zaskar has an alpine, desert-steppe rain shadow climate (Hartmann, 1987). A strong precipitation gradient is marked by higher mean annual precipitation (~400 mm/yr) along the backbone of the High Himalaya in Zaskar to only ~115 mm/yr in the Tso Kar basin (Bookhagen and Burbank, 2006). Precipitation is delivered in the summer months (Jun-Aug) by the Asian summer monsoon that pushes across the High Himalaya into the Tibetan Plateau. In the winter, snow is brought by mid-latitude winter westerlies (Benn and Owen, 1998).

In contrast with the Himalayan foreland, there is little consensus on the impact of monsoon precipitation on erosion in the Transhimalaya. Under modern, normal monsoon conditions, summer rainfall in semi-arid to arid catchments contributes ~40% of the mean annual precipitation and as little as 26% to the total discharge (Bookhagen and Burbank, 2010). Erosion rates in arid catchments receiving overall less rain are commensurately low (<0.1 mm/yr) in comparison to monsoon-dominated catchments (~1–2 mm/yr; Burbank et al., 2012). Despite such low overall erosion and sediment fluxes from arid

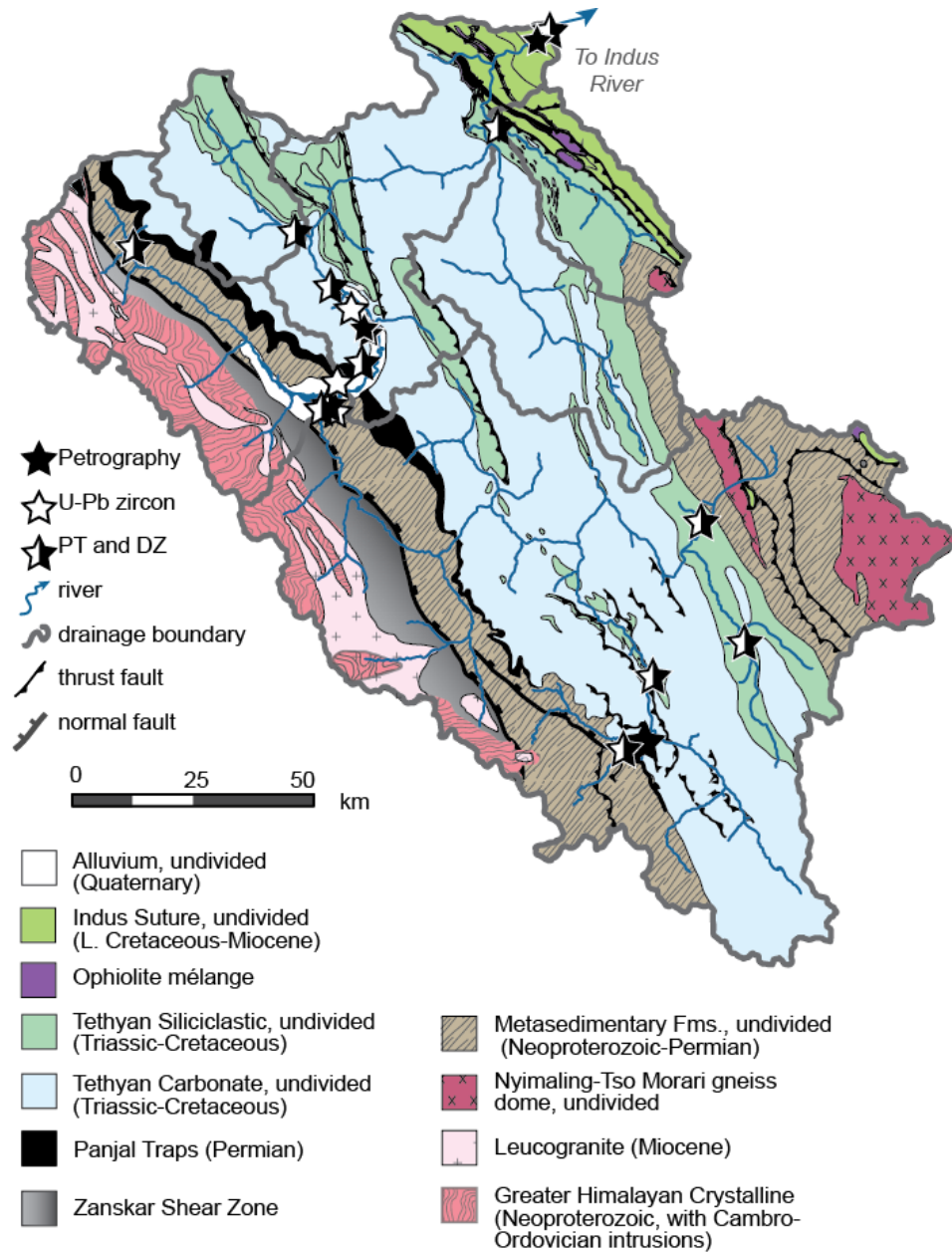


Figure 3.2. Simplified geologic map of the Zaskar River basin after Fuchs (1986; 1987) with additions from Dèzes et al. (1999), southern Zaskar (Lahul) from (Steck et al., 1993) and Tso Kar area (Epard and Steck, 2008). Sample locations denoted by stars. Modified after Jonell et al. (in press).

regions, some observations indicate monsoon storm-triggered hillslope erosion can produce a significant part of the annual suspended sediment flux (30–50%) in only a few events (Wulf et al., 2010; Wulf et al., 2012). Abnormal monsoon events, and potentially

strong monsoon phases, are suggested to play a pivotal role in liberating sediments from arid catchments that otherwise lack sufficient transport capacity (Bookhagen et al., 2005b).

The bedrock geology of the Zaskar River basin (Fig. 3.2) can be grouped into three lithotectonic sequences: (1) the Greater Himalaya; (2) the Tethyan Himalaya; and (3) the Indus Suture Zone. The Greater Himalaya consists of Neoproterozoic-Ordovician paragneiss, metapelite, and orthogneiss (Honegger et al., 1982; Pognante et al., 1990; Spring et al., 1993; Noble and Searle, 1995; Horton and Leech, 2013; Horton et al., 2015). These rocks are largely considered to be the deeply buried, high-grade equivalents of the Tethyan Himalaya sequence, the former passive margin of Greater India.

Neoproterozoic to early Paleocene carbonate and siliciclastic sedimentary rocks comprise the very-low to low-grade metasedimentary Tethyan Himalaya. Locally Tethyan rocks reach lower amphibolite facies adjacent to the Nyimaling-Tso Morari dome and along the Zaskar Shear Zone, the ~150 km-long segment of the South Tibetan Detachment fault segregating the Greater and Tethyan Himalaya (Herren, 1987; Steck et al., 1993; Dèzes et al., 1999). Paleozoic magmatic pulses produced two suites of igneous rocks in Zaskar: 1) Pan-Africa Orogeny Cambro-Ordovician (440–550 Ma) granitic plutons (Cawood et al., 2007; Horton and Leech, 2013) and 2) Gondwanan rifting Panjal Traps flood basalts (~289 Ma) and associated Mississippian-Permian (245–380 Ma) granitic plutons (Shellnutt et al., 2012; Shellnutt et al., 2014). Rocks of the third lithotectonic sequence, the Indus Suture Zone, record sedimentation related to the collision of Greater India and Eurasia (e.g., Searle, 1983; Searle et al., 1990). Ophiolitic mélange, Indus Molasse sandstones, and Cretaceous-Eocene forearc basin strata are

exposed along the easternmost part of Zaskar (Clift et al., 2002; Henderson et al., 2010). The Zaskar River basin and neighboring Ladakh have been relatively tectonically quiescent from the early to mid-Miocene (Schlup et al., 2003; Kirstein et al., 2006; Kirstein et al., 2009; Schlup et al., 2011) with no significant neotectonic activity recorded since that time (Jade et al., 2010).

The many broad, over-deepened intermontane valleys of Zaskar and Ladakh indicate extensive glacial modification in the past (Owen et al., 2006; Korup et al., 2010; Bolch et al., 2012; Blöthe and Korup, 2013), although contemporary glaciers remain strictly confined to north-facing headwalls (Benn and Owen, 1998; Dortch et al., 2011; Kamp et al., 2011; Owen and Dortch, 2014). Glacial valley systems were the most extensive (>50 km from present-day ice margin) during the early last glacial (Mitchell et al., 1999; Hedrick et al., 2011). Since that time, glaciers retreated regionally with only small glacial advances confined <15 km from present-day ice margins in their respective catchments during the Lateglacial, Neoglacial, and Little Ice Age (Burbank and Fort, 1985; Owen, 2009; Owen and Dortch, 2014; Hedrick et al., in press).

3.4 Methods

To assess the provenance of river terrace sediments and constrain timing of sediment aggradation in the Zaskar River basin, field observations, sediment petrography, detrital zircon U-Pb geochronology were integrated with optically stimulated luminescence (OSL) dating. The potential role of sediment buffering in the upper Indus River is addressed using morphometric analysis to identify regions hosting significant Quaternary sediments and calculate stored sediment volumes.

3.4.1 Field Observations and Sampling

All locations, elevations, and heights relative to modern river level of Quaternary alluvial terraces were mapped over three field seasons from 2012 to 2014 using Landsat ETM+ imagery from Google Earth (www.google.com/earth) and handheld Garmin ETrex GPS devices with an estimated vertical accuracy of ± 2 m and horizontal accuracy ± 10 m. Very fine- to medium sands ($>63 \mu\text{m}$) were preferentially sampled from coarse sediment lenses in alluvial terrace stratigraphy (Figs. 3.3–3.5) because the sand-size fraction is commonly targeted for petrographic and detrital mineral provenance analysis. Sample locations are presented in Table 3.1.

3.4.2 Bulk Sediment Petrography

Unsieved bulk terrace sediments were counted in thin section with at least 200 points following the Gazzi-Dickinson method (Ingersoll et al., 1984). All lithic fragments were classified by composition and in reference to the MI Index (Garzanti and Vezzoli, 2003; Vermeesch et al., 2016). Grain mounts were stained with alizarin red-S to distinguish calcite from dolomite. Sediments were classified according to the relative proportion of quartz, feldspar, and lithic material in each sample exceeding 10%.

Environmental bias and intrasample variability as a result of hydrodynamic sorting processes were in part corrected for by applying a “Source Rock Density” (SRD) correction to the bulk petrographic data. SRD corrections adjust the relative abundance of all lithic and mineral phases according to a specified bulk sediment density appropriate for sediment origin and degree of exhumation and erosion (Garzanti and Andò, 2007a, b). Bulk petrographic data were corrected to a SRD value of 2.71 g/cm^3 , considered appropriate for regions of the Himalayan orogen exposing Tethyan and Greater

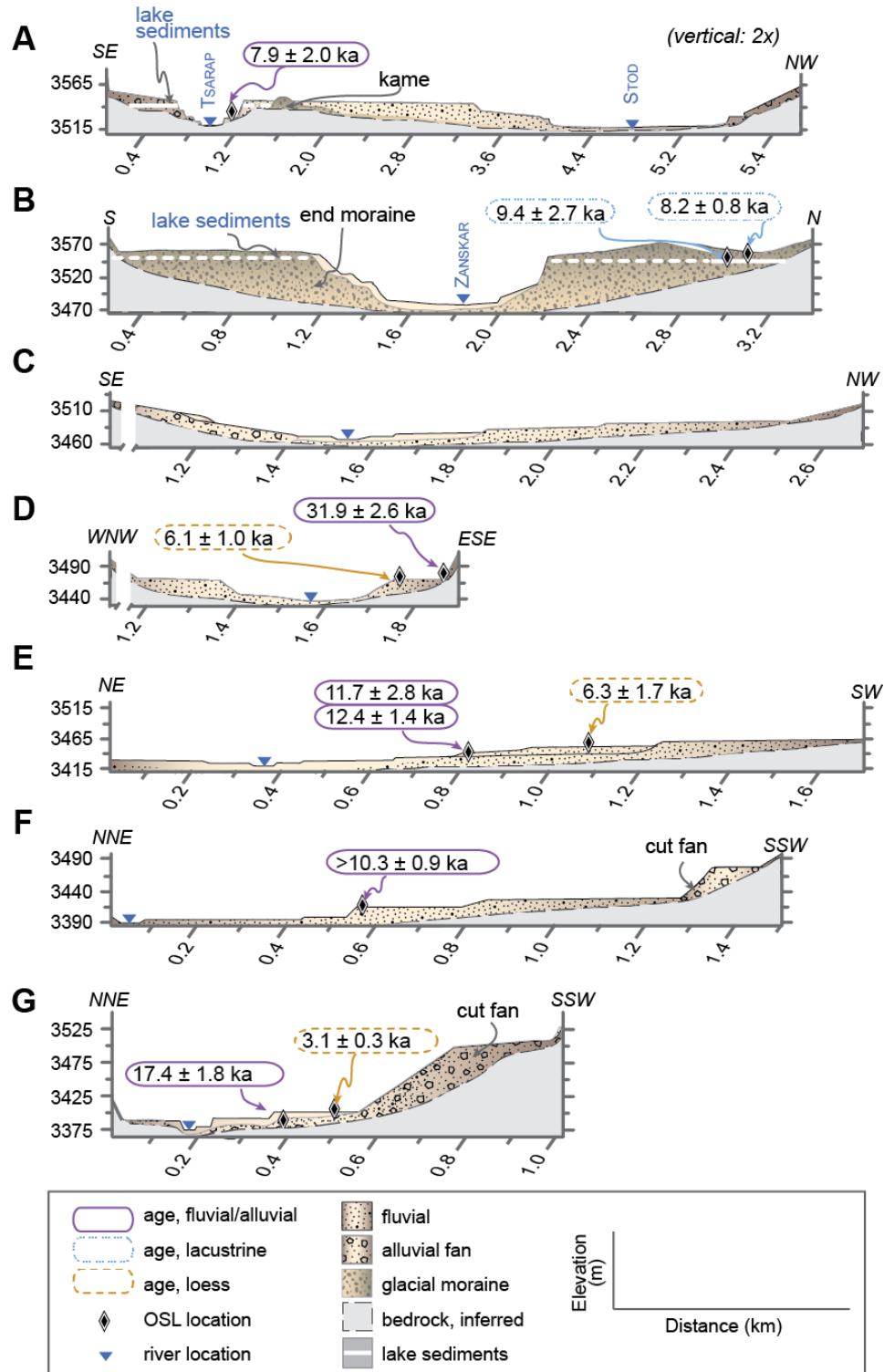
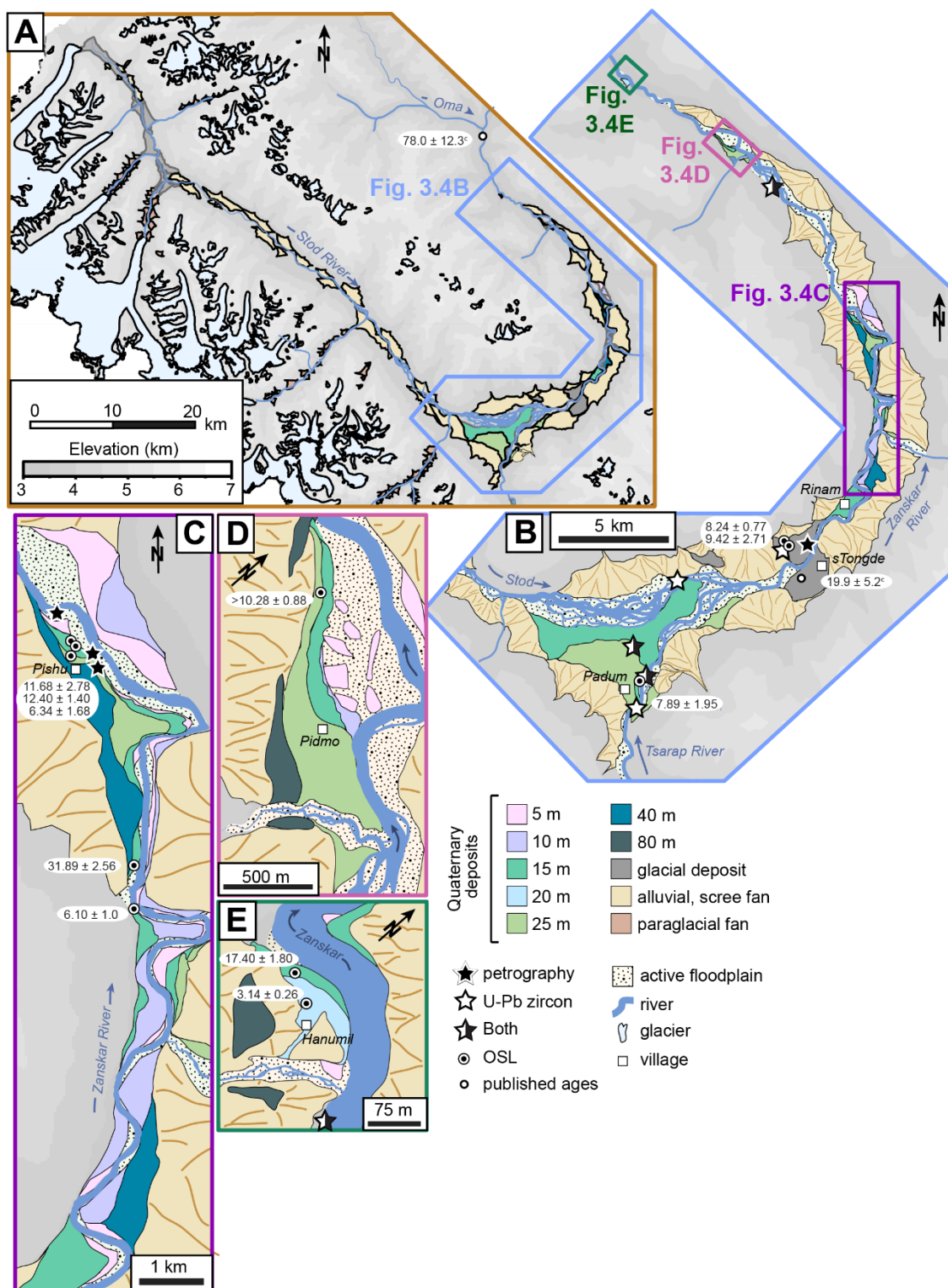


Figure 3.3. Schematic cross-sectional profiles (A–G) of river terraces in the Padum Basin. Profile locations indicated in Figure 3.1C. Diamonds indicate locations of OSL samples.

Figure 3.4. Geomorphologic map of western Zaskar and Padum Basin. (A) Quaternary deposits of Padum Basin and Stod River valley; (B) Quaternary deposits of Padum Basin on trunk Zaskar River (blue lines). Boxes indicate locations of Figs. 3.4C-E; (C) Quaternary deposits at Pishu village; (D) Quaternary deposits at Pidmo village; (E) Quaternary deposits at Hanumil. Reported ages from this study and literature: (a) Saha et al. (2015); (b) Sharma et al. (2016); and (c) Taylor and



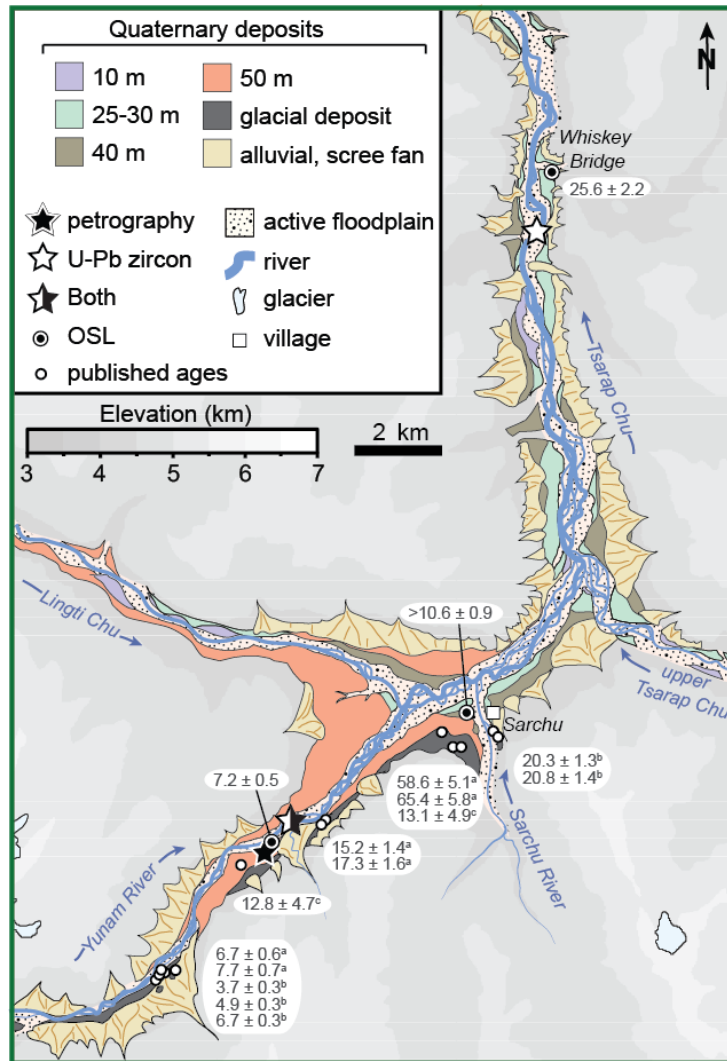


Figure 3.5. Geomorphologic map of eastern Zaskar and Sarchu Basin of upper Tsarap River (blue lines). Reported ages from this study and literature: (a) Saha et al. (2015); (b) Sharma et al. (2016); and (c) Taylor and Mitchell (2000).

Himalayan strata. Bulk petrographic data are reported in Table 3.2 and illustrated in Figure 3.6.

3.4.3 Detrital U-Pb Zircon Geochronology

Detrital zircon is a chemically and mechanically durable mineral phase in siliciclastic sediments such that multiple cycles of erosion do not significantly

Table 3.1. Sample locations for modern and terrace Zaskar River sediments.

ID	Sample	Location	Type	Lat (°N)	Lon (°E)	Elevation (m)	PT	DZ	OSL
1	8081203	Zaskar-Indus	modern	34.162	77.326	3129	x	x	
1b	14072906	Chotski 20	terrace	34.164	77.332	3143	x		
1c	10073101	Chotski 20	terrace	34.164	77.332	3143			x
2	14072807	Markha	modern	33.992	77.241	3311	x	x	
3	12072207	Oma Chu	modern	33.792	76.829	3420	x	x	
4	13071402	Hanumil	modern	33.716	76.877	3407	x	x	
4b	12072302	Hanumil	loess	33.721	76.869	3390			x
4c	13071401	Hanumil	terrace	33.720	76.867	3411			x
4d	13071405	Pidmo 25	terrace	33.700	76.913	3421			x
5	12072401	Pishu	modern	33.682	76.941	3411	x	x	
5b	12072403	Pishu	fan	33.600	76.995	3500			x
6	13071201	Pishu	modern	33.635	76.983	3433	x		
6b	12072402	Pishu	loess	33.630	76.982	3460			x
6c	12072404	Pishu	loess	33.595	76.996	3458			x
6d	12071203	Pishu 15	terrace	33.632	76.984	3447			x
6e	13071205	Pishu 15	terrace	33.632	76.984	3447			x
6f	13071503	Pishu 15	terrace	33.629	76.992	3452	x		
6g	13071206	Pishu 25	terrace	33.628	76.992	3466	x		
R1	13071507	Rinam Lake	lake	33.535	76.954	3571			x
R2	13071504	Rinam 80	terrace	33.531	76.966	3571	x		
R3	12072503	Rinam 80	terrace	33.535	76.955	3571		x	
14	13071607	Padum 15	terrace	33.478	76.892	3545			x
14b	13071609	Padum 15	terrace	33.478	76.892	3545	x	x	
14c	13071602	Padum 25	terrace	33.491	76.885	3553	x	x	
14d	12072501	Padum Lake	lake	33.535	76.955	3577			x
7	12072504	Lower Stod	modern	33.518	76.911	3520	x	x	
8	13071703	Upper Stod	modern	33.817	76.432	4027	x	x	
9	12072507	Lower Tsarap	modern	33.461	76.883	3540	x	x	
10	14080401	Zara	modern	33.342	77.713	4454	x	x	
11	13072301	Toze Lungpa	modern	33.124	77.774	4496	x	x	
12	13072302	Gata	modern	33.008	77.594	4185	x	x	
13	14080609	Yunam	modern	32.885	77.533	4328	x	x	
13b	14080602	Yunam 50	terrace	32.880	77.530	4381	x		
13c	14080601	Yunam 50	terrace	32.880	77.530	4381			x
S	13072304	Sarchu 15	terrace	32.910	77.579	4311			x
W	12072902	Whisky Bridge	fan	33.024	77.592	4196			x

alter U-Th-Pb isotopic compositions (e.g., Gehrels, 2014). U-Pb dating of zircon has become an exceedingly common tool for constraining sediment provenance and there exists a broad chronologic database available for reference on rivers draining the

Table 3.2. Bulk petrography of Zaskar River terrace sediments.

ID	Sample	Location	Framework grains						Mica		Dense minerals									
			Q	F	Lc	Lsm	Lm	Lv	Mu	B	ZTR	Ep	Gt	Ky	Sil	A	Px	Ap	&	
1b	14072906	Choksti 20	18	15	7	85	26	6	2	6	3	1	0	0	5	1	0	0	0	
14c	13071602	Padum 25	14	20	19	105	33	3	1	2	0	0	0	0	1	0	0	0	0	
14b	13071609	Padum 15	6	11	72	76	25	0	2	2	1	0	1	0	1	1	0	0	0	
R2	13071504	Rinam 80	55	48	3	23	43	3	1	4	3	2	0	0	6	5	0	0	0	
6g	13071206	Pishu 25	26	51	26	41	27	7	0	6	0	1	0	1	2	4	0	0	0	
6f	13071503	Pishu 15	18	26	37	39	38	14	1	5	0	0	3	0	5	2	0	0	0	
13b	14080602	Yunam 50	22	12	0	49	65	0	3	12	0	0	0	0	1	1	0	0	0	

Note: Q = all quartz; F = all feldspar; Lc = all carbonate excluding metacarbonate; Lsm = all sedimentary and low rank (1-2) metasedimentary terrigenous fragments after Garzanti and Vezzoli (2003); Lm = all higher rank (3-5) metamorphic fragments; Lv = all volcanic fragments; Mu = muscovite; B = biotite, ZTR = zircon, tourmaline, and rutile; Ep = epidote; Gt = garnet; Ky = kyanite; Sil = sillimanite; A = amphibole; Px = pyroxene; Ap = apatite; and & = andalusite, staurolite, chloritoid, olivine, spinel, and monazite.

Table 3.2 (continued). Bulk petrography of Zanskar River terrace sediments.

ID	Sample	Location	Classification*	Dominant Lithology
1b	14072906	Choksti 20	quartzolithic	(meta-)carbonaticlastic
14c	13071602	Padum 25	feldspatholithic	metamorphiclastic
14b	13071609	Padum 15	lithic	metamorphiclastic
R2	13071504	Rinam 80	feldspatho-quartzolithic	metamorphiclastic
6g	13071206	Pishu 25	quartzo-feldspatholithic	carbonaticlastic
6f	13071503	Pishu 15	quartzo-feldspatholithic	metamorphiclastic
13b	14080602	Yunam 50	quartzolithic	metamorphiclastic

Note:

*Classified according to relative proportion of quartz, feldspar, and lithic material exceeding 10% of QFL total.

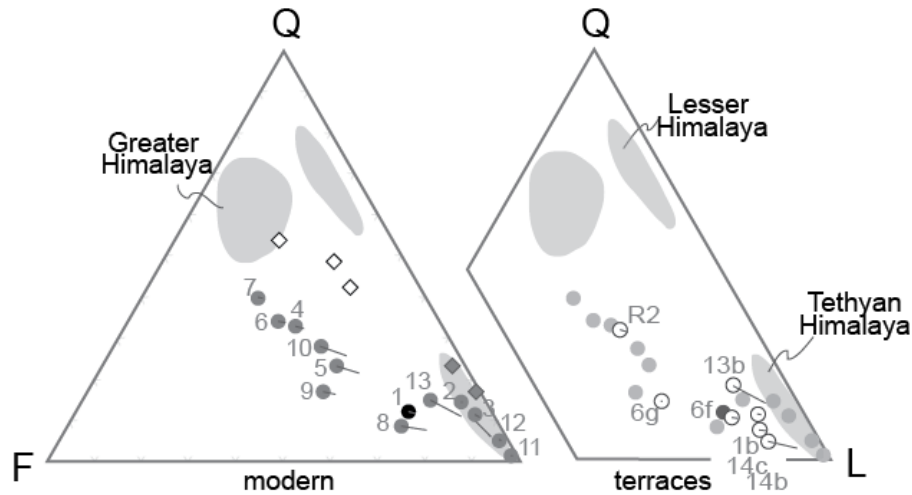


Figure 3.6. Bulk petrographic compositions of modern river and terrace sediments from Zanskar. Compositions are classified by Q(quartz), F(feldspathic), and L(lithic) framework grains following the Gazzi-Dickinson method of point counting (Ingersoll et al., 1984) and classified after Garzanti and Vezzoli (2003). Gray lines indicate data corrections for Source Rock Density (SRD; Vermeesch et al., 2016). Fields for Greater Himalaya and Tethyan Himalaya are after Garzanti et al. (2007). Diamonds indicate trunk Zanskar River samples from Blöthe et al. (2014). Sample numbers follow Table 3.1.

Himalayan-Tibetan orogen (e.g., Amidon et al., 2005; Alizai et al., 2011; Nie et al., 2015). Here the 63–250 μm size fraction is analyzed because this fraction yields all significant U-Pb age populations present in detrital sedimentary samples (Yang et al.,

2012). The application of U-Pb zircon dating to Zanskar River terrace sediments is especially appropriate because modern Zanskar River sediments were recently characterized with this technique (Jonell et al., in press).

Detrital zircon grains were separated using standard magnetic and heavy liquid separation techniques. Extremely magnetic material was removed using a REE hand magnet prior to sieving to 63–250 μm . Zircon grains were mounted in epoxy, polished, and imaged by reflected light and cathodoluminescence before analysis.

U-Th-Pb isotopic compositions were determined at the London Geochronology Centre facilities at University College London using a New Wave 193 nm aperture-imaged frequency-quintupled laser ablation system, coupled to an Agilent 7700 quadrupole-based ICP–MS. An energy density of $\sim 2.5 \text{ J/cm}^2$ and a repetition rate of 10 Hz were used during laser operation. Laser spot diameter was $\sim 30 \mu\text{m}$ with a depth of $\sim 5 \mu\text{m}$. Sample-standard bracketing by measurement of external zircon standard PLESOVICE (Sláma et al., 2008) and NIST 612 silicate glass (Sláma et al., 2008) were used to correct for instrumental mass bias and depth-dependent intra-element fractionation of Pb, Th, and U. Temora (Black et al., 2003) and 91500 (Wiedenbeck et al., 2004) were used as secondary zircon age standards. Over 100 grains were analyzed for each sample to provide a statistically robust dataset for lithologically diverse units (Vermeesch, 2004). Age data were filtered using a + 5 and -15% discordance cut-off. For grains with ages less than 1000 Ma, the $^{206}\text{Pb}/^{238}\text{U}$ ratio was used and the $^{207}\text{Pb}/^{206}\text{Pb}$ ratio for grains older than 1000 Ma. Data were processed using GLITTER 4.4 data reduction software (Griffin et al., 2008). Time-resolved signals recording isotopic ratios with depth in each crystal enabled filtering to remove signatures owing to mixing from overgrowth

boundaries, inclusions and/or fractures. Individual U-Pb ages are reported at 1σ . Analytical data and individual U-Pb ages are presented in Appendix C.

Detrital zircon U-Pb age data are presented in kernel density estimation (KDE) plots in the text for visual analysis of age population distributions and abundance (Fig. 3.7). KDEs are favored in this study to prevent visual bias as traditional probability density functions may smooth older age populations inherently with larger age errors than younger populations at 1σ (Vermeesch, 2012). To quantitatively compare the intersample variability and compare age distributions with bedrock ages from literature the statistical multidimensional scaling (MDS) technique is applied using the open source ‘provenance’ package for R by Vermeesch et al. (2016). MDS analysis produces bivariate maps clustering samples presented here and against bedrock data compiled from literature based on Kolmogorov-Smirnov test dissimilarity.

3.4.4 Optically Stimulated Luminescence Dating

To define the timing of terrace aggradation and relative timing of terrace abandonment and fluvial incision, sediments were dated using OSL. For this investigation sediments likely bearing 63–150 μm quartz grains were sampled because quartz is a commonly targeted mineral in luminescence dating techniques. Furthermore, the 63–150 μm size fraction is the most readily transported and deposited in a fluvial setting (e.g., Rhodes, 2011). Great care was taken during sampling to access sediment facies that received maximum light exposure during transportation, such as shallow channel sediments, to maximize bleaching and minimize inherited signals (Schaetzl and Forman, 2008). OSL samples were collected in hand-cut ~15 cm aluminum tubes, packed and wrapped with newspaper and UV-resistant tape, and double-bagged in opaque media

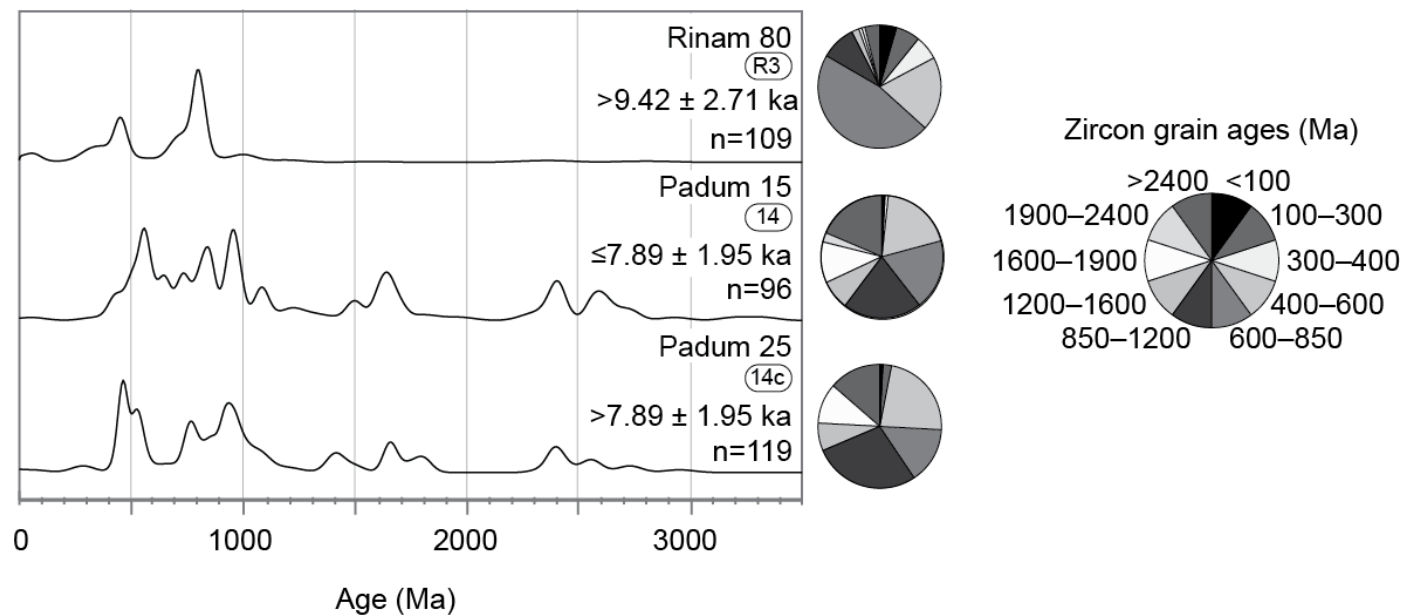


Figure 3.7. Kernel density estimation (KDE) diagrams of detrital zircon U-Pb ages from Zaskar River terrace sediments with age interval ranges illustrated in pie diagrams.

for transport. The majority of OSL samples were processed and analyzed at the luminescence dating laboratories at the University of Cincinnati and the University of Oxford. One sample (10073101) analyzed at Royal Holloway, University of London was incorporated for regional context into this study. Three laboratories were utilized as separation and analysis for OSL dating labor and time intensive but the following standard sample processing and analytical protocols were adhered to by all laboratories.

Quartz grains were isolated from heavy minerals and feldspars using pretreatment with HCl, HF, and fluorosilicic acids, heavy liquid separation, and wet sieving. Modified single-aliquot regeneration (SAR) protocols (Wintle and Murray, 2006) were employed on small aliquots (200–500 grains; 100–150 μm) to estimate equivalent doses and establish signal growth curves. Ultra-small aliquot (5–10 grains) quartz grain dating (Duller, 2008) was undertaken if partial bleaching, a common problem when dealing with fluvial sediments, was noted (i.e., skewed equivalent dose distributions). This allowed age calculations even where populations of grains of various bleaching ages were present (Bailey and Arnold, 2006; Jaiswal et al., 2008; Srivastava et al., 2008). Risø measurement systems were used to calculate paleodoses and dose response curves using a minimum of five SAR cycles under subdued sodium lighting (588 nm). Errors were estimated either with Monte Carlo simulation (2000 repeats) or calculated analytically, based on the difference between the fitted curve and dose points. Analytical uncertainties for OSL ages range typically from 5–10%. Estimations of the contribution of cosmic dose rate accounted for geographic position, elevation, topographic shielding, snow cover and depth, burial depth, and water content (Prescott and Hutton, 1994).

Field observations noted many prominent cut-and-fill aggradational terrace levels

in two glacially-conditioned basins at Padum and Sarchu (Figs. 3.3–3.5). Prominent terrace surfaces were targeted in each region because it was impractical to sample all terrace levels for dating. OSL age analyses are presented in Table 3.3.

3.4.5 Basin Morphology and Sediment Volumes

Digital elevation model (DEM) topographic data were derived from void-filled 30-m grid Shuttle Radar Topography Mission (SRTM30) data. Modern glacial extents are courtesy of Global Land Ice Measurements from Space (GLIMS) Version 1 data (Shrestha et al., 2014). River profile analysis was conducted using ArcGIS and TopoToolbox 2.0 for MATLAB (Schwanghart and Scherler, 2014). Longitudinal river profiles were extracted for all major tributaries ($>500 \text{ km}^2$) and for smaller tributaries featuring significant valley-fills using a carve-and-fill hydrologic conditioning routine. Swath profiles were taken along each river profile confining to confining hillslopes of $>20^\circ$. Elevation and slope values orthogonal to river channels were extracted every 500 m and are plotted in Figure 3.8.

Table 3.4 summarizes volumes of sediments stored as Quaternary alluvial terraces, alluvial and paraglacial fans, and dissected glacial till in the Zaskar River and Tso Kar basins. Alluvial and paraglacial fan volumes were calculated individually for each feature after extracting landform geometries from Landsat ETM+ imagery and SRTM30 data. Terrace volumes and dissected glacial till calculations assumed trapezoidal sediment wedges similar to Clift and Giosan (2014) with planar tread tops and bases. Valley-fill estimates assume sediment thicknesses no deeper than modern river level or exposed adjacent bedrock. Fan volumes were calculated as flat-based semicone volumes after Giles et al. (2010). Volumes for hillslope, paraglacial, nor for glacial valley

Table 3.3. OSL sample results for Zanskar River sediments.

Sample Number	Lab Name	Location	Elevation (m)	Elevation above river (m)	Number of aliquots ^d	Equivalent Dose, De (Gy) ^e	Dose Rate (Gy/ka)	OSL Age (ka, $\pm 1\sigma$) ^f	Depth (m)
10073101	Chotski	Chotski 20 ^a	3143	18	5	7.71 ± 3.65	2.02 ± 0.09	3.8 ± 1.8	4.8
12072302	X6003	Hanumil (L) ^c	3390	15	9	12.11 ± 0.73	3.86 ± 0.13	3.1 ± 0.3	<1
13071401	X6354	Hanumil ^c	3400	25	11	50.06 ± 4.29	2.89 ± 0.10	17.4 ± 1.8	1
13071405	Pidmo Sand	Pidmo 25 ^b	3421	25	6	29.11 ± 2.31	2.92 ± 0.14	* 10.3 ± 0.9	1.5
12072402	X6001	Pishu (L) ^c	3460	40	10	19.14 ± 4.96	3.05 ± 0.10	6.3 ± 1.7	1.5
12072403	UIC3322	Pishu 25 ^b	3500	40	17	123.64 ± 7.70	3.87 ± 0.17	31.9 ± 2.6	3
12072404	X6002	Pishu (L) ^c	3458	25	11	16.30 ± 2.53	2.67 ± 0.09	6.1 ± 1.0	1.5
13071203	Pishu	Pishu 15 ^b	3447	15	24	38.04 ± 7.93	3.37 ± 0.17	11.7 ± 2.8	1.8
13071205	X6351	Pishu 15 ^c	3447	15	9	46.54 ± 4.40	3.75 ± 0.12	12.4 ± 1.4	1.2
13071507	Rinam Lake	Rinam Lake ^b	3571	81	23	38.04 ± 7.76	3.70 ± 0.19	9.4 ± 2.0	1.5
13071607	L-Podum	Padum 15 ^b	3545	10	21	22.26 ± 5.59	2.84 ± 0.03	7.9 ± 2.0	0.5
12072501	X6000	Rinam Lake ^c Whiskey	3577	89	9	31.24 ± 2.44	3.77 ± 0.12	8.2 ± 0.8	0.9
12072902	12072902	Bridge ^c	4196	26	10	66.15 ± 7.49	3.05 ± 0.10	25.6 ± 2.2	3
13072304	L-Sorchu	Sarchu ^b	4311	14	8	27.8 ± 0.93	2.12 ± 0.10	* 10.6 ± 0.9	0.5
14080601	14080601	Yunam 50 ^c	4381	50	11	22.63 ± 1.21	3.13 ± 0.15	7.2 ± 0.5	1.3

Note:

^a Department of Geography, Royal Holloway, University of London

^b Luminescence Dating Lab, Department of Geology, University of Cincinnati

^c Research Laboratory for Archaeology and the History of Art, University of Oxford

^d Number of aliquots used for age calculation. Rejection of aliquots follows standard rejection criteria

^e De calculated using the Minimum Age Model of Galbraith et al. (1999) unless otherwise noted; Excel macros written by Sébastien Huot (UQAM)

^f Error on age is 2-sigma standard error

Table 3.3 (continued). OSL sample results for Zaskar River sediments.

Sample Number	Lab Name	Location	Grain Size (μm)	<i>In-situ</i> H ₂ O (%) ^g	U (ppm)	Th (ppm)	K (%)	Rb (ppm)	Cosmic (mGy/ka) ^h	Notes
10073101	Chotski	Chotski 20 ^a	212-250	0.09	1.95	8.79	0.99	--	0.30 ± 0.150	
12072302	X6003	Hanumil (L) ^c	180-255	6.22	3.90	16.40	2.19	96.0	0.31 ± 0.031	
13071401	X6354	Hanumil ^c	180-255	0.33	2.50	11.40	1.36	76.0	0.32 ± 0.032	
13071405	Pidmo Sand	Pidmo 25 ^b	90-150	0.42	2.80	12.10	1.16	60.0	0.35 ± 0.035	*minimum age; low intensity
12072402	X6001	Pishu (L) ^c	180-255	8.93	3.10	10.00	2.05	61.0	0.28 ± 0.028	
12072403	UIC3322	Pishu 25 ^b	100-150	0.97	3.70	16.50	1.71	--	0.29 ± 0.030	
12072404	X6002	Pishu (L) ^c	180-255	5.43	2.70	12.00	1.34	55.0	0.28 ± 0.028	
13071203	Pishu	Pishu 15 ^b	90-150	--	3.40	15.30	1.25	66.0	0.34 ± 0.035	
13071205	X6351	Pishu 15 ^c	180-255	4.50	3.10	16.90	1.81	59.0	0.31 ± 0.031	
13071507	Rinam Lake	Rinam Lake ^b	90-150	0.63	3.60	18.10	1.34	61.0	0.35 ± 0.036	
13071607	L-Podum	Padum 15 ^b	90-150	3.32	2.5	10.9	1.23	65.0	0.35 ± 0.035	
12072501	X6000	Rinam Lake ^c	180-255	0.20	4.30	22.30	1.35	52.0	0.29 ± 0.029	
12072902	12072902	Whiskey Bridge ^c	180-255	14.73	2.50	12.30	1.37	70.0	0.31 ± 0.031	
13072304	L-Sorchu	Sarchu ^b	90-150	0.07	1.80	8.10	0.84	42.0	0.35 ± 0.035	*minimum age; low intensity
14080601	14080601	Yunam 50 ^c	180-255	0.33	2.40	13.20	1.44	75.0	0.47 ± 0.047	

Note:

^g Assume $5 \pm 2\%$ wt H₂O is representative of burial history^h Contribution of cosmic radiation to the dose rate was calculated by using sample depth, elevation, and longitude/latitude following Prescott and Hutton (1994)

Figure 3.8. Stacked river profiles of all Zaskar River tributaries. (A) Longitudinal river profiles with stacked slope ($<35^\circ$) and elevation values orthogonal to 2-km-wide swath profiles (marked with *). Swath profiles in narrow gorges used 1-km wide swaths (Markha, Khurna, Oma, Kurgiakh, and Tsarap Chu). Lower slope values ($<10^\circ$, blue) are layered above higher slope values. Profile colors and numbers are in reference to (B) for clarity. To best illustrate Rupshu Plateau valley-fills from Munack et al. (2016), the Toze Lungpa and Zara River profiles overlap. Gray shaded regions indicate large valley-fills within the Zaskar River basin from this study. Stored volumes reported in Table 3.4 are indicated next to each valley-fill. (B) Layout of Zaskar River tributaries with longitudinal profile numbers. RP = Rupshu Plateau (includes the More Plain). Confluence marked by “M” notes end of Rupshu Plateau.

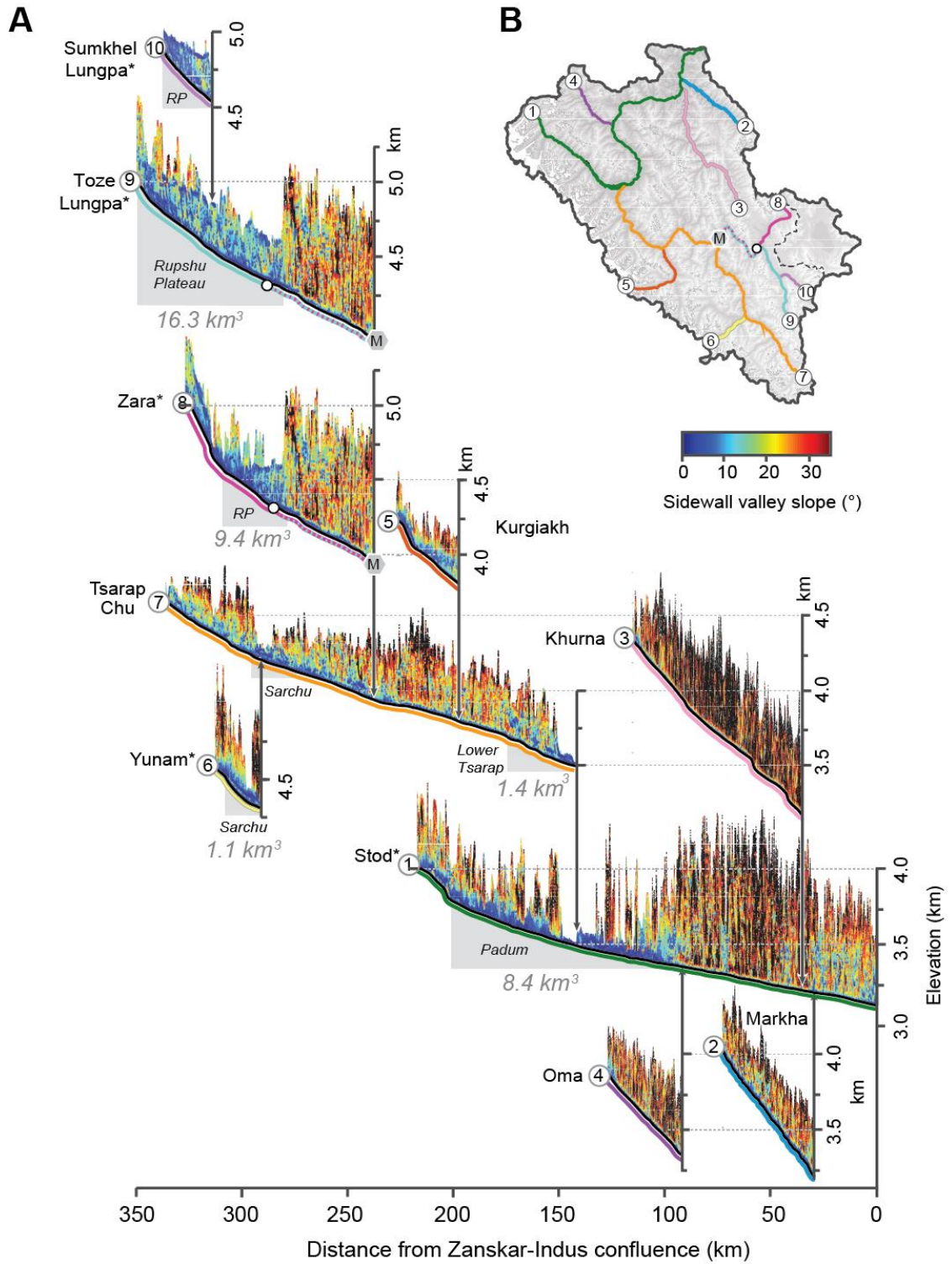


Table 3.4. Stored sediment volumes for Zanskar River and Tso Kar Basins.

Region	Stored Volumes (km ³)	% of Total Stored	Area (km ²)	Area Connected (km ²)	Accessible Volume (km ³) ^a	% of Total Stored ^a
<u>Padum Basin</u>						
Terraces	1.3	4	42			
Glacial deposits	0.7	2	11			
Fans	6.3	17	0.1			
	8.4	23	53.1	53.1	8.4	55
<u>Lower Tsarap</u>						
Glacial deposits	1.2	3	7			
Fans	0.3	1	<0.1			
	1.4	4	7.1	7.1	1.4	9
<u>Sarchu Basin</u>						
Terraces	0.8	2	17			
Fans	0.3	1	<<0.1			
	1.1	3	17	17	1.1	7
<u>Rupshu valley-fill^b</u>						
More Plain	16.3	44	147	26		
Zara	9.4	26	61	11		
	25.7	70	208	37	4.4	29
Zanskar (this study)	36.7	--	--	--	15.3	--
Tso Kar (this study) ^c	6–31	--	124	0	0	0
<u>Blöthe and Korup (2013)</u>						
Padum Basin	12.0					
Sarchu Basin	0.7					
Rupshu valley-fill ^d	20.0					
	32.7					

Note:

^aVolumes within 500-m buffer zone on each side of river drainage

^bMore Plain Surface dated by Munack et al. (2016)

^cTso Kar valley-fill depth ranging 50–250 m

^dIncludes More Plain and Tso Kar only

sediments that have not been incised were not estimated because the assumed depth to bedrock or ice were unknown. This results in this budget represent a robust, albeit minimum, estimate for stored sediment volumes.

3.5 Results

3.5.1 Bulk Sediment Petrography

Zanskar River terrace sediments contain a diverse assemblage of mineral and lithic fragments (Table 3.2). Framework petrography indicates abundant quartz, feldspar, low rank metasedimentary and metacarbonate fragments, and high-rank fibrolite-bearing metafelsite fragments. Minor but notable fragments include serpentinized ultramafic and vesicular, porphyritic metabasite fragments. Abundant mineral phases include calcite and dolomite spar, micas, fibrolitic sillimanite, green and green-brown amphibole with minor garnet, zircon, and titanite. Bulk sediment compositions range from quartzolithic (meta-) carbonaticlastic to lithic metamorphiclastic.

Most terrace sediments more or less fall near rock compositions associated with Tethyan Himalaya provenance on a quartz-feldspar-lithic diagram (Fig. 3.6). Exceptions to this are the reworked Rinam moraine (ID# R2) and ~25 m Pishu terrace (ID# 6g) samples that are more similar to Greater Himalayan sources. This in part is the result of the abundance of carbonate detritus in other sediments and slight enrichment in quartz and/or feldspar fragments, respectively, in Rinam and Pishu (Table 3.2).

3.5.2 Detrital U-Pb Zircon Geochronology

Detrital zircon spectra of the three terrace samples are presented as KDE diagrams following Vermeesch (2004) in Figure 3.7. The ~15 m Padum terrace (ID# 14) sample is characterized by a broad, composite peak of zircon ages from 450 to ~1100 Ma, smaller Proterozoic populations at ~1500 Ma, 1650 Ma, 2400–2600 Ma, with minor Archean ages as old as ~3800 Ma. Within the composite peak are subsidiary peaks at ~950, ~850, ~750, 500–600 Ma (545 Ma peak), and ~450 Ma, Ma. One Miocene zircon yielded an

age of 22.1 ± 0.6 Ma. U-Pb zircon ages from ~25 m Padum terrace (ID# 14c) yielded similar, prominent strong age peaks at ~750, ~530, and ~450 Ma, , with smaller populations at 2400–2600, ~1600–1800, and ~1400 Ma. Younger zircons include one Miocene zircon at 25 ± 0.9 Ma, and two Permo-Triassic zircons at 281 ± 7 Ma and 251 ± 7 Ma. The Rinam moraine sample (ID #R3) contains peaks at ~545, ~440, and 245–380 Ma, with a very strong peak at 650–850 Ma. This sample yielded the most Miocene zircon (n=5) with ages ranging from 21 to 26 Ma.

3.5.3 Optically Stimulated Luminescence Dating

Eleven new OSL samples from the Padum Basin indicate several aggradational events (Figs. 3.3 and 3.4). The confluence of the Stod and Tsarap Rivers near Padum village hosts two prominent terrace surfaces at 25–30 m and 10–15 m above modern river level (Figs. 3.3A and 3.4B). An OSL age of 7.9 ± 2.0 ka was yielded from the ~15 m surface. Downriver from the confluence, lacustrine sediments are perched on an incised, 80–90 m thick glacial moraine and were dated between 8.2 ± 0.8 ka and 9.4 ± 2.7 ka (Figs. 3.3B and 3.4B). Similar lacustrine sediments occurring at the same elevation were mapped upstream of the Rinam moraine at Padum village, south of the Tsarap River (Fig. 3.3A). Immediately upstream of Pishu village (Figs. 3.3C and 3.4C), a ~40 m terrace incorporating an alluvial fan yielded an age at 31.9 ± 2.6 ka. This ~40 m terrace extends upstream to Rinam village and discontinuously to Pidmo village (Figs. 3.3F and 3.4D). Covering this terrace is a thin loess cap dated at 6.1 ± 1.0 ka and at 6.3 ± 1.7 ka, where exposed, on a lower ~25 m surface at Pishu (Figs. 3.3E and 3.4C). This ~25 m surface extends to Pidmo (Figs. 3.3F and 3.4D) and yielded a minimum age of 10.3 ± 0.8 ka. At Pishu (Figs. 3.2E and 3.4C), a lower ~15 m terrace surface yielded two ages at 11.7 ± 2.8

ka and 12.4 ± 1.4 ka. At the end of the Padum Basin, two ages were yielded at Hanumil village (Figs. 3.3G and 3.4E). An incised alluvial fan buried by aggradational terraces yielded an age of 17.4 ± 1.8 ka. A loess cap on a 15–20 m terrace was dated at Hanumil at 3.1 ± 0.3 ka.

From the Sarchu Basin, three samples were dated (Fig. 3.5). One OSL sample from a ~60 m incised alluvial fan yielded an age of 25.6 ± 2.2 ka. A 12–15 m terrace at Sarchu village yielded a minimum age of 10.6 ± 3.6 ka. On the Yunam River, a prominent ~50 m terrace surface yielded an age of 7.2 ± 0.5 ka.

At the Zaskar-Indus River confluence at Choksti, one OSL age was yielded from a ~20 m alluvial terrace perched on a bedrock strath terrace (Fig. 3.1B). The alluvial terrace indicated an age of 3.8 ± 1.8 ka.

3.5.4 Basin Morphology and Sediment Volumes

Four regions storing significant volumes of sediment in the Zaskar River Basin are noted: the Padum Basin, Sarchu Basin, the Rupshu Plateau, and the lower Tsarap River (Table 3.4; Figs. 3.8–3.9). The Padum Basin, which here includes all sediments in the Stod River catchment, is estimated to hold ~ 8.4 km³ of sediment, predominantly as alluvial and paraglacial fans. Latest Pleistocene-earliest Holocene river terraces account for only ~ 1.3 km³ of sediment. In the Sarchu Basin, 1.1 km³ of sediment are held equally between Pleistocene-Holocene terraces and mixed alluvial/scree fans. The greatest volumes of sediment in Zaskar are stored as dissected Pleistocene (~ 135 ka) valley-fills that include the Rupshu Plateau outlined by Munack et al. (2016). Pleistocene Rupshu Plateau valley-fills account for ~ 25.7 km³ of sediments in the Zara River, Toze Lunpa, and Sumkhel Lungpa catchments. New calculations indicate the Tso Kar Basin stores 6–

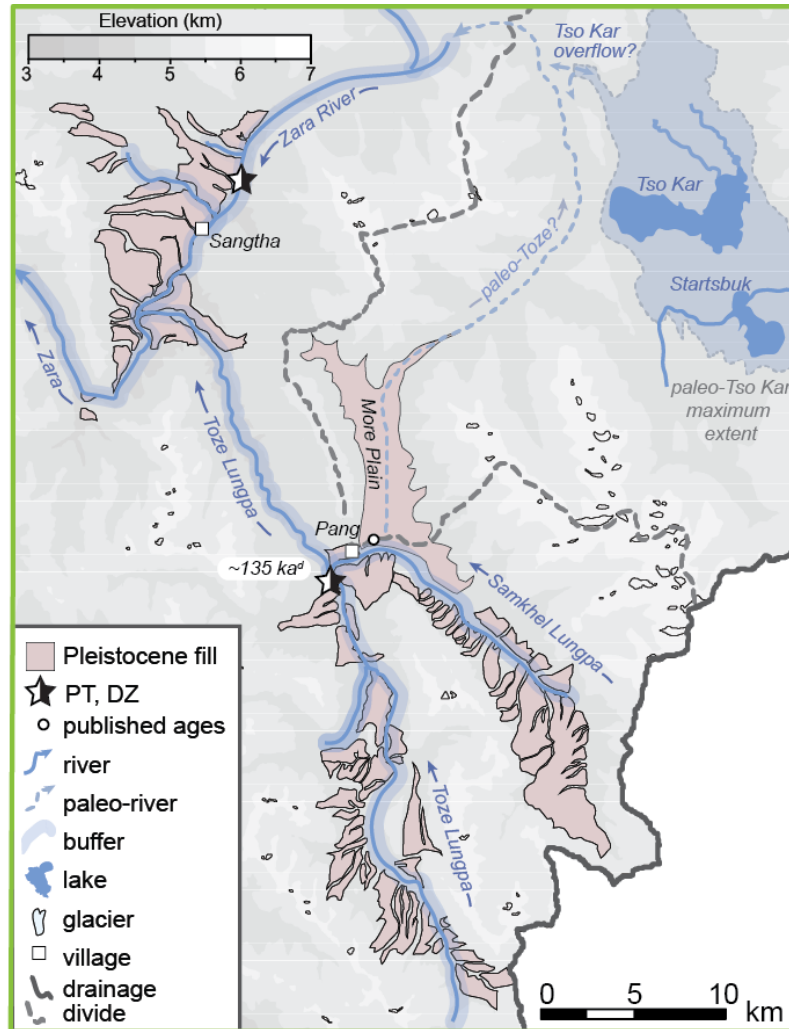


Figure 3.9. Pleistocene Rupshu Plateau valley-fills (pink) of the More Plain and upper Tsarap River tributaries, the Toze Lungpa, Sumkhel Lungpa, and Zara River (blue lines). Tso Kar maximum extent (shaded blue) after Wünnemann et al. (2010). Proposed paleo-Toze Lungpa drainage (dashed blue) and reported ~135 ka age for More Plain terrace (Munack et al., 2016).

31 km³ of sediment depending on estimates for valley-fill thickness (0–250 m). Dissected moraines and paraglacial fans in the lower Tsarap catchment host ~1.4 km³ of sediment.

3.6 Discussion

3.6.1 Provenance and Spatial Patterns of Erosion

By tracking the compositional evolution of both modern river sediment and dated river terrace sediments downstream, spatial patterns of erosion across the basin can be

constructed through time. Data presented here are compared with recent modern sediment analyses (Jonell et al., in press). A major change in Padum Basin sediment provenance (Fig. 3.10) first occurs after ~12 ka, when quartz and feldspar become more abundant in modern sediments downstream of Pishu, as far as Hanumil (ID #4-6). It is likely the more abundant feldspar and quartz are sourced from the Rinam moraine (ID #R2) and/or from the Stod River valley (ID #7). The Stod River has been previously suggested as the most significant source of sediment to the Zaskar River (Jonell et al., in press) but the Rinam moraine cannot be discounted as a source because of its similarity in composition to the modern Stod River. Through MDS analysis, bulk petrography of the Rinam moraine indicates closest similarity to the modern Lower Stod 3.11A). Rinam is discretely grouped with sediments from the modern Zaskar-Indus confluence (ID #1), Hanumil (ID#4), Pishu (ID#5), Upper Stod (ID#8), and Lower Stod (#7) sediments (Fig. 3.11B). All of these sediments have similar U-Pb zircon age spectra to one another, with prominent peaks at 750–850, ~450, and ~350 Ma (Fig. 3.12). The Rinam moraine sediments are likely sourced from Zaskar Greater Himalaya lithologies (Figs. 3.11C and 3.13). Although zircon age frequencies are not identical, all significant age populations in the Zaskar Greater Himalaya are identified at Rinam. It is most likely Rinam sediments were dominantly sourced from a Stod valley glacier carving Zaskar Greater Himalaya lithologies. Although MDS analysis of petrographic data (Fig. 3.10A) suggests the Zara River (ID #10) as a potential source, this is only a product of the abundance of coarse quartz and feldspar grains found in both the Rinam and Zara samples.

Using the fluvial chronology from the Padum Basin, time constraints on the age and incision of the Rinam moraine can be made. Depositional ages from lake sediments

Figure 3.10. Bulk petrography downstream mixing schematic of framework grains from modern river tributary sediments (Jonell et al., in press) and selected terrace sediments. Q = quartz; F = feldspars; Lc = lithic carbonate; Lsm = other sedimentary and low-rank metasedimentary; Lm = medium- to high-rank metamorphic; and Lv = volcanic and metavolcanic. Rank of metamorphic grains and Metamorphic Index (0–500; Garzanti and Vezzoli, 2003). Black line denotes trunk Zaskar River, with gray lines for tributaries. Samples are labelled and numbered after Table 3.1.

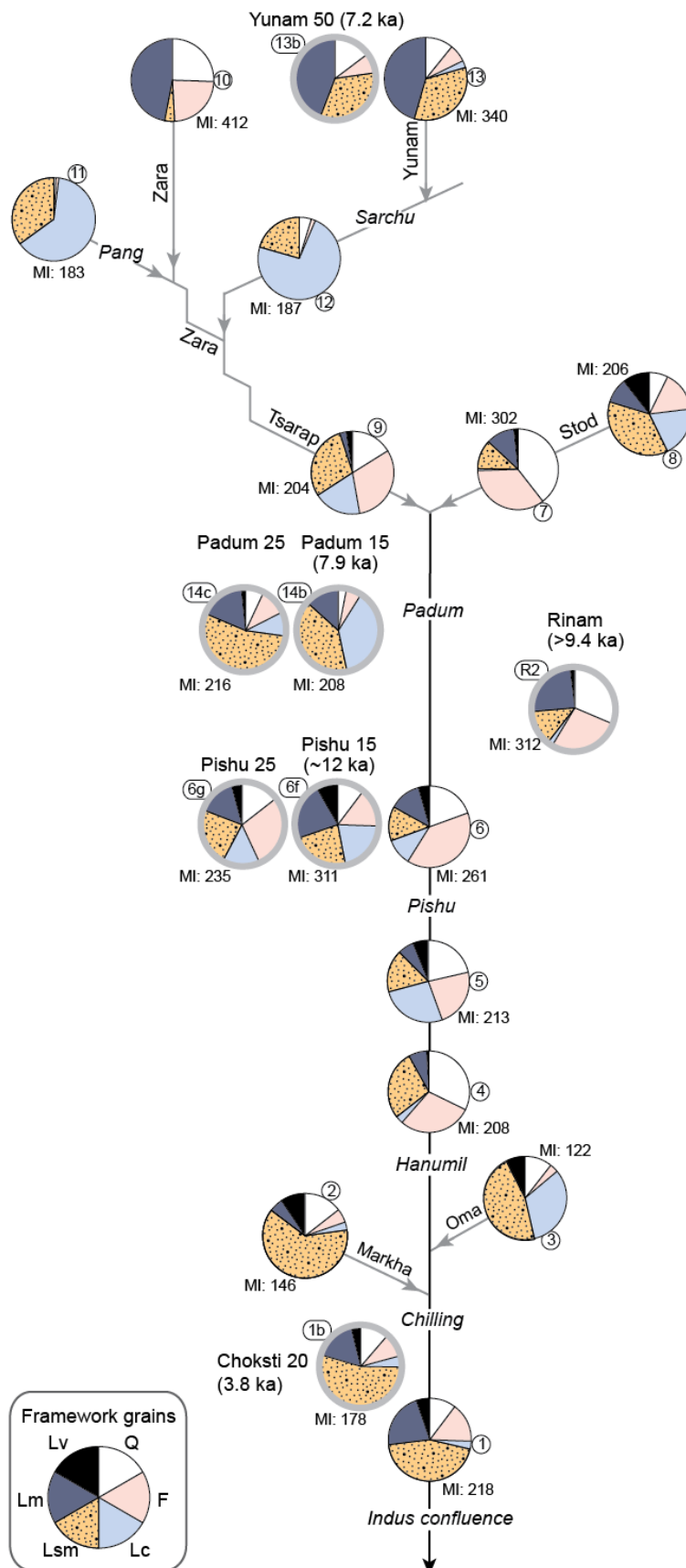
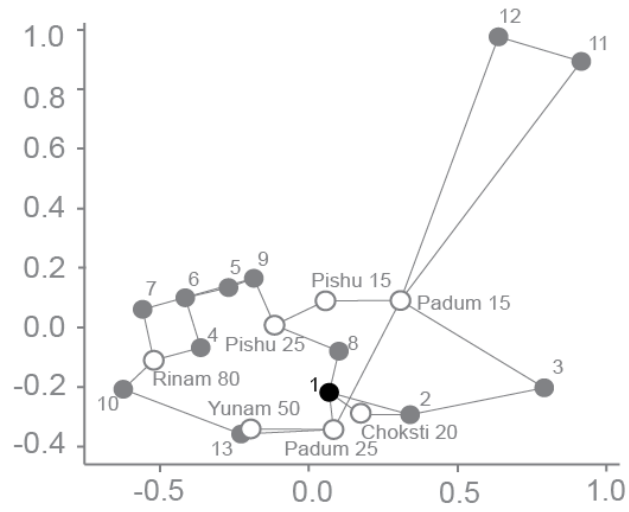
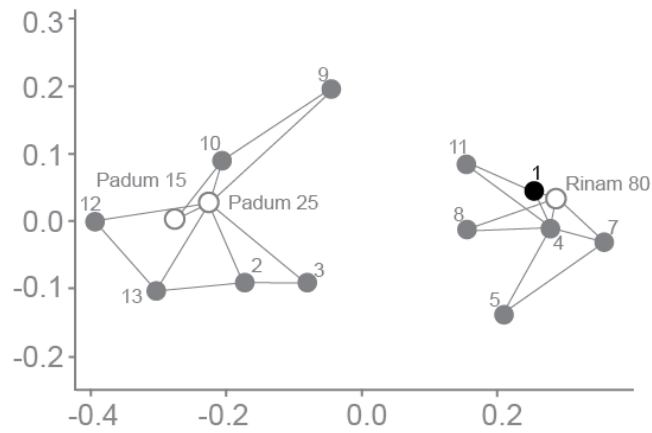


Figure 3.11. Multidimensional scaling (MDS) plots showing the Kolmogorov-Smirnov distances between modern Zaskar River sediments, river terrace sediments, and local bedrock. Number labels follow Table 3.1. (A) Nonmetric MDS plot of source rock density (SRD)-corrected bulk petrographic data; (B) Nonmetric MDS plot of all Zaskar River detrital zircon U-Pb ages; (C) Zaskar River terrace sediments compared with modern Zaskar River sediments and compiled regional Himalayan bedrock U-Pb zircon age from Figure 3.12. Solid lines indicate closest neighbor and dashed lines nearest next neighbors. Data plotted using R ‘provenance’ package by Vermeesch et al. (2016). Bedrock abbreviations mostly follow depositional ages: pC-C = Proterozoic to Cambrian; D-O = Devonian to Ordovician; M-P = Mississippian to Permian; T-J = Triassic to Jurassic; LK = lower Cretaceous; uK-Pg = upper Cretaceous to Paleogene; and ZGH = Zaskar Greater Himalayan bedrock (Horton and Leech, 2013).

A. Bulk Petrography (SRD-corrected)



B. Zanskar River U-Pb zircon



C. Regional Bedrock and Zanskar U-Pb zircon

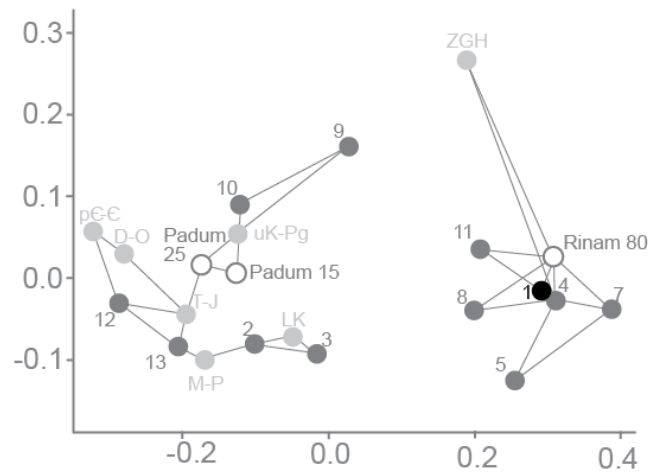


Figure 3.12. KDE diagrams for detrital U-Pb zircon ages for all modern and Quaternary Zaskar River Basin sediments. Color bars indicate age peaks associated with Mississippian-Permian (245–380 Ma) magmatism, Cambro-Ordovician (440–550 Ma) magmatism, and a strong age peak (750–850 Ma) reported in modern Zaskar River sediments (Jonell et al., in press). Labels according to Table 3.1.

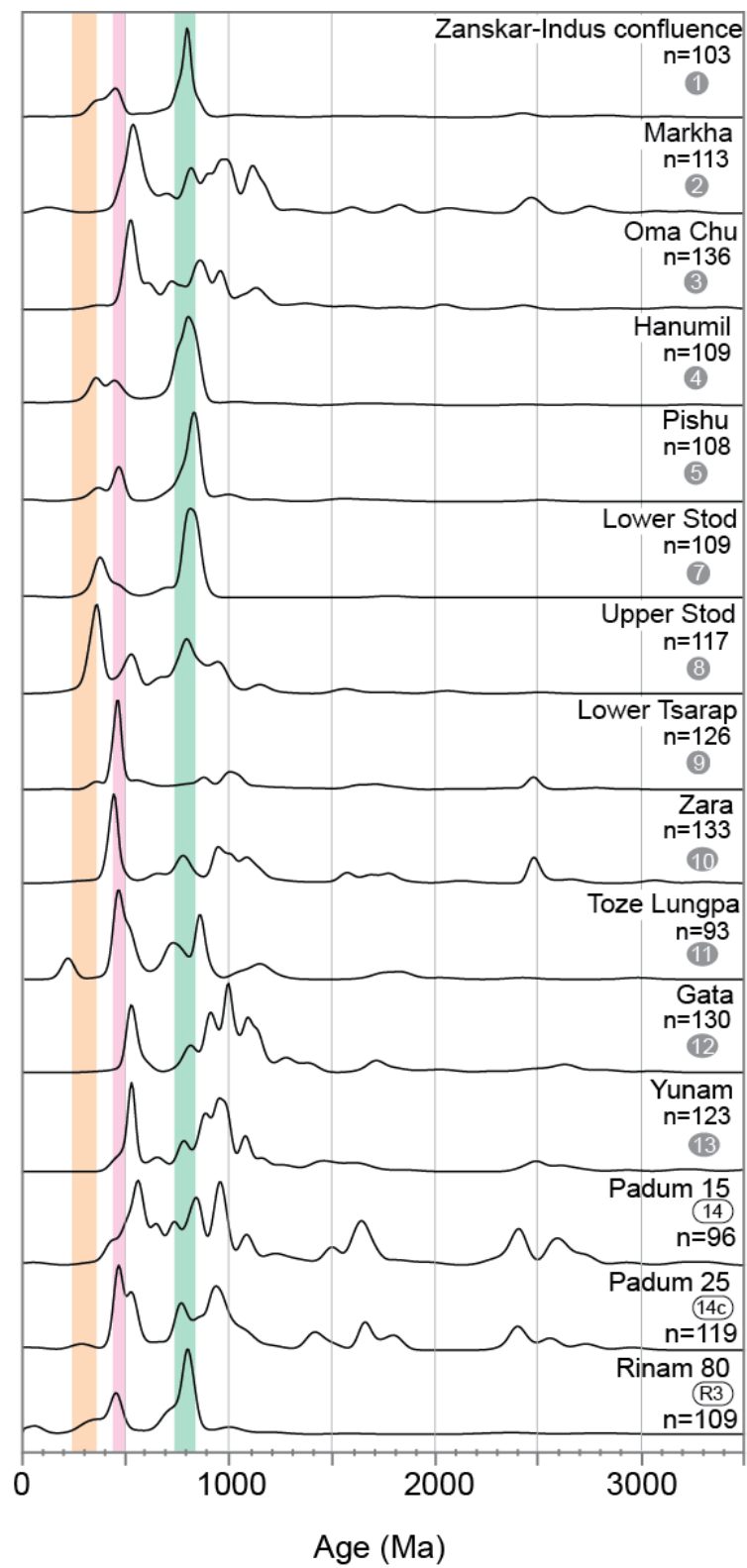
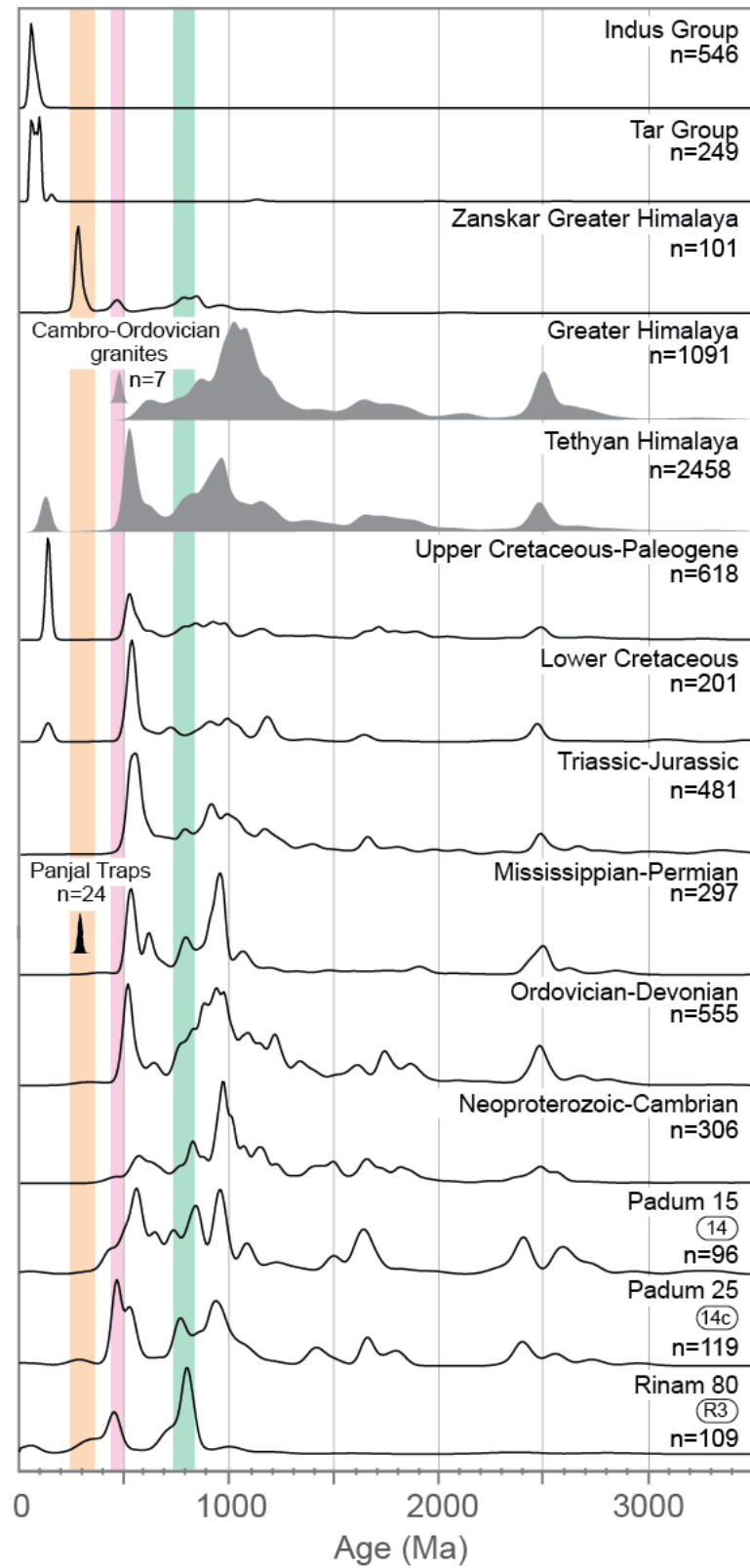


Figure 3.13. KDE diagrams for detrital U-Pb zircon ages from the Zaskar River Basin and selected Himalayan bedrock. Selected samples are from the Indus and Tar Groups (Wu et al., 2007; Henderson et al., 2010), Zaskar region Greater Himalaya (Horton and Leech, 2013), Panjal Traps (Shellnutt et al., 2011), and Cambro-Ordovician granites in Zaskar and the NW Himalaya (Pognante et al., 1990; Girard and Bussy, 1999; Kwatra et al., 1999; Miller et al., 2001; Cawood et al., 2007). Selected bedrock ages for southern Tethyan Himalaya, Greater Himalaya, and correlative strata from the eastern and central Himalaya were plotted (in gray) according to depositional age and compiled into composite KDE diagrams (DeCelles et al., 2000; Myrow et al., 2003; McQuarrie et al., 2008; Myrow et al., 2010; Gehrels et al., 2011; Hu et al., 2012; Clift et al., 2014; Hu et al., 2015). Color bars indicate age peaks associated with Mississippian-Permian (245–380 Ma) magmatism, Cambro-Ordovician (440–500 Ma) magmatism, and a strong age peak (750–850 Ma) reported in modern Zaskar River sediments from references reported above. Labels according to Table 3.1. Figure adapted from Jonell et al. (in press).



dammed behind the Rinam moraine require it to be older than ~9.4 ka (Figs. 3.3 and 3.4B). This is consistent with a previous OSL age of 19.9 ± 5.5 ka from the moraine itself, although that OSL age has been called into question (Owen et al., 2002). Nevertheless, moraine dissection must have occurred after lake sedimentation ended at ~8.2 ka, if not before upstream river incision through correlative lake sediments and before terrace aggradation at ~7.9 ka. If dissection occurred by ~8 ka, and if at least 80 meters of incision occurred over ~4.8 km, an estimated 0.3 km^3 of moraine material was recycled into the Zaskar River downstream of Rinam since that time. This volume equates to ~22% of the total sediment stored in the Padum Basin (Table 3.4). If dissection of glacial valley-fill held in the Stod River was also incised at that time, another ~0.2 km^3 of sediment would have been recycled.

Although buffering significantly controls sediment compositions in the Padum Basin, this effect is moderated downstream through side-valley contributions within the Zaskar Gorge. Sediment compositions at the Zaskar-Indus River confluence are not identical to those in the Padum Basin (Figs. 3.10 and 3.11). This can be observed at least over the last ~3.8 k.y. as recorded at Choksti (ID# 1b), and suggesting that the bulk provenance of sediment fluxed from the Zaskar River to the trunk Indus has not changed significantly since at least that time.

Nonetheless, intrabasinal temporal provenance variations are recorded in river terrace sediments. First, a shift in provenance is noted between the ~25 m Pishu terrace (ID# 6g) and the ~15 m Pishu terrace (ID# 6f). Compositions at ~12 ka included more gneiss, calc-gneiss, fibrolitic sillimanite, and volcanic fragments than younger sediments (Table 3.2; Fig. 3.10). This could either suggest increased erosion of Greater Himalayan

and Panjal Traps bedrock exposed upstream around Padum village and the Stod River, or increased recycling of glaciofluvial outwash sediments derived previously from Greater Himalayan and Panjal Traps bedrock. At present the relative contributions from fresh or reworked sediment can be determined using these new data, but it is most likely that reworking is the dominant supplier of sediment because many deeply incised glaciofluvial gravels are recognized throughout the Stod River valley.

The provenance of terraces near Padum reflects a broad change in erosion patterns across the Tsarap River Basin between 12 and ~7.9 ka. Between construction of the ~25 m (ID# 14c) and ~15 m (ID# 14b) Padum terraces, compositions evolved to include more Tethyan Himalayan lithologies (Figs. 3.10 and 3.11). Sediment compositions changed from dominantly high- and low-grade metamorphic fragments to include abundant carbonate, as also observed in the modern upper Tsarap River (ID# 11, 12). Detrital zircon U-Pb ages also document a subtle shift by ~7.9 ka from populations similar to Triassic-Jurassic strata to populations found more in upper Cretaceous and Paleogene siliciclastic strata (Fig. 3.11B-C). Together these datasets illustrate a general shift from concentrated erosion of lithologies exposed in the High Himalaya in the west and southwest of Zaskar to a broader erosional regime tapping sediment sources in the eastern Zaskar River basin.

Increasing influence of the summer monsoon and winter westerlies drove enhanced erosion and produced this marked intrabasinal shift in sediment provenance by ~7.9 ka. Before deposition of the ~15 m Padum terrace by ~7.9 ka, erosion was concentrated predominantly in regions exposing Greater Himalaya and Neoproterozoic to Jurassic Tethyan Himalaya (Fig. 3.2). This is similar to modern-day conditions where

precipitation and erosion is focused along the High Himalaya (Jonell et al., in press). By 7.9 ka, increased yield from eastern Zaskar lithologies implies stronger erosion of fresh Tethyan Himalaya bedrock and/or large-scale recycling of voluminous Rupshu Plateau sediments held in the upper Tsarap River. Early to Middle Holocene lake records document a very wet, warm interval from 11.8 to 7 ka at Tso Kar (Demske et al., 2009; Wünnemann et al., 2010) and at ~8–11 ka in Tso Morari (Leipe et al., 2014; Mishra et al., 2015). These datasets align with the model presented here, suggesting a shift from isolated erosion along the High Himalaya to broader, more regional erosion across Zaskar during the Holocene Climatic Optimum, as strong moist climate systems penetrated into the Tibetan Plateau.

These observations further suggest considerable reworking over the Holocene by the Yunam River in the Sarchu Basin. Modern river and a prominent ~50 m terrace share similar petrography (Figs. 3.109 and 3.11A), with both containing abundant gneiss, calc-gneiss, and foliated metapelite fragments from deformed, medium- to high-grade Neoproterozoic-Triassic rocks exposed upstream. It is more likely that the modern river is locally recycling glaciofluvial outwash sediments from the ~50 m terrace rather than transporting freshly eroded bedrock. Recent cosmogenic nuclide ages constrain the most recent glacial occupation at ~20 ka in the middle Yunam River valley (Fig. 3.5) and at 7–8 ka in the upper valley (Saha et al., 2015; Sharma et al., 2016). These ages corroborate the OSL age of ~7.2 ka and support the notion that reworking of glacial outwash into the 50 m terrace must have occurred after ~7 ka. Calculations indicate a minimum of ~0.3 km³ of terrace has been exported from the Yunam River and Lingti Chu since that time.

3.6.2 Fluvial Infilling and Incision

The data presented here provide new constraints on Pleistocene and Holocene infilling and erosion that expand prior chronologies across the Zaskar River Basin and adjacent basins (Dortch et al., 2011; Blöthe et al., 2014; Munack et al., 2016). OSL ages in the Padum Basin can be used to establish limits on glacial extent along the trunk Zaskar River. Terrace age data require that the valley glacier system extended no farther than Hanumil village by ~17.4 ka, to Pishu village by ~12 ka, and to Padum village by ~7.9 ka, if not before these times (Fig. 3.4). Many Padum Basin incised alluvial fans ~40–80 m above the modern river imply a much earlier retreat. If an alluvial fan dated at ~32 ka (Table 3.3; Sample 12072403) is considered representative of alluvial fan sedimentation, then the river may have been ice-free downstream of Pishu before the LGM (~20 ka). These data follow along with previous findings from Taylor and Mitchell (2000) arguing for a glacial maximum extent beyond Hanumil village from ~78 ka until at least 40 ka, followed by a retreat to Rinam by ~20 ka.

Pronounced alluvial aggradation occurring up through ~12 ka is preserved in terrace remnants near Pidmo and Pishu (Fig. 3.4), at least downstream of the Rinam moraine. Damming of the Zaskar River behind the Rinam moraine by at least ~9.4 ka resulted in development of a short-lived lake until 8.2 ka. Terrace levels in Padum document two aggradational phases upstream of Rinam >7.9 ka (~25 m terrace) and prior to 7.9 ka (~15 m terrace). Net incision in the Padum Basin may have initiated as early as 7.9 ka, but loess deposits capping terrace levels definitively mark abandonment and incision by ~6.2 ka (Fig. 3.3). A second loess cap at Hanumil indicates abandonment and incision of terrace surfaces there by 3.1 ka (Fig. 3.4).

At least one phase of Pleistocene alluvial fan sedimentation and one phase of aggradation can be defined in the Sarchu Basin. Alluvial fan sedimentation at Whiskey Bridge was active until at least 25.6 ka (Fig. 3.5). Aggradation of glaciofluvial outwash gravels in the Sarchu Basin began before ~10.6 ka. Low intensity of this sample underscores this is a minimum age and therefore valley infilling must have initiated earlier. Sharma et al. (2016) suggest much earlier deposition over Marine Isotope Stage-3 (~29–57 ka) for much of this basin, but data here indicate aggradation up through ~7.2 ka. Incision of the Sarchu Basin can be constrained when considered with the recent glacial landform chronology of Saha et al. (2015). Glaciers extended no farther than Sarchu village as early as ~60 ka, then retreated to the middle Yunam River valley by ~16 ka and the upper Yunam River valley by ~7 ka. With these previous chronologies, a younger Holocene phase of net incision is established in the Sarchu Basin after ~7 ka that worked to shape many of the prominent terraces surfaces ≤ 50 m in height.

From these findings a Late Pleistocene to Holocene sedimentation history can be constructed for the middle and upper Zaskar River basin. Age constraints pinpoint at least two early net phases of aggradation and at least one younger net phase of incision: Late Pleistocene alluvial fan sedimentation from at least ~25–32 ka with potentially concurrent deglacial aggradation; latest Pleistocene-earliest Holocene aggradation (~8–12 ka); and mid-Holocene net incision initiating by ~6–8 ka across the basin and continuing until the present. At the Zaskar-Indus confluence a small phase of Late Holocene local aggradation at Choksti is recorded at ~3.8 ka with ~20 m of incision since that time.

3.6.3 Drivers of Quaternary Sedimentation

Ages from bedrock and alluvial terraces along the Zaskar River Gorge and

Zaskar-Indus confluence illustrate major aggradation at ~20–50 ka, with two younger phases of net incision at 9.5–14 ka and prior to 6.3 ka (Dortch et al., 2011; Blöthe et al., 2014). Terrace and lake sediment ages paint a more complicated picture that contrasts with what is observed downstream at the Zaskar Gorge and in other regions of the Transhimalaya. Instead, phases in the middle and upper Zaskar River correspond well with regional aggradation (~10–15 ka) and incision (<8–10 ka) in the frontal Himalaya that was previously shown to covary with monsoon strength (Pratt et al., 2002; Bookhagen et al., 2006; Srivastava et al., 2008; Thakur et al., 2014; Dey et al., 2016). While temporal correlation between these two regions implies a common driver (i.e., summer monsoon intensity), glaciation and winter mid-latitude westerlies strength also strongly control fluvial and sedimentation dynamics in the Transhimalaya (Demske et al., 2009; Wünnemann et al., 2010; Lee et al., 2014; Owen and Dortch, 2014; Mishra et al., 2015).

Variations in the intensity of the monsoon and westerlies worked in concert with local glaciation to produce late Quaternary aggradation and incision, as recorded in the Zaskar River basin. Enhanced precipitation associated with a strong monsoonal phase during 24–29 ka (Bookhagen et al., 2005a) coincided with local glacial retreat to further promote local aggradation and alluvial fan sedimentation (25–32 ka) along over-steepened Zaskar River valley walls (Sharma et al., 2016). This wet humid interval is recorded throughout the western Tibetan Plateau in lake sediments (Gasse et al., 1991; Gasse et al., 1996; Shi et al., 2001), pollen records (Herzschuh, 2006), and river terraces (Dortch et al., 2011).

Later strengthening of the summer monsoon and westerlies into the early

Holocene corresponded with increased erosion along the High Himalaya and aggradation in the Padum Basin beginning ≥ 12 ka and ending at ~ 8 ka. Expansion of strong precipitation during the Holocene Climatic Optimum further into the Himalayan rain shadow by ~ 8 ka (Demske et al., 2009; Dortch et al., 2009; Leipe et al., 2014) similarly triggered significant erosion of the Zaskar Tethyan Himalaya and reworking of Rupshu Plateau valley-fills. Subsequent weakening of monsoonal and mid-latitude westerlies-derived precipitation through the mid-Holocene decreased sediment flux by 6–7 ka and drove net incision on the northern side of the High Himalaya. With continued weakening of the monsoon and mid-latitude westerlies into the late Holocene, Tethyan Himalaya sediment flux waned. Modern focused glacial erosion and precipitation along the Padum and Sarchu basins support relatively higher Greater Himalayan sediment flux and local reworking of older valley-fills in Zaskar.

The sensitivity this region to climate-modulated buffering may directly reflect its location relative to the Himalaya rainfall maximum. The southwest edge of the Zaskar River basin lies ~ 100 km from the rainfall maximum, compared with >200 km to the Zaskar-Indus River confluence and ~ 180 km to the Rupshu Plateau. Glacial equilibrium line altitude reconstructions suggest that the Zaskar High Himalaya are a permeable topographic barrier that could allow more frequent and/or prolonged moisture transfer into the margins of the rain shadow (Lee et al., 2014). This is in contrast to more arid sectors of the Transhimalaya, deeper into the Tibetan Plateau interior, that only receive limited precipitation during abnormal summer monsoon events and/or over long-term phases of strong monsoon activity. The Zaskar River basin is not unique among Transhimalayan basins in hosting large valley-fills, but it may be that only such marginal

basins, including possibly the upper Sutlej River basin (i.e., Wulf et al., 2012), receive enough moisture to overcome the thresholds for transport capacity, which otherwise is extremely limited in the deeper orogenic interior (Dietsch et al., 2015).

3.6.4 Quaternary Buffering and Sediment Recycling

Quaternary valley-fills account for $\sim 37 \text{ km}^3$ of stored material in the Zaskar River basin, with roughly 70% of this volume ($\sim 26 \text{ km}^3$) held in the Rupshu Plateau (Table 3.4). The overall volumetric estimates presented here are strikingly consistent with previous valley-fill estimates ($\sim 33 \text{ km}^3$) using DEM algorithm-based extraction (Blöthe and Korup, 2013). Previous basin-specific estimates underestimate volumes in the Sarchu Basin (1.1 versus 0.69 km^3) while overestimating volumes in the Padum Basin (8.4 versus 11.9 km^3). This difference likely results from direct field evidence regulating the calculations in this study, especially concerning valley-fill extent and depth. Nevertheless, the general agreement between these studies reinforces the general scale of the sediment budget and furthermore highlights the effectiveness of each technique in assessing sediment volumes over particular spatial scales.

While the results discussed here indicate considerable sediment stored in the Zaskar River basin, not all of the stored sediment is readily accessible for reworking. Some volumes may be relatively disconnected from the drainage network, such as sediments perched $\sim 250\text{--}300 \text{ m}$ above the entrenched rivers of the Rupshu Plateau. This study attempts to account for this connectivity by using a 1-km wide buffer around the drainage network to approximate how much sediment is realistically accessible for reworking into the river through lateral incision, bank failure, and localized debris flows. This width was selected based on observations from modern incision patterns and to

establish a conservative minimum bound. Volumes of erodible sediment adjust to $\sim 16 \text{ km}^3$ for the total Zaskar River. This is comparable to the estimates for the total eroded sediment volumes over the last $\sim 10 \text{ ka}$ of $7\text{--}22 \text{ km}^3$ (Clift and Giosan, 2014), which were based on extrapolation of rates estimated from the trunk Indus, and are thus not very reliable. Further calculations indicate an additional $\sim 4 \text{ km}^3$ of erodible sediment stored in the Rupshu Plateau. These corrected volumes imply that much of the Rupshu Plateau valley-fill is relatively isolated from the modern Zaskar River system. Deep incision and excavation ($11\text{--}19 \text{ km}^3$; Table 3.5) of this region over the last $\sim 135 \text{ k.y}$ reflects considerable reworking (Munack et al., 2016), but provenance data from this study indicate limited contribution of Rupshu Plateau valley-fills to the modern budget since 8 ka . These valley-fills were most likely exported before the mid-Holocene and since then they have been insignificant to the net sediment budget.

To assess how reworking of valley-fills from the Zaskar River might contribute to regional sediment budgets over longer timescales, average yield rates over several possible residence intervals: 10, 20, and 135 k.y. (Table 3.5) were calculated. If all the currently stored river sediments were exported from the Zaskar River basin over the next 10 k.y. , they alone would account for average sediment yield rates of $198\text{--}467 \text{ t/km}^2 \text{ yr}^{-1}$. This is somewhat more than the yield rates of $89\text{--}279 \text{ t/km}^2 \text{ yr}^{-1}$ derived from eroded sediment budgets (Clift and Giosan, 2014). If these eroded budgets are accurate, then the pre-Holocene total stored sediment volume would have reached $\sim 45\text{--}60 \text{ km}^3$. This would indicate that $\sim 42\text{--}77\%$ of stored Zaskar River sediments (excluding the Rupshu Plateau) have been excavated and transported to the trunk Indus since 10 ka .

Blöthe and Korup (2013) estimated $\sim 177 \text{ km}^3$ of stored valley-fill in the upper

Table 3.5. Zanskar River sediment yields.

Basin	Basin Area (km ²)	Volume (km ³)	Bulk Density (g/cm ³)	Yield (10 ⁶ t/km ²)	Average yield rate (t/km ² ·yr) over:		
					10 k.y.	20 k.y.	135 k.y.
Zanskar River	14939	36.7	1.9	4.7	467	233	35
Zanskar River ^a	14939	15.5	1.9	2.0	198	99	15
Sediment <35 ka ^a	14939	11.1	1.9	1.4	142	71	10
Sediment >35 ka ^{ab}	14939	4.4	1.9	0.6	56	28	4
pre-Holocene Zanskar ^c	14939	45–60	1.9	5.7–7.6	570–760	285–380	42–56
Total Export Zanskar ^{ad}	14939	23–38	1.9	3.6–4.9	361–488	181–244	27–36
<u>Clift and Giosan (2014)</u>							
Zanskar River	15000	7–22	1.9	0.8–2.8	89–279	44–139	7–21
<u>Munack et al. (2016)</u>							
Rupshu Plateau ^e	773	11–19	1.9	27.8–46.0	2780–4604	1390– 2302	206–341
RP from Zanskar	14939	11–19	1.9	1.4–2.4	144–238	72–119	11–18
RP* from Tsarap	7619	4.4	1.9	1.1	110	55	8

Note:

RP = Rupshu Plateau

^aadjusted volumes for sediment connectivity

^bSediment >35 ka is Rupshu Plateau valley-fill

^cStored (36.7 km³) + eroded volumes (7–22 km³; Clift and Giosan, 2014) and (11–19 km³; Munack et al., 2016)

^dStored and connected (15.5 km³) + eroded volumes (7–22 km³; Clift and Giosan, 2014)

Indus River basin. The Zaskar River basin comprises ~7% of the upper Indus drainage area and a moderate ~21% of the total stored volume, of which at least ~9% is available for modern erosion. The Zaskar River may have a disproportionate influence on upper Indus River sediment volumes and compositions, especially if other Transhimalaya valley-fills are isolated much like the Rupshu Plateau. Sufficient transport capacity might only be achieved and previously isolated valley-fills recycled significantly into the trunk Indus during episodic wet intervals. In this context, marginal rain shadow river basins, which equally produce and mobilize abundant sediment, strongly modify the Himalayan rain shadow sediment budget. Yet this also underscores that Himalayan valley-fills, although volumetrically significant, likely play a less important role in modulating the total Indus River sediment budget than previously envisaged (Blöthe and Korup, 2013; Clift and Giosan, 2014).

3.7 Conclusions

This study defines patterns of late Quaternary erosion and major phases of valley infilling and dissection in the Zaskar River Basin, which is perched on the margins of the Tibetan Plateau. A new river terrace chronology documents at least two major phases of Late Pleistocene aggradation. The first correlates in part with local deglaciation and a strong phase of South Asian summer monsoon and winter mid-latitude westerlies-driven precipitation at 25–32 ka. A second phase of aggradation initiated before 12 ka and lasted until ~8 ka, correlating with a strengthening summer monsoon. This phase is also documented in valleys in the monsoonal frontal Himalaya (Bookhagen et al., 2006). Net Holocene incision, accompanied by loess sedimentation, initiated by 6–7 ka and was likely continuous through the present. Dynamic changes in Quaternary river provenance

coincide with aggradation and incision. Early Holocene terrace sediments indicate more erosion from the Tethyan Himalaya at that time compared to the modern river. As the monsoon strengthened into the Mid-Holocene, it was able to penetrate farther north beyond the High Himalayan rain shadow into the Transhimalaya. This drove increased erosion and transport of Tethyan Himalayan material between 12 and 8 ka, either directly from the bedrock or from stored valley fill. Much of the bedrock erosion is controlled directly by glaciers, which in turn are fed by monsoon and westerlies precipitation. This material was then subsequently available for transport by the rivers as the summer monsoon strengthened, allowing the valleys to aggrade. Incision of the terraces occurred by 6 ka in the Padum Basin when loess was deposited over the terraces and after ~7 ka in the Sarchu Basin. Both terrace incision and the loess indicate a drying of the climate, consistent with several paleo-monsoon climate records for that time (e.g., Prins et al., 2000; Fleitmann et al., 2003). Results from this study support the concept that regions of the Transhimalaya lying immediately north of the topographic divide may not only be sensitive to abnormal monsoonal excursions (Bookhagen et al., 2005b), but also record strong yet normal monsoon phases over the last ~35 ka. This work highlights the control of the monsoon in addition to glaciation in landscape evolution on the periphery of the Tibetan Plateau.

For the first time the volumes of stored sediment within a major Himalayan rain shadow river basin have been estimated using robust field evidence and remote sensing data. About 37 km³ is stored in the modern Zaskar River basin but only ~16 km³ of this is readily erodible. These values are consistent with previously published budgets, despite being estimated by different methodologies. Zaskar valley-fills host ~18% of the total

upper Indus River sediment ($\sim 177 \text{ km}^3$) in only $\sim 7\%$ of its drainage area, but may disproportionately contribute to the total upper Indus budget over particular climatic regimes. If many Transhimalayan valley-fills within the plateau interior are isolated from the trunk river and/or are without sufficient transport capacity then sedimentary signals to the trunk upper Indus will be fluxed primarily from those basins on the margin and will not be representative for all sectors of the Transhimalaya.

Deconvolving sedimentary signals preserved in offshore archives strictly in terms of climate or tectonically driven-erosion continues to be problematic because sediment buffering occurs over many spatial and temporal scales, and is now documented to occur prolifically even within mountain source regions. This study indicates that climatically-modulated sediment buffering has occurred over 10^3 - 10^5 yr timescales in the upper Indus River and locally presents biases in both sediment compositions and volumes that need to be accounted for when analyzing sequences deposited farther downstream. Climate, and in particular precipitation, plays a more pivotal role governing Himalayan rain shadow erosion than previously recognized. This observation highlights that millennial-scale climate variations can strongly pace landscape evolution in arid mountain belts and even further regulate the long-term dissection and decay of orogenic plateaus.

CHAPTER 4. CONTROLS ON EROSION PATTERNS AND SEDIMENT TRANSPORT IN A MONSOONAL, TECTONICALLY QUIESCENT DRAINAGE, SONG GIANH, CENTRAL VIETNAM

4.1 Abstract

The Song Gianh is a small-sized ($\sim 3500 \text{ km}^2$), monsoon-dominated river in northern central Vietnam that can be used to understand how topography and climate control continental erosion. We present major element concentrations, together with Sr and Nd isotopic compositions, of siliciclastic bulk sediments to define sediment provenance and chemical weathering intensity. These data indicate preferential sediment generation in the steep, wetter upper reaches of the Song Gianh. In contrast, detrital zircon U-Pb ages argue for significant flux from the drier, northern Rao Tro tributary. We propose that this mismatch represents disequilibrium in basin erosion patterns driven by changing monsoon strength and the onset of agriculture across the region. Detrital apatite fission track and ^{10}Be data from modern sediment support slowing of regional bedrock exhumation rates through the Cenozoic. If the Song Gianh is representative of coastal Vietnam then the coastal mountains may have produced around 132,000–158,000 km^3 of the sediment now preserved in the Song Hong-Yinggehai Basin (17–21% of the total), the primary depocenter of the Red River. This flux does not negate the need for drainage capture in the Red River to explain the large Cenozoic sediment volumes in that basin but does partly account for the discrepancy between preserved and eroded sediment volumes. OSL ages from terraces cluster in the Early Holocene (7.4–8.5 ka), Pre-Industrial (550–

This chapter previously appeared as: Jonell, T.N., Clift, P. D., Hoang, L.V., Hoang, T., Carter, A., Wittman, H., Böning, P., Pahnke, K., and Rittenour, T., 2016, Controls on Erosion Patterns in a Monsoonal, Tectonically Quiescent Drainage, Song Gianh, Central Vietnam: Basin Research, doi: 10.1111/bre.12199. It is reprinted by permission of John Wiley and Sons.

320 yr BP) and in the recent past (~150 yr BP). The older terraces reflect high sediment production driven by a strong monsoon, while the younger are the product of anthropogenic impact on the landscape caused by farming. Modern river sediment is consistently more weathered than terrace sediment consistent with reworking of old weathered soils by agricultural disruption.

4.2 Introduction

Erosion of the continental crust is controlled by surface processes that in turn are partly influenced by climate, lithology, and tectonic deformation of the lithosphere. Debate continues about whether climatic or solid Earth forcing dominates the formation of sediment from bedrock (Burbank et al., 2003; Bookhagen et al., 2005a; Clift, 2006; Dortch et al., 2011). Interpretation of the geologic record requires an understanding of modern sediment production and transport processes. Furthermore, long-term recycling of the continental crust is inherently tied to continental erosion, delivering material that can then be reincorporated via subduction back into the mantle (von Huene and Scholl, 1991; Clift et al., 2009).

Previous studies investigating erosion have focused on active mountain belts where tectonic and climatic processes are often intimately linked (Pratt-Sitaula et al., 2004; Kirby and Ouimet, 2011; Blöthe et al., 2014). In many cases, it is hard to separate the relative influence of these primary drivers of erosion. In this study we address this issue by evaluating a fluvial system in a largely tectonically quiescent setting. By doing so we aim to isolate the effects of climate in controlling patterns and rates of erosion. We choose to do so in an Asian monsoonal system because this atmospheric phenomena is often cited as a type example for the influence of surface processes on solid Earth

systems (Beaumont et al., 2001; Hodges et al., 2004). Furthermore, several Quaternary records of monsoonal strength exist across the region (Dykoski et al., 2005; Yancheva et al., 2007; Hu et al., 2012) allowing us to directly correlate landscape evolution and climate variability.

We examine the development of the Song Gianh Basin (Gianh River Basin) since the start of the Holocene (~10 ka) to understand how changing monsoon strength has influenced sediment production and transport. The small size (~3500 km²) and simplicity of its tectonic setting permits a comprehensive basin-wide analysis of sediment production in contrast to logistically more challenging, large fluvial systems (>1000 km in length) such as the Yangtze, Mekong, and Red Rivers, which also have more complex and long sediment transport systems. In addition, the Song Giang originates from the eastern Annamite Range and directly drains into the South China Sea across a relatively high topographic gradient from the mountainous terrain to the narrow coastal plain (Fig. 4.1). This means that sediment could potentially be transported rapidly through the Song Gianh with less possibility for storage and reworking in wide flood plains that can act as sediment buffers and result in signal shredding, as seen in larger rivers (Castelltort and Van Den Driessche, 2003; Wittmann et al., 2011; Simpson and Castelltort, 2012; Bracken et al., 2015).

4.3 Geological Setting

The Song Gianh drains the coastal Annamite Range of central Vietnam and flows to the Gulf of Tonkin. The Song Gianh does not have a well-developed delta but a simple river mouth. Longshore currents remove sediment delivered by the river and transport them southward. North of the river mouth is a large complex of dunes (~40 km²) that

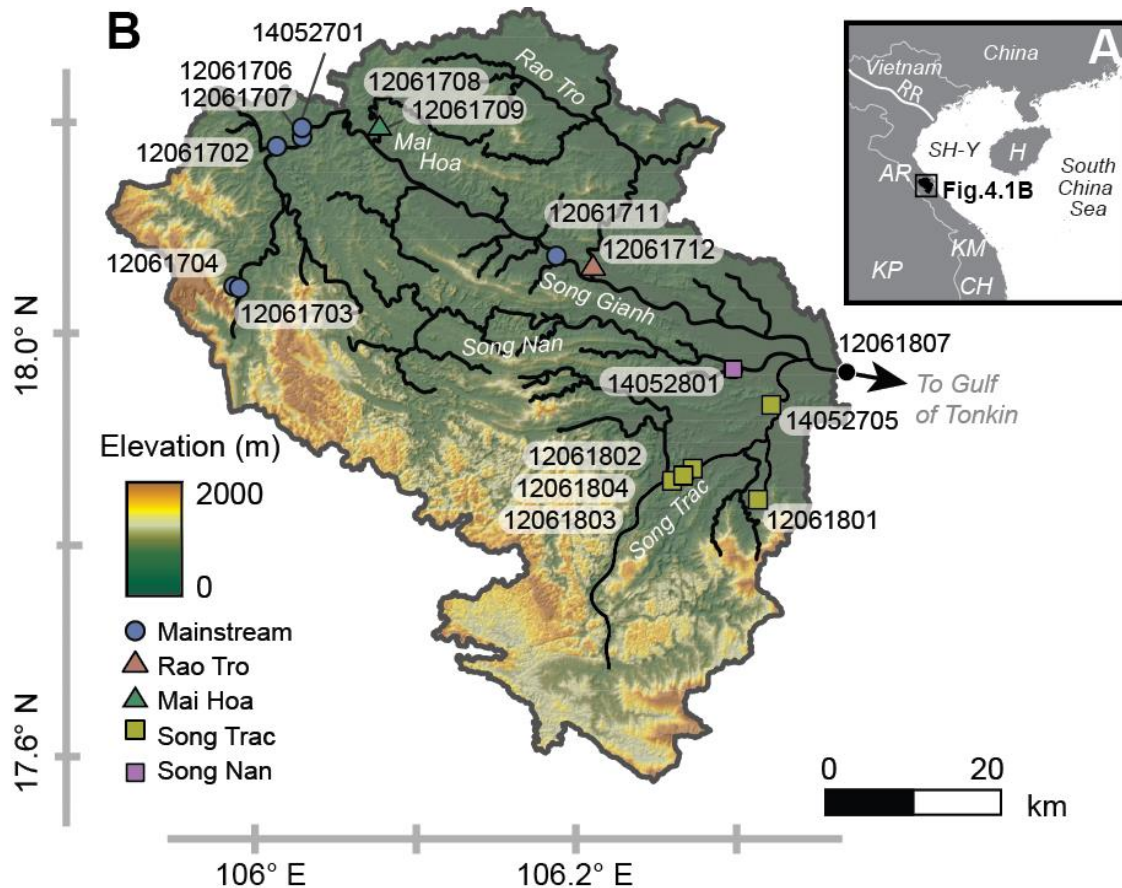


Figure 4.1. Study location in reference to southeast Asia. (A) Regional geographic map of southeast Asia outlining Song Gianh basin (black polygon) and political border of Vietnam (gray line), AR = Annamite Range, CH = Central Highlands, H = Hainan, KM = Kontum Massif, KP = Khorat Plateau, RR = Red River, and SH-Y = Song Hong-Yinggehai Basin; (B) Shaded topographic map derived from void-filled SRTM90 v.4.1 digital elevation model (DEM) grid data with delineated stream network (black line).

might have acted as a source for sediment to the river, but does not appear to influence the modern flux because this complex does not now drain into the Song Gianh (Fig. 4.1). The river has a relatively narrow coastal plain that rises to the SW where the backbone of the Annamite Range separates the Song Gianh from streams that flow to the west and into the Mekong River. The highest topography exceeds 2 km elevation with gorges in the upper reaches ~600–800 m deep although much of the basin is low lying. Aggradational river terraces are found in the upper reaches of the Song Gianh Basin, but

are of very limited extent. However, in the middle reaches, more extensive aggradational terracing, involving at least three separate levels, is recognized. Terraces heights above the modern river level are ≤ 11 m. No terraces extend around or near the river mouth.

The continental margin formed during the opening of the South China Sea, starting in the Eocene (Ru and Pigott, 1986; Franke et al., 2014). Located at the end of the Red River Fault, one of the largest strike-slip systems on Earth, the Song Hong-Yinggehai Basin is a major pull-apart structure linked to that fault (Rangin et al., 1995; Zhong et al., 2004). The Song Hong-Yinggehai Basin is the primary depocenter for the Red River and is also supplied by sediment by the Song Gianh, along with other small rivers draining the northern Ammanite Range. Although active opening of the Song Hong-Yinggehai Basin ceased at ~ 17 Ma, there was modest reactivation after ~ 5 Ma, at least in the northern part of the basin (Rangin et al., 1995; Clift and Sun, 2006). The northern Vietnam margin faces the island of Hainan, which is known to have been affected by volcanism and surface uplift since the Pliocene (Tu et al., 1991; Shi et al., 2011). Further south the Central Highlands of Vietnam were affected by volcanism, uplift and erosion ~ 8 Ma (Carter et al., 2000). Nonetheless, the expectation is that the Song Gianh has been largely unaffected by more recent phases of tectonic activity and is now in a state of slow subsidence linked to passive margin thermal processes. There are no seismic or GPS-related data to indicate active deformation of the bedrock (Michel et al., 2001).

The bedrock of the Song Gianh is largely composed of a variety of Paleozoic to Triassic sedimentary and metasedimentary rocks, intruded by modest volumes of peraluminous granites and rhyolites (Fig. 4.2). The metamorphism and magmatism are

linked to the Permo-Triassic Indosinian Orogeny (Carter et al., 2001; Lepvrier et al., 2004) that affected much of Indochina. It is unclear to what extent the basin was affected by Cenozoic extension, such as that documented further south in the Kontum Massif, but this is also now inactive (Nagy et al., 2001). This means we can interpret erosion more simply, largely in terms of the climate and topography.

Here we address the Song Gianh's development since the start of the Holocene, which is a time over which detailed multiproxy records for monsoon intensity exist in SE Asia. In particular, speleothem records from Dongge Cave in SW China represent the closest high resolution reconstruction (Dykoski et al., 2005; Duan et al., 2014). Although some doubts have been cast concerning the interpretation of such cave records (Clemens et al., 2010) they are broadly in accord with other paleoenvironmental records, such as loess or upwelling productivity proxies (Mohtadi et al., 2011). These show an intensification of the East Asian summer monsoon after ~11 ka, reaching a maximum ~8 ka, followed by a long-term decrease until present, albeit sometimes in steps rather than a continual slow decline. Farther north in the Red River catchment, shifting erosion patterns are tied to Holocene changes in summer rainfall (Hoang et al., 2010a). In general times of strong summer monsoon are associated with faster erosion and sediment supply to deltas across Asia (Goodbred and Kuehl, 2000).

4.4 Methods

We use several methods to constrain the source of sediment in the Song Gianh and to quantify how sediment is mixed downstream before reaching the ocean. Modern river sediments were collected across the basin to characterize the compositions of the major tributaries flowing into the Song Gianh mainstream and assess the relative impact

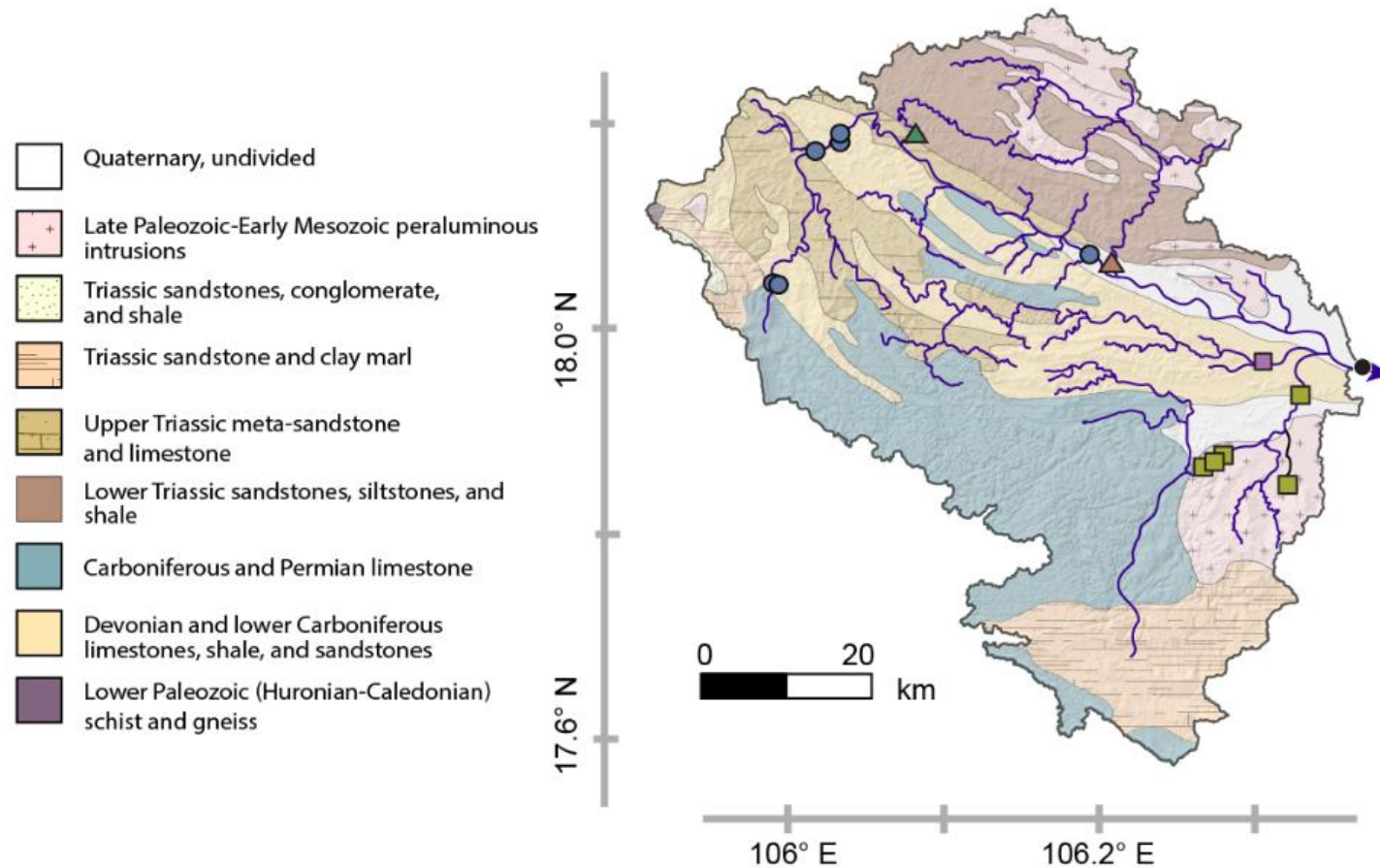


Figure 4.2. Geological map of the Song Gianh basin showing the simplified geology overlain with the modern drainage network. Map is redrawn from Fromaget et al. (1971). Sample colors follow Figure 4.1.

of each tributary to the total budget. Samples were taken from active channel beds and point bars with care to avoid bank material and in facies that were recently reworked by the river (Table 4.1). The very fine- to medium sand fraction ($>63\ \mu\text{m}$) was preferentially sampled because this size fraction is ideal for single-grain mineral provenance techniques, which are limited by the analytical laser spot size. We recognize that by only looking at the bedload in this study we do not consider the suspended load that may have a different provenance and could be volumetrically significant to the marine stratigraphic record (Garzanti et al., 2011). Garzanti et al. (2009) argue that looking at a restricted grainsize fraction can introduce major biases to the bulk sediment provenance analysis. However, these data do represent a wide array of common grain-sizes and provide important initial constraints on the nature of erosion in this river basin. Furthermore, Yang et al. (2012) have indicated that this size fraction is mostly representative of the bulk load, at least for the zircon population. Samples were also taken from selected aggradational terraces for optically stimulated luminescence (OSL) dating.

4.4.1 Topographic Analysis

We evaluated regional patterns of hillslope morphology by extracting topographic parameters from void-filled Shuttle Radar Topography Mission (SRTM) V4 90-m digital elevation model (DEM) data (Jarvis et al., 2008) provided by the Consultative Group on International Agricultural Research (<http://srtm.csi.cgiar.org>) and post-processed with an iterative fill routine (Whipple et al., 2007). Mean local hillslope values were calculated using a 1 km circular moving window. Mean local relief, expressed as maximum elevation difference, was calculated using a 1 km circular moving window. Mean annual

Table 4.1. Sample locations for Song Gianh sediments.

Sample Number	Location	Lat (°N)	Long (°E)	Elevation (m)
Modern river samples				
12061704	Upper reaches mainstream	17.828	105.768	160
12061703	Upper reaches mainstream	17.818	105.775	130
12061702	Upper reaches mainstream	17.960	105.812	48
14052701	Upper reaches mainstream	17.999	105.866	42
12061708	Mai Hoa	17.979	105.929	19
12061711	Middle reaches mainstream	17.843	106.145	1
12061712	Rao Tro	17.825	106.177	0
14052801	Song Nan	17.718	106.353	3
12061802	Song Trac	17.616	106.316	3
12061801	Song Trac	17.597	106.423	10
14052705	Song Trac	17.672	106.392	4
12061807	River Mouth	17.714	106.447	0
Terraces				
12061707	Mainstream terrace	17.999	105.866	51
12061706	Mainstream terrace	17.999	105.866	51
12061709	Mainstream terrace	17.979	105.929	19
12061803	Terrace Southern Song	17.595	106.286	8
	Trac			
12061804	Terrace Southern Song	17.613	106.305	3
	Trac			

rainfall values were generated from the 1998–2009 Tropical Rainfall Measuring Mission (TRMM) 2B31 and 2B42 data products (Bookhagen and Burbank, 2006). Data are presented in Figure 4.3.

Analysis of longitudinal channel river profiles has been a traditional approach to evaluate disequilibrium conditions in fluvial systems. River profiles follow a simple power-law scaling relationship for local slope and upstream drainage area under steady-state conditions (Hack, 1957; Flint, 1974). Perturbation to a river system, such as through active rock uplift or base-level fall, create transient convexities, or knickpoints, that integrate over time and migrate upstream as the river reaches new steady-state conditions

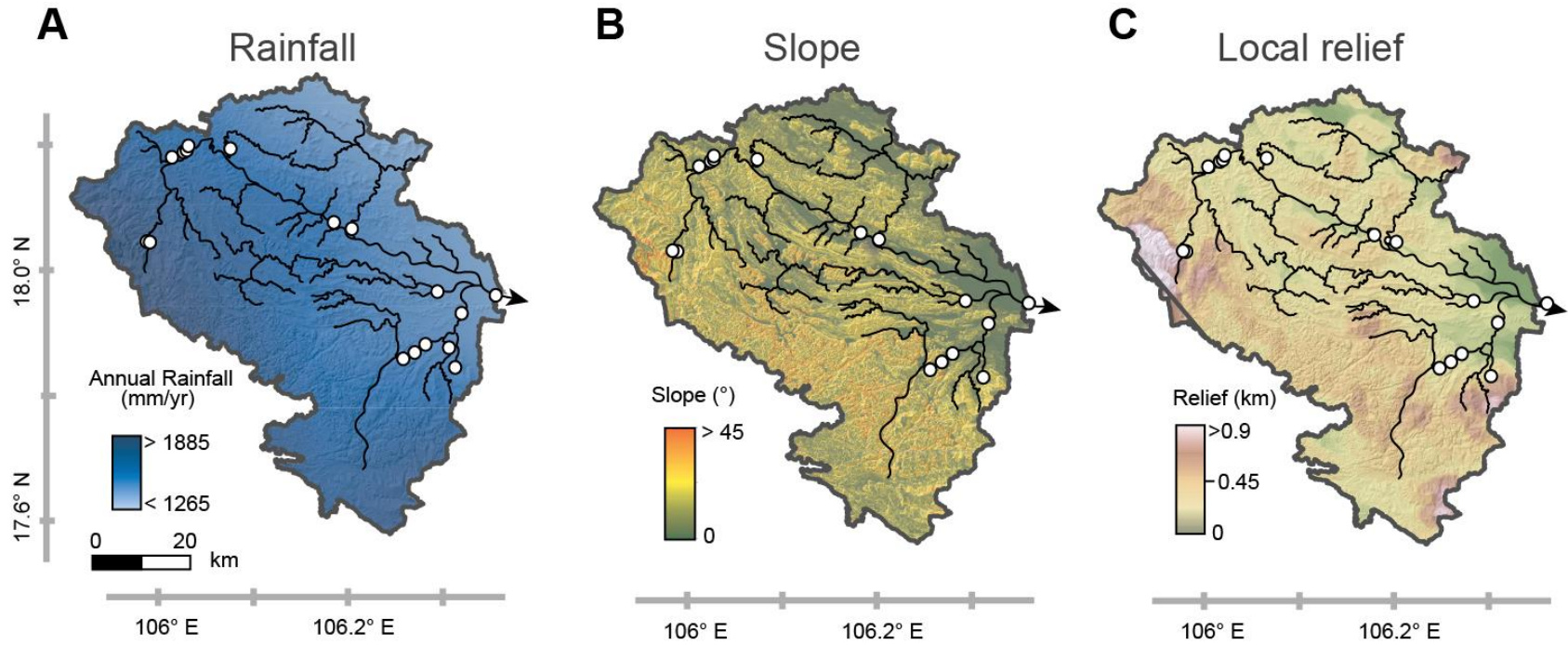


Figure 4.3. Annual rainfall, local mean slope, and local relief maps for the Song Gianh basin. (A) Annual rainfall values derived from TRMM 3B42 data from 1998–2009 at $0.25^\circ \times 0.25^\circ$ resolution (Bookhagen and Burbank, 2006); (B) Average mean local slope calculated from DEM for Song Gianh basin. Black lines and open circles denote stream network and sample locations, respectively; (C) Mean local relief map, expressed as maximum elevation difference, using a moving ~5 km radius moving window.

(Snyder et al., 2000). Significant karst in the Song Nan and upper Song Trac tributaries makes it difficult to perform quantitative analysis of longitudinal channel profiles, to construct hydrologic networks and extract channel data from DEMs. Although calculating parameters to evaluate fluvial equilibrium, such as the widely-applied normalized steepness index (k_{sn}) (Snyder et al., 2000) or χ (Perron and Royden, 2012) would indeed be insightful, we only present first-order observations because detailed quantitative analysis is beyond the scope of this study. We constructed longitudinal channel profiles using ASTER Global DEM ~30 m-grid data crosschecked with LandSat satellite imagery in Google Earth (Fig. 4.4).

4.4.2 Major and Trace Element Geochemistry

Each bulk, unsieved sediment sample was analyzed for major and trace elements to provide a basic characterization of the material that was also assessed with other isotopic and thermochronologic methods and to constrain the degree of chemical weathering. Carbonate was not removed prior to digestion. During chemical weathering the ratios of water-mobile versus water-immobile elements change because of mineral breakdown. Alkali earth elements are commonly used in such proxies because they are relatively mobile, and when compared to immobile elements, track the degree of leaching (e.g., K/Al).

For elemental analysis all samples were freeze-dried and ground before mixing 600 mg of sample with 3600 mg of lithium tetraborate ($\text{Li}_2\text{B}_4\text{O}_7$, Spektromelt). The samples were pre-oxidized at 500°C with NH_4NO_3 and fused to glass-beads. Samples were then analyzed for Si, Al, Ti, Fe, Na, Ca, K, P and Rb by X-Ray Fluorescence (XRF) using a Philips PW 2400 X-Ray spectrometer at the Institut für Chemie und

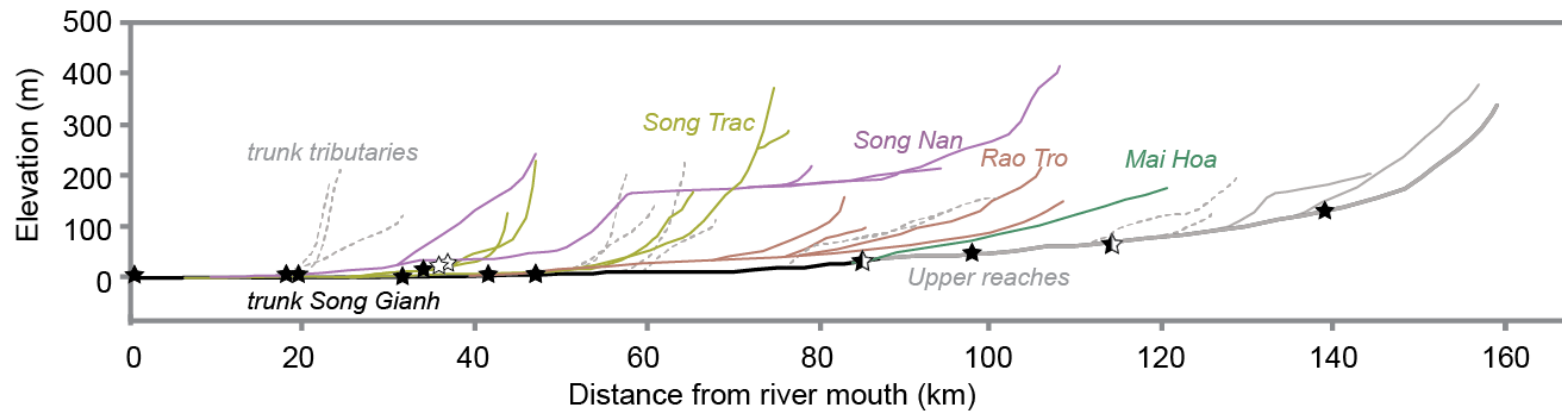


Figure 4.4. Longitudinal river profiles for the main stream and major tributaries of the Song Gianh with sample locations. Black stars mark modern sediment and white stars for terrace samples; black and white stars denote location with dual sampling. Dashed lines mark minor tributaries along the main stream. Colors follow Figure 4.1. Note the large knickpoint as a result of karst terrain and a perched alluvial basin at ~185 m above modern river level on the Song Nan. Also present are smaller perched alluvial basins and corresponding knickpoints in the upper reaches and lower Song Nan at ~50 m above modern river level.

Biologie des Meeres (ICBM) at the Carl von Ossietzky Universität, Oldenburg, Germany. XRF measurements were performed using the method of Böning et al. (2009). Overall analytical precision and accuracy were monitored by measurements of several in-house standards and the certified standard GSD-12, and were better than 3%. All data are presented in Table 3.2. Bulk sediment terrace OSL samples were analyzed separately by ICP-AES methods at the University of Utah, as described below, as part of the OSL methodology.

4.4.3 Isotope Geochemistry

Selected sediments were also analyzed for Sr and Nd isotopes because these systems have an established track record of being reliable provenance and chemical weathering proxies in sedimentary systems and have been applied successfully in the Mekong and Red Rivers (Liu et al., 2007; Clift et al., 2008b). Nd is a water-immobile element and is generally considered not to experience isotopic fractionation during weathering and erosion processes (Goldstein et al., 1984). The Nd isotopic composition broadly reflects the average age and lithology of the crust being eroded so that sediments from ancient continental crust have different signatures compared to those derived from younger igneous bodies. Sr is water mobile and may be affected by weathering processes as well as the provenance (Derry and France-Lanord, 1996). Unweathered rocks show correlation between Nd and Sr isotopes, but $^{87}\text{Sr}/^{86}\text{Sr}$ values tend to increase with stronger alteration (Derry and France-Lanord, 1996; Hu et al., 2013). Sr isotopes are strongly affected by the presence of carbonate and care was taken to decarbonate samples prior to analysis. This was especially important in the Song Gianh because of the presence of common limestone exposures, especially in the southern part of the basin

Table 4.2. Major and trace element geochemistry of Song Gianh sediments.

Sample	Location	SiO ₂	TiO ₂	Al ₂ O ₃	Fe ₂ O ₃	MnO	MgO	CaO	Na ₂ O	K ₂ O	P ₂ O ₅
Modern river samples											
12061704	Upper reaches mainstream	76.2	0.43	9.72	3.82	0.05	1.08	0.35	0.72	1.94	0.06
12061703	Upper reaches mainstream	71.0	0.54	12.66	6.54	0.07	1.37	0.56	0.64	2.42	0.10
12061702	Upper reaches mainstream	72.6	0.43	9.70	4.89	0.05	2.06	2.34	0.38	2.07	0.09
14052701	Upper reaches mainstream	76.5	0.46	10.60	4.94	0.04	0.72	0.20	0.47	2.26	0.09
12061708	Mai Hoa	90.0	0.24	5.08	1.46	0.01	0.13	0.07	0.18	2.42	0.04
	Middle reaches										
12061711	mainstream	84.2	0.36	5.21	2.68	0.02	0.35	0.16	0.38	1.17	0.05
12061712	Rao Tro	90.6	0.34	4.57	1.16	0.02	0.16	0.10	0.23	2.10	0.03
14052801	Song Nan	93.3	0.25	1.56	0.86	0.01	0.20	0.53	0.26	0.27	0.05
12061802	Song Trac	88.2	0.36	5.05	1.93	0.02	0.45	0.49	0.29	0.88	0.05
12061801	Song Trac	79.2	0.42	9.70	3.45	0.03	1.04	0.16	0.26	2.48	0.05
14052705	Song Trac	90.8	0.17	3.83	1.06	0.01	0.33	0.33	0.26	0.82	0.03
12061807	River Mouth	91.0	0.49	3.68	1.47	0.03	0.23	0.15	0.36	1.02	0.03
Terraces											
12061707	Mainstream terrace		0.30	5.77	2.94		0.34	0.08	0.32	1.54	
12061706	Mainstream terrace		0.26	5.58	3.30		0.35	0.07	0.28	1.60	
12061709	Mainstream terrace		0.27	4.60	2.11		0.16	0.03	0.15	2.03	
12061803	Terrace Southern tributary		0.23	3.93	1.92		0.34	0.33	0.27	1.17	
12061804	Terrace Southern tributary		0.15	2.73	1.47		0.20	0.17	0.23	0.86	

Table 4.2 (continued). Major and trace element geochemistry of Song Gianh sediments.

Sample	Location	As	Ba	Ce	Co	Cr	Cu	Ga	Mo	Ni	Nb	Pb	Rb	Sr	Th	Y	V	U	Zn	Zr
Modern river samples																				
12061704	Upper reaches mainstream	5	347	53	12	43	20	12	-5	21	11	17	77	73	9	3	62	13	47	121
12061703	Upper reaches mainstream	11	336	59	15	67	16	17	0	33	13	23	103	83	9	16	86	6	79	132
12061702	Upper reaches mainstream	9	301	50	15	63	13	12	-2	25	12	19	102	58	11	13	60	8	60	142
14052701	Upper reaches mainstream	8	337	57	17	55	13	13	0	24	12	21	112	61	11	15	64	4	65	145
12061708	Mai Hoa	6	321	15	8	15	4	5	0	7	8	13	105	37	7	6	18	7	17	84
12061711	Middle reaches mainstream	3	184	40	8	27	5	6	0	14	10	12	51	42	7	6	33	9	34	104
12061712	Rao Tro	7	317	12	7	13	1	5	0	5	10	8	80	30	6	3	20	7	18	83
14052801	Song Nan	0	40	-30	6	24	0	3	0	7	7	5	16	24	5	11	15	6	16	465
12061802	Song Trac	5	158	10	9	33	7	7	-1	13	9	9	43	39	8	14	34	7	30	271
12061801	Song Trac	0	452	30	10	48	10	12	0	21	11	22	115	45	7	13	61	6	54	95
14052705	Song Trac	0	181	-7	7	20	1	5	-1	6	7	6	36	37	6	5	17	6	14	90
12061807	River Mouth	2	170	38	6	22	2	5	0	13	10	10	36	34	7	11	24	10	25	418
Terraces																				
12061707	Mainstream terrace	7	330	67	13	113	21	14	1	27	12	20	98	56	13	16	67	3	66	60
12061706	Mainstream terrace	8	340	62	13	131	24	14	1	28	9	20	102	54	13	13	67	2	71	51
12061709	Mainstream terrace	8	370	64	8	129	16	11	1	13	9	20	124	36	13	13	48	3	33	42
12061803	Terrace Southern tributary	4	270	67	9	178	16	10	0	19	8	17	70	50	14	14	49	3	50	47
12061804	Terrace Southern tributary	3	230	69	5	171	10	7	0	13	11	12	47	44	14	15	32	4	32	36

(Fig. 4.2). This means that this analysis only constrains the provenance and alteration of the siliciclastic fraction. Much of the carbonate load is in any case dissolved and is not represented in the analyzed bedload (see the low CaO values, Table 3.2).

Prior to total digestion all samples were leached using buffered acetic acid to remove any carbonate-bound Sr. This was followed by a leach with 25% (v/v) acetic acid and 0.02 M hydroxylamine hydrochloride (HH) to remove Sr contained in authigenic Mn-Fe-oxides, which may also concentrate Nd. Hence, the Sr and Nd isotopic signatures is assumed to result solely from the silicate fraction (plus perhaps fractions of dolomite). The leached sediments were then digested in closed PTFE vessels (Böning et al., 2004). The samples and the certified standard BCR-2 (50 mg), as well as a blank, were treated with HNO₃ overnight to oxidize any organic matter. After that HF and HClO₄ were added and the vessels were heated for 12 h at 180°C. All acids were of suprapure quality. After digestion, acids were evaporated on a heated metal block (180°C), residues were redissolved and fumed off three times with 6N HCl, and finally taken up in 1N HNO₃. From the resulting solutions, rare earth elements (REEs) and Sr were isolated from major elements and separated from each other by two-step column chemistry using Eichrom TRU-Spec resin. Nd was then isolated from interfering REEs using Eichrom LN-Spec resin with 0.23–0.25 N HCl as eluant. The TRU-Spec Sr-Rb cut was loaded on Eichrom Sr-Spec columns to isolate Sr using Milli-Q water.

The isotopic compositions of Nd and Sr were analyzed on a Thermo Neptune Plus Multicollector ICP-MS at the ICBM. For Nd isotope analyses, all samples were corrected for internal mass fractionation using $^{146}\text{Nd}/^{144}\text{Nd} = 0.7219$ and an exponential law. Each measurement session was accompanied by multiple analyses of the Nd standard JNdi-1

with sample-like concentrations, and $^{143}\text{Nd}/^{144}\text{Nd}$ ratios of all samples were normalized to the reported JNdi-1 value of $^{143}\text{Nd}/^{144}\text{Nd} = 0.512115$ (Tanaka et al., 2000). The Nd isotopic composition is expressed in ϵNd notation:

$$\epsilon_{\text{Nd}} = \left[\frac{\left(\frac{^{143}\text{Nd}}{^{144}\text{Nd}} \right)_{\text{sample}}}{\left(\frac{^{143}\text{Nd}}{^{144}\text{Nd}} \right)_{\text{CHUR}}} - 1 \right] * 10^4 \quad (4.1)$$

$(^{143}\text{Nd}/^{144}\text{Nd})_{\text{CHUR}}$ is the Chondritic Uniform Reservoir with a value of 0.512638 (Jacobsen & Wasserburg, 1980). The external reproducibility is calculated for each session separately using the analyses of JNdi-1 and was generally better than ± 0.000015 or $\pm 0.3 \epsilon_{\text{Nd}}$ units (2σ). The BCR-2 standard ($n = 4$) had an ϵ_{Nd} value of $0.1 (\pm 0.3, 2\sigma)$ and was well within the reported ϵ_{Nd} value of 0.0 ± 0.2 (Raczek et al., 2003). The procedural blank was $\leq 30 \text{ pg Nd}$.

For Sr isotope analyses, all samples were corrected for mass fractionation using $^{86}\text{Sr}/^{88}\text{Sr} = 0.1194$ and the exponential law. Measurements were accompanied by multiple analyses of NBS987 with sample-like concentrations, and $^{87}\text{Sr}/^{86}\text{Sr}$ ratios of all samples were normalized to the reported value of 0.710248 (Thirlwall, 1991). Furthermore, Kr, Rb and Ba contents were monitored and found to be negligible. The external reproducibility is calculated using the analyses of NBS987 and was generally better than 50 ppm (2σ). The BCR-2 standard ($n = 4$) had a $^{87}\text{Sr}/^{86}\text{Sr}$ ratio of 0.70502 ± 0.00004 (2σ) and was within the reported $^{87}\text{Sr}/^{86}\text{Sr}$ ratio of 0.70496 ± 0.00002 (Raczek et al., 2003). The procedural blanks were negligible throughout. Results are reported in Table 4.3

4.4.4 Detrital U-Pb Zircon Geochronology

Detrital zircon U-Pb dating has become a popular and effective technique for evaluating sediment provenance in clastic systems because zircon is a common mineral in

Table 4.3. Nd and Sr isotope geochemistry of Song Gianh sediments.

Sample ID	Normalized $^{143}\text{Nd}/^{144}\text{Nd}$ §	Internal error $^{143}\text{Nd}/^{144}\text{Nd}$ (2 σ)	ϵ_{Nd}	ϵ_{Nd} external error (2 σ SD)	Propagated error (ϵ_{Nd})	Normalized $^{87}\text{Sr}/^{86}\text{Sr}$ €	Internal error $^{87}\text{Sr}/^{86}\text{Sr}$ (2 σ SD)	External error (2 σ SD)	Propagated error
12061704	0.511874	0.000016	-14.9	0.29	0.42	0.723579	0.000002	0.000021	0.000021
12061703	0.511957	0.000003	-13.3	0.16	0.16	0.724692	0.000020	0.000025	0.000033
12061702	0.511895	0.000013	-14.5	0.29	0.29	0.735913	0.000007	0.000021	0.000022
14052701	0.511871	0.000007	-15.0	0.29	0.29	0.726209	0.000019	0.000021	0.000028
12061708	0.511978	0.000007	-12.9	0.29	0.29	0.750339	0.000018	0.000021	0.000028
12061711	0.511890	0.000009	-14.6	0.18	0.18	0.726481	0.000007	0.000025	0.000026
12061712	0.512014	0.000014	-12.2	0.29	0.29	0.747068	0.000022	0.000021	0.000030
14052801	0.511862	0.000003	-15.1	0.29	0.29	0.734145	0.000018	0.000021	0.000028
12061802	0.511889	0.000042	-14.6	0.29	0.82	0.725182	0.000030	0.000021	0.000037
12061801	0.511857	0.000005	-15.2	0.16	0.16	0.742903	0.000026	0.000025	0.000036
14052705	0.512068	0.000008	-11.1	0.29	0.29	0.725656	0.000020	0.000021	0.000029
12061807	0.511889	0.000008	-14.6	0.22	0.22	0.726791	0.000010	0.000025	0.000027

Notes:

§ measured $^{143}\text{Nd}/^{144}\text{Nd}$ ratios were normalized to the JNdi-1 value of 0.512115 (Tanaka et al., 2000).

€ measured $^{87}\text{Sr}/^{86}\text{Sr}$ ratios were normalized to the NBS987 value of 0.710248 (Thirlwall, 1991).

& reported error, determined as $\sqrt{\{(\text{internal error})^2 + (\text{external error})^2\}}$

continental rocks of many compositions, and is chemically and mechanically durable enough to survive multiple cycles of erosion, transport and sedimentation. Grains $>50\text{ }\mu\text{m}$ across were analyzed, reflecting the spot size of the laser employed. Yang et al. (2012) revealed that younger zircons were larger or more variable in size than the older grains in the Yangtze River, indicating the potential influence of hydrodynamic fractionation on zircon size and age. Yang et al. (2012) concluded that the 63–125 μm size fraction yielded almost the same age distribution as the total zircon population, and can effectively demonstrate all significant age populations. Our analysis may thus be expected to be representative of the bulk composition. Given that the Song Gianh is so much shorter than the Yangtze any grain size effect would be even less significant, because there must be less abrasion of zircons during transport.

Samples were separated for zircon using standard magnetic and heavy liquid separation techniques. The $>40\text{ }\mu\text{m}$ sieve-fraction was separated using a vibrating Gemini® Mineral Separation table. The densest fraction was collected, washed with ethanol, and dried in an oven at 100°C . Once dry, a rare-earth element hand magnet was passed several times over the sample to remove extremely magnetic material and sieved again to 63–250 μm before passing through a Frantz® Magnetic Barrier Laboratory Separator Model LB-1 to isolate nonmagnetic ($>1.6\text{ A}$) grains. Prior to heavy liquid separation, all samples were pre-treated using hydrogen peroxide, acetic acid, and oxalic acid to remove organic material, carbonate, and Fe-oxides, respectively. Extracted detrital zircon were mounted in epoxy resin, polished, and imaged by reflected light and cathodoluminescence.

Detrital zircons were dated using the U-Pb method at the London Geochronology

Centre facilities at University College London, using a New Wave Nd:YAG 193 nm laser ablation system, coupled to an Agilent 7700 quadrupole ICP-MS. Around 100–120 grains are considered generally sufficient for characterizing sand eroded from a geologically complicated drainage basin (Vermeesch, 2004). Real time U-Pb data were processed using GLITTER 4.4 data reduction software. Repeated measurements of external zircon standard PLESOVICE (TIMS reference age 337.13 ± 0.37 Ma; Sláma et al., 2008) and NIST 612 silicate glass (Pearce et al., 1997) were used to correct for instrumental mass bias and depth-dependent inter-element fractionation of Pb, Th and U. For this study $^{206}\text{Pb}/^{238}\text{U}$ ages are used for grains younger than 1000 Ma, and for zircon grains older than 1000 Ma we used the $^{207}\text{Pb}/^{206}\text{Pb}$ ages to calculate the crystallization age. Because some grains are discordant we chose to only plot those grains when the discordance was less than 15% (Appendix E).

4.4.5 Detrital Apatite Fission Track Geochronology

Two samples were analyzed for apatite fission track dating. The low-temperature apatite fission-track method, which records cooling through ~60–125°C over timescales of 1–10 m.y. (Green et al., 1989) is particularly sensitive to exhumation driven by erosion and has been widely used in exhumation studies worldwide. Apatites were picked, mounted, and analyzed after heavy mineral extraction at University College, London, UK. Polished grain mounts of apatite were etched with 5N HNO_3 at 20°C for 20s to reveal the spontaneous fission-tracks. Etched grain mounts were packed with mica external detectors and corning glass (CN5) dosimeters and irradiated in the FRM 11 thermal neutron facility at the University of Munich in Germany. Following irradiation the external detectors were etched using 48% HF at 20°C for 25 minutes. Sample ages

were determined using the zeta calibration method and IUGS recommended age standards (Hurford, 1990). The results of the fission track analyses are presented in Appendix F.

4.4.6 *In situ* ^{10}Be Cosmogenic Nuclides

In situ-produced cosmogenic isotopes (e.g., ^{10}Be) are routinely measured in quartz from river sediment for estimating denudation rates in steady-state hill-slope settings over time scales relevant to soil formation processes, i.e., millennial (Bierman and Steig, 1996; von Blanckenburg, 2005; Granger and Riebe, 2007). These estimates can be compared with other methods, such as fission track to determine the temporal stability of erosion rates. In this study we only analyzed the river mouth sample using this method in order to determine the basin-wide integrated denudation rate in the recent past. Sample processing was done at the Deutsches GeoForschungszentrum (GFZ), in Potsdam, Germany. The sample was dried, sieved into a grain size range of 90 to 300 μm , and pure quartz was separated using magnetic separation followed by etching with weak HF, flotation, and ortho-phosphoric acid treatments until Al concentrations (being indicative of feldspar contents) were below 300 ppm (as subsequently evaluated using optical emission spectroscopy, OES). We used the simplified method of von Blanckenburg et al. (2004) to separate *in situ*-produced ^{10}Be from the sample matrix. Prior to final decomposition using concentrated HF and Fe and Be column chemistry, a final leach in aqua regia was done to remove remaining atmospherically-produced ^{10}Be . About 0.42 g of a ^9Be carrier with a concentration of 372 ppm was added to the sample, determined to contain a $^{10}\text{Be}/^9\text{Be}$ ratio of $3.4 \pm 0.5 \cdot 10^{-15}$, whose amount was subtracted from the measured ^{10}Be concentration. After column chemistry and alkaline precipitation, the sample was

oxidized and pressed into accelerator mass spectrometer (AMS) cathodes and was measured at the Cologne University AMS facility (Dewald et al., 2013) relative to standards KN1-6-2 and KN1-5-3 (having nominal $^{10}\text{Be}/^9\text{Be}$ ratios of $5.35 \cdot 10^{-13}$ and $6.32 \cdot 10^{-12}$, respectively) normalized to a ^{10}Be half-life of 1.39 m.y. (Chmeleff et al., 2010; Korschinek et al., 2010).

Conversion of a blank-corrected ^{10}Be concentration (Table 4.4) to a denudation rate was done using the atmospheric time-independent scaling scheme of Dunai (2000), calculated for pixel-based altitudes derived from SRTM-90 DEM, relative to a total sea level high latitude (SLHL) ^{10}Be nuclide production rate of $4.682 \text{ at/g} \cdot \text{yr}$ (Roller et al., 2012). These calculations resulted in a total mean basin-wide ^{10}Be production rate of $3.37 \text{ at/g} \cdot \text{yr}$ (Table 4.4) for the Song Gianh catchment. This basin-wide production rate is lowered to a rate of $2.90 \text{ at/g} \cdot \text{yr}$ (Table 4.4) when a lithology correction is employed for areas of karstic limestone (not producing any ^{10}Be). These areas, identified mainly as Devonian limestones (Fig. 4.2), were excluded from production rate calculations. An uncertainty of 5% incorporating production rate and scaling errors was propagated into the calculated denudation rate error (yielding an external error for inter-method comparison). Note that a correction for geomagnetic variation in the intensity of Earth's magnetic dipole field was not carried out for the derived production rate. Topographic shielding on production rates was deemed negligible for the studied catchment.

4.4.7 Optically Stimulated Luminescence Dating

Depositional ages of sediment in the terraces were determined by optically stimulated luminescence (OSL) dating of quartz sand. While OSL dating can be challenging in fluvial environments, deposits from these settings can be accurately dated

Table 4.4. Cosmogenic nuclide data for Song Gianh sediments.

Sample	AMS-measured $^{10}\text{Be}/^9\text{Be}$ ratio	Analytical Error (1σ , %)	^{10}Be Production Rate (atoms/g*yr)			^{10}Be (atoms/ g _{qtz})	^{10}Be (atoms/ g _{qtz})	Denudation Rate (mm/ky, $\pm 1\sigma$)	Apparent age (kyr BP)
			Nucleo- genic	stopped muons	fast muons				
12061807	5.52×10^{-13}	3.92	3.18	0.11	0.08	9.55×10^4	3.82×10^3	35.70 ± 2.84	28.50
12061807 ^a			2.75	0.09	0.07			29.50 ± 2.40	33.20

Note:

^a For carbonate correction, the production rate was set to zero for DEM pixels covered by Devonian carbonate lithology.

^b Total error contains a 5% production rate uncertainty and thus represents an external error.

by selecting depositional facies most likely to have been reset by sunlight exposure (Fuchs and Owen, 2008; Rittenour, 2008; Wyshnytzky et al., 2015). We preferentially targeted well-sorted, horizontally bedded sand lenses from fluvial deposits to reduce the influence of incomplete resetting (partial bleaching) of the luminescence signal. Samples for OSL dating were collected by pounding opaque metal pipes into target horizons within the sediment exposures and sealing the ends of the tightly packed tubes to prevent light exposure and sediment mixing. Samples were sent to the Utah State University Luminescence Laboratory for processing to purified quartz separates for analysis. Samples were treated with dilute HCl and chlorine bleach to remove carbonates and organics followed by heavy mineral separation (sodium polytungstate, 2.7 g/cm^3) and treatment in concentrated HF to remove feldspars and etch the quartz grains. The purity of the quartz separates was checked by monitoring response to infra-red stimulation; contaminated aliquots were not used for age calculation.

Samples for environmental dose rate determination were collected from a 30 cm diameter area surrounding the OSL sample tube. Sediments were homogenized and representative samples were analyzed for radioisotope concentration using ICP-MS and ICP-AES techniques (Table 4.5). These concentration values were converted to dose rate following the conversion factors of Guérin et al. (2011) and beta attenuation values of Brennan (2003). Contribution of cosmic radiation to the dose rate was calculated using sample depth, elevation and latitude/longitude following Prescott and Hutton (1994). Total dose rates were calculated based on water content, radioisotope concentration, and cosmic contribution (Adamiec and Aitken, 1998; Aitken, 1998). Small aliquots (50–200 grains) of quartz sand were analyzed using the single-aliquot regenerative-dose (SAR)

Table 4.5. OSL samples results for Song Gianh sediments.

Sample Number	Terrace Location	Elevation (m)	Number of aliquots ^a	Equivalent Dose, De (Gy) ^c	Overdispersion (%) ^d	Dose Rate (Gy/ka)	OSL Age (ka, $\pm 1\sigma$) ^e	Depth (m)
12061803	Southern Song Trac	8	21 (38)	0.84 ± 0.21	58.9 ± 21.7	2.61 ± 0.15	0.32 ± 0.09	1
12061804	Southern Song Trac	3	19 (35)	0.40 ± 0.35	108.0 ± 31.7	2.61 ± 0.16	0.15 ± 0.14	5
12061706	Mainstream	51	23 (28)	23.99 ± 1.79^b	13.1 ± 3.5	2.81 ± 0.16	8.55 ± 1.08	4
12061707	Mainstream	51	20 (28)	21.75 ± 1.74^b	10.7 ± 4.3	2.95 ± 0.17	7.36 ± 0.96	8
12061709	Mainstream	19	20 (41)	1.77 ± 0.58	53.6 ± 10.3	3.24 ± 0.19	0.55 ± 0.19	4

Note:

^a Number of aliquots used for age calculation. Rejection of aliquots follows standard rejection criteria

^b De calculated using the Central Age Model of Galbraith et al (1999); Excel macros written by Sébastien Huot (UQAM). Error on De is 2σ error

^cDe calculated using the Minimum Age Model of Galbraith et al (1999) unless otherwise noted; Excel macros written by Sébastien Huot (UQAM).

^dOverdispersion represents scatter in De beyond calculated uncertainties in data, OD >20% is considered significant.

^eError on age is 2σ standard error.

Table 4.5 (continued). OSL sample results for Song Gianh sediments.

Sample Number	Location	Grain Size (μm)	<i>In-situ</i> H ₂ O (%) ^f	U (ppm)	Th (ppm)	K (%)	Rb (ppm)	Cosmic (mGy/ka) ^g
12061803	Southern Song Trac	90-180	9.4	2.5 ± 0.2	13.8 ± 1.2	1.17 ± 0.03	69.5 ± 2.8	0.14 ± 0.01
12061804	Southern Song Trac	125-212	8.9	4.0 ± 0.3	14.1 ± 1.3	0.86 ± 0.02	47.1 ± 1.9	0.08 ± 0.01
12061706	Mainstream	90-180	10.6	2.3 ± 0.2	12.5 ± 1.1	1.60 ± 0.04	101.5 ± 4.1	0.10 ± 0.01
12061707	Mainstream	90-180	9.8	3.1 ± 0.2	13.1 ± 1.2	1.54 ± 0.04	97.8 ± 3.9	0.06 ± 0.01
12061709	Mainstream	90-180	11.9	2.6 ± 0.2	12.8 ± 1.2	2.03 ± 0.05	124.0 ± 5.0	0.09 ± 0.01

Note:

^f Assume $3 \pm 3\%$ wt H₂O is representative of burial history.

^g Contribution of cosmic radiation to the dose rate was calculated by using sample depth, elevation, and longitude/latitude following Prescott and Hutton (1994).

technique (Murray and Wintle, 2000) on Risø OSL/TL DA-20 luminescence readers with blue-green (470 nm, 36 W/m²) stimulation and detection through 7.5-mm UV filters (U-340). Stimulation was conducted at 125°C following 240°C preheats (10 s) for regenerative and natural doses. OSL ages were calculated from 28–41 aliquots that passed rejection criteria related to feldspar contamination (IRSL signal to background ratio >2) and performance related to repeat-point (>15% difference) and zero-dose tests (>5% signal recuperated). Equivalent dose (DE) values were calculated using either the central age model (CAM) or minimum age model (MAM) of Galbraith and Roberts (2012).

4.5 Results

4.5.1 Topographic Analysis

Key observations from topographic analysis (Figs. 4.3A–C) find that regions containing higher precipitation correlate with regions of higher local relief. Annual rainfall is higher to the west and in the south of the basin. Steep slopes are distributed generally south of the main stream. Regions containing highest local relief lie in the westernmost part of basin. Four regions of low relief are identified along the middle to upper Song Nan, lower to middle Song Nan, the upper Rao Tro, and along the middle and lower reaches of the main stream.

Longitudinal profiles in the Song Gianh are smooth with concavity scaling with drainage area for most tributaries (Fig. 4.4). We identify three major knickpoints, two along the Song Nan and one in upper reaches of the trunk Song Gianh. Two of the three knickpoints lie at ~185 m above sea level (a.s.l.) although they differ in height above the modern river level. In the upper Song Nan, one knickpoint lies at the edge of a perched

basin ~180 m above modern river level (a.r.l.). The second lies much lower with respect to modern river level, at ~45 m a.r.l. Finally, the third lower knickpoint lies at ~35 m a.s.l and ~30 m a.r.l.

4.5.2 Major and Trace Element Geochemistry

The major element compositions of the samples show a typical range for quartz-rich sands. Rarely is the major element geochemistry diagnostic for provenance but it can be effective in determining the intensity of chemical weathering. This can be assessed using the “Chemical Index of Alteration” (CIA) proxy developed by Nesbitt et al. (1980) and expressed as:

$$CIA = \left[\frac{Al_2O_3}{(Al_2O_3 + Na_2O + K_2O + CaO^*)} \right] * 100 \quad (4.2)$$

CIA compares the relative leaching of mobile elements K, Na, and silicate-only Ca against immobile Al as minerals, such as feldspar, weather to clay. CIA values close to 100 indicate intense weathering, where values around 50 indicate negligible weathering. Where excess CaO is present in carbonates and phosphates, a correction is made by assuming reasonable Ca/Na ratios from the silicate material and correcting for CaO in phosphate (Singh et al., 2005).

Figure 4.5 indicates that CIA values range from 57 to 73 and vary in relation to the SiO₂ content, which can serve as a proxy for the quartz content of the sediment. Our samples show negative correlation to CIA with increasing silica content, which is typical of grain size variation in fluvial sediments.

There is a general decrease in CIA variation downstream towards the river mouth as shown in Figure 4.6. The highest values are seen in the upper reaches of the mainstream but decrease rapidly towards the river mouth. The Song Trac is noteworthy in

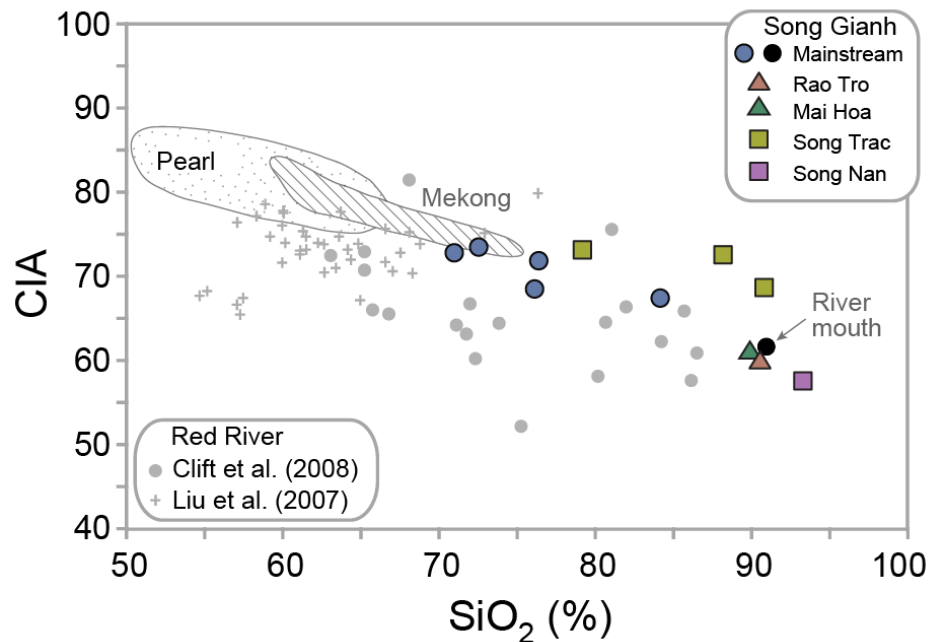


Figure 4.5. Plot of Chemical Index of Alteration (CIA) versus silica content of the samples considered in this study. SiO_2 is used as a proxy for the quartz sand content. Fields showing fine grained material from the Pearl, Mekong, and Red Rivers (gray crosses) are from Liu et al. (2007). Red River fine grained and sandy sediments analyzed by Clift et al. (2008b) are gray circles. Lack of SiO_2 data precludes plotting Song Gianh terraces here.

that it has relatively high CIA values that contrast with the lower values seen in all other tributaries. Sediments in the terraces within the upper reaches and within the Song Trac have lower CIA values than the modern adjacent rivers.

4.5.3 Isotope Geochemistry

Figure 4.7 shows the variation in Sr and Nd isotopes for the Song Gianh and other values than other major SE Asian rivers and generally high $^{87}\text{Sr}/^{86}\text{Sr}$ values. We note that when considering only the Song Gianh samples there is no coherent correlation between the isotopic systems. Along the mainstream, much variation is recognized in $^{87}\text{Sr}/^{86}\text{Sr}$ values of decarbonated sediment (Fig. 4.8A) with most variation occurring in the upper reaches of the mainstream. It is noteworthy that the Rao Tro and Mai Hoa

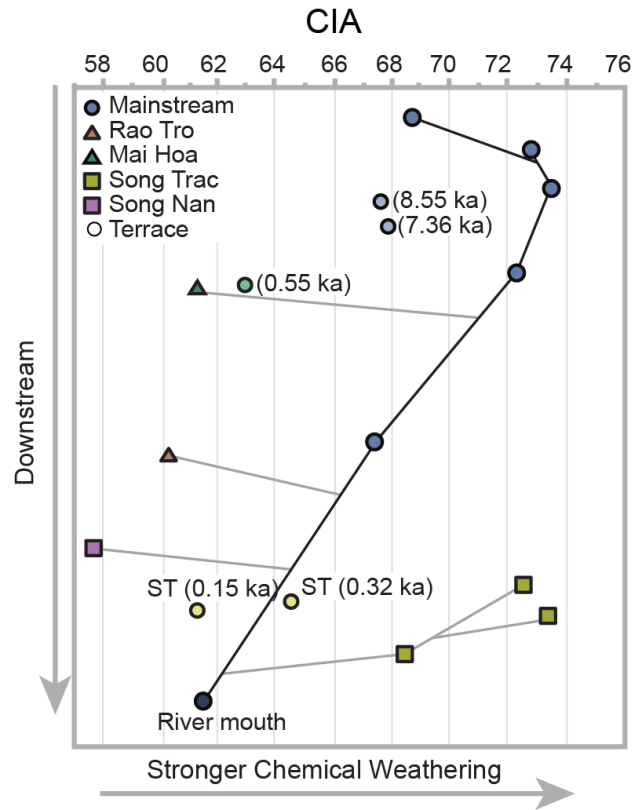


Figure 4.6. Downstream evolution in CIA within the Song Gianh basin. Note the general decrease in CIA downstream and that the terrace sediments are generally lower in CIA compared to the modern river at that location. Terrace samples are from the mainstream, except for those labeled ST that are from the Song Trac. Ages in parentheses are OSL ages. Sample colors follow Figure 4.1.

tributaries have relatively high $^{87}\text{Sr}/^{86}\text{Sr}$ values compared to the mainstream. The $^{87}\text{Sr}/^{86}\text{Sr}$ values of the mainstream fall from upstream to downstream of the Mai Hoa. After this confluence, there is little compositional variability downstream. The Song Trac and Song Nan tributary $^{87}\text{Sr}/^{86}\text{Sr}$ values lie close to the values of the mainstream.

Similar to the Sr isotopes, the ϵ_{Nd} values of the mainstream are stable downstream of the Mai Hoa confluence (Fig. 4.8B). The northern tributaries, the Rao Tro and Mai Hoa, show distinctive, more positive ϵ_{Nd} values than the mainstream river. The mainstream ϵ_{Nd} values do not vary significantly downstream after the confluences of these tributaries. In contrast, the Song Nan and Song Trac have ϵ_{Nd} values that are

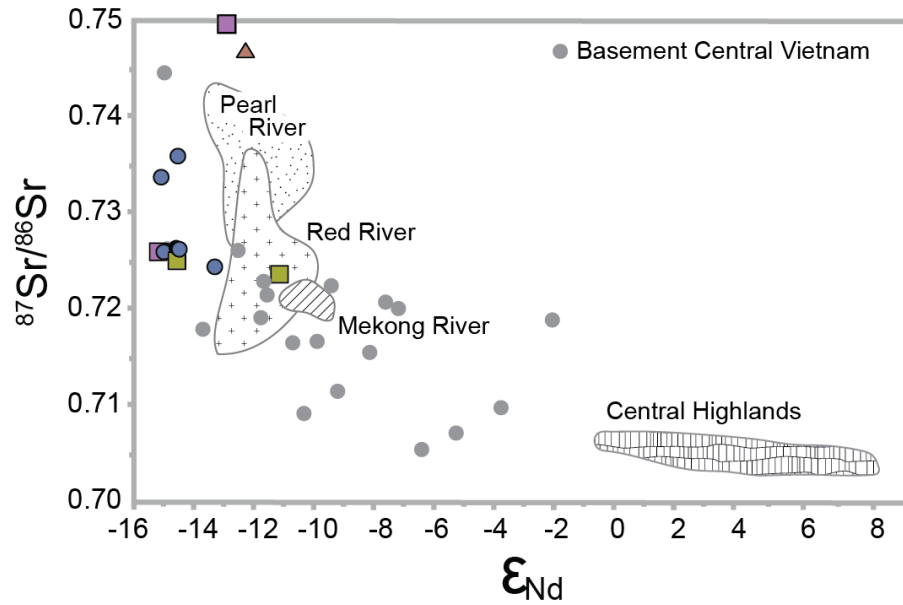


Figure 4.7. Cross plot of Sr versus Nd isotope compositions for the Song Gianh compared with river sediments measured from the Red, Mekong and Pearl Rivers by Liu et al. (2007) and Clift et al. (2008b). Basement samples from central and northern Vietnam are from Hoa et al. (2008), Lan et al. (2003) and Nagy et al. (2000). Central Highland volcanic rocks are compiled from various sources from Hoang et al. (1996). Sample colors follow Figure 4.1.

slightly more negative than the mainstream.

4.5.4 Detrital U-Pb Zircon Geochronology

The distribution of ages for detrital zircons can be best compared graphically with kernel density estimation (KDE) diagrams. Figure 4.9 shows the range of measured zircon ages younger than 3.5 Ga for all the samples in our study, together with basement analyses from the Kontum Massif, Khorat Plateau, and Central Highlands. Although these do not directly source the Song Gianh they represent basement data from the Indochina Block that might have equivalents within our drainage. Each sample has a unique age spectrum but there are resolvable age peaks that can be identified in many samples. One prominent peak spans 100–380 Ma, with a maximum age ~250 Ma; this peak characterizes many rocks in SE Asia and is typically indicative of the Indosinian

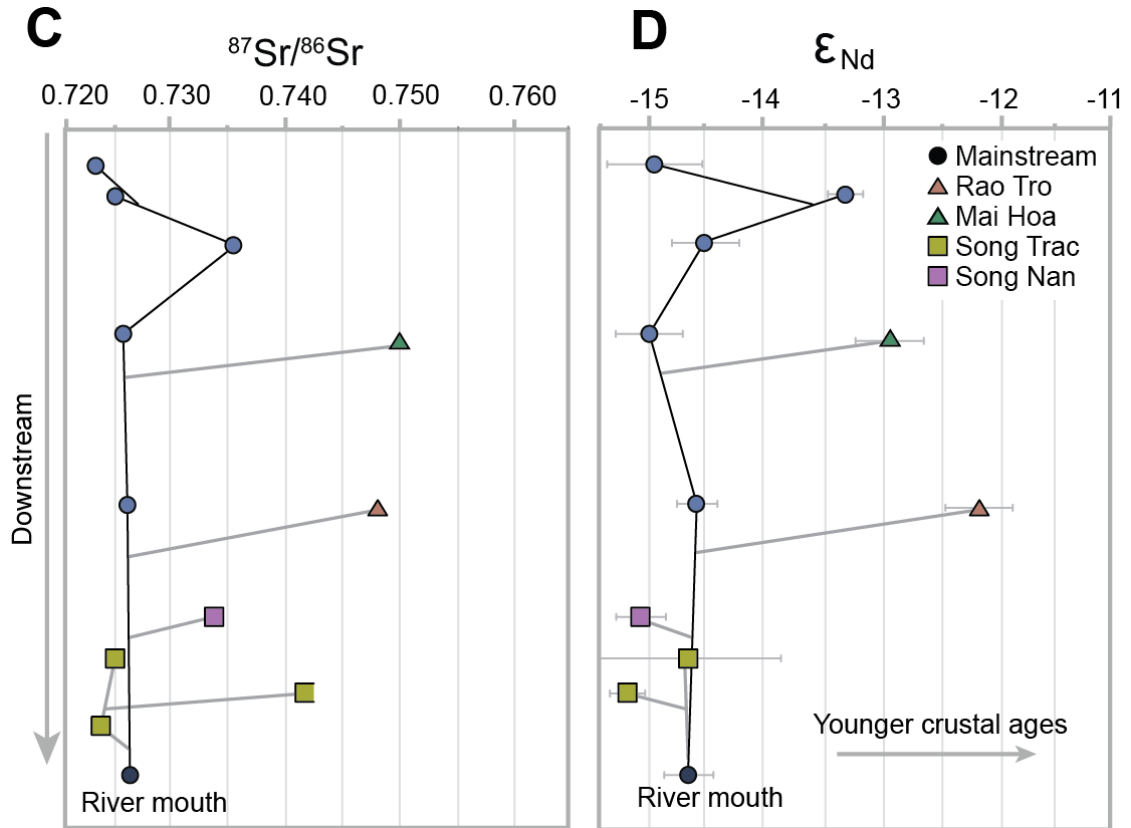


Figure 4.8. Plots showing the downstream evolution in (A) Sr and (B) ϵ_{Nd} isotope compositions within the Song Gianh. Note that the mainstream stabilizes in composition in its middle reaches and does not seem much affected by flow from either of the northern tributaries. Error bars smaller than symbol size for Sr in Fig. 4.8A and propagated error for ϵ_{Nd} in Fig. 4.8B are gray brackets. Sample colors follow Figure 4.1.

Orogeny (Carter et al., 2001; Lepvrier et al., 2004). Another common population at ~450 Ma is sometimes referred to as “the Caledonian event” (Chen and Jahn, 1998) or the Wuyi-Yunkai (or occasionally Kwangsi) Orogeny (Li et al., 2010). A broad population of ages spanning 700–1100 Ma are correlative with rocks of that age from the Yangtze Craton, commonly referred to as the Jinningian (Li, 1999). An older group of zircons ages from 1750–2200 Ma match similar aged rock are referred to as the Luliangian from eastern Asia (Chen and Jahn, 1998). The number of older grains are somewhat fewer, although peaks are identified at ~2500 Ma and rarely ~2800 Ma.

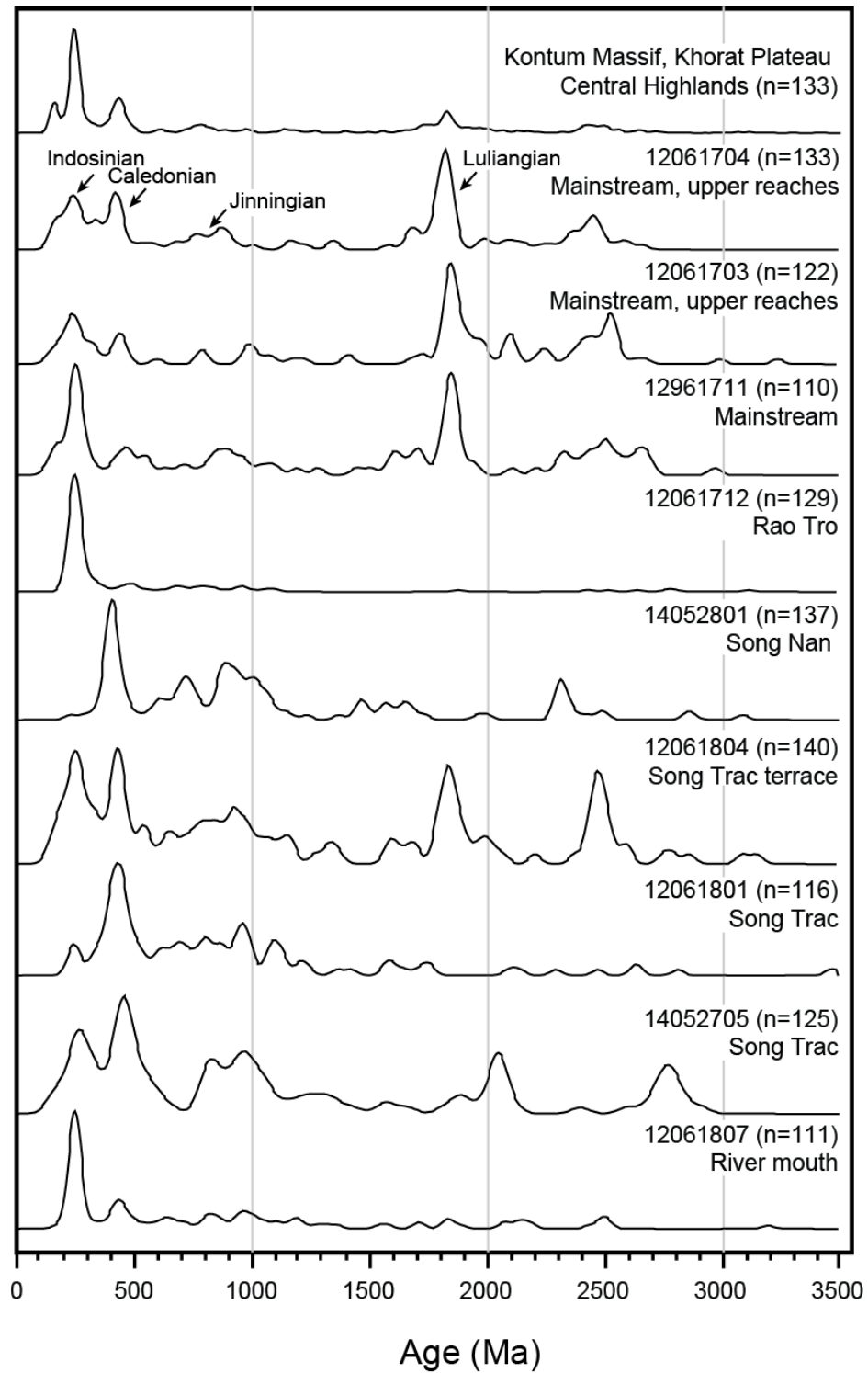


Figure 4.9. KDE plots of U-Pb zircon dates from Song Gianh sediments, compared with bed rock data from the Kontum Massif from Nagy Nagy et al. (2001) and the Khorat Plateau from Carter and Moss (1999) and Carter and Bristow (2003), and the Vietnamese Central Highlands from Carter et al. (2001).

It is noteworthy that the river mouth is characterized by a particularly large peak at ~250 Ma, a characteristic that is shared by the Rao Tro tributary. This peak is common in many of the Song Gianh zircon spectra, but other tributaries' spectra include other prominent, older populations as well. These older peaks are not dominant at the river mouth or Rao Tro spectra.

4.5.5 Detrital Apatite Fission Track Geochronology

A single sample (14052705) yielded sufficient apatite to generate a statistically meaningful result that allows us to examine the average cooling history of bedrock in the Song Trac (Fig. 4.10). A single age population exists in the Song Trac with a central age of 54.5 ± 3.5 Ma as shown by a radial plot (Fig. 4.10A) and a KDE diagram (Fig. 4.10B) that also highlights the tail of older ages back to 120 Ma.

4.5.6 *In situ* ^{10}Be Cosmogenic Nuclides

The measured *in situ* cosmogenic denudation rate at the river mouth is 29.5 ± 2.4 mm/k.y. (calculated using the limestone-corrected production rate). The integration time scale of this denudation rate is 33 k.y., corresponding to the time necessary to erode one attenuation depth scale (60 cm in rock or 100 cm in soil).

4.5.7 Optically Stimulated Luminescence Dating

Results of OSL dating indicate four possible times of terrace construction within the basin (Table 4.5). In the upper reaches two samples within a single prominent, 11 m high terrace, show that it was constructed ~7.4–8.5 ka, during the Early Holocene. This terrace or an equivalent aged surface were not found in the lower reaches. A younger terrace, around 8 m above the modern stream, was identified nearby within the Mai Hoa confluence area and was dated at 550 ± 190 years ago. A slightly younger terrace was

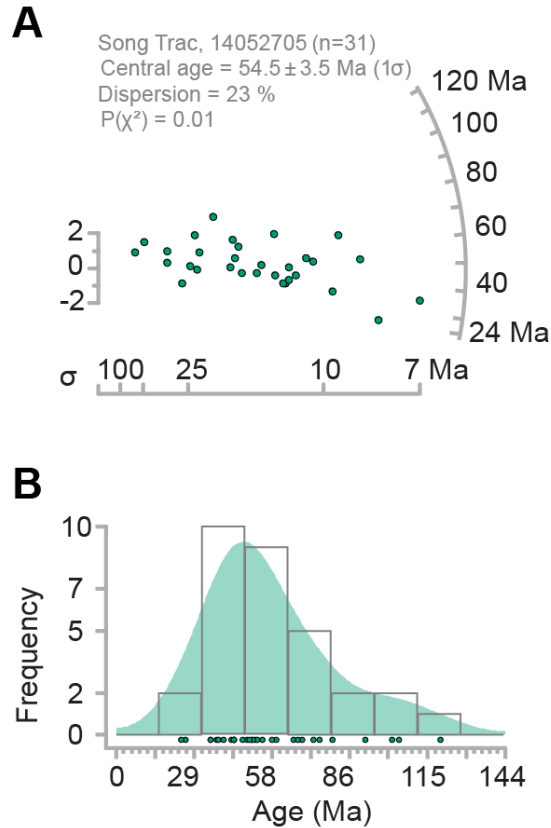


Figure 4.10. (A) Radial plot of apatite fission track data from the Song Trac tributary showing an approximately single population clustered around a central age of 54 Ma. (B) A KDE plot of the apatite fission track data.

dated at $\sim 320 \pm 90$ years ago within the Song Trac, standing 3–4 m above the modern river level. The youngest terrace, also found in the Song Trac, is elevated only ~ 1.5 m above the modern river and constructed against the 320 ± 90 years terrace. This was dated at 150 ± 140 years ago.

4.6 Discussion

4.6.1 Chemical Weathering

The degree of chemical weathering in the Song Gianh is not especially high but is largely a function of the quartz-rich, coarse-grained character of the sediments. Figure 4.5 compares our samples with bulk sediments from the Mekong, Pearl and Red Rivers (Liu

et al., 2007). Analyses from the Pearl and Mekong Rivers are limited to fine-grained sediments and are not surprisingly more altered than Song Gianh sediment. Red River sediments, however, also span sandier compositions and are generally lower in CIA (Clift et al., 2008b) than the Song Gianh at any given silica composition. This implies that the Song Gianh sediments are more altered than those found in the Red River. Sediments from the Song Gianh reach extremely high silica contents by the river mouth. Because the Red River and the Song Gianh have very similar climates, we argue this stronger degree of chemical weathering is a reflection of the long-term tectonic stability of the Song Gianh Basin compared with the still tectonically active drainage basin of the Red River (Michel et al., 2001; Zuchiewicz et al., 2013). This is despite the fact that the Song Gianh is a smaller basin than the Red River, and would be expected to have much shorter sediment transport time. If relief and tectonic activity are lower in the Song Gianh than the Red River then this would favor longer residence of sediment on hillslopes and in unincised river terraces that would allow more alteration to occur.

The downstream variation in CIA might suggest reduced chemical weathering with longer sediment transport (Fig. 4.6), but we believe that this trend is largely a grain-size and quartz content effect. Longer transport typically produces increased chemical weathering in contrast to what we observe here.

It is noteworthy that the terrace sediments, regardless of age, have lower CIA values than the adjacent modern river (Fig. 4.6), although the youngest terraces are the least weathered. This may imply that the modern river is in a state of disequilibrium and presently carries more weathered material than what has been carried in the geologic past. This observation is surprising because sediment stored in terraces has more time to

become weathered than sediment recently derived from bedrock. Evidence from the Amazon Basin suggests that the amount of weathering in flood plains may be rather low (Bouchez et al., 2012), but even if that were true we would not expect terraces to be less weathered than sediment in the adjacent river. We suggest the current highly weathered character of the modern river sediments reflects reworking of old weathered soils as a result of agriculture and/or deforestation, as noted in the Red River and Pearl River systems (Hu et al., 2013; Wan et al., 2015). Although settlement in northern Vietnam is known from ~11 ka population densities remained low and early communities were reliant on hunter-gatherer methods that did not greatly impact erosion (Rabett, 2012). However, rice cultivation spread to the Red River delta after ~3300 yr BP (Li et al., 2006; Sweeney and McCouch, 2007; Fuller, 2011) and would have spread further south after that time. Plowing related to the spread in agriculture into the Song Gianh Basin may have disturbed old, strongly weathered soils that have been reworked into the modern river. This process should continue as the region becomes more densely settled today.

4.6.2 Sediment Provenance

Provenance of the bulk sediment can in part be constrained by the Sr and Nd isotopic values. Although we consider only the bedload our study may have wider applicability to the total load as a global compilation by Turowski et al. (2010) indicates that sandy rivers like the Song Gianh carry 30–50% of their load as bedload. Figure 4.5 shows that one Song Trac sample overlaps, with sediments from the Red Rivers (Liu et al., 2007), suggesting erosion from similar bedrock types. It is clear that there is no sediment derivation from bedrock in the Central Highlands or other equivalent sources because the Song Gianh does not drain these areas. The high $^{87}\text{Sr}/^{86}\text{Sr}$ values may reflect

higher chemical weathering and are not simply provenance driven, as shown by the lack of close correlation between the Sr and Nd isotopes (Fig. 4.7). Sr isotopes do not correlate closely with CIA or other weathering proxies either because there is also a provenance influence on these values. Nonetheless, Song Gianh samples largely have more negative ϵ_{Nd} values compared to the Red River or the basement rocks of the Kontum Massif, which is the closest characterized bedrock exposure known in the literature (Lan et al., 2003). The data from the Red River and Kontum Massif may be interpreted as possibly representative of the average bedrock sources of Indochina. These data suggest that the Song Gianh is preferentially eroding more ancient crustal material (negative ϵ_{Nd}) than is typical of Indochina and may likely represent local compositional heterogeneity within the Indochina Block.

Variability in Sr isotopes in the upper reaches of the Song Gianh is followed by little variation downstream of the Mai Hoa confluence (Fig. 4.8). This pattern suggests that there is significant sediment addition upstream of that point and that there is little addition downstream. In particular, we note that the mainstream does not change substantially downstream of the Mai Hoa and Rao Tro confluences in terms of the Sr isotope compositions. This argues that these tributaries are not significant sources of sediment, although it is possible that influx from the Rao Tro is balanced by the more negative ϵ_{Nd} contributions from the southern tributaries. The $^{87}\text{Sr}/^{86}\text{Sr}$ values for the southern tributaries, however, argue against this possibility because their values lie quite close to the mainstream $^{87}\text{Sr}/^{86}\text{Sr}$ values. If there had been significant sediment input from the Rao Tro, in order to produce the $^{87}\text{Sr}/^{86}\text{Sr}$ values seen at the river mouth, very large quantities of sediment would have to be supplied from the southern tributaries to balance

that addition. We consider this to be unlikely.

To help understand the different influences from individual tributaries Kolmogorov-Smirnov distances between samples were fed into a multidimensional scaling (MDS) algorithm to convert the data into a 'map' (Fig. 4.11) to display the relative distances (similarities) between the data (Vermeesch, 2013). The map shows most samples cluster on the right hand side of the plot reflecting a mixing of sources and similarity in the spectrum of U-Pb ages. A notable exception is the sample from Rao Tro (12061712), which has a narrow range of ages, mostly confined to the early Mesozoic. The upper reaches of the Rao Tro include granites of this age. The drainage of a nearby sample (12061711) from the middle reaches of the mainstream contains a much wider range of older zircon ages reflecting erosion of Triassic clastic sedimentary rocks. Granites also dominate in the southwest of the catchment, however samples from the Song Trac, which drains this area, show a mix with older zircons ages indicating that the Triassic sedimentary rocks from the upper reaches are mixing with eroded granite. Interestingly, the sample from the river mouth only contains a moderate component of the older ages diagnostic of Triassic clastic rocks and shows similarities to the sample from the Rao Tro in containing a larger proportion of granitic ages. This suggests that the granite-rich northeastern part of the catchment is producing a significant amount of the zircons.

This provenance model for at least the 63–250 μm fraction can be further tested by examination of the KDE plots. A wide variety of different spectra are found across the basin (Fig. 4.9) but the Rao Tro and mainstream river show distinctive similarity in having a prominent Indosinian ~250 Ma peak. The source of sediment to the river mouth

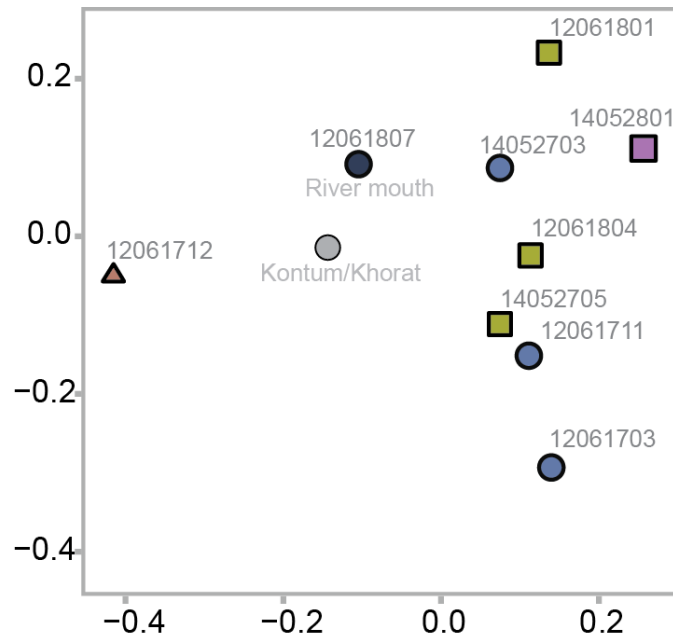


Figure 4.11. Multidimensional scaling (MDS) plot showing the Kolmogorov-Smirnov distances between sample zircon age spectra, following the method of Vermeesch (2013). Sample colors follow Figure 4.1.

is clearly more complicated because of the appearance of older zircon populations that are uncommon in the Rao Tro sample. Note that the river mouth does not plot directly with the Rao Tro sample in Figure 4.11. The ~1800 Ma peak observed in the upper reaches of the mainstream has disappeared in the river mouth sample, suggesting that substantial volumes of zircon-bearing sediment has been added to the mainstream, downstream of sample 12961711. Significant Rao Tro sediment flux to the mainstream is required to dilute the sediment from the upper reaches and generate the spectrum from the river mouth. Modest flux from the Song Nan may account for the smaller age peak at ~450 Ma seen at the river mouth. Likewise, major input from the Song Trac can be ruled out based on the lack of prominent peaks older than ~700 Ma in the river mouth sample but which are typical of the Song Trac.

We can further evaluate the input of sediment if we track the relative abundance

of diagnostic zircon age populations downstream (Figs. 4.12A-E). Using the KDE diagrams we define the following as diagnostic populations, whose abundance can be used to understand sediment mixing: 100–380 Ma, 380–500 Ma, 700–1100 Ma, 1750–2200 Ma, and 2200–2800 Ma. Zircon populations not included in these groups are ubiquitous across samples or very rarely occur. We normalized to 100% the budgets of each sample, excluding zircon outside these five groups. Figure 4.12 demonstrates the evolution of the Song Gianh downstream, as well as the character of each of the major contributing tributaries. We note that there is an increase in the 100–380 Ma (Fig. 4.12A) zircon group from the upper reaches of the mainstream (20%) to the river mouth (50%). Low proportions of these 100–380 Ma grains in the southern tributaries preclude them from driving this trend. The Rao Tro could in part control this evolution because 100–380 Ma grains are prevalent in this tributary. This interpretation is consistent with the trends observed in the 1750–2200 Ma (Fig. 4.12D) and 2200–2800 Ma (Fig. 4.12E) plots, although contribution from the southern tributaries could explain the changes in these two groups downstream.

In contrast, the downstream increase in 380–500 Ma (Fig. 4.12B) and 700–1100 Ma (Fig. 4.12C) zircons would seem to argue for influx from the southern tributaries that are relatively rich in those zircon groups compared to the northern Rao Tro. This inconsistency suggests that our samples are not perfect representatives of the long-term flux of the river. Furthermore, we have not fully characterized all the smaller tributaries contributing to the mainstream, such as along the middle reaches. Nonetheless, based on the data that we do have and statistically supported by MDS, the Rao Tro or other rivers rich in 100–380 Ma zircon must be important contributors to the total zircon budget of

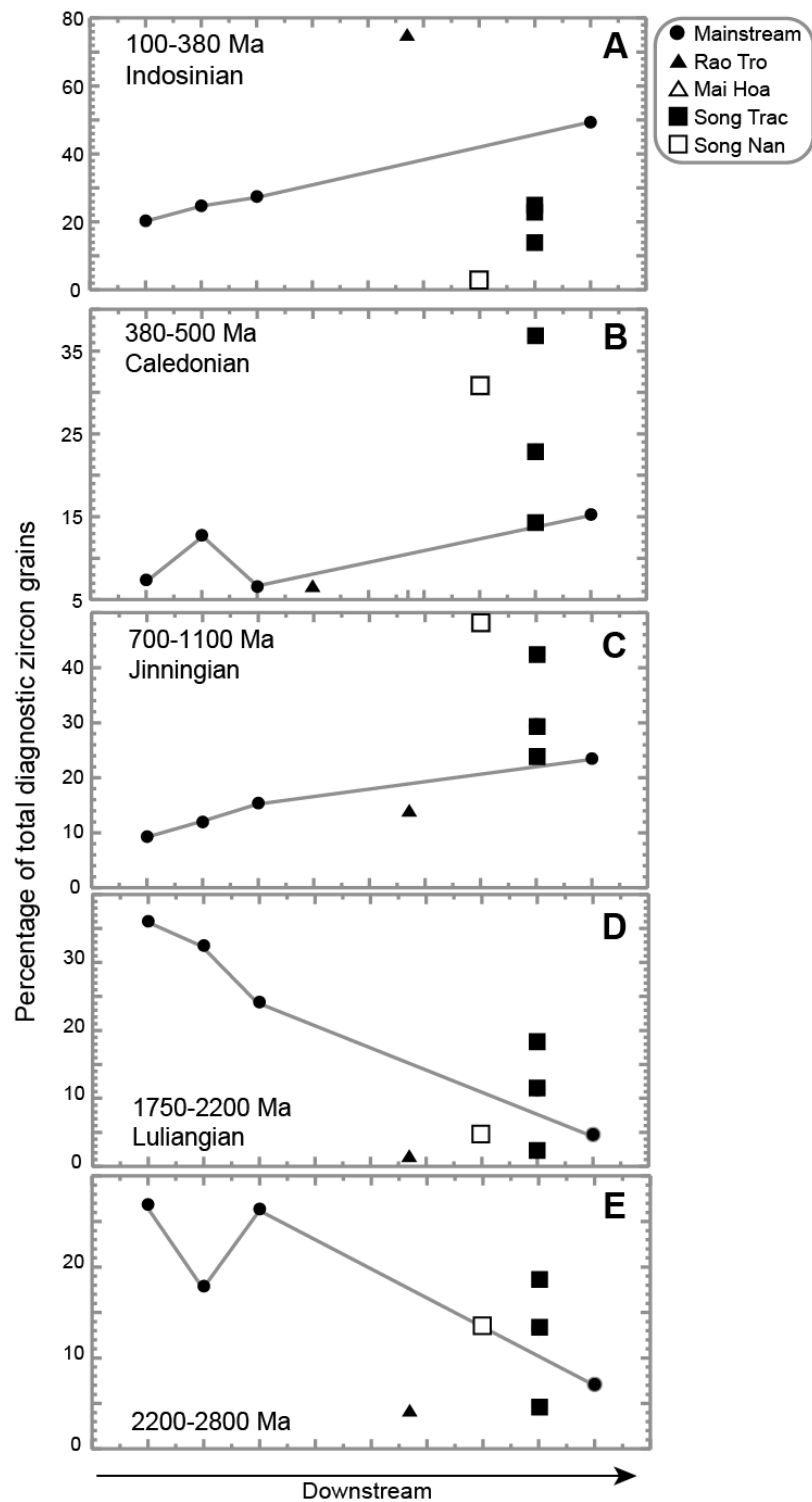


Figure 4.12. Plots showing downstream variation in specific age populations (A-E) within the mainstream (black dots linked by a solid line) and major tributaries showing how addition of sediment from the tributaries acts (or not) to influencing the bulk composition downstream of the confluence.

the 63–250 μm fraction. In particular, the fact that the 100–380 Ma zircon group accounts for almost half of the total zircon at the river mouth is striking. We note that more analyzed grains (Pullen et al., 2014) would provide a more accurate estimate of the frequency of each age population, but we are confident in that no analytical bias can account for the 20% to 50% change in 100–380 Ma zircons.

4.6.3 Fluvial Disequilibrium

If we accept the conclusions of the detrital zircon budget there is clearly a discrepancy between the results of our bulk sediment isotope and zircon data. The former suggests large-scale sediment generation in the upper reaches of the mainstream, while the latter argues for significant input from the Rao Tro (Figs. 4.8 and 4.12). One possible solution to this mismatch is that the bulk sediment is dominated by material finer than the analyzed zircon fraction (63–250 μm). Although possible, our bulk samples tended to be sandy and not contain large amounts of fine material. It is unlikely the upper reaches are misrepresented by considerable fining downstream, as the upper reaches contain higher relief, steeper slopes, and greater precipitation that result in strong hydraulic conditions that can preferentially transport both coarser bulk sediment and finer zircon downstream. This does not preclude fining but suggests its effect is not significant if coarser material is transported more quickly from the upper reaches.

Hydrodynamic sorting should not provide significant bias in our analyzed zircon. Yang et al. (2012) find that the 63–125 μm size fraction of detrital zircon in large river systems is a robust and does not significantly skew the distribution of age populations from those present in the bulk river sediment samples. However, we note that our selected size fraction for zircon analysis (63–250 μm) accounts for all but the coarsest

silt-sized zircon. Zircon populations travelling from the upper reaches that abrade over long distance transport, could concentrate in the suspended load ($<63\text{ }\mu\text{m}$) that we do not analyze here. By analyzing sediment of $63\text{--}250\text{ }\mu\text{m}$ rather than $63\text{--}125\text{ }\mu\text{m}$, it is possible we may also preferentially incorporate more large, young zircons as they have not gone through as many erosion cycles as older populations, although since all our samples were taken in the same way this bias would apply equally to all our analyses.

It is conceivable that phases rich in Nd are travelling through the river at a different rate than the zircons, so that if erosion patterns changed in the past the two systems might not be in agreement in a river that is in disequilibrium. Garçon et al. (2014) showed that monazite strongly controls the Nd content of bulk sediments. Monazite however, has a high density similar to that of zircon, so it is questionable whether these two phases would be separated by hydrodynamic sorting despite moderate differences in crystal morphology.

Garçon et al. (2014) recognized the possible role of biotite, clay, and titanite as other Nd controlling phases. Consequently preferential sorting of biotite compared to zircon could explain this discrepancy provided erosion patterns have changed in the past. Effectively, the lag time in zircon transport relative to micaceous Nd-rich phases is significant because of their morphology and density. Changing monsoon strength might be expected to change erosion patterns. Furthermore settlement/farming patterns would influence the erosion of floodplains and fluvial terraces so that the river sediment compositions could change on millennial timescales. Because these erosional signals travel at variable rates through the river depending on the mineral phase, different proxies yield contrasting results from the same sample. Although we have no independent control

on how quickly the river composition has changed we anticipate that this would be on millennial and centennial time scales if climatic and anthropogenic processes are the primary controls on erosion.

It has been suggested that the sediment loads in rivers may change markedly along the mainstream if sedimentation and capture of material can take place in depocenters along the transport path followed by additional erosion from other sources downstream (Nie et al., 2015). In theory this could explain why the river mouth sediment appears similar to terrace sediments in terms of the CIA, However, this model was developed for the much larger Yellow River where suitable buffering capacity exists. No appropriate depocenter is known in the Song Gianh and the volumes of recycled material from the terraces in this small river systems are insufficient to explain the downstream compositional changes in this way.

There is no suggestion of large-scale drainage capture in the recent past in this basin or its neighbors. While drainage capture is important in the Red River during the Miocene (Clark et al., 2004) this was a time of active deformation in that river basin. In contrast, the Song Gianh appears to be draining a retreating passive margin escarpment and is similar to its neighbors in slowly advancing into the Mekong drainage on the west side of the Annamite Range, but any changes would be slow in the recent past because the margin formation dates from break-up of South China Sea in the Oligocene (Clift and Sun, 2006). We discount drainage reorganization as a key control on fluvial disequilibrium in this study.

Lithological variability between tributaries might be an additional reason why different provenance proxies tell different stories about the source of the sediment. It is

possible that the upper reaches might contain many source rocks rich in Nd while the Rao Tro contains rocks rich in zircon, but we consider this less likely. Using Zr contents as a proxy for zircon abundance (Amidon et al., 2005) would suggest that the Song Nan and parts of the Song Trac might be rich in zircon, not the Rao Tro (Fig. 4.2). It is possible that rocks rich in 100–380 Ma zircons, but with mainstream type ϵ_{Nd} values, are exposed in the slopes that provide sediment directly into the mainstream along its upper reaches and that these might dominate the sediment budget and explain the apparent mismatch. A combination of these factors may explain the contrasting provenance proxies of the Song Gianh.

Bedrock in the Song Gianh comprises rocks deformed in the Indosinian Orogeny so that strata are not generally flat bedded. Steep dipping strata may have generated waves of incision that contribute to fluvial instability (Cook et al., 2009) and we find that three large-scale knickpoints exist in the Song Gianh. The largest knickpoint occurs in the middle to upper Song Nan and we find that this segment of the river is controlled by local bedrock strength, as the river flows underground periodically through karst for several kilometers at that location. The control on a much smaller knickpoint from the upper reaches remains less clear although correlation between local hillslope (Fig. 4.3B) and bedrock orientation and/or rock strength control is possible.

These large areas of karstic limestone that crop out in the central and southern parts of the Song Gianh Basin (Fig. 4.2) clearly do not contribute to the Sr and Nd isotopes or the zircon data presented here. The abundance of limestone in the southern parts of the Song Trac could explain why little sediment is apparently produced from this tributary, despite locally heavy rainfall, high relief and steep slopes (Fig. 4.3). Similarly

in the Song Nan limestone comprises much of the drainage. It is likely that much of the eroded carbonate is carried in solution and so consequently cannot be resolved with the methods nor in the geochemical techniques we employ here.

4.6.4 Exhumation History

With a central age of ~54.5 Ma, the Song Gianh Basin yields apatite ages that are broadly consistent with others in SE Asia (Fig. 4.10). Bedrock ages from the Kontum Massif and Khorat Plateau indicate average central ages at ~43 Ma suggesting that the Song Gianh has a typical Cenozoic exhumation history for the region. If we assume an average geothermal gradient of 25–30°C/km, then cooling from the base of the partial annealing zone (~110°C; Green et al., 1989) would be equivalent to 3.7–4.4 km of exhumation during the Cenozoic. Although central ages can be misleading if exhumation is slow, we lack sufficient number of grains to complete detailed modelling of the process and we assume a relatively simple exhumation history. If we calculate long-term exhumation rates, fission track data suggest rates of 67–81 mm/ky, equivalent to 610–737 t/yr of sediment flux.

Cosmogenic nuclide analysis indicates a denudation rate of ~30 mm/ky (Table 4.4), equivalent to only 273 t/yr discharge. This is somewhat lower than rates derived by fission track analysis. At the first-order level we can say that recent rates of exhumation of the siliciclastic bedrock are slower than the long-term average, so must therefore have decreased over the Cenozoic. This is consistent with thermal models for passive margin evolution with rapid erosion and cooling during the early stages of rifting and break-up followed by a slowing of rates during passive margin thermal subsidence (Gallagher et al., 1995; Brown et al., 2002; Persano et al., 2002).

Constraints on the erosion history for the Song Gianh have implications for our understanding for how the adjacent Song Hong-Yinggehai Basin has been filled since its opening in the Eocene. This basin is typically considered to have been filled by flux from the Red River, and it has been noted that the volume of sediment in the basin far exceeds the amount of erosion within the modern Red River catchment (Clift et al., 2006). This observation was used to argue for a paleo-Red River that far exceeds the modern catchment, in agreement with models that proposed the Red River as a former dominant drainage of East Asia prior to large-scale Tibetan Plateau uplift (Brookfield, 1998; Clark et al., 2004). However, this approach ignored possible flux into the basin from Hainan Island and coastal Vietnam. While fission track studies confirm that erosion from Hainan has been modest (Shi et al., 2011) and largely directed to the south (Clift and Sun, 2006), the same is not true of the coastal ranges of northern Vietnam. Hoang et al. (2010b) noted that clinoforms prograde from the Vietnamese coast into the basin indicating significant flux from Vietnam.

If 3.7–4.4 km of rock has been eroded over the 3500 km² of the Song Gianh then we can estimate the possible flux from the whole Annamite Range adjacent to the Song Hong-Yinggehai Basin, assuming that the Song Gianh is representative of the coastal area. Our fission track data would estimate that 110,000–132,000 km³ of rock have been eroded during the Cenozoic from the Song Gianh and equivalent rivers draining the Annamite Range. This would be equivalent to 132,000–158,000 km³ of sediment produced, assuming an average porosity of ~20%, as previously applied to the Song Hong-Yinggehai Basin by Clift et al. (2006). Using an estimate of 750,000 km³ for the total volume of the Song Hong-Yinggehai Basin, this implies that 17–21% of the total

volume could be accounted for by erosion of coastal Vietnam. While significant, this is insufficient to completely account for the $\sim 455,000 \text{ km}^3$ deficit between eroded and deposited volumes estimated by Clift et al. (2006). Our study suggests that drainage capture for the paleo-Red River must have been important but was perhaps less than previously envisaged (Brookfield, 1998; Clark et al., 2004).

4.6.5 Controls on Erosion Patterns

Our study identifies the upper reaches of the Song Gianh mainstream as the primary source of sediment in the basin. The zircon U-Pb data suggest a potential important contribution from the Rao Tro in the recent geologic past, reflecting the slower transport of zircon downstream relative to other mineral phases. Because the basin is tectonically inactive (Michel et al., 2001) we can exclude active rock uplift as a primary driver of erosion in this particular case, and for the development of knickpoints in the Song Gianh (Fig. 4.4). The majority of Song Gianh longitudinal profiles are without large-scale convexities or steepened lower reaches suggesting constant low uplift rates in the recent geologic past. Channels are at or near equilibrium. Local variation in bedrock lithology, channel hydraulic geometry, or increased sediment supply likely drive the smaller scale variations we observe in tributary morphologies (Lavé and Avouac, 2001; Whipple and Tucker, 2002).

Previous studies have proposed that precipitation distribution can control the efficiency of erosion in fluvial systems (Hodges et al., 2004; Bookhagen et al., 2005a). Figure 4.11A shows that there is a two-fold increase of rainfall annually in the western side of the Song Gianh Basin than in the eastern floodplains. We note that the western part of the basin experiencing the greatest annual rainfall currently produces the bulk of

the sediment delivered to the river mouth. This is despite the fact that unconsolidated sediment in the floodplains would be physically easier to remobilize. We also note that the southern Song Trac experiences heavy precipitation, but contains predominantly carbonate lithologies so does not produce siliciclastic sediment as quantified in this study. Hillslopes in the Song Gianh are also steepest in areas producing the most sediment (Fig. 4.3B) and contain the greatest local relief (Fig. 4.3C). Henck et al. (2011) suggest that erosion patterns in rivers experiencing low rock uplift rates (i.e., Yangtze River) are most strongly influenced by rainfall distribution in contrast to quickly uplifting regions (i.e., Salween and Mekong River basins) where patterns are controlled by local relief. While it is beyond the scope of this study to separate the relative influence of precipitation versus internal basin parameters, the coincidence of rainfall in areas of steeper slope and higher relief suggests correlation between these factors. We additionally note that this may be the case for at least hillslope erosion, as we do not identify contrasting channel morphologies or knickpoints in regions experiencing markedly higher or lesser precipitation and relief.

4.6.6 Terracing

Sedimentation in terraces reflects times when deposition was occurring as a result of the sediment load exceeding the carrying capacity of the river. This requires that the supply of sediment from the sources upstream was particularly high at times of valley filling. The subsequent incision of these sedimented valleys is not well dated but must come after the ages derived from the OSL dating. These ages represent the time of deposition not terrace abandonment and incision. The highest and oldest dated terrace was constructed during the early Holocene (7.4–8.5 ka), which was a time of strong

monsoon precipitation (Dykoski et al., 2005; Hu et al., 2008). Terracing of this age is also known in other monsoonal regions, such as the Western Himalaya (Bookhagen et al., 2006; Srivastava et al., 2008). Stronger erosion often correlates with times of heavy rainfall, which massively increases the sediment supply to the river. Our observation of an Early Holocene terrace is consistent with earlier work suggesting rapid erosion and sediment delivery occurs during times of strong summer monsoon (Goodbred and Kuehl, 2000; Clift et al., 2008a). Early Holocene strong rainfall is reconstructed both in South and East Asia (Enzel et al., 1999; Dykoski et al., 2005; Hu et al., 2008) and we suggest that the landscape response to this climate change was the same in Southeast Asia, as previously demonstrated in the monsoonal Himalayas (Bookhagen et al., 2005a). Although topographic relief is more subdued in northern Vietnam than in examples from South Asia (Dortch et al., 2009), landsliding and debris flows may be important in driving sediment oversupply to the main stream. The correlation between terracing and monsoon strength is clear.

The younger, lower terraces dated in the Song Gianh do not clearly correlate with any known monsoon intensification, although there is some indication of a possible modest strengthening in recent times (Dykoski et al., 2005). We suggest that it is much more likely that the increased sediment flux in the river was instead driven by the establishment of widespread agriculture. The impact of deforestation and farming, especially ploughing, is known to have generated large-scale soil erosion and sediment delivery to rivers both in Asia and worldwide (Syvitski et al., 2005; Montgomery, 2007). The extremely young age of the terracing here suggests that these younger, lower terraces are a direct result of intensified soil erosion driven by human settlement of the basin,

possibly in two phases, one medieval and one 18–19th century. We note that this disruption is too young and volumetrically too small to have greatly impacted the cosmogenic denudation rates reported here.

4.7 Conclusions

Our study highlights the utility of tectonically quiescent, monsoonally-controlled river basins for evaluating connections between the production, weathering, storage and flux of sediment. Study of a small basin moreover allows us to better characterize the erosion patterns throughout the catchment in a way that is impractical in larger river systems, where more complete sampling of all major source terranes is often impossible.

Multiple geochemical datasets from the Song Gianh indicate greatest production of siliciclastic sediment from the steep, wettest upper reaches of the basin and modest input from the tributaries downstream. However, detrital U-Pb zircon dating pinpoints large volumes of sediment flux from the northern Rao Tro tributary in a drier, lower relief part of the catchment. This apparent contrast between U-Pb zircon and bulk sediment Sr and Nd isotopic data requires that the Song Gianh River be in disequilibrium. Bulk sediment composition and flux are largely controlled by topographic and climatic processes. These are modified through the Holocene as a result of a weakening monsoon and are also influenced by sediment reworking triggered by human settlement/farming. Together these result in large scale millennial to centennial scale changes in sediment provenance.

The modern river is marked by more chemically weathered sediment than found in the river terraces. Terrace construction occurred in three pulses, the Early Holocene, 550–320 yrs ago and since ~150 yr ago. We infer that the river was oversupplied by

sediment at those times. The strong monsoon of the Early Holocene correlates with greater sediment supply and terrace construction here, as elsewhere in South Asia.

Younger terraces are most likely a result of anthropogenic erosion related to agriculture because there is no evidence for a strengthening of the monsoon at that time.

Song Gianh exhumation rates derived from detrital apatite fission track and concurrent ^{10}Be -derived denudation rates ^{10}Be are largely consistent with accepted models for a tectonically quiescent passive margin, undergoing thermal subsidence. Exhumation is seen to slow through time since the start of the opening of the Song Hong-Yinggehai Basin in the Eocene. Our study highlights that although rivers along the margins of central Vietnam are small, the total sediment volumes fluxed from these catchments to the Song Hong-Yinggehai Basin are significant (132,000–158,000 km³; 17–21% of the total). If one-fifth of the total sediment budget for the Song Hong-Yinggehai Basin is sourced from central Vietnam and not from the Red River, less significant river capture in the paleo-Red River is required compared to earlier models.

CHAPTER 5. SUMMARY AND CONCLUSIONS

Erosion sculpts, destroys, and recycles the Earth's continental crust in response to a combination of surface processes, controlled by climate, tectonic forcing (including rock uplift and seismic shaking) and, more recently in Earth history, anthropogenic impact. The primary focus of this dissertation was to quantify the erosional signals produced by the dynamic feedback between climate-tectonic-human processes in two mountainous Asian river landscapes. In particular, each main chapter aimed to quantify the connectivity between erosion, climate change, and landscape evolution.

Results from the NW Himalaya illustrate that modern sediment production is controlled by focused combined glacial erosion and monsoon precipitation along the High Himalaya. Glacially liberated sediments strongly dilute most other sediment signals transmitted downstream in the Zaskar River after ~8 ka. These observations demonstrate a contrast between glacial-driven erosion in the Himalayan rain shadow and monsoon-driven erosion in other Indus River tributaries draining the wet, frontal Himalaya. This work, however, recognizes the importance of the monsoon in transporting the sediment generated in the rain shadow.

Chapter 3 further highlights how strong summer monsoon climate phases at 32–25 ka and 8–6 ka coincide with major phases of fluvial aggradation in the Zaskar River. Dynamic changes in basin provenance support reworking of glacially-liberated sediment at these times into terraces as enhanced precipitation pushed farther into the rain shadow. These findings indicate discrepancies in the timing of sediment production, storage, and transport between the wet front and arid interior of the Himalaya. Large valley-fills are identified to hold considerable volumes of sediment, but much of this volume is isolated

from the modern river and not actively recycling. Conclusions from Zaskar indicate that only over significantly wet climatic intervals are these large valley-fills recycled, and it is primarily marginal basins on the edge of the Tibetan Plateau that produce and mobilize much of the total sediment exported from the Himalayan rain shadow.

Chapter 4 presents similar discrepancies between sediment production and transport even in the small, monsoonal Song Gianh. Strong monsoonal rainfall controls modern sediment generation in the steep, upper reaches of the Song Gianh and drove Early Holocene (8.5–7.4 ka) valley aggradation and incision. Late Holocene (pre-Industrial and ~150 yr BP) terrace construction instead reflects aggradation related to anthropogenic erosion rather than in response to climatic or tectonic changes. This implies that modern offshore sediments delivered by larger rivers may be strongly buffered via human-induced erosion and thus may not be representative analogs for long-term geologic processes.

The research presented in this dissertation underlies the importance of climatic processes controlling erosion even in active mountain belts with steep topography where tectonic forces are often presumed to dominate. Results here identify that monsoon intensity is important in controlling the transport of material even in the Himalayan rain shadow, as well as in coastal mountains in Southeast Asia. Although glaciation is generating much of the sediment in the Zaskar River basin, glaciation is intimately linked to moisture supply that again is primarily controlled by the summer monsoon and winter-westerlies. Although the research presented here directly involves relatively short timescales, the results from these chapters have implications for models which have proposed a strong climatic control on erosion and orogenic exhumation over longer

geologic timescales, such as those that connect development of the Greater Himalaya and the onset of the Indian summer monsoon (e.g., the channel flow; Beaumont et al., 2001; Hodges, 2006). This research is generally consistent with such models that link solid Earth tectonics with climatic forcing.

This work additionally proposes that there may be significant buffering over timescales of $>10^4$ yr between initial erosion and final transport of sediment from the high valleys in major mountain belts. This is an integral part of the total transport between source and marine sink. Although the estimated volumes involved appear to be less than those contributed from floodplains located between mountain sources and the offshore delta, the sediment volumes and durations of storage are significant in controlling the overall flux to the ocean, especially during intervals of strong summer precipitation.

Much of this work represents the most detailed investigation yet of a major rain shadow river catchment, but it is dependent on a moderate number of data sets and does not take into account the erosion of the extensive carbonate units found within the Zaskar Tethyan Himalaya or exposed in the Song Gianh. Further investigations are warranted to quantify to what extent the erosional history is influenced by carbonate erosion and dissolution as this contribution is fundamentally unquantified.

Furthermore, quantifying how grain size selections may bias the provenance conclusions derived from this work (and others) is essential. Many studies utilize only one provenance technique (e.g., U-Pb zircon) with a particular size fraction (e.g., 63–250 μm). Reducing the total sediment load to only the fine-medium sand fraction, and utilizing only one mineral phase, likely forces considerable limitations on the accurate assessment of sedimentary deposits and landscape erosion.

REFERENCES

- Adamiec, G., and Aitken, M. J., 1998, Dose rate conversion factors: update: *Ancient TL*, v. 16, p. 37-50.
- Ahmad, T., Harris, N., Bickle, M., Chapman, H., Bunbury, J., and Prince, C., 2000, Isotopic constraints on the structural relationships between the Lesser Himalayan Series and the High Himalayan Crystalline Series, Garhwal Himalaya: *Geological Society of America Bulletin*, v. 112, no. 3, p. 467-477.
- Aitken, M. J., 1998, *An introduction to optical dating*, Oxford, Oxford University Press, 240 p.:
- Alizai, A., Carter, A., Clift, P. D., VanLaningham, S., Williams, J. C., and Kumar, R., 2011, Sediment provenance, reworking and transport processes in the Indus River by U-Pb dating of detrital zircon grains: *Global and Planetary Change*, v. 76, no. 1-2, p. 33-55.
- Allen, P. A., 2008, Time scales of tectonic landscapes and their sediment routing systems: *Geological Society, London, Special Publications*, v. 296, no. 1, p. 7-28.
- Allison, M., Kuehl, S., Martin, T., and Hassan, A., 1998, Importance of flood-plain sedimentation for river sediment budgets and terrigenous input to the oceans: Insights from the Brahmaputra-Jamuna River: *Geology*, v. 26, no. 2, p. 175-178.
- Amidon, W. H., Burbank, D. W., and Gehrels, G. E., 2005, U-Pb zircon ages as a sediment mixing tracer in the Nepal Himalaya: *Earth and Planetary Science Letters*, v. 235, no. 1-2, p. 244-260.
- Anderson, J. L., and Bender, E. E., 1989, Nature and origin of Proterozoic A-type granitic magmatism in the southwestern United States of America: *Lithos*, v. 23, no. 1, p. 19-52.
- Anderson, R. S., Anderson, S. P., MacGregor, K. R., Waddington, E. D., O'Neel, S., Riihimaki, C. A., and Loso, M. G., 2004, Strong feedbacks between hydrology and sliding of a small alpine glacier: *Journal of Geophysical Research: Earth Surface*, v. 109, no. F3, p. F03005.
- Armitage, J. J., Duller, R. A., Whittaker, A. C., and Allen, P. A., 2011, Transformation of tectonic and climatic signals from source to sedimentary archive: *Nature Geoscience*, v. 4, no. 4, p. 231-235.
- Attal, M., and Lavé, J., 2006, Changes of bedload characteristics along the Marsyandi River (central Nepal): Implications for understanding hillslope sediment supply, sediment load evolution along fluvial networks, and denudation in active orogenic belts: *Geological Society of America Special Papers*, v. 398, p. 143-171.

- Bailey, R. M., and Arnold, L. J., 2006, Statistical modelling of single grain quartz De distributions and an assessment of procedures for estimating burial dose: *Quaternary Science Reviews*, v. 25, no. 19, p. 2475-2502.
- Beaumont, C., Jamieson, R. A., Nguyen, M. H., and Lee, B., 2001, Himalayan tectonics explained by extrusion of a low-viscosity crustal channel coupled to focused surface denudation: *Nature*, v. 414, no. 6865, p. 738-742.
- Beaumont, C., Kooi, H., and Willett, S., 2000, Coupled tectonic-surface process models with applications to rifted margins and collisional orogens: *Geomorphology and Global Tectonics*, p. 29-55.
- Benn, D. I., and Owen, L. A., 1998, The role of the Indian summer monsoon and the mid-latitude westerlies in Himalayan glaciation: Review and speculative discussion: *Journal of the Geological Society*, v. 155, p. 11.
- Bernet, M., van der Beek, P., Pik, R., Huyghe, P., Mugnier, J.-L., Labrin, E., and Szulc, A. G., 2006, Miocene to Recent exhumation of the central Himalaya determined from combined detrital zircon fission-track and U/Pb analysis of Siwalik sediments, western Nepal: *Basin Research*, v. 18, p. 393-412.
- Bierman, P. R., and Steig, E., 1996, Estimating rates of denudation and sediment transport using cosmogenic isotope abundances in sediment: *Earth Surface Processes and Landforms*, v. 21, p. 125-139.
- Black, L. P., Kamo, S. L., Allen, C. M., Aleinikoff, J. N., Davis, D. W., Korsch, R. J., and Foudoulis, C., 2003, TEMORA 1: A new zircon standard for Phanerozoic U-Pb geochronology: *Chemical Geology*, v. 200, p. 155-170.
- Blöthe, J. H., and Korup, O., 2013, Millennial lag times in the Himalayan sediment routing system: *Earth and Planetary Science Letters*, v. 382, p. 38-46.
- Blöthe, J. H., Korup, O., and Schwanghart, W., 2015, Large landslides lie low: Excess topography in the Himalaya-Karakoram ranges: *Geology*, v. 43, no. 6, p. 523-526.
- Blöthe, J. H., Munack, H., Korup, O., Fülling, A., Garzanti, E., Resentini, A., and Kubik, P. W., 2014, Late Quaternary valley infill and dissection in the Indus River, western Tibetan Plateau margin: *Quaternary Science Reviews*, v. 94, p. 102-119.
- Bolch, T., Kulkarni, A., Kääb, A., Huggel, C., Paul, F., Cogley, J. G., Frey, H., Kargel, J. S., Fujita, K., Scheel, M., Bajracharya, S., and Stoffel, M., 2012, The State and Fate of Himalayan Glaciers: *Science*, v. 336, no. 6079, p. 310-314.
- Böning, P., Brumsack, H.-J., Böttcher, M. E., Schnetger, B., Kriete, C., Kallmeyer, J., and Borchers, S. L., 2004, Geochemistry of Peruvian near-surface sediments: *Geochimica et Cosmochimica Acta*, v. 68, no. 21, p. 4429-4451.

- Böning, P., Brumsack, H.-J., Schnetger, B., and Grunwald, M., 2009, Trace metal signatures of Chilean upwelling sediments at ~36°S: *Marine Geology*, v. 259, p. 112–121.
- Bookhagen, B., 2010, Appearance of extreme monsoonal rainfall events and their impact on erosion in the Himalaya: *Geomatics Natural Hazards and Risk*, v. 1, no. 1, p. 37–50.
- Bookhagen, B., and Burbank, D. W., 2006, Topography, relief, and TRMM-derived rainfall variations along the Himalaya: *Geophysical Research Letters*, v. 33, no. L08405, p. L08405
- Bookhagen, B., and Burbank, D. W., 2010, Towards a complete Himalayan hydrological budget: The spatiotemporal distribution of snow melt and rainfall and their impact on river discharge: *Journal of Geophysical Research Earth Surface* (2003–2012), v. 115, p. F03019.
- Bookhagen, B., Fleitmann, D., Nishiizumi, K., Strecker, M., and Thiede, R., 2006, Holocene monsoonal dynamics and fluvial terrace formation in the northwest Himalaya, India: *Geology*, v. 34, no. 7, p. 601–604.
- Bookhagen, B., Thiede, R. C., and Strecker, M. R., 2005a, Late Quaternary intensified monsoon phases control landscape evolution in the northwest Himalaya: *Geology*, v. 33, no. 2, p. 149.
- Bookhagen, B., Thiede, R. C., and Strecker, M. R., 2005b, Abnormal monsoon years and their control on erosion and sediment flux in the high, arid northwest Himalaya: *Earth and Planetary Science Letters*, v. 231, no. 1–2, p. 131–146.
- Bouchez, J., Gaillardet, J., Lupker, M., Louvat, P., France-Lanord, C., Maurice, L., Armijos, E., and Moquet, J.-S., 2012, Floodplains of large rivers: Weathering reactors or simple silos?: *Chemical Geology*, v. 332–333, p. 166–184.
- Bracken, L. J., Turnbull, L., Wainwright, J., and Bogaart, P., 2015, Sediment connectivity: A framework for understanding sediment transfer at multiple scales: *Earth Surface Processes and Landforms*, v. 40, p. 177–188.
- Brennan, B. J., 2003, Beta doses to spherical grains: *Radiation Measurements*, v. 37, no. 4–5, p. 299–303.
- Brookfield, M. E., 1998, The evolution of the great river systems of southern Asia during the Cenozoic India-Asia collision: Rivers draining southwards: *Geomorphology*, v. 22, no. 3–4, p. 285–312.
- Brown, R. L., Summerfield, M., and Gleadow, A. J. W., 2002, Denudational history along a transect across the Drakensberg Escarpment of Southern Africa derived from apatite fission track thermochronology: *Journal of Geophysical Research*, v. 107, 2350, no. 12.

- Burbank, D., and Fort, M., 1985, Bedrock control on glacial limits: examples from the Ladakh and Zaskar ranges: North-western Himalaya, India: *Journal of Glaciology*, v. 31, no. 108, p. 143–149.
- Burbank, D. W., Blythe, A. E., Putkonen, J., Pratt-Sitaula, B., Gabet, E. J., Oskin, M., Barros, A., and Ojha, T., 2003, Decoupling of erosion and precipitation in the Himalayas: *Nature*, v. 426, p. 652–655.
- Burbank, D. W., Bookhagen, B., Gabet, E. J., and Putkonen, J., 2012, Modern climate and erosion in the Himalaya: *Comptes Rendus Geoscience*, v. 344, no. 11-12, p. 610–626.
- Burchfiel, B. C., and Royden, L., 1985, North-south extension within the convergent Himalayan region: *Geology*, v. 13, no. 10, p. 679–682.
- Carter, A., and Bristow, C. S., 2003, Linking hinterland evolution and continental basin sedimentation by using detrital zircon thermochronology: A study of the Khorat Plateau basin, eastern Thailand: *Basin Research*, v. 15, p. 271–285.
- Carter, A., and Moss, S. J., 1999, Combined detrital-zircon fission-track and U-Pb dating: A new approach to understanding hinterland evolution: *Geology*, v. 27, p. 235–238.
- Carter, A., Roques, D., Bristow, C., and Kinny, P. D., 2001, Understanding Mesozoic accretion in Southeast Asia: Significance of Triassic thermotectonism (Indosinian orogeny) in Vietnam: *Geology*, v. 29, p. 211–214.
- Carter, A., Roques, D., and Bristow, C. S., 2000, Denudation history of onshore central Vietnam: Constraints on the Cenozoic evolution of the western margin of the South China Sea: *Tectonophysics*, v. 322, p. 265–277.
- Castelltort, S., and Van Den Driessche, J., 2003, How plausible are high-frequency sediment supply-driven cycles in the stratigraphic record?: *Sedimentary Geology*, v. 157, p. 3–13.
- Cawood, P. A., Johnson, M. R., and Nemchin, A. A., 2007, Early Palaeozoic orogenesis along the Indian margin of Gondwana: Tectonic response to Gondwana assembly: *Earth and Planetary Science Letters*, v. 255, no. 1–2, p. 70–84.
- Chen, J., and Jahn, B.-M., 1998, Crustal evolution of southeastern China: Nd and Sr isotopic evidence: *Tectonophysics*, v. 284, p. 101–133.
- Chmeleff, J., von Blanckenburg, F., Kossert, K., and Jakob, D., 2010, Determination of the ^{10}Be half-life by multicollector ICP-MS and liquid scintillation counting: *Nuclear Instruments and Methods in Physics Research Section B: Beam Interactions with Materials and Atoms*, v. 268, p. 192–199.

- Clark, M. K., Schoenbohm, L. M., Royden, L. H., Whipple, K. X., Burchfiel, B. C., Zhang, X., Tang, W., Wang, E., and Chen, L., 2004, Surface uplift, tectonics, and erosion of eastern Tibet from large-scale drainage patterns: *Tectonics*, v. 23, TC1006.
- Clemens, S. C., Prell, W. L., and Sun, Y., 2010, Orbital-scale timing and mechanisms driving Late Pleistocene Indo-Asian summer monsoons: Reinterpreting cave speleothem $\delta^{18}\text{O}$: *Paleoceanography*, v. 25, no. PA4207.
- Clift, P. D., 2006, Controls on the erosion of Cenozoic Asia and the flux of clastic sediment to the ocean: *Earth and Planetary Science Letters*, v. 241, no. 3-4, p. 571-580.
- Clift, P. D., Blusztajn, J., and Nguyen, D. A., 2006, Large-scale drainage capture and surface uplift in eastern Tibet-SW China before 24 Ma inferred from sediments of the Hanoi Basin, Vietnam: *Geophysical Research Letters*, v. 33, no. L19403.
- Clift, P. D., Campbell, I. H., Pringle, M. S., Carter, A., Zhang, X., Hodges, K. V., Khan, A. A., and Allen, C. M., 2004, Thermochronology of the modern Indus River bedload: New insight into the controls on the marine stratigraphic record: *Tectonics*, v. 23, no. 5, p. TC5013.
- Clift, P. D., Carter, A., and Jonell, T. N., 2014, U-Pb dating of detrital zircon grains in the Paleocene Stumpata Formation, Tethyan Himalaya, Zaskar, India: *Journal of Asian Earth Sciences*, v. 82, p. 80–89.
- Clift, P. D., Carter, A., Krol, M., and Kirby, E., 2002, Constraints on India-Eurasia collision in the Arabian Sea region taken from the Indus Group, Ladakh Himalaya, India, *in* Clift, P. D., Kroon, D., Gaedicke, C., and Craig, J., eds., *The tectonic and climatic evolution of the Arabian Sea region*, Volume 195: London, Geological Society, p. 97–116.
- Clift, P. D., and Giosan, L., 2014, Sediment fluxes and buffering in the post-glacial Indus Basin: *Basin Research*, v. 26, no. 3, p. 369-386.
- Clift, P. D., Giosan, L., Blusztajn, J., Campbell, I. H., Allen, C. M., Pringle, M., Tabrez, A., Danish, M., Rabbani, M. M., Carter, A., and Lückge, A., 2008a, Holocene erosion of the Lesser Himalaya triggered by intensified summer monsoon: *Geology*, v. 36, no. 1, p. 79–82.
- Clift, P. D., Hoang, V. L., Hinton, R., Ellam, R., Hannigan, R., Tan, M. T., and Nguyen, D. A., 2008b, Evolving East Asian river systems reconstructed by trace element and Pb and Nd isotope variations in modern and ancient Red River-Song Hong sediments: *Geochemistry Geophysics Geosystems*, v. 9, no. Q04039.
- Clift, P. D., Lee, J. I., Hildebrand, P., Shimizu, N., Layne, G. D., Blusztajn, J., Blum, J. D., Garzanti, E., and Khan, A. A., 2002b, Nd and Pb isotope variability in the Indus River system: Implications for sediment provenance and crustal

- heterogeneity in the western Himalaya: *Earth and Planetary Science Letters*, v. 200, no. 1-2, p. 91–106.
- Clift, P. D., Shimizu, N., Layne, G. D., Blusztajn, J. S., Gaedicke, C., Schlüter, H. U., Clark, M. K., and Amjad, S., 2001, Development of the Indus Fan and its significance for the erosional history of the Western Himalaya and Karakoram: *Geological Society of America Bulletin*, v. 113, no. 8, p. 1039–1051.
- Clift, P. D., and Sun, Z., 2006, The sedimentary and tectonic evolution of the Yinggehai-Song Hong Basin and the southern Hainan margin, South China Sea: Implications for Tibetan uplift and monsoon intensification: *Journal of Geophysical Research*, v. 111, no. B6, 28.
- Clift, P. D., Vannucchi, P., and Phipps Morgan, J., 2009, Crustal redistribution, crust-mantle recycling and Phanerozoic evolution of the continental crust: *Earth Science Reviews*, v. 97, p. 80-104.
- Condie, K. C., 1993, Chemical composition and evolution of the upper continental crust: Contrasting results from surface samples and shales: *Chemical Geology*, v. 104, no. 1–4, p. 1–37.
- Cook, K. L., Whipple, K. X., Heimsath, A. M., and Hanks, T. C., 2009, Rapid incision of the Colorado River in Glen Canyon: Insights from channel profiles, local incision rates, and modeling of lithologic controls: *Earth Surface Processes and Landforms*, v. 34, no. 7, p. 994/1010.
- Craddock, W. H., Burbank, D. W., Bookhagen, B., and Gabet, E. J., 2007, Bedrock channel geometry along an orographic rainfall gradient in the upper Marsyandi River valley in central Nepal: *Journal of Geophysical Research: Earth Surface* v. 112, no. F3, p. F03007.
- Damm, B., 2006, Late Quaternary glacier advances in the upper catchment area of the Indus River (Ladakh and western Tibet): *Quaternary International*, v. 154–155, p. 87–99.
- DeCelles, P. G., Gehrels, G. E., Quade, J., LaReau, B., and Spurlin, M., 2000, Tectonic implications of U-Pb zircon ages of the Himalayan orogenic belt in Nepal: *Science*, v. 288, no. 5465, p. 497–499.
- Demske, D., Tarasov, P. E., Wünnemann, B., and Riedel, F., 2009, Late glacial and Holocene vegetation, Indian monsoon and westerly circulation in the Trans-Himalaya recorded in the lacustrine pollen sequence from Tso Kar, Ladakh, NW India: *Palaeogeography, Palaeoclimatology, Palaeoecology*, v. 279, no. 3-4, p. 172-185.
- Deniel, C., Vidal, P., Fernandez, A., Lefort, P., and Peucat, J. J., 1987, Isotopic Study of the Manaslu Granite (Himalaya, Nepal) - Inferences on the Age and Source of

- Himalayan Leukogranites: Contributions to Mineralogy and Petrology, v. 96, no. 1, p. 78-92.
- Derry, L. A., and France-Lanord, C., 1996, Neogene Himalayan weathering history and river $^{87}\text{Sr}/^{86}\text{Sr}$: Impact on the marine Sr record: Earth and Planetary Science Letters, v. 142, no. 1–2, p. 59–74.
- Dewald, A., Heinze, S., Jolie, J., Zilges, A., Dunai, T., Rethemeyer, J., Melles, M., Staubwasser, M., Kuczewski, B., and Richter, J., 2013, CologneAMS, a dedicated center for accelerator mass spectrometry in Germany: Nuclear Instruments and Methods in Physics Research Section B: Beam Interactions with Materials and Atoms, v. 294, p. 18-23.
- Dey, S., Thiede, R. C., Schildgen, T. F., Wittmann, H., Bookhagen, B., Scherler, D., Jain, V., and Strecker, M. R., 2016, Climate-driven sediment aggradation and incision since the late Pleistocene in the NW Himalaya, India: Earth and Planetary Science Letters, v. 449, p. 321-331.
- Dèzes, P. J., Vannay, J. C., Steck, A., Bussy, F., and Cosca, M., 1999, Synorogenic extension: Quantitative constraints on the age and displacement of the Zaskar shear zone (Northwest Himalaya): Geological Society of America Bulletin, v. 111, no. 3, p. 364–374.
- DiBiase, R. A., Whipple, K. X., Heimsath, A. M., and Ouimet, W. B., 2010, Landscape form and millennial erosion rates in the San Gabriel Mountains, CA: Earth and Planetary Science Letters, v. 289, no. 1–2, p. 134–144.
- Dietsch, C., Dortch, J. M., Reynhout, S. A., Owen, L. A., and Caffee, M. W., 2015, Very slow erosion rates and landscape preservation across the southwestern slope of the Ladakh Range, India: Earth Surface Processes and Landforms, v. 40, no. 3, p. 389–402.
- Dortch, J. M., Dietsch, C., Owen, L. A., Caffee, M. W., and Ruppert, K., 2011, Episodic fluvial incision of rivers and rock uplift in the Himalaya and Transhimalaya: Journal of the Geological Society, v. 168, no. 3, p. 783–804.
- Dortch, J. M., Owen, L. A., and Caffee, M. W., 2010, Quaternary glaciation in the Nubra and Shyok valley confluence, northernmost Ladakh, India: Quaternary Research, v. 74, no. 1, p. 132-144.
- Dortch, J. M., Owen, L. A., and Caffee, M. W., 2013, Timing and climatic drivers for glaciation across semi-arid western Himalayan-Tibetan orogen: Quaternary Science Reviews, v. 78, p. 188–208.
- Dortch, J. M., Owen, L. A., Haneberg, W. C., Caffee, M. W., Dietsch, C., and Kamp, D. U., 2009, Nature and timing of large-landslides in the Himalaya and Transhimalaya of northern India: Quaternary Science Reviews, v. 28, no. 11–12, p. 1037–1054.

- Dortch, J. M., Owen, L. A., Schoenbohm, L. M., and Caffee, M. W., 2011b, Asymmetrical erosion and morphological development of the central Ladakh Range, northern India: *Geomorphology*, v. 135, no. 1-2, p. 167-180.
- Duan, F., Wang, Y., Shen, C.-C., Wang, Y., Cheng, H., Wu, C.-C., Hu, H.-M., Kong, X., Liu, D., and Zhao, K., 2014, Evidence for solar cycles in a late Holocene speleothem record from Dongge Cave, China: *Nature Scientific Reports*, v. 4, no. 5159.
- Duller, G. A. T., 2008, Single-grain optical dating of Quaternary sediments: Why aliquot size matters in luminescence dating: *Boreas*, v. 37, no. 4, p. 589-612.
- Dunai, T. J., 2000, Scaling factors for production rates of *in situ*-produced cosmogenic nuclides: A critical reevaluation: *Earth and Planetary Science Letters*, v. 176, p. 157-169.
- Dykoski, C. A., Edwards, R. L., Cheng, H., Yuan, D., Cai, Y., Zhang, M., Lin, Y., Qing, J., An, Z., and Revenaugh, J., 2005, A high-resolution, absolute-dated Holocene and deglacial Asian monsoon record from Dongge Cave, China: *Earth and Planetary Science Letters*, v. 233, no. 1-2, p. 71-86.
- Dyrgerov, M. B., and Meier, M. F., 2005, *Glaciers and the changing Earth system: A 2004 snapshot*, Institute of Arctic and Alpine Research, University of Colorado Boulder.
- Enzel, Y., Ely, L. L., Mishra, S., Ramesh, R., Amit, R., Lazar, B., Rajaguru, S. N., Baker, V. R., and Sandle, A., 1999, High-resolution Holocene environmental changes in the Thar Desert, northwestern India: *Science*, v. 284, p. 125–128.
- Epard, J.-L., and Steck, A., 2008, Structural development of the Tso Moriri ultra-high pressure nappe of the Ladakh Himalaya: *Tectonophysics*, v. 451, no. 1, p. 242-264.
- Fang, J.-q., 1991, Lake evolution during the past 30,000 years in China, and its implications for environmental change: *Quaternary Research*, v. 36, no. 1, p. 37-60.
- Fedo, C. M., Nesbitt, H. W., and Young, G. M., 1995, Unraveling the effects of potassium metasomatism in sedimentary rocks and paleosols, with implications for paleoweathering conditions and provenance: *Geology*, v. 23, no. 10, p. 921–924.
- Fleitmann, D., Burns, S. J., Mudelsee, M., Neff, U., Kramers, J., Mangini, A., and Matter, A., 2003, Holocene forcing of the Indian monsoon recorded in a stalagmite from southern Oman: *Science*, v. 300, no. 5626, p. 1737-1739.
- Flint, J. J., 1974, Stream gradient as a function of order, magnitude, and discharge: *Water Resources Research*, v. 10, no. 5, p. 969-973.

- Frank, W., Thöni, M., and Purtscheller, F., 1977, Geology and petrography of Kulu-South Lahul area, *Colloquia Internationaux du CNRS* Volume 268, p. 147–160.
- Franke, D., Savva, D., Pubellier, M., Steuer, S., Mouly, B., Auxietre, J.-L., Meresse, F., and Chamot-Rooke, N., 2014, The final rifting evolution in the South China Sea: *Marine and Petroleum Geology*, v. 58B, p. 704–720.
- Frihy, O., Lotfy, M., and Komar, P., 1995, Spatial variations in heavy minerals and patterns of sediment sorting along the Nile Delta, Egypt: *Sedimentary Geology*, v. 97, no. 1, p. 33–41.
- Fromaget, J., Saurin, E., and Fontaine, H., 1971, Geological Map of Vietnam, Cambodia and Laos: National Geographic Directorate of Vietnam.
- Fuchs, G., 1987, The Geology of Southern Zaskar (Ladakh) - Evidence for the Autochthony of the Tethys Zone of the Himalaya: *Jahrbuch der Geologischen Bundesanstalt*, v. 130, no. 4, p. 465–491.
- Fuchs, M., and Owen, L. A., 2008, Luminescence dating of glacial and associated sediments: Review, recommendations and future directions: *Boreas*, v. 37, p. 636–659.
- Fuller, D., 2011, Pathways to Asian Civilizations: Tracing the Origins and Spread of Rice and Rice Cultures: *Rice*, v. 4, no. 3, p. 78–92.
- Gabet, E. J., Burbank, D. W., Pratt-Sitaula, B., Putkonen, J., and Bookhagen, B., 2008, Modern erosion rates in the High Himalayas of Nepal: *Earth and Planetary Science Letters*, v. 267, no. 3–4, p. 482–494.
- Gaetani, M., Casnedi, P., Fois, E., Garzanti, E., Jadoul, F., Nicora, A., and Tintori, A., 1986, Stratigraphy of the Tethys Himalaya in Zaskar, Ladakh: *Rivista Italiana di Paleontologia e Stratigrafia*, v. 91, no. 4, p. 443–478.
- Gaetani, M., Nicora, A., Silva, I. P., Fois, E., Garzanti, E., and Tintori, A., 1983, Upper Cretaceous and Paleocene in Zaskar Range (NW Himalaya), Milano, Istituti di geologia e paleontologia dell'Università degli studi di Milano, *Rivista Italiana di Paleontologia e Stratigrafia*.
- Galbraith, H., Hatch, J. J., Nisbet, I. C., and Kunz, T. H., 1999, Age-related changes in efficiency among breeding common terns *Sterna hirundo*: measurement of energy expenditure using doubly-labelled water: *Journal of Avian Biology*, p. 85–96.
- Galbraith, R. F., and Roberts, R. G., 2012, Statistical aspects of equivalent dose and error calculation and display in OSL dating: An overview and some recommendations: *Quaternary Geochronology*, v. 11, p. 1–27.
- Gallagher, K., Hawkesworth, C. J., and Mantovani, M. S. M., 1995, Denudation, fission track analysis and the long-term evolution of passive margin topography:

- Application to the SE Brazilian margin: *Journal of South American Earth Sciences*, v. 8, p. 65-77.
- Galy, A., and France-Lanord, C., 2001, Higher erosion rates in the Himalaya: Geochemical constraints on riverine fluxes: *Geology*, v. 29, no. 1, p. 23-26.
- Garçon, M., Chauvel, C., France-Lanord, C., Limonta, M., and Garzanti, E., 2014, Which minerals control the Nd-Hf-Sr-Pb isotopic compositions of river sediments?: *Chemical Geology*, v. 364, p. 42–55.
- Garzanti, E., and Andò, S., 2007a, Heavy mineral concentration in modern sands: Implications for provenance interpretation, *in* Mange, M. A., and Wright, D. T., eds., *Heavy Minerals in Use*, Volume 58, Elsevier, p. 517–545.
- Garzanti, E., and Andò, S., 2007b, Plate tectonics and heavy mineral suites of modern sands, *in* Mange, M. A., and Wright, D. T., eds., *Heavy Minerals in Use*, Volume 58, Elsevier, p. 741–763.
- Garzanti, E., Andò, S., France-Lanord, C., Censi, P., Vignola, P., Galy, V., and Lupker, M., 2011, Mineralogical and chemical variability of fluvial sediments 2. Suspended-load silt (Ganga-Brahmaputra, Bangladesh): *Earth and Planetary Science Letters*, v. 302, no. 1–2, p. 107–120.
- Garzanti, E., Andò, S., and Vezzoli, G., 2009, Grain-size dependence of sediment composition and environmental bias in provenance studies: *Earth and Planetary Science Letters*, v. 277, no. 3–4, p. 422–432.
- Garzanti, E., Casnedi, R., and Jadoul, F., 1986, Sedimentary evidence of a Cambro-Ordovician orogenic event in the northwestern Himalaya: *Sedimentary Geology*, v. 48, no. 3–4, p. 237–265.
- Garzanti, E., and Vezzoli, G., 2003, A classification of metamorphic grains in sands based on their composition and grade: *Journal of Sedimentary Research*, v. 73, no. 5, p. 830–837.
- Garzanti, E., Vezzoli, G., Andò, S., Lavé, J. r. m., Attal, M. l., France-Lanord, C., and DeCelles, P., 2007, Quantifying sand provenance and erosion (Marsyandi River, Nepal Himalaya): *Earth and Planetary Science Letters*, v. 258, no. 3–4, p. 500–515.
- Gasse, F., Arnold, M., Fontes, J. C., Fort, M., Gibert, E., Huc, A., Bingyan, L., Yuanfang, L., Qing, L., and Melieres, F., 1991, A 13, 000-year climate record from western Tibet: *Nature*, v. 353, no. 6346, p. 742-745.
- Gasse, F., Fontes, J. C., Van Campo, E., and Wei, K., 1996, Holocene environmental changes in Bangong Co basin (Western Tibet). Part 4: Discussion and conclusions: *Palaeogeography, Palaeoclimatology, Palaeoecology*, v. 120, no. 1, p. 79-92.

- Gazzi, P., Zuffa, G. G., Gandolfi, G., and Paganelli, L., 1973, Provenienza e dispersione litoranea delle sabbie delle spiagge adriatiche fra le foci dell'Isonzo e del Foglia: Inquadramento regionale: Memorie della Società Geologica Italiana, v. 12, p. 1–37.
- Gehrels, G. E., 2014, Detrital zircon U-Pb geochronology applied to tectonics: Annual Review of Earth and Planetary Sciences, v. 42, p. 127–149.
- Gehrels, G. E., Kapp, P., DeCelles, P., Pullen, A., Blakely, R., Weisgel, A., Ding, L., Guynn, J., Marin, A., McQuarrie, N., and Yin, A., 2011, Detrital zircon geochronology of pre-Tertiary strata in the Tibetan-Himalayan orogen: Tectonics, v. 30, no. 5, p. TC5016.
- Giles, P., Nichols, G., and Wilford, D., 2010, Alluvial Fans: From reconstructing past environments to identifying contemporary hazards: Geomorphology, v. 118, no. 1, p. 224.
- Giosan, L., Clift, P. D., Macklin, M. G., Fuller, D. Q., Constantinescu, S., Durcan, J. A., Stevens, T., Duller, G. A. T., Tabrez, A. R., Gangal, K., Adhikari, R., Alizai, A., Filip, F., VanLaningham, S., and Syvitski, J. P. M., 2012, Fluvial landscapes of the Harappan civilization: Proceedings of the National Academy of Sciences, v. 109, no. 26, p. E1688-E1694.
- Girard, M., and Bussy, F., 1999, Late Pan-African magmatism in the Himalaya: New geochronological and geochemical data from the Ordovician Tso Moriri metagranites (Ladakh, NW India): Schweizerische Mineralogische und Petrographische Mitteilungen, v. 79, no. 3, p. 399–418.
- Godard, V., Burbank, D. W., Bourlès, D. L., Bookhagen, B., Braucher, R., and Fisher, G. B., 2012, Impact of glacial erosion on ^{10}Be concentrations in fluvial sediments of the Marsyandi catchment, central Nepal: Journal of Geophysical Research: Earth Surface, v. 117, no. F3, p. F03013.
- Godin, L., 2001, The Chako Dome: An enigmatic structure in the hanging wall of the South Tibetan detachment, Nar Valley central Nepal: Journal of Asian Earth Sciences, v. 19, no. 3A, p. 22–23.
- Goldstein, S. L., O'Nions, R. K., and Hamilton, P. J., 1984, A Sm-Nd isotopic study of atmospheric dusts and particulates from major river systems: Earth and Planetary Science Letters, v. 70, no. 2, p. 221–236.
- Goodbred, S. L., 2003, Response of the Ganges dispersal system to climate change: A source-to-sink view since the last interstade: Sedimentary Geology, v. 162, no. 1–2, p. 83–104.
- Goodbred, S. L., and Kuehl, S. A., 2000, Enormous Ganges-Brahmaputra sediment discharge during strengthened early Holocene monsoon: Geology, v. 28, no. 12, p. 1083–1086.

- Granger, D. E., and Riebe, C. S., 2007, Cosmogenic Nuclides in Weathering and Erosion, *in* Drever, J. I., ed., Surface and Ground Water, Weathering, and Soils, Volume 5: London, Elsevier.
- Green, O. R., Searle, M. P., Corfield, R. I., and Corfield, R. M., 2008, Cretaceous-Tertiary carbonate platform evolution and the age of the India-Asia collision along the Ladakh Himalaya (northwest India): *Journal of Geology*, v. 116, no. 4, p. 331–353.
- Green, P. F., Duddy, I. R., Laslett, G. M., Hegarty, K. A., Gleadow, A. J. W., and Lovering, J. F., 1989, Thermal annealing of fission tracks in apatite, 4: Quantitative modelling techniques and extension to geological timescales: *Chemical Geology*, v. 79, no. 2, p. 155-182.
- Griffin, W. L., Powell, W. J., Pearson, N. J., and O'Reilly, S. Y., GLITTER: data reduction software for laser ablation ICP-MS: *Laser Ablation-ICP-MS in the earth sciences*, *in* Proceedings Mineralogical association of Canada Short Course Series 2008, Volume 40, p. 204–207.
- Guérin, G., Mercier, N., and Adamiec, G., 2011, Dose rate conversion factors: Update: *Ancient Thermo Luminescence*, v. 29, no. 1, p. 5-8.
- Gupta, A. K., Anderson, D. M., and Overpeck, J. T., 2003, Abrupt changes in the Asian southwest monsoon during the Holocene and their links to North Atlantic Ocean: *Nature*, v. 421.
- Hack, J. T., 1957, Studies of longitudinal stream profiles in Virginia and Maryland, 2330-7102.
- Hales, T., and Roering, J. J., 2007, Climatic controls on frost cracking and implications for the evolution of bedrock landscapes: *Journal of Geophysical Research: Earth Surface*, v. 112, no. F2.
- Hartmann, H., 1987, Pflanzengesellschaften trockener Standorte aus der subalpinen und alpinen Stufe im südlichen und östlichen Ladakh: *Candollea*, v. 42, no. 1, p. 277-326.
- He, M., Zheng, H., and Clift, P. D., 2013, Zircon U-Pb geochronology and Hf isotope data from the Yangtze River sands: Implications for major magmatic events and crustal evolution in Central China: *Chemical Geology*, v. 360–261, p. 186–203.
- Hedrick, K. A., Owen, L. A., Chen, J., Robinson, A., Yuan, Z., Yang, X., Imrecke, D. B., Li, W., Caffee, M. W., Schoenbohm, L. M., and Zhang, B., in press, Quaternary history and landscape evolution of a high-altitude intermountain basin at the western end of the Himalayan-Tibetan orogen, Waqia Valley, Chinese Pamir: *Geomorphology*.

- Hedrick, K. A., Seong, Y. B., Owen, L. A., Caffee, M. W., and Dietsch, C., 2011, Towards defining the transition in style and timing of Quaternary glaciation between the monsoon-influenced Greater Himalaya and the semi-arid Transhimalaya of Northern India: *Quaternary International*, v. 236, no. 1–2, p. 21–33.
- Henck, A. C., Huntington, K. W., Stone, J. O., Montgomery, D. R., and Hallet, B., 2011, Spatial controls on erosion in the Three Rivers Region, southeastern Tibet and southwestern China: *Earth and Planetary Science Letters*, v. 303, p. 71–83.
- Henderson, A. L., Najman, Y., Parrish, R., BouDagher-Fadel, M., Barford, D., Garzanti, E., and Andò, S., 2010, Geology of the Cenozoic Indus Basin sedimentary rocks: Paleoenvironmental interpretation of sedimentation from the western Himalaya during the early phases of India-Eurasia collision Tectonics, v. 29, no. 6, p. TC6015.
- Herren, E., 1987, Zaskar Shear Zone: Northeast-south-west extension within the Higher Himalaya: *Geology*, v. 15, no. 5, p. 409–413.
- Herzschuh, U., 2006, Palaeo-moisture evolution in monsoonal Central Asia during the last 50,000 years: *Quaternary Science Reviews*, v. 25, no. 1–2, p. 163–178.
- Hewitt, K., 1998, Catastrophic landslides and their effects on the Upper Indus streams, Karakoram Himalaya, northern Pakistan: *Geomorphology*, v. 26, no. 1–3, p. 47–80.
- Hewitt, K., 2002, Postglacial landform and sediment associations in a landslide-fragmented river system: The Transhimalayan Indus streams, Central Asia, *in* Hewitt, K., Byrne, M.-L., English, M., and Young, G., eds., *Landscapes of Transition: Landform Assemblages and Transformations in Cold Regions*: Dordrecht, Springer Netherlands, p. 63–91.
- Hoa, T. T., Anh, T. T., Phuong, N. T., Dung, P. T., Anh, T. V., Izokh, A. E., Borisenko, A. S., Lan, C. Y., Chung, S. L., and Lo, C. H., 2008, Permo-Triassic intermediate-felsic magmatism of the Truong Son belt, eastern margin of Indochina: *Comptes Rendus Geoscience*, v. 340, no. 2–3, p. 112–126.
- Hoang, L. V., Clift, P. D., Mark, D., Zheng, H., and Tan, M. T., 2010a, Ar-Ar Muscovite dating as a constraint on sediment provenance and erosion processes in the Red and Yangtze River systems, SE Asia: *Earth and Planetary Science Letters*, v. 295, p. 379–389.
- Hoang, L. V., Clift, P. D., Schwab, A. M., Huuse, M., Nguyen, D. A., and Zhen, S., 2010b, Large-scale erosional response of SE Asia to monsoon evolution reconstructed from sedimentary records of the Song Hong-Yinggehai and Qiongdongnan Basins, South China Sea, *in* Clift, P. D., Tada, R., and Zheng, H., eds., *Monsoon evolution and tectonic-climate linkage in Asia*, Volume 342: London, Geological Society, p. 219–244.

- Hoang, N., Flower, M. F. J., and Carlson, R. W., 1996, Major, trace element, and isotopic compositions of Vietnamese basalts: Interaction of hydrous EM1-rich asthenosphere with thinned Eurasian lithosphere: *Geochimica et Cosmochimica Acta*, v. 60, p. 4329–4351.
- Hobley, D. E., Sinclair, H. D., and Mudd, S. M., 2012, Reconstruction of a major storm event from its geomorphic signature: The Ladakh floods, 6 August 2010: *Geology*, v. 40, no. 6, p. 483–486.
- Hodges, K., 2006, A synthesis of the channel flow-extrusion hypothesis as developed for the Himalayan-Tibetan orogenic system: Geological Society, London, Special Publications, v. 268, no. 1, p. 71–90.
- Hodges, K. V., Wobus, C., Ruhl, K., Schildgen, T., and Whipple, K., 2004, Quaternary deformation, river steepening, and heavy precipitation at the front of the Higher Himalayan ranges: *Earth and Planetary Science Letters*, v. 220, no. 3–4, p. 379–389.
- Honegger, K., Dietrich, V., Frank, W., Gansser, A., Thoni, M., and Trommsdorf, V. F., 1982, Magmatism and metamorphism in the Ladakh Himalayas (The Indus-Tsangpo suture zone): *Earth and Planetary Science Letters*, v. 60, no. 2, p. 253–292.
- Horton, F., Lee, J., Hacker, B., Bowman-Kamaha'o, M., and Cosca, M., 2015, Himalayan gneiss dome formation in the middle crust and exhumation by normal faulting: New geochronology of Gianbul dome, northwestern India: *Geological Society of America Bulletin*, v. 127, no. 1–2, p. 162–180.
- Horton, F., and Leech, M. L., 2013, Age and origin of granites in the Karakoram shear zone and Greater Himalaya Sequence, NW India: *Lithosphere*, v. 5, no. 3, p. 300–320.
- Hu, C., Henderson, G. M., Huang, J., Xie, S., Sun, Y., and Johnson, K. R., 2008, Quantification of Holocene Asian monsoon rainfall from spatially separated cave records: *Earth and Planetary Science Letters*, v. 266, p. 221–232.
- Hu, D., Clift, P. D., Böning, P., Hannigan, R., Hillier, S., Blusztajn, J., Wang, S., and Fuller, D. Q., 2013, Holocene evolution in weathering and erosion patterns in the Pearl River delta: *Geochemistry Geophysics Geosystems*, v. 14.
- Hu, X.-M., Garzanti, E., An, W., and Hu, X.-F., 2015, Provenance and drainage system of the Early Cretaceous volcanic detritus in the Himalaya as constrained by detrital zircon geochronology: *Journal of Palaeogeography*, v. 4, no. 1, p. 85–98.
- Hu, X.-M., Sinclair, H. D., Wang, J., Jiang, H., and Wu, F., 2012, Late Cretaceous-Palaeogene stratigraphic and basin evolution in the Zhepure Mountain of southern Tibet: Implications for the timing of India-Asia initial collision: *Basin Research*, v. 24, no. 5, p. 520–543.

- Hurford, A., 1990, Standardization of fission track dating calibration: Recommendation by the Fission Track Working Group of the IUGS subcommission on geochronology: *Chemical Geology*, v. 80, p. 177–178.
- Inger, S., and Harris, N., 1993, Geochemical Constraints on Leucogranite Magmatism in the Langtang Valley, Nepal Himalaya: *Journal of Petrology*, v. 34, no. 2, p. 345–368.
- Ingersoll, R. V., Bullard, T. F., Ford, R. L., Grimm, J. P., Pickle, J. D., and Sares, S. W., 1984, The effect of grain size on detrital modes: A test of the Gazzi-Dickinson point-counting method: *Journal of Sedimentary Petrology*, v. 54, no. 1, p. 103–116.
- Jacobsen, S. B., and Wasserburg, G. J., 1980, Sm-Nd isotopic evolution of chondrites: *Earth and Planetary Science Letters* v. 50, no. 1, p. 139–155.
- Jade, S., Rao, H. J. R., Vijayan, M. S. M., Gaur, V. K., Bhatt, B. C., Kumar, K., Jaganathan, S., Ananda, M. B., and Kumar, P. D., 2010, GPS-derived deformation rates in northwestern Himalaya and Ladakh: *International Journal of Earth Sciences*, v. 100, no. 6, p. 1293–1301.
- Jaiswal, M., Srivastava, P., Tripathi, J., and Islam, R., 2008, Feasibility of the SAR technique on quartz sand of terraces of NW Himalaya: a case study from Devprayag: *Geochronometria*, v. 31, no. 1, p. 45–52.
- Jarvis, A., Reuter, H. I., Nelson, A., and Guevara, E., 2008, Hole-filled SRTM for the globe Version 4, *in* Research, C. G. o. I. A., ed., CGIAR-CSI SRTM 90m Database <http://srtm.csi.cgiar.org>.
- Jerolmack, D. J., and Paola, C., 2010, Shredding of environmental signals by sediment transport: *Geophysical Research Letters*, v. 37, no. 19.
- Jonell, T. N., Carter, A., Böning, P., Pahnke, K., and Clift, P. D., in press, Climatic and glacial impact on erosion patterns and sediment provenance in the Himalayan rain shadow, Zaskar River, NW India: *Geological Society of America Bulletin*.
- Kamp, U., Byrne, M., and Bolch, T., 2011, Glacier fluctuations between 1975 and 2008 in the Greater Himalaya Range of Zaskar, southern Ladakh: *Journal of Mountain Science*, v. 8, no. 3, p. 374–389.
- Kirby, E., and Ouimet, W., 2011, Tectonic geomorphology along the eastern margin of Tibet: Insights into the pattern and processes of active deformation adjacent to the Sichuan Basin, *in* Gloaguen, R., and Ratschbacher, L., eds., *Growth and Collapse of the Tibetan Plateau*, Volume 353: London, Geological Society, p. 165–188.
- Kirby, E., and Whipple, K., 2001, Quantifying differential rock-uplift rates via stream profile analysis: *Geology*, v. 29, no. 5, p. 415–418.

- Kirstein, L. A., Foeken, J. P. T., Van Der Beek, P., Stuart, F. M., and Phillips, R. J., 2009, Cenozoic unroofing history of the Ladakh Batholith, western Himalaya, constrained by thermochronology and numerical modelling: *Journal of the Geological Society*, v. 166, no. 4, p. 667-678.
- Kirstein, L. A., Sinclair, H. D., Stuart, F. M., and Dobson, K., 2006, Rapid early Miocene exhumation of the Ladakh batholith, western Himalaya: *Geology*, v. 34, no. 12, p. 1049-1052.
- Korschinek, G., Bergmaier, A., Faestermann, T., Gerstmann, U. C., Knie, K., Rugel, G., Wallner, A., Dillmann, I., Dollinger, G., von Gostonski, C. L., Kossert, K., Maiti, M., Poutivtsev, M., and Remmert, A., 2010, A new value for the half-life of ^{10}Be by heavy-ion elastic recoil detection and liquid scintillation counting., : *Nuclear Instruments and Methods in Physics Research Section B: Beam Interactions with Materials and Atoms*, v. 268, p. 187-191.
- Korup, O., Montgomery, D. R., and Hewitt, K., 2010, Glacier and landslide feedbacks to topographic relief in the Himalayan syntaxes: *Proceedings of the National Academy of Sciences*, v. 107, no. 12, p. 5317-5322.
- Kwatra, S. K., Singh, S., Singh, V. P., Sharma, R. K., Rai, B., and Kishor, N., 1999, Geochemical and geochronological characteristics of the Early Paleozoic granitoids from Sutlej-Baspa Valleys, Himachal Himalayas: *Gondwana Research Group Memoirs*, v. 6, p. 145–158.
- Lan, C.-Y., Chung, S.-L., Trinh, V. L., Lo, C.-H., Lee, T.-Y., Mertzman, S. A., and Shen, J. J.-S., 2003, Geochemical and Sr-Nd isotopic constraints from the Kontum massif, central Vietnam on the crustal evolution of the Indochina block: *Precambrian Research*, v. 122, p. 7-27.
- Lavé, J., and Avouac, J. P., 2001, Fluvial incision and tectonic uplift across the Himalaya of central Nepal: *Journal of Geophysical Research*, v. 106, p. 26,561–526,592.
- Lee, S. Y., Seong, Y. B., Owen, L. A., Murari, M. K., Lim, H. S., Yoon, H. I., and Yoo, K. C., 2014, Late Quaternary glaciation in the Nun-Kun massif, northwestern India: *Boreas*, v. 43, no. 1, p. 67-89.
- Leipe, C., Demske, D., and Tarasov, P. E., 2014, A Holocene pollen record from the northwestern Himalayan lake Tso Moriri: Implications for palaeoclimatic and archaeological research: *Quaternary International*, v. 348, p. 93-112.
- Leloup, P. H., Mahéo, G., Arnaud, N., Kali, E., Boutonnet, E., Liu, D., Xiaohan, L., and Haibing, L., 2010, The South Tibet detachment shear zone in the Dinggye area: Time constraints on extrusion models of the Himalayas: *Earth and Planetary Science Letters*, v. 292, no. 1–2, p. 1–16.
- Lepvrier, C., Maluski, H., Vu, V. T., Leyreloup, A., Phan, T. T., and Vuong, N. V., 2004, The Early Triassic Indosinian orogeny in Vietnam (Truong Son Belt and Kontum

Massif): Implications for the geodynamic evolution of Indochina:
Tectonophysics, v. 393, p. 87-118.

- Li, X. H., 1999, U-Pb zircon ages of granites from the southern margin of the Yangtze Block: Timing of Neoproterozoic Jinning orogeny in SE China and implications for Rodinia assembly: *Precambrian Research*, v. 97, p. 43–57.
- Li, Z., Saito, Y., Matsumoto, E., Wang, Y., Tanabe, S., and Vu, Q. L., 2006, Climate change and human impact on the Song Hong (Red River) Delta, Vietnam, during the Holocene: *Quaternary International*, v. 144, p. 4–28.
- Li, Z. X., Li, X. H., Wartho, J. A., Clark, C., Li, W. X., Zhang, C. L., and Bao, C., 2010, Magmatic and metamorphic events during the early Paleozoic Wuyi-Yunkai orogeny, southeastern South China: New age constraints and pressure-temperature conditions: *Geological Society of America Bulletin*, v. 122, p. 772–793.
- Liu, Z., Colin, C., Huang, W., Le, K. P., Tong, S., Chen, Z., and Trentesaux, A., 2007, Climatic and tectonic controls on weathering in south China and Indochina Peninsula: Clay mineralogical and geochemical investigations from the Pearl, Red, and Mekong drainage basins: *Geochemistry Geophysics Geosystems*, v. 8, Q05005.
- McQuarrie, N., Robinson, D., Long, S., Tobgay, T., Grujic, D., Gehrels, G., and Ducea, M., 2008, Preliminary stratigraphic and structural architecture of Bhutan: Implications for the along strike architecture of the Himalayan system: *Earth and Planetary Science Letters*, v. 272, no. 1–2, p. 105–117.
- Mehta, P. K., 1977, Rb-Sr geochronology of the Kulu-Mandi belt: Its implications for the Himalayan tectogenesis: *Geologische Rundschau*, v. 66, no. 1, p. 156–175.
- Métivier, F., and Gaudemer, Y., 1999, Stability of output fluxes of large rivers in South and East Asia during the last 2 million years: Implications on floodplain processes: *Basin Research*, v. 11, no. 4, p. 293-303.
- Michel, G. W., Yu, Y. Q., Zhu, S. Y., Christoph, R., Becker, M., Reinhart, E., Simons, W., Ambrosius, B., Vigny, C., Chamot-Rooke, N., Le-Pichon, X., Morgan, P., and Matheussen, S., 2001, Crustal motion and block behaviour in SE Asia from GPS measurements: *Earth and Planetary Science Letters*, v. 187, no. 3-4.
- Miller, C., Thöni, M., Frank, W., Grasemann, B., Klötzli, U., Guntli, P., and Draganits, E., 2001, The early Palaeozoic magmatic event in the northwest Himalaya, India: Source, tectonic setting and age of emplacement: *Geological Magazine*, v. 138, no. 03, p. 237–251.
- Milliman, J. D., and Meade, R. H., 1983, World-wide delivery of sediment to the oceans: *Journal of Geology*, v. 91, no. 1, p. 1–21.

- Mishra, P. K., Anoop, A., Schettler, G., Prasad, S., Jehangir, A., Menzel, P., Naumann, R., Yousuf, A., Basavaiah, N., and Deenadayalan, K., 2015, Reconstructed late Quaternary hydrological changes from lake Tso Moriri, NW Himalaya: *Quaternary International*, v. 371, p. 76-86.
- Mitchell, W. A., Taylor, P. J., and Osmaston, H., 1999, Quaternary geology in Zaskar, NW Indian Himalaya: Evidence for restricted glaciation and preglacial topography: *Journal of Asian Earth Sciences*, v. 17, no. 3, p. 307–318.
- Mohtadi, M., Oppo, D. W., Steinke, S., Stuut, J.-B. W., Pol-Holz, R. D., Hebbeln, D., and Lückge, A., 2011, Glacial to Holocene swings of the Australian-Indonesian monsoon: *Nature Geoscience*, v. 4, p. 540-544.
- Montgomery, D. R., 2007, *Dirt: The erosion of civilizations*, Berkeley, University of California Press, 285 p.:
- Munack, H., Blöthe, J. H., Fülöp, R. H., Codilean, A. T., Fink, D., and Korup, O., 2016, Recycling of Pleistocene valley fills dominates 135 ka of sediment flux, upper Indus River: *Quaternary Science Reviews*, v. 149, p. 122-134.
- Munack, H., Korup, O., Resentini, A., Limonta, M., Garzanti, E., Blöthe, J. H., Scherler, D., Wittmann, H., and Kubik, P. W., 2014, Postglacial denudation of western Tibetan Plateau margin outpaced by long-term exhumation: *Geological Society of America Bulletin*, v. 126, no. 11–12, p. 1580–1594.
- Murray, A. S., and Wintle, A. G., 2000, Luminescence dating of quartz using an improved single-aliquot regenerative-dose protocol: *Radiation Measurements*, v. 32, p. 57-72.
- Myrow, P. M., Hughes, N. C., Goodge, J. W., Fanning, C. M., Williams, I. S., Peng, S., Bhargava, O. N., Parcha, S. K., and Pogue, K. R., 2010, Extraordinary transport and mixing of sediment across Himalayan central Gondwana during the Cambrian-Ordovician: *Geological Society of America Bulletin*, v. 122, no. 9–10, p. 1660–1670.
- Myrow, P. M., Hughes, N. C., Paulsen, T., Williams, I., Parcha, S. K., Thompson, K. R., Bowring, S. A., Peng, S.-C., and Ahluwalia, A. D., 2003, Integrated tectonostratigraphic analysis of the Himalaya and implications for its tectonic reconstruction: *Earth and Planetary Science Letters*, v. 212, no. 3–4, p. 433–441.
- Nagy, E. A., Maluski, H., Lepvrier, C., Schärer, U., Phan, T. T., Leyreloup, A., and Vu, V. T., 2001, Geodynamic significance of the Kontum Massif in central Vietnam: Composite $^{40}\text{Ar}/^{39}\text{Ar}$ and U-Pb ages from Paleozoic to Triassic: *Journal of Geology*, v. 109, p. 755–770.
- Nagy, E. A., Schärer, U., and Nguyen, T. M., 2000, Oligo-Miocene granitic magmatism in central Vietnam and implications for continental deformation in Indochina: *Terra Nova*, v. 12, p. 67–76.

- Nesbitt, H. W., Markovics, G., and Price, R. C., 1980, Chemical processes affecting alkalis and alkaline earths during continental weathering: *Geochimica et Cosmochimica Acta*, v. 44, no. 11, p. 1659–1666.
- Nie, J., Stevens, T., Rittner, M., Stockli, D., Garzanti, E., Limonta, M., Bird, A., Ando, S., Vermeesch, P., Saylor, J., Lu, H., Breecker, D., Hu, X., Liu, S., Resentini, A., Vezzoli, G., Peng, W., Carter, A., Ji, S., and Pan, B., 2015, Loess Plateau storage of northeastern Tibetan Plateau-derived Yellow River sediment: *Nature Communications*, v. 6.
- Noble, S. R., and Searle, M. P., 1995, Age of crustal melting and leukogranite formation from U-Pb zircon and monazite dating in the western Himalaya, Zaskar, India: *Geology*, v. 23, no. 12, p. 1135–1138.
- Noble, S. R., Searle, M. P., and Walker, C. B., 2001, Age and tectonic significance of Permian granites in western Zaskar, High Himalaya: *Journal of Geology*, v. 109, no. 1, p. 127–135.
- Ouimet, W. B., Whipple, K. X., and Granger, D. E., 2009, Beyond threshold hillslopes: Channel adjustment to base-level fall in tectonically active mountain ranges: *Geology*, v. 37, no. 7, p. 579–582.
- Owen, L., Gualtieri, L., Finkel, R., Caffee, M., Benn, D., and Sharma, M., 2002, Reply: Cosmogenic radionuclide dating of glacial landforms in the Lahul Himalaya, northern India: Defining the timing of Late Quaternary glaciation: *Journal of Quaternary Science*, v. 17, no. 3, p. 279–281.
- Owen, L. A., 2009, Latest Pleistocene and Holocene glacier fluctuations in the Himalaya and Tibet: *Quaternary Science Reviews*, v. 28, no. 21–22, p. 2150–2164.
- Owen, L. A., 2011, Quaternary Glaciation of Northern India, *Developments in Quaternary Science*, Volume 15, Elsevier, p. 14.
- Owen, L. A., and Benn, D. I., 2005, Equilibrium-line altitudes of the last glacial maximum for the Himalaya and Tibet: An assessment and evaluation of results: *Quaternary International*, v. 138–139, p. 55–78.
- Owen, L. A., Caffee, M. W., Bovard, K. R., Finkel, R. C., and Sharma, M. C., 2006, Terrestrial cosmogenic nuclide surface exposure dating of the oldest glacial successions in the Himalayan orogen: Ladakh Range, northern India: *Geological Society of America Bulletin*, v. 118, no. 3–4, p. 383–392.
- Owen, L. A., and Dortch, J. M., 2014, Nature and timing of Quaternary glaciation in the Himalayan-Tibetan orogen: *Quaternary Science Reviews*, v. 88, p. 14–54.
- Owen, L. A., Finkel, R. C., Barnard, P. L., Ma, H., Asahi, K., Caffee, M. W., and Derbyshire, E., 2005, Climatic and topographic controls on the style and timing of late Quaternary glaciation throughout Tibet and the Himalaya defined by ^{10}Be

- cosmogenic radionuclide surface exposure dating: *Quaternary Science Reviews*, v. 24, no. 12–13, p. 1391–1411.
- Owen, L. A., Finkel, R. C., and Caffee, M. W., 2002b, A note on the extent of glaciation throughout the Himalaya during the global Last Glacial Maximum: *Quaternary Science Reviews*, v. 21, no. 1–3, p. 147–157.
- Pant, R., Phadtare, N., Chamyal, L., and Juyal, N., 2005, Quaternary deposits in Ladakh and Karakoram Himalaya: A treasure trove of the palaeoclimate records: *Current Science*, v. 88, no. 11, p. 1789–1798.
- Parrish, R. R., and Hodges, K. V., 1996, Isotopic constraints on the age and provenance of the Lesser and Greater Himalayan sequences, *Nepalese Himalaya: Geological Society of America Bulletin*, v. 108, no. 7, p. 904–911.
- Pearce, N. J. G., Perkins, W. T., Westgate, J. A., Gorton, M. P., Jackson, S. E., Neal, C. R., and Chenery, S. P., 1997, A compilation of new and published major and trace element data for NIST SRM 610 and NIST SRM 612 glass reference materials: *Journal of Geostandards and Geoanalysis*, v. 21, no. 1, p. 115–144.
- Pedersen, R. B., Searle, M. P., and Corfield, R. I., 2001, U-Pb zircon ages from the Spontang Ophiolite, Ladakh Himalaya: *Journal of the Geological Society*, v. 158, no. 3, p. 513–520.
- Perron, J. T., and Royden, L., 2012, An integral approach to bedrock river profile analysis: *Earth Surface Processes and Landforms*, v. 38, no. 6, p. 570–576.
- Persano, C., Stuart, F. M., Bishop, P., and Barfod, D. N., 2002, Apatite (U-Th)/He age constraints on the development of the Great Escarpment on the southeastern Australian passive margin: *Earth and Planetary Science Letters*, v. 200, no. 1–2, p. 79–90.
- Phartiyal, B., Sharma, A., and Upadhyay, R., 2005, Quaternary geology, tectonics and distribution of palaeo-and present fluvio/glacio lacustrine deposits in Ladakh, NW Indian Himalaya: A study based on field observations: *Geomorphology*, v. 65, p. 241–256.
- Pognante, U., Castelli, D., Benna, P., Genovese, G., Oberli, F., Meier, M., and Tonarini, S., 1990, The crystalline units of the High Himalayas in the Lahul-Zaskar region (northwest India): Metamorphic-tectonic history and geochronology of the collided and imbricated Indian plate: *Geological Magazine*, v. 127, no. 02, p. 101–116.
- Pognante, U., and Lombardo, B., 1989, Metamorphic evolution of the High Himalayan Crystallines in SE Zaskar, India: *Journal of Metamorphic Geology*, v. 7, no. 1, p. 9–17.

- Pratt-Sitaula, B., Burbank, D. W., Heimsath, A., and Ojha, T., 2004, Landscape disequilibrium on 1000-10,000 year scales Marsyandi River, Nepal, central Himalaya: *Geomorphology*, v. 58, no. 1-4, p. 223-241.
- Pratt, B., Burbank, D. W., Heimsath, A., and Ojha, T., 2002, Impulsive alluviation during early Holocene strengthened monsoons, central Nepal Himalaya: *Geology*, v. 30, no. 10, p. 911.
- Prescott, J. R., and Hutton, J. T., 1994, Cosmic ray contributions to dose rates for luminescence and ESR dating: Large depths and long-term time variations: *Radiation measurements*, v. 23, no. 2, p. 497-500.
- Prins, M., Postma, G., and Weltje, G. J., 2000, Controls on terrigenous sediment supply to the Arabian Sea during the late Quaternary: The Makran continental slope: *Marine Geology*, v. 169, no. 3, p. 351-371.
- Pullen, A., Ibanez-Mejia, M., Gehrels, G. E., Ibanez-Mejia, J. C., and Pecha, M., 2014, What happens when n=1000? Creating large-n geochronological datasets with LA-ICP-MS for geologic investigations: *Journal of Analytical Atomic Spectrometry*, v. 29, p. 971-980.
- Rabett, R. J., 2012, *Human Adaptation in the Asian Palaeolithic*, Cambridge University Press, 372 p.:
- Raczek, I., Jochum, K. P., and Hofmann, A. W., 2003, Neodymium and strontium isotope data for USGS reference materials BCR-1, BCR-2, BHVO-1, BHVO-2, AGV-1, AGV-2, GSP-1, GSP-2 and eight MPI-DING reference glasses: *Journal of Geostandards and Geoanalysis*, v. 27, no. 2, p. 173-179.
- Rangin, C., Klein, M., Roques, D., Le Pichon, X., and Trong, L. V., 1995, The Red River fault system in the Tonkin Gulf, Vietnam: *Tectonophysics*, v. 243, p. 209-222.
- Rhodes, E. J., 2011, Optically stimulated luminescence dating of sediments over the past 200,000 years: *Annual Review of Earth and Planetary Sciences*, v. 39, p. 461-488.
- Richards, A., Argles, T., Harris, N., Parrish, R., Ahmad, T., Darbyshire, F., and Draganits, E., 2005, Himalayan architecture constrained by isotopic tracers from clastic sediments: *Earth and Planetary Science Letters*, v. 236, no. 3, p. 773-796.
- Rittenour, T. M., 2008, Luminescence dating of fluvial deposits: Applications to geomorphic, palaeoseismic and archaeological research: *Boreas* v. 37, p. 613-635.
- Robinson, D. M., DeCelles, P. G., and Copeland, P., 2006, Tectonic evolution of the Himalayan thrust belt in western Nepal: Implications for channel flow models: *Geological Society of America Bulletin*, v. 118, no. 7-8, p. 865-885.

- Robinson, D. M., DeCelles, P. G., Patchett, P. J., and Garzione, C. N., 2001, The kinematic evolution of the Nepalese Himalaya interpreted from Nd isotopes: *Earth and Planetary Science Letters*, v. 192, no. 4, p. 507–521.
- Robinson, R. A. J., Brezina, C. A., Parrish, R. R., Horstwood, M. S. A., Oo, N. W., Bird, M. I., Thein, M., Walters, A. S., Oliver, G. J., and Zaw, K., 2014, Large rivers and orogens: The evolution of the Yarlung Tsangpo-Irrawaddy system and the eastern Himalayan syntaxis: *Gondwana Research*, v. 26, no. 1, p. 112–121.
- Robyr, M., Hacker, B. R., and Mattinson, J. M., 2006, Doming in compressional orogenic settings: New geochronological constraints from the NW Himalaya: *Tectonics*, v. 25, no. 2, p. TC2007.
- Roe, G. H., Montgomery, D. R., and Hallet, B., 2002, Effects of orographic precipitation variations on the concavity of steady-state river profiles: *Geology*, v. 30, no. 2, p. 143–146.
- Rolland, Y., Picard, C., Pecher, A., Lapierre, H., Bosch, D., and Keller, F., 2002, The Cretaceous Ladakh arc of NW Himalaya: Slab melting and melt-mantle interaction during fast northward drift of Indian Plate: *Chemical Geology*, v. 182, no. 2–4, p. 139–178.
- Roller, S., Wittmann, H., Kastowski, M., and Hinderer, M., 2012, Erosion of the Rwenzori Mountains, East African Rift: From *in situ*-produced cosmogenic ^{10}Be : *Journal of Geophysical Research*, v. 117, no. F03003.
- Ru, K., and Pigott, J. D., 1986, Episodic rifting and subsidence in the South China Sea: *AAPG Bulletin*, v. 70, no. 9, p. 1136–1155.
- Saha, S., Sharma, M. C., Murari, M. K., Owen, L. A., and Caffee, M. W., 2015, Geomorphology, sedimentology and minimum exposure ages of streamlined subglacial landforms in the NW Himalaya, India: *Boreas*, v. 45, p. 284–303.
- Schaetzl, R. J., and Forman, S. L., 2008, OSL ages on glaciofluvial sediment in northern Lower Michigan constrain expansion of the Laurentide ice sheet: *Quaternary Research*, v. 70, no. 1, p. 81–90.
- Scherler, D., 2014, Climatic limits to headwall retreat in the Khumbu Himalaya, eastern Nepal: *Geology*, v. 42, no. 11, p. 1019–1022.
- Scherler, D., Bookhagen, B., Wulf, H., Preusser, F., and Strecker, M. R., 2015, Increased late Pleistocene erosion rates during fluvial aggradation in the Garhwal Himalaya, northern India: *Earth and Planetary Science Letters*, v. 428, p. 255–266.
- Schlup, M., Carter, A., Cosca, M., and Steck, A., 2003, Exhumation history of eastern Ladakh revealed by ^{40}Ar - ^{39}Ar and fission track ages: The Indus River-Tso Morari transect, NW Himalaya: *Journal of the Geological Society*, v. 160, p. 385–399.

- Schlup, M., Steck, A., Carter, A., Cosca, M., Epard, J.-L., and Hunziker, J., 2011, Exhumation history of the NW Indian Himalaya revealed by fission track and $^{40}\text{Ar}/^{39}\text{Ar}$ ages: *Journal of Asian Earth Sciences*, v. 40, no. 1, p. 334–350.
- Schwanghart, W., and Scherler, D., 2014, Short Communication: TopoToolbox 2: MATLAB-based software for topographic analysis and modeling in Earth surface sciences: *Earth Surface Dynamics*, v. 2, no. 1, p. 1-7.
- Searle, M. P., 1983, On the Tectonics of the Western Himalaya: *Episodes*, no. 4, p. 21-26.
- Searle, M. P., Pickering, K. T., and Cooper, D. J. W., 1990, Restoration and evolution of the intermontane Indus Molasse Basin, Ladakh Himalaya, India: *Tectonophysics*, v. 174, no. 3–4, p. 301–314.
- Searle, M. P., Waters, D. J., Rex, D. C., and Wilson, R., N., 1992, Pressure, temperature and time constraints on Himalayan metamorphism from eastern Kashmir and western Zaskar: *Journal of the Geological Society*, v. 149, no. 5, p. 753–773.
- Sharma, S., Chand, P., Bisht, P., Shukla, A. D., Bartarya, S., Sundriyal, Y., and Juyal, N., 2016, Factors responsible for driving the glaciation in the Sarchu Plain, eastern Zaskar Himalaya, during the late Quaternary: *Journal of Quaternary Science*, v. 31, no. 5, p. 495-511.
- Shellnutt, J., Bhat, G., Brookfield, M., and Jahn, B. M., 2011, No link between the Panjal Traps (Kashmir) and the Late Permian mass extinctions: *Geophysical Research Letters*, v. 38, no. 19, p. L19308.
- Shellnutt, J. G., Bhat, G. M., Wang, K.-L., Brookfield, M. E., Dostal, J., and Jahn, B.-M., 2012, Origin of the silicic volcanic rocks of the Early Permian Panjal Traps, Kashmir, India: *Chemical Geology*, v. 334, p. 154-170.
- Shellnutt, J. G., Bhat, G. M., Wang, K.-L., Brookfield, M. E., Jahn, B.-M., and Dostal, J., 2014, Petrogenesis of the flood basalts from the Early Permian Panjal Traps, Kashmir, India: Geochemical evidence for shallow melting of the mantle: *Lithos*, v. 204, p. 159–171.
- Shi, X., Kohn, B., Spencer, S., Guo, X., Li, Y., Yang, X., Shi, H., and Gleadow, A., 2011, Cenozoic denudation history of southern Hainan Island, South China Sea: Constraints from low temperature thermochronology: *Tectonophysics*, v. 504, p. 100–115.
- Shi, Y., Yu, G., Liu, X., Li, B., and Yao, T., 2001, Reconstruction of the 30–40 ka BP enhanced Indian monsoon climate based on geological records from the Tibetan Plateau: *Palaeogeography, Palaeoclimatology, Palaeoecology*, v. 169, no. 1, p. 69-83.

- Shrestha, F., Bajracharya, S., Maharjan, S., and Guo, W., 2014, GLIMS Glacier Database Version 1: Boulder, Colorado USA, NSIDC: National Snow and Ice Data Center.
- Simpson, G., and Castelltort, S., 2012, Model shows that rivers transmit high-frequency climate cycles to the sedimentary record: *Geology*, v. 40, no. 12, p. 1131-1134.
- Singh, M., Sharma, M., and Tobschall, H. J., 2005, Weathering of the Ganga alluvial plain, northern India: Implications from fluvial geochemistry of the Gomati River: *Applied Geochemistry*, v. 20, p. 1–21.
- Singh, M. P., Manda, M. M., and Sinha, P. K., 1976, The Ralaking volcanics of the Zaskar valley (Ladakh): Its geological setting, petrography, petrogeochemistry and a comparative study with the Panjal volcanics of the NW Himalaya: Geological Survey of India Miscellaneous Publications, v. 41, p. 218–228.
- Sklar, L., and Dietrich, W. E., 1998, River longitudinal profiles and bedrock incision models: Stream power and the influence of sediment supply, *in* Tinkler, K. J., and Wohl, E. E., eds., *Rivers Over Rock: Fluvial Processes in Bedrock Channels*, Volume Geophysical Monograph: Washington, D.C., American Geophysical Union, p. 237–260.
- Sláma, J., Košler, J., Condon, D. J., Crowley, J. L., Gerdes, A., Hanchar, J. M., Horstwood, M. S. A., Morris, G. A., Nasdala, L., Norberg, N., Schaltegger, U., Schoene, B., Tubrett, M. N., and Whitehouse, M. J., 2008, Plezovice zircon: A new natural reference material for U-Pb and Hf isotopic microanalysis: *Chemical Geology*, v. 249, no. 1–2, p. 1–35.
- Snyder, N. P., Whipple, K. X., Tucker, G. E., and Merritts, D. J., 2000, Landscape response to tectonic forcing: Digital elevation model analysis of stream profiles in the Mendocino triple junction region, northern California: *Geological Society of America Bulletin*, v. 112, no. 8, p. 1250-1263.
- Spring, L., Bussy, F., Vannay, J.-C., Huon, S., and Cosca, M., 1993, Early Permian granitic dykes of alkaline affinity in the Indian High Himalaya of Upper Lahul and SE Zaskar: Geochemical characterization and geotectonic implications: Geological Society, London, Special Publications, v. 74, no. 1, p. 251–264.
- Srivastava, P., Tripathi, J. K., Islam, R., and Jaiswal, M. K., 2008, Fashion and phases of late Pleistocene aggradation and incision in Alaknanda River, western Himalaya India: *Quaternary Research*, v. 70, no. 1, p. 68–80.
- Staubwasser, M., and Weiss, H., 2006, Holocene climate and cultural evolution in late prehistoric-early historic West Asia: *Quaternary Research*, v. 66, no. 3, p. 372-387.
- Steck, A., Spring, L., Vannay, J. C., Masson, H., Stutz, E., Bucher, H., Marchant, R., and Tèche, J. C., 1993, Geological transect across the northwestern Himalaya in

- eastern Ladakh and Lahul (a model for the continental collision of India and Asia): *Eclogae Geologicae Helvetiae* v. 86, no. 1, p. 219–263.
- Stolle, A., Langer, M., Blöthe, J. H., and Korup, O., 2015, On predicting debris flows in arid mountain belts: *Global and Planetary Change*, v. 126, p. 1–13.
- Stutz, E., and Thöni, M., 1987, The lower Paleozoic Nyimaling granite in the Indian Himalaya (Ladakh): New Rb/Sr data versus zircon typology: *Geologische Rundschau*, v. 76, no. 2, p. 307–315.
- Sweeney, M., and McCouch, S., 2007, The complex history of the domestication of rice: *Annals of Botany*, v. 100, no. 5, p. 951–957.
- Syvitski, J. P. M., C., V., Kettner, A. J., and Green, P., 2005, Impact of humans on the flux of terrestrial sediment to the global coastal ocean: *Science*, v. 308, p. 376–380.
- Tanaka, T., Togashi, S., Kamioka, H., Amakawa, H., Kagami, H., Hamamoto, T., Yuhara, M., Orihashi, Y., Yoneda, S., Shimizu, H., Kunimaru, T., Takahashi, K., Yanagi, T., Nakano, T., Fujimaki, H., Shinjo, R., Asahara, Y., Tanimizu, M., and Dragusanu, C., 2000, JNdi-1: A neodymium isotopic reference in consistency with LaJolla neodymium: *Chemical Geology*, v. 168, no. 3–4, p. 279–281.
- Taylor, P. J., and Mitchell, W. A., 2000, The Quaternary glacial history of the Zaskar Range, north-west Indian Himalaya: *Quaternary International*, v. 65–66, p. 81–99.
- Thakur, V., Joshi, M., Sahoo, D., Suresh, N., Jayangondapermal, R., and Singh, A., 2014, Partitioning of convergence in Northwest Sub-Himalaya: Estimation of late Quaternary uplift and convergence rates across the Kangra reentrant, North India: *International Journal of Earth Sciences*, v. 103, no. 4, p. 1037–1056.
- Thiede, R. C., Bookhagen, B., Arrowsmith, J. R., Sobel, E. R., and Strecker, M. R., 2004, Climatic control on rapid exhumation along the Southern Himalayan Front: *Earth and Planetary Science Letters*, v. 222, no. 3–4, p. 791–806.
- Thirlwall, M. F., 1991, Long-term reproducibility of multicollector Sr and Nd isotope ratio analysis: *Chemical Geology*, v. 94, no. 2, p. 85–104.
- Tu, K., Flower, M. F. J., Carlson, R. W., Zhang, M., and Xie, G., 1991, Sr, Nd, and Pb isotopic compositions of Hainan basalts (south China): Implications for a subcontinental lithosphere Dupal source: *Geology*, v. 19, p. 567–569.
- Tucker, G. E., and Whipple, K. X., 2002, Topographic outcomes predicted by stream erosion models: Sensitivity analysis and intermodel comparison: *Journal of Geophysical Research: Solid Earth*, v. 107, no. B9, p. ETG 1-1–ETG 1-16.

- Turowski, J. M., Rickenmann, D., and Dadson, S. J., 2010, The partitioning of the total sediment load of a river into suspended load and bedload: A review of empirical data: *Sedimentology*, v. 57, no. 4, p. 1126–1146.
- Vermeesch, P., 2004, How many grains are needed for a provenance study?: *Earth and Planetary Science Letters*, v. 224, p. 351–441.
- Vermeesch, P., 2012, On the visualisation of detrital age distributions: *Chemical Geology*, v. 312–313, p. 190–194.
- Vermeesch, P., 2013, Multi-sample comparison of detrital age distributions: *Chemical Geology*, v. 341, p. 140–146.
- Vermeesch, P., Resentini, A., and Garzanti, E., 2016, An R package for statistical provenance analysis: *Sedimentary Geology*, v. 336, p. 14–25.
- von Blanckenburg, F., 2005, The control mechanisms of erosion and weathering at basin scale from cosmogenic nuclides in river sediment: *Earth and Planetary Science Letters*, v. 237, p. 462–479.
- von Blanckenburg, F., Hewawasam, T., and Kubik, P., 2004, Cosmogenic nuclide evidence for low weathering and denudation in the wet tropical Highlands of Sri Lanka: *Journal of Geophysical Research*, v. 109.
- von Huene, R., and Scholl, D. W., 1991, Observations at convergent margins concerning sediment subduction, subduction erosion, and the growth of continental crust: *Reviews of Geophysics*, v. 29, no. 3, p. 279–316.
- Walker, C. B., Searle, M. P., and Waters, D. J., 2001, An integrated tectonothermal model for the evolution of the High Himalaya in western Zaskar with constraints from thermobarometry and metamorphic modeling: *Tectonics*, v. 20, no. 6, p. 810–833.
- Walker, J., Martin, M. W., Bowring, S. A., Searle, M., Waters, D. J., and Hodges, K., 1999, Metamorphism, melting, and extension: Age constraints from the High Himalayan Slab of southeast Zaskar and northwest Lahaul: *Journal of Geology*, v. 107, no. 4, p. 473–495.
- Wallis, D., Carter, A., Phillips, R. J., Parsons, A. J., and Searle, M. P., 2016, Spatial variation in exhumation rates across Ladakh and the Karakoram: New apatite fission track data from the Eastern Karakoram, NW India: *Tectonics*, v. 35, no. 3, p. 704–721.
- Wan, S., Toucanne, S., Clift, P. D., Zhao, D., Bayon, G., Yu, Z., Cai, G., Yin, X., Révillon, S., Wang, D., Li, A., and Li, T., 2015, Human impact overwhelms long-term climate control of weathering and erosion in southwest China: *Geology*, v. 43, no. 5, p. 439–442.

- Whipple, K., Wobus, C., Crosby, B., Kirby, E., and Sheehan, D., 2007, New tools for quantitative geomorphology: Extraction and interpretation of stream profiles from digital topographic data, Geological Society of America Short Course, Volume 506: Boulder, CO, GSA.
- Whipple, K. X., and Tucker, G. E., 2002, Implications of sediment-flux-dependent river incision models for landscape evolution: *Journal of Geophysical Research Solid Earth*, v. 107, no. B2, p. ETG 3-1-ETG 3-20.
- White, L. T., Ahmad, T., Ireland, T. R., Lister, G. S., and Forster, M. A., 2011, Deconvolving episodic age spectra from zircons of the Ladakh Batholith, northwest Indian Himalaya: *Chemical Geology*, v. 289, no. 3–4, p. 179–196.
- Wiedenbeck, M., Hanchar, J. M., Peck, W. H., Sylvester, P., Valley, J., Whitehouse, M., Kronz, A., Morishita, Y., Nasdala, L., Fiebig, J., Franchi, I., Girard, J. P., Greenwood, R. C., Hinton, R., Kita, N., Mason, P. R. D., Norman, M., Ogasawara, M., Piccoli, P. M., Rhede, D., Satoh, H., Schulz-Dobrick, B., Skår, O., Spicuzza, M. J., Terada, K., Tindle, A., Togashi, S., Vennemann, T., Xie, Q., and Zheng, Y. F., 2004, Further characterisation of the 91500 zircon crystal: *Geostandards and Geoanalytical Research*, v. 28, no. 1, p. 9–39.
- Winter, J. D., 2010, *Principles of Igneous and Metamorphic Petrology*, New York, Pearson, 720 p.:
- Wintle, A. G., and Murray, A. S., 2006, A review of quartz optically stimulated luminescence characteristics and their relevance in single-aliquot regeneration dating protocols: *Radiation Measurements*, v. 41, no. 4, p. 369-391.
- Wittmann, H., von Blanckenburg, F., Maurice, L., Guyot, J. L., Filizola, N., and Kubik, P. W., 2011, Sediment production and delivery in the Amazon River basin quantified by *in situ*-produced cosmogenic nuclides and recent river loads: *Geological Society of America Bulletin*, v. 123, no. 5/6, p. 934–950.
- Wobus, C., Whipple, K. X., Kirby, E., Snyder, N., Johnson, J., Spyropolou, K., Crosby, B., and Sheehan, D., 2006, Tectonics from topography: Procedures, promise, and pitfalls, *in* Willett, S. D., Hovius, N., Brandon, M. T., and Fisher, D. M., eds., *Tectonics, Climate, and Landscape Evolution*, Volume 398: Boulder, CO, Geological Society of America, p. 55-74.
- Wu, F. Y., Clift, P. D., and Yang, J. H., 2007, Zircon Hf isotopic constraints on the sources of the Indus Molasse, Ladakh Himalaya, India: *Tectonics*, v. 26, no. 2, p. TC2014.
- Wulf, H., Bookhagen, B., and Scherler, D., 2010, Seasonal precipitation gradients and their impact on fluvial sediment flux in the northwest Himalaya: *Geomorphology*, v. 118, no. 1–2, p. 13-21.

- Wulf, H., Bookhagen, B., and Scherler, D., 2012, Climatic and geologic controls on suspended sediment flux in the Sutlej River Valley, western Himalaya: *Hydrology and Earth System Sciences Discussions*, v. 9, p. 541–594.
- Wünnemann, B., Demske, D., Tarasov, P., Kotlia, B. S., Reinhardt, C., Bloemendal, J., Diekmann, B., Hartmann, K., Krois, J., and Riedel, F., 2010, Hydrological evolution during the last 15 kyr in the Tso Kar lake basin (Ladakh, India), derived from geomorphological, sedimentological and palynological records: *Quaternary Science Reviews*, v. 29, no. 9-10, p. 1138-1155.
- Wyshnytzky, C. E., Rittenour, T. M., Nelson, M. S., and Thackray, G., 2015, Luminescence dating of late Pleistocene proximal glacial sediments in the Olympic Mountains, Washington: *Quaternary International*, v. 362, p. 116–123.
- Yancheva, G., Nowaczyk, N. R., Mingram, J., Dulski, P., Schettler, G., Negendank, J. F. W., Liu, J., Sigman, D. M., Peterson, L. C., and Haug, G. H., 2007, Influence of the intertropical convergence zone on the East Asian monsoon: *Nature*, v. 445, p. 74-77.
- Yang, S., Zhang, F., and Wang, Z., 2012, Grain size distribution and age population of detrital zircons from the Changjiang (Yangtze) River system, China: *Chemical Geology*, v. 296-297, p. 26–38.
- Zhong, Z., Wang, L., Xia, B., Dong, W., Sun, Z., and Shi, Y., 2004, The dynamics of Yinggehai basin formation and its tectonic significance: *Acta Geologica Sinica*, v. 78, no. 3, p. 302-309.
- Zuchiewicz, W., Nguyen, Q. C., Zasadni, J., and Nguyen, T. Y., 2013, Late Cenozoic tectonics of the Red River Fault Zone, Vietnam, in the light of geomorphic studies: *Journal of Geodynamics*, v. 69, p. 11– 30.

APPENDIX A. CONSENT FOR CHAPTER 2



THE GEOLOGICAL SOCIETY
OF AMERICA®

SCIENCE ■ STEWARDSHIP ■ SERVICE

6 February 2016

Tara N. Jonell
Geology & Geophysics
E235 Howe-Russell-Kniffen Complex
Louisiana State University
Baton Rouge, LA 70803

Dear Tara,

Permission is granted for your use of the following material in your dissertation at Louisiana State University. In addition, LSU and its agents are granted non-exclusive license to archive and make accessible the paper, in whole or in part, in all forms of media now or hereafter known, and you have the right to use the paper in future works.

Jonell, T.N., Carter, A., Böning P., Pahnke, K. and Clift, P.D., 2016, Climatic and glacial impact on erosion patterns and sediment provenance in the Himalayan rain shadow, Zaskar River, NW India: Geological Society of America Bulletin, doi:10.1130/B31573.

Best regards,

Jeanette Hammann
Director, GSA Publications
(303) 357-1048
jhammann@geosociety.org

3300 Penrose Place, P.O. Box 9140, Boulder, Colorado 80301-9140, USA

Tel +1.303.357.1000 ■ Toll Free +1.800.472.1988 ■ Fax +1.303.357.1070 ■ www.geosociety.org

APPENDIX B. U-Pb ZIRCON AGES OF ZANSKAR RIVER SEDIMENTS

Grain No.	Pb (ppm)	U (ppm)	Ratios						Ages (Ma)						Best Age (Ma)	± 2σ
			²⁰⁶ Pb/ ²³⁸ U	± 1 σ	²⁰⁷ Pb/ ²³⁵ U	± s.e.	²⁰⁷ Pb/ ²⁰⁶ Pb	± s.e.	²⁰⁶ Pb/ ²³⁸ U	± 2σ	²⁰⁷ Pb/ ²³⁵ U	± 2σ	²⁰⁷ Pb/ ²⁰⁶ Pb	± 2σ		
Sample 08081203 Zanskar-Indus Confluence																
G53	3.4	346.7	0.0090	0.0001	0.0661	0.0026	0.0532	0.0021	57.8	1.2	65.0	5.0	337.8	25.6	57.76	1.15
G10	47.2	1149.1	0.0388	0.0002	0.2910	0.0047	0.0529	0.0008	245.5	2.9	259.3	7.1	326.2	11.7	245.51	2.85
G112	20.5	390.3	0.0478	0.0003	0.3735	0.0093	0.0565	0.0013	301.0	4.2	322.3	12.8	472.5	20.2	301.00	4.18
G52	53.5	938.6	0.0536	0.0003	0.4201	0.0070	0.0554	0.0008	336.6	3.9	356.1	9.5	427.6	13.9	336.65	3.92
G11	13.0	211.4	0.0539	0.0004	0.3858	0.0089	0.0526	0.0011	338.4	4.5	331.3	12.3	309.4	14.3	338.42	4.53
G20	59.8	890.1	0.0544	0.0003	0.4185	0.0067	0.0551	0.0008	341.3	3.9	355.0	9.2	417.1	13.3	341.30	3.91
G70	43.8	628.0	0.0557	0.0004	0.4120	0.0081	0.0530	0.0009	349.2	4.3	350.3	10.9	326.7	13.3	349.18	4.27
G110	96.7	1391.2	0.0568	0.0003	0.4549	0.0081	0.0551	0.0009	356.0	4.1	380.7	10.5	417.5	14.5	356.01	4.15
G16	18.4	266.1	0.0569	0.0004	0.4606	0.0110	0.0575	0.0012	356.6	4.9	384.7	13.9	509.6	20.2	356.62	4.88
G55	38.1	559.0	0.0585	0.0004	0.4383	0.0081	0.0547	0.0009	366.3	4.4	369.0	10.9	399.2	14.4	366.31	4.39
G50	10.5	140.6	0.0607	0.0005	0.4552	0.0121	0.0557	0.0013	379.6	5.5	380.9	15.8	439.6	20.1	379.58	5.47
G33	164.0	2772.1	0.0638	0.0004	0.5106	0.0074	0.0562	0.0007	398.6	4.5	418.9	9.6	461.9	13.1	398.63	4.48
G65	38.7	537.6	0.0639	0.0004	0.4732	0.0085	0.0543	0.0009	399.4	4.7	393.4	11.3	382.3	13.7	399.36	4.73
G106	65.2	1095.7	0.0639	0.0004	0.5525	0.0103	0.0596	0.0010	399.4	4.7	446.6	12.4	590.5	18.4	399.42	4.73
G21	71.7	927.5	0.0642	0.0004	0.5176	0.0087	0.0575	0.0009	400.9	4.7	423.5	11.1	509.2	15.5	400.94	4.72
G79	427.4	6837.1	0.0676	0.0004	0.5521	0.0083	0.0566	0.0008	421.9	4.7	446.4	10.4	477.5	13.8	421.86	4.71
G45	133.9	2081.0	0.0683	0.0004	0.5518	0.0082	0.0556	0.0007	426.1	4.7	446.2	10.1	438.0	12.9	426.09	4.71
G88	41.3	567.4	0.0686	0.0004	0.5912	0.0112	0.0616	0.0010	427.7	5.2	471.6	13.4	659.2	19.7	427.66	5.19
G80	66.6	947.5	0.0687	0.0004	0.5822	0.0102	0.0595	0.0009	428.5	5.1	465.9	12.3	584.7	17.4	428.50	5.07
G4	54.6	555.0	0.0709	0.0004	0.5714	0.0107	0.0577	0.0009	441.5	5.3	458.9	12.8	516.9	16.7	441.46	5.30
G62	425.2	6478.4	0.0717	0.0004	0.5720	0.0082	0.0556	0.0007	446.3	4.9	459.3	10.2	437.6	12.7	446.27	4.93
G104	93.5	1386.3	0.0726	0.0004	0.6089	0.0107	0.0574	0.0009	451.5	5.3	482.9	12.5	508.5	16.0	451.50	5.29
G99	46.6	517.1	0.0728	0.0005	0.6454	0.0129	0.0635	0.0011	453.0	5.5	505.7	14.7	724.0	21.6	453.00	5.53
G17	8.7	106.8	0.0745	0.0006	0.5837	0.0164	0.0575	0.0014	462.9	6.7	466.8	18.8	510.8	22.6	462.91	6.72
G89	90.0	1243.4	0.0745	0.0004	0.6056	0.0103	0.0565	0.0009	463.2	5.3	480.8	12.2	472.9	15.0	463.21	5.28
G32	85.1	1157.5	0.0746	0.0004	0.6774	0.0100	0.0640	0.0008	464.0	5.2	525.2	11.6	741.0	17.3	464.05	5.16
G40	134.5	1684.5	0.0753	0.0004	0.6096	0.0093	0.0573	0.0008	467.8	5.3	483.3	11.2	501.6	14.3	467.83	5.28
G94	67.7	942.1	0.0755	0.0005	0.6503	0.0120	0.0581	0.0009	469.0	5.5	508.7	13.2	532.8	16.9	468.97	5.51
G72	25.3	288.4	0.0755	0.0005	0.5763	0.0117	0.0557	0.0010	469.4	5.8	462.1	14.1	441.6	16.2	469.39	5.75
G25	47.3	640.0	0.0766	0.0005	0.6152	0.0097	0.0578	0.0008	475.7	5.4	486.9	11.6	522.2	14.8	475.68	5.39
G48	73.8	769.9	0.0893	0.0005	0.7244	0.0120	0.0572	0.0008	551.5	6.3	553.2	13.2	499.3	14.9	551.46	6.27

APPENDIX B (continued). U-Pb ZIRCON AGES OF ZANSKAR RIVER SEDIMENTS

Grain No.	Pb (ppm)	U (ppm)	Ratios						Ages (Ma)						Best Age (Ma)	$\pm 2\sigma$
			$^{206}\text{Pb}/^{238}\text{U}$	$\pm 1\sigma$	$^{207}\text{Pb}/^{235}\text{U}$	$\pm \text{s.e.}$	$^{207}\text{Pb}/^{206}\text{Pb}$	$\pm \text{s.e.}$	$^{206}\text{Pb}/^{238}\text{U}$	$\pm 2\sigma$	$^{207}\text{Pb}/^{235}\text{U}$	$\pm 2\sigma$	$^{207}\text{Pb}/^{206}\text{Pb}$	$\pm 2\sigma$		
G46	32.5	313.3	0.0928	0.0006	0.7128	0.0136	0.0568	0.0009	572.1	6.8	546.4	15.0	483.0	16.1	572.13	6.84
G59	15.6	169.6	0.0931	0.0007	0.8357	0.0209	0.0649	0.0013	573.6	7.8	616.8	20.0	770.8	25.6	573.61	7.78
G27	64.4	605.7	0.1075	0.0007	0.9343	0.0160	0.0642	0.0009	658.3	7.6	669.9	15.5	746.6	18.8	658.33	7.57
G9	59.9	500.7	0.1161	0.0007	1.0485	0.0165	0.0663	0.0009	707.9	8.0	728.1	15.3	816.5	18.5	707.90	7.97
G19	47.2	378.7	0.1184	0.0007	1.0724	0.0200	0.0670	0.0010	721.3	8.5	739.9	17.6	837.2	21.0	721.35	8.53
G14	133.4	725.4	0.1208	0.0007	1.2215	0.0207	0.0725	0.0010	735.2	8.4	810.5	17.0	1001.1	21.4	735.22	8.40
G82	154.6	749.9	0.1225	0.0007	1.1509	0.0199	0.0683	0.0010	744.9	8.5	777.7	17.5	876.2	21.0	744.94	8.50
G35	165.6	1178.9	0.1235	0.0007	1.1576	0.0166	0.0665	0.0008	750.7	8.1	780.8	15.0	821.5	17.7	750.68	8.15
G58	148.3	838.9	0.1237	0.0007	1.1506	0.0178	0.0660	0.0009	752.1	8.3	777.5	15.8	805.4	18.5	752.05	8.26
G24	45.2	337.3	0.1238	0.0008	1.1127	0.0190	0.0654	0.0009	752.5	8.6	759.5	16.6	786.6	19.1	752.51	8.60
G78	184.0	1037.8	0.1238	0.0007	1.1891	0.0188	0.0673	0.0009	752.6	8.3	795.5	16.4	848.0	19.5	752.63	8.26
G43	59.1	337.3	0.1251	0.0008	1.1258	0.0225	0.0670	0.0011	759.9	9.2	765.8	19.0	837.5	22.0	759.91	9.17
G12	58.3	352.9	0.1251	0.0008	1.1259	0.0190	0.0658	0.0009	760.1	8.6	765.8	16.6	800.3	19.1	760.08	8.59
G108	60.3	373.8	0.1257	0.0008	1.1488	0.0233	0.0674	0.0012	763.2	9.2	776.7	19.9	849.9	23.1	763.17	9.16
G23	133.2	896.8	0.1271	0.0007	1.1809	0.0180	0.0651	0.0009	771.2	8.5	791.7	15.5	776.9	17.7	771.24	8.46
G75	199.0	1480.6	0.1273	0.0007	1.2283	0.0188	0.0668	0.0009	772.2	8.5	813.6	16.2	831.9	19.0	772.22	8.46
G2	205.3	1598.6	0.1273	0.0007	1.1716	0.0157	0.0648	0.0008	772.3	8.2	787.4	14.2	766.5	16.3	772.33	8.23
G47	191.1	1104.6	0.1287	0.0007	1.1970	0.0180	0.0661	0.0009	780.2	8.5	799.2	15.7	810.2	18.2	780.22	8.45
G39	53.6	288.8	0.1294	0.0008	1.2760	0.0252	0.0717	0.0011	784.7	9.4	835.1	19.5	978.3	23.4	784.67	9.36
G29	157.3	1053.0	0.1297	0.0008	1.2428	0.0183	0.0680	0.0009	786.1	8.6	820.1	15.6	869.2	18.4	786.10	8.56
G1	235.8	989.3	0.1306	0.0008	1.2102	0.0170	0.0662	0.0008	791.5	8.6	805.3	15.1	813.0	17.3	791.46	8.55
G91	128.2	796.2	0.1308	0.0008	1.2384	0.0206	0.0676	0.0010	792.5	8.8	818.2	17.6	857.2	20.4	792.48	8.78
G66	144.1	721.0	0.1310	0.0008	1.2436	0.0216	0.0685	0.0010	793.4	9.0	820.5	17.7	884.6	20.7	793.40	9.01
G68	55.7	421.0	0.1311	0.0008	1.1987	0.0215	0.0668	0.0010	794.0	9.1	800.0	18.1	830.9	20.7	794.02	9.12
G44	224.3	1522.5	0.1312	0.0008	1.2514	0.0180	0.0661	0.0008	794.7	8.5	824.0	15.4	808.9	17.7	794.65	8.55
G15	87.2	433.9	0.1313	0.0008	1.1774	0.0190	0.0654	0.0009	795.0	8.9	790.1	16.3	786.9	18.4	795.05	8.89
G117	28.2	134.4	0.1315	0.0009	1.3574	0.0346	0.0745	0.0015	796.6	10.6	870.7	24.8	1054.5	29.7	796.64	10.60
G54	81.1	447.7	0.1316	0.0008	1.3062	0.0235	0.0739	0.0011	796.9	9.2	848.5	18.7	1038.7	22.8	796.93	9.23
G96	234.1	1691.6	0.1317	0.0008	1.2628	0.0210	0.0670	0.0010	797.6	8.9	829.2	17.6	837.8	20.2	797.56	8.89
G28	115.3	768.1	0.1317	0.0008	1.2151	0.0181	0.0666	0.0009	797.8	8.7	807.5	15.7	825.6	18.1	797.78	8.66
G42	50.0	315.5	0.1319	0.0008	1.2183	0.0223	0.0662	0.0010	798.5	9.2	809.0	18.1	812.4	20.4	798.47	9.23
G67	140.6	942.6	0.1320	0.0008	1.2310	0.0200	0.0649	0.0009	799.4	8.9	814.8	16.7	769.8	18.6	799.38	8.88

APPENDIX B (continued). U-Pb ZIRCON AGES OF ZANSKAR RIVER SEDIMENTS

Grain No.	Pb (ppm)	U (ppm)	Ratios						Ages (Ma)						Best Age (Ma)	$\pm 2\sigma$
			$^{206}\text{Pb}/^{238}\text{U}$	$\pm 1\sigma$	$^{207}\text{Pb}/^{235}\text{U}$	$\pm \text{s.e.}$	$^{207}\text{Pb}/^{206}\text{Pb}$	$\pm \text{s.e.}$	$^{206}\text{Pb}/^{238}\text{U}$	$\pm 2\sigma$	$^{207}\text{Pb}/^{235}\text{U}$	$\pm 2\sigma$	$^{207}\text{Pb}/^{206}\text{Pb}$	$\pm 2\sigma$		
G7	204.1	1250.6	0.1324	0.0008	1.2473	0.0179	0.0657	0.0008	801.3	8.7	822.2	15.2	797.8	17.3	801.31	8.65
G34	76.4	443.7	0.1325	0.0008	1.2147	0.0195	0.0660	0.0009	802.1	8.9	807.3	16.5	806.1	18.7	802.05	8.88
G107	69.0	308.4	0.1326	0.0008	1.2447	0.0236	0.0675	0.0011	802.9	9.3	821.0	19.4	853.9	22.1	802.91	9.33
G92	40.7	273.7	0.1327	0.0008	1.2216	0.0248	0.0662	0.0011	803.1	9.6	810.5	19.9	814.0	22.3	803.14	9.56
G83	125.0	657.8	0.1334	0.0008	1.2575	0.0215	0.0674	0.0010	806.9	9.1	826.8	17.8	850.2	20.4	806.95	9.10
G61	116.3	652.9	0.1335	0.0008	1.2716	0.0219	0.0690	0.0010	807.8	9.1	833.1	17.8	898.4	20.8	807.80	9.10
G49	94.2	626.2	0.1338	0.0008	1.2677	0.0212	0.0677	0.0010	809.4	9.1	831.3	17.2	859.4	19.8	809.39	9.10
G26	41.5	273.3	0.1340	0.0008	1.2361	0.0216	0.0666	0.0010	810.7	9.2	817.1	17.5	824.3	19.8	810.70	9.21
G56	80.8	579.0	0.1345	0.0008	1.2336	0.0198	0.0661	0.0009	813.4	9.0	816.0	16.7	809.9	18.8	813.43	8.98
G103	150.6	901.2	0.1346	0.0008	1.3305	0.0242	0.0681	0.0011	814.3	9.3	859.1	18.9	872.8	21.7	814.28	9.32
G3	111.4	613.3	0.1348	0.0008	1.2243	0.0182	0.0648	0.0008	815.1	8.9	811.7	15.6	768.5	17.3	815.13	8.86
G118	32.6	189.1	0.1365	0.0009	1.4205	0.0304	0.0751	0.0013	825.0	10.1	897.6	22.3	1070.6	26.8	824.95	10.10
G77	55.3	382.7	0.1384	0.0009	1.3002	0.0238	0.0674	0.0010	835.7	9.6	845.8	18.8	849.5	21.1	835.72	9.63
G115	50.6	202.5	0.1393	0.0009	1.3014	0.0277	0.0670	0.0012	840.6	10.2	846.3	21.4	837.2	23.6	840.59	10.18
G113	77.2	539.4	0.1393	0.0009	1.2905	0.0236	0.0670	0.0011	840.6	9.6	841.5	19.4	839.0	21.5	840.65	9.62
G105	19.2	105.0	0.1412	0.0010	1.3466	0.0344	0.0695	0.0014	851.4	11.2	866.1	24.8	912.7	27.6	851.44	11.18
G13	42.6	224.7	0.1416	0.0009	1.3931	0.0271	0.0727	0.0011	853.8	10.1	886.0	19.8	1005.0	23.1	853.82	10.05
G81	55.9	400.1	0.1418	0.0009	1.2926	0.0229	0.0661	0.0010	854.9	9.7	842.5	18.5	808.6	20.2	854.89	9.71
G93	16.6	90.8	0.1420	0.0011	1.4741	0.0442	0.0716	0.0016	855.7	12.3	919.8	27.8	975.7	31.3	855.74	12.31
G71	49.3	332.4	0.1455	0.0009	1.4065	0.0264	0.0710	0.0011	875.8	10.1	891.7	19.7	958.0	22.5	875.80	10.13
G6	120.4	628.0	0.1733	0.0010	1.7640	0.0268	0.0740	0.0009	1030.3	11.1	1032.3	18.1	1040.1	20.0	1040.10	20.03
G114	67.5	396.1	0.1615	0.0010	1.6666	0.0341	0.0741	0.0012	965.0	11.3	995.9	22.6	1043.1	25.3	1043.10	25.32
G101	117.7	702.7	0.1671	0.0010	1.8429	0.0315	0.0768	0.0011	995.9	11.0	1060.9	20.8	1115.2	23.6	1115.22	23.59
G60	111.6	514.0	0.1781	0.0011	2.0002	0.0339	0.0810	0.0011	1056.8	11.6	1115.6	20.5	1220.5	23.3	1220.47	23.31
G109	90.0	337.3	0.2438	0.0015	3.2201	0.0621	0.0938	0.0015	1406.6	15.5	1462.0	25.8	1503.7	27.9	1503.69	27.91
G38	67.8	225.6	0.2818	0.0017	3.8313	0.0711	0.0987	0.0014	1600.2	17.3	1599.3	24.1	1599.3	25.5	1599.33	25.52
G97	179.3	687.6	0.2659	0.0016	3.9390	0.0704	0.1070	0.0016	1520.0	16.3	1621.7	25.8	1749.6	28.1	1749.62	28.11
G18	100.7	287.1	0.3055	0.0018	4.7773	0.0823	0.1141	0.0015	1718.3	18.1	1780.9	23.7	1865.9	25.3	1865.87	25.33
G37	894.8	2163.8	0.4070	0.0023	8.7598	0.1204	0.1516	0.0018	2201.0	21.1	2313.3	24.2	2364.3	25.6	2364.28	25.61
G36	170.3	306.2	0.4319	0.0025	9.4071	0.1570	0.1566	0.0020	2314.1	22.9	2378.5	25.4	2419.2	26.6	2419.17	26.56
G30	101.7	210.1	0.4402	0.0027	9.7503	0.1826	0.1569	0.0020	2351.4	23.8	2411.5	25.8	2422.0	26.9	2421.98	26.88
G76	86.1	194.5	0.3941	0.0025	8.7311	0.1826	0.1584	0.0023	2141.6	22.8	2310.3	28.2	2438.9	29.7	2438.87	29.72

APPENDIX B (continued). U-Pb ZIRCON AGES OF ZANSKAR RIVER SEDIMENTS

Grain No.	Pb (ppm)	U (ppm)	Ratios						Ages (Ma)						Best Age (Ma)	$\pm 2\sigma$
			$^{206}\text{Pb}/^{238}\text{U}$	$\pm 1\sigma$	$^{207}\text{Pb}/^{235}\text{U}$	$\pm \text{s.e.}$	$^{207}\text{Pb}/^{206}\text{Pb}$	$\pm \text{s.e.}$	$^{206}\text{Pb}/^{238}\text{U}$	$\pm 2\sigma$	$^{207}\text{Pb}/^{235}\text{U}$	$\pm 2\sigma$	$^{207}\text{Pb}/^{206}\text{Pb}$	$\pm 2\sigma$		
G22	118.6	198.9	0.4972	0.0029	11.8948	0.1971	0.1755	0.0021	2601.6	25.1	2596.2	25.3	2610.7	26.3	2610.70	26.25
G116	112.5	185.1	0.5228	0.0034	14.0805	0.3280	0.1909	0.0030	2711.1	28.6	2755.1	31.9	2749.5	33.0	2749.50	32.98
G95	34.4	46.3	0.5355	0.0036	15.5570	0.4222	0.1996	0.0031	2764.6	30.6	2850.0	31.8	2822.8	32.6	2822.76	32.60
G87	58.9	97.5	0.5134	0.0034	14.4351	0.3469	0.2049	0.0030	2671.0	28.6	2778.7	30.6	2865.3	31.5	2865.31	31.55
G57	127.1	177.6	0.6100	0.0036	20.1761	0.3522	0.2395	0.0031	3070.0	28.9	3099.8	27.2	3116.5	28.2	3116.45	28.23
G69	8.6	3043.6	0.0031	0.0000	0.0263	0.0007	0.0583	0.0015	20.1	0.3	26.3	1.3	539.6	24.3		
G86	7.1	529.6	0.0121	0.0001	0.0956	0.0024	0.0573	0.0014	77.3	1.1	92.7	4.5	504.6	22.6		
G64	0.6	4.5	0.1288	0.0033	1.3886	0.1583	0.1016	0.0084	780.8	38.1	884.1	113.0	1653.7	138.1	780.84	38.15
G98	28.1	380.1	0.0747	0.0005	0.7272	0.0146	0.0708	0.0012	464.6	5.8	554.9	15.9	951.9	24.9		
G73	342.4	877.2	0.3943	0.0023	17.7312	0.2780	0.3159	0.0041	2142.9	21.2	2975.3	27.5	3550.2	29.3		
G111	269.8	1580.8	0.1816	0.0011	2.6896	0.0451	0.1022	0.0015	1075.8	11.8	1325.6	23.3	1665.2	27.7		
G41	208.6	1908.3	0.1069	0.0006	1.0694	0.0154	0.0704	0.0009	655.0	7.1	738.5	14.5	940.3	19.2	654.95	7.10
G102	51.9	434.4	0.1242	0.0008	1.3077	0.0237	0.0752	0.0012	754.7	8.7	849.1	19.1	1074.9	24.1	754.75	8.72
G63	52.4	253.2	0.1733	0.0011	2.0899	0.0389	0.0881	0.0013	1030.3	11.8	1145.5	22.0	1383.8	25.8		
G100	309.5	850.5	0.3531	0.0021	8.4577	0.1488	0.1703	0.0025	1949.6	20.1	2281.4	28.4	2560.9	30.6		
G8	700.0	1820.7	0.3482	0.0020	7.8516	0.1050	0.1603	0.0019	1926.0	18.8	2214.1	23.2	2458.8	25.0		
G84	225.4	566.1	0.3777	0.0023	8.8151	0.1570	0.1706	0.0024	2065.3	21.2	2319.1	27.7	2563.3	29.6		
G31	87.9	322.2	0.2695	0.0016	4.3420	0.0704	0.1156	0.0015	1538.3	16.1	1701.4	23.1	1889.4	25.3		
G5	33.2	139.3	0.2190	0.0015	2.8898	0.0658	0.0968	0.0015	1276.8	15.4	1379.2	25.5	1563.7	28.2		
G51	195.7	534.9	0.3337	0.0019	6.3762	0.0993	0.1377	0.0018	1856.3	18.8	2029.0	24.5	2198.5	26.3		
Sample 14072807 Markha																
G20	0.3	18.6	0.0152	0.0002	0.1011	0.0044	0.0483	0.0021	97.2	2.8	97.8	8.7	112.5	9.4	97.2	2.8
G33	0.6	25.6	0.0205	0.0003	0.1369	0.0045	0.0486	0.0016	130.5	3.4	130.3	8.7	127.6	7.9	130.5	3.4
G59	0.5	14.5	0.0305	0.0005	0.2162	0.0092	0.0514	0.0022	193.7	5.8	198.8	16.4	260.6	19.7	193.7	5.8
G118	10.1	167.8	0.0644	0.0008	0.5017	0.0096	0.0565	0.0010	402.6	10.2	412.8	14.7	471.3	13.1	402.6	10.2
G98	8.9	130.0	0.0732	0.0009	0.5750	0.0098	0.0570	0.0009	455.5	11.2	461.2	14.8	491.1	12.0	455.5	11.2
G90	0.5	15.5	0.0768	0.0011	0.6278	0.0171	0.0593	0.0016	476.9	12.6	494.7	23.6	579.2	23.7	476.9	12.6
G39	1.6	21.0	0.0771	0.0010	0.5984	0.0123	0.0563	0.0011	478.9	11.5	476.2	18.0	465.0	15.0	478.9	11.5
G21	2.6	35.0	0.0774	0.0009	0.6045	0.0107	0.0567	0.0010	480.6	11.1	480.1	16.0	478.7	13.1	480.6	11.1
G2	4.2	55.6	0.0791	0.0009	0.6142	0.0102	0.0564	0.0009	490.6	11.1	486.2	15.3	466.2	11.9	490.6	11.1
G16	1.6	16.2	0.0798	0.0010	0.6150	0.0145	0.0559	0.0013	494.9	11.9	486.7	20.5	449.6	17.0	494.9	11.9

APPENDIX B (continued). U-Pb ZIRCON AGES OF ZANSKAR RIVER SEDIMENTS

Grain No.	Pb (ppm)	U (ppm)	Ratios						Ages (Ma)						Best Age (Ma)	$\pm 2\sigma$
			$^{206}\text{Pb}/^{238}\text{U}$	$\pm 1\sigma$	$^{207}\text{Pb}/^{235}\text{U}$	$\pm \text{s.e.}$	$^{207}\text{Pb}/^{206}\text{Pb}$	$\pm \text{s.e.}$	$^{206}\text{Pb}/^{238}\text{U}$	$\pm 2\sigma$	$^{207}\text{Pb}/^{235}\text{U}$	$\pm 2\sigma$	$^{207}\text{Pb}/^{206}\text{Pb}$	$\pm 2\sigma$		
G111	1.1	12.8	0.0823	0.0011	0.6622	0.0178	0.0584	0.0015	510.0	13.5	515.9	23.9	543.7	22.1	510.0	13.5
G76	0.4	3.2	0.0827	0.0014	0.6466	0.0327	0.0568	0.0029	512.1	16.6	506.4	43.0	482.2	39.4	512.1	16.6
G82	0.8	6.3	0.0835	0.0012	0.6729	0.0231	0.0585	0.0020	516.8	14.0	522.4	30.2	548.9	29.0	516.8	14.0
G34	1.7	14.4	0.0846	0.0011	0.6784	0.0148	0.0582	0.0013	523.8	12.6	525.8	20.4	536.2	17.9	523.8	12.6
G36	1.7	20.3	0.0852	0.0011	0.6641	0.0164	0.0566	0.0014	527.1	12.9	517.1	22.3	474.8	18.5	527.1	12.9
G14	1.6	18.8	0.0856	0.0011	0.6645	0.0154	0.0563	0.0013	529.3	12.7	517.3	21.2	465.8	17.1	529.3	12.7
G72	1.4	14.3	0.0857	0.0011	0.6777	0.0154	0.0574	0.0013	529.9	13.2	525.4	20.9	507.7	17.5	529.9	13.2
G121	1.8	18.1	0.0858	0.0012	0.7277	0.0186	0.0615	0.0015	530.6	14.0	555.2	24.1	658.2	23.8	530.6	14.0
G46	1.4	13.3	0.0863	0.0011	0.6854	0.0156	0.0576	0.0013	533.9	13.1	530.0	21.2	515.3	18.0	533.9	13.1
G30	1.3	14.1	0.0881	0.0011	0.7087	0.0155	0.0584	0.0013	544.0	13.0	544.0	21.0	545.5	18.2	544.0	13.0
G61	3.2	30.5	0.0885	0.0011	0.6969	0.0133	0.0572	0.0010	546.4	13.0	536.9	18.4	498.5	14.3	546.4	13.0
G62	2.3	19.9	0.0889	0.0012	0.7145	0.0164	0.0584	0.0013	548.7	13.6	547.4	21.9	543.7	18.9	548.7	13.6
G116	0.7	7.0	0.0893	0.0013	0.7153	0.0211	0.0581	0.0017	551.2	14.9	547.9	27.2	535.0	24.0	551.2	14.9
G12	2.8	30.0	0.0897	0.0011	0.7498	0.0152	0.0607	0.0012	553.5	13.0	568.1	20.3	628.3	18.5	553.5	13.0
G122	2.0	21.1	0.0918	0.0013	0.7734	0.0194	0.0611	0.0015	566.1	14.8	581.7	24.5	643.8	22.9	566.1	14.8
G29	1.4	11.2	0.0921	0.0012	0.7274	0.0192	0.0573	0.0015	567.9	14.2	555.0	25.1	504.3	20.9	567.9	14.2
G68	1.9	15.9	0.0923	0.0012	0.7510	0.0162	0.0591	0.0012	569.1	13.9	568.8	21.3	569.3	18.2	569.1	13.9
G85	2.8	31.3	0.0925	0.0012	0.7729	0.0181	0.0606	0.0014	570.4	14.4	581.4	23.2	626.1	21.1	570.4	14.4
G49	3.2	33.2	0.0949	0.0012	0.8005	0.0138	0.0612	0.0010	584.4	13.7	597.1	18.4	647.3	15.6	584.4	13.7
G11	1.5	12.7	0.0958	0.0013	0.7695	0.0228	0.0583	0.0017	589.7	15.1	579.4	28.9	540.3	25.0	589.7	15.1
G51	3.9	35.8	0.0972	0.0012	0.8386	0.0155	0.0626	0.0011	598.2	14.2	618.4	20.0	694.3	17.7	598.2	14.2
G32	5.4	48.1	0.1003	0.0012	0.8615	0.0142	0.0623	0.0010	616.2	14.2	631.0	18.6	685.8	15.7	616.2	14.2
G13	5.6	48.1	0.1004	0.0012	0.8411	0.0130	0.0608	0.0009	616.8	13.9	619.7	17.5	631.5	13.8	616.8	13.9
G79	3.5	31.0	0.1025	0.0013	0.9461	0.0203	0.0670	0.0014	628.9	15.6	676.1	24.0	838.1	23.5	628.9	15.6
G24	7.9	57.6	0.1089	0.0013	0.9166	0.0138	0.0611	0.0009	666.1	15.0	660.6	17.9	643.1	13.4	666.1	15.0
G15	3.9	36.5	0.1101	0.0013	0.9276	0.0163	0.0611	0.0010	673.3	15.3	666.4	20.2	644.2	16.1	673.3	15.3
G27	3.1	27.5	0.1125	0.0014	0.9704	0.0164	0.0626	0.0010	687.3	15.6	688.6	20.1	694.3	16.2	687.3	15.6
G75	5.1	44.7	0.1177	0.0015	1.0879	0.0203	0.0671	0.0012	717.2	17.1	747.5	22.9	840.9	20.1	717.2	17.1
G35	5.7	43.3	0.1181	0.0014	1.0784	0.0175	0.0663	0.0010	719.7	16.4	742.9	20.5	814.6	17.1	719.7	16.4
G25	1.0	5.9	0.1182	0.0016	1.0680	0.0300	0.0656	0.0019	720.4	18.3	737.8	32.8	792.0	31.0	720.4	18.3
G55	2.9	21.7	0.1277	0.0016	1.1753	0.0222	0.0668	0.0012	774.6	18.3	789.1	24.0	832.2	20.4	774.6	18.3
G54	1.5	9.4	0.1296	0.0017	1.2908	0.0297	0.0723	0.0016	785.8	19.5	841.7	30.0	993.6	28.8	785.8	19.5

APPENDIX B (continued). U-Pb ZIRCON AGES OF ZANSKAR RIVER SEDIMENTS

Grain No.	Pb (ppm)	U (ppm)	Ratios						Ages (Ma)						Best Age (Ma)	$\pm 2\sigma$
			$^{206}\text{Pb}/^{238}\text{U}$	$\pm 1\sigma$	$^{207}\text{Pb}/^{235}\text{U}$	$\pm \text{s.e.}$	$^{207}\text{Pb}/^{206}\text{Pb}$	$\pm \text{s.e.}$	$^{206}\text{Pb}/^{238}\text{U}$	$\pm 2\sigma$	$^{207}\text{Pb}/^{235}\text{U}$	$\pm 2\sigma$	$^{207}\text{Pb}/^{206}\text{Pb}$	$\pm 2\sigma$		
G94	5.4	42.1	0.1318	0.0017	1.3268	0.0227	0.0731	0.0011	798.1	18.9	857.5	23.1	1015.6	19.9	798.1	18.9
G17	10.1	77.0	0.1325	0.0016	1.4121	0.0202	0.0773	0.0010	802.2	17.8	894.1	21.0	1129.7	18.0	802.2	17.8
G3	2.4	17.5	0.1327	0.0016	1.1829	0.0236	0.0647	0.0013	803.1	18.4	792.7	25.3	764.3	20.9	803.1	18.4
G97	1.9	13.2	0.1347	0.0018	1.2748	0.0306	0.0687	0.0016	814.6	20.6	834.5	30.6	889.1	27.6	814.6	20.6
G100	1.8	13.4	0.1368	0.0018	1.2775	0.0298	0.0678	0.0015	826.8	20.8	835.8	29.8	860.9	26.0	826.8	20.8
G87	4.5	32.1	0.1369	0.0017	1.3303	0.0249	0.0706	0.0012	826.8	19.7	859.0	25.0	944.4	21.4	826.8	19.7
G28	3.1	20.2	0.1377	0.0017	1.3243	0.0245	0.0698	0.0013	831.5	19.2	856.4	25.1	922.8	21.7	831.5	19.2
G80	3.9	28.1	0.1378	0.0017	1.3218	0.0230	0.0696	0.0011	832.0	19.6	855.3	23.6	917.8	19.4	832.0	19.6
G108	5.2	35.9	0.1424	0.0018	1.3329	0.0253	0.0679	0.0012	858.3	20.8	860.1	25.3	865.8	20.4	858.3	20.8
G38	0.3	1.5	0.1442	0.0023	1.3345	0.0568	0.0672	0.0029	868.3	25.9	860.8	53.4	843.0	49.5	868.3	25.9
G104	2.9	14.9	0.1532	0.0020	1.4438	0.0286	0.0684	0.0013	918.8	22.2	907.3	27.1	880.4	21.7	880.4	21.7
G92	3.6	22.4	0.1486	0.0019	1.4972	0.0273	0.0731	0.0012	893.2	21.2	929.3	25.7	1017.0	21.6	893.2	21.2
G81	7.1	49.3	0.1493	0.0019	1.4691	0.0249	0.0714	0.0011	896.9	21.0	917.7	24.1	969.7	19.4	896.9	21.0
G37	1.4	8.4	0.1494	0.0019	1.4119	0.0291	0.0686	0.0014	897.4	21.1	894.0	28.2	887.0	23.8	897.4	21.1
G89	5.2	34.8	0.1519	0.0019	1.4493	0.0248	0.0693	0.0011	911.4	21.4	909.6	24.1	906.8	18.7	906.8	18.7
G109	4.0	27.0	0.1543	0.0020	1.4761	0.0273	0.0694	0.0012	924.9	22.2	920.6	25.7	911.5	20.3	911.5	20.3
G22	0.5	2.0	0.1693	0.0025	1.6326	0.0556	0.0700	0.0024	1008.0	27.1	982.8	47.1	928.4	41.9	928.4	41.9
G103	9.0	60.6	0.1510	0.0019	1.4648	0.0255	0.0704	0.0011	906.3	21.5	916.0	24.3	940.6	19.2	940.6	19.2
G23	3.0	13.8	0.1695	0.0021	1.6497	0.0315	0.0706	0.0013	1009.5	23.0	989.4	28.2	946.4	22.8	946.4	22.8
G71	7.4	43.0	0.1710	0.0021	1.6653	0.0272	0.0707	0.0011	1017.8	23.2	995.4	24.6	947.9	18.5	947.9	18.5
G48	5.2	26.9	0.1600	0.0020	1.5629	0.0254	0.0709	0.0011	956.7	21.7	955.6	24.0	954.8	18.7	954.8	18.7
G124	3.0	18.8	0.1608	0.0021	1.5728	0.0309	0.0709	0.0013	961.4	23.4	959.5	27.6	955.7	22.2	955.7	22.2
G63	1.7	8.5	0.1733	0.0022	1.6999	0.0354	0.0712	0.0014	1030.3	24.5	1008.5	30.5	962.9	25.0	962.9	25.0
G7	2.3	12.3	0.1621	0.0020	1.6010	0.0331	0.0717	0.0015	968.5	22.4	970.6	29.9	976.3	25.6	976.3	25.6
G45	3.5	20.9	0.1716	0.0021	1.6989	0.0299	0.0719	0.0012	1020.9	23.2	1008.1	26.5	981.7	21.0	981.7	21.0
G18	3.5	21.9	0.1645	0.0020	1.6293	0.0260	0.0719	0.0011	981.8	21.7	981.6	24.3	982.3	19.1	982.3	19.1
G58	2.0	10.1	0.1705	0.0022	1.6934	0.0366	0.0721	0.0015	1014.6	24.2	1006.1	31.6	989.0	26.6	989.0	26.6
G66	7.9	37.7	0.1798	0.0022	1.7941	0.0298	0.0724	0.0011	1065.8	24.3	1043.3	25.7	998.0	19.5	998.0	19.5
G119	5.1	32.3	0.1631	0.0021	1.6343	0.0314	0.0727	0.0013	974.2	23.6	983.5	27.5	1005.0	22.3	1005.0	22.3
G123	7.9	43.2	0.1684	0.0022	1.6912	0.0326	0.0729	0.0013	1003.2	24.3	1005.2	27.9	1010.1	22.5	1010.1	22.5
G107	3.8	21.1	0.1761	0.0023	1.7723	0.0357	0.0730	0.0014	1045.6	25.2	1035.4	29.7	1014.8	24.1	1014.8	24.1
G88	5.7	35.2	0.1532	0.0020	1.5434	0.0295	0.0731	0.0013	919.0	21.9	947.8	27.1	1017.0	23.0	1017.0	23.0

APPENDIX B (continued). U-Pb ZIRCON AGES OF ZANSKAR RIVER SEDIMENTS

Grain No.	Pb (ppm)	U (ppm)	Ratios						Ages (Ma)						Best Age (Ma)	$\pm 2\sigma$
			$^{206}\text{Pb}/^{238}\text{U}$	$\pm 1\sigma$	$^{207}\text{Pb}/^{235}\text{U}$	$\pm \text{s.e.}$	$^{207}\text{Pb}/^{206}\text{Pb}$	$\pm \text{s.e.}$	$^{206}\text{Pb}/^{238}\text{U}$	$\pm 2\sigma$	$^{207}\text{Pb}/^{235}\text{U}$	$\pm 2\sigma$	$^{207}\text{Pb}/^{206}\text{Pb}$	$\pm 2\sigma$		
G117	4.1	23.4	0.1707	0.0022	1.7300	0.0331	0.0735	0.0013	1015.9	24.6	1019.8	28.0	1028.9	22.5	1028.9	22.5
G86	3.0	18.6	0.1539	0.0020	1.5629	0.0283	0.0737	0.0012	922.6	21.8	955.6	26.1	1033.8	21.8	1033.8	21.8
G50	10.7	59.5	0.1544	0.0019	1.6023	0.0253	0.0753	0.0011	925.6	21.0	971.1	23.8	1077.1	19.4	1077.1	19.4
G10	4.8	23.3	0.1959	0.0023	2.0382	0.0323	0.0755	0.0011	1153.4	25.1	1128.4	26.2	1081.6	20.1	1081.6	20.1
G53	1.7	8.5	0.1816	0.0024	1.8975	0.0414	0.0759	0.0016	1075.5	25.8	1080.2	33.3	1091.1	28.6	1091.1	28.6
G19	4.9	25.4	0.1703	0.0021	1.7886	0.0295	0.0762	0.0012	1013.9	22.6	1041.3	25.8	1100.3	21.2	1100.3	21.2
G47	4.8	23.5	0.1826	0.0022	1.9174	0.0305	0.0762	0.0011	1081.3	24.2	1087.1	25.6	1100.3	19.9	1100.3	19.9
G65	3.4	17.3	0.2068	0.0026	2.1854	0.0406	0.0767	0.0014	1211.6	27.9	1176.4	30.2	1113.7	23.8	1113.7	23.8
G41	5.9	31.6	0.1933	0.0023	2.0480	0.0309	0.0769	0.0011	1139.2	25.1	1131.6	25.1	1118.6	18.9	1118.6	18.9
G84	3.7	19.9	0.1843	0.0023	1.9539	0.0340	0.0769	0.0012	1090.5	25.3	1099.8	27.5	1119.6	21.9	1119.6	21.9
G114	5.4	30.1	0.1828	0.0024	1.9452	0.0353	0.0772	0.0013	1082.0	25.7	1096.8	27.9	1126.9	22.2	1126.9	22.2
G64	12.1	69.0	0.1858	0.0023	1.9810	0.0319	0.0774	0.0011	1098.6	24.9	1109.1	25.9	1131.3	20.1	1131.3	20.1
G93	6.0	31.2	0.1824	0.0023	1.9632	0.0353	0.0781	0.0013	1080.1	25.3	1103.0	28.2	1149.7	22.9	1149.7	22.9
G105	3.3	18.4	0.1762	0.0023	1.9080	0.0385	0.0786	0.0015	1046.0	25.3	1083.9	30.6	1161.8	26.1	1161.8	26.1
G106	3.4	13.3	0.2070	0.0027	2.2484	0.0428	0.0788	0.0014	1212.7	28.6	1196.3	30.6	1167.6	24.3	1167.6	24.3
G40	7.7	41.0	0.1691	0.0020	1.8420	0.0275	0.0791	0.0011	1007.2	22.4	1060.6	24.1	1173.4	19.2	1173.4	19.2
G102	3.4	19.1	0.1873	0.0024	2.0558	0.0374	0.0797	0.0013	1106.6	26.2	1134.2	28.8	1188.6	23.4	1188.6	23.4
G120	1.9	7.2	0.2020	0.0028	2.2190	0.0521	0.0797	0.0018	1186.2	29.7	1187.1	36.7	1189.3	31.3	1189.3	31.3
G110	2.7	10.4	0.2122	0.0029	2.4450	0.0537	0.0836	0.0017	1240.7	30.4	1255.9	35.7	1283.0	30.3	1283.0	30.3
G78	10.1	46.1	0.2116	0.0027	2.5142	0.0455	0.0863	0.0015	1237.1	28.5	1276.2	30.7	1344.0	25.2	1344.0	25.2
G70	4.4	11.3	0.2910	0.0037	3.9406	0.0673	0.0983	0.0016	1646.5	36.5	1622.1	32.8	1591.9	25.5	1591.9	25.5
G9	6.5	20.4	0.2831	0.0034	3.8486	0.0582	0.0987	0.0014	1606.8	33.9	1603.0	30.0	1598.9	23.0	1598.9	23.0
G112	6.6	17.8	0.3240	0.0042	4.8989	0.0863	0.1097	0.0017	1809.0	40.7	1802.1	34.4	1794.8	26.6	1794.8	26.6
G56	3.4	7.8	0.3313	0.0042	5.1079	0.0935	0.1119	0.0020	1844.6	41.1	1837.4	36.7	1830.7	29.6	1830.7	29.6
G42	2.7	5.8	0.3372	0.0042	5.2225	0.0887	0.1124	0.0018	1873.0	40.5	1856.3	34.7	1838.9	27.4	1838.9	27.4
G99	9.5	22.8	0.3563	0.0045	6.1859	0.1026	0.1260	0.0019	1964.7	43.0	2002.5	34.0	2042.8	26.0	2042.8	26.0
G69	7.5	19.6	0.3670	0.0045	6.4876	0.0993	0.1283	0.0018	2015.3	42.6	2044.2	32.6	2074.9	24.5	2074.9	24.5
G5	5.9	12.6	0.4140	0.0049	7.7432	0.1130	0.1357	0.0019	2233.3	45.0	2201.6	32.7	2173.0	24.6	2173.0	24.6
G8	10.5	20.5	0.4411	0.0052	9.5009	0.1343	0.1563	0.0021	2355.5	46.8	2387.6	32.6	2416.0	24.3	2416.0	24.3
G43	33.1	75.3	0.4262	0.0051	9.3005	0.1287	0.1584	0.0020	2288.5	46.0	2368.1	31.6	2438.5	23.0	2438.5	23.0
G95	13.1	30.6	0.4161	0.0052	9.1520	0.1464	0.1596	0.0023	2242.8	47.6	2353.3	34.7	2451.6	26.3	2451.6	26.3
G6	17.6	30.4	0.4621	0.0054	10.2886	0.1376	0.1615	0.0020	2449.0	47.6	2461.1	31.4	2471.8	22.8	2471.8	22.8

APPENDIX B (continued). U-Pb ZIRCON AGES OF ZANSKAR RIVER SEDIMENTS

Grain No.	Pb (ppm)	U (ppm)	Ratios						Ages (Ma)						Best Age (Ma)	$\pm 2\sigma$
			$^{206}\text{Pb}/^{238}\text{U}$	$\pm 1\sigma$	$^{207}\text{Pb}/^{235}\text{U}$	$\pm \text{s.e.}$	$^{207}\text{Pb}/^{206}\text{Pb}$	$\pm \text{s.e.}$	$^{206}\text{Pb}/^{238}\text{U}$	$\pm 2\sigma$	$^{207}\text{Pb}/^{235}\text{U}$	$\pm 2\sigma$	$^{207}\text{Pb}/^{206}\text{Pb}$	$\pm 2\sigma$		
G57	8.5	18.0	0.4570	0.0056	10.3528	0.1536	0.1644	0.0022	2426.2	49.5	2466.8	33.7	2501.8	25.0	2501.8	25.0
G113	13.9	30.6	0.4362	0.0056	9.8986	0.1700	0.1647	0.0025	2333.4	50.4	2425.4	36.8	2504.2	28.3	2504.2	28.3
G91	10.5	19.4	0.4725	0.0060	12.3556	0.1996	0.1898	0.0028	2494.6	52.4	2631.8	36.1	2740.2	27.4	2740.2	27.4
G67	3.8	6.4	0.5195	0.0066	13.5831	0.2169	0.1898	0.0028	2696.9	55.7	2721.1	36.7	2740.3	27.8	2740.3	27.8
G60	2.5	4.1	0.5361	0.0068	14.7103	0.2368	0.1992	0.0030	2767.3	57.2	2796.7	37.3	2819.2	28.4	2819.2	28.4
G77	18.8	26.7	0.5962	0.0074	19.0633	0.2852	0.2321	0.0031	3014.6	59.4	3045.0	35.0	3066.4	25.7	3066.4	25.7
G83	9.8	17.1	0.5609	0.0070	19.9047	0.3044	0.2576	0.0035	2870.1	57.6	3086.7	35.7	3232.0	26.5	3232.0	26.5
G31	3.7	55.9	0.0658	0.0008	0.5834	0.0095	0.0644	0.0010	410.6	9.6	466.6	14.6	754.1	16.4	410.6	9.6
G44	7.7	112.6	0.0741	0.0009	0.6788	0.0109	0.0665	0.0010	460.8	10.8	526.1	15.9	821.8	16.9	460.8	10.8
G115	1.4	18.6	0.0799	0.0011	0.7418	0.0188	0.0674	0.0017	495.5	13.1	563.4	24.3	849.2	28.2	495.5	13.1
G96	1.2	12.6	0.0859	0.0011	0.8108	0.0186	0.0685	0.0015	531.4	13.5	602.9	23.4	883.4	26.0	531.4	13.5
G4	1.7	14.1	0.0932	0.0012	0.8672	0.0212	0.0675	0.0017	574.4	14.0	634.1	26.0	854.2	28.2	574.4	14.0
G52	1.4	10.3	0.1181	0.0016	1.1938	0.0312	0.0734	0.0019	719.6	18.4	797.7	32.4	1024.5	33.6	719.6	18.4
G101	1.8	10.5	0.1354	0.0019	1.4676	0.0375	0.0787	0.0020	818.6	21.3	917.1	34.5	1163.6	34.5	818.6	21.3
G1	3.8	39.7	0.0764	0.0009	0.5761	0.0102	0.0547	0.0009	474.7	10.9	462.0	15.5	400.0	11.4	474.7	10.9
G74	0.4	42.5	0.0081	0.0001	0.0521	0.0021	0.0469	0.0019	51.8	1.5	51.6	4.3	42.6	3.4	51.8	1.5
G73	0.1	5.9	0.0091	0.0002	0.0586	0.0067	0.0469	0.0055	58.1	2.9	57.8	13.4	44.6	10.2	58.1	2.9
G26	0.5	33.4	0.0150	0.0002	0.0971	0.0033	0.0469	0.0016	96.1	2.5	94.1	6.6	45.7	3.0	96.1	2.5
Sample 12072207 Oma Chu																
G79	24.5	346.4	0.0566	0.0004	0.4289	0.0091	0.0554	0.0010	355.2	4.6	362.4	12.2	428.8	206.1	355.16	4.64
G58	33.4	528.7	0.0588	0.0004	0.4333	0.0073	0.0549	0.0008	368.1	4.4	365.5	10.2	409.4	203.2	368.08	4.38
G23	14.9	149.2	0.0671	0.0005	0.5148	0.0143	0.0561	0.0013	418.7	6.0	421.7	17.4	455.5	19.4	418.66	6.04
G46	14.3	119.5	0.0747	0.0006	0.6672	0.0178	0.0667	0.0015	464.3	6.8	519.0	19.5	827.8	218.3	464.35	6.84
G38	39.3	497.6	0.0767	0.0005	0.5991	0.0093	0.0577	0.0008	476.5	5.4	476.6	11.5	519.5	204.1	476.51	5.39
G53	100.9	1126.3	0.0783	0.0005	0.6375	0.0093	0.0577	0.0008	486.0	5.5	500.8	11.1	519.1	203.6	486.03	5.50
G103	36.1	354.5	0.0789	0.0006	0.6336	0.0167	0.0596	0.0013	489.6	7.1	498.3	18.7	588.4	212.8	489.61	7.05
G82	60.7	678.6	0.0794	0.0005	0.6238	0.0110	0.0580	0.0009	492.7	5.9	492.2	13.0	530.5	205.7	492.72	5.85
G63	11.0	113.4	0.0796	0.0006	0.6197	0.0169	0.0591	0.0014	493.9	7.2	489.6	19.2	571.9	213.0	493.85	7.17
G67	45.0	490.9	0.0810	0.0005	0.6386	0.0103	0.0583	0.0008	501.9	5.8	501.4	12.3	541.4	204.8	501.91	5.84
G1	35.7	247.8	0.0811	0.0005	0.6407	0.0141	0.0576	0.0011	502.7	6.4	502.7	15.8	513.8	15.1	502.69	6.44
G75	36.8	403.1	0.0813	0.0005	0.6506	0.0109	0.0592	0.0009	504.1	6.0	508.8	12.8	573.4	205.7	504.06	5.96

APPENDIX B (continued). U-Pb ZIRCON AGES OF ZANSKAR RIVER SEDIMENTS

Grain No.	Pb (ppm)	U (ppm)	Ratios						Ages (Ma)						Best Age (Ma)	$\pm 2\sigma$
			$^{206}\text{Pb}/^{238}\text{U}$	$\pm 1\sigma$	$^{207}\text{Pb}/^{235}\text{U}$	$\pm \text{s.e.}$	$^{207}\text{Pb}/^{206}\text{Pb}$	$\pm \text{s.e.}$	$^{206}\text{Pb}/^{238}\text{U}$	$\pm 2\sigma$	$^{207}\text{Pb}/^{235}\text{U}$	$\pm 2\sigma$	$^{207}\text{Pb}/^{206}\text{Pb}$	$\pm 2\sigma$		
G37	50.4	555.7	0.0814	0.0005	0.6502	0.0097	0.0591	0.0008	504.5	5.7	508.6	11.8	569.3	204.7	504.53	5.72
G47	9.1	64.1	0.0817	0.0008	0.6739	0.0261	0.0604	0.0019	506.4	9.2	523.1	27.1	616.5	222.2	506.44	9.18
G11	13.4	103.3	0.0821	0.0007	0.6522	0.0197	0.0594	0.0015	508.7	7.7	509.8	21.6	582.9	24.2	508.70	7.74
G132	25.7	214.7	0.0836	0.0006	0.6393	0.0141	0.0564	0.0011	517.5	6.8	501.9	15.9	467.8	207.0	517.46	6.78
G93	37.4	437.6	0.0836	0.0005	0.6656	0.0116	0.0592	0.0009	517.8	6.2	518.1	13.4	573.7	206.2	517.75	6.19
G15	6.2	43.2	0.0845	0.0009	0.6676	0.0332	0.0563	0.0023	522.6	10.9	519.3	34.0	465.4	32.3	522.63	10.94
G108	15.4	129.6	0.0846	0.0006	0.6959	0.0174	0.0616	0.0013	523.5	7.3	536.4	18.7	661.6	213.2	523.46	7.25
G141	28.2	219.5	0.0846	0.0006	0.6737	0.0152	0.0573	0.0011	523.5	6.9	523.0	16.5	501.9	208.1	523.46	6.89
G106	25.5	195.8	0.0846	0.0006	0.6558	0.0147	0.0555	0.0011	523.7	6.8	512.0	16.2	434.0	206.5	523.70	6.78
G100	14.4	95.9	0.0849	0.0007	0.6353	0.0179	0.0566	0.0013	525.0	7.7	499.4	20.1	477.5	211.0	525.01	7.72
G104	78.2	833.9	0.0851	0.0005	0.6658	0.0114	0.0586	0.0009	526.3	6.3	518.2	13.3	551.9	205.6	526.31	6.30
G109	20.2	256.6	0.0854	0.0006	0.6955	0.0152	0.0586	0.0011	528.4	6.9	536.1	16.3	550.8	208.7	528.39	6.89
G14	91.9	923.7	0.0861	0.0005	0.6837	0.0106	0.0574	0.0008	532.3	5.9	529.0	12.3	506.9	12.8	532.25	5.94
G137	10.5	75.6	0.0863	0.0008	0.7443	0.0293	0.0616	0.0020	533.6	9.9	564.9	28.6	658.5	223.9	533.62	9.85
G8	89.9	962.2	0.0874	0.0005	0.7070	0.0111	0.0577	0.0008	540.0	6.0	543.0	12.5	519.9	13.1	539.96	6.05
G136	20.4	154.6	0.0876	0.0007	0.7231	0.0202	0.0598	0.0014	541.3	7.9	552.5	20.6	596.3	213.7	541.33	7.94
G13	65.6	783.3	0.0879	0.0005	0.7117	0.0124	0.0593	0.0009	543.2	6.3	545.8	13.7	576.3	15.0	543.22	6.28
G120	12.9	112.1	0.0882	0.0007	0.7114	0.0208	0.0599	0.0014	544.8	8.3	545.6	21.7	600.3	214.8	544.82	8.29
G31	54.9	538.2	0.0893	0.0005	0.7454	0.0127	0.0591	0.0009	551.5	6.4	565.5	13.6	572.3	14.7	551.46	6.39
G144	21.8	171.5	0.0895	0.0006	0.7350	0.0168	0.0616	0.0012	552.6	7.5	559.5	17.8	659.2	211.4	552.58	7.46
G86	10.4	72.9	0.0897	0.0008	0.7931	0.0280	0.0638	0.0018	553.6	9.3	592.9	26.6	735.7	222.7	553.64	9.35
G17	124.9	1286.3	0.0898	0.0005	0.7718	0.0122	0.0632	0.0009	554.5	6.3	580.8	13.4	715.3	15.9	554.47	6.27
G123	373.5	4364.7	0.0910	0.0010	0.7397	0.0369	0.0610	0.0025	561.4	12.2	562.2	37.0	638.2	231.4	561.45	12.17
G119	78.7	725.2	0.0930	0.0006	0.7626	0.0130	0.0597	0.0009	573.1	6.8	575.5	14.0	590.9	206.1	573.14	6.84
G35	50.4	459.2	0.0940	0.0006	0.7525	0.0113	0.0595	0.0008	578.9	6.5	569.7	12.8	584.3	204.8	578.86	6.48
G57	16.2	164.1	0.0963	0.0006	0.7857	0.0164	0.0609	0.0011	592.7	7.4	588.8	16.9	636.1	209.4	592.69	7.41
G139	17.9	161.4	0.0972	0.0007	0.8561	0.0220	0.0629	0.0013	598.0	8.5	628.0	20.5	703.2	214.1	598.04	8.46
G74	62.5	480.8	0.0992	0.0006	0.8064	0.0125	0.0604	0.0008	609.4	6.9	600.4	13.5	617.2	205.4	609.43	6.92
G73	54.3	564.5	0.0994	0.0006	0.8254	0.0126	0.0605	0.0008	611.0	6.9	611.0	13.5	621.9	205.4	610.95	6.92
G85	552.7	5918.4	0.1001	0.0007	0.9263	0.0211	0.0675	0.0012	614.9	8.1	665.7	19.2	853.5	214.2	614.94	8.09
G55	56.1	530.7	0.1012	0.0006	0.8540	0.0133	0.0633	0.0009	621.4	7.0	626.9	14.0	719.7	206.8	621.38	7.02
G2	16.0	111.4	0.1027	0.0008	0.8627	0.0231	0.0613	0.0013	629.9	8.8	631.6	21.5	648.7	22.5	629.92	8.77

APPENDIX B (continued). U-Pb ZIRCON AGES OF ZANSKAR RIVER SEDIMENTS

Grain No.	Pb (ppm)	U (ppm)	Ratios						Ages (Ma)						Best Age (Ma)	$\pm 2\sigma$
			$^{206}\text{Pb}/^{238}\text{U}$	$\pm 1\sigma$	$^{207}\text{Pb}/^{235}\text{U}$	$\pm \text{s.e.}$	$^{207}\text{Pb}/^{206}\text{Pb}$	$\pm \text{s.e.}$	$^{206}\text{Pb}/^{238}\text{U}$	$\pm 2\sigma$	$^{207}\text{Pb}/^{235}\text{U}$	$\pm 2\sigma$	$^{207}\text{Pb}/^{206}\text{Pb}$	$\pm 2\sigma$		
G126	143.7	1386.9	0.1047	0.0006	0.9094	0.0147	0.0619	0.0009	641.8	7.5	656.7	14.5	669.6	206.6	641.84	7.47
G115	8.6	66.2	0.1062	0.0010	0.9105	0.0356	0.0647	0.0020	650.6	11.8	657.3	31.7	765.9	225.9	650.58	11.77
G125	84.1	763.7	0.1075	0.0007	0.8802	0.0144	0.0607	0.0009	658.0	7.7	641.1	14.8	629.3	206.3	658.04	7.68
G133	23.0	198.5	0.1126	0.0008	1.0265	0.0269	0.0657	0.0014	687.6	9.6	717.2	22.5	797.8	215.9	687.60	9.62
G54	104.8	964.2	0.1156	0.0007	1.0332	0.0145	0.0639	0.0008	705.2	7.7	720.5	14.0	739.0	206.0	705.19	7.74
G113	57.7	482.8	0.1168	0.0007	1.0200	0.0177	0.0649	0.0010	712.0	8.4	713.9	16.5	769.5	208.8	712.00	8.43
G26	254.4	1772.5	0.1168	0.0007	1.1117	0.0153	0.0690	0.0008	712.1	7.6	759.0	14.3	899.0	16.3	712.12	7.62
G72	46.8	345.7	0.1169	0.0007	1.0234	0.0179	0.0660	0.0010	712.5	8.3	715.6	16.5	807.0	209.2	712.52	8.31
G69	107.6	898.1	0.1183	0.0007	1.1672	0.0161	0.0710	0.0009	720.8	7.8	785.3	14.6	956.5	208.0	720.83	7.84
G76	26.5	196.5	0.1192	0.0008	1.1266	0.0211	0.0691	0.0011	726.0	8.6	766.1	17.8	902.9	211.2	726.02	8.64
G34	73.9	642.1	0.1195	0.0007	1.0848	0.0163	0.0661	0.0009	727.9	8.1	746.0	15.1	810.8	14.5	727.92	8.06
G36	106.4	889.3	0.1221	0.0007	1.1657	0.0162	0.0684	0.0008	742.9	8.0	784.6	14.7	880.4	207.5	742.87	8.04
G147	85.5	581.4	0.1259	0.0008	1.1142	0.0207	0.0651	0.0010	764.7	9.3	760.2	17.9	777.2	209.7	764.66	9.28
G50	31.7	190.4	0.1266	0.0008	1.2114	0.0229	0.0711	0.0011	768.6	9.2	805.9	18.5	960.9	211.9	768.55	9.16
G131	49.2	343.7	0.1268	0.0008	1.0919	0.0223	0.0636	0.0011	769.4	9.6	749.4	19.0	728.7	210.2	769.36	9.61
G16	38.1	281.6	0.1270	0.0008	1.1310	0.0221	0.0657	0.0010	770.4	9.2	768.2	18.5	797.8	19.3	770.44	9.15
G111	59.9	397.7	0.1287	0.0008	1.1002	0.0192	0.0640	0.0009	780.3	9.1	753.4	17.1	740.6	208.3	780.33	9.14
G59	56.5	385.6	0.1315	0.0008	1.1871	0.0188	0.0679	0.0009	796.2	8.9	794.6	16.4	865.2	208.6	796.19	8.89
G9	36.0	217.4	0.1326	0.0009	1.1613	0.0243	0.0652	0.0011	802.7	9.8	782.6	19.8	779.2	20.0	802.68	9.79
G114	38.9	232.3	0.1347	0.0009	1.2324	0.0242	0.0685	0.0011	814.8	9.9	815.4	19.5	883.7	211.8	814.79	9.88
G24	5991.6	47049.5	0.1368	0.0010	1.2487	0.0319	0.0675	0.0013	826.4	11.0	822.8	23.7	854.2	24.4	826.43	11.00
G95	57.0	361.2	0.1379	0.0009	1.2656	0.0216	0.0672	0.0010	832.8	9.6	830.4	17.6	844.3	209.2	832.78	9.63
G52	40.9	274.8	0.1383	0.0008	1.2741	0.0211	0.0682	0.0009	834.9	9.4	834.2	17.1	874.0	209.0	834.87	9.40
G87	54.3	382.9	0.1383	0.0008	1.2518	0.0207	0.0673	0.0009	835.2	9.5	824.2	17.2	848.3	208.9	835.21	9.51
G77	591.9	1501.7	0.1397	0.0008	1.4526	0.0198	0.0734	0.0009	842.9	9.2	911.0	15.8	1026.1	208.5	842.85	9.16
G29	205.3	941.3	0.1398	0.0008	1.2737	0.0187	0.0660	0.0008	843.5	9.0	834.0	15.9	806.7	16.0	843.47	9.05
G51	30.5	187.0	0.1398	0.0009	1.2919	0.0257	0.0695	0.0011	843.5	10.2	842.1	19.7	914.8	211.9	843.53	10.18
G18	116.2	733.3	0.1413	0.0008	1.4227	0.0239	0.0733	0.0010	852.2	9.5	898.5	17.9	1021.7	19.6	852.18	9.49
G41	14.2	89.1	0.1422	0.0011	1.5174	0.0470	0.0757	0.0017	857.0	12.8	937.4	28.3	1086.6	222.3	856.98	12.76
G61	32.1	183.0	0.1434	0.0009	1.4025	0.0251	0.0725	0.0010	864.0	10.0	890.0	18.7	1000.6	211.2	863.97	10.04
G98	35.6	205.3	0.1441	0.0009	1.3277	0.0257	0.0694	0.0011	867.9	10.5	857.9	19.7	910.1	211.5	867.86	10.48
G49	42.2	265.4	0.1446	0.0009	1.3638	0.0225	0.0701	0.0010	870.6	9.8	873.5	17.6	931.9	209.5	870.62	9.80

APPENDIX B (continued). U-Pb ZIRCON AGES OF ZANSKAR RIVER SEDIMENTS

Grain No.	Pb (ppm)	U (ppm)	Ratios						Ages (Ma)						Best Age (Ma)	$\pm 2\sigma$
			$^{206}\text{Pb}/^{238}\text{U}$	$\pm 1\sigma$	$^{207}\text{Pb}/^{235}\text{U}$	$\pm \text{s.e.}$	$^{207}\text{Pb}/^{206}\text{Pb}$	$\pm \text{s.e.}$	$^{206}\text{Pb}/^{238}\text{U}$	$\pm 2\sigma$	$^{207}\text{Pb}/^{235}\text{U}$	$\pm 2\sigma$	$^{207}\text{Pb}/^{206}\text{Pb}$	$\pm 2\sigma$		
G122	42.7	249.2	0.1520	0.0010	1.4391	0.0288	0.0681	0.0011	911.9	11.1	905.4	20.5	871.3	211.5	871.29	211.55
G138	35.0	228.2	0.1459	0.0010	1.3495	0.0264	0.0686	0.0011	877.7	10.7	867.3	20.1	885.8	211.6	877.71	10.69
G66	118.9	811.0	0.1460	0.0009	1.4649	0.0228	0.0721	0.0009	878.4	9.8	916.0	17.2	989.3	209.5	878.45	9.79
G60	3.4	18.9	0.1485	0.0018	1.5125	0.0852	0.0698	0.0027	892.4	19.8	935.4	48.2	923.7	239.7	892.38	19.76
G44	36.4	197.2	0.1488	0.0009	1.4400	0.0245	0.0724	0.0010	894.1	10.1	905.7	18.3	997.5	210.5	894.06	10.10
G149	77.4	463.2	0.1523	0.0010	1.4356	0.0273	0.0689	0.0011	913.8	11.0	903.9	20.2	894.8	211.5	894.85	211.47
G22	27.5	155.3	0.1491	0.0010	1.3519	0.0298	0.0674	0.0012	895.8	11.0	868.4	21.6	848.9	21.5	895.80	11.00
G107	62.3	391.0	0.1495	0.0009	1.3661	0.0247	0.0681	0.0010	897.9	10.5	874.5	18.9	870.7	210.2	897.94	10.54
G116	65.4	353.1	0.1622	0.0010	1.5273	0.0285	0.0700	0.0011	969.0	11.4	941.4	20.2	928.6	211.2	928.65	211.25
G143	36.2	214.0	0.1538	0.0010	1.4721	0.0300	0.0701	0.0011	922.0	11.4	919.0	21.2	930.4	212.6	930.41	212.64
G110	108.3	652.3	0.1525	0.0009	1.4452	0.0244	0.0704	0.0010	915.0	10.5	907.9	18.6	939.8	210.2	939.75	210.24
G62	40.5	202.6	0.1530	0.0010	1.4627	0.0267	0.0706	0.0010	917.6	10.6	915.1	19.1	945.3	210.8	945.27	210.77
G92	53.5	334.2	0.1583	0.0010	1.5273	0.0269	0.0706	0.0010	947.3	10.9	941.4	19.0	947.0	210.4	947.01	210.43
G105	25.2	119.5	0.1639	0.0011	1.6011	0.0352	0.0709	0.0012	978.5	12.2	970.6	22.4	953.7	213.6	953.67	213.59
G6	79.6	517.9	0.1588	0.0010	1.5615	0.0273	0.0712	0.0010	950.3	10.7	955.0	18.9	961.7	19.3	961.73	19.28
G112	109.5	707.6	0.1604	0.0010	1.5657	0.0249	0.0712	0.0010	959.1	10.8	956.7	18.4	962.6	209.8	962.59	209.77
G102	50.2	234.3	0.1628	0.0011	1.5929	0.0321	0.0712	0.0011	972.5	11.8	967.4	21.1	963.4	212.4	963.45	212.39
G90	13.8	66.8	0.1663	0.0012	1.6320	0.0424	0.0714	0.0014	991.8	13.3	982.6	25.5	968.9	216.6	968.89	216.60
G5	80.1	413.2	0.1646	0.0010	1.6285	0.0264	0.0715	0.0010	982.1	10.7	981.3	18.3	972.6	18.4	972.60	18.43
G68	38.5	188.4	0.1556	0.0010	1.5154	0.0277	0.0716	0.0010	932.4	10.8	936.6	19.4	975.2	211.2	975.16	211.20
G43	85.4	478.7	0.1529	0.0009	1.4992	0.0228	0.0722	0.0009	917.4	10.1	930.1	17.2	990.5	209.1	990.46	209.12
G99	35.5	176.9	0.1502	0.0010	1.4393	0.0292	0.0724	0.0012	902.2	11.0	905.4	20.9	996.9	213.2	996.93	213.17
G81	87.4	505.7	0.1651	0.0010	1.6415	0.0252	0.0737	0.0010	985.3	10.8	986.3	18.1	1031.9	209.7	1031.89	209.71
G48	153.1	911.6	0.1634	0.0009	1.6806	0.0239	0.0742	0.0009	975.4	10.4	1001.2	17.1	1046.9	208.8	1046.91	208.84
G129	46.6	212.0	0.1838	0.0012	1.8794	0.0370	0.0748	0.0012	1087.9	13.0	1073.8	22.2	1062.9	213.3	1062.86	213.26
G84	41.8	226.9	0.1690	0.0011	1.7314	0.0335	0.0749	0.0011	1006.3	11.9	1020.3	21.0	1064.7	212.7	1064.75	212.73
G7	96.9	490.9	0.1792	0.0011	1.8776	0.0341	0.0753	0.0011	1062.4	11.9	1073.2	20.4	1076.8	20.7	1076.79	20.67
G118	79.4	376.8	0.1819	0.0011	1.8537	0.0317	0.0759	0.0011	1077.2	12.3	1064.7	20.4	1091.1	211.7	1091.11	211.68
G28	30.2	114.8	0.1663	0.0011	1.7816	0.0433	0.0769	0.0014	991.5	12.6	1038.7	24.4	1118.9	25.6	1118.86	25.61
G142	40.4	202.6	0.1851	0.0012	1.9863	0.0419	0.0771	0.0012	1094.8	13.4	1110.9	23.4	1123.8	214.9	1123.78	214.86
G71	23.5	112.8	0.1811	0.0012	1.8743	0.0388	0.0772	0.0012	1072.7	12.9	1072.0	22.4	1127.4	214.0	1127.39	213.97
G3	90.1	409.2	0.1911	0.0011	2.0406	0.0327	0.0773	0.0010	1127.5	12.1	1129.2	19.5	1127.9	19.6	1127.91	19.61

APPENDIX B (continued). U-Pb ZIRCON AGES OF ZANSKAR RIVER SEDIMENTS

Grain No.	Pb (ppm)	U (ppm)	Ratios						Ages (Ma)						Best Age (Ma)	$\pm 2\sigma$
			$^{206}\text{Pb}/^{238}\text{U}$	$\pm 1\sigma$	$^{207}\text{Pb}/^{235}\text{U}$	$\pm \text{s.e.}$	$^{207}\text{Pb}/^{206}\text{Pb}$	$\pm \text{s.e.}$	$^{206}\text{Pb}/^{238}\text{U}$	$\pm 2\sigma$	$^{207}\text{Pb}/^{235}\text{U}$	$\pm 2\sigma$	$^{207}\text{Pb}/^{206}\text{Pb}$	$\pm 2\sigma$		
G80	97.5	455.1	0.1966	0.0012	2.1063	0.0329	0.0776	0.0010	1157.1	12.6	1150.9	19.4	1137.2	210.4	1137.16	210.44
G134	76.9	310.6	0.2050	0.0013	2.1878	0.0393	0.0785	0.0011	1201.9	13.8	1177.2	22.0	1158.3	212.9	1158.29	212.90
G89	15.8	67.5	0.1764	0.0014	1.8054	0.0537	0.0787	0.0016	1047.3	15.0	1047.4	29.5	1163.6	221.7	1163.59	221.70
G21	66.7	278.9	0.2046	0.0013	2.3102	0.0441	0.0793	0.0011	1200.0	13.5	1215.4	21.8	1179.4	21.7	1179.38	21.69
G33	132.8	569.9	0.1971	0.0012	2.1760	0.0365	0.0794	0.0011	1159.8	12.6	1173.4	20.3	1183.1	20.5	1183.12	20.46
G140	85.8	409.2	0.2041	0.0013	2.2443	0.0394	0.0807	0.0012	1197.0	13.7	1195.0	22.0	1213.7	213.2	1213.66	213.18
G130	36.5	142.5	0.2167	0.0015	2.4208	0.0534	0.0826	0.0013	1264.4	15.5	1248.8	25.2	1259.8	216.2	1259.78	216.24
G30	133.4	540.9	0.2137	0.0012	2.5119	0.0385	0.0844	0.0011	1248.4	13.2	1275.5	20.0	1300.6	20.2	1300.64	20.24
G12	89.7	361.9	0.2275	0.0014	2.6788	0.0461	0.0863	0.0012	1321.6	14.3	1322.6	21.7	1344.7	21.7	1344.69	21.67
G10	24.2	92.5	0.2385	0.0016	2.8879	0.0702	0.0877	0.0014	1378.7	16.8	1378.8	26.5	1375.9	26.2	1375.92	26.21
G128	109.6	413.9	0.2422	0.0015	2.8945	0.0486	0.0889	0.0012	1398.0	15.5	1380.5	22.7	1400.9	213.7	1400.93	213.69
G4	53.2	189.7	0.2577	0.0016	3.2500	0.0581	0.0912	0.0012	1478.1	15.9	1469.2	22.6	1451.0	22.3	1450.99	22.30
G117	110.3	377.5	0.2544	0.0016	3.2077	0.0547	0.0942	0.0013	1461.0	16.1	1459.0	23.1	1512.7	214.2	1512.73	214.19
G97	69.4	217.4	0.2844	0.0018	3.7855	0.0661	0.0983	0.0013	1613.4	17.6	1589.7	23.5	1592.5	214.2	1592.50	214.25
G27	60.8	190.4	0.2910	0.0018	4.0995	0.0775	0.0998	0.0013	1646.6	17.7	1654.2	23.8	1620.2	23.4	1620.17	23.39
G25	48.9	136.4	0.3185	0.0020	4.8213	0.1053	0.1091	0.0015	1782.5	19.9	1788.6	26.0	1784.6	25.5	1784.61	25.53
G83	40.7	91.2	0.3129	0.0021	4.7969	0.1142	0.1139	0.0017	1755.0	20.8	1784.4	27.4	1863.2	218.2	1863.18	218.16
G91	212.0	528.7	0.3457	0.0021	5.7736	0.0919	0.1250	0.0016	1913.9	19.8	1942.5	24.0	2028.1	214.8	2028.09	214.77
G127	66.2	133.0	0.4070	0.0026	6.8302	0.1404	0.1255	0.0018	2201.3	24.1	2089.6	27.6	2036.0	217.8	2036.00	217.78
G39	105.6	279.5	0.3271	0.0019	5.6588	0.0910	0.1278	0.0015	1824.1	18.7	1925.1	23.1	2068.3	214.1	2068.34	214.13
G145	19.4	37.1	0.4138	0.0031	8.2341	0.2438	0.1518	0.0025	2232.1	28.5	2257.1	32.9	2366.1	223.1	2366.08	223.07
G101	268.4	503.0	0.4392	0.0026	9.4591	0.1503	0.1577	0.0020	2346.8	23.6	2383.6	25.4	2431.5	215.9	2431.47	215.93
G94	123.1	241.7	0.4402	0.0027	9.4395	0.1566	0.1583	0.0020	2351.3	23.7	2381.7	25.3	2437.4	215.9	2437.37	215.86
G32	19.6	25.0	0.5463	0.0044	15.5857	0.5883	0.2050	0.0031	2809.8	36.6	2851.7	32.9	2866.3	31.0	2866.27	30.98
G20	218.2	231.6	0.6321	0.0037	21.2096	0.3580	0.2402	0.0029	3157.7	29.1	3148.2	25.6	3121.0	24.8	3120.96	24.79
G88	57.4	85.1	0.5571	0.0039	17.8938	0.4723	0.2512	0.0033	2854.5	32.0	2984.0	28.8	3192.5	218.7	3192.47	218.67
G146	192.2	277.5	0.6004	0.0038	22.7174	0.4264	0.2785	0.0038	3031.5	30.6	3214.9	29.5	3354.4	219.9	3354.43	219.90
G45	182.3	274.8	0.5970	0.0035	22.5344	0.3557	0.2893	0.0033	3017.8	28.0	3207.1	24.8	3413.7	215.2	3413.69	215.22
G65	81.8	2740.8	0.0268	0.0004	10.8194	0.9108	0.3161	0.0097	170.7	5.1	2507.7	37.5	3551.0	253.4		
G19	1.4	50.0	0.0230	0.0004	0.5512	0.0257	0.1746	0.0073	146.3	4.7	445.8	32.2	2602.6	79.7		
G148	173.5	1847.4	0.0956	0.0008	1.0911	0.0346	0.0873	0.0021	588.5	9.8	749.0	28.3	1367.8	229.8		
G124	24.5	203.9	0.0862	0.0006	0.8900	0.0200	0.0757	0.0014	533.1	7.2	646.4	19.0	1086.4	217.7		

APPENDIX B (continued). U-Pb ZIRCON AGES OF ZANSKAR RIVER SEDIMENTS

Grain No.	Pb (ppm)	U (ppm)	Ratios						Ages (Ma)						Best Age (Ma)	$\pm 2\sigma$
			$^{206}\text{Pb}/^{238}\text{U}$	$\pm 1\sigma$	$^{207}\text{Pb}/^{235}\text{U}$	$\pm \text{s.e.}$	$^{207}\text{Pb}/^{206}\text{Pb}$	$\pm \text{s.e.}$	$^{206}\text{Pb}/^{238}\text{U}$	$\pm 2\sigma$	$^{207}\text{Pb}/^{235}\text{U}$	$\pm 2\sigma$	$^{207}\text{Pb}/^{206}\text{Pb}$	$\pm 2\sigma$		
G70	29.6	287.0	0.0803	0.0005	0.7912	0.0134	0.0728	0.0011	498.0	6.0	591.9	14.4	1007.3	211.6		
G121	100.6	1163.4	0.0870	0.0005	0.8557	0.0145	0.0713	0.0010	537.9	6.4	627.8	14.8	965.2	211.2	537.95	6.40
G96	37.0	236.3	0.1312	0.0009	1.5353	0.0311	0.0871	0.0014	794.8	9.9	944.6	21.2	1362.7	216.6		
G78	186.7	1126.3	0.1470	0.0009	1.9122	0.0261	0.0915	0.0011	884.1	9.6	1085.4	17.6	1456.8	211.6		
G56	9.6	58.7	0.1485	0.0011	1.6402	0.0459	0.0866	0.0017	892.5	12.8	985.8	27.8	1351.4	222.8	892.55	12.80
G42	11.7	91.8	0.0900	0.0006	0.7909	0.0192	0.0671	0.0013	555.8	7.6	591.7	19.6	839.9	215.8	555.77	7.57
G40	19.3	141.1	0.0812	0.0006	0.6929	0.0197	0.0635	0.0015	503.3	7.5	534.5	20.9	724.7	217.3	503.34	7.51
G64	71.9	163.4	0.3642	0.0022	8.2728	0.1586	0.1556	0.0019	2001.8	21.1	2261.3	24.9	2408.8	215.8		
G135	69.9	185.0	0.2856	0.0019	5.4987	0.1159	0.1416	0.0021	1619.4	19.0	1900.4	27.6	2246.3	219.4		

Sample 13071402 Hanumil

G1	5.6	1679.4	0.0040	0.0001	0.0252	0.0012	0.0466	0.0022	25.4	0.8	25.3	2.5	27.2	69.7	25.4	0.8
G79	1.6	416.8	0.0041	0.0001	0.0275	0.0023	0.0501	0.0042	26.5	1.2	27.5	4.9	197.3	97.6	26.5	1.2
G93	42.8	1406.4	0.0238	0.0003	0.1839	0.0055	0.0569	0.0016	151.8	4.0	171.4	9.7	488.0	88.3	151.8	4.0
G16	3.8	150.8	0.0262	0.0005	0.1912	0.0141	0.0559	0.0039	167.0	6.4	177.7	24.7	447.6	117.7	167.0	6.4
G101	73.9	1609.2	0.0408	0.0005	0.3020	0.0080	0.0542	0.0013	257.9	6.6	268.0	12.8	378.1	82.1	257.9	6.6
G23	35.4	752.9	0.0424	0.0005	0.3174	0.0083	0.0538	0.0013	267.6	6.7	279.9	13.0	363.5	81.6	267.6	6.7
G90	20.2	228.0	0.0500	0.0007	0.3622	0.0125	0.0545	0.0017	314.7	8.5	313.8	18.6	393.4	87.0	314.7	8.5
G48	10.5	176.5	0.0502	0.0007	0.3558	0.0125	0.0542	0.0017	315.8	8.5	309.1	19.0	378.1	87.0	315.8	8.5
G97	70.4	1191.9	0.0528	0.0007	0.3908	0.0101	0.0533	0.0012	331.8	8.3	335.0	14.8	339.9	80.3	331.8	8.3
G35	9.7	157.8	0.0554	0.0008	0.4054	0.0145	0.0539	0.0017	347.7	9.3	345.6	20.4	366.9	86.6	347.7	9.3
G74	86.2	1096.6	0.0557	0.0007	0.4159	0.0087	0.0544	0.0010	349.5	8.5	353.1	13.1	388.1	78.8	349.5	8.5
G55	8.9	137.9	0.0561	0.0008	0.4125	0.0156	0.0547	0.0018	351.8	9.5	350.7	21.8	399.6	89.2	351.8	9.5
G12	47.9	682.7	0.0567	0.0007	0.4219	0.0090	0.0541	0.0010	355.6	8.5	357.4	13.6	376.9	79.1	355.6	8.5
G103	29.4	498.0	0.0580	0.0008	0.4272	0.0109	0.0538	0.0012	363.1	9.1	361.2	15.6	361.4	80.7	363.1	9.1
G22	89.2	1146.3	0.0583	0.0007	0.4447	0.0083	0.0544	0.0009	365.2	8.6	373.6	12.6	386.0	77.7	365.2	8.6
G96	2.1	26.3	0.0592	0.0015	0.4357	0.0528	0.0485	0.0052	370.8	18.4	367.2	63.1	121.8	91.7	370.8	18.4
G47	65.9	1125.8	0.0606	0.0008	0.4525	0.0094	0.0542	0.0010	379.0	9.1	379.0	13.9	378.1	78.6	379.0	9.1
G65	53.2	740.6	0.0636	0.0008	0.5218	0.0121	0.0598	0.0012	397.6	9.7	426.4	16.5	596.3	85.3	397.6	9.7
G10	150.9	2441.0	0.0662	0.0008	0.5440	0.0095	0.0600	0.0009	413.3	9.7	441.0	13.9	603.2	81.0	413.3	9.7
G15	80.1	1083.7	0.0683	0.0008	0.5327	0.0099	0.0571	0.0009	426.1	10.0	433.6	14.3	494.2	79.8	426.1	10.0
G77	111.6	1709.2	0.0691	0.0009	0.5406	0.0108	0.0566	0.0010	430.9	10.4	438.8	15.1	476.4	80.2	430.9	10.4

APPENDIX B (continued). U-Pb ZIRCON AGES OF ZANSKAR RIVER SEDIMENTS

Grain No.	Pb (ppm)	U (ppm)	Ratios						Ages (Ma)						Best Age (Ma)	$\pm 2\sigma$
			$^{206}\text{Pb}/^{238}\text{U}$	$\pm 1\sigma$	$^{207}\text{Pb}/^{235}\text{U}$	$\pm \text{s.e.}$	$^{207}\text{Pb}/^{206}\text{Pb}$	$\pm \text{s.e.}$	$^{206}\text{Pb}/^{238}\text{U}$	$\pm 2\sigma$	$^{207}\text{Pb}/^{235}\text{U}$	$\pm 2\sigma$	$^{207}\text{Pb}/^{206}\text{Pb}$	$\pm 2\sigma$		
G37	127.2	1571.8	0.0703	0.0009	0.5563	0.0107	0.0574	0.0010	437.7	10.4	449.1	14.9	506.9	80.4	437.7	10.4
G58	126.9	1937.7	0.0703	0.0009	0.5409	0.0105	0.0566	0.0010	438.1	10.5	439.0	15.0	474.4	79.9	438.1	10.5
G3	71.8	923.0	0.0713	0.0009	0.5518	0.0113	0.0562	0.0010	444.0	10.5	446.1	15.5	458.3	80.2	444.0	10.5
G4	47.7	590.4	0.0735	0.0009	0.5679	0.0116	0.0566	0.0010	457.0	10.7	456.6	15.7	476.8	80.5	457.0	10.7
G108	51.1	569.9	0.0746	0.0010	0.7002	0.0191	0.0689	0.0016	463.5	11.8	538.9	22.2	894.2	94.3	463.5	11.8
G7	90.3	1187.2	0.0759	0.0009	0.6165	0.0122	0.0591	0.0010	471.5	11.0	487.7	16.3	570.4	82.1	471.5	11.0
G69	46.1	603.8	0.0770	0.0010	0.5958	0.0141	0.0570	0.0012	478.4	11.6	474.6	18.2	491.1	82.9	478.4	11.6
G91	11.4	85.3	0.0791	0.0011	0.5986	0.0239	0.0566	0.0019	490.4	13.4	476.3	28.2	476.4	92.7	490.4	13.4
G60	111.2	1011.8	0.0808	0.0010	0.6275	0.0143	0.0561	0.0011	500.7	12.0	494.5	18.0	456.3	81.5	500.7	12.0
G67	32.0	325.6	0.0876	0.0011	0.6881	0.0181	0.0589	0.0013	541.0	13.3	531.6	21.5	563.8	86.3	541.0	13.3
G11	57.3	652.9	0.0879	0.0011	0.7258	0.0155	0.0599	0.0011	542.9	12.8	554.1	18.5	598.2	83.4	542.9	12.8
G75	83.0	781.5	0.0931	0.0012	0.8609	0.0233	0.0655	0.0014	573.7	14.3	630.6	23.7	789.8	91.3	573.7	14.3
G107	169.6	1550.2	0.0995	0.0013	0.8993	0.0192	0.0659	0.0012	611.7	14.8	651.3	21.1	803.2	87.1	611.7	14.8
G51	283.9	2652.0	0.1029	0.0013	0.9263	0.0166	0.0647	0.0010	631.4	14.7	665.7	18.9	763.0	83.5	631.4	14.7
G83	114.8	1104.8	0.1053	0.0013	0.9655	0.0201	0.0665	0.0012	645.6	15.4	686.1	21.3	823.4	86.7	645.6	15.4
G63	68.2	571.1	0.1086	0.0014	0.9712	0.0231	0.0639	0.0012	664.7	15.9	689.1	23.0	739.0	87.6	664.7	15.9
G17	353.1	2372.6	0.1140	0.0014	1.0596	0.0179	0.0674	0.0010	696.0	15.9	733.6	19.5	848.9	83.6	696.0	15.9
G39	65.9	415.0	0.1147	0.0015	1.0429	0.0262	0.0678	0.0014	700.1	16.8	725.4	24.9	862.1	90.5	700.1	16.8
G21	12.4	92.4	0.1157	0.0016	1.0025	0.0376	0.0662	0.0019	705.5	18.3	705.1	33.4	814.0	99.6	705.5	18.3
G80	245.9	1462.5	0.1178	0.0015	1.1399	0.0224	0.0698	0.0012	717.6	16.8	772.4	22.2	922.5	87.2	717.6	16.8
G87	33.3	197.0	0.1198	0.0016	1.0477	0.0325	0.0658	0.0016	729.4	18.3	727.8	29.3	798.7	94.1	729.4	18.3
G110	242.8	1530.3	0.1209	0.0015	1.1415	0.0248	0.0670	0.0012	735.9	17.6	773.2	23.6	836.5	87.8	735.9	17.6
G62	311.8	1510.4	0.1212	0.0015	1.0879	0.0212	0.0657	0.0011	737.5	17.1	747.5	21.7	797.8	85.2	737.5	17.1
G19	211.3	1390.6	0.1218	0.0015	1.1433	0.0191	0.0673	0.0010	740.6	16.8	774.1	20.0	846.5	83.4	740.6	16.8
G20	299.7	1680.5	0.1223	0.0015	1.1514	0.0191	0.0675	0.0010	743.8	16.9	777.9	20.0	854.5	83.4	743.8	16.9
G89	109.1	681.6	0.1234	0.0016	1.1594	0.0257	0.0684	0.0012	749.9	17.8	781.7	24.1	880.1	88.5	749.9	17.8
G42	50.0	304.0	0.1235	0.0016	1.0584	0.0317	0.0659	0.0015	750.9	18.5	733.0	28.7	804.2	93.1	750.9	18.5
G32	66.5	479.3	0.1236	0.0015	1.1095	0.0220	0.0669	0.0011	751.0	17.3	757.9	22.0	834.7	85.7	751.0	17.3
G100	118.7	897.3	0.1242	0.0016	1.1323	0.0235	0.0656	0.0011	754.6	17.9	768.8	22.9	792.7	86.2	754.6	17.9
G33	68.0	451.8	0.1247	0.0015	1.1220	0.0231	0.0675	0.0011	757.3	17.5	764.0	22.6	853.9	86.5	757.3	17.5
G31	57.7	443.1	0.1254	0.0015	1.1224	0.0226	0.0670	0.0011	761.8	17.5	764.1	22.3	838.7	85.9	761.8	17.5
G52	198.3	925.9	0.1257	0.0016	1.1606	0.0230	0.0666	0.0011	763.4	17.8	782.2	22.3	824.3	85.7	763.4	17.8

APPENDIX B (continued). U-Pb ZIRCON AGES OF ZANSKAR RIVER SEDIMENTS

Grain No.	Pb (ppm)	U (ppm)	Ratios						Ages (Ma)						Best Age (Ma)	$\pm 2\sigma$
			$^{206}\text{Pb}/^{238}\text{U}$	$\pm 1\sigma$	$^{207}\text{Pb}/^{235}\text{U}$	$\pm \text{s.e.}$	$^{207}\text{Pb}/^{206}\text{Pb}$	$\pm \text{s.e.}$	$^{206}\text{Pb}/^{238}\text{U}$	$\pm 2\sigma$	$^{207}\text{Pb}/^{235}\text{U}$	$\pm 2\sigma$	$^{207}\text{Pb}/^{206}\text{Pb}$	$\pm 2\sigma$		
G34	56.5	399.8	0.1259	0.0016	1.1395	0.0235	0.0675	0.0011	764.4	17.7	772.3	22.8	851.7	86.5	764.4	17.7
G61	115.7	889.7	0.1263	0.0016	1.1826	0.0246	0.0661	0.0011	766.6	18.0	792.5	22.8	809.9	86.1	766.6	18.0
G6	23.8	157.2	0.1281	0.0017	1.1497	0.0353	0.0681	0.0016	777.0	19.0	777.1	29.8	871.9	94.7	777.0	19.0
G56	117.4	758.7	0.1285	0.0016	1.1652	0.0227	0.0654	0.0011	779.1	18.1	784.4	22.2	786.9	84.9	779.1	18.1
G30	35.9	250.2	0.1292	0.0016	1.1306	0.0265	0.0651	0.0012	783.1	18.4	768.0	24.4	778.9	87.4	783.1	18.4
G46	80.6	634.8	0.1297	0.0016	1.1954	0.0233	0.0671	0.0011	785.9	18.1	798.5	22.3	840.3	85.4	785.9	18.1
G2	82.7	582.8	0.1297	0.0016	1.1904	0.0218	0.0673	0.0010	786.0	17.8	796.1	21.5	848.0	84.6	786.0	17.8
G111	85.3	579.3	0.1297	0.0017	1.1969	0.0270	0.0664	0.0012	786.1	18.8	799.1	24.8	820.3	88.0	786.1	18.8
G13	124.0	816.6	0.1304	0.0016	1.1889	0.0211	0.0678	0.0010	790.3	17.9	795.4	21.2	861.8	84.3	790.3	17.9
G102	100.4	658.2	0.1315	0.0017	1.2086	0.0263	0.0668	0.0012	796.1	18.9	804.6	24.4	831.5	87.6	796.1	18.9
G92	165.4	1006.6	0.1315	0.0016	1.2117	0.0243	0.0665	0.0011	796.3	18.7	806.0	23.1	823.4	86.0	796.3	18.7
G54	99.3	746.4	0.1316	0.0016	1.2196	0.0237	0.0663	0.0011	796.8	18.5	809.6	22.4	814.3	85.1	796.8	18.5
G8	76.1	585.7	0.1316	0.0016	1.2331	0.0245	0.0685	0.0011	796.9	18.1	815.7	22.6	884.3	86.1	796.9	18.1
G45	90.4	420.3	0.1318	0.0017	1.1601	0.0280	0.0662	0.0013	798.0	18.8	782.0	25.3	811.1	88.5	798.0	18.8
G98	93.0	682.1	0.1318	0.0017	1.2271	0.0261	0.0662	0.0012	798.2	18.8	813.0	23.9	813.3	86.8	798.2	18.8
G71	66.9	426.1	0.1324	0.0017	1.2147	0.0267	0.0674	0.0012	801.6	18.9	807.4	24.4	848.9	87.7	801.6	18.9
G68	273.4	2100.2	0.1330	0.0016	1.2311	0.0228	0.0663	0.0010	804.9	18.5	814.8	22.0	816.8	84.6	804.9	18.5
G50	59.2	436.6	0.1332	0.0017	1.2027	0.0250	0.0666	0.0011	806.2	18.8	801.8	23.3	826.2	86.2	806.2	18.8
G95	146.2	1103.0	0.1339	0.0017	1.2226	0.0262	0.0662	0.0012	810.3	19.1	811.0	24.2	813.3	87.0	810.3	19.1
G38	107.8	674.5	0.1343	0.0016	1.2291	0.0231	0.0664	0.0010	812.3	18.6	813.9	22.1	818.1	84.6	812.3	18.6
G27	131.6	881.5	0.1345	0.0017	1.2211	0.0263	0.0658	0.0011	813.7	18.8	810.3	23.6	801.3	86.2	813.7	18.8
G82	122.3	855.2	0.1359	0.0017	1.2445	0.0250	0.0658	0.0011	821.5	19.2	820.9	23.4	801.3	85.7	821.5	19.2
G85	44.7	299.3	0.1360	0.0018	1.2207	0.0382	0.0668	0.0016	822.2	20.4	810.1	30.9	830.0	94.4	822.2	20.4
G94	478.0	2633.3	0.1361	0.0017	1.2549	0.0252	0.0666	0.0011	822.8	19.3	825.6	23.6	825.6	86.2	822.8	19.3
G5	136.7	894.3	0.1362	0.0017	1.2670	0.0260	0.0674	0.0011	823.1	18.7	831.1	23.2	850.8	86.2	823.1	18.7
G99	85.8	410.3	0.1363	0.0017	1.2284	0.0280	0.0667	0.0012	823.8	19.6	813.6	25.4	826.9	88.2	823.8	19.6
G73	46.4	236.1	0.1367	0.0018	1.2921	0.0336	0.0703	0.0014	825.9	19.8	842.2	27.8	937.7	92.1	825.9	19.8
G57	268.6	1806.2	0.1375	0.0017	1.5334	0.0298	0.0781	0.0012	830.6	19.2	943.8	24.3	1149.7	89.0	830.6	19.2
G81	50.4	341.9	0.1382	0.0017	1.2482	0.0291	0.0666	0.0012	834.4	19.7	822.6	25.5	823.7	88.2	834.4	19.7
G49	149.2	906.0	0.1387	0.0017	1.2674	0.0242	0.0664	0.0010	837.5	19.2	831.2	22.6	818.7	84.8	837.5	19.2
G84	79.8	413.3	0.1390	0.0018	1.2911	0.0308	0.0678	0.0013	839.2	19.9	841.8	26.1	860.9	89.1	839.2	19.9
G29	130.6	745.3	0.1393	0.0017	1.2723	0.0230	0.0668	0.0010	840.6	19.1	833.4	22.0	832.5	84.2	840.6	19.1

APPENDIX B (continued). U-Pb ZIRCON AGES OF ZANSKAR RIVER SEDIMENTS

Grain No.	Pb (ppm)	U (ppm)	Ratios						Ages (Ma)						Best Age (Ma)	$\pm 2\sigma$
			$^{206}\text{Pb}/^{238}\text{U}$	$\pm 1\sigma$	$^{207}\text{Pb}/^{235}\text{U}$	$\pm \text{s.e.}$	$^{207}\text{Pb}/^{206}\text{Pb}$	$\pm \text{s.e.}$	$^{206}\text{Pb}/^{238}\text{U}$	$\pm 2\sigma$	$^{207}\text{Pb}/^{235}\text{U}$	$\pm 2\sigma$	$^{207}\text{Pb}/^{206}\text{Pb}$	$\pm 2\sigma$		
G76	92.8	443.1	0.1395	0.0018	1.2978	0.0284	0.0692	0.0012	841.9	19.8	844.8	25.1	903.5	88.3	841.9	19.8
G41	56.0	395.7	0.1399	0.0018	1.2663	0.0309	0.0671	0.0013	844.3	19.9	830.8	26.2	840.9	89.0	844.3	19.9
G112	87.0	413.3	0.1411	0.0018	1.2769	0.0305	0.0661	0.0013	850.7	20.3	835.5	26.5	810.5	88.8	850.7	20.3
G66	88.4	476.4	0.1416	0.0018	1.3304	0.0309	0.0684	0.0013	853.7	20.1	859.1	25.9	880.1	88.9	853.7	20.1
G59	172.9	631.9	0.1422	0.0018	1.2876	0.0266	0.0666	0.0011	857.0	19.9	840.2	24.0	825.0	86.2	857.0	19.9
G70	22.0	132.1	0.1426	0.0019	1.3201	0.0436	0.0695	0.0017	859.1	21.4	854.6	33.0	914.8	97.0	859.1	21.4
G72	84.1	631.9	0.1427	0.0018	1.3861	0.0316	0.0691	0.0013	859.7	20.2	883.1	25.8	902.9	88.8	859.7	20.2
G25	57.0	352.5	0.1435	0.0018	1.2494	0.0329	0.0650	0.0013	864.1	20.4	823.1	27.2	772.7	89.0	864.1	20.4
G86	194.3	1227.5	0.1439	0.0018	1.3179	0.0256	0.0660	0.0011	866.5	20.1	853.6	23.5	807.6	85.2	866.5	20.1
G53	126.2	468.2	0.1450	0.0018	1.3978	0.0337	0.0718	0.0014	872.6	20.5	888.0	27.1	980.6	90.8	872.6	20.5
G64	49.6	305.1	0.1497	0.0019	1.3695	0.0342	0.0678	0.0013	899.0	21.3	875.9	27.4	862.1	89.6	899.0	21.3
G24	123.9	778.0	0.1653	0.0020	1.6220	0.0320	0.0707	0.0011	986.0	22.2	978.8	24.7	949.6	86.4	949.6	86.4
G9	30.8	149.6	0.1751	0.0022	1.7534	0.0500	0.0735	0.0015	1040.0	24.2	1028.4	31.2	1026.4	93.6	1026.4	93.6
G106	93.7	488.7	0.1658	0.0021	1.6570	0.0414	0.0740	0.0014	988.7	23.6	992.2	29.8	1042.6	92.5	1042.6	92.5
G78	91.7	427.9	0.1954	0.0025	2.0536	0.0474	0.0772	0.0014	1150.7	26.5	1133.5	29.7	1126.1	91.2	1126.1	91.2
G109	42.1	180.0	0.2067	0.0027	2.2372	0.0589	0.0806	0.0016	1210.9	28.5	1192.8	33.4	1211.5	95.1	1211.5	95.1
G26	184.9	881.5	0.2147	0.0026	2.4625	0.0416	0.0836	0.0012	1253.8	27.4	1261.1	26.4	1282.8	87.2	1282.8	87.2
G28	80.1	234.4	0.2717	0.0033	3.5995	0.0770	0.0985	0.0015	1549.3	33.7	1549.4	31.2	1595.2	91.7	1595.2	91.7
G88	127.1	414.4	0.2912	0.0036	4.0070	0.0842	0.1026	0.0017	1647.3	36.2	1635.6	33.5	1671.5	93.9	1671.5	93.9
G40	160.8	441.9	0.3076	0.0038	4.4347	0.0993	0.1078	0.0017	1728.9	37.4	1718.8	33.0	1763.2	93.1	1763.2	93.1
G105	84.1	258.4	0.2928	0.0037	4.5702	0.1133	0.1167	0.0021	1655.3	37.2	1743.9	36.8	1905.7	98.0	1905.7	98.0
G43	868.2	2264.5	0.3960	0.0048	8.5538	0.1438	0.1582	0.0022	2150.6	44.2	2291.7	33.3	2436.3	92.5	2436.3	92.5
G44	84.6	158.4	0.4902	0.0062	12.0256	0.3333	0.1862	0.0029	2571.6	53.2	2606.4	37.4	2709.1	96.3	2709.1	96.3
G36	36.9	43.8	0.6562	0.0084	22.7902	0.8017	0.2615	0.0040	3252.5	65.3	3218.0	39.0	3255.6	97.2	3255.6	97.2
G104	61.2	466.5	0.0903	0.0013	0.9058	0.0334	0.0747	0.0022	557.5	15.1	654.8	32.0	1059.9	106.0	557.5	15.1
G14	97.3	1112.9	0.0835	0.0010	0.8005	0.0152	0.0691	0.0011	517.1	12.0	597.1	18.1	900.8	86.4	517.1	12.0
G18	189.5	2114.2	0.0921	0.0011	0.8677	0.0150	0.0676	0.0010	567.8	13.1	634.3	17.8	856.0	84.1	567.8	13.1
Sample 12072401 Pishu																
G67	6.5	2082.3	0.0034	0.0000	0.0224	0.0008	0.0469	0.0016	22.1	0.4	22.5	1.5	42.1	16.8	22.14	0.39
G27	1.1	231.4	0.0049	0.0001	0.0313	0.0033	0.0480	0.0051	31.6	1.4	31.3	6.9	97.3	33.6	31.64	1.41
G44	36.2	948.4	0.0405	0.0003	0.2988	0.0074	0.0537	0.0012	255.7	3.6	265.4	11.1	358.5	27.6	255.68	3.59

APPENDIX B (continued). U-Pb ZIRCON AGES OF ZANSKAR RIVER SEDIMENTS

Grain No.	Pb (ppm)	U (ppm)	Ratios						Ages (Ma)						Best Age (Ma)	$\pm 2\sigma$
			$^{206}\text{Pb}/^{238}\text{U}$	$\pm 1\sigma$	$^{207}\text{Pb}/^{235}\text{U}$	$\pm \text{s.e.}$	$^{207}\text{Pb}/^{206}\text{Pb}$	$\pm \text{s.e.}$	$^{206}\text{Pb}/^{238}\text{U}$	$\pm 2\sigma$	$^{207}\text{Pb}/^{235}\text{U}$	$\pm 2\sigma$	$^{207}\text{Pb}/^{206}\text{Pb}$	$\pm 2\sigma$		
G71	5.5	102.4	0.0462	0.0005	0.3451	0.0160	0.0570	0.0024	291.1	6.2	301.1	23.2	492.7	46.5	291.09	6.16
G94	15.4	224.9	0.0513	0.0004	0.3775	0.0112	0.0540	0.0014	322.2	4.9	325.2	15.5	372.7	24.0	322.19	4.91
G66	37.4	657.9	0.0558	0.0004	0.4327	0.0098	0.0557	0.0011	349.9	4.5	365.1	13.0	440.0	28.5	349.91	4.52
G86	22.9	322.3	0.0558	0.0004	0.4297	0.0116	0.0569	0.0014	350.2	5.0	363.0	15.7	487.3	32.8	350.22	5.01
G49	12.3	190.4	0.0573	0.0006	0.4514	0.0180	0.0574	0.0020	359.1	6.7	378.2	22.9	507.3	41.8	359.12	6.71
G41	9.2	135.0	0.0598	0.0006	0.4828	0.0213	0.0572	0.0022	374.3	7.5	400.0	25.6	500.4	44.0	374.29	7.54
G108	208.9	3548.1	0.0601	0.0004	0.4747	0.0078	0.0553	0.0008	375.9	4.4	394.4	10.1	425.2	17.6	375.93	4.38
G95	19.6	259.0	0.0604	0.0005	0.4527	0.0161	0.0559	0.0017	377.8	6.4	379.2	20.7	448.4	29.9	377.75	6.44
G8	29.7	451.3	0.0611	0.0004	0.4699	0.0104	0.0554	0.0011	382.1	5.0	391.1	13.2	427.6	27.5	382.13	4.98
G11	3.1	41.0	0.0645	0.0011	0.4801	0.0380	0.0560	0.0038	402.9	13.0	398.1	47.6	450.4	64.0	402.93	12.96
G43	99.5	1505.1	0.0715	0.0004	0.5513	0.0098	0.0561	0.0009	444.9	5.3	445.8	12.3	457.5	25.7	444.89	5.29
G10	69.0	1029.7	0.0716	0.0004	0.5504	0.0095	0.0562	0.0009	445.5	5.3	445.3	11.8	460.3	25.2	445.49	5.29
G26	34.4	509.7	0.0724	0.0005	0.5345	0.0119	0.0548	0.0011	450.8	5.9	434.8	14.7	405.3	26.9	450.78	5.89
G24	71.8	869.4	0.0727	0.0005	0.5724	0.0110	0.0581	0.0010	452.2	5.5	459.5	13.3	533.5	27.9	452.16	5.53
G42	30.2	326.6	0.0734	0.0005	0.5730	0.0139	0.0575	0.0012	456.3	6.1	460.0	16.5	510.4	30.9	456.31	6.13
G18	55.5	759.8	0.0747	0.0005	0.7123	0.0156	0.0703	0.0013	464.5	6.1	546.1	16.8	935.7	36.7	464.47	6.12
G64	87.4	924.3	0.0747	0.0005	0.5733	0.0110	0.0564	0.0010	464.5	5.6	460.1	13.8	466.6	27.0	464.47	5.64
G6	163.6	2351.0	0.0751	0.0004	0.5816	0.0084	0.0559	0.0007	467.0	5.3	465.5	10.5	448.0	23.4	467.05	5.28
G93	70.3	1007.5	0.0758	0.0005	0.5741	0.0104	0.0564	0.0009	470.8	5.6	460.7	12.8	466.6	19.3	470.76	5.63
G15	43.2	591.1	0.0761	0.0005	0.5963	0.0111	0.0576	0.0009	472.6	5.8	474.9	13.4	514.6	27.2	472.62	5.75
G47	84.8	1200.8	0.0767	0.0005	0.6063	0.0118	0.0572	0.0010	476.3	5.7	481.2	14.0	500.4	27.6	476.34	5.75
G22	67.9	832.1	0.0767	0.0005	0.5870	0.0103	0.0558	0.0009	476.5	5.6	469.0	12.5	442.4	25.1	476.51	5.63
G19	146.2	2064.2	0.0767	0.0005	0.5993	0.0090	0.0567	0.0008	476.6	5.4	476.8	11.1	481.4	24.3	476.63	5.39
G4	79.8	867.0	0.0770	0.0005	0.6122	0.0105	0.0573	0.0009	478.1	5.6	484.9	12.4	504.3	26.0	478.13	5.63
G103	135.1	1862.2	0.0772	0.0005	0.6022	0.0093	0.0554	0.0008	479.4	5.4	478.6	11.2	429.6	17.1	479.39	5.39
G37	56.0	739.9	0.0801	0.0005	0.6405	0.0141	0.0578	0.0011	496.8	6.3	502.6	15.8	523.7	29.4	496.84	6.33
G98	71.9	723.9	0.0988	0.0007	0.9139	0.0254	0.0660	0.0015	607.2	8.7	659.1	22.5	806.1	32.1	607.20	8.68
G104	82.3	522.4	0.1120	0.0009	1.0794	0.0335	0.0667	0.0016	684.2	10.3	743.3	25.7	827.2	34.3	684.24	10.32
G48	175.3	1627.4	0.1126	0.0007	1.0305	0.0198	0.0666	0.0011	687.9	8.1	719.2	18.2	826.5	32.7	687.95	8.11
G52	56.1	433.2	0.1149	0.0008	0.9913	0.0246	0.0647	0.0013	700.9	9.3	699.4	22.0	764.6	35.8	700.85	9.25
G56	7.6	51.2	0.1159	0.0012	1.0235	0.0459	0.0669	0.0023	707.0	13.7	715.7	37.5	835.3	53.0	707.04	13.75
G54	25.2	203.0	0.1201	0.0009	1.0535	0.0295	0.0673	0.0015	731.3	10.4	730.6	25.2	847.4	39.6	731.25	10.36

APPENDIX B (continued). U-Pb ZIRCON AGES OF ZANSKAR RIVER SEDIMENTS

Grain No.	Pb (ppm)	U (ppm)	Ratios						Ages (Ma)						Best Age (Ma)	$\pm 2\sigma$
			$^{206}\text{Pb}/^{238}\text{U}$	$\pm 1\sigma$	$^{207}\text{Pb}/^{235}\text{U}$	$\pm \text{s.e.}$	$^{207}\text{Pb}/^{206}\text{Pb}$	$\pm \text{s.e.}$	$^{206}\text{Pb}/^{238}\text{U}$	$\pm 2\sigma$	$^{207}\text{Pb}/^{235}\text{U}$	$\pm 2\sigma$	$^{207}\text{Pb}/^{206}\text{Pb}$	$\pm 2\sigma$		
G92	80.7	572.3	0.1204	0.0008	1.1110	0.0215	0.0673	0.0011	732.6	8.7	758.6	18.2	846.8	25.5	732.58	8.75
G102	60.2	401.7	0.1204	0.0008	1.0756	0.0267	0.0665	0.0013	732.9	9.7	741.5	22.0	821.8	29.3	732.87	9.67
G25	40.7	294.6	0.1235	0.0010	1.1327	0.0346	0.0655	0.0015	750.8	11.1	769.0	26.4	791.4	39.7	750.79	11.13
G72	67.1	326.0	0.1242	0.0008	1.1304	0.0265	0.0675	0.0013	754.7	9.6	767.9	22.5	854.5	36.6	754.69	9.63
G61	137.5	792.9	0.1256	0.0008	1.1668	0.0252	0.0675	0.0012	762.5	9.4	785.2	21.0	852.3	34.9	762.54	9.39
G73	13.0	88.6	0.1268	0.0012	1.1313	0.0455	0.0647	0.0020	769.8	13.4	768.4	34.5	763.3	46.9	769.81	13.39
G17	58.4	458.5	0.1275	0.0008	1.1759	0.0220	0.0670	0.0010	773.4	9.1	789.4	18.2	836.8	31.6	773.36	9.15
G80	44.6	215.7	0.1276	0.0010	1.2330	0.0380	0.0721	0.0017	773.9	11.4	815.7	28.8	988.8	44.5	773.87	11.43
G99	53.1	346.2	0.1276	0.0008	1.1313	0.0235	0.0649	0.0011	774.1	9.4	768.4	19.3	772.4	25.4	774.10	9.38
G21	73.2	597.1	0.1280	0.0009	1.2435	0.0269	0.0702	0.0012	776.7	9.7	820.5	20.6	933.3	34.9	776.67	9.71
G101	57.3	388.5	0.1283	0.0008	1.1498	0.0228	0.0646	0.0010	778.3	9.3	777.2	18.6	760.7	24.5	778.27	9.26
G46	22.1	148.2	0.1303	0.0010	1.1724	0.0326	0.0664	0.0014	789.3	11.0	787.8	25.3	817.8	38.4	789.35	10.95
G31	19.4	122.9	0.1303	0.0010	1.2327	0.0362	0.0669	0.0015	789.6	11.3	815.6	26.1	833.7	39.4	789.58	11.29
G100	362.0	2020.1	0.1318	0.0008	1.2049	0.0187	0.0650	0.0009	798.1	8.8	802.9	16.1	775.0	22.0	798.07	8.77
G81	142.9	999.0	0.1322	0.0008	1.1793	0.0235	0.0666	0.0012	800.3	9.5	791.0	20.9	826.5	34.1	800.29	9.45
G84	69.4	400.7	0.1323	0.0009	1.3202	0.0308	0.0722	0.0014	801.0	10.1	854.6	24.0	992.4	38.9	800.97	10.13
G88	69.4	520.6	0.1323	0.0009	1.2500	0.0281	0.0677	0.0013	801.1	9.9	823.4	22.9	858.8	36.5	801.14	9.91
G78	197.6	1342.4	0.1335	0.0008	1.2145	0.0228	0.0672	0.0011	807.7	9.3	807.3	20.1	843.4	33.3	807.69	9.33
G9	81.4	419.4	0.1336	0.0009	1.2247	0.0264	0.0669	0.0011	808.4	10.0	811.9	20.5	835.3	33.4	808.37	10.01
G12	99.4	558.5	0.1344	0.0008	1.2205	0.0227	0.0665	0.0010	812.7	9.5	810.0	18.4	820.6	31.1	812.69	9.55
G70	63.4	345.8	0.1349	0.0009	1.2293	0.0269	0.0677	0.0013	816.0	10.0	814.0	22.2	859.1	35.4	815.99	10.00
G75	75.6	513.9	0.1352	0.0009	1.2440	0.0270	0.0670	0.0012	817.2	10.0	820.7	22.1	838.7	35.1	817.24	9.99
G83	112.9	895.9	0.1353	0.0009	1.2328	0.0255	0.0663	0.0012	817.8	9.8	815.6	21.7	814.9	34.5	817.80	9.77
G38	182.9	1079.7	0.1354	0.0008	1.2338	0.0211	0.0670	0.0010	818.5	9.3	816.1	17.9	837.5	30.7	818.48	9.31
G91	102.0	634.8	0.1354	0.0008	1.2361	0.0215	0.0661	0.0010	818.7	9.3	817.1	17.5	809.2	23.5	818.65	9.31
G74	146.1	896.5	0.1357	0.0009	1.2652	0.0250	0.0678	0.0012	820.2	9.6	830.2	20.8	861.8	34.1	820.24	9.65
G85	129.4	939.9	0.1358	0.0009	1.3753	0.0277	0.0742	0.0013	820.9	9.8	878.4	22.4	1046.9	37.4	820.93	9.76
G79	57.3	432.0	0.1358	0.0009	1.2427	0.0278	0.0671	0.0013	821.1	10.1	820.1	22.7	840.9	35.7	821.10	10.10
G77	90.9	587.5	0.1359	0.0009	1.2497	0.0262	0.0678	0.0012	821.4	9.9	823.3	21.7	861.2	34.9	821.44	9.87
G55	48.6	348.9	0.1364	0.0009	1.2580	0.0298	0.0692	0.0013	824.4	10.6	827.0	23.3	905.3	36.9	824.44	10.55
G58	36.7	188.0	0.1373	0.0011	1.2719	0.0390	0.0647	0.0015	829.3	12.0	833.3	27.6	765.2	39.3	829.32	12.02
G53	92.7	469.4	0.1374	0.0009	1.2643	0.0264	0.0680	0.0012	830.0	10.0	829.8	21.2	867.0	34.3	830.00	9.98

APPENDIX B (continued). U-Pb ZIRCON AGES OF ZANSKAR RIVER SEDIMENTS

Grain No.	Pb (ppm)	U (ppm)	Ratios						Ages (Ma)						Best Age (Ma)	$\pm 2\sigma$
			$^{206}\text{Pb}/^{238}\text{U}$	$\pm 1\sigma$	$^{207}\text{Pb}/^{235}\text{U}$	$\pm \text{s.e.}$	$^{207}\text{Pb}/^{206}\text{Pb}$	$\pm \text{s.e.}$	$^{206}\text{Pb}/^{238}\text{U}$	$\pm 2\sigma$	$^{207}\text{Pb}/^{235}\text{U}$	$\pm 2\sigma$	$^{207}\text{Pb}/^{206}\text{Pb}$	$\pm 2\sigma$		
G39	89.5	567.0	0.1379	0.0009	1.2668	0.0265	0.0672	0.0011	832.7	10.1	830.9	20.7	843.4	33.5	832.72	10.08
G87	114.9	845.9	0.1380	0.0009	1.2540	0.0260	0.0668	0.0012	833.2	10.0	825.2	22.1	832.8	34.9	833.23	9.97
G1	125.0	557.3	0.1380	0.0008	1.2739	0.0215	0.0665	0.0009	833.5	9.5	834.1	17.3	823.4	15.8	833.51	9.52
G33	51.0	291.6	0.1381	0.0010	1.2804	0.0348	0.0678	0.0014	833.7	11.4	837.0	25.1	862.4	38.0	833.68	11.44
G97	168.6	924.1	0.1392	0.0008	1.2825	0.0212	0.0666	0.0009	840.0	9.3	838.0	17.1	823.7	23.1	840.02	9.28
G5	124.1	848.9	0.1393	0.0008	1.2782	0.0204	0.0670	0.0009	840.7	9.4	836.0	16.8	836.2	29.3	840.70	9.39
G2	101.8	617.0	0.1395	0.0008	1.2797	0.0209	0.0674	0.0009	841.7	9.5	836.7	17.1	851.1	29.8	841.72	9.50
G29	102.0	536.8	0.1395	0.0009	1.2813	0.0240	0.0666	0.0010	841.8	9.8	837.4	19.0	825.6	31.5	841.83	9.84
G107	144.5	862.9	0.1402	0.0009	1.2844	0.0227	0.0663	0.0010	845.5	9.6	838.8	17.9	817.1	23.7	845.51	9.61
G90	96.7	389.1	0.1404	0.0010	1.3912	0.0343	0.0708	0.0013	847.0	11.1	885.2	23.4	952.8	23.0	847.04	11.08
G23	272.6	1726.8	0.1406	0.0008	1.3202	0.0202	0.0671	0.0009	847.9	9.3	854.6	16.6	841.2	29.2	847.88	9.27
G28	78.3	417.5	0.1406	0.0009	1.2804	0.0240	0.0662	0.0010	848.1	9.9	837.0	19.0	811.1	31.3	848.05	9.95
G3	69.1	439.2	0.1411	0.0009	1.3162	0.0234	0.0665	0.0010	851.0	9.8	852.8	18.0	820.6	30.3	851.05	9.83
G65	74.4	504.9	0.1412	0.0009	1.2898	0.0275	0.0676	0.0012	851.6	10.3	841.2	22.0	856.3	34.7	851.56	10.28
G34	117.5	786.3	0.1416	0.0009	1.3332	0.0242	0.0702	0.0011	853.7	9.8	860.3	19.1	933.9	32.5	853.70	9.83
G59	107.2	676.6	0.1419	0.0009	1.2964	0.0262	0.0678	0.0012	855.2	10.2	844.1	21.1	861.5	33.9	855.23	10.16
G68	95.7	559.1	0.1419	0.0009	1.2958	0.0266	0.0675	0.0012	855.6	10.2	843.9	21.5	852.3	34.2	855.62	10.16
G76	126.7	785.7	0.1425	0.0009	1.3105	0.0260	0.0674	0.0012	858.6	10.0	850.4	21.3	850.5	34.0	858.56	10.04
G63	47.0	312.1	0.1427	0.0010	1.3258	0.0325	0.0682	0.0013	859.6	11.1	857.1	24.2	875.2	37.1	859.63	11.06
G82	168.2	1064.0	0.1435	0.0009	1.2912	0.0262	0.0665	0.0012	864.1	10.1	841.8	22.0	822.5	34.4	864.14	10.15
G106	174.0	1083.3	0.1437	0.0009	1.4232	0.0260	0.0710	0.0011	865.3	9.9	898.7	19.0	957.7	25.8	865.27	9.92
G51	131.1	830.9	0.1443	0.0009	1.5603	0.0284	0.0790	0.0012	868.9	9.9	954.6	20.9	1172.6	35.9	868.93	9.91
G20	44.5	271.7	0.1469	0.0010	1.4010	0.0298	0.0711	0.0012	883.5	10.8	889.3	21.4	960.9	34.6	883.45	10.79
G16	156.7	1069.5	0.1498	0.0009	1.4218	0.0223	0.0697	0.0009	899.6	10.0	898.1	17.5	918.9	30.2	899.56	9.98
G69	182.0	1007.4	0.1515	0.0009	1.4682	0.0280	0.0709	0.0012	909.4	10.5	917.4	21.5	954.0	34.6	953.95	34.62
G50	93.6	589.9	0.1526	0.0010	1.4605	0.0277	0.0709	0.0011	915.3	10.6	914.2	21.0	955.7	33.9	955.69	33.93
G62	39.6	206.1	0.1632	0.0012	1.6358	0.0480	0.0721	0.0016	974.6	13.6	984.1	28.9	989.3	41.6	989.33	41.55
G57	43.3	202.4	0.1690	0.0012	1.6812	0.0474	0.0724	0.0015	1006.5	13.7	1001.4	28.4	996.9	40.7	996.93	40.69
G14	14.1	80.1	0.1672	0.0014	1.6789	0.0549	0.0732	0.0017	996.7	14.9	1000.6	30.9	1018.1	43.4	1018.11	43.38
G7	108.2	659.2	0.1523	0.0009	1.5240	0.0255	0.0734	0.0010	913.8	10.3	940.1	18.5	1025.0	31.8	1025.02	31.79
G35	37.0	183.2	0.1712	0.0012	1.6905	0.0388	0.0747	0.0013	1018.5	12.7	1004.9	24.2	1059.1	36.9	1059.09	36.93
G40	38.4	181.4	0.1882	0.0014	2.0836	0.0603	0.0795	0.0016	1111.3	15.2	1143.4	29.3	1184.1	42.2	1184.11	42.17

APPENDIX B (continued). U-Pb ZIRCON AGES OF ZANSKAR RIVER SEDIMENTS

Grain No.	Pb (ppm)	U (ppm)	Ratios						Ages (Ma)						Best Age (Ma)	$\pm 2\sigma$
			$^{206}\text{Pb}/^{238}\text{U}$	$\pm 1\sigma$	$^{207}\text{Pb}/^{235}\text{U}$	$\pm \text{s.e.}$	$^{207}\text{Pb}/^{206}\text{Pb}$	$\pm \text{s.e.}$	$^{206}\text{Pb}/^{238}\text{U}$	$\pm 2\sigma$	$^{207}\text{Pb}/^{235}\text{U}$	$\pm 2\sigma$	$^{207}\text{Pb}/^{206}\text{Pb}$	$\pm 2\sigma$		
G30	145.0	574.2	0.2075	0.0013	2.2591	0.0394	0.0798	0.0011	1215.3	13.3	1199.6	21.6	1191.1	33.7	1191.06	33.72
G60	64.3	253.7	0.2216	0.0015	2.7250	0.0629	0.0940	0.0016	1290.3	15.6	1335.3	28.1	1508.5	41.4	1508.52	41.43
G105	126.5	459.9	0.2280	0.0014	3.0097	0.0595	0.0955	0.0014	1324.1	14.9	1410.1	23.7	1537.8	30.0	1537.76	30.02
G13	75.9	239.2	0.2804	0.0019	3.8314	0.0903	0.0977	0.0015	1593.1	18.8	1599.4	26.9	1579.7	38.6	1579.72	38.64
G45	200.4	664.6	0.2947	0.0018	4.1238	0.0735	0.1008	0.0015	1665.1	17.7	1659.0	25.6	1638.5	37.6	1638.52	37.59
G32	159.7	367.5	0.3076	0.0020	4.5068	0.0986	0.1047	0.0016	1728.7	19.5	1732.2	26.9	1708.2	38.7	1708.17	38.67
G96	196.5	479.4	0.2979	0.0019	4.5776	0.0969	0.1092	0.0015	1680.7	18.8	1745.2	25.7	1786.4	31.2	1786.44	31.16
G36	311.2	560.9	0.4683	0.0028	10.4185	0.1813	0.1635	0.0022	2475.9	24.6	2472.7	27.0	2491.9	38.7	2491.87	38.67
G89	417.3	808.6	0.4205	0.0026	9.7157	0.1946	0.1678	0.0029	2262.7	23.8	2408.2	34.1	2536.0	46.6	2536.02	46.57

Sample 12072504 Lower Stod

G71	22.4	8459.9	0.0029	0.0000	0.0198	0.0004	0.0482	0.0010	18.7	0.3	19.9	0.8	108.6	11.8	18.67	0.26
G67	1.0	263.6	0.0041	0.0001	0.0274	0.0020	0.0469	0.0035	26.5	0.8	27.4	4.0	45.2	14.2	26.50	0.77
G68	31.0	552.6	0.0482	0.0003	0.3513	0.0077	0.0536	0.0011	303.5	4.1	305.7	11.1	352.2	19.3	303.52	4.06
G2	60.4	884.0	0.0509	0.0003	0.3809	0.0072	0.0532	0.0009	319.9	4.0	327.7	9.9	339.0	17.3	319.92	4.05
G49	136.0	1764.8	0.0515	0.0003	0.3898	0.0061	0.0537	0.0007	323.4	3.8	334.2	8.4	358.1	15.9	323.42	3.80
G8	105.4	1410.5	0.0524	0.0003	0.3856	0.0057	0.0522	0.0007	329.5	3.9	331.1	8.0	295.5	14.3	329.48	3.92
G80	62.6	743.5	0.0559	0.0004	0.4636	0.0085	0.0595	0.0010	350.3	4.4	386.8	11.1	585.8	22.0	350.34	4.40
G28	244.7	3010.6	0.0562	0.0003	0.4300	0.0060	0.0542	0.0007	352.2	4.0	363.1	8.1	381.0	15.3	352.17	4.03
G99	60.9	821.2	0.0575	0.0004	0.4313	0.0077	0.0540	0.0009	360.2	4.5	364.1	10.3	371.0	17.4	360.16	4.51
G98	37.9	518.4	0.0575	0.0004	0.4287	0.0092	0.0534	0.0010	360.4	4.8	362.2	12.0	344.6	18.6	360.40	4.75
G108	3.1	42.3	0.0588	0.0007	0.4413	0.0220	0.0541	0.0024	368.0	8.2	371.2	28.0	376.9	35.2	368.02	8.16
G19	126.9	864.7	0.0589	0.0004	0.4349	0.0070	0.0528	0.0007	369.1	4.4	366.6	9.3	319.4	15.3	369.11	4.38
G111	18.2	264.8	0.0590	0.0004	0.4671	0.0120	0.0573	0.0013	369.7	5.4	389.2	15.3	501.9	25.5	369.66	5.36
G60	5.6	82.1	0.0598	0.0005	0.4968	0.0163	0.0585	0.0017	374.3	6.2	409.5	19.6	548.2	31.7	374.29	6.20
G51	72.1	976.6	0.0599	0.0004	0.4436	0.0071	0.0536	0.0008	375.0	4.5	372.8	9.6	354.7	16.1	374.96	4.50
G58	13.3	184.0	0.0600	0.0004	0.4292	0.0109	0.0525	0.0012	375.4	5.4	362.6	14.4	309.0	19.5	375.44	5.35
G104	11.8	143.6	0.0602	0.0005	0.4328	0.0131	0.0534	0.0014	376.5	5.8	365.2	17.2	344.6	23.1	376.54	5.84
G15	57.4	839.8	0.0605	0.0004	0.4520	0.0071	0.0533	0.0007	378.8	4.5	378.7	9.5	341.2	15.7	378.79	4.50
G91	35.9	471.2	0.0613	0.0004	0.4573	0.0087	0.0542	0.0009	383.5	4.9	382.4	11.4	377.7	18.1	383.47	4.86
G30	40.1	591.8	0.0620	0.0004	0.4681	0.0086	0.0544	0.0009	387.6	4.9	389.9	11.2	386.4	18.0	387.59	4.86
G81	5.8	76.5	0.0622	0.0006	0.4952	0.0205	0.0572	0.0020	388.9	7.5	408.5	24.6	498.9	35.6	388.93	7.53

APPENDIX B (continued). U-Pb ZIRCON AGES OF ZANSKAR RIVER SEDIMENTS

Grain No.	Pb (ppm)	U (ppm)	Ratios						Ages (Ma)						Best Age (Ma)	$\pm 2\sigma$
			$^{206}\text{Pb}/^{238}\text{U}$	$\pm 1\sigma$	$^{207}\text{Pb}/^{235}\text{U}$	$\pm \text{s.e.}$	$^{207}\text{Pb}/^{206}\text{Pb}$	$\pm \text{s.e.}$	$^{206}\text{Pb}/^{238}\text{U}$	$\pm 2\sigma$	$^{207}\text{Pb}/^{235}\text{U}$	$\pm 2\sigma$	$^{207}\text{Pb}/^{206}\text{Pb}$	$\pm 2\sigma$		
G64	87.4	1184.8	0.0623	0.0004	0.4958	0.0082	0.0575	0.0008	389.5	4.7	408.9	10.6	508.8	19.2	389.48	4.73
G79	46.6	611.7	0.0626	0.0004	0.4721	0.0088	0.0537	0.0009	391.2	4.9	392.7	11.2	358.1	17.4	391.18	4.85
G92	11.6	166.0	0.0626	0.0006	0.4543	0.0158	0.0522	0.0016	391.2	6.7	380.3	19.9	295.9	23.1	391.24	6.67
G96	2.8	38.5	0.0635	0.0008	0.5083	0.0297	0.0583	0.0029	396.8	10.2	417.3	35.7	540.3	49.7	396.82	10.18
G93	121.4	1768.0	0.0702	0.0004	0.5655	0.0095	0.0563	0.0008	437.1	5.3	455.1	11.5	465.8	18.6	437.12	5.30
G5	139.9	2057.0	0.0723	0.0004	0.5615	0.0077	0.0546	0.0007	449.9	5.2	452.5	9.6	395.5	15.5	449.94	5.17
G63	48.3	511.0	0.0724	0.0005	0.5620	0.0106	0.0571	0.0009	450.5	5.7	452.8	12.9	496.6	20.4	450.54	5.65
G100	99.5	1232.1	0.0730	0.0005	0.5760	0.0104	0.0553	0.0009	454.3	5.5	461.9	12.3	423.6	18.5	454.32	5.53
G46	137.4	2029.0	0.0732	0.0004	0.5683	0.0080	0.0558	0.0007	455.3	5.2	456.9	10.0	442.4	16.5	455.29	5.17
G24	30.0	387.3	0.0737	0.0005	0.5773	0.0117	0.0568	0.0010	458.6	5.9	462.7	13.9	481.8	21.0	458.59	5.88
G88	270.5	2549.4	0.0743	0.0005	0.5966	0.0093	0.0565	0.0008	462.1	5.4	475.1	11.1	471.7	17.9	462.13	5.40
G75	33.5	393.5	0.0758	0.0005	0.6185	0.0138	0.0578	0.0011	470.9	6.2	488.9	15.5	523.3	23.2	470.94	6.23
G18	42.5	514.7	0.0803	0.0005	0.6339	0.0109	0.0566	0.0008	497.6	6.0	498.5	12.5	474.0	18.7	497.61	5.97
G70	43.0	419.0	0.0878	0.0006	0.7062	0.0143	0.0581	0.0010	542.7	6.9	542.5	15.3	534.7	21.8	542.75	6.87
G31	53.2	514.7	0.1046	0.0007	0.9275	0.0151	0.0641	0.0009	641.0	7.6	666.3	14.7	743.6	22.1	641.02	7.59
G11	130.0	1879.2	0.1064	0.0007	1.0341	0.0159	0.0687	0.0009	651.7	7.6	721.0	14.5	888.8	22.8	651.69	7.57
G82	110.0	783.9	0.1112	0.0007	1.0340	0.0181	0.0659	0.0010	679.6	8.1	720.9	16.3	803.8	24.0	679.60	8.12
G12	90.1	558.9	0.1135	0.0007	1.0324	0.0165	0.0660	0.0009	693.0	8.1	720.1	15.2	804.8	22.4	693.04	8.11
G29	561.2	5039.7	0.1144	0.0007	1.0622	0.0140	0.0656	0.0008	698.0	7.8	734.9	13.4	794.0	20.4	698.02	7.75
G65	72.2	530.3	0.1153	0.0007	1.1137	0.0188	0.0698	0.0010	703.6	8.3	759.9	16.4	921.3	24.6	703.57	8.32
G101	109.7	830.5	0.1159	0.0007	1.0920	0.0199	0.0663	0.0010	706.9	8.5	749.5	17.3	817.1	24.7	706.92	8.55
G62	73.9	484.3	0.1193	0.0008	1.1210	0.0199	0.0678	0.0010	726.5	8.8	763.4	17.1	862.8	24.6	726.53	8.75
G59	79.3	499.8	0.1195	0.0007	1.1163	0.0180	0.0671	0.0009	727.9	8.4	761.2	15.9	840.6	23.1	727.92	8.41
G42	214.2	1082.3	0.1265	0.0008	1.2732	0.0193	0.0716	0.0009	768.1	8.8	833.8	15.9	974.6	23.5	768.10	8.81
G74	127.4	1065.5	0.1272	0.0008	1.2096	0.0182	0.0662	0.0009	771.7	8.8	805.0	15.6	814.0	22.2	771.70	8.81
G105	90.0	651.5	0.1276	0.0008	1.1579	0.0205	0.0659	0.0010	774.0	9.1	781.0	17.6	803.8	24.1	773.99	9.15
G54	51.2	352.5	0.1282	0.0009	1.2089	0.0245	0.0665	0.0011	777.8	9.7	804.7	19.1	821.5	25.7	777.82	9.71
G16	49.4	400.3	0.1296	0.0008	1.1547	0.0185	0.0653	0.0009	785.5	9.0	779.5	15.9	784.7	22.0	785.53	9.02
G78	285.2	2006.0	0.1298	0.0008	1.2192	0.0177	0.0660	0.0008	786.6	8.8	809.4	15.3	806.7	21.6	786.61	8.79
G77	55.5	275.4	0.1298	0.0009	1.2725	0.0254	0.0718	0.0011	786.8	9.8	833.5	19.6	980.0	27.6	786.84	9.81
G26	153.1	1248.3	0.1301	0.0008	1.2061	0.0176	0.0660	0.0008	788.2	8.9	803.4	15.0	805.1	21.3	788.21	8.90
G14	170.0	1160.0	0.1303	0.0008	1.2301	0.0170	0.0663	0.0008	789.5	8.8	814.4	14.5	814.3	20.8	789.52	8.78

APPENDIX B (continued). U-Pb ZIRCON AGES OF ZANSKAR RIVER SEDIMENTS

Grain No.	Pb (ppm)	U (ppm)	Ratios						Ages (Ma)						Best Age (Ma)	$\pm 2\sigma$
			$^{206}\text{Pb}/^{238}\text{U}$	$\pm 1\sigma$	$^{207}\text{Pb}/^{235}\text{U}$	$\pm \text{s.e.}$	$^{207}\text{Pb}/^{206}\text{Pb}$	$\pm \text{s.e.}$	$^{206}\text{Pb}/^{238}\text{U}$	$\pm 2\sigma$	$^{207}\text{Pb}/^{235}\text{U}$	$\pm 2\sigma$	$^{207}\text{Pb}/^{206}\text{Pb}$	$\pm 2\sigma$		
G97	72.5	486.1	0.1303	0.0008	1.2512	0.0222	0.0702	0.0010	789.6	9.4	823.9	18.2	934.2	25.7	789.63	9.35
G110	97.1	688.2	0.1303	0.0008	1.2187	0.0222	0.0674	0.0010	789.8	9.5	809.2	18.4	849.2	25.2	789.80	9.47
G39	546.5	3831.2	0.1305	0.0008	1.1903	0.0161	0.0656	0.0008	790.6	8.8	796.1	14.4	794.6	20.5	790.60	8.78
G106	54.2	276.6	0.1306	0.0009	1.1797	0.0228	0.0664	0.0011	791.0	9.7	791.2	19.1	820.0	25.6	791.00	9.69
G25	142.4	755.3	0.1308	0.0008	1.2046	0.0189	0.0668	0.0009	792.3	9.1	802.7	16.0	831.9	22.4	792.26	9.12
G1	74.6	458.8	0.1311	0.0008	1.1602	0.0202	0.0648	0.0009	794.1	9.3	782.0	16.8	768.2	22.7	794.08	9.35
G94	102.9	668.9	0.1311	0.0008	1.2305	0.0216	0.0668	0.0010	794.2	9.3	814.6	17.7	831.9	24.3	794.19	9.35
G7	119.9	901.4	0.1311	0.0008	1.1914	0.0174	0.0647	0.0008	794.3	8.9	796.6	14.9	763.0	20.7	794.25	8.89
G21	473.3	3259.9	0.1312	0.0008	1.2357	0.0166	0.0652	0.0008	794.8	8.8	816.9	14.3	779.2	20.3	794.82	8.78
G86	266.8	2129.1	0.1314	0.0008	1.2319	0.0188	0.0657	0.0009	795.6	9.0	815.2	16.0	798.1	22.2	795.62	9.00
G33	148.9	946.8	0.1316	0.0008	1.1795	0.0185	0.0661	0.0009	797.0	9.1	791.1	15.9	809.9	22.1	797.04	9.11
G61	86.8	474.3	0.1321	0.0008	1.1930	0.0197	0.0671	0.0009	799.8	9.3	797.4	16.8	839.9	23.3	799.78	9.34
G50	293.0	1634.9	0.1326	0.0008	1.2069	0.0169	0.0657	0.0008	802.8	9.0	803.8	15.0	795.2	21.1	802.79	8.99
G53	110.4	548.3	0.1334	0.0008	1.2598	0.0201	0.0681	0.0009	807.5	9.3	827.8	16.5	870.1	23.1	807.46	9.33
G22	154.5	996.5	0.1336	0.0008	1.2338	0.0180	0.0659	0.0008	808.1	9.1	816.0	15.2	803.8	21.3	808.14	9.10
G40	156.5	678.2	0.1336	0.0008	1.2372	0.0192	0.0677	0.0009	808.3	9.2	817.6	16.2	859.4	22.7	808.26	9.21
G103	78.9	476.8	0.1338	0.0009	1.2665	0.0248	0.0680	0.0011	809.6	9.9	830.8	19.5	869.2	26.3	809.62	9.89
G87	283.2	1475.8	0.1339	0.0008	1.3150	0.0211	0.0687	0.0009	810.2	9.3	852.3	16.9	889.4	23.7	810.25	9.32
G73	143.9	895.8	0.1343	0.0008	1.2312	0.0199	0.0656	0.0009	812.3	9.3	814.9	16.6	793.3	22.6	812.35	9.32
G34	113.3	662.7	0.1351	0.0008	1.2471	0.0201	0.0676	0.0009	816.8	9.4	822.1	16.6	856.6	23.0	816.84	9.43
G69	193.5	1484.5	0.1355	0.0008	1.2526	0.0187	0.0653	0.0008	819.4	9.2	824.6	15.8	783.1	21.7	819.39	9.20
G27	67.2	470.0	0.1356	0.0008	1.2356	0.0194	0.0651	0.0009	819.9	9.4	816.9	16.1	778.2	21.8	819.90	9.42
G89	84.3	616.7	0.1358	0.0009	1.3002	0.0230	0.0689	0.0010	820.9	9.8	845.8	18.3	895.7	25.1	820.93	9.76
G35	183.2	1229.6	0.1368	0.0008	1.2487	0.0175	0.0657	0.0008	826.3	9.2	822.8	15.1	795.6	20.9	826.26	9.19
G109	70.7	514.1	0.1368	0.0009	1.2485	0.0227	0.0667	0.0010	826.7	9.9	822.7	18.6	827.5	24.8	826.71	9.87
G20	159.3	1183.0	0.1375	0.0008	1.2880	0.0191	0.0659	0.0008	830.2	9.3	840.4	15.6	804.5	21.4	830.23	9.29
G37	54.9	300.3	0.1375	0.0009	1.2775	0.0227	0.0671	0.0010	830.6	9.9	835.7	17.8	841.2	24.0	830.57	9.86
G47	51.0	297.1	0.1377	0.0009	1.3431	0.0292	0.0699	0.0012	831.6	10.5	864.6	20.9	924.8	27.9	831.59	10.54
G48	111.8	729.8	0.1379	0.0008	1.2563	0.0194	0.0663	0.0009	833.0	9.5	826.2	16.2	815.2	22.2	833.00	9.52
G45	265.3	1206.0	0.1387	0.0008	1.3242	0.0193	0.0684	0.0009	837.1	9.4	856.4	15.9	881.3	22.3	837.14	9.40
G52	180.1	995.9	0.1388	0.0008	1.2799	0.0188	0.0666	0.0008	837.7	9.4	836.8	15.7	826.2	21.7	837.70	9.40
G83	132.5	826.2	0.1389	0.0009	1.2801	0.0203	0.0654	0.0009	838.6	9.6	836.9	16.7	787.2	22.4	838.55	9.62

APPENDIX B (continued). U-Pb ZIRCON AGES OF ZANSKAR RIVER SEDIMENTS

Grain No.	Pb (ppm)	U (ppm)	Ratios						Ages (Ma)						Best Age (Ma)	$\pm 2\sigma$
			$^{206}\text{Pb}/^{238}\text{U}$	$\pm 1\sigma$	$^{207}\text{Pb}/^{235}\text{U}$	$\pm \text{s.e.}$	$^{207}\text{Pb}/^{206}\text{Pb}$	$\pm \text{s.e.}$	$^{206}\text{Pb}/^{238}\text{U}$	$\pm 2\sigma$	$^{207}\text{Pb}/^{235}\text{U}$	$\pm 2\sigma$	$^{207}\text{Pb}/^{206}\text{Pb}$	$\pm 2\sigma$		
G55	232.9	1410.5	0.1389	0.0008	1.2983	0.0193	0.0669	0.0008	838.6	9.4	845.0	15.9	833.7	21.9	838.61	9.40
G72	78.0	509.1	0.1390	0.0009	1.2757	0.0206	0.0669	0.0009	839.1	9.6	834.9	16.9	834.7	22.9	839.12	9.62
G13	130.8	946.1	0.1394	0.0008	1.2750	0.0187	0.0649	0.0008	841.0	9.4	834.6	15.4	770.8	20.9	840.99	9.39
G17	141.1	1046.2	0.1396	0.0008	1.2938	0.0184	0.0655	0.0008	842.1	9.4	843.0	15.2	790.1	20.9	842.12	9.39
G107	65.6	301.5	0.1401	0.0009	1.4857	0.0304	0.0766	0.0013	845.1	10.5	924.6	21.4	1109.5	29.7	845.11	10.52
G84	131.5	641.5	0.1402	0.0009	1.2712	0.0206	0.0664	0.0009	845.9	9.7	832.9	17.1	817.4	23.0	845.91	9.72
G85	169.5	865.9	0.1402	0.0009	1.2909	0.0204	0.0662	0.0009	846.0	9.6	841.7	16.8	811.8	22.6	845.96	9.61
G23	91.1	559.5	0.1404	0.0009	1.2825	0.0195	0.0665	0.0008	846.9	9.6	837.9	16.0	820.6	21.8	846.87	9.61
G43	299.6	1823.9	0.1406	0.0008	1.2997	0.0179	0.0666	0.0008	847.9	9.4	845.6	15.2	825.3	21.0	847.88	9.38
G95	83.4	502.9	0.1410	0.0009	1.3042	0.0229	0.0666	0.0010	850.3	10.1	847.6	18.2	824.3	24.1	850.31	10.06
G41	186.6	1170.6	0.1420	0.0008	1.3296	0.0189	0.0672	0.0008	856.0	9.5	858.7	15.6	845.2	21.6	855.96	9.48
G57	272.3	1626.8	0.1420	0.0009	1.3122	0.0190	0.0668	0.0008	856.1	9.6	851.1	15.9	831.9	21.7	856.07	9.60
G4	249.6	1367.0	0.1422	0.0008	1.3305	0.0184	0.0659	0.0008	857.1	9.5	859.1	15.0	802.9	20.6	857.09	9.48
G6	103.7	540.2	0.1429	0.0009	1.3249	0.0201	0.0675	0.0009	860.9	9.7	856.7	16.2	852.3	22.1	860.93	9.70
G32	83.8	454.4	0.1435	0.0009	1.2750	0.0222	0.0655	0.0009	864.5	10.1	834.6	17.6	791.4	23.0	864.48	10.15
G56	139.6	741.6	0.1437	0.0009	1.3395	0.0204	0.0681	0.0009	865.6	9.8	863.0	16.5	870.7	22.6	865.61	9.81
G102	69.2	289.1	0.1439	0.0009	1.3483	0.0267	0.0662	0.0011	866.5	10.6	866.8	19.9	812.1	25.5	866.51	10.59
G44	197.5	1102.2	0.1445	0.0009	1.4346	0.0213	0.0714	0.0009	870.2	9.8	903.4	16.5	969.5	23.2	870.17	9.80
G38	238.5	1679.1	0.1449	0.0009	1.3477	0.0191	0.0663	0.0008	872.4	9.7	866.6	15.6	815.2	21.1	872.42	9.68
G90	27.2	147.3	0.1464	0.0010	1.4172	0.0324	0.0702	0.0012	880.9	11.4	896.2	22.6	933.6	29.2	880.92	11.36
G66	73.8	353.7	0.1479	0.0009	1.3514	0.0237	0.0668	0.0010	889.1	10.4	868.1	18.2	831.9	23.8	889.12	10.45
G10	217.9	1289.9	0.1482	0.0009	1.3987	0.0201	0.0657	0.0008	891.1	9.9	888.4	15.6	797.5	20.9	891.09	9.88
G9	105.4	292.2	0.3161	0.0019	4.6375	0.0736	0.1088	0.0013	1770.8	18.7	1756.0	22.3	1778.6	27.5	1778.58	27.52
G36	94.6	267.3	0.3141	0.0020	4.7214	0.0866	0.1088	0.0014	1760.9	19.3	1771.1	23.8	1779.3	29.1	1779.25	29.06
G76	25.3	236.8	0.0996	0.0007	0.9031	0.0222	0.0682	0.0014	611.8	8.6	653.4	20.9	875.9	31.0	611.83	8.56
G3	61.3	305.2	0.1242	0.0008	1.2612	0.0241	0.0751	0.0011	754.9	9.3	828.4	18.7	1070.1	27.5	754.92	9.29
G9	3.5	102.8	0.0316	0.0004	0.2452	0.0090	0.0546	0.0019	200.4	4.9	222.6	14.1	395.9	26.0	200.37	4.87
G54	19.6	483.0	0.0409	0.0003	0.3391	0.0066	0.0604	0.0010	258.5	3.7	296.5	9.3	619.0	18.8	258.53	3.72
G31	18.9	226.8	0.0444	0.0004	0.3407	0.0080	0.0560	0.0011	280.2	4.6	297.7	11.2	451.6	18.2	280.17	4.57
G38	9.7	196.6	0.0488	0.0004	0.3781	0.0080	0.0545	0.0010	307.0	4.5	325.7	10.4	390.1	15.1	307.03	4.55
G27	25.0	465.9	0.0491	0.0003	0.3621	0.0070	0.0532	0.0009	309.2	4.2	313.8	9.4	338.6	12.8	309.24	4.18
G91	3.3	62.0	0.0510	0.0007	0.3575	0.0140	0.0520	0.0018	320.5	8.0	310.3	20.1	285.8	21.0	320.54	7.97

APPENDIX B (continued). U-Pb ZIRCON AGES OF ZANSKAR RIVER SEDIMENTS

Grain No.	Pb (ppm)	U (ppm)	Ratios						Ages (Ma)						Best Age (Ma)	$\pm 2\sigma$
			$^{206}\text{Pb}/^{238}\text{U}$	$\pm 1\sigma$	$^{207}\text{Pb}/^{235}\text{U}$	$\pm \text{s.e.}$	$^{207}\text{Pb}/^{206}\text{Pb}$	$\pm \text{s.e.}$	$^{206}\text{Pb}/^{238}\text{U}$	$\pm 2\sigma$	$^{207}\text{Pb}/^{235}\text{U}$	$\pm 2\sigma$	$^{207}\text{Pb}/^{206}\text{Pb}$	$\pm 2\sigma$		
G102	8.7	176.2	0.0511	0.0004	0.4011	0.0082	0.0575	0.0010	321.4	4.8	342.4	10.8	510.8	17.0	321.39	4.78
G89	17.4	312.5	0.0525	0.0004	0.3934	0.0068	0.0544	0.0007	329.7	4.3	336.8	8.7	387.2	12.4	329.67	4.29
G62	3.3	61.2	0.0526	0.0005	0.3855	0.0118	0.0540	0.0014	330.2	6.6	331.1	16.1	371.5	20.0	330.16	6.61
G1	18.9	326.4	0.0526	0.0003	0.4590	0.0072	0.0624	0.0008	330.5	3.9	383.5	8.5	687.8	12.0	330.53	3.92
G43	162.3	2277.2	0.0530	0.0003	0.3944	0.0042	0.0533	0.0003	332.7	3.1	337.6	4.5	341.2	7.3	332.67	3.06
G18	24.6	399.0	0.0532	0.0003	0.3873	0.0054	0.0540	0.0006	333.8	3.6	332.4	6.7	372.3	10.1	333.83	3.55
G76	6.5	110.1	0.0544	0.0004	0.4269	0.0095	0.0562	0.0010	341.4	5.3	361.0	12.0	461.1	17.2	341.42	5.26
G58	60.4	940.7	0.0560	0.0003	0.4200	0.0050	0.0537	0.0004	351.1	3.5	356.1	5.7	356.4	8.5	351.07	3.54
G81	21.2	368.8	0.0561	0.0004	0.4100	0.0085	0.0536	0.0009	352.1	5.1	348.9	10.9	356.0	13.7	352.11	5.13
G3	5.8	97.1	0.0569	0.0005	0.4219	0.0109	0.0525	0.0011	356.9	6.0	357.4	13.7	308.1	15.1	356.93	5.98
G2	2.3	35.9	0.0570	0.0007	0.4265	0.0160	0.0541	0.0018	357.4	8.3	360.7	21.0	373.5	24.0	357.36	8.29
G72	31.3	540.1	0.0571	0.0003	0.4550	0.0061	0.0576	0.0005	358.0	3.9	380.7	6.9	515.0	11.2	357.96	3.90
G48	6.2	108.5	0.0576	0.0004	0.4361	0.0093	0.0549	0.0010	360.7	5.2	367.5	11.7	406.5	15.4	360.71	5.24
G25	46.0	694.3	0.0576	0.0003	0.4265	0.0054	0.0542	0.0005	361.1	3.7	360.7	6.2	377.3	9.1	361.07	3.66
G109	32.0	480.6	0.0577	0.0003	0.4271	0.0061	0.0554	0.0006	361.4	4.1	361.1	7.4	427.2	10.8	361.38	4.14
G8	20.9	288.0	0.0582	0.0003	0.4264	0.0066	0.0522	0.0006	364.5	4.1	360.6	7.8	293.3	9.6	364.49	4.14
G90	7.6	98.7	0.0583	0.0006	0.5001	0.0131	0.0637	0.0014	365.3	6.7	411.8	16.2	732.7	26.3	365.34	6.70
G19	58.6	809.4	0.0583	0.0003	0.4375	0.0055	0.0548	0.0005	365.5	3.7	368.5	6.2	402.8	9.4	365.46	3.65
G84	22.8	360.6	0.0585	0.0004	0.4259	0.0065	0.0548	0.0006	366.5	4.3	360.2	8.0	402.0	11.2	366.50	4.26
G75	3.9	62.0	0.0604	0.0007	0.4903	0.0160	0.0590	0.0016	378.1	8.1	405.1	19.9	567.1	27.7	378.06	8.15
G80	6.8	92.2	0.0604	0.0005	0.4196	0.0111	0.0526	0.0012	378.3	6.6	355.8	14.9	312.4	15.7	378.30	6.57
G65	150.7	2047.1	0.0607	0.0003	0.5119	0.0057	0.0606	0.0004	379.8	3.6	419.7	5.7	623.3	10.0	379.82	3.65
Sample 13071703 Upper Stod																
G96	47.8	691.9	0.0611	0.0003	0.4603	0.0063	0.0545	0.0005	382.1	4.1	384.5	7.1	392.6	9.9	382.07	4.13
G66	9.5	133.0	0.0618	0.0005	0.4739	0.0101	0.0563	0.0010	386.6	5.7	393.9	12.3	463.0	16.3	386.62	5.71
G50	3.3	53.0	0.0619	0.0007	0.4767	0.0158	0.0538	0.0015	387.0	8.0	395.8	19.2	361.8	20.7	387.05	8.01
G88	2.3	28.6	0.0666	0.0009	0.4548	0.0205	0.0502	0.0020	415.8	11.1	380.7	26.5	203.8	18.1	415.76	11.12
G104	150.1	2003.9	0.0682	0.0004	0.5317	0.0066	0.0565	0.0005	425.3	4.5	433.0	6.9	472.5	9.8	425.30	4.47
G22	86.3	1121.1	0.0682	0.0003	0.5323	0.0059	0.0565	0.0004	425.4	4.0	433.3	5.9	472.5	8.9	425.42	3.98
G42	22.3	285.6	0.0738	0.0004	0.5805	0.0082	0.0574	0.0006	458.8	4.9	464.8	8.6	505.8	11.7	458.77	4.92
G52	58.0	786.5	0.0744	0.0004	0.6813	0.0095	0.0647	0.0006	462.7	5.0	527.6	9.0	765.2	13.9	462.67	5.04

APPENDIX B (continued). U-Pb ZIRCON AGES OF ZANSKAR RIVER SEDIMENTS

Grain No.	Pb (ppm)	U (ppm)	Ratios						Ages (Ma)						Best Age (Ma)	$\pm 2\sigma$
			$^{206}\text{Pb}/^{238}\text{U}$	$\pm 1\sigma$	$^{207}\text{Pb}/^{235}\text{U}$	$\pm \text{s.e.}$	$^{207}\text{Pb}/^{206}\text{Pb}$	$\pm \text{s.e.}$	$^{206}\text{Pb}/^{238}\text{U}$	$\pm 2\sigma$	$^{207}\text{Pb}/^{235}\text{U}$	$\pm 2\sigma$	$^{207}\text{Pb}/^{206}\text{Pb}$	$\pm 2\sigma$		
G57	102.2	1221.4	0.0770	0.0004	0.7134	0.0086	0.0665	0.0005	478.1	4.8	546.7	7.8	823.1	12.3	478.13	4.79
G59	12.8	123.2	0.0785	0.0005	0.6139	0.0115	0.0571	0.0008	486.9	6.3	486.0	12.2	493.5	14.7	486.86	6.34
G101	7.0	61.2	0.0808	0.0008	0.7146	0.0208	0.0629	0.0014	501.1	9.5	547.5	20.8	703.5	26.7	501.08	9.54
G17	31.2	380.2	0.0813	0.0004	0.6855	0.0089	0.0595	0.0005	503.6	5.1	530.1	8.3	586.9	11.4	503.58	5.13
G24	92.4	1130.8	0.0814	0.0004	0.6714	0.0074	0.0586	0.0004	504.4	4.6	521.6	6.6	551.9	9.3	504.41	4.65
G111	24.1	250.5	0.0828	0.0005	0.6551	0.0103	0.0582	0.0007	512.6	6.1	511.6	10.3	536.5	13.0	512.58	6.07
G105	72.9	826.5	0.0839	0.0005	0.6689	0.0091	0.0588	0.0005	519.1	5.6	520.0	8.8	558.6	11.5	519.06	5.59
G10	16.9	142.0	0.0856	0.0006	0.6950	0.0132	0.0579	0.0008	529.6	6.9	535.8	12.9	527.1	15.3	529.64	6.89
G11	22.5	248.9	0.0864	0.0005	0.7036	0.0102	0.0582	0.0006	534.4	5.7	540.9	9.5	538.1	12.0	534.45	5.70
G39	59.1	708.2	0.0869	0.0005	0.7161	0.0089	0.0587	0.0005	537.1	5.3	548.4	8.0	556.0	10.5	537.06	5.34
G49	15.2	142.0	0.0880	0.0006	0.6866	0.0126	0.0578	0.0008	543.6	6.9	530.7	12.7	520.7	14.8	543.64	6.87
G82	45.3	496.1	0.0882	0.0005	0.7170	0.0098	0.0584	0.0005	544.8	5.8	548.9	9.0	545.9	11.3	544.82	5.81
G107	40.1	453.6	0.0885	0.0005	0.6876	0.0097	0.0578	0.0006	546.9	6.0	531.3	9.3	523.3	11.4	546.90	6.04
G85	18.7	190.1	0.0896	0.0006	0.7027	0.0124	0.0572	0.0007	553.2	7.0	540.4	12.2	498.5	13.8	553.23	6.98
G21	26.2	308.4	0.0909	0.0005	0.7408	0.0100	0.0582	0.0005	560.7	5.7	562.9	9.0	538.8	11.3	560.74	5.67
G98	5.4	31.8	0.1010	0.0019	0.9670	0.0594	0.0679	0.0033	620.0	22.3	686.9	50.9	865.2	59.6	619.97	22.25
G45	46.6	474.9	0.1029	0.0005	0.8685	0.0105	0.0616	0.0005	631.5	6.1	634.7	8.5	661.3	10.9	631.50	6.08
G56	84.3	834.7	0.1048	0.0006	0.9697	0.0129	0.0669	0.0006	642.7	6.7	688.3	10.1	835.9	13.3	642.65	6.65
G63	14.2	140.3	0.1075	0.0007	0.9231	0.0162	0.0634	0.0008	658.2	8.0	664.0	13.7	721.7	16.4	658.21	8.03
G115	12.4	114.2	0.1086	0.0008	1.0369	0.0214	0.0696	0.0010	664.7	9.4	722.4	16.9	916.6	21.2	664.73	9.42
G12	19.6	162.4	0.1124	0.0007	1.0616	0.0181	0.0675	0.0008	686.9	8.1	734.6	13.6	854.2	17.0	686.90	8.11
G99	24.2	179.5	0.1141	0.0007	0.9818	0.0154	0.0632	0.0007	696.6	8.0	694.5	12.4	716.0	14.5	696.63	7.98
G94	97.6	798.0	0.1147	0.0006	1.0184	0.0123	0.0652	0.0005	700.2	6.9	713.1	9.4	780.5	11.8	700.22	6.94
G47	122.9	1037.8	0.1182	0.0006	1.1082	0.0127	0.0667	0.0005	720.1	6.7	757.3	8.8	828.7	11.3	720.08	6.69
G86	49.7	404.7	0.1224	0.0007	1.1405	0.0167	0.0694	0.0007	744.1	8.2	772.7	12.2	911.8	15.1	744.13	8.16
G103	52.0	421.8	0.1224	0.0007	1.2199	0.0177	0.0737	0.0007	744.2	8.3	809.7	12.4	1032.7	15.8	744.19	8.27
G95	13.0	89.7	0.1237	0.0009	1.1403	0.0236	0.0675	0.0010	751.8	10.3	772.6	17.4	852.9	20.1	751.77	10.33
G97	180.1	1110.4	0.1241	0.0007	1.1364	0.0139	0.0661	0.0005	754.3	7.6	770.8	10.0	809.2	12.1	754.29	7.57
G26	61.1	440.6	0.1244	0.0007	1.1803	0.0161	0.0673	0.0006	755.6	7.7	791.5	11.1	848.0	13.6	755.61	7.68
G70	99.6	501.8	0.1252	0.0007	1.2194	0.0160	0.0698	0.0006	760.3	7.8	809.5	10.9	921.0	13.5	760.31	7.79
G113	49.6	269.2	0.1273	0.0008	1.1246	0.0172	0.0661	0.0007	772.5	8.8	765.2	12.9	808.3	15.0	772.50	8.81
G6	53.0	286.4	0.1286	0.0007	1.2532	0.0181	0.0684	0.0006	779.6	8.1	824.8	11.8	879.2	14.3	779.65	8.11

APPENDIX B (continued). U-Pb ZIRCON AGES OF ZANSKAR RIVER SEDIMENTS

Grain No.	Pb (ppm)	U (ppm)	Ratios						Ages (Ma)						Best Age (Ma)	$\pm 2\sigma$
			$^{206}\text{Pb}/^{238}\text{U}$	$\pm 1\sigma$	$^{207}\text{Pb}/^{235}\text{U}$	$\pm \text{s.e.}$	$^{207}\text{Pb}/^{206}\text{Pb}$	$\pm \text{s.e.}$	$^{206}\text{Pb}/^{238}\text{U}$	$\pm 2\sigma$	$^{207}\text{Pb}/^{235}\text{U}$	$\pm 2\sigma$	$^{207}\text{Pb}/^{206}\text{Pb}$	$\pm 2\sigma$		
G87	28.4	215.4	0.1296	0.0008	1.1855	0.0191	0.0668	0.0007	785.4	9.0	793.9	13.5	831.9	15.7	785.35	9.02
G116	51.7	296.2	0.1305	0.0008	1.1850	0.0176	0.0670	0.0007	790.5	8.8	793.6	12.6	837.2	14.7	790.55	8.78
G40	54.3	431.6	0.1307	0.0007	1.2956	0.0171	0.0703	0.0006	792.1	7.9	843.8	11.0	937.7	13.6	792.09	7.87
G41	23.6	155.8	0.1309	0.0008	1.2235	0.0185	0.0666	0.0006	792.8	8.6	811.4	12.4	825.6	14.5	792.83	8.55
G13	53.0	288.8	0.1311	0.0007	1.2067	0.0172	0.0662	0.0006	794.3	8.1	803.7	11.5	811.8	13.6	794.31	8.09
G117	12.1	80.8	0.1313	0.0010	1.1922	0.0240	0.0681	0.0009	795.1	10.8	797.0	17.5	871.9	19.8	795.11	10.83
G106	42.1	266.0	0.1320	0.0008	1.1792	0.0175	0.0667	0.0006	799.0	8.9	791.0	12.5	829.7	14.5	799.04	8.88
G32	36.2	272.5	0.1340	0.0007	1.3428	0.0184	0.0712	0.0006	810.5	8.2	864.4	11.5	962.3	14.1	810.53	8.19
G71	24.1	167.3	0.1355	0.0008	1.2341	0.0203	0.0676	0.0007	819.0	9.4	816.2	14.1	857.2	16.1	819.00	9.42
G74	36.2	241.5	0.1360	0.0008	1.2856	0.0188	0.0676	0.0006	821.8	8.9	839.3	12.3	857.5	14.3	821.83	8.85
G55	23.7	160.7	0.1364	0.0008	1.2774	0.0217	0.0670	0.0007	824.2	9.5	835.7	14.3	836.5	16.2	824.22	9.53
G46	59.2	409.6	0.1374	0.0007	1.3010	0.0156	0.0677	0.0005	829.7	7.8	846.2	9.9	859.7	11.9	829.72	7.82
G33	138.5	957.9	0.1404	0.0007	1.4671	0.0167	0.0753	0.0005	846.8	7.7	917.0	9.8	1076.8	12.3	846.81	7.69
G53	26.2	181.1	0.1406	0.0008	1.2654	0.0195	0.0666	0.0007	847.8	9.3	830.3	13.2	824.7	14.8	847.77	9.27
G64	18.9	107.7	0.1418	0.0010	1.2701	0.0261	0.0660	0.0009	854.9	11.4	832.4	17.6	807.0	18.8	854.95	11.40
G4	59.1	425.1	0.1421	0.0007	1.3596	0.0161	0.0678	0.0005	856.4	7.8	871.7	9.8	863.1	11.7	856.36	7.79
G36	25.6	181.1	0.1427	0.0008	1.3114	0.0207	0.0660	0.0007	859.6	9.4	850.7	13.3	806.1	14.8	859.63	9.37
G7	36.3	225.2	0.1454	0.0008	1.4631	0.0230	0.0719	0.0007	875.3	9.5	915.3	13.6	983.4	15.9	875.29	9.45
G5	7.9	53.0	0.1468	0.0012	1.4544	0.0359	0.0696	0.0011	882.9	13.2	911.7	21.3	916.0	23.1	882.94	13.15
G23	45.4	278.2	0.1474	0.0008	1.4048	0.0178	0.0714	0.0005	886.1	8.5	890.9	11.0	967.7	13.1	886.09	8.54
G44	49.1	335.3	0.1494	0.0009	1.2912	0.0196	0.0647	0.0006	897.8	9.5	841.8	12.9	765.9	13.9	897.77	9.53
G93	41.7	250.5	0.1545	0.0010	1.4397	0.0251	0.0694	0.0008	926.3	11.1	905.6	15.5	909.2	17.0	909.17	16.98
G114	41.5	223.6	0.1551	0.0009	1.4602	0.0223	0.0695	0.0007	929.4	10.4	914.1	13.8	913.9	15.3	913.91	15.26
G108	30.4	187.7	0.1510	0.0010	1.3830	0.0243	0.0696	0.0008	906.3	11.1	881.7	15.9	917.8	17.5	917.76	17.53
G112	100.6	710.7	0.1518	0.0009	1.4486	0.0233	0.0701	0.0007	910.9	10.5	909.3	14.5	930.7	16.2	930.70	16.17
G20	19.7	123.2	0.1504	0.0009	1.4537	0.0232	0.0704	0.0007	903.0	9.9	911.4	13.9	939.2	15.8	939.17	15.84
G79	41.1	214.6	0.1622	0.0010	1.5504	0.0242	0.0704	0.0007	969.0	10.6	950.7	14.1	939.8	15.5	939.75	15.49
G67	122.3	767.0	0.1653	0.0008	1.6535	0.0196	0.0708	0.0005	986.1	9.3	990.9	10.8	950.5	12.2	950.49	12.19
G61	12.8	65.3	0.1682	0.0012	1.6410	0.0358	0.0711	0.0010	1002.4	13.6	986.1	19.7	959.1	20.8	959.14	20.76
G68	31.4	161.5	0.1609	0.0010	1.6022	0.0290	0.0713	0.0008	961.6	11.6	971.1	16.3	966.3	17.8	966.31	17.81
G83	86.1	439.8	0.1589	0.0009	1.5473	0.0200	0.0713	0.0006	950.4	9.5	949.4	11.6	966.9	13.3	966.89	13.26
G35	126.8	775.1	0.1625	0.0008	1.6227	0.0183	0.0717	0.0005	970.5	8.8	979.0	10.1	976.3	11.7	976.30	11.70

APPENDIX B (continued). U-Pb ZIRCON AGES OF ZANSKAR RIVER SEDIMENTS

Grain No.	Pb (ppm)	U (ppm)	Ratios						Ages (Ma)						Best Age (Ma)	$\pm 2\sigma$
			$^{206}\text{Pb}/^{238}\text{U}$	$\pm 1\sigma$	$^{207}\text{Pb}/^{235}\text{U}$	$\pm \text{s.e.}$	$^{207}\text{Pb}/^{206}\text{Pb}$	$\pm \text{s.e.}$	$^{206}\text{Pb}/^{238}\text{U}$	$\pm 2\sigma$	$^{207}\text{Pb}/^{235}\text{U}$	$\pm 2\sigma$	$^{207}\text{Pb}/^{206}\text{Pb}$	$\pm 2\sigma$		
G37	4.8	24.5	0.1607	0.0023	1.6444	0.0787	0.0719	0.0022	960.8	25.4	987.4	42.4	983.7	42.5	983.68	42.54
G30	39.6	218.7	0.1708	0.0009	1.6636	0.0233	0.0723	0.0006	1016.6	10.1	994.8	12.7	993.6	14.2	993.55	14.17
G29	39.3	216.2	0.1762	0.0010	1.8457	0.0265	0.0733	0.0006	1045.9	10.5	1061.9	12.9	1020.9	14.4	1020.88	14.37
G78	186.8	1134.9	0.1635	0.0008	1.7596	0.0205	0.0734	0.0005	976.3	9.2	1030.7	10.8	1026.1	12.4	1026.12	12.44
G73	85.7	490.4	0.1660	0.0009	1.8080	0.0220	0.0775	0.0006	989.9	9.5	1048.3	11.4	1133.8	13.3	1133.83	13.34
G69	60.9	310.9	0.1965	0.0011	2.0831	0.0282	0.0777	0.0006	1156.6	11.4	1143.3	13.1	1139.5	14.4	1139.47	14.40
G77	96.7	474.0	0.1980	0.0010	2.1326	0.0270	0.0782	0.0006	1164.5	11.2	1159.4	12.4	1153.0	13.7	1152.97	13.69
G51	65.1	323.9	0.1920	0.0010	2.1434	0.0267	0.0789	0.0006	1132.1	10.6	1162.9	11.9	1169.1	13.3	1169.13	13.33
G15	63.5	333.7	0.1819	0.0010	2.0577	0.0275	0.0815	0.0006	1077.2	10.4	1134.8	12.6	1234.5	14.5	1234.49	14.51
G14	122.4	406.3	0.2608	0.0013	3.4822	0.0420	0.0960	0.0006	1494.0	13.1	1523.2	12.5	1548.2	13.6	1548.16	13.57
G34	32.5	116.7	0.2518	0.0015	3.5817	0.0582	0.0965	0.0008	1447.9	14.9	1545.5	15.8	1558.3	16.8	1558.30	16.85
G28	65.4	244.8	0.2561	0.0013	3.5650	0.0455	0.0987	0.0007	1469.7	13.3	1541.8	13.1	1599.9	14.3	1599.89	14.25
G16	83.4	271.7	0.3073	0.0016	4.6588	0.0610	0.1080	0.0007	1727.4	15.4	1759.9	13.7	1765.3	14.5	1765.27	14.50
G100	70.2	173.0	0.3695	0.0021	6.2269	0.0880	0.1257	0.0009	2026.9	19.4	2008.2	16.3	2038.4	16.7	2038.40	16.66
G92	424.1	1002.7	0.3708	0.0019	6.6057	0.0757	0.1284	0.0008	2033.1	17.7	2060.1	14.5	2076.0	15.1	2076.04	15.08
G60	119.1	217.8	0.4658	0.0024	10.9713	0.1456	0.1650	0.0010	2465.1	21.2	2520.7	15.0	2507.1	15.3	2507.15	15.25
G110	22.3	155.0	0.1346	0.0010	1.5339	0.0292	0.0861	0.0011	813.9	10.8	944.1	17.7	1339.3	22.0	813.94	10.80
Sample 12072507 Lower Tsarap																
G18	7.7	237.0	0.0273	0.0002	0.2007	0.0053	0.0544	0.0014	173.8	2.5	185.7	9.0	385.6	18.0	173.82	2.51
G45	77.4	1140.5	0.0551	0.0003	0.4395	0.0076	0.0586	0.0009	345.5	4.0	369.9	10.4	551.5	15.1	345.51	4.03
G54	119.8	1768.4	0.0558	0.0003	0.4630	0.0067	0.0599	0.0008	350.2	3.9	386.4	9.2	601.4	13.9	350.22	3.91
G118	124.4	1890.6	0.0562	0.0003	0.4505	0.0072	0.0579	0.0009	352.7	4.0	377.6	9.9	526.7	14.0	352.72	4.03
G111	161.5	2561.8	0.0565	0.0003	0.4475	0.0066	0.0571	0.0008	354.1	3.9	375.5	9.1	495.8	12.5	354.06	3.91
G64	56.4	863.6	0.0601	0.0004	0.4896	0.0083	0.0588	0.0009	376.3	4.4	404.6	10.8	560.8	14.9	376.29	4.38
G9	95.3	1357.9	0.0625	0.0004	0.5175	0.0071	0.0603	0.0008	391.1	4.2	423.5	9.5	614.7	13.4	391.05	4.25
G90	66.8	977.1	0.0678	0.0004	0.5349	0.0089	0.0577	0.0009	422.9	4.8	435.0	11.4	518.8	14.0	422.89	4.83
G21	47.9	609.7	0.0681	0.0004	0.5613	0.0085	0.0602	0.0008	424.9	4.7	452.3	10.8	611.8	14.4	424.88	4.71
G24	77.3	903.5	0.0690	0.0004	0.5854	0.0091	0.0612	0.0009	430.2	4.8	467.9	11.2	646.6	15.2	430.19	4.82
G136	43.6	657.0	0.0695	0.0004	0.5531	0.0102	0.0573	0.0009	433.2	5.1	447.0	12.6	503.5	14.9	433.20	5.06
G1	114.5	1457.8	0.0696	0.0004	0.5340	0.0072	0.0559	0.0007	433.8	4.7	434.5	9.6	448.8	9.0	433.81	4.70
G122	125.5	1947.4	0.0696	0.0004	0.5743	0.0090	0.0603	0.0009	433.9	4.8	460.8	11.4	612.6	15.0	433.87	4.82

APPENDIX B (continued). U-Pb ZIRCON AGES OF ZANSKAR RIVER SEDIMENTS

Grain No.	Pb (ppm)	U (ppm)	Ratios						Ages (Ma)						Best Age (Ma)	$\pm 2\sigma$
			$^{206}\text{Pb}/^{238}\text{U}$	$\pm 1\sigma$	$^{207}\text{Pb}/^{235}\text{U}$	$\pm \text{s.e.}$	$^{207}\text{Pb}/^{206}\text{Pb}$	$\pm \text{s.e.}$	$^{206}\text{Pb}/^{238}\text{U}$	$\pm 2\sigma$	$^{207}\text{Pb}/^{235}\text{U}$	$\pm 2\sigma$	$^{207}\text{Pb}/^{206}\text{Pb}$	$\pm 2\sigma$		
G126	42.2	564.5	0.0701	0.0004	0.5748	0.0117	0.0605	0.0011	436.8	5.3	461.1	14.2	622.9	18.5	436.82	5.30
G57	88.6	1353.8	0.0702	0.0004	0.5619	0.0086	0.0581	0.0008	437.6	4.8	452.8	10.9	532.4	13.3	437.60	4.82
G55	85.8	1275.5	0.0705	0.0004	0.5633	0.0083	0.0581	0.0008	439.3	4.8	453.7	10.6	532.8	12.9	439.35	4.82
G40	65.9	953.4	0.0716	0.0004	0.5592	0.0086	0.0565	0.0008	445.5	4.9	451.0	10.9	473.2	12.3	445.55	4.93
G19	90.9	1245.8	0.0716	0.0004	0.5567	0.0077	0.0568	0.0007	445.8	4.8	449.4	10.0	483.0	11.5	445.79	4.81
G105	71.4	1023.0	0.0718	0.0004	0.5501	0.0085	0.0561	0.0008	446.7	4.9	445.1	10.9	457.1	12.1	446.69	4.93
G47	73.7	979.1	0.0724	0.0004	0.5631	0.0083	0.0568	0.0008	450.4	4.9	453.5	10.7	484.6	12.2	450.42	4.93
G58	147.1	2133.1	0.0731	0.0004	0.5786	0.0082	0.0571	0.0007	454.9	4.9	463.6	10.5	494.6	12.1	454.87	4.93
G102	89.8	982.5	0.0732	0.0004	0.5839	0.0092	0.0573	0.0008	455.1	5.0	467.0	11.3	503.9	13.1	455.11	5.05
G61	104.3	1000.7	0.0734	0.0004	0.5752	0.0086	0.0567	0.0008	456.7	5.0	461.4	10.9	480.3	12.3	456.73	5.04
G82	113.2	1529.4	0.0735	0.0004	0.6101	0.0093	0.0597	0.0008	457.4	5.0	483.6	11.4	591.3	14.2	457.45	5.04
G121	112.4	1415.3	0.0737	0.0004	0.6256	0.0091	0.0617	0.0008	458.4	4.9	493.4	11.3	663.4	14.9	458.41	4.92
G123	128.2	1808.3	0.0738	0.0004	0.5792	0.0085	0.0569	0.0008	458.8	4.9	464.0	10.9	486.5	12.4	458.77	4.92
G38	112.2	1634.7	0.0738	0.0004	0.5723	0.0077	0.0562	0.0007	459.1	4.9	459.5	10.0	461.1	11.0	459.07	4.92
G130	83.4	1054.0	0.0738	0.0004	0.5736	0.0088	0.0568	0.0008	459.1	5.0	460.3	11.3	483.4	12.7	459.13	5.04
G144	64.4	605.0	0.0741	0.0004	0.5761	0.0102	0.0578	0.0009	460.6	5.3	462.0	12.8	521.0	14.9	460.57	5.28
G44	558.2	8220.9	0.0742	0.0004	0.5742	0.0071	0.0564	0.0007	461.4	4.8	460.7	9.5	469.7	10.6	461.41	4.80
G32	77.3	1017.6	0.0742	0.0004	0.5775	0.0082	0.0568	0.0007	461.6	5.0	462.9	10.5	481.8	11.8	461.65	5.04
G31	120.5	1733.3	0.0744	0.0004	0.5950	0.0084	0.0575	0.0007	462.6	5.0	474.0	10.5	510.4	12.1	462.61	5.04
G112	93.9	1147.2	0.0748	0.0004	0.5776	0.0086	0.0562	0.0008	464.7	5.0	462.9	10.9	460.7	11.9	464.71	5.04
G56	73.6	899.4	0.0748	0.0004	0.5925	0.0088	0.0587	0.0008	465.0	5.2	472.5	11.2	556.4	13.4	465.01	5.16
G117	73.8	1062.1	0.0750	0.0004	0.5866	0.0090	0.0574	0.0008	466.1	5.2	468.7	11.4	505.4	13.0	466.09	5.16
G51	75.9	1066.2	0.0750	0.0004	0.5910	0.0086	0.0577	0.0008	466.2	5.0	471.5	10.9	517.6	12.6	466.21	5.04
G39	51.4	715.1	0.0754	0.0005	0.6025	0.0101	0.0583	0.0009	468.8	5.4	478.8	12.2	540.7	14.3	468.85	5.39
G88	49.1	568.5	0.0757	0.0005	0.6050	0.0104	0.0581	0.0009	470.4	5.4	480.4	12.5	533.9	14.5	470.41	5.39
G8	82.1	973.0	0.0758	0.0004	0.5876	0.0083	0.0560	0.0007	470.9	5.2	469.3	10.4	453.2	11.2	470.88	5.15
G79	95.3	1191.1	0.0758	0.0004	0.5960	0.0089	0.0572	0.0008	471.0	5.2	474.7	11.1	497.3	12.5	471.00	5.15
G97	54.5	717.1	0.0762	0.0005	0.6110	0.0103	0.0580	0.0009	473.1	5.4	484.2	12.4	529.4	14.3	473.10	5.39
G86	33.3	429.4	0.0763	0.0005	0.6528	0.0123	0.0620	0.0010	474.1	5.6	510.2	14.1	674.8	18.1	474.12	5.63
G106	189.6	2174.9	0.0765	0.0004	0.6027	0.0084	0.0568	0.0007	475.3	5.0	478.9	10.6	484.9	11.8	475.26	5.03
G92	75.3	960.9	0.0771	0.0005	0.6523	0.0104	0.0610	0.0009	479.0	5.4	509.9	12.3	639.9	15.4	478.97	5.39
G36	81.9	1043.2	0.0774	0.0005	0.6409	0.0099	0.0601	0.0008	480.5	5.4	502.9	11.8	606.5	14.4	480.47	5.39

APPENDIX B (continued). U-Pb ZIRCON AGES OF ZANSKAR RIVER SEDIMENTS

Grain No.	Pb (ppm)	U (ppm)	Ratios						Ages (Ma)						Best Age (Ma)	$\pm 2\sigma$
			$^{206}\text{Pb}/^{238}\text{U}$	$\pm 1\sigma$	$^{207}\text{Pb}/^{235}\text{U}$	$\pm \text{s.e.}$	$^{207}\text{Pb}/^{206}\text{Pb}$	$\pm \text{s.e.}$	$^{206}\text{Pb}/^{238}\text{U}$	$\pm 2\sigma$	$^{207}\text{Pb}/^{235}\text{U}$	$\pm 2\sigma$	$^{207}\text{Pb}/^{206}\text{Pb}$	$\pm 2\sigma$		
G52	116.8	1571.3	0.0793	0.0004	0.6188	0.0084	0.0566	0.0007	491.6	5.3	489.1	10.5	474.4	11.3	491.64	5.26
G137	45.4	532.8	0.0797	0.0005	0.6127	0.0105	0.0568	0.0009	494.5	5.6	485.3	12.8	485.3	13.7	494.51	5.61
G69	56.5	746.1	0.0799	0.0005	0.6379	0.0107	0.0572	0.0009	495.3	5.6	501.0	12.5	498.1	13.6	495.35	5.61
G109	45.0	528.0	0.0842	0.0005	0.6959	0.0128	0.0596	0.0010	521.3	6.1	536.3	14.3	589.1	16.3	521.26	6.06
G91	43.5	422.0	0.0847	0.0005	0.6958	0.0130	0.0593	0.0010	523.9	6.2	536.3	14.4	579.2	16.2	523.94	6.18
G11	56.6	606.4	0.0887	0.0005	0.7721	0.0114	0.0632	0.0008	547.7	6.0	580.9	12.6	713.3	15.2	547.67	6.04
G71	13.0	100.6	0.0887	0.0008	0.7606	0.0262	0.0603	0.0017	547.9	8.9	574.3	25.1	615.4	27.6	547.90	8.88
G131	73.4	870.4	0.0905	0.0005	0.7363	0.0113	0.0588	0.0008	558.6	6.0	560.3	12.9	559.0	13.9	558.55	6.03
G20	95.0	986.5	0.0936	0.0005	0.7734	0.0106	0.0596	0.0007	576.9	6.1	581.7	12.0	588.7	13.0	576.85	6.13
G150	65.5	667.8	0.0948	0.0006	0.8408	0.0148	0.0636	0.0010	584.0	6.6	619.6	15.2	728.4	17.9	583.98	6.59
G37	152.3	1580.7	0.0989	0.0006	0.8721	0.0123	0.0643	0.0008	608.1	6.6	636.7	13.1	751.2	15.3	608.14	6.57
G132	127.2	1266.7	0.0999	0.0006	0.8359	0.0127	0.0611	0.0008	613.6	6.6	616.9	13.8	642.4	15.0	613.65	6.56
G70	19.5	168.1	0.1054	0.0008	0.9416	0.0264	0.0650	0.0014	646.0	9.1	673.7	23.0	774.3	25.9	645.98	9.10
G127	26.8	239.0	0.1100	0.0007	1.0061	0.0224	0.0657	0.0012	672.7	8.4	706.9	19.5	795.9	21.9	672.75	8.36
G93	33.5	259.3	0.1178	0.0007	1.0864	0.0207	0.0670	0.0011	717.8	8.3	746.8	17.8	838.1	19.8	717.77	8.30
G66	82.9	667.1	0.1191	0.0007	1.0922	0.0171	0.0665	0.0009	725.3	7.8	749.6	15.6	823.1	17.2	725.32	7.83
G72	72.7	480.8	0.1274	0.0007	1.1647	0.0193	0.0657	0.0009	772.7	8.5	784.2	16.5	796.2	17.4	772.73	8.46
G98	19.8	133.0	0.1289	0.0009	1.1820	0.0284	0.0666	0.0013	781.5	9.9	792.3	21.9	826.5	23.1	781.47	9.94
G125	13.8	79.7	0.1335	0.0010	1.1875	0.0326	0.0651	0.0014	807.5	10.9	794.8	24.6	777.2	24.8	807.52	10.92
G143	48.1	321.4	0.1361	0.0008	1.2890	0.0249	0.0697	0.0011	822.7	9.4	840.8	19.6	918.9	21.2	822.74	9.42
G128	443.2	2222.2	0.1373	0.0008	1.2644	0.0181	0.0668	0.0009	829.5	8.6	829.9	16.0	831.5	16.7	829.55	8.62
G6	264.0	1665.8	0.1447	0.0008	1.3814	0.0183	0.0695	0.0008	871.2	9.0	881.0	15.4	913.0	16.1	871.19	9.01
G34	20.9	83.7	0.1453	0.0011	1.4629	0.0421	0.0723	0.0015	874.4	12.2	915.2	26.6	993.0	28.4	874.39	12.16
G84	100.0	503.7	0.1461	0.0008	1.3974	0.0227	0.0694	0.0010	878.8	9.4	887.9	17.6	909.5	18.4	878.84	9.45
G94	38.8	218.1	0.1463	0.0009	1.4287	0.0299	0.0721	0.0012	880.2	10.5	901.0	21.1	988.8	22.6	880.19	10.46
G104	25.9	133.7	0.1470	0.0010	1.4122	0.0339	0.0688	0.0013	884.0	11.0	894.1	22.9	893.0	23.5	884.01	11.02
G124	30.0	170.8	0.1482	0.0009	1.3997	0.0286	0.0688	0.0011	890.6	10.3	888.8	20.7	893.9	21.2	890.64	10.33
G103	47.3	294.4	0.1542	0.0009	1.4987	0.0281	0.0694	0.0011	924.2	10.4	929.9	19.7	909.8	20.1	909.76	20.10
G135	72.7	382.9	0.1686	0.0010	1.6529	0.0279	0.0708	0.0010	1004.3	10.8	990.7	19.5	951.4	19.5	951.36	19.53
G99	91.5	569.2	0.1584	0.0009	1.5981	0.0255	0.0713	0.0010	948.0	10.1	969.5	18.1	965.5	18.7	965.45	18.69
G134	57.0	293.1	0.1616	0.0010	1.5792	0.0294	0.0715	0.0011	965.8	10.8	962.1	20.4	972.3	21.0	972.31	20.98
G145	73.9	406.5	0.1650	0.0010	1.6229	0.0271	0.0720	0.0010	984.7	10.5	979.1	19.4	985.7	20.0	985.66	19.96

APPENDIX B (continued). U-Pb ZIRCON AGES OF ZANSKAR RIVER SEDIMENTS

Grain No.	Pb (ppm)	U (ppm)	Ratios						Ages (Ma)						Best Age (Ma)	$\pm 2\sigma$
			$^{206}\text{Pb}/^{238}\text{U}$	$\pm 1\sigma$	$^{207}\text{Pb}/^{235}\text{U}$	$\pm \text{s.e.}$	$^{207}\text{Pb}/^{206}\text{Pb}$	$\pm \text{s.e.}$	$^{206}\text{Pb}/^{238}\text{U}$	$\pm 2\sigma$	$^{207}\text{Pb}/^{235}\text{U}$	$\pm 2\sigma$	$^{207}\text{Pb}/^{206}\text{Pb}$	$\pm 2\sigma$		
G101	104.4	678.6	0.1585	0.0009	1.5627	0.0237	0.0721	0.0010	948.2	10.0	955.5	17.8	989.6	18.6	989.61	18.56
G16	82.3	474.0	0.1623	0.0009	1.6280	0.0236	0.0722	0.0009	969.7	10.2	981.1	17.0	991.9	17.5	991.87	17.51
G43	97.5	532.1	0.1590	0.0009	1.5909	0.0253	0.0725	0.0010	951.3	10.2	966.7	17.9	1000.8	18.6	1000.85	18.58
G63	70.1	395.0	0.1664	0.0010	1.6545	0.0256	0.0726	0.0009	992.4	10.5	991.3	18.0	1002.8	18.4	1002.81	18.41
G133	19.8	93.9	0.1628	0.0011	1.6663	0.0396	0.0727	0.0013	972.4	12.0	995.8	24.0	1005.6	24.7	1005.60	24.73
G115	77.0	440.3	0.1656	0.0010	1.6556	0.0265	0.0730	0.0010	988.0	10.5	991.7	18.8	1015.1	19.5	1015.06	19.48
G4	179.5	841.3	0.1701	0.0010	1.7111	0.0230	0.0738	0.0009	1012.4	10.5	1012.7	16.8	1036.6	17.2	1036.55	17.22
G87	46.6	257.9	0.1622	0.0010	1.6166	0.0309	0.0739	0.0011	968.8	11.0	976.7	20.5	1037.4	21.4	1037.37	21.44
G5	93.7	518.6	0.1696	0.0010	1.7291	0.0261	0.0739	0.0009	1009.7	10.7	1019.4	17.8	1039.0	18.3	1039.01	18.28
G74	54.2	346.4	0.1528	0.0009	1.5282	0.0266	0.0741	0.0011	916.8	10.2	941.8	19.0	1045.3	20.4	1045.28	20.39
G12	37.7	207.3	0.1587	0.0009	1.6291	0.0281	0.0746	0.0010	949.5	10.5	981.5	18.9	1057.2	20.1	1057.20	20.05
G107	18.1	89.8	0.1744	0.0012	1.8589	0.0502	0.0748	0.0014	1036.3	13.5	1066.6	26.6	1062.6	27.1	1062.59	27.10
G15	118.7	610.4	0.1729	0.0010	1.7725	0.0245	0.0748	0.0009	1027.9	10.7	1035.4	17.1	1063.4	17.6	1063.40	17.59
G148	60.5	312.6	0.1757	0.0011	1.8344	0.0363	0.0764	0.0012	1043.7	11.8	1057.9	22.2	1106.6	23.1	1106.62	23.07
G89	17.6	93.9	0.1632	0.0012	1.7109	0.0503	0.0772	0.0016	974.5	13.5	1012.6	28.4	1125.8	30.1	1125.84	30.12
G29	41.2	185.7	0.1786	0.0011	1.9235	0.0379	0.0783	0.0012	1059.5	12.1	1089.3	21.5	1153.7	22.3	1153.73	22.34
G96	103.5	517.2	0.1867	0.0011	2.0672	0.0313	0.0794	0.0010	1103.3	11.4	1138.0	19.1	1181.4	19.9	1181.38	19.85
G110	44.0	182.3	0.2120	0.0013	2.4514	0.0472	0.0821	0.0012	1239.6	13.6	1257.8	22.7	1248.6	22.9	1248.62	22.90
G46	126.3	586.8	0.1856	0.0010	2.1310	0.0303	0.0832	0.0010	1097.7	11.3	1158.9	18.5	1272.7	19.5	1272.74	19.53
G75	99.4	403.1	0.2354	0.0013	2.8658	0.0451	0.0873	0.0011	1362.6	14.0	1373.0	20.9	1366.9	21.0	1366.90	21.01
G149	65.6	270.1	0.2278	0.0014	2.8001	0.0518	0.0894	0.0013	1323.2	14.3	1355.6	23.7	1413.2	24.3	1413.17	24.26
G76	62.6	243.1	0.2512	0.0015	3.1940	0.0602	0.0947	0.0013	1444.5	15.6	1455.7	23.3	1522.9	23.6	1522.91	23.55
G85	334.7	896.0	0.2799	0.0016	3.7910	0.0535	0.0985	0.0012	1590.7	15.6	1590.8	21.5	1595.2	21.5	1595.16	21.51
G10	64.4	223.5	0.2575	0.0015	3.6348	0.0585	0.1000	0.0012	1477.2	15.3	1557.2	21.5	1624.1	21.8	1624.08	21.84
G73	37.0	106.0	0.2786	0.0019	3.9474	0.1048	0.1001	0.0016	1584.4	19.3	1623.5	28.3	1625.9	28.1	1625.94	28.15
G62	90.4	294.4	0.2477	0.0015	3.4820	0.0615	0.1013	0.0013	1426.6	15.1	1523.1	22.7	1648.6	23.3	1648.62	23.31
G120	288.2	981.8	0.2948	0.0016	4.1819	0.0588	0.1045	0.0013	1665.3	16.2	1670.5	22.5	1704.7	22.6	1704.65	22.62
G108	297.2	921.0	0.2890	0.0016	4.1888	0.0617	0.1045	0.0013	1636.4	16.1	1671.8	22.5	1705.0	22.6	1705.00	22.62
G139	42.7	144.5	0.2640	0.0017	3.7438	0.0836	0.1050	0.0016	1510.4	17.1	1580.8	26.9	1715.0	27.4	1715.02	27.44
G49	206.0	661.1	0.2799	0.0016	4.0774	0.0595	0.1069	0.0013	1590.8	15.8	1649.8	21.6	1747.1	21.9	1747.05	21.87
G53	240.2	690.8	0.3102	0.0017	4.7020	0.0654	0.1090	0.0013	1741.5	16.9	1767.6	21.7	1782.1	21.6	1782.10	21.64
G50	350.8	1029.1	0.3258	0.0018	4.9784	0.0660	0.1106	0.0013	1817.9	17.4	1815.7	21.5	1809.1	21.3	1809.13	21.30

APPENDIX B (continued). U-Pb ZIRCON AGES OF ZANSKAR RIVER SEDIMENTS

Grain No.	Pb (ppm)	U (ppm)	Ratios						Ages (Ma)						Best Age (Ma)	$\pm 2\sigma$
			$^{206}\text{Pb}/^{238}\text{U}$	$\pm 1\sigma$	$^{207}\text{Pb}/^{235}\text{U}$	$\pm \text{s.e.}$	$^{207}\text{Pb}/^{206}\text{Pb}$	$\pm \text{s.e.}$	$^{206}\text{Pb}/^{238}\text{U}$	$\pm 2\sigma$	$^{207}\text{Pb}/^{235}\text{U}$	$\pm 2\sigma$	$^{207}\text{Pb}/^{206}\text{Pb}$	$\pm 2\sigma$		
G83	179.1	655.7	0.2573	0.0015	3.7742	0.0577	0.1128	0.0014	1475.8	15.0	1587.3	22.3	1845.0	23.2	1845.01	23.2
G78	268.3	683.3	0.3260	0.0018	5.8391	0.0829	0.1287	0.0015	1818.7	17.6	1952.2	22.8	2079.6	23.1	2079.61	23.08
G119	216.8	490.2	0.4091	0.0023	7.8168	0.1149	0.1402	0.0018	2210.8	20.9	2210.1	24.8	2229.1	24.6	2229.06	24.57
G147	5.2	10.8	0.3628	0.0046	6.3971	0.4011	0.1499	0.0041	1995.5	43.6	2031.9	54.5	2345.0	52.4	2345.01	52.42
G95	521.7	1326.8	0.3688	0.0020	7.8045	0.1082	0.1528	0.0018	2023.7	19.1	2208.7	23.8	2377.5	24.0	2377.50	24.01
G3	248.6	500.3	0.4631	0.0026	10.2048	0.1495	0.1601	0.0018	2453.1	23.0	2453.5	23.6	2456.4	23.1	2456.40	23.06
G146	379.2	545.6	0.4714	0.0026	10.5159	0.1605	0.1610	0.0021	2489.9	23.1	2481.3	26.4	2466.3	26.2	2466.29	26.17
G27	123.5	242.4	0.4136	0.0024	9.1298	0.1525	0.1610	0.0019	2231.2	21.8	2351.1	24.2	2466.6	23.9	2466.61	23.87
G14	120.0	222.2	0.4464	0.0025	9.7440	0.1493	0.1617	0.0019	2379.2	22.6	2410.9	23.8	2473.5	23.3	2473.51	23.34
G22	542.2	1137.1	0.4581	0.0025	10.2242	0.1298	0.1621	0.0018	2431.2	22.2	2455.3	23.0	2477.7	22.6	2477.68	22.61
G2	205.5	376.1	0.4673	0.0027	10.6365	0.1647	0.1624	0.0019	2471.7	23.4	2491.9	23.8	2480.6	23.3	2480.59	23.26
G68	52.4	119.5	0.3920	0.0027	8.5349	0.2228	0.1631	0.0023	2132.1	24.5	2289.6	28.6	2488.4	28.2	2488.36	28.18
G59	89.2	222.8	0.3707	0.0021	8.2795	0.1376	0.1652	0.0020	2032.5	20.1	2262.1	24.4	2509.6	24.4	2509.6	24.4
G142	318.6	628.6	0.4695	0.0027	11.6550	0.1843	0.1829	0.0024	2481.5	23.2	2577.1	26.7	2679.4	26.5	2679.43	26.55
G129	72.7	121.5	0.5239	0.0031	13.9753	0.2810	0.1937	0.0026	2715.6	26.6	2748.0	27.6	2774.1	27.1	2774.09	27.09
G113	325.3	476.0	0.5262	0.0029	14.1653	0.2164	0.1968	0.0025	2725.4	24.8	2760.8	25.9	2799.5	25.6	2799.51	25.59
G114	68.4	83.1	0.5817	0.0036	17.4957	0.4012	0.2162	0.0029	2955.8	29.5	2962.4	28.0	2952.8	27.2	2952.75	27.21
G77	1.5	111.4	0.0124	0.0002	0.5980	0.0201	0.3488	0.0109	79.7	2.5	476.0	26.7	3701.6	63.7		
G65	3.8	965.6	0.0043	0.0001	0.0337	0.0014	0.0561	0.0024	27.7	0.6	33.7	2.9	457.9	33.4		
G100	-1.3	6.1	0.0939	0.0025	45.0084	4.9649	2.0809	0.0651	578.7	29.1	3887.7	80.0	6248.2	65.3		
G30	8.9	721.8	0.0129	0.0001	0.1217	0.0038	0.0672	0.0020	82.9	1.4	116.6	6.8	844.3	36.5		
G60	4.2	49.3	0.0782	0.0010	3.8431	0.1540	0.3802	0.0090	485.2	12.1	1601.8	44.1	3832.4	49.0		
G13	72.4	1100.0	0.0746	0.0004	2.8444	0.0370	0.2767	0.0032	463.7	5.0	1367.3	19.2	3344.6	24.4		
G116	168.0	2227.6	0.0692	0.0004	0.9965	0.0140	0.1049	0.0014	431.2	4.7	702.0	14.3	1712.4	23.2		
G67	1.0	16.9	0.0583	0.0011	0.6729	0.0560	0.0819	0.0057	365.3	13.6	522.5	58.0	1242.4	101.4		
G25	95.4	973.7	0.0723	0.0004	0.9247	0.0131	0.0934	0.0012	450.1	4.9	664.8	13.5	1496.2	21.5		
G138	22.0	208.6	0.0875	0.0006	1.0776	0.0218	0.0915	0.0015	540.6	6.6	742.5	19.2	1456.4	28.0		
G28	154.8	1084.4	0.1271	0.0007	1.7339	0.0236	0.0998	0.0012	771.3	8.1	1021.2	17.0	1620.4	21.2		
G41	162.8	1994.6	0.0711	0.0004	0.6744	0.0096	0.0695	0.0009	443.0	4.8	523.4	11.5	914.2	17.3		
G23	11.7	82.4	0.1272	0.0009	1.6580	0.0394	0.0943	0.0017	772.1	10.2	992.6	23.9	1513.1	29.4		
G7	1.5	11.5	0.1210	0.0020	1.4491	0.1148	0.0856	0.0048	736.5	23.5	909.5	69.6	1328.0	84.5		
G26	11.1	77.7	0.1224	0.0010	1.3244	0.0418	0.0788	0.0018	744.4	11.4	856.4	28.5	1165.9	34.1	744.42	11.37

APPENDIX B (continued). U-Pb ZIRCON AGES OF ZANSKAR RIVER SEDIMENTS

Grain No.	Pb (ppm)	U (ppm)	Ratios						Ages (Ma)						Best Age (Ma)	$\pm 2\sigma$
			$^{206}\text{Pb}/^{238}\text{U}$	$\pm 1\sigma$	$^{207}\text{Pb}/^{235}\text{U}$	$\pm \text{s.e.}$	$^{207}\text{Pb}/^{206}\text{Pb}$	$\pm \text{s.e.}$	$^{206}\text{Pb}/^{238}\text{U}$	$\pm 2\sigma$	$^{207}\text{Pb}/^{235}\text{U}$	$\pm 2\sigma$	$^{207}\text{Pb}/^{206}\text{Pb}$	$\pm 2\sigma$		
G141	73.5	736.0	0.1021	0.0006	0.9936	0.0180	0.0718	0.0011	626.5	7.1	700.5	17.1	978.9	21.5	626.53	7.14
G17	35.6	367.3	0.0848	0.0005	0.7740	0.0127	0.0656	0.0009	524.9	5.9	582.1	13.5	793.0	17.5	524.89	5.94
G42	1.9	18.9	0.0969	0.0018	0.9511	0.0842	0.0690	0.0047	595.9	21.2	678.7	68.6	898.7	83.0	595.92	21.16
G35	14.1	118.2	0.0948	0.0007	0.9089	0.0270	0.0683	0.0016	583.7	8.7	656.5	23.8	878.3	29.6	583.74	8.71
G48	140.8	389.6	0.3782	0.0021	12.3415	0.1741	0.2378	0.0027	2067.7	19.7	2630.7	24.0	3105.6	24.1		
G140	88.3	903.5	0.0949	0.0006	0.8944	0.0155	0.0683	0.0010	584.5	6.6	648.7	15.7	876.2	19.8	584.45	6.59
G81	50.1	260.0	0.1796	0.0012	2.4797	0.0548	0.0980	0.0015	1064.6	12.8	1266.1	24.3	1586.4	27.0		
G33	435.3	1099.3	0.3703	0.0020	8.7494	0.1170	0.1712	0.0019	2030.8	19.2	2312.2	23.0	2569.6	23.1		
G80	550.0	1438.9	0.3890	0.0021	8.9062	0.1190	0.1660	0.0020	2118.0	19.8	2328.4	23.7	2517.5	23.8		

Sample 14080401 Zara

G100	12.0	297.3	0.0395	0.0005	0.2772	0.0076	0.0509	0.0014	249.8	6.3	248.5	13.3	236.8	11.5	249.79	6.33
G34	92.4	1521.6	0.0498	0.0006	0.3726	0.0078	0.0543	0.0011	313.0	7.5	321.6	13.2	384.3	13.2	313.05	7.49
G55	45.0	723.2	0.0582	0.0007	0.4579	0.0107	0.0571	0.0013	364.4	8.9	382.8	16.9	496.2	18.3	364.36	8.89
G24	99.5	1263.0	0.0633	0.0008	0.4782	0.0078	0.0548	0.0009	395.5	9.1	396.8	12.9	404.9	10.5	395.54	9.09
G69	50.3	784.6	0.0651	0.0008	0.4969	0.0091	0.0554	0.0010	406.3	9.4	409.6	14.5	428.4	12.5	406.32	9.44
G87	72.3	959.9	0.0657	0.0008	0.5085	0.0095	0.0562	0.0010	410.1	9.6	417.4	14.8	458.7	13.3	410.14	9.56
G39	48.7	524.7	0.0661	0.0008	0.5052	0.0097	0.0555	0.0010	412.5	9.7	415.2	15.2	430.8	13.2	412.50	9.67
G68	33.3	376.1	0.0665	0.0008	0.5018	0.0106	0.0547	0.0011	415.1	9.9	412.9	16.4	401.2	13.8	415.10	9.91
G61	20.6	249.2	0.0675	0.0008	0.5153	0.0120	0.0554	0.0013	420.8	10.1	422.0	18.0	428.8	16.0	420.83	10.15
G38	18.0	246.1	0.0675	0.0009	0.5072	0.0120	0.0545	0.0013	421.3	10.3	416.6	18.1	390.9	15.1	421.32	10.27
G64	29.9	349.4	0.0679	0.0009	0.5285	0.0135	0.0565	0.0014	423.6	10.5	430.8	20.0	470.5	19.2	423.55	10.50
G33	22.8	284.8	0.0696	0.0009	0.5354	0.0117	0.0558	0.0012	433.6	10.4	435.4	17.6	445.2	15.5	433.62	10.37
G22	12.1	145.5	0.0697	0.0009	0.5219	0.0153	0.0543	0.0016	434.4	11.1	426.4	22.5	383.9	18.8	434.41	11.09
G12	24.5	320.4	0.0701	0.0009	0.5335	0.0113	0.0552	0.0012	436.9	10.4	434.1	17.1	419.5	14.3	436.88	10.36
G89	22.8	260.8	0.0702	0.0009	0.5425	0.0157	0.0561	0.0016	437.2	11.2	440.1	22.7	455.9	21.2	437.18	11.20
G16	23.4	331.1	0.0703	0.0009	0.5436	0.0115	0.0561	0.0012	438.1	10.5	440.8	17.2	455.1	15.2	438.08	10.48
G90	45.0	559.4	0.0704	0.0009	0.5414	0.0109	0.0558	0.0011	438.5	10.4	439.4	16.4	444.8	14.1	438.50	10.36
G79	32.9	418.3	0.0708	0.0009	0.5438	0.0113	0.0558	0.0011	440.7	10.5	440.9	17.1	442.8	14.7	440.67	10.48
G125	32.3	388.1	0.0711	0.0009	0.5530	0.0125	0.0564	0.0013	442.7	10.6	447.0	18.4	469.7	16.7	442.72	10.59
G99	11.0	142.9	0.0713	0.0009	0.5382	0.0154	0.0547	0.0016	444.2	11.3	437.2	22.4	401.2	19.0	444.22	11.31
G77	36.7	404.1	0.0716	0.0009	0.5550	0.0116	0.0563	0.0012	445.5	10.6	448.3	17.3	463.0	15.2	445.49	10.59

APPENDIX B (continued). U-Pb ZIRCON AGES OF ZANSKAR RIVER SEDIMENTS

Grain No.	Pb (ppm)	U (ppm)	Ratios						Ages (Ma)						Best Age (Ma)	$\pm 2\sigma$
			$^{206}\text{Pb}/^{238}\text{U}$	$\pm 1\sigma$	$^{207}\text{Pb}/^{235}\text{U}$	$\pm \text{s.e.}$	$^{207}\text{Pb}/^{206}\text{Pb}$	$\pm \text{s.e.}$	$^{206}\text{Pb}/^{238}\text{U}$	$\pm 2\sigma$	$^{207}\text{Pb}/^{235}\text{U}$	$\pm 2\sigma$	$^{207}\text{Pb}/^{206}\text{Pb}$	$\pm 2\sigma$		
G123	37.4	453.0	0.0720	0.0009	0.5484	0.0120	0.0553	0.0012	448.0	10.7	443.9	17.9	423.6	14.9	448.01	10.70
G37	15.0	178.9	0.0723	0.0009	0.5584	0.0141	0.0560	0.0014	450.2	11.1	450.5	20.4	452.0	18.2	450.24	11.06
G122	10.6	108.6	0.0727	0.0010	0.5756	0.0176	0.0575	0.0018	452.2	11.7	461.6	24.9	509.6	24.7	452.22	11.66
G105	30.9	374.7	0.0728	0.0009	0.5525	0.0122	0.0550	0.0012	453.2	10.8	446.6	18.0	413.4	14.7	453.24	10.82
G81	30.2	368.5	0.0730	0.0009	0.5820	0.0124	0.0578	0.0012	454.1	10.8	465.7	18.1	523.7	17.1	454.14	10.81
G83	18.5	225.2	0.0730	0.0009	0.5729	0.0137	0.0569	0.0014	454.1	11.1	459.9	19.9	489.2	18.4	454.14	11.05
G130	18.8	230.5	0.0730	0.0010	0.5806	0.0161	0.0577	0.0016	454.4	11.4	464.8	22.9	517.6	22.5	454.38	11.41
G05	54.5	582.6	0.0744	0.0009	0.5699	0.0104	0.0556	0.0010	462.7	10.8	458.0	15.8	434.8	12.5	462.67	10.80
G120	16.2	206.5	0.0746	0.0010	0.6117	0.0172	0.0595	0.0017	463.5	11.8	484.6	24.0	586.9	25.2	463.51	11.76
G128	10.7	118.4	0.0772	0.0011	0.6050	0.0215	0.0569	0.0021	479.3	13.0	480.4	29.6	486.5	27.9	479.33	13.05
G109	14.7	158.4	0.0783	0.0010	0.5994	0.0159	0.0555	0.0015	486.1	12.1	476.9	22.4	433.6	18.7	486.09	12.08
G106	43.8	523.4	0.0791	0.0010	0.6330	0.0128	0.0580	0.0012	490.9	11.6	498.0	18.3	531.3	16.4	490.93	11.59
G53	37.3	335.6	0.0833	0.0010	0.6524	0.0131	0.0568	0.0011	515.8	12.1	510.0	18.6	484.2	15.2	515.85	12.14
G85	16.1	89.0	0.0936	0.0013	0.7919	0.0230	0.0614	0.0018	576.7	14.7	592.2	28.8	652.6	28.1	576.73	14.74
G41	31.2	317.8	0.1013	0.0012	0.8479	0.0161	0.0607	0.0011	622.0	14.4	623.5	20.6	629.3	17.3	622.02	14.40
G49	6.5	60.5	0.1054	0.0014	0.8694	0.0274	0.0599	0.0019	645.9	16.8	635.2	32.6	598.2	28.7	645.86	16.80
G95	45.9	373.4	0.1066	0.0013	0.8984	0.0196	0.0612	0.0013	652.8	15.4	650.9	23.8	645.2	20.5	652.80	15.38
G15	128.1	1235.9	0.1072	0.0013	1.0132	0.0154	0.0685	0.0010	656.6	14.8	710.5	19.0	884.9	16.9	656.64	14.79
G92	10.0	73.9	0.1145	0.0016	0.9974	0.0311	0.0632	0.0020	699.0	18.2	702.5	34.7	714.3	32.1	699.00	18.16
G46	50.8	453.5	0.1165	0.0014	1.0293	0.0179	0.0641	0.0011	710.4	16.2	718.6	21.2	744.6	17.6	710.39	16.17
G65	25.8	209.6	0.1199	0.0015	1.0828	0.0243	0.0655	0.0015	730.1	17.4	745.0	26.9	790.4	24.3	730.10	17.38
G35	20.6	156.7	0.1235	0.0015	1.0936	0.0232	0.0642	0.0013	750.7	17.7	750.3	25.8	749.5	22.1	750.68	17.67
G124	12.9	87.2	0.1235	0.0016	1.0981	0.0294	0.0645	0.0017	750.8	18.6	752.4	31.7	757.7	28.6	750.85	18.59
G14	11.9	76.5	0.1245	0.0018	1.2084	0.0403	0.0704	0.0024	756.2	20.5	804.5	40.8	940.9	41.5	756.18	20.52
G48	12.2	77.0	0.1269	0.0017	1.1591	0.0295	0.0662	0.0017	770.4	18.9	781.5	31.1	814.0	28.4	770.39	18.88
G102	25.0	129.5	0.1271	0.0016	1.1370	0.0268	0.0649	0.0015	771.5	18.4	771.1	28.8	770.4	25.3	771.47	18.42
G19	34.7	217.6	0.1275	0.0016	1.1619	0.0224	0.0661	0.0012	773.6	17.8	782.8	24.4	809.5	20.9	773.59	17.84
G30	26.7	177.1	0.1292	0.0016	1.1901	0.0240	0.0668	0.0013	783.4	18.2	796.0	25.7	831.5	22.4	783.41	18.15
G62	5.4	36.5	0.1311	0.0021	1.3057	0.0548	0.0723	0.0031	793.9	24.1	848.2	52.5	993.8	54.2	793.85	24.05
G129	10.2	96.6	0.1312	0.0017	1.1879	0.0303	0.0657	0.0017	794.9	19.4	795.0	31.5	796.2	28.1	794.88	19.38
G107	24.5	147.8	0.1330	0.0017	1.2036	0.0273	0.0657	0.0015	804.9	19.0	802.3	28.5	795.6	24.7	804.90	19.00
G56	21.8	113.5	0.1334	0.0018	1.2212	0.0331	0.0664	0.0018	807.5	20.1	810.3	33.7	818.7	30.5	807.46	20.13

APPENDIX B (continued). U-Pb ZIRCON AGES OF ZANSKAR RIVER SEDIMENTS

Grain No.	Pb (ppm)	U (ppm)	Ratios						Ages (Ma)						Best Age (Ma)	$\pm 2\sigma$
			$^{206}\text{Pb}/^{238}\text{U}$	$\pm 1\sigma$	$^{207}\text{Pb}/^{235}\text{U}$	$\pm \text{s.e.}$	$^{207}\text{Pb}/^{206}\text{Pb}$	$\pm \text{s.e.}$	$^{206}\text{Pb}/^{238}\text{U}$	$\pm 2\sigma$	$^{207}\text{Pb}/^{235}\text{U}$	$\pm 2\sigma$	$^{207}\text{Pb}/^{206}\text{Pb}$	$\pm 2\sigma$		
G60	114.7	757.9	0.1365	0.0016	1.2996	0.0212	0.0691	0.0011	825.0	18.4	845.5	22.5	900.2	18.7	825.01	18.38
G131	26.2	172.7	0.1389	0.0017	1.4004	0.0313	0.0732	0.0016	838.2	19.7	889.1	30.1	1018.9	28.5	838.16	19.70
G11	64.3	398.3	0.1423	0.0018	1.3163	0.0259	0.0671	0.0013	857.4	19.8	852.9	26.3	841.2	22.0	857.43	19.75
G132	21.9	122.8	0.1473	0.0019	1.4304	0.0338	0.0705	0.0017	885.7	21.0	901.7	31.8	942.1	28.7	885.70	21.01
G01	125.2	757.0	0.1569	0.0019	1.5051	0.0230	0.0696	0.0010	939.2	20.6	932.5	22.7	916.6	17.3	916.58	17.35
G10	12.2	69.9	0.1635	0.0021	1.5787	0.0386	0.0701	0.0017	975.9	23.5	961.9	34.2	930.1	29.6	930.11	29.56
G58	55.8	320.4	0.1556	0.0019	1.5040	0.0266	0.0701	0.0012	932.4	21.0	932.0	25.6	931.3	20.9	931.28	20.87
G25	99.9	567.0	0.1589	0.0019	1.5411	0.0243	0.0703	0.0011	950.8	21.0	946.9	23.5	938.3	18.3	938.29	18.28
G21	43.6	259.9	0.1501	0.0018	1.4570	0.0260	0.0704	0.0012	901.5	20.4	912.8	25.5	940.3	21.2	940.33	21.25
G32	24.8	138.9	0.1664	0.0021	1.6168	0.0323	0.0705	0.0014	992.4	22.8	976.8	29.1	942.1	24.0	942.08	24.04
G71	49.3	244.3	0.1683	0.0020	1.6343	0.0303	0.0705	0.0013	1002.5	22.5	983.5	27.4	942.1	22.1	942.08	22.13
G17	105.4	551.0	0.1514	0.0018	1.4735	0.0233	0.0706	0.0011	908.8	20.2	919.6	23.2	945.9	18.5	945.85	18.48
G50	60.4	318.6	0.1695	0.0020	1.6512	0.0284	0.0707	0.0012	1009.6	22.5	990.0	25.9	947.3	20.4	947.30	20.40
G70	58.0	369.8	0.1565	0.0019	1.5357	0.0305	0.0712	0.0014	937.0	21.5	944.8	28.3	963.4	24.1	963.45	24.12
G28	78.2	445.0	0.1547	0.0018	1.5230	0.0246	0.0714	0.0011	927.0	20.5	939.7	23.9	969.7	19.2	969.74	19.24
G111	108.9	573.7	0.1626	0.0020	1.6045	0.0298	0.0716	0.0013	971.1	21.7	971.9	27.1	974.6	22.6	974.59	22.58
G43	38.8	213.6	0.1526	0.0019	1.5101	0.0308	0.0718	0.0014	915.5	21.3	934.5	28.8	980.0	25.2	979.99	25.22
G23	31.5	161.1	0.1623	0.0020	1.6074	0.0308	0.0719	0.0013	969.4	22.1	973.1	27.9	981.7	23.5	981.69	23.47
G134	35.2	206.9	0.1643	0.0020	1.6294	0.0348	0.0720	0.0015	980.7	22.6	981.6	30.7	984.5	26.5	984.53	26.46
G101	13.7	67.6	0.1736	0.0023	1.7413	0.0441	0.0728	0.0018	1031.6	24.9	1024.0	36.7	1008.4	32.3	1008.39	32.31
G47	67.5	397.4	0.1656	0.0020	1.6625	0.0300	0.0728	0.0013	987.9	22.2	994.3	26.9	1008.9	22.3	1008.95	22.31
G117	68.6	381.4	0.1654	0.0020	1.6606	0.0321	0.0728	0.0014	986.9	22.2	993.6	28.4	1009.2	24.1	1009.23	24.06
G06	19.5	94.3	0.1599	0.0020	1.6066	0.0363	0.0729	0.0016	956.1	22.7	972.8	32.2	1010.9	28.6	1010.90	28.63
G84	49.9	240.3	0.1712	0.0021	1.7240	0.0367	0.0730	0.0015	1018.9	23.6	1017.5	31.4	1015.1	26.9	1015.06	26.89
G94	78.3	473.1	0.1727	0.0021	1.7458	0.0328	0.0734	0.0013	1026.9	23.1	1025.6	28.3	1023.6	23.6	1023.64	23.56
G74	27.6	135.3	0.1791	0.0022	1.8193	0.0366	0.0737	0.0015	1062.2	24.3	1052.4	30.5	1032.7	25.5	1032.72	25.51
G113	62.4	309.3	0.1611	0.0021	1.6456	0.0390	0.0741	0.0017	962.7	22.9	987.9	33.8	1044.7	30.6	1044.74	30.63
G98	46.9	203.4	0.1862	0.0023	1.9175	0.0385	0.0747	0.0015	1100.8	24.9	1087.2	31.0	1060.7	25.9	1060.71	25.90
G121	84.0	441.5	0.1788	0.0022	1.8441	0.0355	0.0748	0.0014	1060.3	23.7	1061.3	29.4	1064.2	24.7	1064.21	24.67
G135	70.6	360.5	0.1819	0.0023	1.8813	0.0394	0.0750	0.0015	1077.5	24.5	1074.5	31.8	1069.6	27.1	1069.57	27.14
G72	72.5	341.3	0.1863	0.0022	1.9283	0.0335	0.0751	0.0013	1101.1	24.3	1091.0	27.6	1071.4	22.2	1071.45	22.21
G67	88.1	482.9	0.1762	0.0021	1.8368	0.0314	0.0756	0.0012	1046.0	23.1	1058.7	26.7	1085.6	21.9	1085.56	21.86

APPENDIX B (continued). U-Pb ZIRCON AGES OF ZANSKAR RIVER SEDIMENTS

Grain No.	Pb (ppm)	U (ppm)	Ratios						Ages (Ma)						Best Age (Ma)	$\pm 2\sigma$
			$^{206}\text{Pb}/^{238}\text{U}$	$\pm 1\sigma$	$^{207}\text{Pb}/^{235}\text{U}$	$\pm \text{s.e.}$	$^{207}\text{Pb}/^{206}\text{Pb}$	$\pm \text{s.e.}$	$^{206}\text{Pb}/^{238}\text{U}$	$\pm 2\sigma$	$^{207}\text{Pb}/^{235}\text{U}$	$\pm 2\sigma$	$^{207}\text{Pb}/^{206}\text{Pb}$	$\pm 2\sigma$		
G108	113.1	652.4	0.1791	0.0022	1.8725	0.0340	0.0759	0.0013	1061.8	23.6	1071.4	28.2	1091.6	23.5	1091.64	23.45
G29	24.0	116.6	0.1664	0.0022	1.7474	0.0450	0.0762	0.0020	992.4	24.5	1026.2	37.4	1099.3	34.6	1099.28	34.56
G86	24.0	104.1	0.1991	0.0026	2.0920	0.0540	0.0762	0.0020	1170.3	28.4	1146.2	39.9	1101.4	34.7	1101.38	34.74
G97	174.4	851.8	0.1767	0.0021	1.8580	0.0331	0.0763	0.0013	1049.1	23.2	1066.3	27.7	1102.2	23.1	1102.17	23.10
G114	9.3	51.2	0.1767	0.0024	1.8737	0.0536	0.0769	0.0022	1048.8	26.5	1071.8	42.1	1119.6	39.0	1119.63	38.97
G66	30.7	123.7	0.1912	0.0024	2.0453	0.0401	0.0776	0.0015	1128.1	25.5	1130.7	31.1	1136.4	26.3	1136.39	26.26
G51	48.7	183.8	0.1912	0.0023	2.0492	0.0372	0.0778	0.0014	1127.8	25.2	1132.0	29.2	1140.5	24.1	1140.49	24.15
G54	79.6	362.7	0.1918	0.0023	2.0651	0.0344	0.0781	0.0012	1130.8	24.8	1137.3	27.2	1150.2	21.8	1150.18	21.85
G137	66.2	271.5	0.1873	0.0023	2.0189	0.0413	0.0782	0.0016	1106.6	25.0	1121.9	32.0	1152.5	27.7	1152.47	27.66
G91	52.3	221.2	0.2003	0.0024	2.1884	0.0413	0.0793	0.0015	1176.7	26.2	1177.4	30.6	1179.1	25.5	1179.13	25.51
G96	103.9	352.5	0.2054	0.0025	2.2852	0.0413	0.0807	0.0014	1204.0	26.5	1207.7	30.0	1215.1	24.7	1215.12	24.75
G52	121.7	549.6	0.2074	0.0025	2.3430	0.0372	0.0820	0.0012	1215.0	26.3	1225.4	27.2	1244.3	21.5	1244.32	21.53
G136	43.1	178.0	0.2188	0.0027	2.5771	0.0536	0.0855	0.0017	1275.7	28.7	1294.2	34.9	1325.8	30.1	1325.77	30.15
G126	24.1	85.9	0.2533	0.0032	3.2175	0.0703	0.0922	0.0020	1455.5	32.9	1461.4	38.8	1470.7	33.5	1470.68	33.55
G78	87.6	289.3	0.2678	0.0032	3.5651	0.0605	0.0966	0.0016	1529.8	32.7	1541.8	32.1	1558.7	25.9	1558.69	25.91
G26	115.5	402.8	0.2722	0.0032	3.6380	0.0549	0.0970	0.0014	1551.8	32.6	1557.9	29.5	1566.4	22.7	1566.44	22.72
G115	149.1	606.1	0.2538	0.0031	3.3998	0.0616	0.0972	0.0017	1457.9	31.5	1504.3	33.3	1571.1	28.0	1571.08	27.96
G31	61.7	186.5	0.2796	0.0034	3.7603	0.0612	0.0976	0.0015	1589.2	33.9	1584.3	31.4	1578.0	24.8	1578.00	24.79
G75	48.9	128.6	0.2812	0.0034	3.8342	0.0695	0.0989	0.0017	1597.3	34.6	1600.0	34.5	1604.0	28.4	1604.05	28.36
G93	53.5	163.8	0.2924	0.0036	4.1279	0.0793	0.1024	0.0019	1653.7	36.1	1659.8	36.7	1668.3	30.7	1668.25	30.71
G40	88.6	247.4	0.2881	0.0034	4.0741	0.0644	0.1026	0.0015	1632.2	34.4	1649.1	31.3	1671.0	24.6	1670.96	24.61
G104	75.9	210.1	0.3032	0.0037	4.3412	0.0795	0.1039	0.0018	1707.1	36.4	1701.2	35.4	1694.6	29.2	1694.57	29.19
G07	66.3	189.6	0.3034	0.0036	4.3550	0.0691	0.1041	0.0016	1708.0	36.0	1703.8	31.8	1698.8	24.9	1698.82	24.87
G08	70.0	197.2	0.3218	0.0039	4.7377	0.0747	0.1068	0.0016	1798.5	37.6	1773.9	32.2	1745.3	25.0	1745.34	24.97
G44	23.8	61.4	0.3054	0.0038	4.5681	0.0873	0.1085	0.0020	1718.1	37.9	1743.5	37.6	1774.4	31.4	1774.38	31.38
G09	240.6	700.0	0.3192	0.0038	4.7827	0.0692	0.1087	0.0015	1785.7	36.7	1781.9	30.1	1777.4	22.7	1777.41	22.70
G03	82.5	252.3	0.2792	0.0034	4.1836	0.0704	0.1087	0.0018	1587.2	34.3	1670.8	33.2	1777.6	27.2	1777.58	27.17
G36	40.0	128.6	0.2935	0.0037	4.4876	0.0850	0.1109	0.0021	1659.0	36.8	1728.7	37.1	1814.4	31.2	1814.38	31.25
G82	91.6	236.8	0.3332	0.0040	5.2275	0.0889	0.1138	0.0019	1853.9	38.8	1857.1	34.6	1861.3	27.9	1861.28	27.88
G112	57.8	116.6	0.4027	0.0049	7.2287	0.1356	0.1302	0.0024	2181.6	45.4	2140.1	39.2	2101.1	32.3	2101.07	32.29
G116	56.6	119.3	0.3920	0.0048	7.2177	0.1366	0.1336	0.0025	2132.1	44.6	2138.7	39.5	2145.7	32.9	2145.69	32.88
G45	54.4	93.9	0.4554	0.0055	10.0920	0.1624	0.1607	0.0025	2419.3	49.0	2443.2	36.2	2463.5	28.4	2463.46	28.45

APPENDIX B (continued). U-Pb ZIRCON AGES OF ZANSKAR RIVER SEDIMENTS

Grain No.	Pb (ppm)	U (ppm)	Ratios						Ages (Ma)						Best Age (Ma)	$\pm 2\sigma$
			$^{206}\text{Pb}/^{238}\text{U}$	$\pm 1\sigma$	$^{207}\text{Pb}/^{235}\text{U}$	$\pm \text{s.e.}$	$^{207}\text{Pb}/^{206}\text{Pb}$	$\pm \text{s.e.}$	$^{206}\text{Pb}/^{238}\text{U}$	$\pm 2\sigma$	$^{207}\text{Pb}/^{235}\text{U}$	$\pm 2\sigma$	$^{207}\text{Pb}/^{206}\text{Pb}$	$\pm 2\sigma$		
G18	76.8	107.7	0.4394	0.0054	9.7428	0.1575	0.1608	0.0025	2348.0	48.3	2410.8	36.4	2464.4	28.7	2464.40	28.66
G42	388.3	906.1	0.4249	0.0050	9.4211	0.1383	0.1608	0.0022	2282.6	45.2	2379.9	33.2	2464.5	25.4	2464.51	25.44
G63	102.9	190.9	0.4444	0.0054	9.8621	0.1597	0.1610	0.0025	2370.5	47.8	2422.0	36.1	2465.9	28.5	2465.87	28.53
G103	145.2	192.3	0.4609	0.0056	10.2327	0.1805	0.1611	0.0027	2443.5	49.2	2456.0	38.6	2467.0	31.5	2467.03	31.50
G80	81.7	135.7	0.4592	0.0056	10.2717	0.1735	0.1623	0.0026	2435.9	49.1	2459.6	37.4	2479.7	30.0	2479.66	30.05
G04	226.1	440.1	0.4663	0.0055	10.4786	0.1500	0.1630	0.0022	2467.4	48.4	2478.0	33.0	2486.9	24.7	2486.92	24.70
G59	233.5	415.7	0.4457	0.0053	10.0405	0.1543	0.1634	0.0024	2376.1	47.2	2438.5	34.6	2491.4	26.9	2491.36	26.92
G118	134.0	231.4	0.4777	0.0058	10.7900	0.1972	0.1639	0.0029	2517.2	50.4	2505.2	39.7	2496.2	32.7	2496.19	32.75
G133	59.0	96.6	0.4553	0.0058	10.4010	0.2135	0.1658	0.0033	2418.7	51.1	2471.1	44.1	2515.3	37.5	2515.28	37.48
G73	109.3	177.6	0.5041	0.0061	11.6851	0.1895	0.1682	0.0026	2631.5	51.9	2579.5	36.6	2539.3	28.8	2539.31	28.83
G27	370.8	646.6	0.4700	0.0056	11.3018	0.1653	0.1744	0.0024	2483.6	48.8	2548.4	33.8	2600.5	25.7	2600.51	25.68
G127	48.2	88.1	0.4760	0.0061	11.8463	0.2400	0.1806	0.0036	2510.0	52.8	2592.3	44.2	2658.0	37.4	2658.02	37.43
G88	72.0	110.4	0.5241	0.0064	13.1822	0.2278	0.1825	0.0030	2716.7	54.1	2692.8	38.9	2675.4	31.3	2675.45	31.30
G76	128.4	193.6	0.5345	0.0065	16.9115	0.2761	0.2296	0.0036	2760.2	54.2	2929.8	37.7	3049.0	30.0	3048.98	30.01
G110	146.5	232.3	0.5878	0.0071	18.8884	0.3332	0.2331	0.0040	2980.5	57.6	3036.1	40.2	3073.7	32.8	3073.73	32.82
G13	150.1	212.7	0.6346	0.0075	23.6373	0.3397	0.2702	0.0036	3167.9	59.3	3253.6	34.9	3307.0	26.2	3306.95	26.16
G57	29.4	230.1	0.1111	0.0015	1.1674	0.0291	0.0762	0.0019	679.1	16.8	785.4	30.8	1100.9	33.5	679.13	16.83
G119	10.3	117.0	0.0723	0.0010	0.6248	0.0188	0.0627	0.0019	449.9	11.7	492.8	25.9	698.4	30.6	449.94	11.66
G20	39.5	529.6	0.0688	0.0008	0.5123	0.0097	0.0540	0.0010	428.7	10.0	420.0	15.2	372.7	11.5	428.74	10.01
G02	22.2	212.7	0.0851	0.0011	0.6522	0.0158	0.0556	0.0013	526.3	12.8	509.8	21.8	436.8	17.1	526.25	12.83
G104	12.1	336.5	0.0293	0.0004	0.2375	0.0045	0.0562	0.0010	186.4	4.4	216.3	8.1	461.5	20.5	186.35	4.38
G10	20.8	661.4	0.0322	0.0004	0.2224	0.0040	0.0513	0.0009	204.2	4.7	203.9	7.7	254.3	14.7	204.18	4.75
G75	17.7	473.8	0.0329	0.0004	0.2177	0.0040	0.0484	0.0008	208.4	5.0	200.0	7.6	116.9	11.0	208.36	4.99
G66	17.1	523.5	0.0330	0.0004	0.2323	0.0039	0.0511	0.0008	209.2	4.9	212.1	7.4	244.9	13.9	209.23	4.87
G7	27.7	858.8	0.0336	0.0004	0.2471	0.0036	0.0523	0.0007	213.1	4.7	224.2	6.9	299.0	14.2	213.10	4.74
G40	15.5	451.2	0.0351	0.0004	0.2520	0.0047	0.0517	0.0009	222.6	5.2	228.2	8.5	273.5	15.5	222.64	5.23
G29	146.7	2430.9	0.0598	0.0007	0.4820	0.0060	0.0588	0.0007	374.1	8.0	399.4	10.4	559.0	16.9	374.10	8.03
G17	16.3	196.9	0.0661	0.0008	0.5385	0.0105	0.0578	0.0010	412.8	9.6	437.4	14.5	522.9	21.1	412.80	9.55
G11	23.0	258.1	0.0682	0.0008	0.5887	0.0111	0.0617	0.0010	425.3	9.8	470.0	15.0	664.8	23.1	425.30	9.78
G4	54.0	767.8	0.0689	0.0008	0.5614	0.0074	0.0584	0.0007	429.5	9.2	452.5	11.7	546.3	17.3	429.46	9.17
G92	44.8	604.0	0.0702	0.0008	0.5666	0.0089	0.0589	0.0008	437.6	10.0	455.8	13.4	564.1	19.2	437.60	10.00
G81	12.4	139.0	0.0703	0.0009	0.5865	0.0142	0.0584	0.0012	438.2	11.1	468.6	17.9	545.9	24.6	438.20	11.08

APPENDIX B (continued). U-Pb ZIRCON AGES OF ZANSKAR RIVER SEDIMENTS

Grain No.	Pb (ppm)	U (ppm)	Ratios						Ages (Ma)						Best Age (Ma)	$\pm 2\sigma$
			$^{206}\text{Pb}/^{238}\text{U}$	$\pm 1\sigma$	$^{207}\text{Pb}/^{235}\text{U}$	$\pm \text{s.e.}$	$^{207}\text{Pb}/^{206}\text{Pb}$	$\pm \text{s.e.}$	$^{206}\text{Pb}/^{238}\text{U}$	$\pm 2\sigma$	$^{207}\text{Pb}/^{235}\text{U}$	$\pm 2\sigma$	$^{207}\text{Pb}/^{206}\text{Pb}$	$\pm 2\sigma$		
G56	26.4	276.4	0.0704	0.0009	0.5867	0.0112	0.0600	0.0010	438.5	10.4	468.8	15.3	604.3	22.3	438.50	10.36
G79	19.5	194.7	0.0705	0.0009	0.6031	0.0115	0.0620	0.0010	439.3	10.5	479.2	15.7	673.4	23.5	439.29	10.48
G28	13.4	137.9	0.0712	0.0009	0.5927	0.0112	0.0589	0.0010	443.3	10.2	472.6	15.0	563.0	21.4	443.32	10.23
G85	8.7	100.4	0.0718	0.0010	0.5932	0.0142	0.0608	0.0012	447.0	11.4	472.9	18.6	631.1	26.5	446.99	11.43
G14	42.3	488.7	0.0719	0.0008	0.6096	0.0091	0.0617	0.0008	447.4	9.7	483.3	13.2	663.4	19.9	447.35	9.74
G23	46.3	554.9	0.0728	0.0008	0.5705	0.0082	0.0582	0.0007	453.1	9.9	458.3	12.7	535.4	17.9	453.12	9.85
G68	25.7	295.7	0.0730	0.0009	0.5834	0.0103	0.0582	0.0009	453.9	10.5	466.7	14.5	536.5	20.0	453.90	10.45
G78	11.5	105.9	0.0736	0.0010	0.6587	0.0154	0.0646	0.0013	457.9	11.5	513.8	19.0	761.7	28.4	457.93	11.53
G57	24.5	195.8	0.0743	0.0009	0.6141	0.0124	0.0592	0.0010	462.1	10.9	486.1	16.2	573.4	22.4	462.13	10.92
G25	27.9	329.9	0.0746	0.0009	0.6016	0.0100	0.0577	0.0008	463.8	10.3	478.2	13.9	519.5	19.0	463.81	10.32
G18	30.6	372.9	0.0753	0.0009	0.5915	0.0090	0.0577	0.0008	468.1	10.2	471.9	13.3	518.8	18.1	468.07	10.19
G59	90.9	659.7	0.0753	0.0009	0.6162	0.0096	0.0586	0.0008	468.2	10.6	487.4	13.7	553.4	18.8	468.25	10.55
G34	35.3	468.9	0.0754	0.0009	0.7153	0.0115	0.0676	0.0009	468.3	10.4	547.9	15.0	856.3	23.2	468.31	10.43
G87	10.1	95.4	0.0775	0.0010	0.6309	0.0143	0.0574	0.0011	481.4	12.0	496.7	17.8	506.2	22.6	481.36	11.97
G102	6.9	69.5	0.0777	0.0000	0.6793	0.0000	0.0611	0.0000	482.4	0.0	526.3	0.0	644.2	7.3	482.38	0.00
G26	25.9	289.0	0.0797	0.0009	0.7183	0.0112	0.0628	0.0009	494.4	10.9	549.6	14.7	700.4	21.0	494.39	10.87
Sample 13072301 Toze Lungpa																
G70	951.7	12925.6	0.0802	0.0014	0.6659	0.0286	0.0602	0.0021	497.1	16.4	518.2	31.9	610.1	39.7	497.14	16.35
G98	19.8	247.7	0.0804	0.0010	0.6885	0.0126	0.0613	0.0010	498.7	11.8	531.9	16.3	649.4	22.2	498.69	11.81
G76	47.1	477.1	0.0809	0.0009	0.6251	0.0095	0.0573	0.0008	501.7	11.2	493.1	14.0	501.2	17.8	501.67	11.21
G47	80.2	1031.5	0.0816	0.0009	0.6977	0.0094	0.0613	0.0007	505.7	11.0	537.4	13.6	650.5	18.7	505.73	10.97
G2	1.9	23.7	0.0835	0.0013	0.6727	0.0272	0.0595	0.0020	516.9	15.9	522.4	30.6	585.4	37.0	516.92	15.95
G64	27.0	297.9	0.0838	0.0010	0.7304	0.0119	0.0597	0.0008	518.5	11.7	556.8	15.1	591.6	19.8	518.53	11.66
G41	27.9	332.6	0.0842	0.0010	0.6997	0.0113	0.0590	0.0008	521.4	11.7	538.6	15.0	567.8	19.4	521.38	11.65
G93	32.9	403.2	0.0857	0.0010	0.7407	0.0115	0.0633	0.0009	530.1	12.1	562.8	15.6	717.7	21.1	530.12	12.11
G49	132.9	1611.8	0.0875	0.0010	0.6933	0.0092	0.0580	0.0007	540.7	11.7	534.8	13.6	529.8	17.0	540.73	11.74
G95	31.4	336.5	0.0887	0.0011	0.7972	0.0134	0.0650	0.0009	547.8	12.7	595.3	16.7	775.6	22.6	547.78	12.67
G44	210.7	2238.4	0.0919	0.0010	0.7821	0.0098	0.0617	0.0007	566.5	12.2	586.7	14.1	664.4	18.2	566.47	12.16
G69	25.0	262.6	0.0963	0.0011	0.8832	0.0148	0.0653	0.0009	592.8	13.4	642.7	17.4	783.1	22.7	592.81	13.41
G27	382.7	2912.4	0.1050	0.0012	0.9983	0.0119	0.0687	0.0007	643.5	13.4	703.0	15.6	890.9	20.1	643.47	13.42
G101	35.5	358.5	0.1053	0.0013	0.9610	0.0162	0.0667	0.0009	645.3	14.8	683.8	18.5	827.2	23.2	645.34	14.81
G88	49.3	455.1	0.1102	0.0013	1.0310	0.0154	0.0685	0.0009	674.1	15.0	719.4	17.9	882.2	22.3	674.08	14.98

APPENDIX B (continued). U-Pb ZIRCON AGES OF ZANSKAR RIVER SEDIMENTS

Grain No.	Pb (ppm)	U (ppm)	Ratios						Ages (Ma)						Best Age (Ma)	$\pm 2\sigma$
			$^{206}\text{Pb}/^{238}\text{U}$	$\pm 1\sigma$	$^{207}\text{Pb}/^{235}\text{U}$	$\pm \text{s.e.}$	$^{207}\text{Pb}/^{206}\text{Pb}$	$\pm \text{s.e.}$	$^{206}\text{Pb}/^{238}\text{U}$	$\pm 2\sigma$	$^{207}\text{Pb}/^{235}\text{U}$	$\pm 2\sigma$	$^{207}\text{Pb}/^{206}\text{Pb}$	$\pm 2\sigma$		
G22	27.5	248.2	0.1110	0.0013	1.0413	0.0175	0.0683	0.0010	678.6	14.9	724.5	18.8	878.9	23.6	678.55	14.85
G80	23.9	200.8	0.1141	0.0014	1.0757	0.0189	0.0671	0.0010	696.7	15.9	741.6	19.5	841.5	23.7	696.69	15.85
G42	33.3	284.1	0.1148	0.0013	1.1031	0.0174	0.0701	0.0009	700.3	15.3	754.8	18.5	929.8	23.1	700.28	15.27
G39	47.3	386.7	0.1148	0.0013	1.1240	0.0167	0.0691	0.0009	700.3	15.2	764.9	17.9	902.3	22.2	700.28	15.15
G24	89.8	818.0	0.1157	0.0013	1.0734	0.0144	0.0685	0.0008	705.5	14.9	740.4	17.0	884.0	20.9	705.48	14.91
G89	41.5	348.6	0.1176	0.0014	1.0833	0.0168	0.0665	0.0009	716.5	16.0	745.2	18.5	821.2	21.9	716.50	16.04
G6	138.9	1078.4	0.1194	0.0013	1.1763	0.0148	0.0714	0.0008	727.0	15.0	789.6	17.0	967.5	21.1	726.99	14.97
G32	84.8	738.6	0.1215	0.0014	1.1076	0.0148	0.0654	0.0008	739.4	15.6	757.0	17.1	787.9	20.0	739.42	15.63
G1	107.8	785.5	0.1220	0.0013	1.0936	0.0144	0.0647	0.0007	741.9	15.3	750.3	16.7	764.9	12.3	741.89	15.28
G12	82.6	654.7	0.1225	0.0014	1.2925	0.0172	0.0721	0.0008	745.0	15.5	842.4	17.7	989.0	21.7	744.99	15.51
G13	97.6	794.9	0.1253	0.0014	1.2614	0.0162	0.0734	0.0008	760.7	15.8	828.5	17.8	1024.5	21.7	760.71	15.81
G15	109.9	794.3	0.1253	0.0014	1.2549	0.0167	0.0716	0.0008	761.0	15.9	825.6	17.9	973.7	21.6	761.00	15.93
G38	141.6	1115.9	0.1285	0.0014	1.3131	0.0171	0.0731	0.0008	779.2	16.3	851.5	18.1	1017.3	21.7	779.19	16.34
G16	92.3	519.6	0.1298	0.0014	1.3085	0.0178	0.0743	0.0009	786.8	16.4	849.4	18.6	1048.3	22.4	786.84	16.43
G51	109.8	870.4	0.1305	0.0015	1.2763	0.0173	0.0711	0.0008	790.7	16.9	835.2	18.6	961.2	21.8	790.72	16.88
G71	17.6	116.9	0.1342	0.0016	1.2859	0.0253	0.0687	0.0011	811.7	18.6	839.5	22.4	890.3	25.6	811.72	18.64
G84	98.4	752.9	0.1377	0.0016	1.3893	0.0195	0.0727	0.0009	831.8	18.1	884.4	19.6	1005.6	22.6	831.76	18.13
G21	90.7	659.7	0.1390	0.0015	1.3411	0.0175	0.0696	0.0008	839.0	17.4	863.7	18.3	915.4	20.8	839.01	17.43
G97	76.2	403.2	0.1392	0.0017	1.3591	0.0210	0.0711	0.0009	840.0	18.7	871.5	20.4	958.9	23.2	840.02	18.67
G63	200.2	1502.6	0.1393	0.0016	1.4488	0.0185	0.0745	0.0008	840.6	17.8	909.4	18.9	1054.8	21.9	840.65	17.77
G43	101.3	756.8	0.1398	0.0016	1.3687	0.0185	0.0697	0.0008	843.8	17.8	875.6	18.8	920.4	21.3	843.76	17.76
G82	55.0	348.6	0.1400	0.0016	1.4301	0.0220	0.0731	0.0009	844.8	18.5	901.6	20.6	1016.4	23.6	844.83	18.55
G8	71.2	509.7	0.1406	0.0016	1.3852	0.0197	0.0715	0.0009	848.0	17.6	882.7	19.2	972.3	22.2	848.00	17.63
G86	31.3	225.6	0.1406	0.0017	1.4306	0.0244	0.0719	0.0010	848.1	19.0	901.8	21.4	982.3	24.5	848.05	18.99
G36	108.5	803.1	0.1409	0.0016	1.3355	0.0177	0.0686	0.0008	849.6	17.7	861.3	18.5	887.0	20.7	849.64	17.74
G65	73.4	486.5	0.1420	0.0016	1.3696	0.0196	0.0701	0.0008	856.1	18.4	876.0	19.5	931.3	21.9	856.07	18.40
G74	24.1	134.6	0.1440	0.0017	1.4649	0.0272	0.0737	0.0011	867.4	19.6	916.0	22.8	1033.8	26.1	867.41	19.61
G19	28.6	187.0	0.1445	0.0018	1.4100	0.0299	0.0693	0.0011	870.1	19.7	893.1	23.6	908.0	26.5	870.12	19.71
G91	13.3	79.4	0.1453	0.0019	1.4612	0.0339	0.0743	0.0013	874.5	21.2	914.5	26.3	1049.6	30.0	874.45	21.16
G99	91.9	642.6	0.1489	0.0018	1.4431	0.0207	0.0708	0.0009	894.8	19.6	907.0	20.3	952.5	22.3	894.79	19.64
G37	25.0	171.5	0.1496	0.0018	1.5707	0.0300	0.0715	0.0010	898.7	20.0	958.7	22.7	971.2	25.5	898.72	19.96
G33	40.2	222.3	0.1719	0.0020	1.7956	0.0288	0.0737	0.0009	1022.7	21.7	1043.9	22.0	1033.8	23.7	1033.81	23.65

APPENDIX B (continued). U-Pb ZIRCON AGES OF ZANSKAR RIVER SEDIMENTS

Grain No.	Pb (ppm)	U (ppm)	Ratios						Ages (Ma)						Best Age (Ma)	$\pm 2\sigma$
			$^{206}\text{Pb}/^{238}\text{U}$	$\pm 1\sigma$	$^{207}\text{Pb}/^{235}\text{U}$	$\pm \text{s.e.}$	$^{207}\text{Pb}/^{206}\text{Pb}$	$\pm \text{s.e.}$	$^{206}\text{Pb}/^{238}\text{U}$	$\pm 2\sigma$	$^{207}\text{Pb}/^{235}\text{U}$	$\pm 2\sigma$	$^{207}\text{Pb}/^{206}\text{Pb}$	$\pm 2\sigma$		
G61	42.9	260.9	0.1562	0.0018	1.6268	0.0251	0.0739	0.0009	935.6	20.2	980.6	21.2	1038.7	23.5	1038.74	23.48
G58	38.6	222.8	0.1576	0.0019	1.6892	0.0300	0.0750	0.0010	943.4	20.7	1004.4	22.8	1067.7	25.4	1067.70	25.44
G60	35.1	188.6	0.1605	0.0019	1.6949	0.0270	0.0766	0.0010	959.6	20.8	1006.6	22.1	1110.5	24.6	1110.53	24.57
G55	54.3	347.5	0.1598	0.0018	1.7492	0.0266	0.0768	0.0009	955.4	20.5	1026.9	21.4	1116.5	23.9	1116.52	23.86
G83	74.2	363.0	0.1786	0.0021	1.9491	0.0298	0.0775	0.0010	1059.0	22.9	1098.2	22.7	1134.3	24.2	1134.34	24.21
G77	79.7	447.3	0.1802	0.0021	1.9664	0.0282	0.0784	0.0009	1068.1	22.7	1104.1	22.2	1156.8	23.7	1156.77	23.67
G62	35.1	177.1	0.1722	0.0020	1.9231	0.0331	0.0786	0.0010	1024.2	22.3	1089.2	23.4	1161.8	25.6	1161.83	25.60
G9	67.6	335.9	0.1755	0.0020	2.0102	0.0292	0.0799	0.0009	1042.4	21.4	1118.9	21.7	1193.3	23.8	1193.29	23.81
G48	76.8	410.4	0.1781	0.0020	2.0112	0.0288	0.0812	0.0010	1056.3	22.1	1119.3	22.0	1226.5	23.9	1226.53	23.94
G50	69.7	228.4	0.2948	0.0034	4.2117	0.0610	0.1035	0.0012	1665.7	33.4	1676.3	26.4	1686.9	26.1	1686.92	26.05
G94	68.4	230.6	0.2725	0.0032	3.9588	0.0633	0.1063	0.0013	1553.3	32.6	1625.8	27.7	1736.9	27.8	1736.91	27.79
G53	32.9	128.5	0.2593	0.0030	3.8261	0.0583	0.1065	0.0013	1486.2	30.4	1598.2	26.4	1739.7	26.8	1739.67	26.83
G45	111.7	314.4	0.2978	0.0034	4.7648	0.0746	0.1114	0.0013	1680.6	33.9	1778.7	27.2	1822.4	27.0	1822.38	27.05
G20	338.6	1143.5	0.2741	0.0030	4.2685	0.0516	0.1114	0.0012	1561.7	30.4	1687.3	25.0	1822.5	25.2	1822.54	25.22
G35	101.9	309.4	0.2896	0.0033	4.6379	0.0677	0.1138	0.0013	1639.4	32.7	1756.1	26.6	1861.6	26.6	1861.60	26.62
G46	95.8	248.2	0.3235	0.0037	5.6932	0.0866	0.1240	0.0014	1806.8	35.9	1930.3	27.8	2015.0	27.3	2014.99	27.34
G72	174.7	381.7	0.4071	0.0047	8.7691	0.1267	0.1557	0.0018	2201.8	42.8	2314.3	29.3	2409.2	28.1	2409.16	28.11
G100	50.6	78.3	0.5349	0.0067	15.6263	0.3583	0.2184	0.0028	2762.2	56.4	2854.2	34.3	2968.6	31.9	2968.56	31.93
G30	57.9	690.6	0.0861	0.0010	0.8222	0.0113	0.0683	0.0008	532.5	11.5	609.3	15.0	876.8	21.4	532.55	11.51
G90	49.0	511.3	0.0924	0.0011	0.9147	0.0145	0.0703	0.0009	569.4	13.0	659.6	17.2	936.3	23.6	569.42	12.98
G73	97.5	787.7	0.1299	0.0015	1.4708	0.0203	0.0814	0.0010	787.1	17.0	918.5	19.8	1230.2	24.1	787.12	17.00
G31	18.2	151.1	0.1033	0.0012	1.0500	0.0204	0.0717	0.0011	633.7	14.5	728.9	20.2	976.0	26.9	633.66	14.49
G96	15.6	115.8	0.1143	0.0015	1.1867	0.0252	0.0749	0.0013	697.4	16.8	794.4	23.0	1065.8	29.3	697.44	16.78
G67	114.5	1171.6	0.0955	0.0011	0.9019	0.0120	0.0688	0.0008	587.8	12.8	652.8	15.7	891.2	21.1	587.81	12.83
G5	89.8	1171.6	0.0819	0.0009	0.7289	0.0092	0.0648	0.0007	507.6	10.6	555.9	13.4	766.2	19.4	507.57	10.61
G52	41.4	359.6	0.1022	0.0012	0.9710	0.0150	0.0695	0.0009	627.3	13.8	689.0	17.5	913.3	23.1	627.29	13.80
G54	126.0	989.0	0.1159	0.0013	1.1642	0.0157	0.0733	0.0009	706.9	15.1	783.9	17.7	1023.1	22.2	706.92	15.14
Sample 13072302 Gata																
G82	137.8	2113.9	0.0649	0.0008	0.5818	0.0123	0.0649	0.0012	405.2	9.9	465.6	16.6	772.1	20.3	405.24	9.93
G75	42.1	591.1	0.0759	0.0010	0.5965	0.0167	0.0576	0.0014	471.7	11.9	475.0	20.6	513.8	19.5	471.66	11.86
G92	36.0	317.9	0.0807	0.0011	0.6368	0.0201	0.0590	0.0016	500.1	12.9	500.3	24.0	567.8	23.6	500.12	12.88

APPENDIX B (continued). U-Pb ZIRCON AGES OF ZANSKAR RIVER SEDIMENTS

Grain No.	Pb (ppm)	U (ppm)	Ratios						Ages (Ma)						Best Age (Ma)	$\pm 2\sigma$
			$^{206}\text{Pb}/^{238}\text{U}$	$\pm 1\sigma$	$^{207}\text{Pb}/^{235}\text{U}$	$\pm \text{s.e.}$	$^{207}\text{Pb}/^{206}\text{Pb}$	$\pm \text{s.e.}$	$^{206}\text{Pb}/^{238}\text{U}$	$\pm 2\sigma$	$^{207}\text{Pb}/^{235}\text{U}$	$\pm 2\sigma$	$^{207}\text{Pb}/^{206}\text{Pb}$	$\pm 2\sigma$		
G17	17.3	153.0	0.0820	0.0012	0.6392	0.0258	0.0562	0.0019	508.0	13.8	501.8	28.9	461.5	25.5	508.05	13.82
G56	30.3	311.5	0.0822	0.0011	0.6410	0.0194	0.0571	0.0015	509.1	13.0	502.9	22.9	495.0	20.4	509.12	12.99
G117	27.1	286.0	0.0826	0.0012	0.6613	0.0252	0.0589	0.0019	511.7	13.9	515.4	28.3	562.3	27.9	511.68	13.93
G29	109.9	1247.8	0.0828	0.0010	0.6481	0.0125	0.0574	0.0009	512.9	12.3	507.3	16.5	505.8	13.5	512.93	12.26
G110	21.6	235.0	0.0829	0.0011	0.6390	0.0226	0.0572	0.0017	513.4	13.6	501.7	26.2	497.3	23.7	513.41	13.57
G39	13.4	122.0	0.0837	0.0012	0.6618	0.0301	0.0566	0.0021	517.9	14.8	515.7	32.6	476.0	29.2	517.93	14.75
G125	52.7	601.1	0.0838	0.0011	0.6542	0.0178	0.0575	0.0013	518.6	13.0	511.1	21.5	509.6	19.0	518.59	12.97
G34	13.7	147.5	0.0845	0.0012	0.6717	0.0267	0.0578	0.0019	522.6	14.3	521.8	29.4	523.3	27.5	522.63	14.27
G70	45.3	470.0	0.0852	0.0011	0.6878	0.0179	0.0596	0.0013	527.3	13.1	531.5	21.2	587.6	19.9	527.26	13.07
G66	24.2	249.6	0.0858	0.0012	0.6989	0.0231	0.0597	0.0016	530.7	13.8	538.1	25.6	593.1	25.0	530.71	13.77
G43	14.9	163.9	0.0863	0.0012	0.7022	0.0268	0.0595	0.0019	533.6	14.4	540.1	29.0	586.2	28.4	533.56	14.36
G42	47.1	573.8	0.0864	0.0011	0.6949	0.0164	0.0585	0.0012	534.0	13.1	535.8	19.7	548.5	17.3	534.03	13.05
G84	41.8	461.8	0.0874	0.0011	0.6942	0.0185	0.0582	0.0013	540.2	13.4	535.3	21.6	537.3	19.1	540.20	13.40
G102	9.1	92.0	0.0883	0.0014	0.7177	0.0359	0.0616	0.0025	545.6	16.2	549.3	38.2	661.3	40.4	545.59	16.23
G1	111.2	1104.8	0.0888	0.0011	0.7158	0.0138	0.0593	0.0010	548.4	13.0	548.2	17.4	578.9	14.3	548.44	13.03
G101	36.7	398.9	0.0933	0.0012	0.7565	0.0213	0.0598	0.0014	575.1	14.4	572.0	23.7	597.4	21.6	575.08	14.39
G108	28.8	279.6	0.0934	0.0013	0.7225	0.0229	0.0584	0.0015	575.7	14.7	552.1	25.8	545.5	22.7	575.73	14.74
G28	44.1	459.9	0.0970	0.0013	0.8668	0.0290	0.0651	0.0017	596.9	15.5	633.8	28.3	778.9	29.5	596.92	15.51
G120	8.8	96.5	0.0973	0.0015	0.7846	0.0380	0.0612	0.0024	598.3	17.4	588.1	38.6	647.3	38.1	598.33	17.39
G45	91.2	725.0	0.1238	0.0016	1.1436	0.0261	0.0691	0.0013	752.2	18.0	774.2	24.4	902.9	22.3	752.23	18.01
G111	121.7	866.1	0.1249	0.0016	1.1078	0.0286	0.0669	0.0014	758.7	18.5	757.1	26.7	834.0	24.3	758.71	18.45
G118	89.8	643.0	0.1303	0.0017	1.3081	0.0406	0.0737	0.0018	789.3	19.8	849.3	31.8	1033.3	31.6	789.35	19.85
G54	55.0	363.4	0.1305	0.0017	1.1759	0.0304	0.0653	0.0013	790.8	19.0	789.4	26.2	783.4	22.5	790.77	19.05
G72	127.1	832.5	0.1330	0.0017	1.2840	0.0268	0.0703	0.0012	805.0	19.0	838.6	24.1	936.8	21.2	805.01	19.00
G55	11.1	69.2	0.1334	0.0020	1.3684	0.0672	0.0768	0.0027	807.0	23.2	875.5	46.0	1115.7	48.6	807.01	23.21
G62	132.7	1023.7	0.1334	0.0017	1.3783	0.0270	0.0732	0.0012	807.5	18.9	879.7	23.6	1018.1	21.0	807.46	18.88
G80	13.0	95.6	0.1346	0.0021	1.3122	0.0668	0.0712	0.0027	814.3	23.5	851.1	46.6	962.9	46.8	814.28	23.52
G119	162.6	1132.1	0.1388	0.0018	1.3517	0.0296	0.0712	0.0013	837.8	19.8	868.3	26.0	962.3	23.2	837.82	19.81
G99	161.9	1210.4	0.1397	0.0018	1.5049	0.0319	0.0775	0.0014	843.0	19.9	932.4	26.1	1133.8	24.3	843.02	19.91
G38	114.9	750.5	0.1403	0.0018	1.3886	0.0277	0.0727	0.0012	846.3	19.8	884.1	24.0	1005.0	20.8	846.30	19.79
G44	171.0	1245.0	0.1459	0.0018	1.4154	0.0259	0.0706	0.0011	877.8	20.3	895.4	23.0	945.0	18.8	877.83	20.25
G31	48.6	306.9	0.1502	0.0019	1.3983	0.0359	0.0685	0.0013	901.9	21.5	888.2	27.7	884.6	23.4	884.63	23.38

APPENDIX B (continued). U-Pb ZIRCON AGES OF ZANSKAR RIVER SEDIMENTS

Grain No.	Pb (ppm)	U (ppm)	Ratios						Ages (Ma)						Best Age (Ma)	$\pm 2\sigma$
			$^{206}\text{Pb}/^{238}\text{U}$	$\pm 1\sigma$	$^{207}\text{Pb}/^{235}\text{U}$	$\pm \text{s.e.}$	$^{207}\text{Pb}/^{206}\text{Pb}$	$\pm \text{s.e.}$	$^{206}\text{Pb}/^{238}\text{U}$	$\pm 2\sigma$	$^{207}\text{Pb}/^{235}\text{U}$	$\pm 2\sigma$	$^{207}\text{Pb}/^{206}\text{Pb}$	$\pm 2\sigma$		
G79	86.8	516.4	0.1481	0.0019	1.4597	0.0378	0.0731	0.0015	890.3	21.4	913.9	28.9	1015.9	26.1	890.30	21.45
G30	269.0	1911.7	0.1487	0.0018	1.5439	0.0276	0.0740	0.0011	893.9	20.5	948.0	23.2	1040.4	19.3	893.90	20.54
G51	95.5	572.0	0.1490	0.0019	1.4601	0.0318	0.0714	0.0012	895.1	21.0	914.1	25.6	970.0	21.8	895.07	20.98
G16	100.5	645.7	0.1552	0.0019	1.4709	0.0298	0.0689	0.0011	930.2	21.5	918.5	24.3	895.7	19.3	895.75	19.29
G8	18.3	118.4	0.1492	0.0021	1.4232	0.0528	0.0709	0.0019	896.2	23.0	898.7	36.4	954.0	33.8	896.20	23.00
G21	96.7	603.8	0.1493	0.0019	1.4432	0.0300	0.0709	0.0012	896.9	20.9	907.0	24.6	955.4	20.5	896.93	20.87
G115	17.6	120.2	0.1500	0.0022	1.4418	0.0648	0.0693	0.0023	901.1	24.6	906.5	42.8	906.5	39.6	906.49	39.59
G33	67.0	425.3	0.1514	0.0019	1.4338	0.0334	0.0695	0.0012	908.8	21.4	903.2	26.3	912.4	22.0	912.43	21.95
G52	42.9	210.4	0.1675	0.0022	1.5531	0.0456	0.0695	0.0015	998.4	24.2	951.7	31.6	914.5	26.5	914.51	26.47
G116	60.1	366.1	0.1598	0.0021	1.4868	0.0397	0.0697	0.0015	955.7	23.0	925.0	30.3	920.1	25.8	920.12	25.80
G98	145.2	977.3	0.1529	0.0019	1.4634	0.0311	0.0699	0.0012	917.0	21.5	915.4	26.0	925.7	21.7	925.71	21.66
G13	70.4	403.5	0.1603	0.0020	1.4977	0.0340	0.0700	0.0012	958.6	22.4	929.4	26.4	927.2	21.5	927.18	21.49
G122	31.2	172.1	0.1586	0.0022	1.5077	0.0519	0.0700	0.0018	949.0	23.9	933.5	35.7	928.4	31.7	928.35	31.75
G126	24.7	122.0	0.1659	0.0023	1.5791	0.0616	0.0702	0.0020	989.3	25.5	962.0	39.5	933.6	35.1	933.62	35.08
G114	39.2	226.8	0.1653	0.0022	1.5412	0.0471	0.0707	0.0016	986.3	24.2	947.0	33.5	947.3	29.1	947.30	29.05
G91	65.5	405.3	0.1609	0.0021	1.5963	0.0401	0.0709	0.0014	961.5	22.9	968.8	28.9	955.4	24.5	955.40	24.55
G49	52.5	313.3	0.1698	0.0022	1.6334	0.0413	0.0710	0.0013	1011.0	23.9	983.2	28.9	957.1	23.9	957.13	23.86
G103	64.4	289.6	0.1749	0.0023	1.6576	0.0492	0.0711	0.0016	1039.1	25.2	992.5	33.1	960.9	28.1	960.86	28.06
G85	12.9	73.8	0.1630	0.0024	1.6071	0.0753	0.0715	0.0024	973.4	26.6	973.0	45.1	972.6	41.6	972.60	41.58
G14	71.2	383.4	0.1609	0.0020	1.5719	0.0369	0.0718	0.0013	961.9	22.5	959.2	27.1	978.9	22.7	978.86	22.70
G106	36.1	205.8	0.1714	0.0024	1.6447	0.0649	0.0718	0.0020	1020.0	26.4	987.5	40.3	981.1	36.0	981.13	36.01
G124	74.1	492.7	0.1597	0.0021	1.5376	0.0389	0.0718	0.0015	955.1	22.8	945.5	29.8	981.4	25.9	981.41	25.85
G27	96.9	654.8	0.1524	0.0019	1.4822	0.0300	0.0719	0.0012	914.2	21.3	923.1	24.8	983.4	20.6	983.39	20.60
G76	124.0	732.3	0.1626	0.0020	1.5552	0.0338	0.0719	0.0012	971.4	22.6	952.6	26.7	984.2	22.2	984.24	22.18
G11	70.9	427.2	0.1558	0.0020	1.5309	0.0345	0.0721	0.0012	933.3	21.9	942.9	26.3	989.0	22.2	989.05	22.19
G36	91.6	629.3	0.1526	0.0019	1.4859	0.0304	0.0722	0.0012	915.5	21.3	924.6	24.9	991.9	20.8	991.87	20.80
G64	93.5	653.9	0.1528	0.0019	1.4945	0.0348	0.0722	0.0013	916.4	21.6	928.2	27.1	991.9	23.4	991.87	23.43
G113	77.8	405.3	0.1652	0.0021	1.5854	0.0407	0.0723	0.0015	985.8	23.6	964.5	30.3	993.3	26.1	993.27	26.06
G131	55.8	339.7	0.1662	0.0022	1.6300	0.0451	0.0723	0.0016	990.9	23.9	981.8	31.9	994.1	27.8	994.12	27.82
G63	185.1	1020.1	0.1632	0.0020	1.6280	0.0315	0.0724	0.0011	974.7	22.5	981.1	25.1	998.3	20.3	998.33	20.29
G26	97.2	619.3	0.1576	0.0020	1.5496	0.0317	0.0725	0.0012	943.6	21.8	950.3	25.2	998.6	20.8	998.61	20.81
G10	20.7	120.2	0.1504	0.0021	1.4731	0.0532	0.0725	0.0019	903.1	23.0	919.4	35.9	1001.1	33.6	1001.13	33.63

APPENDIX B (continued). U-Pb ZIRCON AGES OF ZANSKAR RIVER SEDIMENTS

Grain No.	Pb (ppm)	U (ppm)	Ratios						Ages (Ma)						Best Age (Ma)	$\pm 2\sigma$
			$^{206}\text{Pb}/^{238}\text{U}$	$\pm 1\sigma$	$^{207}\text{Pb}/^{235}\text{U}$	$\pm \text{s.e.}$	$^{207}\text{Pb}/^{206}\text{Pb}$	$\pm \text{s.e.}$	$^{206}\text{Pb}/^{238}\text{U}$	$\pm 2\sigma$	$^{207}\text{Pb}/^{235}\text{U}$	$\pm 2\sigma$	$^{207}\text{Pb}/^{206}\text{Pb}$	$\pm 2\sigma$		
G41	96.6	465.4	0.1709	0.0021	1.6729	0.0370	0.0725	0.0012	1017.0	23.6	998.3	27.0	1001.1	22.0	1001.13	22.05
G25	19.3	85.6	0.1723	0.0024	1.7274	0.0705	0.0730	0.0021	1024.9	26.5	1018.8	40.6	1014.5	36.7	1014.51	36.65
G57	37.3	232.2	0.1518	0.0020	1.4928	0.0425	0.0731	0.0016	911.1	22.2	927.4	30.6	1017.6	27.7	1017.56	27.70
G77	48.7	222.2	0.1693	0.0022	1.6625	0.0480	0.0734	0.0016	1008.0	24.4	994.3	32.1	1024.5	28.1	1024.47	28.07
G112	54.0	303.3	0.1727	0.0022	1.7072	0.0473	0.0735	0.0016	1026.8	24.6	1011.2	32.0	1026.4	27.7	1026.39	27.72
G68	41.1	260.5	0.1560	0.0020	1.5622	0.0434	0.0736	0.0015	934.3	22.5	955.4	30.5	1031.3	27.4	1031.34	27.37
G6	230.1	1347.0	0.1675	0.0021	1.7270	0.0317	0.0738	0.0011	998.2	22.7	1018.6	24.3	1035.5	19.3	1035.46	19.29
G121	109.0	560.1	0.1754	0.0022	1.7681	0.0431	0.0739	0.0014	1041.6	24.6	1033.8	30.2	1039.8	25.6	1039.83	25.63
G47	85.0	445.4	0.1843	0.0023	1.8564	0.0419	0.0746	0.0013	1090.5	25.3	1065.7	28.1	1058.8	22.8	1058.82	22.83
G100	156.2	1059.2	0.1570	0.0020	1.6431	0.0374	0.0748	0.0014	940.1	22.2	986.9	27.8	1063.1	24.4	1063.13	24.42
G24	90.1	505.5	0.1585	0.0020	1.6584	0.0363	0.0751	0.0013	948.4	22.1	992.7	26.3	1072.0	22.5	1071.98	22.49
G3	78.4	407.1	0.1841	0.0023	1.8607	0.0408	0.0753	0.0012	1089.4	25.0	1067.2	27.4	1076.0	22.1	1075.99	22.14
G19	68.8	383.4	0.1836	0.0023	1.9126	0.0430	0.0753	0.0013	1086.5	25.1	1085.5	27.8	1076.3	22.7	1076.25	22.67
G40	132.4	795.1	0.1632	0.0020	1.7109	0.0334	0.0754	0.0012	974.4	22.4	1012.6	25.2	1079.5	20.9	1079.45	20.91
G35	55.9	269.6	0.1843	0.0024	1.9137	0.0492	0.0757	0.0014	1090.6	25.6	1085.9	30.2	1086.4	25.3	1086.35	25.32
G58	67.3	415.3	0.1669	0.0021	1.8678	0.0456	0.0757	0.0014	995.1	23.3	1069.7	28.2	1088.2	24.3	1088.21	24.26
G90	40.0	199.5	0.1871	0.0025	1.9788	0.0608	0.0758	0.0017	1105.4	26.7	1108.3	34.5	1089.3	29.9	1089.26	29.90
G109	148.6	868.0	0.1775	0.0022	1.8397	0.0405	0.0759	0.0014	1053.1	24.5	1059.7	28.9	1093.2	24.4	1093.23	24.44
G50	35.9	152.1	0.1922	0.0025	1.9410	0.0617	0.0760	0.0017	1133.2	27.5	1095.3	35.1	1096.1	30.3	1096.12	30.26
G12	166.5	654.8	0.1830	0.0023	1.8929	0.0375	0.0761	0.0012	1083.3	24.7	1078.6	26.2	1096.4	20.9	1096.39	20.91
G65	33.0	175.8	0.1902	0.0025	1.9567	0.0597	0.0768	0.0017	1122.6	27.1	1100.7	34.2	1116.8	29.6	1116.78	29.55
G18	66.2	318.8	0.1863	0.0024	1.8639	0.0439	0.0771	0.0013	1101.0	25.5	1068.4	29.0	1123.3	24.1	1123.26	24.08
G132	44.6	213.1	0.1968	0.0000	2.0138	0.0000	0.0773	0.0000	1157.8	0.0	1120.2	0.0	1128.2	0.5	1128.17	0.46
G74	51.7	265.0	0.1815	0.0024	1.9403	0.0615	0.0774	0.0017	1075.3	26.2	1095.1	34.8	1130.7	31.0	1130.74	30.96
G107	26.7	123.9	0.1979	0.0027	2.0316	0.0729	0.0774	0.0019	1164.2	29.0	1126.1	39.3	1131.0	34.7	1131.00	34.66
G20	78.5	318.8	0.1959	0.0025	2.0257	0.0485	0.0775	0.0014	1153.1	26.6	1124.2	29.5	1134.9	24.3	1134.86	24.25
G48	36.8	188.5	0.1976	0.0026	2.0925	0.0611	0.0778	0.0016	1162.5	27.7	1146.4	33.4	1142.0	28.5	1142.03	28.48
G37	66.4	305.1	0.2026	0.0026	2.1145	0.0514	0.0778	0.0014	1189.1	27.4	1153.5	30.1	1142.0	24.6	1142.03	24.60
G53	88.3	381.6	0.2029	0.0026	2.1621	0.0499	0.0785	0.0013	1190.8	27.4	1168.9	29.6	1160.6	24.1	1160.57	24.06
G87	117.4	568.3	0.1851	0.0023	2.0233	0.0452	0.0787	0.0014	1094.8	25.3	1123.4	29.1	1165.6	24.6	1165.61	24.58
G67	67.2	371.6	0.1798	0.0023	1.9389	0.0464	0.0789	0.0014	1065.9	24.9	1094.6	29.6	1170.1	25.5	1170.13	25.46
G9	92.4	483.6	0.1827	0.0023	2.0301	0.0430	0.0809	0.0013	1081.9	24.9	1125.6	27.4	1219.7	22.9	1219.75	22.92

APPENDIX B (continued). U-Pb ZIRCON AGES OF ZANSKAR RIVER SEDIMENTS

Grain No.	Pb (ppm)	U (ppm)	Ratios						Ages (Ma)						Best Age (Ma)	$\pm 2\sigma$
			$^{206}\text{Pb}/^{238}\text{U}$	$\pm 1\sigma$	$^{207}\text{Pb}/^{235}\text{U}$	$\pm \text{s.e.}$	$^{207}\text{Pb}/^{206}\text{Pb}$	$\pm \text{s.e.}$	$^{206}\text{Pb}/^{238}\text{U}$	$\pm 2\sigma$	$^{207}\text{Pb}/^{235}\text{U}$	$\pm 2\sigma$	$^{207}\text{Pb}/^{206}\text{Pb}$	$\pm 2\sigma$		
G78	142.1	633.9	0.1932	0.0024	2.1267	0.0450	0.0812	0.0013	1138.4	26.1	1157.5	28.8	1227.3	24.0	1227.26	23.95
G94	94.2	399.8	0.2029	0.0026	2.3356	0.0567	0.0826	0.0015	1190.7	27.7	1223.2	31.6	1259.1	26.8	1259.07	26.85
G93	74.4	306.9	0.2192	0.0028	2.4237	0.0621	0.0828	0.0016	1277.4	29.6	1249.7	33.0	1264.7	27.7	1264.74	27.71
G96	55.6	240.4	0.2161	0.0028	2.4717	0.0693	0.0835	0.0017	1261.2	29.7	1263.8	34.5	1280.7	29.6	1280.70	29.57
G46	105.4	439.9	0.2207	0.0028	2.5343	0.0551	0.0840	0.0014	1285.5	29.2	1281.9	29.7	1292.1	24.0	1292.09	23.96
G32	74.1	322.4	0.2163	0.0027	2.4618	0.0572	0.0846	0.0014	1262.5	28.8	1260.9	30.4	1306.6	25.0	1306.62	24.95
G88	59.5	231.3	0.2408	0.0031	2.8470	0.0786	0.0871	0.0017	1391.1	32.3	1368.0	34.9	1361.8	29.2	1361.82	29.22
G81	88.6	345.2	0.2360	0.0030	2.8047	0.0675	0.0876	0.0015	1366.0	31.2	1356.8	32.4	1373.9	26.8	1373.95	26.76
G129	74.1	314.2	0.2273	0.0030	2.7458	0.0831	0.0886	0.0019	1320.3	31.4	1340.9	37.7	1396.0	33.2	1395.96	33.16
G71	154.5	628.4	0.2443	0.0030	2.8859	0.0593	0.0889	0.0014	1409.1	31.5	1378.2	30.6	1401.1	24.4	1401.14	24.40
G73	61.3	198.5	0.2859	0.0037	3.9407	0.1078	0.1013	0.0018	1621.1	36.8	1622.1	35.9	1648.6	29.7	1648.62	29.74
G86	138.9	463.6	0.2709	0.0034	3.7472	0.0823	0.1033	0.0017	1545.3	34.5	1581.5	33.3	1684.6	27.4	1684.60	27.35
G2	20.0	92.0	0.3064	0.0040	4.4223	0.1525	0.1046	0.0020	1722.7	39.9	1716.5	39.0	1706.6	32.7	1706.59	32.70
G130	153.6	452.7	0.3054	0.0039	4.3168	0.1058	0.1048	0.0019	1718.1	38.4	1696.6	37.2	1710.1	31.1	1710.11	31.09
G95	66.6	172.1	0.3269	0.0043	4.6140	0.1457	0.1052	0.0021	1823.2	41.6	1751.8	39.6	1717.8	33.1	1717.81	33.06
G60	207.8	704.0	0.2732	0.0034	4.0368	0.0784	0.1090	0.0016	1557.0	34.3	1641.6	31.5	1782.8	25.3	1782.77	25.27
G61	1116.8	1766.9	0.2826	0.0035	4.2744	0.0742	0.1096	0.0016	1604.5	35.0	1688.4	30.9	1793.3	24.3	1793.27	24.26
G89	110.8	322.4	0.3335	0.0042	5.1707	0.1241	0.1153	0.0019	1855.4	40.7	1847.8	35.8	1884.9	29.1	1884.89	29.13
G69	202.3	619.3	0.3125	0.0039	5.2346	0.1127	0.1230	0.0019	1752.9	38.3	1858.3	33.8	2000.6	27.3	2000.63	27.31
G59	105.1	253.2	0.3750	0.0047	6.4729	0.1572	0.1269	0.0020	2052.8	44.3	2042.2	35.3	2055.0	28.0	2055.05	27.96
G23	363.1	742.3	0.4133	0.0051	8.2587	0.1620	0.1448	0.0020	2230.0	46.4	2259.8	33.2	2284.8	25.1	2284.81	25.06
G123	231.4	466.3	0.4606	0.0058	9.7505	0.2280	0.1588	0.0028	2442.4	51.4	2411.5	39.6	2442.9	32.5	2442.92	32.45
G128	204.9	385.3	0.4632	0.0059	9.9470	0.2410	0.1621	0.0029	2453.8	51.8	2429.9	40.3	2477.5	33.3	2477.48	33.28
G105	77.9	159.4	0.4610	0.0059	10.4876	0.3060	0.1696	0.0030	2443.9	52.4	2478.8	40.6	2553.2	33.4	2553.21	33.37
G7	91.0	186.7	0.4185	0.0053	9.7511	0.2464	0.1730	0.0025	2253.6	47.8	2411.5	35.4	2587.0	27.5	2586.98	27.51
G83	77.1	131.2	0.5120	0.0066	12.1414	0.3659	0.1763	0.0029	2665.1	56.1	2615.4	39.5	2618.2	31.7	2618.18	31.65
G15	541.6	1083.8	0.4637	0.0057	11.5136	0.1930	0.1787	0.0023	2455.8	49.9	2565.7	33.0	2640.7	24.6	2640.75	24.55
G5	317.5	567.4	0.4922	0.0060	11.9942	0.2240	0.1813	0.0024	2580.2	52.2	2604.0	33.6	2664.7	25.0	2664.71	24.98
G104	108.1	156.7	0.5783	0.0074	15.0883	0.4439	0.1939	0.0033	2941.8	60.6	2820.8	40.7	2775.5	32.9	2775.53	32.87
G127	56.6	95.6	0.5284	0.0070	13.9350	0.4889	0.2011	0.0038	2734.5	59.0	2745.3	44.2	2835.1	36.9	2835.06	36.86
G22	272.8	399.8	0.5800	0.0072	18.5942	0.3794	0.2303	0.0030	2948.7	58.3	3021.0	34.7	3054.1	25.9	3054.13	25.86
G4	19.3	148.5	0.0962	0.0013	0.9661	0.0346	0.0753	0.0021	592.0	15.8	686.5	31.9	1076.0	37.8	592.04	15.76

APPENDIX B (continued). U-Pb ZIRCON AGES OF ZANSKAR RIVER SEDIMENTS

Grain No.	Pb (ppm)	U (ppm)	Ratios						Ages (Ma)						Best Age (Ma)	$\pm 2\sigma$
			$^{206}\text{Pb}/^{238}\text{U}$	$\pm 1\sigma$	$^{207}\text{Pb}/^{235}\text{U}$	$\pm \text{s.e.}$	$^{207}\text{Pb}/^{206}\text{Pb}$	$\pm \text{s.e.}$	$^{206}\text{Pb}/^{238}\text{U}$	$\pm 2\sigma$	$^{207}\text{Pb}/^{235}\text{U}$	$\pm 2\sigma$	$^{207}\text{Pb}/^{206}\text{Pb}$	$\pm 2\sigma$		
G97	27.2	272.3	0.0975	0.0014	0.7515	0.0272	0.0577	0.0017	599.9	15.9	569.1	29.0	518.0	24.5	599.92	15.86
Sample 14080609 Yunam																
G26	141.4	2026.5	0.0712	0.0009	0.5892	0.0092	0.0601	0.0009	443.3	10.2	470.3	14.2	605.4	13.4	443.32	10.23
G103	41.3	471.5	0.0727	0.0009	0.5694	0.0124	0.0568	0.0012	452.5	11.1	457.6	18.3	483.8	16.4	452.52	11.06
G93	49.1	546.0	0.0742	0.0009	0.5846	0.0117	0.0572	0.0011	461.3	11.2	467.4	17.3	498.1	15.3	461.29	11.16
G114	20.7	268.0	0.0752	0.0010	0.5859	0.0142	0.0566	0.0014	467.1	11.8	468.2	20.4	474.4	18.1	467.11	11.75
G15	78.9	965.3	0.0798	0.0010	0.6513	0.0113	0.0592	0.0010	494.7	11.5	509.2	16.4	575.6	14.5	494.75	11.46
G78	24.7	227.3	0.0799	0.0010	0.6308	0.0151	0.0573	0.0014	495.7	12.3	496.6	21.1	501.2	18.7	495.70	12.30
G17	37.9	403.2	0.0823	0.0010	0.6534	0.0131	0.0576	0.0011	509.8	12.2	510.6	18.5	514.6	15.7	509.84	12.15
G95	27.2	262.6	0.0839	0.0011	0.6494	0.0153	0.0561	0.0013	519.6	12.8	508.1	21.2	457.1	17.1	519.60	12.85
G74	9.3	104.4	0.0842	0.0012	0.6667	0.0207	0.0575	0.0018	520.8	13.8	518.7	27.7	510.0	25.0	520.85	13.79
G53	134.1	1269.4	0.0849	0.0010	0.6800	0.0111	0.0581	0.0009	525.5	12.2	526.8	16.1	532.8	12.7	525.48	12.24
G33	54.2	585.1	0.0851	0.0011	0.7091	0.0151	0.0605	0.0013	526.2	12.7	544.2	20.5	620.8	19.4	526.20	12.71
G50	60.8	497.6	0.0854	0.0011	0.6879	0.0131	0.0584	0.0011	528.2	12.5	531.6	18.3	546.3	15.5	528.22	12.47
G32	44.3	185.8	0.0855	0.0011	0.6800	0.0168	0.0577	0.0014	529.1	13.1	526.8	22.7	517.2	19.8	529.11	13.06
G68	9.3	77.6	0.0857	0.0014	0.7002	0.0331	0.0593	0.0028	530.1	16.6	538.9	42.3	577.0	42.2	530.06	16.63
G99	35.5	389.3	0.0857	0.0011	0.6670	0.0140	0.0564	0.0012	530.2	12.8	518.9	19.5	469.7	15.3	530.23	12.82
G21	8.5	81.4	0.0858	0.0012	0.6921	0.0235	0.0585	0.0020	530.5	14.2	534.0	30.7	550.0	29.0	530.53	14.25
G47	54.2	542.9	0.0861	0.0011	0.6938	0.0128	0.0585	0.0010	532.5	12.6	535.1	18.0	546.7	15.0	532.49	12.58
G5	10.3	103.7	0.0866	0.0012	0.6917	0.0222	0.0580	0.0019	535.3	14.1	533.8	29.1	527.9	26.6	535.34	14.12
G24	61.0	598.2	0.0869	0.0011	0.7012	0.0139	0.0585	0.0011	537.4	12.7	539.5	19.2	549.3	16.4	537.36	12.69
G35	92.5	1078.9	0.0871	0.0011	0.7151	0.0123	0.0596	0.0010	538.2	12.6	547.8	17.2	588.4	14.5	538.24	12.57
G11	61.9	548.3	0.0871	0.0011	0.7215	0.0152	0.0601	0.0012	538.5	12.9	551.5	20.5	606.5	18.8	538.54	12.93
G1	10.0	67.6	0.0918	0.0013	0.7559	0.0280	0.0598	0.0022	566.1	15.7	571.7	35.1	594.5	33.7	566.11	15.71
G108	71.3	741.0	0.0939	0.0012	0.7813	0.0144	0.0604	0.0011	578.4	13.7	586.2	19.1	617.2	16.2	578.38	13.67
G89	5.4	51.5	0.1028	0.0016	0.8575	0.0342	0.0605	0.0024	630.9	18.2	628.7	40.4	621.5	37.5	630.86	18.24
G13	27.9	247.3	0.1056	0.0013	0.8867	0.0187	0.0609	0.0013	647.3	15.4	644.6	23.1	636.1	19.6	647.26	15.39
G90	46.1	370.1	0.1058	0.0014	0.9025	0.0195	0.0619	0.0013	648.5	15.7	653.0	23.7	669.3	20.6	648.54	15.74
G100	115.2	957.6	0.1083	0.0013	0.9382	0.0163	0.0629	0.0010	662.8	15.5	671.9	20.1	703.2	16.6	662.75	15.47
G38	136.9	1288.6	0.1111	0.0013	1.0408	0.0163	0.0680	0.0010	679.2	15.5	724.3	19.6	867.3	17.0	679.19	15.55
G4	232.9	2103.3	0.1198	0.0014	1.1659	0.0171	0.0706	0.0010	729.6	16.3	784.7	19.6	945.6	16.6	729.64	16.35

APPENDIX B (continued). U-Pb ZIRCON AGES OF ZANSKAR RIVER SEDIMENTS

Grain No.	Pb (ppm)	U (ppm)	Ratios						Ages (Ma)						Best Age (Ma)	$\pm 2\sigma$
			$^{206}\text{Pb}/^{238}\text{U}$	$\pm 1\sigma$	$^{207}\text{Pb}/^{235}\text{U}$	$\pm \text{s.e.}$	$^{207}\text{Pb}/^{206}\text{Pb}$	$\pm \text{s.e.}$	$^{206}\text{Pb}/^{238}\text{U}$	$\pm 2\sigma$	$^{207}\text{Pb}/^{235}\text{U}$	$\pm 2\sigma$	$^{207}\text{Pb}/^{206}\text{Pb}$	$\pm 2\sigma$		
G34	116.9	924.6	0.1250	0.0015	1.2508	0.0211	0.0726	0.0012	759.2	17.4	823.8	22.7	1002.8	20.4	759.16	17.42
G124	102.4	853.1	0.1268	0.0016	1.1551	0.0227	0.0661	0.0012	769.8	18.3	779.6	24.6	808.3	20.9	769.81	18.31
G19	26.6	174.3	0.1270	0.0016	1.1425	0.0245	0.0653	0.0014	770.7	18.3	773.7	26.5	783.1	22.9	770.73	18.30
G45	26.5	149.0	0.1286	0.0017	1.1780	0.0280	0.0665	0.0016	779.7	19.1	790.4	29.5	821.2	26.4	779.70	19.08
G104	85.8	688.0	0.1288	0.0016	1.2679	0.0253	0.0714	0.0014	780.9	18.6	831.4	26.2	969.5	24.1	780.90	18.62
G25	48.9	343.3	0.1295	0.0016	1.1534	0.0207	0.0646	0.0011	784.7	18.0	778.8	22.9	762.6	18.4	784.73	18.04
G80	61.4	367.1	0.1324	0.0016	1.2141	0.0223	0.0665	0.0012	801.5	18.7	807.1	23.8	822.8	19.7	801.54	18.67
G76	241.0	1915.2	0.1327	0.0016	1.2623	0.0198	0.0690	0.0010	803.5	18.3	828.9	21.4	898.1	17.3	803.48	18.32
G84	27.6	168.2	0.1363	0.0018	1.1931	0.0279	0.0635	0.0015	823.5	20.0	797.4	29.1	725.4	23.8	823.54	19.97
G125	56.3	388.6	0.1400	0.0018	1.2950	0.0250	0.0671	0.0012	844.5	19.9	843.5	25.6	841.5	21.1	844.49	19.91
G118	51.2	363.2	0.1407	0.0018	1.3756	0.0286	0.0709	0.0014	848.8	20.2	878.6	27.9	954.5	24.8	848.85	20.23
G113	68.1	462.3	0.1426	0.0018	1.3657	0.0257	0.0695	0.0012	859.1	20.1	874.3	25.5	913.3	21.5	859.12	20.09
G81	61.1	182.0	0.1428	0.0018	1.4442	0.0316	0.0734	0.0016	860.6	20.8	907.4	30.0	1023.6	27.6	860.65	20.76
G30	57.4	291.0	0.1530	0.0019	1.4307	0.0276	0.0678	0.0013	917.9	21.2	901.8	26.9	863.4	21.8	863.36	21.78
G59	151.8	1052.8	0.1454	0.0018	1.4739	0.0244	0.0735	0.0012	875.4	19.9	919.7	24.0	1028.0	20.2	875.35	19.92
G37	13.9	90.6	0.1458	0.0020	1.5308	0.0399	0.0762	0.0020	877.3	22.3	942.8	36.2	1099.5	35.1	877.32	22.28
G94	35.9	193.5	0.1517	0.0019	1.4289	0.0295	0.0683	0.0014	910.3	21.5	901.1	28.3	878.9	23.6	878.88	23.58
G91	100.9	709.5	0.1462	0.0018	1.3662	0.0232	0.0678	0.0011	879.6	20.1	874.5	23.6	862.1	18.5	879.63	20.13
G122	76.2	505.3	0.1470	0.0019	1.3818	0.0292	0.0682	0.0014	884.1	21.1	881.2	28.4	874.6	23.9	884.07	21.13
G18	164.0	1133.4	0.1484	0.0018	1.5818	0.0255	0.0773	0.0012	892.2	20.1	963.1	24.2	1129.2	20.8	892.21	20.10
G127	36.9	228.1	0.1497	0.0019	1.3858	0.0304	0.0672	0.0014	899.1	21.6	882.9	29.4	843.0	24.4	899.11	21.64
G116	99.4	698.8	0.1497	0.0019	1.4224	0.0261	0.0689	0.0012	899.5	20.9	898.4	25.5	896.0	20.7	899.51	20.86
G56	33.1	167.4	0.1637	0.0021	1.5604	0.0335	0.0691	0.0015	977.5	23.2	954.6	30.4	902.6	25.1	902.62	25.08
G27	97.5	626.6	0.1509	0.0018	1.4404	0.0226	0.0693	0.0010	905.8	20.3	905.9	22.8	906.5	17.7	906.49	17.66
G110	28.7	183.5	0.1551	0.0020	1.4858	0.0335	0.0695	0.0015	929.4	22.4	924.6	31.0	913.6	26.5	913.62	26.53
G85	107.4	724.1	0.1559	0.0019	1.4997	0.0248	0.0698	0.0011	934.0	21.2	930.3	24.0	921.9	18.8	921.89	18.75
G101	130.5	672.7	0.1558	0.0019	1.5024	0.0259	0.0700	0.0011	933.4	21.4	931.3	24.8	926.9	19.6	926.89	19.64
G36	83.4	534.5	0.1593	0.0019	1.5413	0.0265	0.0702	0.0011	952.9	21.6	947.0	25.0	933.9	19.8	933.92	19.84
G16	49.7	273.4	0.1556	0.0019	1.5060	0.0269	0.0702	0.0012	932.4	21.2	932.8	25.6	934.5	20.9	934.50	20.88
G82	46.8	241.9	0.1625	0.0021	1.5767	0.0313	0.0704	0.0014	970.8	22.7	961.1	28.5	939.5	23.5	939.46	23.51
G87	43.3	251.9	0.1583	0.0020	1.5378	0.0291	0.0705	0.0013	947.3	22.0	945.6	27.1	942.1	22.3	942.08	22.30
G12	131.5	793.3	0.1537	0.0018	1.4930	0.0226	0.0705	0.0010	921.4	20.5	927.5	22.4	943.0	17.3	942.95	17.25

APPENDIX B (continued). U-Pb ZIRCON AGES OF ZANSKAR RIVER SEDIMENTS

Grain No.	Pb (ppm)	U (ppm)	Ratios						Ages (Ma)						Best Age (Ma)	$\pm 2\sigma$
			$^{206}\text{Pb}/^{238}\text{U}$	$\pm 1\sigma$	$^{207}\text{Pb}/^{235}\text{U}$	$\pm \text{s.e.}$	$^{207}\text{Pb}/^{206}\text{Pb}$	$\pm \text{s.e.}$	$^{206}\text{Pb}/^{238}\text{U}$	$\pm 2\sigma$	$^{207}\text{Pb}/^{235}\text{U}$	$\pm 2\sigma$	$^{207}\text{Pb}/^{206}\text{Pb}$	$\pm 2\sigma$		
G121	22.1	237.3	0.1502	0.0019	1.4660	0.0299	0.0708	0.0014	902.1	21.4	916.5	28.2	951.6	24.3	951.64	24.25
G67	45.9	273.4	0.1621	0.0020	1.5816	0.0291	0.0708	0.0013	968.2	22.3	963.0	26.8	951.6	21.8	951.64	21.81
G123	70.4	443.9	0.1560	0.0020	1.5235	0.0286	0.0708	0.0013	934.6	21.7	939.9	26.7	952.8	22.0	952.80	21.99
G120	26.4	138.2	0.1580	0.0021	1.5432	0.0348	0.0708	0.0016	945.8	22.8	947.8	31.5	952.8	27.2	952.80	27.22
G105	43.0	235.7	0.1549	0.0020	1.5149	0.0348	0.0710	0.0016	928.1	22.6	936.4	31.9	956.3	27.9	956.26	27.93
G52	147.1	963.7	0.1578	0.0019	1.5538	0.0247	0.0714	0.0011	944.4	21.3	952.0	23.7	970.0	18.5	970.03	18.54
G44	143.8	712.6	0.1663	0.0020	1.6387	0.0281	0.0715	0.0012	991.9	22.4	985.2	25.6	970.9	20.3	970.89	20.29
G41	52.7	291.8	0.1658	0.0021	1.6350	0.0301	0.0716	0.0013	988.8	22.7	983.8	27.3	973.2	22.2	973.17	22.22
G106	49.9	278.0	0.1726	0.0022	1.7052	0.0325	0.0717	0.0013	1026.5	23.7	1010.5	28.2	976.3	22.8	976.30	22.76
G39	77.9	452.3	0.1607	0.0020	1.5912	0.0262	0.0718	0.0011	960.7	21.7	966.8	24.5	981.1	19.4	981.13	19.44
G3	83.4	460.0	0.1529	0.0019	1.5192	0.0268	0.0721	0.0012	917.4	20.8	938.2	25.5	987.9	21.4	987.92	21.38
G62	29.4	133.6	0.1768	0.0023	1.7563	0.0412	0.0721	0.0017	1049.4	25.3	1029.5	34.4	987.9	29.3	987.92	29.27
G7	115.3	653.5	0.1675	0.0020	1.6643	0.0270	0.0721	0.0011	998.4	22.3	995.0	24.7	988.5	19.3	988.48	19.28
G20	101.5	411.6	0.1649	0.0020	1.6444	0.0297	0.0724	0.0013	983.9	22.4	987.4	26.7	995.8	21.9	995.80	21.93
G66	182.5	943.0	0.1641	0.0020	1.6366	0.0264	0.0724	0.0011	979.2	22.0	984.4	24.4	996.4	19.1	996.36	19.12
G107	37.2	216.6	0.1505	0.0019	1.5044	0.0327	0.0725	0.0015	904.0	21.7	932.2	30.2	1000.0	26.8	1000.01	26.85
G31	69.3	364.8	0.1738	0.0021	1.7390	0.0289	0.0726	0.0011	1032.7	23.2	1023.1	25.6	1003.1	20.0	1003.09	20.01
G51	108.5	497.6	0.1724	0.0021	1.7316	0.0282	0.0729	0.0011	1025.3	23.0	1020.4	25.1	1010.1	19.5	1010.06	19.50
G29	24.1	98.3	0.1725	0.0023	1.7337	0.0438	0.0729	0.0018	1025.9	25.2	1021.1	36.6	1011.5	32.1	1011.45	32.15
G77	73.8	357.1	0.1798	0.0022	1.8434	0.0318	0.0744	0.0012	1065.6	24.2	1061.1	26.8	1052.3	21.3	1052.34	21.31
G8	35.4	164.3	0.1938	0.0024	1.9992	0.0406	0.0749	0.0015	1141.8	26.4	1115.3	31.7	1064.7	26.1	1064.75	26.08
G55	75.1	370.1	0.1783	0.0022	1.8444	0.0310	0.0750	0.0012	1057.8	23.9	1061.4	26.4	1069.3	21.0	1069.31	20.97
G46	98.4	452.3	0.1806	0.0022	1.8752	0.0303	0.0753	0.0011	1070.0	23.9	1072.4	25.7	1077.6	20.1	1077.59	20.10
G54	153.6	829.3	0.1911	0.0023	1.9875	0.0308	0.0754	0.0011	1127.5	25.0	1111.3	25.5	1080.2	19.2	1080.25	19.22
G40	186.1	952.2	0.1793	0.0022	1.8657	0.0288	0.0755	0.0011	1063.3	23.6	1069.0	24.7	1081.3	19.0	1081.31	19.04
G92	152.9	856.2	0.1806	0.0022	1.8845	0.0308	0.0757	0.0012	1070.0	24.0	1075.6	25.8	1087.4	20.3	1087.41	20.28
G9	127.0	670.4	0.1817	0.0022	1.8980	0.0286	0.0758	0.0011	1076.5	23.7	1080.4	24.5	1089.0	18.7	1089.00	18.69
G58	113.3	593.6	0.1780	0.0022	1.8613	0.0325	0.0759	0.0013	1056.1	24.0	1067.5	27.3	1091.1	22.2	1091.11	22.22
G49	163.3	793.3	0.1900	0.0023	2.0451	0.0328	0.0781	0.0012	1121.2	24.9	1130.7	26.3	1149.4	20.6	1149.42	20.61
G119	98.3	479.9	0.1828	0.0023	1.9761	0.0378	0.0784	0.0014	1082.0	25.1	1107.4	29.9	1158.0	25.2	1158.04	25.19
G65	90.9	384.7	0.2000	0.0024	2.1630	0.0360	0.0785	0.0012	1175.2	26.2	1169.2	27.6	1158.8	21.7	1158.80	21.66
G111	27.0	134.4	0.1855	0.0026	2.0089	0.0563	0.0785	0.0022	1097.1	28.3	1118.5	42.5	1160.6	38.7	1160.57	38.75

APPENDIX B (continued). U-Pb ZIRCON AGES OF ZANSKAR RIVER SEDIMENTS

Grain No.	Pb (ppm)	U (ppm)	Ratios						Ages (Ma)						Best Age (Ma)	$\pm 2\sigma$
			$^{206}\text{Pb}/^{238}\text{U}$	$\pm 1\sigma$	$^{207}\text{Pb}/^{235}\text{U}$	$\pm \text{s.e.}$	$^{207}\text{Pb}/^{206}\text{Pb}$	$\pm \text{s.e.}$	$^{206}\text{Pb}/^{238}\text{U}$	$\pm 2\sigma$	$^{207}\text{Pb}/^{235}\text{U}$	$\pm 2\sigma$	$^{207}\text{Pb}/^{206}\text{Pb}$	$\pm 2\sigma$		
G86	203.1	1024.4	0.1887	0.0023	2.1177	0.0335	0.0814	0.0012	1114.2	24.8	1154.6	26.2	1231.6	20.9	1231.60	20.86
G79	91.7	401.6	0.2119	0.0026	2.4000	0.0396	0.0822	0.0013	1239.0	27.6	1242.6	28.3	1249.1	22.2	1249.09	22.22
G73	45.0	177.4	0.2156	0.0027	2.4879	0.0453	0.0837	0.0015	1258.6	28.5	1268.5	31.1	1285.8	25.4	1285.82	25.44
G70	114.0	479.2	0.2078	0.0026	2.4506	0.0409	0.0856	0.0013	1216.9	27.2	1257.6	28.7	1328.3	23.2	1328.26	23.21
G64	32.8	121.3	0.2473	0.0034	3.0444	0.0766	0.0893	0.0022	1424.3	35.0	1418.8	43.7	1411.0	38.2	1411.03	38.24
G6	204.3	746.4	0.2497	0.0030	3.0911	0.0445	0.0898	0.0012	1436.7	30.5	1430.5	27.3	1421.9	20.3	1421.92	20.27
G23	87.6	289.5	0.2375	0.0030	2.9763	0.0558	0.0909	0.0017	1373.6	31.0	1401.6	33.5	1444.9	28.0	1444.93	27.97
G72	176.7	661.2	0.2502	0.0030	3.1856	0.0492	0.0924	0.0013	1439.2	31.2	1453.7	29.0	1475.2	22.2	1475.21	22.23
G115	126.0	418.5	0.2384	0.0030	3.0566	0.0537	0.0930	0.0015	1378.5	30.8	1421.9	31.7	1487.9	25.9	1487.89	25.86
G102	335.8	1560.4	0.2287	0.0028	2.9948	0.0492	0.0950	0.0015	1327.7	29.4	1406.3	29.9	1527.9	24.3	1527.88	24.28
G71	177.4	566.7	0.2350	0.0029	3.1047	0.0495	0.0958	0.0014	1360.7	29.9	1433.8	29.6	1544.4	23.7	1544.44	23.68
G42	180.2	530.6	0.2832	0.0034	3.8334	0.0582	0.0982	0.0014	1607.5	34.3	1599.8	29.8	1590.0	22.6	1590.03	22.58
G83	95.7	293.3	0.3002	0.0037	4.1006	0.0708	0.0991	0.0016	1692.4	37.0	1654.4	33.5	1606.9	26.4	1606.87	26.38
G61	59.3	179.7	0.3094	0.0038	4.3059	0.0722	0.1010	0.0016	1737.6	37.5	1694.5	33.1	1642.0	25.8	1642.02	25.79
G28	234.9	788.6	0.2944	0.0035	4.1503	0.0593	0.1023	0.0013	1663.6	35.0	1664.3	29.0	1665.7	21.4	1665.72	21.45
G63	71.4	197.4	0.3214	0.0040	4.6545	0.0806	0.1051	0.0017	1796.6	39.0	1759.1	34.5	1715.4	27.3	1715.37	27.27
G60	84.2	209.6	0.3468	0.0043	5.4410	0.0921	0.1138	0.0018	1919.1	41.3	1891.3	34.7	1861.4	27.3	1861.44	27.28
G112	56.3	104.4	0.4575	0.0058	9.9137	0.1754	0.1572	0.0026	2428.6	51.1	2426.8	38.7	2425.7	30.9	2425.66	30.86
G14	55.2	102.9	0.4380	0.0056	9.5908	0.1659	0.1589	0.0026	2341.7	50.1	2396.3	38.5	2443.7	30.7	2443.67	30.70
G69	183.4	316.4	0.4763	0.0058	10.7227	0.1620	0.1633	0.0023	2511.0	50.5	2499.4	34.3	2490.3	25.8	2490.32	25.80
G22	29.3	49.1	0.4521	0.0061	10.1879	0.2008	0.1635	0.0032	2404.7	54.2	2452.0	43.6	2492.0	35.9	2491.97	35.88
G97	308.3	698.8	0.4270	0.0052	9.6971	0.1563	0.1647	0.0025	2292.2	47.3	2406.4	35.7	2504.9	27.9	2504.90	27.86
G88	288.3	592.1	0.4702	0.0058	11.2336	0.1770	0.1733	0.0025	2484.6	50.4	2542.7	35.5	2589.8	27.3	2589.77	27.33
G2	115.8	227.3	0.4614	0.0056	11.1037	0.1683	0.1746	0.0025	2445.9	49.7	2531.9	34.9	2602.2	26.6	2602.23	26.62
G57	662.4	1496.7	0.4386	0.0053	10.8791	0.1575	0.1799	0.0024	2344.5	47.1	2512.8	33.2	2652.1	24.9	2652.13	24.89
G96	340.5	548.3	0.5217	0.0064	13.3752	0.2097	0.1860	0.0027	2706.4	53.9	2706.5	35.7	2706.9	27.3	2706.93	27.33
G109	466.5	743.3	0.5702	0.0070	16.7444	0.2716	0.2130	0.0032	2908.7	57.3	2920.3	37.1	2928.7	28.8	2928.66	28.80
G10	104.4	132.8	0.6405	0.0077	21.9196	0.3134	0.2483	0.0033	3191.1	60.8	3180.2	34.7	3173.8	25.6	3173.83	25.57
G43	51.1	59.9	0.6522	0.0082	23.6625	0.3635	0.2632	0.0038	3236.8	63.6	3254.6	37.0	3266.0	27.9	3265.96	27.92
G98	72.0	556.0	0.7271	0.0089	30.5792	0.4819	0.3051	0.0044	3522.7	66.4	3505.6	37.4	3496.2	28.6	3496.16	28.61
G48	8.4	81.4	0.0771	0.0012	0.6959	0.0292	0.0655	0.0028	478.7	14.5	536.3	37.8	790.1	46.8	478.73	14.48
G117	114.8	1451.4	0.0792	0.0010	0.7196	0.0133	0.0659	0.0012	491.2	11.7	550.4	18.2	804.2	19.4	491.23	11.71

APPENDIX B (continued). U-Pb ZIRCON AGES OF ZANSKAR RIVER SEDIMENTS

Grain No.	Pb (ppm)	U (ppm)	Ratios						Ages (Ma)						Best Age (Ma)	$\pm 2\sigma$
			$^{206}\text{Pb}/^{238}\text{U}$	$\pm 1\sigma$	$^{207}\text{Pb}/^{235}\text{U}$	$\pm \text{s.e.}$	$^{207}\text{Pb}/^{206}\text{Pb}$	$\pm \text{s.e.}$	$^{206}\text{Pb}/^{238}\text{U}$	$\pm 2\sigma$	$^{207}\text{Pb}/^{235}\text{U}$	$\pm 2\sigma$	$^{207}\text{Pb}/^{206}\text{Pb}$	$\pm 2\sigma$		
<i>G126</i>	84.5	584.4	0.1401	0.0018	1.6435	0.0301	0.0851	0.0015	845.4	19.8	987.0	27.0	1317.4	25.7	845.40	19.79
<i>G75</i>	32.7	246.5	0.1264	0.0016	1.0584	0.0234	0.0607	0.0013	767.3	18.4	733.0	26.2	630.0	20.2	767.30	18.43

APPENDIX C. U-Pb ZIRCON AGES OF ZANSKAR RIVER TERRACE SEDIMENTS

Grain No.	Pb (ppm)	U (ppm)	Ratios						Ages (Ma)						Best Age (Ma)	± 2σ
			²⁰⁶ Pb/ ²³⁸ U	± 1 σ	²⁰⁷ Pb/ ²³⁵ U	± s.e.	²⁰⁷ Pb/ ²⁰⁶ Pb	± s.e.	²⁰⁶ Pb/ ²³⁸ U	± 2σ	²⁰⁷ Pb/ ²³⁵ U	± 2σ	²⁰⁷ Pb/ ²⁰⁶ Pb	± 2σ		
Sample 13071602 Padum 25 m Terrace																
G43	2.5	689.7	0.0039	0.0001	0.0249	0.0015	0.0466	0.0029	25.3	0.9	25.0	3.2	26.2	4.4	25.3	0.9
G54	13.0	337.2	0.0397	0.0005	0.2734	0.0073	0.0503	0.0012	250.8	6.6	245.4	12.1	209.3	10.4	250.8	6.6
G9	31.0	689.7	0.0446	0.0006	0.3230	0.0061	0.0526	0.0009	281.0	6.9	284.2	10.3	312.9	10.1	281.0	6.9
G90	44.7	718.0	0.0665	0.0009	0.5254	0.0109	0.0576	0.0010	415.3	10.5	428.8	15.4	515.7	15.4	415.3	10.5
G68	46.2	676.7	0.0700	0.0009	0.6483	0.0140	0.0670	0.0012	436.4	11.0	507.4	17.7	838.1	21.8	436.4	11.0
G5	102.2	1566.5	0.0701	0.0009	0.5386	0.0079	0.0564	0.0007	437.0	10.4	437.5	12.5	466.6	10.5	437.0	10.4
G7	104.5	1499.1	0.0716	0.0009	0.6193	0.0091	0.0631	0.0008	445.5	10.6	489.4	13.6	712.9	13.9	445.5	10.6
G46	69.9	1037.8	0.0719	0.0009	0.5584	0.0091	0.0563	0.0008	447.7	10.8	450.5	13.6	464.2	11.6	447.7	10.8
G78	79.0	1148.8	0.0721	0.0009	0.6032	0.0122	0.0599	0.0010	449.0	11.2	479.2	16.1	598.5	16.5	449.0	11.2
G70	45.8	628.8	0.0724	0.0009	0.5578	0.0103	0.0561	0.0009	450.4	11.1	450.1	14.7	455.1	12.7	450.4	11.1
G93	92.6	1251.1	0.0730	0.0009	0.5524	0.0095	0.0567	0.0008	454.0	11.3	446.6	14.3	479.1	12.3	454.0	11.3
G13	134.5	1873.3	0.0737	0.0009	0.5776	0.0082	0.0571	0.0007	458.5	10.9	462.9	12.9	495.4	10.7	458.5	10.9
G98	63.2	900.8	0.0738	0.0010	0.5601	0.0100	0.0558	0.0008	458.8	11.4	451.6	14.6	442.4	12.0	458.8	11.4
G53	141.5	2051.7	0.0746	0.0009	0.5806	0.0085	0.0565	0.0007	463.5	11.2	464.8	13.0	473.2	10.5	463.5	11.2
G65	36.6	459.1	0.0767	0.0010	0.5926	0.0158	0.0582	0.0013	476.3	12.2	472.5	20.2	538.4	20.0	476.3	12.2
G14	16.9	198.0	0.0798	0.0010	0.6185	0.0153	0.0575	0.0012	494.7	12.3	488.9	19.3	512.3	18.0	494.7	12.3
G87	43.5	543.9	0.0813	0.0011	0.6415	0.0121	0.0576	0.0009	503.7	12.5	503.2	16.3	515.0	14.0	503.7	12.5
G36	7.0	71.8	0.0820	0.0013	0.6375	0.0319	0.0587	0.0025	507.8	15.4	500.7	36.1	557.5	37.0	507.8	15.4
G92	18.7	171.9	0.0827	0.0012	0.6175	0.0252	0.0563	0.0019	512.2	14.5	488.3	29.6	463.0	26.7	512.2	14.5
G31	10.8	91.4	0.0845	0.0012	0.7074	0.0268	0.0609	0.0019	522.9	14.3	543.2	28.8	635.4	30.6	522.9	14.3
G44	8.9	78.3	0.0848	0.0013	0.6189	0.0273	0.0546	0.0020	524.8	15.0	489.2	31.4	397.5	25.4	524.8	15.0
G38	13.6	126.2	0.0863	0.0012	0.6529	0.0208	0.0579	0.0015	533.5	13.9	510.2	24.6	524.1	22.9	533.5	13.9
G61	25.7	274.1	0.0867	0.0012	0.6763	0.0181	0.0579	0.0013	536.1	13.6	524.5	21.4	527.1	19.4	536.1	13.6
G81	33.3	385.1	0.0880	0.0012	0.7181	0.0170	0.0601	0.0012	543.7	13.7	549.5	20.1	606.8	19.0	543.7	13.7
G16	10.2	104.4	0.0912	0.0012	0.7378	0.0242	0.0580	0.0016	562.3	14.7	561.1	25.7	529.4	23.3	562.3	14.7
G39	17.8	137.1	0.0999	0.0014	0.7999	0.0314	0.0604	0.0019	614.1	16.8	596.8	31.9	617.6	30.3	614.1	16.8
G55	221.6	2101.8	0.1070	0.0013	0.9491	0.0134	0.0636	0.0008	655.1	15.5	677.7	16.8	728.4	13.5	655.1	15.5
G69	25.8	221.9	0.1145	0.0015	0.9626	0.0224	0.0617	0.0011	698.5	17.2	684.6	22.6	662.0	19.2	698.5	17.2
G48	253.5	2099.6	0.1227	0.0015	1.1103	0.0168	0.0658	0.0008	746.3	17.6	758.3	18.7	800.7	14.9	746.3	17.6
G33	83.8	628.8	0.1243	0.0016	1.1489	0.0194	0.0655	0.0009	755.3	17.8	776.7	19.7	790.1	16.0	755.3	17.8
G18	120.4	1005.2	0.1246	0.0015	1.1270	0.0169	0.0670	0.0008	757.2	17.7	766.3	18.9	838.7	15.2	757.2	17.7
G35	42.4	324.2	0.1259	0.0016	1.1491	0.0246	0.0668	0.0011	764.3	18.3	776.8	22.8	832.5	20.1	764.3	18.3
G49	86.4	702.8	0.1267	0.0016	1.2209	0.0224	0.0697	0.0010	769.1	18.3	810.2	21.3	918.3	18.6	769.1	18.3
G21	14.1	108.8	0.1288	0.0018	1.1827	0.0391	0.0656	0.0016	781.0	20.0	792.6	30.9	794.6	28.6	781.0	20.0
G41	23.7	174.1	0.1291	0.0017	1.1478	0.0339	0.0660	0.0015	782.8	19.6	776.2	28.5	805.1	26.0	782.8	19.6

APPENDIX C (continued). U-Pb ZIRCON AGES OF ZANSKAR RIVER TERRACE SEDIMENTS

Grain No.	Pb (ppm)	U (ppm)	Ratios						Ages (Ma)						Best Age (Ma)	± 2σ
			²⁰⁶ Pb/ ²³⁸ U	± 1 σ	²⁰⁷ Pb/ ²³⁵ U	± s.e.	²⁰⁷ Pb/ ²⁰⁶ Pb	± s.e.	²⁰⁶ Pb/ ²³⁸ U	± 2σ	²⁰⁷ Pb/ ²³⁵ U	± 2σ	²⁰⁷ Pb/ ²⁰⁶ Pb	± 2σ		
G10	21.1	150.1	0.1324	0.0017	1.1501	0.0312	0.0647	0.0013	801.5	19.6	777.3	26.9	764.3	23.5	801.5	19.6
G74	20.9	141.4	0.1352	0.0018	1.2066	0.0308	0.0655	0.0013	817.3	20.2	803.6	26.2	790.1	22.5	817.3	20.2
G84	66.5	435.1	0.1377	0.0018	1.2614	0.0238	0.0667	0.0010	831.9	20.1	828.5	22.3	828.7	18.0	831.9	20.1
G67	260.3	1890.7	0.1404	0.0018	1.3273	0.0201	0.0694	0.0009	846.8	19.9	857.7	20.4	911.8	16.0	846.8	19.9
G50	68.3	452.6	0.1432	0.0018	1.4522	0.0261	0.0736	0.0010	863.0	20.4	910.8	22.6	1029.7	19.2	863.0	20.4
G63	115.4	794.1	0.1442	0.0018	1.3668	0.0224	0.0688	0.0009	868.4	20.5	874.8	21.2	893.6	16.6	868.4	20.5
G20	32.5	204.5	0.1466	0.0019	1.4250	0.0336	0.0710	0.0012	881.9	21.1	899.5	25.9	956.0	22.9	881.9	21.1
G73	58.1	385.1	0.1473	0.0019	1.4135	0.0283	0.0698	0.0011	885.6	21.2	894.6	23.8	922.2	19.8	885.6	21.2
G57	114.7	641.8	0.1543	0.0019	1.4570	0.0241	0.0695	0.0009	924.8	21.7	912.8	21.9	914.5	16.8	914.5	16.8
G59	85.7	498.2	0.1543	0.0020	1.5177	0.0317	0.0699	0.0011	925.0	22.1	937.5	24.5	923.9	20.2	923.9	20.2
G76	71.1	480.8	0.1539	0.0020	1.4380	0.0257	0.0699	0.0010	922.6	21.9	904.9	22.8	924.2	18.1	924.2	18.1
G95	143.9	970.4	0.1544	0.0020	1.4600	0.0230	0.0699	0.0009	925.6	22.0	914.0	21.9	926.3	16.7	926.3	16.7
G94	85.8	415.6	0.1620	0.0021	1.5313	0.0282	0.0702	0.0010	967.9	23.2	943.0	23.8	933.3	18.6	933.3	18.6
G58	54.2	326.4	0.1584	0.0020	1.5609	0.0315	0.0706	0.0011	948.1	22.5	954.8	24.4	945.3	19.9	945.3	19.9
G47	39.2	241.5	0.1569	0.0020	1.5014	0.0300	0.0706	0.0011	939.5	22.2	931.0	24.1	946.7	19.7	946.7	19.7
G71	131.9	596.2	0.1595	0.0020	1.6051	0.0293	0.0709	0.0010	953.8	22.6	972.2	23.4	954.2	18.5	954.2	18.5
G62	34.4	180.6	0.1757	0.0023	1.6571	0.0393	0.0713	0.0012	1043.7	25.0	992.3	27.6	964.9	22.6	964.9	22.6
G2	165.0	1137.9	0.1528	0.0019	1.5145	0.0215	0.0716	0.0008	916.4	20.9	936.3	20.5	975.2	15.6	975.2	15.6
G28	15.7	82.7	0.1621	0.0023	1.6568	0.0628	0.0716	0.0019	968.5	25.1	992.2	37.1	975.7	34.1	975.7	34.1
G30	40.5	250.2	0.1526	0.0019	1.4910	0.0321	0.0717	0.0012	915.7	21.7	926.7	25.0	978.3	21.4	978.3	21.4
G45	--	89.2	0.1614	0.0021	1.6022	0.0451	0.0723	0.0015	964.7	23.6	971.1	30.1	993.8	26.7	993.8	26.7
G75	190.8	1074.8	0.1690	0.0021	1.7186	0.0262	0.0724	0.0009	1006.4	23.5	1015.5	22.3	998.3	16.7	998.3	16.7
G91	63.9	409.0	0.1549	0.0020	1.5071	0.0284	0.0731	0.0011	928.1	22.3	933.2	24.0	1017.0	19.9	1017.0	19.9
G11	31.4	174.1	0.1599	0.0020	1.5731	0.0331	0.0732	0.0011	956.2	22.5	959.7	25.1	1019.5	21.3	1019.5	21.3
G22	119.4	650.5	0.1757	0.0022	1.7537	0.0278	0.0740	0.0009	1043.3	23.8	1028.5	22.7	1040.1	17.3	1040.1	17.3
G89	121.1	617.9	0.1737	0.0022	1.7972	0.0300	0.0746	0.0010	1032.6	24.4	1044.4	23.7	1057.7	18.3	1057.7	18.3
G29	20.6	93.6	0.1813	0.0024	1.8834	0.0586	0.0751	0.0016	1074.3	26.4	1075.3	33.2	1070.4	29.3	1070.4	29.3
G40	102.1	578.7	0.1703	0.0021	1.8096	0.0335	0.0761	0.0011	1013.8	23.6	1048.9	24.3	1097.7	19.7	1097.7	19.7
G1	134.5	787.6	0.1725	0.0021	1.7948	0.0259	0.0766	0.0009	1025.8	23.2	1043.6	22.0	1111.3	15.5	1111.3	15.5
G42	159.8	798.5	0.1912	0.0024	2.0747	0.0325	0.0773	0.0009	1127.9	25.8	1140.5	23.7	1129.5	17.8	1129.5	17.8
G17	165.0	485.2	0.1773	0.0022	1.9748	0.0340	0.0796	0.0010	1052.1	24.1	1106.9	24.0	1186.8	19.4	1186.8	19.4
G82	181.4	718.0	0.2186	0.0028	2.4753	0.0401	0.0822	0.0010	1274.6	29.4	1264.8	25.7	1249.6	19.1	1249.6	19.1
G25	75.1	306.8	0.2358	0.0030	2.9407	0.0610	0.0897	0.0013	1364.6	31.0	1392.4	28.5	1419.4	22.7	1419.4	22.7
G88	55.8	200.2	0.2508	0.0033	3.0555	0.0639	0.0905	0.0013	1442.4	33.5	1421.6	29.8	1436.9	23.3	1436.9	23.3
G51	60.3	217.6	0.2577	0.0033	3.2070	0.0618	0.0911	0.0012	1477.8	33.4	1458.8	28.5	1449.3	21.7	1449.3	21.7
G37	18.2	63.1	0.2518	0.0038	3.2134	0.1610	0.0919	0.0026	1447.9	38.6	1460.4	49.7	1465.5	45.5	1465.5	45.5

APPENDIX C (continued). U-Pb ZIRCON AGES OF ZANSKAR RIVER TERRACE SEDIMENTS

Grain No.	Pb (ppm)	U (ppm)	Ratios						Ages (Ma)						Best Age (Ma)	± 2σ
			²⁰⁶ Pb/ ²³⁸ U	± 1 σ	²⁰⁷ Pb/ ²³⁵ U	± s.e.	²⁰⁷ Pb/ ²⁰⁶ Pb	± s.e.	²⁰⁶ Pb/ ²³⁸ U	± 2σ	²⁰⁷ Pb/ ²³⁵ U	± 2σ	²⁰⁷ Pb/ ²⁰⁶ Pb	± 2σ		
G23	49.7	178.4	0.2509	0.0032	3.2684	0.0672	0.0944	0.0013	1443.0	32.5	1473.6	29.0	1516.7	22.9	1516.7	22.9
G60	238.4	898.6	0.2461	0.0031	3.2416	0.0516	0.0957	0.0011	1418.1	32.0	1467.2	26.9	1541.5	20.1	1541.5	20.1
G83	150.7	476.5	0.3003	0.0038	4.2288	0.0716	0.1037	0.0013	1692.8	37.9	1679.6	29.1	1690.8	21.4	1690.8	21.4
G26	106.2	337.2	0.2605	0.0033	3.6467	0.0714	0.1041	0.0014	1492.2	33.4	1559.8	29.1	1699.2	22.9	1699.2	22.9
G15	28.6	69.6	0.2990	0.0039	4.2509	0.1179	0.1042	0.0017	1686.2	38.3	1683.9	34.0	1699.7	27.8	1699.7	27.8
G56	67.5	211.0	0.2795	0.0036	4.0172	0.0807	0.1047	0.0014	1588.8	35.8	1637.7	29.9	1708.9	23.2	1708.9	23.2
G32	43.4	119.7	0.3029	0.0039	4.3865	0.1097	0.1048	0.0016	1705.6	38.4	1709.8	32.5	1711.5	25.9	1711.5	25.9
G19	79.6	254.6	0.3106	0.0039	4.5483	0.0803	0.1086	0.0013	1743.5	37.9	1739.9	28.9	1776.2	21.5	1776.2	21.5
G96	138.8	439.5	0.2776	0.0036	4.0551	0.0721	0.1093	0.0014	1579.5	35.9	1645.3	29.6	1787.1	22.6	1787.1	22.6
G3	174.8	550.5	0.3163	0.0039	4.9212	0.0832	0.1132	0.0013	1771.6	38.1	1805.9	28.7	1852.1	21.2	1852.1	21.2
G12	65.2	187.1	0.3186	0.0040	4.7999	0.0894	0.1134	0.0014	1783.0	38.7	1784.9	29.6	1854.6	22.3	1854.6	22.3
G77	83.4	226.3	0.3489	0.0045	5.5142	0.1260	0.1142	0.0016	1929.2	43.0	1902.8	32.5	1867.1	24.9	1867.1	24.9
G85	237.6	435.1	0.4354	0.0056	9.2620	0.1887	0.1565	0.0020	2330.1	50.2	2364.3	32.9	2418.5	24.3	2418.5	24.3
G52	102.1	202.3	0.4636	0.0058	9.9817	0.1840	0.1604	0.0019	2455.3	51.3	2433.1	31.7	2460.3	22.8	2460.3	22.8
G64	189.5	359.0	0.4682	0.0059	10.0043	0.1996	0.1612	0.0020	2475.7	52.2	2435.2	32.5	2468.3	23.6	2468.3	23.6
G97	203.6	402.5	0.4551	0.0059	10.1510	0.2052	0.1616	0.0020	2417.7	52.0	2448.6	33.3	2472.9	24.5	2472.9	24.5
G8	90.6	184.9	0.4211	0.0053	9.3023	0.1953	0.1647	0.0020	2265.4	47.6	2368.2	32.0	2504.3	23.8	2504.3	23.8
G72	45.6	82.7	0.4800	0.0062	10.8507	0.2811	0.1650	0.0022	2527.2	54.2	2510.4	34.6	2507.0	26.0	2507.0	26.0
G27	309.7	644.0	0.4583	0.0057	10.8381	0.1729	0.1704	0.0019	2432.0	50.0	2509.3	30.8	2561.2	21.8	2561.2	21.8
G6	142.6	265.4	0.4996	0.0062	11.9222	0.2207	0.1777	0.0020	2612.2	53.0	2598.3	31.6	2631.9	22.7	2631.9	22.7
G4	145.0	252.4	0.4973	0.0061	12.0784	0.2047	0.1792	0.0020	2602.3	52.6	2610.5	31.2	2645.7	22.2	2645.7	22.2
G80	78.7	139.2	0.5081	0.0065	12.8957	0.2838	0.1819	0.0023	2648.5	55.7	2672.1	33.6	2670.6	24.6	2670.6	24.6
G79	181.7	287.2	0.5315	0.0068	14.0843	0.3166	0.1980	0.0025	2747.7	57.5	2755.4	33.9	2809.7	24.8	2809.7	24.8
G34	50.0	76.2	0.5566	0.0071	15.6898	0.4094	0.2017	0.0025	2852.6	58.6	2858.1	34.0	2839.9	25.1	2839.9	25.1
G66	114.4	195.8	0.5310	0.0070	16.6142	0.4906	0.2308	0.0031	2745.7	58.5	2912.8	35.7	3057.8	26.8	3057.8	26.8
G24	21.6	221.9	0.0976	0.0013	0.9633	0.0283	0.0723	0.0017	600.4	15.4	685.0	26.8	993.6	30.5	600.4	15.4
G86	--	106.6	0.1277	0.0019	1.3393	0.0512	0.0762	0.0021	774.6	21.2	862.9	36.6	1101.4	38.8	774.6	21.2
Sample 13071609 Padum 15 m Terrace																
G1	6.5	2067.9	0.0034	0.0001	0.0229	0.0012	0.0465	0.0024	22.1	0.6	23.0	2.4	22.1	2.3	22.1	0.6
G71	116.9	2315.6	0.0521	0.0006	0.4154	0.0083	0.0568	0.0010	327.6	7.8	352.7	12.6	484.6	23.4	327.6	7.8
G15	57.5	948.2	0.0649	0.0008	0.5162	0.0110	0.0584	0.0011	405.2	9.4	422.6	15.4	544.8	25.4	405.2	9.4
G80	96.7	1331.0	0.0669	0.0008	0.5168	0.0111	0.0569	0.0011	417.5	10.0	423.0	15.6	485.7	24.2	417.5	10.0
G4	308.5	4818.8	0.0676	0.0008	0.5283	0.0084	0.0574	0.0008	421.7	9.5	430.7	12.9	505.0	20.9	421.7	9.5
G78	75.0	1150.6	0.0690	0.0008	0.5419	0.0108	0.0565	0.0010	430.1	10.1	439.7	15.0	471.3	22.9	430.1	10.1
G98	16.2	199.7	0.0767	0.0011	0.6339	0.0220	0.0612	0.0018	476.5	12.6	498.5	25.7	646.6	37.7	476.5	12.6

APPENDIX C (continued). U-Pb ZIRCON AGES OF ZANSKAR RIVER TERRACE SEDIMENTS

Grain No.	Pb (ppm)	U (ppm)	Ratios						Ages (Ma)						Best Age (Ma)	± 2σ
			²⁰⁶ Pb/ ²³⁸ U	± 1 σ	²⁰⁷ Pb/ ²³⁵ U	± s.e.	²⁰⁷ Pb/ ²⁰⁶ Pb	± s.e.	²⁰⁶ Pb/ ²³⁸ U	± 2σ	²⁰⁷ Pb/ ²³⁵ U	± 2σ	²⁰⁷ Pb/ ²⁰⁶ Pb	± 2σ		
G17	23.4	244.4	0.0772	0.0010	0.6372	0.0203	0.0601	0.0016	479.3	12.0	500.6	23.5	607.5	34.2	479.3	12.0
G115	24.2	274.7	0.0785	0.0011	0.6067	0.0202	0.0559	0.0016	487.2	12.7	481.5	23.9	448.0	30.2	487.2	12.7
G57	99.3	1107.6	0.0805	0.0010	0.6796	0.0147	0.0605	0.0011	499.2	11.8	526.5	18.0	621.9	26.9	499.2	11.8
G86	10.0	80.0	0.0820	0.0012	0.6416	0.0266	0.0579	0.0020	507.8	13.8	503.3	30.0	525.6	38.2	507.8	13.8
G113	22.8	251.5	0.0828	0.0011	0.6564	0.0193	0.0592	0.0015	512.8	13.0	512.4	23.0	573.7	31.6	512.8	13.0
G84	17.0	121.9	0.0857	0.0013	0.7221	0.0328	0.0635	0.0024	530.1	15.1	551.9	34.8	724.0	48.3	530.1	15.1
G35	23.9	276.9	0.0875	0.0011	0.7374	0.0236	0.0600	0.0016	540.9	13.5	560.9	25.1	604.3	33.8	540.9	13.5
G91	112.7	1207.4	0.0877	0.0011	0.7408	0.0151	0.0618	0.0011	541.7	12.8	562.9	18.6	666.2	26.9	541.7	12.8
G108	73.5	862.1	0.0877	0.0011	0.6768	0.0167	0.0569	0.0012	542.0	13.2	524.8	20.2	486.5	26.0	542.0	13.2
G97	110.0	1209.7	0.0890	0.0011	0.7284	0.0159	0.0590	0.0011	549.5	13.1	555.6	19.1	566.0	26.0	549.5	13.1
G68	10.6	75.6	0.0900	0.0014	0.7705	0.0424	0.0636	0.0028	555.8	17.0	580.0	42.2	729.4	56.0	555.8	17.0
G10	6.2	44.7	0.0907	0.0014	0.7472	0.0436	0.0581	0.0028	559.7	17.0	566.6	42.7	534.7	49.2	559.7	17.0
G123	21.5	177.1	0.0912	0.0012	0.7726	0.0253	0.0628	0.0017	562.6	14.5	581.3	27.1	700.1	37.3	562.6	14.5
G101	24.1	180.9	0.0926	0.0013	0.7146	0.0283	0.0578	0.0019	571.0	15.3	547.5	30.6	521.0	36.4	571.0	15.3
G124	43.7	432.5	0.0934	0.0012	0.7910	0.0215	0.0636	0.0015	575.4	14.3	591.7	24.0	728.4	33.5	575.4	14.3
G12	28.0	297.9	0.0951	0.0012	0.8439	0.0245	0.0641	0.0015	585.7	14.1	621.3	24.8	746.3	34.7	585.7	14.1
G3	3.9	39.7	0.0971	0.0016	0.7944	0.0481	0.0583	0.0028	597.2	18.2	593.7	45.6	540.7	50.7	597.2	18.2
G75	29.3	262.6	0.1000	0.0013	0.8130	0.0220	0.0601	0.0013	614.1	14.9	604.1	23.6	607.2	30.2	614.1	14.9
G43	28.2	263.1	0.1047	0.0013	0.8993	0.0248	0.0630	0.0014	641.9	15.4	651.3	24.7	709.6	32.5	641.9	15.4
G118	49.5	381.2	0.1052	0.0014	1.0009	0.0279	0.0689	0.0016	644.9	16.0	704.3	26.6	895.4	37.0	644.9	16.0
G107	19.4	173.8	0.1056	0.0014	0.8506	0.0278	0.0618	0.0016	647.0	16.4	625.0	28.6	668.6	35.8	647.0	16.4
G45	46.1	349.2	0.1058	0.0013	0.8571	0.0235	0.0598	0.0013	648.4	15.5	628.5	24.2	594.9	29.9	648.4	15.5
G85	77.8	530.1	0.1072	0.0013	0.9540	0.0208	0.0644	0.0012	656.5	15.5	680.2	21.8	754.5	29.2	656.5	15.5
G30	13.3	97.1	0.1145	0.0016	1.0644	0.0446	0.0686	0.0022	698.8	18.5	736.0	36.8	885.5	47.6	698.8	18.5
G74	18.7	125.2	0.1159	0.0015	1.0319	0.0338	0.0659	0.0017	707.2	17.7	719.9	30.0	802.6	38.3	707.2	17.7
G77	236.8	1458.4	0.1204	0.0015	1.1192	0.0204	0.0662	0.0010	732.7	16.8	762.6	21.0	811.1	27.2	732.7	16.8
G21	50.0	388.3	0.1204	0.0015	1.1436	0.0276	0.0694	0.0013	732.9	16.9	774.2	24.6	910.9	32.7	732.9	16.9
G110	63.7	494.8	0.1210	0.0015	1.1482	0.0279	0.0689	0.0014	736.2	17.7	776.4	25.8	896.3	33.7	736.2	17.7
G105	48.8	390.0	0.1212	0.0015	1.0633	0.0257	0.0660	0.0013	737.6	17.6	735.4	25.1	807.3	31.9	737.6	17.6
G93	25.9	182.0	0.1244	0.0016	1.1295	0.0328	0.0665	0.0015	756.0	18.5	767.5	28.4	821.2	35.6	756.0	18.5
G60	55.8	429.1	0.1289	0.0016	1.2795	0.0311	0.0702	0.0013	781.8	18.3	836.6	25.7	935.4	33.2	781.8	18.3
G18	3.1	22.1	0.1308	0.0025	1.1937	0.1007	0.0648	0.0040	792.3	28.6	797.7	71.1	767.8	76.7	792.3	28.6
G8	7.9	49.1	0.1326	0.0021	1.2410	0.0720	0.0693	0.0029	802.7	23.8	819.3	51.2	908.9	60.6	802.7	23.8
G2	53.3	383.4	0.1350	0.0016	1.3046	0.0308	0.0697	0.0013	816.5	18.5	847.7	25.2	920.1	32.1	816.5	18.5
G38	42.5	305.6	0.1356	0.0017	1.4007	0.0353	0.0751	0.0015	819.8	19.1	889.2	27.2	1071.4	35.4	819.8	19.1
G5	63.3	437.4	0.1377	0.0017	1.3090	0.0315	0.0698	0.0013	831.5	18.9	849.7	25.7	923.1	32.4	831.5	18.9

APPENDIX C (continued). U-Pb ZIRCON AGES OF ZANSKAR RIVER TERRACE SEDIMENTS

Grain No.	Pb (ppm)	U (ppm)	Ratios						Ages (Ma)						Best Age (Ma)	± 2σ
			²⁰⁶ Pb/ ²³⁸ U	± 1 σ	²⁰⁷ Pb/ ²³⁵ U	± s.e.	²⁰⁷ Pb/ ²⁰⁶ Pb	± s.e.	²⁰⁶ Pb/ ²³⁸ U	± 2σ	²⁰⁷ Pb/ ²³⁵ U	± 2σ	²⁰⁷ Pb/ ²⁰⁶ Pb	± 2σ		
G76	31.9	197.5	0.1377	0.0018	1.2322	0.0358	0.0674	0.0015	831.6	20.1	815.3	29.4	851.1	35.7	831.6	20.1
G88	107.3	736.9	0.1406	0.0017	1.4182	0.0285	0.0745	0.0013	847.9	19.6	896.6	25.0	1055.3	31.9	847.9	19.6
G94	3.8	24.8	0.1420	0.0027	1.3277	0.1048	0.0698	0.0040	855.7	30.4	857.9	70.1	922.8	78.6	855.7	30.4
G83	46.0	231.1	0.1423	0.0018	1.2787	0.0362	0.0683	0.0015	857.6	20.7	836.3	29.6	876.8	35.7	857.6	20.7
G114	124.9	696.1	0.1426	0.0018	1.3801	0.0354	0.0695	0.0014	859.2	20.5	880.5	28.4	913.6	34.6	859.2	20.5
G104	18.4	117.5	0.1440	0.0020	1.3863	0.0491	0.0698	0.0019	867.3	22.0	883.1	35.1	922.2	42.0	867.3	22.0
G23	3.0	18.8	0.1450	0.0029	1.4234	0.1251	0.0701	0.0043	872.6	32.3	898.8	77.0	930.1	85.3	872.6	32.3
G25	30.1	150.6	0.1470	0.0019	1.3601	0.0391	0.0691	0.0015	884.2	20.8	871.9	29.6	900.5	35.6	884.2	20.8
G125	95.6	572.0	0.1514	0.0019	1.4465	0.0354	0.0700	0.0014	909.0	21.6	908.4	28.6	926.9	34.2	926.9	34.2
G81	64.8	397.7	0.1574	0.0020	1.4786	0.0334	0.0701	0.0013	942.1	21.7	921.6	26.8	930.1	31.8	930.1	31.8
G56	24.8	147.3	0.1549	0.0020	1.4969	0.0493	0.0704	0.0017	928.5	22.5	929.1	33.3	939.2	39.3	939.2	39.3
G47	180.0	382.3	0.1599	0.0020	1.5358	0.0338	0.0707	0.0012	956.2	21.7	944.8	26.0	949.0	31.0	949.0	31.0
G42	35.0	192.5	0.1609	0.0021	1.6112	0.0495	0.0708	0.0016	961.9	22.8	974.6	31.9	952.2	37.4	952.2	37.4
G61	109.0	627.7	0.1590	0.0019	1.5946	0.0313	0.0712	0.0011	951.1	21.4	968.1	24.8	962.3	29.8	962.3	29.8
G62	47.5	279.1	0.1510	0.0019	1.4351	0.0324	0.0712	0.0013	906.3	20.8	903.7	26.3	963.7	32.0	963.7	32.0
G72	70.8	428.0	0.1591	0.0020	1.5331	0.0324	0.0712	0.0012	951.6	21.7	943.7	25.9	963.7	31.0	963.7	31.0
G109	62.1	313.9	0.1647	0.0021	1.5985	0.0435	0.0715	0.0015	982.6	23.4	969.6	31.0	972.9	36.3	972.9	36.3
G24	34.0	195.3	0.1628	0.0020	1.6133	0.0424	0.0718	0.0014	972.0	22.3	975.4	28.9	981.4	34.4	981.4	34.4
G55	522.3	2639.9	0.1580	0.0019	1.5801	0.0266	0.0721	0.0010	945.8	20.9	962.4	23.1	987.6	27.9	987.6	27.9
G7	24.1	146.2	0.1499	0.0019	1.4787	0.0443	0.0721	0.0016	900.1	21.1	921.7	30.7	989.0	37.5	989.0	37.5
G73	71.7	378.4	0.1707	0.0021	1.6559	0.0400	0.0724	0.0014	1016.0	23.3	991.8	28.7	996.6	33.5	996.6	33.5
G54	4.8	24.8	0.1673	0.0028	1.5965	0.1086	0.0728	0.0034	997.3	31.4	968.8	63.4	1008.4	69.7	1008.4	69.7
G64	20.3	109.8	0.1683	0.0022	1.6083	0.0553	0.0728	0.0018	1003.0	24.5	973.4	35.7	1008.7	41.5	1008.7	41.5
G51	172.9	853.3	0.1659	0.0020	1.7226	0.0315	0.0752	0.0011	989.4	22.0	1017.0	24.7	1072.5	29.8	1072.5	29.8
G9	22.3	91.0	0.1569	0.0021	1.6835	0.0666	0.0761	0.0021	939.7	23.5	1002.3	38.6	1096.9	46.7	1096.9	46.7
G92	83.5	454.5	0.1668	0.0021	1.7288	0.0368	0.0762	0.0013	994.2	22.8	1019.3	27.5	1100.3	33.1	1100.3	33.1
G13	40.7	217.9	0.1681	0.0021	1.8223	0.0465	0.0764	0.0014	1001.9	22.7	1053.5	28.9	1104.3	34.9	1104.3	34.9
G70	134.5	655.8	0.1648	0.0020	1.7654	0.0355	0.0767	0.0013	983.5	22.2	1032.8	26.3	1112.6	31.9	1112.6	31.9
G37	40.7	149.5	0.1933	0.0024	2.0679	0.0606	0.0780	0.0016	1139.0	26.3	1138.2	32.8	1145.9	37.9	1145.9	37.9
G36	101.6	328.8	0.1892	0.0023	2.0457	0.0446	0.0813	0.0013	1116.9	24.8	1130.9	28.1	1229.2	33.2	1229.2	33.2
G121	39.0	153.9	0.2010	0.0026	2.1715	0.0600	0.0818	0.0017	1180.6	27.9	1172.0	34.7	1239.5	39.8	1239.5	39.8
G117	96.4	403.8	0.2038	0.0026	2.3012	0.0620	0.0839	0.0017	1195.6	28.1	1212.7	34.2	1290.2	39.4	1290.2	39.4
G26	169.5	756.8	0.2191	0.0026	2.6588	0.0494	0.0861	0.0012	1277.0	27.5	1317.1	27.4	1340.4	31.3	1340.4	31.3
G59	161.3	751.3	0.2114	0.0026	2.6337	0.0543	0.0898	0.0014	1236.1	27.2	1310.1	29.3	1420.2	34.0	1420.2	34.0
G48	112.5	370.7	0.2645	0.0032	3.4056	0.0717	0.0952	0.0015	1512.6	32.5	1505.7	30.9	1531.4	34.3	1531.4	34.3
G82	10.0	82.7	0.2632	0.0034	3.3777	0.1073	0.0953	0.0020	1506.1	34.7	1499.2	38.3	1533.2	42.4	1533.2	42.4

APPENDIX C (continued). U-Pb ZIRCON AGES OF ZANSKAR RIVER TERRACE SEDIMENTS

Grain No.	Pb (ppm)	U (ppm)	Ratios						Ages (Ma)						Best Age (Ma)	± 2σ
			²⁰⁶ Pb/ ²³⁸ U	± 1 σ	²⁰⁷ Pb/ ²³⁵ U	± s.e.	²⁰⁷ Pb/ ²⁰⁶ Pb	± s.e.	²⁰⁶ Pb/ ²³⁸ U	± 2σ	²⁰⁷ Pb/ ²³⁵ U	± 2σ	²⁰⁷ Pb/ ²⁰⁶ Pb	± 2σ		
G11	329.6	1018.8	0.2551	0.0030	3.4237	0.0586	0.0953	0.0013	1464.9	30.7	1509.9	28.0	1534.8	31.3	1534.8	31.3
G22	114.1	445.1	0.2493	0.0030	3.3801	0.0616	0.0978	0.0014	1435.0	30.4	1499.8	28.7	1583.0	32.3	1583.0	32.3
G90	30.1	75.0	0.2870	0.0038	4.0043	0.1373	0.1011	0.0022	1626.5	37.7	1635.1	40.6	1643.9	44.5	1643.9	44.5
G14	125.5	390.5	0.2877	0.0034	3.9863	0.0787	0.1012	0.0015	1630.0	34.0	1631.4	30.2	1645.5	33.2	1645.5	33.2
G52	12.0	44.1	0.3030	0.0040	4.2015	0.1632	0.1016	0.0022	1706.2	39.7	1674.3	42.3	1653.0	45.8	1653.0	45.8
G89	46.1	135.1	0.2799	0.0036	3.7786	0.1100	0.1025	0.0020	1590.7	36.1	1588.2	37.6	1669.3	41.5	1669.3	41.5
G46	60.9	194.2	0.2798	0.0035	3.9344	0.1111	0.1033	0.0019	1590.5	35.2	1620.8	35.4	1684.6	39.3	1684.6	39.3
G111	418.0	1505.3	0.2901	0.0036	4.1666	0.0845	0.1036	0.0018	1642.1	36.0	1667.5	34.4	1689.6	37.8	1689.6	37.8
G69	106.8	342.0	0.2688	0.0033	3.7800	0.0783	0.1041	0.0016	1534.5	33.2	1588.5	32.0	1698.6	35.7	1698.6	35.7
G67	102.8	340.3	0.2741	0.0034	3.8066	0.1003	0.1047	0.0019	1561.4	34.6	1594.1	35.1	1708.9	39.1	1708.9	39.1
G16	59.2	174.9	0.2732	0.0034	3.9488	0.1203	0.1058	0.0020	1557.2	34.5	1623.7	36.1	1729.0	40.4	1729.0	40.4
G28	123.0	329.3	0.3197	0.0038	4.7560	0.0980	0.1068	0.0016	1788.4	37.2	1777.2	31.5	1746.0	34.0	1746.0	34.0
G33	91.9	253.2	0.3140	0.0038	4.5624	0.1028	0.1071	0.0016	1760.3	37.1	1742.4	32.4	1750.1	35.2	1750.1	35.2
G32	88.4	256.5	0.3346	0.0042	5.1054	0.1546	0.1117	0.0020	1860.6	40.3	1837.0	36.6	1827.9	39.6	1827.9	39.6
G44	123.3	376.2	0.3099	0.0038	4.9321	0.1186	0.1159	0.0018	1740.4	37.2	1807.8	33.8	1893.9	37.1	1893.9	37.1
G65	269.5	796.5	0.3474	0.0042	6.1124	0.1204	0.1254	0.0019	1922.1	40.2	1992.0	33.4	2034.0	36.1	2034.0	36.1
G95	59.3	110.3	0.4432	0.0058	9.2883	0.3314	0.1497	0.0029	2364.7	51.6	2366.9	42.5	2341.9	44.9	2341.9	44.9
G53	98.1	211.3	0.4096	0.0050	8.7548	0.2237	0.1537	0.0024	2213.2	45.9	2312.8	36.1	2387.6	38.4	2387.6	38.4
G119	176.3	355.8	0.4285	0.0054	9.1290	0.2238	0.1579	0.0028	2298.7	48.8	2351.0	40.1	2433.0	42.8	2433.0	42.8
G6	484.3	916.8	0.4386	0.0051	9.7593	0.1582	0.1602	0.0021	2344.4	45.7	2412.3	31.9	2458.1	33.6	2458.1	33.6
G41	240.0	550.5	0.4062	0.0049	9.0071	0.1912	0.1604	0.0023	2197.3	44.7	2338.7	34.2	2459.6	36.4	2459.6	36.4
G49	103.7	199.1	0.4619	0.0056	10.3846	0.2300	0.1628	0.0024	2447.8	49.1	2469.7	35.0	2485.4	36.8	2485.4	36.8
G27	807.2	1555.5	0.4798	0.0056	10.8291	0.1703	0.1633	0.0021	2526.6	49.0	2508.6	32.5	2489.6	33.9	2489.6	33.9
G103	367.4	770.6	0.4647	0.0057	10.5323	0.2157	0.1641	0.0027	2460.3	50.4	2482.8	38.1	2498.0	40.4	2498.0	40.4
G58	538.6	1134.6	0.4503	0.0054	10.3108	0.1935	0.1654	0.0024	2396.7	48.0	2463.1	34.5	2511.4	36.4	2511.4	36.4
G63	216.4	348.6	0.4304	0.0052	9.9858	0.2194	0.1675	0.0025	2307.3	47.1	2433.5	35.6	2533.2	37.8	2533.2	37.8
G112	164.3	277.5	0.4911	0.0062	11.8322	0.2772	0.1792	0.0031	2575.4	53.2	2591.2	40.0	2645.4	42.3	2645.4	42.3
G19	182.3	323.8	0.4944	0.0059	11.9656	0.2546	0.1796	0.0025	2589.7	50.6	2601.7	34.0	2649.0	35.5	2649.0	35.5
G102	382.1	802.6	0.4198	0.0052	10.6918	0.2246	0.1796	0.0030	2259.7	47.1	2496.7	38.2	2649.4	40.8	2649.4	40.8
G39	207.9	393.3	0.4305	0.0052	10.5782	0.2414	0.1836	0.0026	2307.8	46.8	2486.8	34.9	2685.4	37.0	2685.4	37.0
G116	252.3	419.2	0.5041	0.0063	12.5897	0.2833	0.1851	0.0032	2631.2	54.0	2649.4	40.2	2698.8	42.5	2698.8	42.5
G96	359.0	597.4	0.5235	0.0065	13.4329	0.2885	0.1864	0.0030	2713.8	54.6	2710.6	38.5	2710.2	40.5	2710.2	40.5
G122	27.8	45.2	0.5121	0.0069	13.0345	0.5267	0.1900	0.0039	2665.4	58.9	2682.2	46.3	2742.3	48.6	2742.3	48.6
G120	212.8	382.8	0.5268	0.0067	13.8851	0.3732	0.1931	0.0035	2728.0	56.5	2741.9	41.7	2768.4	44.0	2768.4	44.0
G29	48.8	71.7	0.5440	0.0068	15.1803	0.5279	0.2005	0.0032	2800.2	56.9	2826.6	38.3	2830.3	39.9	2830.3	39.9
G40	260.3	472.2	0.4828	0.0058	13.1706	0.2594	0.2006	0.0028	2539.5	50.0	2692.0	34.3	2831.3	36.0	2831.3	36.0

APPENDIX C (continued). U-Pb ZIRCON AGES OF ZANSKAR RIVER TERRACE SEDIMENTS

Grain No.	Pb (ppm)	U (ppm)	Ratios						Ages (Ma)						Best Age (Ma)	± 2σ
			²⁰⁶ Pb/ ²³⁸ U	± 1 σ	²⁰⁷ Pb/ ²³⁵ U	± s.e.	²⁰⁷ Pb/ ²⁰⁶ Pb	± s.e.	²⁰⁶ Pb/ ²³⁸ U	± 2σ	²⁰⁷ Pb/ ²³⁵ U	± 2σ	²⁰⁷ Pb/ ²⁰⁶ Pb	± 2σ		
G79	406.5	736.9	0.5485	0.0067	17.0695	0.3354	0.2274	0.0034	2818.9	55.5	2938.7	37.1	3033.8	38.8	3033.8	38.8
G106	185.9	282.4	0.6033	0.0075	20.7716	0.5068	0.2714	0.0046	3043.1	60.6	3128.0	40.7	3314.2	42.7	3314.2	42.7
G99	526.3	642.1	0.6837	0.0084	28.4200	0.6012	0.2965	0.0048	3358.4	64.5	3433.7	39.8	3451.8	41.6	3451.8	41.6
G20	203.2	259.8	0.7505	0.0089	39.5609	0.8104	0.3797	0.0050	3609.5	65.3	3759.8	34.8	3830.4	35.7	3830.4	35.7
G87	11.3	87.7	0.0813	0.0012	0.7391	0.0288	0.0680	0.0022	503.8	13.7	561.9	30.8	867.0	47.3	503.8	13.7
G50	11.8	81.6	0.0869	0.0014	0.7889	0.0444	0.0673	0.0030	537.2	16.7	590.5	43.5	847.4	61.8	537.2	16.7
G66	198.6	1404.9	0.1195	0.0015	1.2852	0.0248	0.0776	0.0012	727.6	16.7	839.2	22.9	1136.1	31.7	727.6	16.7
G34	91.7	971.9	0.0997	0.0012	1.0141	0.0203	0.0695	0.0012	612.5	14.1	710.9	20.3	914.8	29.8	612.5	14.1
G31	41.0	278.6	0.1205	0.0015	1.2278	0.0362	0.0752	0.0017	733.2	17.7	813.3	29.2	1074.4	39.6	733.2	17.7
G100	10.7	69.5	0.1246	0.0019	1.0284	0.0507	0.0612	0.0023	757.1	21.3	718.1	42.4	644.9	46.1	757.1	21.3
Sample 13071609 Padum 15 m Terrace																
G47	8.5	2791.4	0.0033	0.0000	0.0229	0.0008	0.0504	0.0018	21.4	0.5	23.0	1.7	213.9	15.9	21.4	0.5
G78	9.3	2709.7	0.0037	0.0000	0.0264	0.0006	0.0509	0.0011	23.6	0.4	26.5	1.2	238.1	11.6	23.6	0.4
G82	3.2	880.5	0.0040	0.0001	0.0282	0.0012	0.0501	0.0021	25.8	0.8	28.2	2.4	199.2	17.4	25.8	0.8
G111	2.4	637.4	0.0040	0.0000	0.0265	0.0000	0.0491	0.0000	25.9	0.0	26.6	0.0	152.1	2.4	25.9	0.0
G28	1.7	441.6	0.0041	0.0001	0.0285	0.0016	0.0512	0.0029	26.6	0.9	28.5	3.4	248.5	27.2	26.6	0.9
G26	11.2	420.7	0.0251	0.0002	0.1740	0.0042	0.0521	0.0012	159.6	2.8	162.9	7.4	288.9	13.5	159.6	2.8
G60	5.6	128.3	0.0397	0.0004	0.2748	0.0083	0.0515	0.0014	251.0	5.1	246.5	13.0	261.0	14.9	251.0	5.1
G56	3.8	89.1	0.0401	0.0006	0.2591	0.0114	0.0476	0.0019	253.5	6.8	233.9	18.1	78.4	8.5	253.5	6.8
G102	22.6	440.3	0.0457	0.0003	0.3403	0.0069	0.0557	0.0009	287.8	4.2	297.4	9.6	441.2	14.3	287.8	4.2
G43	54.0	1267.4	0.0463	0.0003	0.3652	0.0062	0.0562	0.0008	291.5	3.8	316.1	8.0	460.7	12.3	291.5	3.8
G41	36.9	852.1	0.0465	0.0003	0.3666	0.0058	0.0572	0.0007	292.9	3.6	317.1	7.3	499.6	11.8	292.9	3.6
G101	59.3	987.2	0.0476	0.0003	0.3609	0.0062	0.0559	0.0007	300.0	3.8	312.9	8.0	446.8	12.0	300.0	3.8
G29	5.3	83.7	0.0531	0.0008	0.4101	0.0188	0.0567	0.0023	333.7	9.8	348.9	25.8	477.9	33.3	333.7	9.8
G69	17.8	263.3	0.0537	0.0004	0.4114	0.0083	0.0561	0.0009	337.2	4.9	349.9	10.6	454.3	14.3	337.2	4.9
G59	69.4	989.2	0.0562	0.0003	0.4262	0.0062	0.0536	0.0006	352.7	4.0	360.5	7.1	356.0	8.7	352.7	4.0
G21	29.1	426.7	0.0566	0.0004	0.4258	0.0076	0.0551	0.0008	354.6	4.6	360.2	9.5	417.9	12.0	354.6	4.6
G58	19.5	276.2	0.0576	0.0004	0.4287	0.0085	0.0539	0.0009	361.1	5.1	362.2	10.6	368.1	12.1	361.1	5.1
G46	151.1	1968.3	0.0604	0.0003	0.4836	0.0065	0.0583	0.0005	377.9	4.1	400.5	7.2	541.1	10.2	377.9	4.1
G76	285.1	4981.2	0.0622	0.0003	0.5016	0.0064	0.0574	0.0005	389.1	4.1	412.8	6.7	507.3	9.1	389.1	4.1
G70	55.4	885.2	0.0661	0.0004	0.5278	0.0089	0.0598	0.0008	412.4	5.2	430.3	10.1	597.8	13.7	412.4	5.2
G71	16.9	215.4	0.0664	0.0006	0.5511	0.0148	0.0620	0.0014	414.3	7.6	445.7	17.6	675.1	24.0	414.3	7.6
G100	67.2	1079.7	0.0669	0.0004	0.5183	0.0083	0.0575	0.0007	417.7	5.1	424.0	9.4	512.3	11.9	417.7	5.1
G37	72.2	1032.4	0.0676	0.0004	0.5263	0.0071	0.0564	0.0005	421.4	4.6	429.3	7.6	467.0	9.3	421.4	4.6
G17	300.3	4257.3	0.0684	0.0004	0.5472	0.0065	0.0568	0.0004	426.2	4.3	443.2	6.3	483.4	7.9	426.2	4.3

APPENDIX C (continued). U-Pb ZIRCON AGES OF ZANSKAR RIVER TERRACE SEDIMENTS

Grain No.	Pb (ppm)	U (ppm)	Ratios						Ages (Ma)						Best Age (Ma)	± 2σ
			²⁰⁶ Pb/ ²³⁸ U	± 1 σ	²⁰⁷ Pb/ ²³⁵ U	± s.e.	²⁰⁷ Pb/ ²⁰⁶ Pb	± s.e.	²⁰⁶ Pb/ ²³⁸ U	± 2σ	²⁰⁷ Pb/ ²³⁵ U	± 2σ	²⁰⁷ Pb/ ²⁰⁶ Pb	± 2σ		
G65	98.6	1129.7	0.0702	0.0004	0.5408	0.0075	0.0555	0.0005	437.3	4.8	439.0	7.9	432.8	9.1	437.3	4.8
G12	136.7	2006.8	0.0703	0.0004	0.5528	0.0071	0.0571	0.0005	437.8	4.7	446.8	7.3	496.9	9.0	437.8	4.7
G77	178.8	2710.4	0.0703	0.0004	0.5619	0.0076	0.0569	0.0005	438.1	4.8	452.7	7.8	487.3	9.5	438.1	4.8
G87	429.8	6597.0	0.0707	0.0004	0.5600	0.0074	0.0570	0.0005	440.1	4.7	451.5	7.4	493.1	9.1	440.1	4.7
G27	35.0	428.8	0.0712	0.0005	0.5526	0.0091	0.0575	0.0007	443.4	5.4	446.7	9.9	509.2	12.0	443.4	5.4
G80	88.0	1317.4	0.0715	0.0004	0.5559	0.0081	0.0559	0.0006	445.4	5.1	448.9	8.5	450.0	9.8	445.4	5.1
G73	156.6	2337.0	0.0716	0.0004	0.5642	0.0074	0.0564	0.0005	446.0	4.8	454.3	7.5	469.3	8.9	446.0	4.8
G8	38.5	538.8	0.0726	0.0005	0.6259	0.0112	0.0645	0.0009	451.9	6.0	493.5	12.0	757.4	16.6	451.9	6.0
G48	97.5	1383.6	0.0732	0.0004	0.5806	0.0076	0.0566	0.0005	455.3	4.8	464.9	7.4	475.6	8.8	455.3	4.8
G19	129.4	1866.3	0.0743	0.0004	0.5765	0.0071	0.0562	0.0004	461.8	4.8	462.2	7.0	458.3	8.2	461.8	4.8
G42	63.1	753.6	0.0753	0.0004	0.5855	0.0083	0.0573	0.0006	468.1	5.3	468.0	8.6	503.9	10.2	468.1	5.3
G31	60.8	790.0	0.0760	0.0004	0.6053	0.0086	0.0570	0.0006	472.3	5.3	480.6	8.7	491.1	10.0	472.3	5.3
G25	30.3	415.3	0.0770	0.0005	0.5790	0.0096	0.0559	0.0007	478.3	5.9	463.8	10.4	449.6	11.2	478.3	5.9
G5	112.3	1363.3	0.0880	0.0005	0.7316	0.0090	0.0607	0.0005	543.5	5.6	557.5	8.0	629.0	9.5	543.5	5.6
G36	189.3	1801.5	0.0886	0.0005	0.7889	0.0111	0.0644	0.0006	547.1	6.0	590.5	9.9	754.8	12.5	547.1	6.0
G92	50.6	555.0	0.0912	0.0006	0.7134	0.0118	0.0587	0.0007	562.5	6.9	546.7	11.7	556.4	12.6	562.5	6.9
G84	152.2	1193.8	0.1075	0.0006	1.0117	0.0147	0.0669	0.0007	658.2	7.3	709.7	11.5	835.9	13.5	658.2	7.3
G53	178.2	1646.2	0.1081	0.0006	1.0253	0.0142	0.0693	0.0006	661.5	7.2	716.6	11.0	908.0	13.1	661.5	7.2
G97	191.3	1858.9	0.1088	0.0006	0.9650	0.0139	0.0653	0.0006	665.6	7.3	685.9	11.4	783.7	13.1	665.6	7.3
G91	113.5	974.4	0.1127	0.0007	1.0384	0.0180	0.0673	0.0008	688.6	8.6	723.1	14.4	848.0	16.4	688.6	8.6
G50	145.8	1245.1	0.1132	0.0006	1.0526	0.0144	0.0675	0.0006	691.4	7.4	730.2	10.8	853.2	12.5	691.4	7.4
G99	61.6	494.9	0.1138	0.0008	1.0335	0.0198	0.0669	0.0009	694.7	9.3	720.7	15.9	833.1	17.9	694.7	9.3
G13	55.4	418.0	0.1141	0.0007	1.0070	0.0173	0.0646	0.0008	696.7	8.6	707.4	13.8	761.0	15.0	696.7	8.6
G20	142.3	1016.9	0.1149	0.0006	1.0385	0.0132	0.0659	0.0005	701.3	7.2	723.2	9.8	801.9	11.0	701.3	7.2
G64	99.6	892.7	0.1167	0.0007	1.0858	0.0149	0.0668	0.0006	711.5	7.6	746.5	11.0	830.3	12.4	711.5	7.6
G81	144.1	1082.4	0.1190	0.0007	1.1094	0.0162	0.0673	0.0007	724.8	8.1	757.9	12.1	845.5	13.5	724.8	8.1
G62	63.2	457.8	0.1199	0.0007	1.0636	0.0158	0.0662	0.0007	729.8	8.2	735.6	12.2	813.7	13.4	729.8	8.2
G2	131.5	1056.1	0.1212	0.0007	1.1253	0.0150	0.0674	0.0006	737.6	7.7	765.5	10.7	850.5	12.0	737.6	7.7
G54	137.0	1116.2	0.1215	0.0007	1.1200	0.0148	0.0670	0.0006	739.0	7.7	763.0	10.8	838.4	11.9	739.0	7.7
G96	349.7	2856.9	0.1220	0.0007	1.1405	0.0157	0.0676	0.0006	742.3	7.9	772.7	11.6	855.4	13.0	742.3	7.9
G14	37.4	239.0	0.1231	0.0009	1.1366	0.0219	0.0689	0.0009	748.6	10.0	770.9	16.4	894.8	18.1	748.6	10.0
G55	41.5	283.6	0.1253	0.0008	1.1343	0.0204	0.0660	0.0008	761.1	9.5	769.8	15.1	806.1	16.0	761.1	9.5
G4	73.8	526.0	0.1255	0.0007	1.1333	0.0157	0.0666	0.0006	762.2	8.1	769.3	11.3	824.7	12.2	762.2	8.1
G45	164.2	1116.2	0.1270	0.0007	1.1366	0.0156	0.0661	0.0006	770.9	8.2	770.9	11.2	810.2	12.0	770.9	8.2
G18	64.7	477.4	0.1275	0.0008	1.1011	0.0190	0.0668	0.0008	773.5	9.5	753.9	14.5	830.3	15.5	773.5	9.5
G11	37.6	290.3	0.1282	0.0008	1.1988	0.0190	0.0691	0.0007	777.5	9.0	800.0	13.4	901.1	14.7	777.5	9.0

APPENDIX C (continued). U-Pb ZIRCON AGES OF ZANSKAR RIVER TERRACE SEDIMENTS

Grain No.	Pb (ppm)	U (ppm)	Ratios						Ages (Ma)						Best Age (Ma)	± 2σ
			²⁰⁶ Pb/ ²³⁸ U	± 1 σ	²⁰⁷ Pb/ ²³⁵ U	± s.e.	²⁰⁷ Pb/ ²⁰⁶ Pb	± s.e.	²⁰⁶ Pb/ ²³⁸ U	± 2σ	²⁰⁷ Pb/ ²³⁵ U	± 2σ	²⁰⁷ Pb/ ²⁰⁶ Pb	± 2σ		
G7	147.9	950.7	0.1284	0.0007	1.1983	0.0149	0.0662	0.0005	778.4	7.9	799.8	10.0	813.3	10.7	778.4	7.9
G52	112.2	668.5	0.1290	0.0008	1.2407	0.0186	0.0742	0.0007	782.3	8.8	819.2	13.2	1048.0	15.1	782.3	8.8
G75	273.9	1836.0	0.1299	0.0007	1.2182	0.0159	0.0671	0.0006	787.5	8.1	808.9	11.1	840.6	11.9	787.5	8.1
G93	131.0	611.8	0.1300	0.0008	1.2112	0.0188	0.0686	0.0007	787.6	9.0	805.7	13.6	886.7	14.8	787.6	9.0
G33	84.3	486.2	0.1307	0.0008	1.1746	0.0168	0.0670	0.0006	791.6	8.6	788.8	12.0	837.5	12.8	791.6	8.6
G103	55.2	376.8	0.1311	0.0008	1.1973	0.0203	0.0684	0.0008	794.0	9.6	799.4	15.0	880.7	16.2	794.0	9.6
G10	200.2	1235.0	0.1312	0.0007	1.1744	0.0143	0.0658	0.0005	794.8	7.9	788.7	9.8	800.0	10.3	794.8	7.9
G51	208.6	1192.5	0.1312	0.0007	1.2265	0.0160	0.0667	0.0005	794.9	8.2	812.7	10.9	828.1	11.6	794.9	8.2
G89	32.5	243.8	0.1314	0.0010	1.1978	0.0252	0.0706	0.0010	795.8	11.3	799.6	18.9	946.1	20.5	795.8	11.3
G1	132.3	896.7	0.1321	0.0007	1.1916	0.0149	0.0668	0.0005	800.1	8.1	796.7	10.3	830.6	8.5	800.1	8.1
G34	61.7	426.1	0.1322	0.0008	1.1766	0.0173	0.0669	0.0006	800.1	8.9	789.7	12.4	835.9	13.1	800.1	8.9
G61	63.9	426.1	0.1322	0.0008	1.2111	0.0183	0.0674	0.0007	800.2	9.0	805.7	12.8	849.2	13.7	800.2	9.0
G72	103.8	745.5	0.1327	0.0008	1.2154	0.0171	0.0671	0.0006	803.4	8.7	807.6	12.0	842.1	12.8	803.4	8.7
G30	185.3	1231.6	0.1332	0.0007	1.2307	0.0153	0.0670	0.0005	806.0	8.1	814.7	10.3	839.0	10.9	806.0	8.1
G3	89.5	648.9	0.1333	0.0007	1.1921	0.0156	0.0663	0.0005	806.4	8.3	797.0	10.8	814.3	11.4	806.4	8.3
G107	56.0	350.4	0.1333	0.0010	1.2125	0.0250	0.0677	0.0010	806.4	11.1	806.3	18.3	859.7	19.2	806.4	11.1
G15	135.2	883.2	0.1333	0.0007	1.2061	0.0158	0.0663	0.0005	806.5	8.3	803.4	10.8	815.9	11.4	806.5	8.3
G83	51.1	377.5	0.1337	0.0010	1.2070	0.0246	0.0693	0.0010	808.8	11.1	803.8	18.1	908.9	19.4	808.8	11.1
G109	116.8	600.3	0.1352	0.0009	1.2495	0.0212	0.0659	0.0008	817.3	9.8	823.2	14.9	801.6	15.4	817.3	9.8
G68	90.4	635.4	0.1357	0.0008	1.2389	0.0178	0.0668	0.0006	820.2	9.0	818.4	12.4	830.9	12.9	820.2	9.0
G32	77.5	474.7	0.1358	0.0008	1.2276	0.0179	0.0673	0.0006	821.0	9.0	813.2	12.3	846.5	13.0	821.0	9.0
G106	136.3	834.6	0.1362	0.0009	1.2338	0.0208	0.0664	0.0008	823.2	9.9	816.1	14.9	818.4	15.4	823.2	9.9
G105	206.6	1440.3	0.1365	0.0008	1.2992	0.0191	0.0685	0.0007	824.8	9.1	845.4	13.2	882.5	14.1	824.8	9.1
G108	202.0	1580.0	0.1374	0.0008	1.3588	0.0205	0.0730	0.0008	830.1	9.3	871.4	14.0	1014.0	15.6	830.1	9.3
G104	43.3	280.2	0.1377	0.0009	1.2764	0.0229	0.0672	0.0008	831.5	10.3	835.3	15.9	843.4	16.5	831.5	10.3
G38	49.8	290.3	0.1379	0.0009	1.3036	0.0209	0.0687	0.0007	832.9	9.6	847.3	13.8	890.0	14.6	832.9	9.6
G66	110.7	675.9	0.1382	0.0008	1.2780	0.0191	0.0664	0.0006	834.5	9.3	836.0	12.8	820.3	13.2	834.5	9.3
G39	139.3	927.1	0.1385	0.0008	1.3236	0.0171	0.0689	0.0005	836.2	8.6	856.1	11.0	895.7	11.7	836.2	8.6
G88	113.8	657.7	0.1389	0.0009	1.3163	0.0213	0.0698	0.0008	838.4	9.8	852.9	14.6	923.7	15.6	838.4	9.8
G23	106.6	784.6	0.1390	0.0008	1.2766	0.0168	0.0670	0.0005	839.0	8.7	835.4	11.2	837.5	11.6	839.0	8.7
G63	157.5	672.5	0.1398	0.0009	1.3166	0.0221	0.0698	0.0008	843.6	10.1	853.0	14.8	923.7	15.8	843.6	10.1
G9	34.8	213.4	0.1419	0.0009	1.3115	0.0226	0.0683	0.0008	855.3	10.3	850.8	15.1	878.3	15.6	855.3	10.3
G86	156.3	1019.6	0.1451	0.0008	1.3493	0.0190	0.0669	0.0006	873.5	9.3	867.2	12.7	835.0	12.9	873.5	9.3
G79	102.3	582.0	0.1476	0.0009	1.3821	0.0211	0.0688	0.0007	887.4	9.9	881.3	13.8	892.1	14.3	887.4	9.9
G22	66.8	436.2	0.1628	0.0009	1.5722	0.0226	0.0712	0.0006	972.5	10.4	959.3	13.1	961.7	13.2	961.7	13.2
G16	19.5	112.1	0.1661	0.0013	1.6466	0.0374	0.0716	0.0010	990.4	14.2	988.3	20.7	975.4	20.6	975.4	20.6

APPENDIX C (continued). U-Pb ZIRCON AGES OF ZANSKAR RIVER TERRACE SEDIMENTS

Grain No.	Pb (ppm)	U (ppm)	Ratios						Ages (Ma)						Best Age (Ma)	± 2σ
			²⁰⁶ Pb/ ²³⁸ U	± 1 σ	²⁰⁷ Pb/ ²³⁵ U	± s.e.	²⁰⁷ Pb/ ²⁰⁶ Pb	± s.e.	²⁰⁶ Pb/ ²³⁸ U	± 2σ	²⁰⁷ Pb/ ²³⁵ U	± 2σ	²⁰⁷ Pb/ ²⁰⁶ Pb	± 2σ		
G24	75.8	440.9	0.1655	0.0010	1.6336	0.0233	0.0727	0.0006	987.4	10.5	983.3	13.2	1004.5	13.4	1004.5	13.4
G40	173.0	1025.7	0.1661	0.0009	1.6840	0.0212	0.0731	0.0006	990.5	9.8	1002.5	11.7	1016.2	12.1	1016.2	12.1
G85	52.5	299.1	0.1566	0.0010	1.5547	0.0266	0.0741	0.0008	937.8	11.3	952.4	16.2	1043.4	17.0	1043.4	17.0
G74	27.6	146.5	0.1716	0.0012	1.7467	0.0337	0.0743	0.0009	1021.1	13.0	1026.0	18.3	1049.1	18.6	1049.1	18.6
G6	496.5	3016.9	0.1644	0.0008	1.7636	0.0198	0.0766	0.0005	981.3	9.3	1032.2	10.4	1110.8	10.9	1110.8	10.9
G98	93.2	434.8	0.1877	0.0012	2.0605	0.0351	0.0808	0.0009	1108.7	13.0	1135.8	17.5	1217.3	18.0	1217.3	18.0
G110	31.5	154.6	0.1911	0.0014	2.1509	0.0441	0.0822	0.0011	1127.3	14.9	1165.4	21.0	1250.3	21.5	1250.3	21.5
G57	84.6	228.9	0.2786	0.0018	3.7074	0.0637	0.1000	0.0010	1584.2	17.6	1573.0	18.4	1623.5	17.8	1623.5	17.8
G44	301.5	731.3	0.3722	0.0020	7.4475	0.0966	0.1491	0.0011	2039.5	18.9	2166.7	15.9	2335.4	15.3	2335.4	15.3
G90	259.4	518.6	0.4379	0.0026	9.5389	0.1458	0.1589	0.0014	2341.0	23.0	2391.3	19.4	2443.5	18.6	2443.5	18.6
G67	275.0	480.1	0.4514	0.0026	10.4001	0.1521	0.1663	0.0013	2401.3	22.8	2471.1	18.0	2520.4	17.1	2520.4	17.1
G35	141.9	241.1	0.5243	0.0030	13.9490	0.2119	0.2003	0.0014	2717.4	25.5	2746.3	17.3	2828.2	15.9	2828.2	15.9
G49	93.6	116.1	0.5757	0.0036	17.1763	0.3078	0.2191	0.0017	2931.0	29.2	2944.7	19.1	2973.9	17.3	2973.9	17.3
G94	15.4	120.2	0.0906	0.0008	0.8759	0.0217	0.0707	0.0013	559.1	9.3	638.8	19.6	948.2	25.4	559.1	9.3
G95	296.6	253.2	0.0934	0.0008	0.8640	0.0196	0.0703	0.0012	575.3	9.0	632.3	18.1	936.0	23.1	575.3	9.0

APPENDIX D. CONSENT FOR CHAPTER 4

JOHN WILEY AND SONS LICENSE TERMS AND CONDITIONS

This Agreement between Tara N Jonell ("You") and John Wiley and Sons ("John Wiley and Sons") consists of your license details and the terms and conditions provided by John Wiley and Sons and Copyright Clearance Center.

License Number	4035621171042
License date	
Licensed Content Publisher	John Wiley and Sons
Licensed Content Publication	Basin Research
Licensed Content Title	Controls on erosion patterns and sediment transport in a monsoonal, tectonically quiescent drainage, Song Gianh, central Vietnam
Licensed Content Author	Tara N. Jonell, Peter D. Clift, Long V. Hoang, Tina Hoang, Andrew Carter, Hella Wittmann, Philipp Böning, Katharina Pahnke, Tammy Rittenour
Licensed Content Date	Jul 6, 2016
Licensed Content Pages	1
Type of use	Dissertation/Thesis
Requestor type	Author of this Wiley article
Format	Print and electronic
Portion	Full article
Will you be translating?	No
Title of your thesis / dissertation	Quaternary river erosion, provenance, and climate variability in NW Himalaya and Vietnam
Expected completion date	May 2017
Expected size (number of pages)	200
Publisher Tax ID	EU826007151
Billing Type	Invoice
Total	0.00 USD

APPENDIX E. U-Pb ZIRCON AGES OF SONG GIANH SEDIMENTS

Grain No.	Pb (ppm)	U (ppm)	Ratios						Ages (Ma)						Best Age (Ma)	± 2σ
			²⁰⁶ Pb/ ²³⁸ U	± 1 σ	²⁰⁷ Pb/ ²³⁵ U	± s.e.	²⁰⁷ Pb/ ²⁰⁶ Pb	± s.e.	²⁰⁶ Pb/ ²³⁸ U	± 2σ	²⁰⁷ Pb/ ²³⁵ U	± 2σ	²⁰⁷ Pb/ ²⁰⁶ Pb	± 2σ		
Sample 12061711 Middle reaches																
G71	7	253	0.0222	0.0058	0.1510	0.2292	0.0488	0.0017	141.7	72.9	142.8	69.3	137.8	10.6	141.7	72.9
G24	30	984	0.0275	0.0054	0.1881	0.2188	0.0502	0.0016	174.7	67.6	175.0	64.5	205.2	13.6	174.7	67.6
G26	21	616	0.0275	0.0003	0.1963	0.0029	0.0517	0.0006	174.9	4.1	182.0	5.3	270.8	6.8	174.9	4.1
G106	7	214	0.0283	0.0039	0.1976	0.0910	0.0506	0.0012	180.1	49.3	183.1	47.2	221.7	11.4	180.1	49.3
G80	6	192	0.0300	0.0018	0.2105	0.0225	0.0503	0.0007	190.8	22.9	194.0	21.8	208.0	6.8	190.8	22.9
G110	9	165	0.0365	0.0004	0.2543	0.0056	0.0507	0.0013	231.2	4.9	230.1	11.5	227.7	12.3	231.2	4.9
G92	8	202	0.0381	0.0005	0.3147	0.0054	0.0584	0.0008	240.9	6.1	277.8	9.0	545.9	13.3	240.9	6.1
G28	14	344	0.0393	0.0003	0.2832	0.0033	0.0516	0.0007	248.5	4.1	253.2	6.7	267.7	7.7	248.5	4.1
G81	34	893	0.0394	0.0010	0.2780	0.0144	0.0510	0.0010	249.2	12.4	249.0	14.3	240.8	10.5	249.2	12.4
G47	15	343	0.0395	0.0047	0.2796	0.1270	0.0513	0.0012	249.5	57.9	250.4	53.4	252.5	12.2	249.5	57.9
G90	11	278	0.0396	0.0010	0.2786	0.0104	0.0509	0.0006	250.5	12.8	249.6	12.5	234.5	6.5	250.5	12.8
G66	8	209	0.0396	0.0039	0.2811	0.0833	0.0512	0.0010	250.5	48.6	251.5	44.8	249.4	10.6	250.5	48.6
G105	12	307	0.0401	0.0014	0.2866	0.0180	0.0514	0.0008	253.5	17.1	255.8	17.0	259.7	9.0	253.5	17.1
G14	40	1016	0.0403	0.0006	0.2907	0.0096	0.0517	0.0015	254.9	7.2	259.1	14.4	272.2	15.2	254.9	7.2
G82	59	1507	0.0404	0.0004	0.2872	0.0059	0.0512	0.0013	255.2	5.1	256.4	12.0	250.3	12.6	255.2	5.1
G49	40	797	0.0405	0.0005	0.2885	0.0051	0.0517	0.0007	256.1	5.9	257.4	8.4	270.4	8.4	256.1	5.9
G12	9	154	0.0414	0.0012	0.3263	0.0210	0.0573	0.0012	261.6	14.2	286.8	17.6	502.7	18.9	261.6	14.2
G15	38	920	0.0417	0.0035	0.2985	0.0627	0.0519	0.0008	263.6	43.2	265.2	39.7	282.8	9.2	263.6	43.2
G34	6	120	0.0423	0.0017	0.3016	0.0192	0.0510	0.0006	267.2	20.4	267.7	18.9	241.7	6.7	267.2	20.4
G5	17	418	0.0425	0.0006	0.3111	0.0097	0.0519	0.0013	268.0	7.9	275.0	13.5	279.7	13.6	268.0	7.9
G86	11	208	0.0436	0.0059	0.3278	0.2483	0.0543	0.0018	274.8	73.0	287.9	69.8	383.9	23.3	274.8	73.0
G74	5	94	0.0462	0.0062	0.3252	0.2533	0.0522	0.0018	291.0	76.3	285.9	70.1	295.1	19.3	291.0	76.3
G3	10	204	0.0470	0.0044	0.3462	0.1557	0.0525	0.0016	295.8	54.7	301.9	51.3	308.5	18.2	295.8	54.7
G97	24	525	0.0479	0.0043	0.3553	0.1367	0.0532	0.0016	301.6	52.4	308.7	49.4	335.2	18.4	301.6	52.4
G83	29	492	0.0566	0.0005	0.4671	0.0044	0.0590	0.0006	355.1	5.7	389.2	8.3	565.2	10.4	355.1	5.7
G68	17	211	0.0670	0.0005	0.4913	0.0064	0.0535	0.0010	418.2	6.2	405.8	13.3	350.1	12.6	418.2	6.2
G27	32	398	0.0703	0.0045	0.5370	0.1199	0.0545	0.0011	437.8	54.7	436.4	47.6	389.7	15.0	437.8	54.7

APPENDIX E (continued). U-Pb ZIRCON AGES OF SONG GIANH SEDIMENTS

Grain No.	Pb (ppm)	U (ppm)	Ratios						Ages (Ma)						Best Age (Ma)	± 2σ
			²⁰⁶ Pb/ ²³⁸ U	± 1 σ	²⁰⁷ Pb/ ²³⁵ U	± s.e.	²⁰⁷ Pb/ ²⁰⁶ Pb	± s.e.	²⁰⁶ Pb/ ²³⁸ U	± 2σ	²⁰⁷ Pb/ ²³⁵ U	± 2σ	²⁰⁷ Pb/ ²⁰⁶ Pb	± 2σ		
G76	16	198	0.0748	0.0006	0.5784	0.0097	0.0564	0.0014	464.9	7.7	463.4	19.1	467.0	19.8	464.9	7.7
G58	18	180	0.0772	0.0035	0.6374	0.0842	0.0583	0.0011	479.1	42.3	500.7	38.7	541.4	18.1	479.1	42.3
G79	8	91	0.0783	0.0055	0.6177	0.1570	0.0570	0.0015	485.7	65.3	488.4	57.4	489.6	21.5	485.7	65.3
G104	16	185	0.0803	0.0036	0.6975	0.0791	0.0634	0.0012	497.9	43.2	537.3	40.8	720.3	20.9	497.9	43.2
G88	119	1278	0.0884	0.0005	0.7024	0.0069	0.0575	0.0009	545.9	6.4	540.2	14.5	511.9	14.7	545.9	6.4
G21	10	71	0.0894	0.0018	0.7724	0.0269	0.0617	0.0008	552.0	21.7	581.2	21.1	663.0	14.0	552.0	21.7
G29	67	755	0.0929	0.0008	0.8364	0.0085	0.0659	0.0006	572.8	9.9	617.2	11.7	802.6	11.5	572.8	9.9
G67	23	215	0.1046	0.0062	0.8843	0.3330	0.0595	0.0021	641.2	71.9	643.3	64.2	584.3	32.8	641.2	71.9
G101	33	271	0.1153	0.0031	1.0220	0.0528	0.0642	0.0010	703.5	35.8	714.9	31.6	747.2	17.6	703.5	35.8
G52	18	128	0.1227	0.0057	1.0923	0.2318	0.0641	0.0017	745.9	65.0	749.6	55.9	745.6	29.1	745.9	65.0
G20	23	130	0.1325	0.0038	1.4056	0.0824	0.0758	0.0010	802.2	43.5	891.3	37.1	1089.0	18.5	802.2	43.5
G32	67	393	0.1401	0.0039	1.2923	0.0782	0.0664	0.0009	845.1	44.2	842.3	35.3	818.7	16.6	845.1	44.2
G11	92	584	0.1415	0.0058	1.3669	0.1760	0.0675	0.0012	853.1	65.4	874.8	51.8	852.9	22.9	853.1	65.4
G41	48	283	0.1434	0.0056	1.3803	0.1717	0.0681	0.0013	864.1	63.5	880.6	50.9	871.9	24.1	864.1	63.5
G61	30	167	0.1484	0.0060	1.4638	0.2251	0.0701	0.0016	892.2	66.8	915.6	55.2	929.8	29.6	892.2	66.8
G19	22	135	0.1513	0.0042	1.5206	0.0813	0.0709	0.0008	908.5	46.5	938.7	36.2	955.4	16.4	908.5	46.5
G9	104	625	0.1519	0.0024	1.4922	0.0488	0.0697	0.0010	911.3	27.0	927.2	25.2	918.1	18.2	911.3	27.0
G78	137	829	0.1567	0.0009	1.5100	0.0120	0.0705	0.0009	938.5	10.4	934.5	17.1	942.7	17.2	938.5	10.4
G89	51	258	0.1630	0.0035	1.6251	0.0779	0.0711	0.0011	973.3	39.2	980.0	33.6	959.4	21.5	973.3	39.2
G93	15	81	0.1631	0.0022	1.6419	0.0307	0.0712	0.0008	973.8	23.8	986.5	21.7	963.4	15.7	973.8	23.8
G43	105	528	0.1743	0.0017	1.7752	0.0212	0.0726	0.0006	1035.5	18.6	1036.4	16.9	1001.7	13.0	1035.5	18.6
G91	61	308	0.1822	0.0019	1.9018	0.0273	0.0755	0.0008	1079.0	21.0	1081.7	19.9	1080.8	15.8	1079.0	21.0
G2	116	441	0.1905	0.0032	2.0712	4.1212	0.0767	0.0088	1123.9	34.5	1139.3	158.0	1113.9	157.6	1113.9	157.6
G42	118	497	0.2066	0.0067	2.3049	0.3779	0.0802	0.0021	1210.7	71.2	1213.8	58.3	1202.2	38.1	1202.2	38.1
G4	114	420	0.2028	0.0022	2.3616	0.0298	0.0841	0.0006	1190.6	24.0	1231.1	18.8	1293.9	12.3	1293.9	12.3
G23	56	225	0.2252	0.0021	2.8645	0.0495	0.0916	0.0011	1309.3	22.0	1372.6	22.4	1458.1	19.8	1458.1	19.8
G99	186	601	0.2647	0.0006	3.4640	0.0062	0.0944	0.0007	1513.7	5.8	1519.1	12.1	1516.9	13.4	1516.9	13.4
G103	130	338	0.2827	0.0014	3.8520	0.0180	0.0986	0.0008	1604.8	13.9	1603.7	15.4	1597.6	15.0	1597.6	15.0
G45	43	127	0.2827	0.0020	3.9583	0.0257	0.0991	0.0006	1604.8	20.5	1625.7	15.4	1607.8	11.8	1607.8	11.8
G53	123	492	0.2477	0.0054	3.4873	0.1855	0.1001	0.0014	1426.6	55.4	1524.3	40.7	1626.5	24.7	1626.5	24.7

APPENDIX E (continued). U-Pb ZIRCON AGES OF SONG GIANH SEDIMENTS

Grain No.	Pb (ppm)	U (ppm)	Ratios						Ages (Ma)						Best Age (Ma)	± 2σ
			²⁰⁶ Pb/ ²³⁸ U	± 1 σ	²⁰⁷ Pb/ ²³⁵ U	± s.e.	²⁰⁷ Pb/ ²⁰⁶ Pb	± s.e.	²⁰⁶ Pb/ ²³⁸ U	± 2σ	²⁰⁷ Pb/ ²³⁵ U	± 2σ	²⁰⁷ Pb/ ²⁰⁶ Pb	± 2σ		
G56	31	76	0.2896	0.0040	4.0854	0.0812	0.1009	0.0010	1639.5	39.9	1651.4	27.3	1639.8	17.4	1639.8	17.4
G13	121	359	0.2969	0.0017	4.2707	0.0210	0.1027	0.0006	1676.1	16.7	1687.7	13.6	1673.1	11.6	1673.1	11.6
G100	45	116	0.3034	0.0060	4.3246	0.2021	0.1043	0.0018	1708.0	59.7	1698.1	43.7	1701.8	30.5	1701.8	30.5
G38	9	24	0.3055	0.0043	4.4554	0.1390	0.1054	0.0015	1718.6	42.0	1722.7	33.1	1721.1	25.5	1721.1	25.5
G55	6	15	0.3079	0.0029	4.4180	0.0492	0.1055	0.0008	1730.3	28.5	1715.7	20.2	1723.4	14.6	1723.4	14.6
G70	20	58	0.3058	0.0008	4.4025	0.0096	0.1064	0.0008	1720.0	8.1	1712.8	13.3	1738.5	14.2	1738.5	14.2
G109	14	34	0.3203	0.0005	4.8563	0.0060	0.1098	0.0009	1791.3	4.9	1794.7	13.7	1795.8	15.2	1795.8	15.2
G33	97	227	0.3345	0.0022	5.2215	0.0340	0.1120	0.0007	1860.3	21.3	1856.1	15.9	1831.6	12.9	1831.6	12.9
G96	206	556	0.3210	0.0061	4.9731	0.2441	0.1122	0.0018	1794.4	59.3	1814.8	41.8	1835.4	28.7	1835.4	28.7
G36	13	29	0.3304	0.0005	5.1016	0.0089	0.1123	0.0021	1840.5	4.4	1836.4	32.4	1837.3	34.1	1837.3	34.1
G87	100	326	0.3001	0.0056	4.7407	0.1852	0.1124	0.0016	1691.6	55.7	1774.5	39.3	1838.6	25.9	1838.6	25.9
G75	138	448	0.2926	0.0066	4.5508	0.2483	0.1125	0.0017	1654.7	66.2	1740.3	45.3	1840.2	27.3	1840.2	27.3
G18	94	211	0.3218	0.0039	5.0152	0.0823	0.1127	0.0009	1798.4	38.0	1821.9	24.5	1843.1	15.2	1843.1	15.2
G108	33	87	0.3321	0.0010	5.1842	0.0131	0.1128	0.0009	1848.5	9.5	1850.0	14.3	1844.2	15.2	1844.2	15.2
G8	217	677	0.3147	0.0041	4.9501	0.0792	0.1133	0.0008	1764.0	39.9	1810.8	25.0	1853.5	14.1	1853.5	14.1
G64	71	179	0.3334	0.0050	5.2686	0.1417	0.1135	0.0014	1854.8	48.3	1863.8	32.7	1856.8	22.2	1856.8	22.2
G48	115	308	0.3364	0.0005	5.4176	0.0080	0.1138	0.0011	1869.3	4.9	1887.6	16.8	1861.4	18.4	1861.4	18.4
G102	115	322	0.3317	0.0036	5.2863	0.0791	0.1140	0.0012	1846.8	35.0	1866.6	25.6	1864.3	19.4	1864.3	19.4
G35	166	335	0.3455	0.0007	5.5649	0.0111	0.1145	0.0017	1912.9	6.2	1910.7	25.4	1872.3	26.8	1872.3	26.8
G54	96	262	0.3407	0.0015	5.3962	0.0202	0.1147	0.0008	1889.9	14.3	1884.2	14.1	1875.6	13.7	1875.6	13.7
G17	157	437	0.3539	0.0005	5.7042	0.0045	0.1149	0.0005	1953.1	4.7	1932.0	8.2	1878.2	9.5	1878.2	9.5
G1	19	48	0.3369	0.0033	5.2922	3.6232	0.1149	0.0087	1871.8	31.4	1867.6	130.7	1878.5	131.5	1878.5	131.5
G7	145	411	0.3473	0.0005	5.6465	0.0062	0.1151	0.0008	1921.5	5.1	1923.2	12.5	1881.1	13.9	1881.1	13.9
G31	108	307	0.3338	0.0011	5.4111	0.0117	0.1151	0.0006	1856.5	10.5	1886.6	9.9	1881.3	9.9	1881.3	9.9
G16	131	349	0.3309	0.0005	5.4303	0.0046	0.1151	0.0006	1842.5	4.7	1889.7	8.9	1881.9	10.4	1881.9	10.4
G62	164	466	0.3349	0.0042	5.6156	0.1025	0.1189	0.0012	1862.3	40.7	1918.5	27.2	1940.1	18.5	1940.1	18.5
G60	68	126	0.3543	0.0010	5.8330	0.0143	0.1203	0.0010	1954.9	9.3	1951.3	15.2	1961.3	16.2	1961.3	16.2
G44	385	957	0.3252	0.0024	5.9702	0.0339	0.1315	0.0007	1815.3	23.5	1971.5	15.7	2117.4	10.9	2117.4	10.9
G95	63	158	0.3546	0.0021	6.9770	0.0394	0.1394	0.0012	1956.6	19.6	2108.5	17.9	2220.0	16.6	2220.0	16.6
G46	142	333	0.3977	0.0038	8.2402	0.0812	0.1463	0.0010	2158.5	34.9	2257.8	21.1	2303.0	14.2	2303.0	14.2

APPENDIX E (continued). U-Pb ZIRCON AGES OF SONG GIANH SEDIMENTS

Grain No.	Pb (ppm)	U (ppm)	Ratios						Ages (Ma)						Best Age (Ma)	± 2σ
			²⁰⁶ Pb/ ²³⁸ U	± 1 σ	²⁰⁷ Pb/ ²³⁵ U	± s.e.	²⁰⁷ Pb/ ²⁰⁶ Pb	± s.e.	²⁰⁶ Pb/ ²³⁸ U	± 2σ	²⁰⁷ Pb/ ²³⁵ U	± 2σ	²⁰⁷ Pb/ ²⁰⁶ Pb	± 2σ		
G51	51	83	0.4455	0.0005	9.2787	0.0044	0.1487	0.0006	2375.2	4.3	2365.9	7.1	2331.3	8.5	2331.3	8.5
G6	70	119	0.4388	0.0024	9.1038	0.0381	0.1502	0.0008	2345.4	21.7	2348.5	13.7	2348.2	11.0	2348.2	11.0
G25	103	236	0.3873	0.0027	8.2190	0.0434	0.1508	0.0008	2110.2	24.7	2255.4	15.5	2354.5	11.1	2354.5	11.1
G37	397	913	0.4313	0.0040	9.2576	0.0810	0.1541	0.0009	2311.4	36.4	2363.8	20.2	2391.5	12.4	2391.5	12.4
G22	16	30	0.4337	0.0012	9.1829	0.0183	0.1563	0.0011	2322.5	10.4	2356.4	13.8	2415.9	14.7	2415.9	14.7
G63	209	405	0.4270	0.0019	9.3800	0.0323	0.1593	0.0010	2292.3	16.7	2375.9	14.4	2447.9	13.8	2447.9	13.8
G77	159	290	0.4668	0.0034	10.2672	0.0703	0.1602	0.0011	2469.6	30.1	2459.2	18.2	2457.2	13.9	2457.2	13.9
G50	36	68	0.4605	0.0040	10.0902	0.0844	0.1608	0.0010	2441.8	34.9	2443.1	19.4	2463.6	12.9	2463.6	12.9
G85	94	163	0.4749	0.0007	10.5824	0.0085	0.1638	0.0008	2505.1	6.0	2487.2	9.6	2495.5	10.9	2495.5	10.9
G39	110	183	0.4795	0.0050	11.1188	0.1257	0.1656	0.0011	2525.1	43.7	2533.1	23.3	2513.9	14.5	2513.9	14.5
G69	39	62	0.4780	0.0013	10.9160	0.0159	0.1659	0.0008	2518.7	11.0	2516.0	9.7	2516.8	10.1	2516.8	10.1
G94	74	115	0.5067	0.0005	11.9661	0.0085	0.1660	0.0014	2642.5	4.4	2601.8	15.7	2517.9	17.2	2517.9	17.2
G30	80	119	0.4987	0.0005	11.3395	0.0051	0.1673	0.0007	2608.1	4.1	2551.5	8.2	2530.5	9.8	2530.5	9.8
G65	22	34	0.4812	0.0010	11.3997	0.0168	0.1702	0.0009	2532.3	8.8	2556.4	10.7	2560.0	11.7	2560.0	11.7
G57	6	9	0.4795	0.0043	10.7268	0.1580	0.1719	0.0019	2525.2	37.5	2499.7	26.9	2575.9	22.8	2575.9	22.8
G10	257	465	0.4932	0.0037	12.0799	0.0710	0.1746	0.0008	2584.6	31.9	2610.6	16.7	2602.5	10.7	2602.5	10.7
G107	222	378	0.5072	0.0033	12.3334	0.0625	0.1776	0.0011	2644.5	28.5	2630.1	16.6	2630.2	12.8	2630.2	12.8
G59	85	146	0.5015	0.0071	12.5985	0.4785	0.1794	0.0029	2620.4	60.9	2650.1	40.7	2647.1	32.6	2647.1	32.6
G72	34	56	0.5151	0.0037	12.5969	0.0936	0.1819	0.0013	2678.5	31.8	2650.0	18.8	2669.9	14.7	2669.9	14.7
G84	69	123	0.4951	0.0005	12.8926	0.0045	0.1825	0.0006	2592.8	4.1	2671.8	6.1	2675.8	7.6	2675.8	7.6
G98	357	646	0.5166	0.0038	13.1953	0.0774	0.1851	0.0011	2684.7	32.0	2693.7	17.9	2699.1	13.3	2699.1	13.3
G73	132	202	0.5644	0.0003	14.7021	0.0041	0.1857	0.0012	2884.7	2.5	2796.2	12.4	2704.2	14.0	2704.2	14.0
G40	52	77	0.5429	0.0040	16.2770	0.1313	0.2199	0.0016	2795.6	33.6	2893.2	19.8	2979.8	15.6	2979.8	15.6
12061804 Terrace Song Trac																
G8	7.5	295.6	0.0230	0.0004	0.1523	0.0082	0.0505	0.0026	146.8	4.7	143.9	15.2	219.9	21.2	146.8	4.66
G82	10.2	378.6	0.0249	0.0003	0.1703	0.0055	0.0510	0.0015	158.5	4.3	159.7	10.0	239.0	13.6	158.5	4.28
G55	1.8	55.9	0.0300	0.0007	0.1949	0.0199	0.0480	0.0047	190.4	8.6	180.8	33.5	98.8	19.0	190.4	8.64
G66	57.0	1812.7	0.0307	0.0004	0.2159	0.0042	0.0505	0.0009	194.9	4.8	198.5	7.7	219.4	7.7	194.9	4.75
G18	2.4	72.7	0.0311	0.0005	0.2079	0.0136	0.0486	0.0030	197.6	6.8	191.8	22.5	128.1	15.6	197.6	6.75

APPENDIX E (continued). U-Pb ZIRCON AGES OF SONG GIANH SEDIMENTS

Grain No.	Pb (ppm)	U (ppm)	Ratios						Ages (Ma)						Best Age (Ma)	± 2σ
			²⁰⁶ Pb/ ²³⁸ U	± 1 σ	²⁰⁷ Pb/ ²³⁵ U	± s.e.	²⁰⁷ Pb/ ²⁰⁶ Pb	± s.e.	²⁰⁶ Pb/ ²³⁸ U	± 2σ	²⁰⁷ Pb/ ²³⁵ U	± 2σ	²⁰⁷ Pb/ ²⁰⁶ Pb	± 2σ		
G87	28.8	970.7	0.0313	0.0004	0.2430	0.0065	0.0556	0.0014	198.6	5.1	220.9	10.9	436.0	18.1	198.6	5.13
G92	6.5	151.1	0.0346	0.0005	0.2489	0.0105	0.0517	0.0020	219.5	6.2	225.7	16.7	269.9	19.3	219.5	6.23
G118	21.3	573.5	0.0360	0.0005	0.2618	0.0088	0.0526	0.0016	228.2	6.1	236.1	14.1	309.8	17.1	228.2	6.10
G97	16.6	347.8	0.0373	0.0005	0.2578	0.0075	0.0517	0.0014	235.8	6.1	232.9	12.6	271.3	13.4	235.8	6.09
G38	12.3	255.5	0.0389	0.0006	0.2801	0.0115	0.0526	0.0020	246.3	6.9	250.7	17.9	312.0	20.8	246.3	6.95
G133	13.4	356.2	0.0392	0.0005	0.2792	0.0088	0.0523	0.0015	247.6	6.6	250.0	14.2	298.1	15.6	247.6	6.58
G119	14.4	364.6	0.0395	0.0005	0.2858	0.0084	0.0538	0.0014	249.5	6.4	255.2	13.7	362.7	17.1	249.5	6.45
G31	75.2	1823.0	0.0401	0.0005	0.2864	0.0049	0.0517	0.0008	253.7	6.1	255.8	8.8	270.4	8.0	253.7	6.07
G113	28.8	691.0	0.0409	0.0005	0.3228	0.0085	0.0571	0.0013	258.3	6.6	284.0	13.3	494.2	19.1	258.3	6.56
G105	15.5	363.7	0.0410	0.0005	0.2786	0.0080	0.0511	0.0013	258.8	6.7	249.6	13.3	246.7	12.1	258.8	6.69
G46	10.0	194.9	0.0426	0.0006	0.2904	0.0106	0.0508	0.0017	268.8	7.3	258.9	16.7	233.6	14.5	268.8	7.30
G41	23.3	500.7	0.0433	0.0006	0.2824	0.0069	0.0474	0.0011	273.5	6.8	252.5	11.4	66.9	3.6	273.5	6.80
G102	16.5	366.5	0.0433	0.0006	0.3292	0.0090	0.0565	0.0014	273.5	6.9	289.0	14.2	470.9	19.1	273.5	6.92
G88	17.2	377.6	0.0455	0.0006	0.3223	0.0090	0.0526	0.0013	286.5	7.3	283.6	14.1	310.3	14.1	286.5	7.28
G69	14.7	326.4	0.0458	0.0006	0.3366	0.0095	0.0536	0.0014	288.7	7.4	294.6	14.6	354.3	15.8	288.7	7.40
G36	18.2	394.4	0.0461	0.0006	0.3388	0.0086	0.0533	0.0012	290.8	7.3	296.3	13.4	341.6	13.9	290.8	7.27
G29	27.1	579.1	0.0497	0.0006	0.3678	0.0084	0.0544	0.0011	312.8	7.6	318.1	13.2	386.0	13.8	312.8	7.61
G126	8.3	168.8	0.0505	0.0008	0.3898	0.0205	0.0552	0.0026	317.3	9.9	334.3	27.8	419.9	32.9	317.3	9.94
G47	16.7	281.6	0.0537	0.0007	0.3865	0.0110	0.0534	0.0013	337.0	8.6	331.8	16.3	344.6	15.4	337.0	8.57
G130	3.8	69.9	0.0537	0.0011	0.3917	0.0326	0.0541	0.0040	337.1	13.5	335.6	44.6	374.4	47.1	337.1	13.46
G138	12.4	208.9	0.0552	0.0008	0.4175	0.0174	0.0560	0.0021	346.6	9.8	354.3	24.0	453.6	27.6	346.6	9.77
G77	9.8	149.2	0.0584	0.0008	0.4208	0.0143	0.0541	0.0016	365.7	9.6	356.6	20.2	373.5	19.5	365.7	9.62
G49	112.3	1957.2	0.0602	0.0007	0.4946	0.0093	0.0598	0.0010	376.7	9.0	408.1	13.7	596.0	15.4	376.7	9.00
G75	13.4	204.2	0.0658	0.0009	0.5384	0.0169	0.0565	0.0015	410.9	10.5	437.4	20.5	470.9	20.9	410.9	10.52
G115	48.9	749.7	0.0670	0.0009	0.5177	0.0126	0.0564	0.0012	418.1	10.3	423.6	17.0	468.1	16.4	418.1	10.27
G101	26.8	365.5	0.0677	0.0009	0.5574	0.0134	0.0604	0.0013	422.0	10.4	449.8	17.8	619.4	19.9	422.0	10.39
G7	81.0	1244.8	0.0687	0.0008	0.5097	0.0088	0.0542	0.0008	428.3	10.0	418.3	13.2	381.0	10.2	428.3	10.01
G98	13.1	178.1	0.0687	0.0010	0.5664	0.0201	0.0600	0.0018	428.6	11.5	455.7	24.4	604.7	28.2	428.6	11.46
G107	22.1	306.8	0.0691	0.0009	0.5338	0.0141	0.0573	0.0013	430.6	10.7	434.3	18.6	501.9	18.6	430.6	10.73

APPENDIX E (continued). U-Pb ZIRCON AGES OF SONG GIANH SEDIMENTS

Grain No.	Pb (ppm)	U (ppm)	Ratios						Ages (Ma)						Best Age (Ma)	$\pm 2\sigma$
			$^{206}\text{Pb}/^{238}\text{U}$	$\pm 1\sigma$	$^{207}\text{Pb}/^{235}\text{U}$	$\pm \text{s.e.}$	$^{207}\text{Pb}/^{206}\text{Pb}$	$\pm \text{s.e.}$	$^{206}\text{Pb}/^{238}\text{U}$	$\pm 2\sigma$	$^{207}\text{Pb}/^{235}\text{U}$	$\pm 2\sigma$	$^{207}\text{Pb}/^{206}\text{Pb}$	$\pm 2\sigma$		
G20	16.5	237.8	0.0692	0.0009	0.5146	0.0143	0.0535	0.0013	431.1	10.7	421.5	18.5	347.9	14.7	431.1	10.73
G111	11.3	163.2	0.0699	0.0009	0.6472	0.0203	0.0709	0.0019	435.6	11.3	506.8	24.4	955.7	33.4	435.6	11.33
G34	35.2	488.6	0.0715	0.0009	0.5523	0.0116	0.0558	0.0010	445.2	10.6	446.5	15.8	445.6	13.8	445.2	10.59
G58	7.6	99.8	0.0715	0.0010	0.5575	0.0236	0.0572	0.0021	445.3	12.4	449.9	28.4	498.5	29.1	445.3	12.39
G2	67.8	884.0	0.0716	0.0009	0.5403	0.0101	0.0546	0.0009	445.7	10.5	438.6	14.4	395.1	11.3	445.7	10.47
G67	35.9	452.2	0.0726	0.0009	0.5337	0.0129	0.0544	0.0011	451.5	10.9	434.2	17.4	389.3	14.2	451.5	10.94
G114	41.5	548.3	0.0748	0.0010	0.6020	0.0157	0.0584	0.0013	465.1	11.5	478.5	19.5	542.9	19.3	465.1	11.52
G125	27.7	309.6	0.0748	0.0010	0.6080	0.0191	0.0596	0.0016	465.2	12.0	482.3	23.0	588.4	24.4	465.2	12.00
G62	83.5	1124.6	0.0777	0.0010	0.7330	0.0142	0.0677	0.0011	482.1	11.5	558.3	17.5	858.2	19.7	482.1	11.49
G95	159.4	1979.6	0.0809	0.0010	0.6426	0.0110	0.0577	0.0009	501.7	11.8	503.9	15.2	517.2	12.7	501.7	11.81
G90	10.9	104.4	0.0868	0.0013	0.7997	0.0331	0.0673	0.0022	536.5	14.8	596.7	32.9	846.1	39.0	536.5	14.83
G43	36.5	176.2	0.0896	0.0012	0.7078	0.0202	0.0586	0.0014	552.9	13.6	543.5	22.9	552.3	20.8	552.9	13.61
G74	11.3	103.5	0.0906	0.0012	0.7233	0.0258	0.0601	0.0018	559.1	14.7	552.6	28.0	606.1	27.3	559.1	14.66
G16	11.4	97.9	0.0907	0.0013	0.7638	0.0344	0.0600	0.0022	559.9	15.6	576.2	34.1	604.7	33.8	559.9	15.60
G10	12.8	93.2	0.1003	0.0014	0.8081	0.0315	0.0592	0.0018	615.9	16.2	601.4	31.1	572.6	28.0	615.9	16.17
G48	19.8	188.4	0.1059	0.0014	0.8947	0.0239	0.0611	0.0013	649.0	15.7	648.9	23.9	642.8	21.2	649.0	15.74
G136	63.1	586.5	0.1066	0.0014	1.0166	0.0280	0.0683	0.0015	653.0	16.2	712.2	26.1	876.2	26.7	653.0	16.19
G85	38.7	354.3	0.1093	0.0014	0.9865	0.0212	0.0659	0.0012	668.8	15.8	696.9	21.7	801.9	20.1	668.8	15.81
G78	25.6	213.5	0.1140	0.0015	1.0161	0.0301	0.0654	0.0015	695.6	17.2	712.0	27.4	786.3	26.2	695.6	17.25
G72	36.7	315.2	0.1187	0.0015	0.9706	0.0220	0.0616	0.0011	723.2	17.1	688.8	22.6	660.3	18.5	723.2	17.06
G56	13.4	105.4	0.1208	0.0017	1.0511	0.0442	0.0655	0.0021	735.1	19.8	729.4	37.2	791.7	36.0	735.1	19.79
G128	10.8	68.1	0.1259	0.0018	1.1023	0.0443	0.0657	0.0020	764.4	20.4	754.5	36.6	797.2	34.7	764.4	20.38
G68	32.6	253.6	0.1264	0.0016	1.1181	0.0307	0.0656	0.0014	767.3	18.5	762.1	26.8	793.6	24.1	767.3	18.54
G99	66.8	456.0	0.1315	0.0016	1.2081	0.0256	0.0670	0.0011	796.2	18.6	804.3	23.5	836.2	20.1	796.2	18.57
G64	60.3	412.1	0.1324	0.0016	1.2094	0.0251	0.0677	0.0011	801.3	18.6	804.9	23.1	858.5	19.9	801.3	18.56
G129	71.6	537.1	0.1338	0.0017	1.3990	0.0316	0.0761	0.0014	809.5	19.2	888.5	26.1	1098.0	24.9	809.5	19.22
G76	44.3	315.2	0.1375	0.0017	1.2650	0.0271	0.0686	0.0012	830.3	19.3	830.1	24.0	887.3	20.7	830.3	19.27
G93	27.6	173.4	0.1408	0.0018	1.3147	0.0335	0.0679	0.0013	849.1	20.2	852.2	27.0	865.8	23.5	849.1	20.23
G108	92.7	687.2	0.1430	0.0018	1.3783	0.0264	0.0706	0.0011	861.4	19.9	879.7	23.6	944.4	20.1	861.4	19.85
G52	108.2	750.6	0.1438	0.0017	1.3418	0.0232	0.0668	0.0010	866.3	19.6	864.0	21.6	831.9	16.9	866.3	19.61

APPENDIX E (continued). U-Pb ZIRCON AGES OF SONG GIANH SEDIMENTS

Grain No.	Pb (ppm)	U (ppm)	Ratios						Ages (Ma)						Best Age (Ma)	± 2σ
			²⁰⁶ Pb/ ²³⁸ U	± 1 σ	²⁰⁷ Pb/ ²³⁵ U	± s.e.	²⁰⁷ Pb/ ²⁰⁶ Pb	± s.e.	²⁰⁶ Pb/ ²³⁸ U	± 2σ	²⁰⁷ Pb/ ²³⁵ U	± 2σ	²⁰⁷ Pb/ ²⁰⁶ Pb	± 2σ		
G51	65.4	413.1	0.1540	0.0019	1.4520	0.0284	0.0687	0.0011	923.4	21.0	910.7	23.7	889.4	19.0	889.4	19.02
G89	30.9	167.8	0.1647	0.0022	1.5332	0.0478	0.0690	0.0016	983.0	23.8	943.8	32.5	899.6	27.9	899.6	27.88
G32	125.8	873.7	0.1504	0.0018	1.4793	0.0242	0.0699	0.0009	903.2	20.3	921.9	21.7	924.8	17.1	924.8	17.06
G59	19.2	115.6	0.1549	0.0020	1.4733	0.0479	0.0700	0.0017	928.4	22.8	919.5	32.9	927.8	29.4	927.8	29.41
G12	37.7	217.3	0.1634	0.0020	1.5835	0.0361	0.0702	0.0012	975.8	22.3	963.7	26.1	932.7	21.4	932.7	21.43
G30	106.9	663.9	0.1595	0.0019	1.5334	0.0264	0.0702	0.0010	954.1	21.3	943.9	22.6	932.7	17.6	932.7	17.61
G70	40.3	243.4	0.1560	0.0019	1.4719	0.0326	0.0706	0.0012	934.3	21.6	918.9	25.9	947.0	21.8	947.0	21.83
G5	55.8	317.0	0.1667	0.0020	1.6610	0.0344	0.0716	0.0011	994.1	22.4	993.7	25.0	973.7	20.3	973.7	20.33
G112	77.8	400.0	0.1707	0.0021	1.6721	0.0355	0.0722	0.0012	1015.9	23.3	998.0	26.7	991.6	21.9	991.6	21.95
G103	57.7	332.0	0.1652	0.0021	1.6141	0.0348	0.0723	0.0012	985.5	22.7	975.7	26.5	993.0	22.1	993.0	22.13
G23	46.6	274.1	0.1705	0.0021	1.6681	0.0348	0.0724	0.0011	1014.6	22.9	996.5	25.5	996.6	20.7	996.6	20.73
G140	68.0	428.9	0.1578	0.0022	1.5747	0.0574	0.0741	0.0020	944.5	24.1	960.3	37.3	1043.6	35.2	1043.6	35.24
G27	81.3	428.0	0.1853	0.0022	1.8497	0.0341	0.0742	0.0011	1095.8	24.4	1063.3	24.9	1046.9	19.4	1046.9	19.40
G132	157.1	806.6	0.1738	0.0022	1.8451	0.0360	0.0757	0.0012	1033.0	23.6	1061.7	26.5	1087.9	22.1	1087.9	22.07
G25	76.5	416.8	0.1734	0.0021	1.8130	0.0337	0.0760	0.0011	1030.5	23.1	1050.2	24.6	1095.3	20.0	1095.3	19.95
G110	77.1	398.2	0.1851	0.0023	1.9613	0.0418	0.0776	0.0013	1094.9	25.0	1102.3	27.9	1135.9	23.3	1135.9	23.29
G35	101.1	576.3	0.1811	0.0022	1.9159	0.0330	0.0781	0.0011	1072.8	23.8	1086.6	24.5	1149.7	19.6	1149.7	19.58
G1	248.1	1215.9	0.1926	0.0023	2.1147	0.0318	0.0791	0.0010	1135.6	24.8	1153.6	23.6	1174.6	17.2	1174.6	17.25
G65	107.4	486.7	0.2108	0.0026	2.2616	0.0436	0.0794	0.0012	1233.2	27.4	1200.4	27.1	1183.1	21.3	1183.1	21.31
G100	112.7	507.3	0.2119	0.0026	2.4473	0.0463	0.0833	0.0013	1239.0	27.7	1256.6	27.9	1276.3	22.5	1276.3	22.53
G11	57.5	209.8	0.2390	0.0029	2.9128	0.0651	0.0857	0.0013	1381.4	30.4	1385.2	29.4	1330.5	23.4	1330.5	23.41
G28	152.2	672.3	0.2283	0.0027	2.7040	0.0443	0.0865	0.0011	1325.6	28.8	1329.6	26.2	1348.7	20.1	1348.7	20.07
G127	170.7	714.3	0.2339	0.0029	2.8092	0.0556	0.0879	0.0014	1354.6	30.3	1358.0	30.0	1380.3	24.4	1380.3	24.43
G83	145.1	487.7	0.2630	0.0032	3.5513	0.0642	0.0979	0.0014	1505.0	32.7	1538.7	29.4	1584.3	23.2	1584.3	23.18
G139	140.9	511.0	0.2667	0.0033	3.5364	0.0738	0.0991	0.0016	1523.9	33.8	1535.4	32.6	1606.3	27.0	1606.3	26.95
G44	6.1	18.6	0.3014	0.0051	4.1108	0.3013	0.0999	0.0037	1698.2	50.2	1656.4	66.9	1622.0	61.1	1622.0	61.05
G24	114.6	362.7	0.2955	0.0036	4.0650	0.0736	0.1022	0.0014	1669.0	35.4	1647.3	29.3	1663.9	22.4	1663.9	22.35
G71	10.5	31.7	0.3014	0.0043	4.3010	0.2046	0.1038	0.0026	1698.3	42.3	1693.5	47.7	1693.5	42.3	1693.5	42.31
G33	50.9	158.5	0.2984	0.0037	4.2163	0.0961	0.1046	0.0016	1683.2	36.3	1677.2	31.7	1707.6	25.2	1707.6	25.22
G21	43.3	123.1	0.3310	0.0041	4.9716	0.1334	0.1094	0.0017	1843.0	39.9	1814.5	33.9	1788.8	27.2	1788.8	27.19

APPENDIX E (continued). U-Pb ZIRCON AGES OF SONG GIANH SEDIMENTS

Grain No.	Pb (ppm)	U (ppm)	Ratios						Ages (Ma)						Best Age (Ma)	± 2σ
			²⁰⁶ Pb/ ²³⁸ U	± 1 σ	²⁰⁷ Pb/ ²³⁵ U	± s.e.	²⁰⁷ Pb/ ²⁰⁶ Pb	± s.e.	²⁰⁶ Pb/ ²³⁸ U	± 2σ	²⁰⁷ Pb/ ²³⁵ U	± 2σ	²⁰⁷ Pb/ ²⁰⁶ Pb	± 2σ		
G39	30.7	97.0	0.2919	0.0038	4.3153	0.1462	0.1102	0.0021	1651.1	37.9	1696.3	38.4	1802.5	33.0	1802.5	33.03
G4	139.2	401.9	0.3190	0.0038	4.8413	0.0825	0.1105	0.0014	1785.0	37.2	1792.1	29.2	1807.8	22.0	1807.8	21.97
G13	262.3	853.2	0.3128	0.0037	4.7722	0.0789	0.1106	0.0014	1754.4	36.7	1780.0	29.0	1808.5	21.8	1808.5	21.81
G3	34.8	94.2	0.3414	0.0043	5.1182	0.1613	0.1123	0.0019	1893.4	41.6	1839.1	36.6	1837.0	30.1	1837.0	30.07
G79	134.5	478.4	0.2915	0.0036	4.4978	0.0838	0.1124	0.0016	1649.1	35.4	1730.6	30.8	1838.1	24.5	1838.1	24.46
G131	85.6	271.3	0.3088	0.0039	4.7459	0.1263	0.1125	0.0020	1734.6	38.7	1775.4	36.5	1840.5	30.6	1840.5	30.63
G109	205.1	650.9	0.3182	0.0039	4.9401	0.0979	0.1130	0.0017	1781.0	38.3	1809.1	32.6	1847.6	26.0	1847.6	26.04
G57	237.2	586.5	0.3250	0.0039	5.0405	0.0865	0.1130	0.0015	1814.2	38.1	1826.1	30.2	1848.7	23.0	1848.7	23.02
G63	70.9	214.5	0.3222	0.0040	4.8550	0.1081	0.1130	0.0017	1800.2	38.7	1794.5	32.6	1848.7	25.9	1848.7	25.88
G80	100.7	309.6	0.3228	0.0039	4.9381	0.0954	0.1131	0.0016	1803.3	38.4	1808.8	31.7	1850.1	24.8	1850.1	24.81
G19	209.5	759.0	0.2871	0.0035	4.5825	0.0855	0.1136	0.0015	1627.2	34.7	1746.1	29.7	1857.0	23.2	1857.0	23.25
G94	120.3	388.8	0.3047	0.0037	4.7234	0.0891	0.1141	0.0016	1714.7	36.9	1771.4	31.6	1865.2	25.1	1865.2	25.13
G96	119.4	392.6	0.3088	0.0038	4.9000	0.1017	0.1152	0.0017	1734.7	37.5	1802.3	32.6	1882.2	26.2	1882.2	26.16
G84	66.6	205.1	0.3257	0.0040	5.1437	0.1095	0.1154	0.0017	1817.7	39.0	1843.3	32.7	1886.8	26.0	1886.8	25.97
G45	52.4	160.4	0.2946	0.0037	4.6940	0.1386	0.1165	0.0020	1664.3	37.2	1766.2	35.8	1902.7	30.2	1902.7	30.25
G26	167.6	515.7	0.3273	0.0039	5.3035	0.0893	0.1168	0.0015	1825.4	38.1	1869.4	29.7	1908.0	22.4	1908.0	22.38
G120	31.9	89.5	0.3410	0.0044	5.3732	0.1565	0.1184	0.0021	1891.3	42.0	1880.6	37.8	1932.1	31.5	1932.1	31.53
G104	172.2	484.9	0.3495	0.0043	5.7394	0.1067	0.1215	0.0018	1932.4	40.9	1937.3	32.8	1977.9	25.8	1977.9	25.82
G61	103.4	270.4	0.3539	0.0044	6.1952	0.1499	0.1224	0.0018	1953.2	41.7	2003.8	33.7	1991.1	26.7	1991.1	26.68
G40	16.8	44.8	0.3613	0.0049	6.1926	0.2590	0.1239	0.0025	1988.5	46.0	2003.4	42.7	2013.7	36.5	2013.7	36.48
G91	22.7	59.7	0.3466	0.0047	5.8724	0.2303	0.1252	0.0026	1918.2	44.6	1957.2	42.5	2030.9	36.5	2030.9	36.51
G15	106.4	330.1	0.3279	0.0039	5.7442	0.1049	0.1287	0.0017	1828.2	38.3	1938.1	30.5	2079.6	23.4	2079.6	23.42
G122	85.0	197.7	0.3959	0.0049	7.3109	0.1679	0.1392	0.0022	2150.1	45.6	2150.1	35.9	2217.0	29.0	2217.0	28.96
G42	220.4	427.1	0.4369	0.0053	9.1600	0.1798	0.1537	0.0020	2336.6	47.5	2354.1	32.6	2387.1	24.6	2387.1	24.64
G17	111.4	230.3	0.4688	0.0057	10.1262	0.2113	0.1588	0.0021	2478.3	49.8	2446.4	32.7	2442.5	24.6	2442.5	24.59
G50	19.4	36.4	0.4432	0.0058	9.6200	0.3714	0.1602	0.0028	2364.9	52.1	2399.1	40.4	2457.6	33.2	2457.6	33.19
G137	57.6	107.2	0.4590	0.0058	10.0419	0.2797	0.1602	0.0027	2434.9	51.6	2438.6	39.0	2458.2	31.9	2458.2	31.91
G60	99.3	189.3	0.4736	0.0059	10.3123	0.2917	0.1605	0.0024	2499.3	51.9	2463.2	36.2	2461.3	28.4	2461.3	28.40
G121	386.8	898.0	0.4202	0.0052	9.3923	0.1831	0.1621	0.0024	2261.5	47.0	2377.1	35.4	2477.9	28.2	2477.9	28.18
G124	189.0	347.8	0.4698	0.0059	10.3368	0.2362	0.1622	0.0025	2482.6	51.3	2465.4	36.7	2478.4	29.3	2478.4	29.31

APPENDIX E (continued). U-Pb ZIRCON AGES OF SONG GIANH SEDIMENTS

Grain No.	Pb (ppm)	U (ppm)	Ratios						Ages (Ma)						Best Age (Ma)	± 2σ
			²⁰⁶ Pb/ ²³⁸ U	± 1 σ	²⁰⁷ Pb/ ²³⁵ U	± s.e.	²⁰⁷ Pb/ ²⁰⁶ Pb	± s.e.	²⁰⁶ Pb/ ²³⁸ U	± 2σ	²⁰⁷ Pb/ ²³⁵ U	± 2σ	²⁰⁷ Pb/ ²⁰⁶ Pb	± 2σ		
G86	106.8	209.8	0.4409	0.0055	9.3673	0.2288	0.1627	0.0024	2354.5	49.0	2374.6	35.6	2483.8	28.1	2483.8	28.09
G117	26.3	43.8	0.4553	0.0060	9.9346	0.3703	0.1635	0.0030	2418.7	53.3	2428.7	41.9	2492.2	34.8	2492.2	34.79
G123	194.4	381.4	0.4577	0.0057	10.0576	0.2001	0.1636	0.0024	2429.5	50.0	2440.1	35.8	2493.6	28.4	2493.6	28.41
G73	145.6	258.3	0.4760	0.0058	10.6259	0.2239	0.1637	0.0022	2509.9	50.8	2491.0	34.1	2494.3	26.1	2494.3	26.14
G14	45.6	79.3	0.4840	0.0061	10.7579	0.3567	0.1640	0.0025	2544.6	53.3	2502.4	37.1	2497.7	29.4	2497.7	29.38
G22	50.0	93.2	0.4826	0.0062	10.8269	0.3920	0.1656	0.0027	2538.7	54.0	2508.4	38.5	2513.5	30.8	2513.5	30.84
G135	117.7	232.2	0.4630	0.0059	10.1534	0.2624	0.1661	0.0027	2452.9	51.6	2448.8	38.4	2518.8	31.2	2518.8	31.20
G134	106.3	201.4	0.4703	0.0059	10.7807	0.2489	0.1678	0.0027	2484.9	51.6	2504.4	37.5	2536.1	30.2	2536.1	30.16
G6	87.1	140.8	0.4804	0.0058	11.0598	0.2496	0.1684	0.0022	2529.1	50.8	2528.2	33.2	2541.6	25.1	2541.6	25.09
G54	107.5	230.3	0.4482	0.0055	10.6440	0.2477	0.1749	0.0024	2387.3	49.1	2492.5	34.3	2605.3	26.6	2605.3	26.56
G37	139.9	307.7	0.4219	0.0052	9.9433	0.2320	0.1752	0.0024	2269.2	46.9	2429.5	33.9	2608.1	26.3	2608.1	26.31
G53	64.0	107.2	0.5246	0.0065	13.5604	0.3384	0.1921	0.0026	2718.6	54.7	2719.5	35.0	2760.6	26.8	2760.6	26.79
G106	251.7	436.4	0.5271	0.0065	14.2785	0.2696	0.1971	0.0028	2729.1	54.5	2768.4	35.4	2802.2	27.6	2802.2	27.56
G81	96.3	162.2	0.5411	0.0068	14.9183	0.4360	0.2057	0.0031	2788.2	57.1	2810.0	37.2	2872.2	29.2	2872.2	29.15
G9	57.5	274.1	0.6856	0.0083	22.8134	0.5376	0.2371	0.0030	3365.7	63.5	3219.0	33.9	3100.8	25.0	3100.8	24.97
G116	131.6	178.1	0.6173	0.0077	20.6797	0.4683	0.2464	0.0036	3099.2	61.0	3123.7	37.3	3161.7	29.2	3161.7	29.24
Sample A9412061703 Upper reaches mainstream																
G61	11	435	0.0221	0.0003	0.1566	0.0033	0.0513	0.0009	141.0	3.5	147.7	6.1	253.4	9.6	141.0	3.5
G29	22	795	0.0261	0.0003	0.1852	0.0033	0.0523	0.0007	166.2	3.9	172.5	5.9	297.7	8.7	166.2	3.9
G27	29	982	0.0272	0.0003	0.1962	0.0033	0.0531	0.0007	172.7	4.0	181.9	6.0	331.4	8.8	172.7	4.0
G25	6	181	0.0291	0.0004	0.2010	0.0062	0.0503	0.0014	185.0	5.1	186.0	10.8	207.0	12.0	185.0	5.1
G133	144	4010	0.0321	0.0048	0.2546	0.1345	0.0573	0.0014	203.6	59.6	230.3	61.9	504.3	20.6	203.6	59.6
G112	28	745	0.0350	0.0004	0.2484	0.0044	0.0518	0.0007	222.0	5.2	225.3	7.5	275.3	8.2	222.0	5.2
G144	27	633	0.0360	0.0036	0.2779	0.0692	0.0561	0.0010	228.1	45.3	249.0	45.3	454.7	13.9	228.1	45.3
G30	13	333	0.0363	0.0004	0.2530	0.0049	0.0510	0.0008	229.9	5.5	229.0	8.3	239.5	8.2	229.9	5.5
G51	9	201	0.0364	0.0005	0.2854	0.0073	0.0579	0.0013	230.2	6.0	254.9	11.8	527.1	19.7	230.2	6.0
G18	37	829	0.0369	0.0004	0.2768	0.0043	0.0547	0.0006	233.5	5.3	248.1	7.1	398.3	8.7	233.5	5.3
G125	9	207	0.0391	0.0024	0.2736	0.0604	0.0511	0.0013	247.1	29.2	245.6	28.6	244.9	12.4	247.1	29.2
G38	23	589	0.0405	0.0005	0.2877	0.0047	0.0516	0.0006	255.7	5.9	256.8	7.8	269.5	7.2	255.7	5.9

APPENDIX E (continued). U-Pb ZIRCON AGES OF SONG GIANH SEDIMENTS

Grain No.	Pb (ppm)	U (ppm)	Ratios						Ages (Ma)						Best Age (Ma)	± 2σ
			²⁰⁶ Pb/ ²³⁸ U	± 1 σ	²⁰⁷ Pb/ ²³⁵ U	± s.e.	²⁰⁷ Pb/ ²⁰⁶ Pb	± s.e.	²⁰⁶ Pb/ ²³⁸ U	± 2σ	²⁰⁷ Pb/ ²³⁵ U	± 2σ	²⁰⁷ Pb/ ²⁰⁶ Pb	± 2σ		
G114	10	199	0.0405	0.0004	0.3217	0.0044	0.0578	0.0007	256.0	5.2	283.2	8.1	521.8	11.7	256.0	5.2
G96	21	498	0.0407	0.0005	0.2918	0.0057	0.0522	0.0008	257.1	6.2	260.0	9.2	292.9	9.4	257.1	6.2
G138	20	350	0.0407	0.0034	0.3041	0.0735	0.0543	0.0011	257.2	42.0	269.6	40.7	385.2	14.3	257.2	42.0
G97	16	312	0.0415	0.0005	0.2982	0.0058	0.0527	0.0008	262.2	6.3	265.0	9.5	314.6	10.0	262.2	6.3
G46	17	320	0.0434	0.0005	0.3182	0.0059	0.0532	0.0008	274.1	6.5	280.5	9.4	338.6	9.8	274.1	6.5
G23	17	378	0.0472	0.0006	0.3632	0.0071	0.0566	0.0009	297.4	7.1	314.6	10.8	476.4	13.1	297.4	7.1
G32	19	311	0.0503	0.0006	0.3636	0.0062	0.0529	0.0007	316.2	7.4	314.9	9.6	325.8	8.5	316.2	7.4
G94	23	471	0.0514	0.0006	0.3657	0.0065	0.0522	0.0007	323.0	7.6	316.4	10.0	294.6	8.4	323.0	7.6
G141	24	350	0.0533	0.0029	0.4226	0.0492	0.0567	0.0009	334.8	35.0	357.9	33.4	480.7	13.4	334.8	35.0
G105	15	210	0.0554	0.0007	0.4347	0.0098	0.0578	0.0011	347.7	8.6	366.5	13.9	523.7	16.4	347.7	8.6
G121	1	16	0.0628	0.0042	0.4973	0.0982	0.0568	0.0011	392.4	50.5	409.9	46.2	483.4	16.4	392.4	50.5
G69	14	178	0.0699	0.0009	0.5301	0.0102	0.0569	0.0008	435.4	10.2	431.9	13.8	486.9	12.8	435.4	10.2
G8	37	480	0.0705	0.0008	0.5389	0.0078	0.0555	0.0005	439.2	9.9	437.7	10.6	432.8	8.0	439.2	9.9
G101	23	287	0.0708	0.0009	0.5633	0.0117	0.0590	0.0010	441.2	10.6	453.6	15.1	567.5	15.4	441.2	10.6
G77	48	604	0.0717	0.0008	0.5525	0.0081	0.0558	0.0005	446.1	10.0	446.7	10.9	444.8	8.3	446.1	10.0
G65	28	363	0.0718	0.0008	0.5462	0.0088	0.0558	0.0006	446.8	10.1	442.5	11.8	444.4	9.6	446.8	10.1
G76	27	339	0.0727	0.0009	0.5536	0.0092	0.0559	0.0007	452.3	10.3	447.4	12.2	449.2	9.9	452.3	10.3
G7	17	187	0.0763	0.0009	0.5945	0.0113	0.0568	0.0008	474.1	11.1	473.7	14.1	484.9	12.2	474.1	11.1
G24	95	959	0.0986	0.0011	0.8646	0.0122	0.0637	0.0006	606.0	13.4	632.6	13.6	730.4	10.4	606.0	13.4
G129	31	170	0.1308	0.0023	1.2288	0.0324	0.0676	0.0007	792.6	26.5	813.8	23.2	854.8	13.9	792.6	26.5
G2	67	541	0.1313	0.0015	1.2203	0.0166	0.0667	0.0005	795.3	17.2	809.9	15.4	827.2	10.2	795.3	17.2
G93	104	663	0.1331	0.0015	1.2921	0.0181	0.0714	0.0006	805.3	17.4	842.2	16.5	968.9	12.0	805.3	17.4
G120	105	572	0.1627	0.0006	1.5883	0.0142	0.0715	0.0019	971.6	6.2	965.6	33.7	972.9	34.8	972.9	34.8
G40	120	767	0.1616	0.0019	1.5946	0.0209	0.0721	0.0005	965.7	20.5	968.1	17.0	989.3	10.7	989.3	10.7
G33	75	363	0.1665	0.0019	1.6488	0.0231	0.0724	0.0006	992.5	21.2	989.1	17.8	996.1	11.5	996.1	11.5
G86	73	396	0.1692	0.0020	1.6912	0.0245	0.0729	0.0006	1007.9	21.5	1005.2	18.4	1010.9	12.4	1010.9	12.4
G80	38	175	0.1650	0.0020	1.6640	0.0299	0.0733	0.0008	984.5	21.7	994.9	20.7	1021.7	15.8	1021.7	15.8
G116	153	900	0.1575	0.0006	1.6573	0.0087	0.0751	0.0014	942.8	6.1	992.4	23.2	1070.6	25.3	1070.6	25.3
G3	55	287	0.1919	0.0022	2.0321	0.0289	0.0763	0.0006	1131.4	24.0	1126.3	19.0	1102.2	12.0	1102.2	12.0
G127	77	340	0.2000	0.0005	2.1579	0.0070	0.0793	0.0011	1175.5	5.5	1167.6	20.4	1178.6	21.4	1178.6	21.4

APPENDIX E (continued). U-Pb ZIRCON AGES OF SONG GIANH SEDIMENTS

Grain No.	Pb (ppm)	U (ppm)	Ratios						Ages (Ma)						Best Age (Ma)	± 2σ
			²⁰⁶ Pb/ ²³⁸ U	± 1 σ	²⁰⁷ Pb/ ²³⁵ U	± s.e.	²⁰⁷ Pb/ ²⁰⁶ Pb	± s.e.	²⁰⁶ Pb/ ²³⁸ U	± 2σ	²⁰⁷ Pb/ ²³⁵ U	± 2σ	²⁰⁷ Pb/ ²⁰⁶ Pb	± 2σ		
G11	155	675	0.2205	0.0025	2.4727	0.0333	0.0814	0.0006	1284.3	26.7	1264.1	19.5	1230.6	11.5	1230.6	11.5
G139	65	274	0.2444	0.0049	2.9931	0.1474	0.0894	0.0014	1409.7	50.4	1405.9	38.6	1411.7	25.3	1411.7	25.3
G143	88	315	0.2477	0.0007	2.9764	0.0088	0.0900	0.0010	1426.7	6.8	1401.6	16.7	1425.7	17.5	1425.7	17.5
G78	42	132	0.2961	0.0035	4.1619	0.0688	0.1036	0.0009	1672.0	34.4	1666.6	24.0	1688.7	15.8	1688.7	15.8
G28	12	42	0.2725	0.0034	4.0420	0.0974	0.1061	0.0013	1553.4	34.2	1642.7	28.3	1733.3	21.7	1733.3	21.7
G92	32	94	0.3080	0.0037	4.5067	0.0971	0.1067	0.0012	1731.1	36.7	1732.2	27.4	1742.9	20.0	1742.9	20.0
G21	128	435	0.2950	0.0034	4.4878	0.0647	0.1113	0.0008	1666.3	33.9	1728.7	22.7	1819.9	13.7	1819.9	13.7
G15	123	320	0.3263	0.0037	4.9868	0.0673	0.1118	0.0008	1820.5	36.4	1817.1	22.6	1828.4	12.9	1828.4	12.9
G19	423	1304	0.3198	0.0037	4.9834	0.0633	0.1122	0.0007	1788.7	35.7	1816.5	22.1	1835.0	12.3	1835.0	12.3
G79	140	412	0.3233	0.0037	4.9911	0.0702	0.1124	0.0009	1805.8	36.1	1817.8	23.3	1837.9	14.2	1837.9	14.2
G108	351	1017	0.3201	0.0037	4.9420	0.0663	0.1127	0.0009	1790.3	35.7	1809.5	23.3	1844.0	14.5	1844.0	14.5
G99	134	392	0.3234	0.0037	5.0071	0.0738	0.1128	0.0009	1806.2	36.3	1820.5	23.8	1844.8	15.1	1844.8	15.1
G142	328	1053	0.3171	0.0050	4.9796	0.1300	0.1128	0.0013	1775.6	49.3	1815.9	33.1	1845.0	21.0	1845.0	21.0
G106	223	673	0.3311	0.0038	5.0941	0.0702	0.1129	0.0009	1843.6	36.8	1835.1	23.6	1846.0	14.6	1846.0	14.6
G67	156	432	0.3318	0.0038	5.1346	0.0740	0.1129	0.0009	1847.0	37.0	1841.9	23.4	1846.1	14.2	1846.1	14.2
G53	347	1055	0.3306	0.0038	5.1153	0.0652	0.1130	0.0008	1841.0	36.5	1838.6	22.5	1847.9	12.8	1847.9	12.8
G134	214	638	0.3229	0.0045	4.9141	0.1632	0.1131	0.0016	1803.9	43.8	1804.7	33.7	1849.0	25.6	1849.0	25.6
G73	210	611	0.3252	0.0037	5.0867	0.0705	0.1133	0.0008	1814.8	36.3	1833.9	23.2	1853.3	14.0	1853.3	14.0
G47	185	533	0.3260	0.0037	5.0902	0.0680	0.1133	0.0008	1819.1	36.3	1834.5	22.7	1853.6	13.1	1853.6	13.1
G31	15	42	0.2950	0.0037	4.7245	0.1200	0.1135	0.0014	1666.6	36.7	1771.6	29.4	1855.6	22.5	1855.6	22.5
G87	92	234	0.3350	0.0039	5.1582	0.0826	0.1136	0.0010	1862.7	37.6	1845.7	24.5	1858.3	15.8	1858.3	15.8
G63	214	563	0.3342	0.0038	5.2543	0.0716	0.1137	0.0008	1858.7	37.0	1861.5	23.0	1859.5	13.5	1859.5	13.5
G70	164	530	0.3039	0.0035	4.7631	0.0623	0.1142	0.0008	1710.7	34.3	1778.4	22.6	1867.1	13.5	1867.1	13.5
G74	320	999	0.3241	0.0037	5.1226	0.0656	0.1143	0.0008	1809.7	36.0	1839.9	22.7	1868.7	13.3	1868.7	13.3
G75	54	144	0.3370	0.0040	5.4380	0.0985	0.1145	0.0010	1872.4	38.2	1890.9	25.4	1871.4	16.9	1871.4	16.9
G104	135	394	0.3354	0.0039	5.2424	0.0771	0.1145	0.0009	1864.4	37.4	1859.5	24.1	1871.4	15.3	1871.4	15.3
G36	106	307	0.3374	0.0039	5.4038	0.0751	0.1147	0.0008	1874.1	37.3	1885.5	23.0	1874.5	13.3	1874.5	13.3
G54	149	435	0.3364	0.0039	5.3131	0.0705	0.1149	0.0008	1869.4	37.1	1871.0	22.9	1877.8	13.3	1877.8	13.3
G35	217	630	0.3321	0.0038	5.2275	0.0692	0.1151	0.0008	1848.4	36.8	1857.1	22.7	1880.7	13.0	1880.7	13.0
G81	218	614	0.3384	0.0039	5.3108	0.0706	0.1151	0.0008	1879.1	37.3	1870.6	23.1	1881.9	13.7	1881.9	13.7

APPENDIX E (continued). U-Pb ZIRCON AGES OF SONG GIANH SEDIMENTS

Grain No.	Pb (ppm)	U (ppm)	Ratios						Ages (Ma)						Best Age (Ma)	± 2σ
			²⁰⁶ Pb/ ²³⁸ U	± 1 σ	²⁰⁷ Pb/ ²³⁵ U	± s.e.	²⁰⁷ Pb/ ²⁰⁶ Pb	± s.e.	²⁰⁶ Pb/ ²³⁸ U	± 2σ	²⁰⁷ Pb/ ²³⁵ U	± 2σ	²⁰⁷ Pb/ ²⁰⁶ Pb	± 2σ		
G50	78	213	0.3404	0.0039	5.3860	0.0780	0.1151	0.0009	1888.5	37.7	1882.6	23.4	1882.1	14.0	1882.1	14.0
G37	123	346	0.3438	0.0039	5.4646	0.0741	0.1166	0.0008	1904.7	37.8	1895.1	23.0	1904.3	13.2	1904.3	13.2
G58	181	496	0.3325	0.0038	5.3718	0.0720	0.1178	0.0008	1850.6	36.9	1880.4	23.0	1923.7	13.5	1923.7	13.5
G85	348	1177	0.3060	0.0035	4.9994	0.0640	0.1179	0.0008	1720.8	34.5	1819.2	22.7	1924.0	13.7	1924.0	13.7
G126	199	549	0.3388	0.0067	5.4759	0.3680	0.1180	0.0020	1880.9	64.1	1896.8	44.9	1925.7	31.1	1925.7	31.1
G6	71	174	0.3503	0.0041	5.6654	0.0854	0.1181	0.0009	1935.8	38.7	1926.1	23.7	1927.8	14.1	1927.8	14.1
G62	85	220	0.3546	0.0041	5.8341	0.0855	0.1199	0.0009	1956.5	38.9	1951.5	23.9	1955.3	14.4	1955.3	14.4
G132	17	36	0.3553	0.0044	5.9255	0.1013	0.1208	0.0011	1960.0	42.0	1965.0	26.8	1967.5	17.2	1967.5	17.2
G111	214	546	0.3596	0.0041	5.9245	0.0808	0.1216	0.0010	1980.4	39.1	1964.8	24.2	1979.5	15.0	1979.5	15.0
G49	102	260	0.3605	0.0042	5.9552	0.0898	0.1219	0.0009	1984.6	39.4	1969.3	24.0	1983.8	14.5	1983.8	14.5
G150	140	357	0.3650	0.0056	6.1940	0.1630	0.1233	0.0015	2005.6	52.5	2003.6	33.7	2004.1	21.9	2004.1	21.9
G64	117	314	0.3618	0.0042	6.0448	0.0899	0.1233	0.0009	1990.9	39.5	1982.3	24.1	2004.5	14.6	2004.5	14.6
G71	26	65	0.3816	0.0045	6.6380	0.1310	0.1290	0.0012	2083.5	42.3	2064.4	26.8	2084.1	18.0	2084.1	18.0
G149	172	475	0.3353	0.0055	5.8376	0.2183	0.1305	0.0017	1864.1	53.1	1952.0	36.3	2105.1	24.2	2105.1	24.2
G119	113	312	0.3596	0.0053	6.3433	0.1575	0.1306	0.0013	1980.5	50.4	2024.5	31.5	2105.6	19.3	2105.6	19.3
G115	176	533	0.3245	0.0045	5.8809	0.1244	0.1310	0.0013	1811.6	43.5	1958.4	29.2	2111.8	18.6	2111.8	18.6
G128	107	293	0.3318	0.0039	5.9841	0.0818	0.1312	0.0010	1847.2	37.9	1973.5	24.5	2114.6	15.1	2114.6	15.1
G130	283	664	0.3840	0.0039	6.9625	0.1011	0.1316	0.0012	2094.9	36.1	2106.7	24.3	2119.0	17.7	2119.0	17.7
G83	68	163	0.3715	0.0043	6.7949	0.1119	0.1324	0.0011	2036.3	40.6	2085.1	25.2	2129.8	16.0	2129.8	16.0
G57	123	273	0.4102	0.0047	7.9410	0.1113	0.1397	0.0010	2215.8	43.1	2224.3	24.3	2223.0	14.0	2223.0	14.0
G20	517	1212	0.3999	0.0046	7.9008	0.0990	0.1416	0.0009	2168.6	42.0	2219.8	23.4	2247.1	12.7	2247.1	12.7
G98	460	1325	0.3505	0.0040	6.8748	0.0903	0.1429	0.0011	1936.8	38.2	2095.4	24.1	2263.0	14.7	2263.0	14.7
G55	228	540	0.4222	0.0048	8.2920	0.1092	0.1436	0.0010	2270.4	43.7	2263.4	24.1	2270.6	13.6	2270.6	13.6
G137	117	215	0.4143	0.0056	8.3435	0.1947	0.1509	0.0015	2234.6	50.9	2269.1	30.7	2356.0	20.1	2356.0	20.1
G48	88	177	0.4478	0.0052	9.4370	0.1496	0.1535	0.0011	2385.5	46.1	2381.4	25.2	2385.7	14.9	2385.7	14.9
G113	167	358	0.3872	0.0041	8.1442	0.0808	0.1549	0.0010	2109.7	38.3	2247.2	22.3	2400.3	12.7	2400.3	12.7
G56	175	412	0.3936	0.0045	8.4202	0.1133	0.1564	0.0011	2139.7	41.7	2277.4	24.2	2416.8	14.0	2416.8	14.0
G140	378	771	0.4400	0.0005	9.4163	0.0066	0.1565	0.0010	2350.4	4.6	2379.4	11.8	2418.2	13.0	2418.2	13.0
G117	135	216	0.4593	0.0038	9.9574	0.0894	0.1583	0.0011	2436.6	33.1	2430.8	19.8	2437.4	14.2	2437.4	14.2
G89	161	379	0.3963	0.0045	8.5621	0.1178	0.1601	0.0012	2152.0	41.9	2292.5	24.8	2456.4	15.0	2456.4	15.0

APPENDIX E (continued). U-Pb ZIRCON AGES OF SONG GIANH SEDIMENTS

Grain No.	Pb (ppm)	U (ppm)	Ratios						Ages (Ma)						Best Age (Ma)	± 2σ
			²⁰⁶ Pb/ ²³⁸ U	± 1 σ	²⁰⁷ Pb/ ²³⁵ U	± s.e.	²⁰⁷ Pb/ ²⁰⁶ Pb	± s.e.	²⁰⁶ Pb/ ²³⁸ U	± 2σ	²⁰⁷ Pb/ ²³⁵ U	± 2σ	²⁰⁷ Pb/ ²⁰⁶ Pb	± 2σ		
G146	50	82	0.4567	0.0004	9.8590	0.0049	0.1601	0.0008	2424.9	3.8	2421.7	9.1	2456.4	10.3	2456.4	10.3
G82	420	798	0.4576	0.0052	10.2939	0.1376	0.1608	0.0011	2428.8	46.3	2461.6	24.9	2464.4	14.5	2464.4	14.5
G22	100	174	0.4686	0.0054	10.3861	0.1602	0.1618	0.0011	2477.6	47.6	2469.8	25.1	2474.6	14.4	2474.6	14.4
G95	57	90	0.4710	0.0056	10.7888	0.2190	0.1632	0.0015	2487.7	49.0	2505.1	27.7	2489.4	18.2	2489.4	18.2
G135	63	121	0.4742	0.0004	10.4823	0.0035	0.1654	0.0005	2501.8	3.2	2478.4	6.0	2512.0	7.2	2512.0	7.2
G14	51	76	0.4796	0.0057	10.7667	0.2035	0.1667	0.0013	2525.6	49.2	2503.2	26.5	2525.0	16.2	2525.0	16.2
G72	160	297	0.4794	0.0055	11.0423	0.1626	0.1668	0.0012	2524.8	48.0	2526.7	25.3	2525.8	14.9	2525.8	14.9
G41	365	603	0.4806	0.0055	11.0826	0.1453	0.1677	0.0011	2530.1	47.8	2530.1	24.5	2535.0	13.5	2535.0	13.5
G66	82	147	0.4772	0.0056	10.9195	0.1873	0.1678	0.0013	2515.2	48.5	2516.3	26.1	2535.6	15.9	2535.6	15.9
G10	53	97	0.4827	0.0056	11.2491	0.1897	0.1681	0.0012	2538.9	48.9	2544.0	25.6	2538.4	15.0	2538.4	15.0
G34	36	60	0.4767	0.0056	10.7926	0.2060	0.1682	0.0014	2513.1	49.1	2505.4	26.6	2540.0	16.4	2540.0	16.4
G131	294	652	0.4147	0.0016	9.4565	0.0230	0.1687	0.0009	2236.5	14.3	2383.3	11.7	2544.6	10.9	2544.6	10.9
G147	253	412	0.4828	0.0029	11.1006	0.0538	0.1688	0.0010	2539.6	24.9	2531.6	15.4	2546.1	12.1	2546.1	12.1
G16	82	147	0.4829	0.0056	11.1910	0.1780	0.1691	0.0012	2540.0	48.6	2539.2	25.3	2548.3	14.6	2548.3	14.6
G52	30	55	0.4910	0.0058	11.4486	0.2271	0.1699	0.0014	2575.2	50.2	2560.4	27.1	2557.0	17.0	2557.0	17.0
G26	129	206	0.4860	0.0056	11.3947	0.1621	0.1714	0.0011	2553.4	48.4	2556.0	24.8	2571.4	13.8	2571.4	13.8
G39	56	95	0.4894	0.0058	11.6346	0.2164	0.1784	0.0014	2567.9	49.8	2575.5	26.6	2638.2	16.2	2638.2	16.2
G68	62	92	0.5171	0.0061	13.2105	0.2540	0.1841	0.0015	2687.0	51.8	2694.8	27.1	2689.8	16.9	2689.8	16.9
G124	57	87	0.5617	0.0030	17.6672	0.0668	0.2230	0.0011	2873.5	24.4	2971.8	14.0	3002.7	11.0	3002.7	11.0
G60	92	126	0.6309	0.0073	22.7002	0.3958	0.2601	0.0019	3153.3	58.0	3214.2	26.7	3247.4	15.5	3247.4	15.5
Sample A23014052705 Song Trac																
G96	35	1242	0.0257	0.0003	0.1766	0.0040	0.0495	0.0010	163.7	4.1	165.1	7.1	173.0	10.8	163.7	4.1
G81	57	2018	0.0264	0.0003	0.1872	0.0034	0.0503	0.0007	167.9	4.0	174.2	5.9	206.6	10.1	167.9	4.0
G105	18	632	0.0268	0.0055	0.1840	0.1786	0.0499	0.0018	170.6	68.7	171.5	65.4	188.0	16.7	170.6	68.7
G94	5	148	0.0271	0.0005	0.1935	0.0091	0.0527	0.0024	172.2	6.0	179.6	16.1	317.2	29.0	172.2	6.0
G73	4	125	0.0273	0.0005	0.1811	0.0091	0.0501	0.0024	173.3	6.3	169.0	16.4	197.3	21.8	173.3	6.3
G127	30	1077	0.0273	0.0030	0.1864	0.0870	0.0495	0.0020	173.5	38.2	173.6	37.7	172.1	17.1	173.5	38.2
G58	47	1399	0.0325	0.0004	0.2337	0.0043	0.0520	0.0008	206.4	5.0	213.3	7.3	283.2	11.8	206.4	5.0
G86	5	124	0.0342	0.0005	0.2441	0.0087	0.0504	0.0017	217.0	6.4	221.8	14.0	213.0	17.2	217.0	6.4

APPENDIX E (continued). U-Pb ZIRCON AGES OF SONG GIANH SEDIMENTS

Grain No.	Pb (ppm)	U (ppm)	Ratios						Ages (Ma)						Best Age (Ma)	± 2σ
			²⁰⁶ Pb/ ²³⁸ U	± 1 σ	²⁰⁷ Pb/ ²³⁵ U	± s.e.	²⁰⁷ Pb/ ²⁰⁶ Pb	± s.e.	²⁰⁶ Pb/ ²³⁸ U	± 2σ	²⁰⁷ Pb/ ²³⁵ U	± 2σ	²⁰⁷ Pb/ ²⁰⁶ Pb	± 2σ		
G46	9	201	0.0351	0.0005	0.2481	0.0078	0.0518	0.0015	222.1	6.2	225.0	12.8	276.1	18.3	222.1	6.2
G99	10	195	0.0366	0.0006	0.2654	0.0094	0.0536	0.0017	232.0	6.8	239.0	15.3	354.3	23.9	232.0	6.8
G91	6	126	0.0374	0.0006	0.2639	0.0091	0.0504	0.0016	236.4	6.8	237.8	14.4	212.1	16.6	236.4	6.8
G124	42	1039	0.0377	0.0010	0.3022	0.0177	0.0579	0.0014	238.4	12.5	268.1	17.0	526.0	24.5	238.4	12.5
G61	24	641	0.0378	0.0005	0.2924	0.0069	0.0563	0.0011	239.1	6.1	260.4	11.0	465.0	19.6	239.1	6.1
G82	11	221	0.0390	0.0006	0.2909	0.0099	0.0549	0.0017	246.3	7.2	259.2	15.7	409.8	25.3	246.3	7.2
G37	19	418	0.0401	0.0005	0.3148	0.0070	0.0561	0.0010	253.1	6.3	277.9	10.7	456.7	18.2	253.1	6.3
G64	21	413	0.0401	0.0005	0.2675	0.0061	0.0484	0.0009	253.6	6.3	240.7	10.0	117.4	9.0	253.6	6.3
G83	4	66	0.0413	0.0007	0.2950	0.0144	0.0504	0.0023	260.9	9.0	262.5	21.8	212.1	21.8	260.9	9.0
G102	24	561	0.0420	0.0008	0.3207	0.0122	0.0547	0.0010	265.3	10.1	282.4	13.2	400.8	17.0	265.3	10.1
G43	15	290	0.0424	0.0006	0.3060	0.0085	0.0523	0.0013	267.8	7.2	271.1	13.3	299.9	17.3	267.8	7.2
G89	3	69	0.0431	0.0007	0.3068	0.0146	0.0500	0.0022	272.0	9.1	271.7	21.8	194.1	20.1	272.0	9.1
G130	8	137	0.0436	0.0028	0.2998	0.0888	0.0519	0.0019	275.2	34.8	266.3	35.7	282.3	22.2	275.2	34.8
G28	24	475	0.0454	0.0006	0.3516	0.0077	0.0548	0.0010	286.3	7.2	305.9	11.5	404.1	16.7	286.3	7.2
G75	22	350	0.0480	0.0006	0.3810	0.0099	0.0570	0.0013	302.5	7.9	327.8	14.3	490.8	21.7	302.5	7.9
G109	70	1238	0.0524	0.0056	0.4182	0.2100	0.0575	0.0019	329.1	69.0	354.7	67.0	511.5	30.9	329.1	69.0
G108	10	142	0.0539	0.0057	0.4366	0.2692	0.0588	0.0022	338.5	69.2	367.8	68.6	558.2	36.1	338.5	69.2
G123	25	416	0.0550	0.0016	0.4102	0.0216	0.0541	0.0009	345.4	19.1	349.0	19.3	376.9	14.8	345.4	19.1
G8	6	94	0.0551	0.0009	0.3996	0.0165	0.0518	0.0019	346.0	10.9	341.3	22.9	278.4	22.4	346.0	10.9
G10	28	365	0.0556	0.0007	0.4113	0.0100	0.0534	0.0011	348.8	8.9	349.8	14.1	344.1	16.4	348.8	8.9
G67	6	88	0.0573	0.0008	0.4135	0.0144	0.0530	0.0016	359.4	10.2	351.4	20.0	330.5	21.6	359.4	10.2
G38	14	220	0.0613	0.0008	0.4591	0.0107	0.0544	0.0010	383.3	9.6	383.6	14.6	388.5	16.9	383.3	9.6
G90	22	331	0.0660	0.0008	0.5192	0.0110	0.0573	0.0010	412.0	9.9	424.6	14.4	503.9	17.8	412.0	9.9
G100	28	399	0.0663	0.0008	0.5772	0.0122	0.0617	0.0010	413.7	9.9	462.7	15.1	664.8	20.8	413.7	9.9
G118	56	814	0.0665	0.0036	0.5047	0.0885	0.0550	0.0014	415.0	43.8	414.9	40.9	412.6	21.8	415.0	43.8
G77	23	284	0.0671	0.0009	0.6149	0.0153	0.0657	0.0013	418.8	10.6	486.7	18.3	795.9	26.7	418.8	10.6
G51	34	443	0.0672	0.0008	0.5102	0.0105	0.0547	0.0009	419.1	10.0	418.6	13.9	400.8	15.3	419.1	10.0
G50	43	594	0.0682	0.0008	0.5491	0.0105	0.0573	0.0008	425.3	10.1	444.4	13.5	504.3	16.2	425.3	10.1
G11	30	393	0.0685	0.0009	0.5489	0.0114	0.0573	0.0009	426.9	10.4	444.3	14.5	503.9	17.4	426.9	10.4
G101	53	702	0.0694	0.0006	0.5326	0.0094	0.0558	0.0017	432.6	6.6	433.5	22.5	446.0	26.9	432.6	6.6

APPENDIX E (continued). U-Pb ZIRCON AGES OF SONG GIANH SEDIMENTS

Grain No.	Pb (ppm)	U (ppm)	Ratios						Ages (Ma)						Best Age (Ma)	± 2σ
			²⁰⁶ Pb/ ²³⁸ U	± 1 σ	²⁰⁷ Pb/ ²³⁵ U	± s.e.	²⁰⁷ Pb/ ²⁰⁶ Pb	± s.e.	²⁰⁶ Pb/ ²³⁸ U	± 2σ	²⁰⁷ Pb/ ²³⁵ U	± 2σ	²⁰⁷ Pb/ ²⁰⁶ Pb	± 2σ		
G42	89	1209	0.0699	0.0008	0.5355	0.0084	0.0556	0.0006	435.7	10.0	435.4	11.4	434.4	12.3	435.7	10.0
G44	28	352	0.0704	0.0009	0.5412	0.0099	0.0559	0.0008	438.6	10.4	439.2	13.1	449.2	14.5	438.6	10.4
G45	27	334	0.0709	0.0009	0.5658	0.0105	0.0572	0.0008	441.5	10.4	455.3	13.4	500.4	15.6	441.5	10.4
G62	32	375	0.0713	0.0009	0.5524	0.0111	0.0565	0.0009	444.2	10.6	446.5	14.3	472.9	16.3	444.2	10.6
G1	33	324	0.0721	0.0009	0.5224	0.0104	0.0543	0.0008	449.0	10.8	426.8	13.9	384.3	9.7	449.0	10.8
G122	15	169	0.0743	0.0043	0.5949	0.1268	0.0566	0.0017	461.8	51.6	474.0	48.4	475.2	26.9	461.8	51.6
G115	70	633	0.0834	0.0037	0.6718	0.0859	0.0580	0.0013	516.4	43.6	521.8	40.2	527.9	23.6	516.4	43.6
G39	42	410	0.0903	0.0011	0.7605	0.0157	0.0617	0.0009	557.5	13.4	574.3	17.4	664.8	19.5	557.5	13.4
G53	10	87	0.0975	0.0014	0.9181	0.0298	0.0671	0.0017	599.6	16.3	661.3	27.5	839.3	32.9	599.6	16.3
G40	19	143	0.1109	0.0014	0.9610	0.0237	0.0621	0.0011	678.0	16.6	683.8	21.9	675.8	22.5	678.0	16.6
G5	247	2139	0.1146	0.0014	1.1862	0.0178	0.0759	0.0007	699.3	15.7	794.2	16.6	1092.2	17.0	699.3	15.7
G19	16	80	0.1237	0.0017	1.0960	0.0323	0.0619	0.0013	751.9	19.3	751.4	26.4	668.9	25.6	751.9	19.3
G111	29	101	0.1270	0.0006	1.1444	0.0077	0.0669	0.0008	770.7	7.2	774.6	14.5	833.4	18.6	770.7	7.2
G20	78	473	0.1278	0.0015	1.1464	0.0184	0.0652	0.0007	775.5	17.4	775.5	17.1	779.5	15.8	775.5	17.4
G121	164	960	0.1318	0.0039	1.2032	0.1100	0.0664	0.0015	797.8	44.8	802.0	41.9	820.0	30.6	797.8	44.8
G110	32	176	0.1366	0.0008	1.2595	0.0153	0.0669	0.0019	825.2	8.7	827.7	31.9	835.0	36.1	825.2	8.7
G18	15	78	0.1417	0.0019	1.3124	0.0382	0.0652	0.0013	854.0	21.6	851.2	27.7	781.1	26.7	854.0	21.6
G26	23	149	0.1442	0.0019	1.5336	0.0387	0.0763	0.0013	868.4	21.2	943.9	26.1	1102.2	27.4	868.4	21.2
G117	157	1058	0.1447	0.0010	1.3816	0.0122	0.0699	0.0008	871.0	11.3	881.1	15.7	924.2	18.4	871.0	11.3
G88	137	913	0.1485	0.0018	1.4363	0.0237	0.0707	0.0008	892.6	19.6	904.2	19.5	949.6	18.4	892.6	19.6
G30	111	770	0.1493	0.0018	1.4254	0.0217	0.0686	0.0006	897.1	19.7	899.6	17.9	887.9	15.7	897.1	19.7
G16	44	284	0.1523	0.0018	1.4149	0.0247	0.0694	0.0008	913.6	20.5	895.2	19.7	910.4	18.0	910.4	18.0
G60	101	590	0.1672	0.0020	1.6286	0.0271	0.0704	0.0008	996.5	21.9	981.3	20.0	941.2	17.7	941.2	17.7
G31	73	387	0.1699	0.0021	1.7236	0.0316	0.0731	0.0008	1011.3	22.6	1017.4	21.4	1015.3	19.4	1015.3	19.4
G2	46	183	0.2001	0.0025	2.1439	0.0412	0.0788	0.0009	1176.0	26.3	1163.1	23.4	1166.1	20.7	1166.1	20.7
G32	386	1909	0.1744	0.0020	1.9209	0.0261	0.0793	0.0006	1036.3	22.3	1088.4	18.8	1180.1	15.7	1180.1	15.7
G126	11	40	0.2103	0.0005	2.3135	0.0064	0.0816	0.0010	1230.3	5.0	1216.4	18.1	1235.5	22.5	1235.5	22.5
G95	76	275	0.2371	0.0029	2.8324	0.0550	0.0867	0.0011	1371.8	29.7	1364.2	25.9	1353.4	23.1	1353.4	23.1
G104	53	178	0.2212	0.0005	2.6080	0.0071	0.0870	0.0010	1288.0	5.6	1302.9	17.5	1360.9	22.1	1360.9	22.1
G33	89	249	0.2802	0.0033	3.7033	0.0625	0.0983	0.0009	1592.5	33.5	1572.1	24.3	1591.7	19.7	1591.7	19.7

APPENDIX E (continued). U-Pb ZIRCON AGES OF SONG GIANH SEDIMENTS

Grain No.	Pb (ppm)	U (ppm)	Ratios						Ages (Ma)						Best Age (Ma)	± 2σ
			²⁰⁶ Pb/ ²³⁸ U	± 1 σ	²⁰⁷ Pb/ ²³⁵ U	± s.e.	²⁰⁷ Pb/ ²⁰⁶ Pb	± s.e.	²⁰⁶ Pb/ ²³⁸ U	± 2σ	²⁰⁷ Pb/ ²³⁵ U	± 2σ	²⁰⁷ Pb/ ²⁰⁶ Pb	± 2σ		
G72	13	34	0.3235	0.0045	4.4345	0.1614	0.1027	0.0019	1806.7	43.9	1718.8	38.9	1673.8	35.3	1673.8	35.3
G57	21	59	0.3032	0.0039	4.3692	0.1234	0.1032	0.0015	1707.4	38.8	1706.5	32.4	1682.6	29.0	1682.6	29.0
G129	42	118	0.2955	0.0040	4.3169	0.1190	0.1037	0.0017	1669.1	40.2	1696.6	34.6	1692.1	31.0	1692.1	31.0
G132	95	336	0.2677	0.0022	3.9575	0.0499	0.1043	0.0014	1529.0	22.6	1625.5	25.3	1702.2	26.7	1702.2	26.7
G85	20	50	0.2892	0.0039	4.5106	0.1467	0.1045	0.0018	1637.4	38.7	1732.9	35.6	1704.7	33.0	1704.7	33.0
G21	32	81	0.3077	0.0038	4.5361	0.0985	0.1062	0.0012	1729.3	37.4	1737.6	27.7	1734.8	23.3	1734.8	23.3
G71	3	9	0.3122	0.0061	4.5825	0.3215	0.1077	0.0037	1751.3	60.0	1746.1	66.3	1760.2	62.4	1760.2	62.4
G65	47	134	0.3157	0.0038	4.6705	0.0959	0.1086	0.0012	1768.5	37.4	1762.0	27.8	1776.7	23.7	1776.7	23.7
G70	143	516	0.2764	0.0033	4.1846	0.0689	0.1095	0.0011	1753.0	32.9	1671.0	25.2	1790.4	21.3	1790.4	21.3
G119	58	156	0.3193	0.0008	4.7309	0.0091	0.1099	0.0008	1786.2	7.7	1772.7	12.4	1797.6	16.3	1797.6	16.3
G23	86	204	0.3237	0.0039	4.9081	0.0865	0.1100	0.0010	1807.6	37.6	1803.6	25.5	1799.1	20.3	1799.1	20.3
G9	100	92	0.3096	0.0039	4.5377	0.1102	0.1101	0.0014	1738.8	38.5	1737.9	29.7	1800.9	25.6	1800.9	25.6
G128	29	75	0.3228	0.0008	4.7380	0.0218	0.1108	0.0019	1803.5	8.1	1774.0	29.9	1812.7	34.2	1812.7	34.2
G112	347	1085	0.3186	0.0017	4.8972	0.0348	0.1109	0.0015	1782.8	16.9	1801.8	24.6	1813.6	27.5	1813.6	27.5
G113	39	95	0.3252	0.0031	4.9755	0.1752	0.1109	0.0031	1814.9	29.9	1815.2	50.5	1813.7	52.5	1813.7	52.5
G114	163	400	0.3088	0.0037	4.6821	0.0810	0.1112	0.0012	1734.8	36.7	1764.1	27.6	1819.3	23.5	1819.3	23.5
G98	101	265	0.3223	0.0039	4.9236	0.1022	0.1112	0.0014	1801.1	37.9	1806.3	29.0	1819.8	25.4	1819.8	25.4
G56	55	142	0.3217	0.0039	4.8314	0.0941	0.1113	0.0012	1797.9	37.8	1790.4	27.1	1819.9	22.6	1819.9	22.6
G14	90	59	0.3253	0.0042	4.9219	0.1347	0.1116	0.0015	1815.8	40.9	1806.0	31.8	1824.8	27.7	1824.8	27.7
G52	78	191	0.3303	0.0040	4.9561	0.1003	0.1118	0.0012	1839.7	38.8	1811.9	27.6	1829.2	23.0	1829.2	23.0
G22	159	518	0.2846	0.0033	4.4251	0.0648	0.1122	0.0009	1614.2	33.5	1717.1	23.5	1835.7	18.3	1835.7	18.3
G41	218	691	0.3229	0.0038	4.9618	0.0763	0.1123	0.0010	1804.1	36.9	1812.8	24.6	1836.3	19.2	1836.3	19.2
G47	51	160	0.2852	0.0035	4.3427	0.0935	0.1125	0.0013	1617.7	35.1	1701.5	28.0	1840.2	24.4	1840.2	24.4
G49	126	370	0.3278	0.0039	5.0573	0.0795	0.1125	0.0010	1827.6	37.4	1829.0	25.0	1840.8	19.8	1840.8	19.8
G48	92	251	0.3265	0.0039	5.0711	0.0922	0.1126	0.0011	1821.5	37.9	1831.3	26.3	1842.1	21.4	1842.1	21.4
G17	99	244	0.3374	0.0040	5.2768	0.0948	0.1127	0.0010	1874.1	38.9	1865.1	25.8	1843.2	20.4	1843.2	20.4
G63	127	375	0.3036	0.0036	4.7007	0.0814	0.1127	0.0011	1709.2	35.6	1767.4	25.8	1843.4	21.4	1843.4	21.4
G59	16	46	0.2947	0.0041	4.8635	0.1704	0.1127	0.0020	1665.0	40.4	1796.0	37.2	1843.6	34.5	1843.6	34.5
G93	34	107	0.2827	0.0036	4.4576	0.1162	0.1127	0.0016	1604.8	36.1	1723.1	31.9	1843.6	29.4	1843.6	29.4
G79	122	348	0.3303	0.0039	4.9608	0.0919	0.1129	0.0012	1839.8	38.2	1812.7	27.3	1846.6	22.9	1846.6	22.9

APPENDIX E (continued). U-Pb ZIRCON AGES OF SONG GIANH SEDIMENTS

Grain No.	Pb (ppm)	U (ppm)	Ratios						Ages (Ma)						Best Age (Ma)	$\pm 2\sigma$
			$^{206}\text{Pb}/^{238}\text{U}$	$\pm 1\sigma$	$^{207}\text{Pb}/^{235}\text{U}$	$\pm \text{s.e.}$	$^{207}\text{Pb}/^{206}\text{Pb}$	$\pm \text{s.e.}$	$^{206}\text{Pb}/^{238}\text{U}$	$\pm 2\sigma$	$^{207}\text{Pb}/^{235}\text{U}$	$\pm 2\sigma$	$^{207}\text{Pb}/^{206}\text{Pb}$	$\pm 2\sigma$		
G7	279	1034	0.2799	0.0033	4.4119	0.0600	0.1129	0.0008	1591.1	32.9	1714.6	22.9	1846.8	17.3	1846.8	17.3
G97	173	489	0.3325	0.0039	5.2130	0.0903	0.1130	0.0012	1850.3	37.9	1854.7	27.3	1848.2	23.2	1848.2	23.2
G24	245	724	0.3333	0.0039	5.2270	0.0751	0.1130	0.0009	1854.6	37.7	1857.0	23.9	1848.5	17.9	1848.5	17.9
G25	137	347	0.3271	0.0039	5.1015	0.0848	0.1134	0.0010	1824.5	37.7	1836.4	25.1	1854.0	19.7	1854.0	19.7
G4	106	276	0.3343	0.0040	5.2041	0.0862	0.1142	0.0010	1859.0	38.5	1853.3	25.0	1867.8	19.3	1867.8	19.3
G116	117	355	0.3043	0.0014	4.7421	0.0249	0.1143	0.0011	1712.7	13.9	1774.7	17.7	1868.6	20.8	1868.6	20.8
G74	213	666	0.2895	0.0034	4.5916	0.0744	0.1155	0.0011	1639.2	34.0	1747.8	25.5	1888.3	21.4	1888.3	21.4
G34	155	429	0.3479	0.0041	5.9070	0.0956	0.1222	0.0011	1924.6	39.2	1962.3	25.3	1989.2	19.6	1989.2	19.6
G78	113	301	0.3337	0.0041	5.7620	0.1227	0.1225	0.0014	1856.1	39.2	1940.7	28.8	1993.5	24.7	1993.5	24.7
G68	44	105	0.3138	0.0039	5.4832	0.1346	0.1251	0.0016	1759.2	38.6	1898.0	30.6	2030.2	27.0	2030.2	27.0
G6	212	585	0.3422	0.0040	6.1505	0.0869	0.1293	0.0010	1897.3	38.5	1997.4	24.3	2088.6	17.9	2088.6	17.9
G66	166	362	0.3630	0.0043	6.5222	0.1153	0.1307	0.0013	1996.5	40.7	2048.9	27.1	2107.5	22.1	2107.5	22.1
G92	248	614	0.3665	0.0043	6.6381	0.1179	0.1333	0.0014	2013.1	40.9	2064.4	28.1	2142.2	23.7	2142.2	23.7
G12	258	566	0.3920	0.0046	7.4881	0.1140	0.1359	0.0011	2132.3	42.7	2171.6	25.2	2175.0	18.6	2175.0	18.6
G120	326	783	0.3645	0.0027	7.1833	0.0538	0.1412	0.0012	2003.5	25.1	2134.4	19.8	2242.2	19.9	2242.2	19.9
G54	161	352	0.4295	0.0051	8.5510	0.1444	0.1450	0.0013	2303.4	45.6	2291.4	26.9	2287.8	21.0	2287.8	21.0
G55	87	173	0.4230	0.0050	8.9755	0.1683	0.1501	0.0014	2274.2	45.7	2335.5	27.8	2347.1	22.1	2347.1	22.1
G80	175	359	0.3950	0.0047	8.2028	0.1411	0.1518	0.0015	2146.0	43.1	2253.7	27.9	2366.3	22.8	2366.3	22.8
G27	194	382	0.4630	0.0055	9.8546	0.1569	0.1524	0.0012	2452.9	48.0	2421.3	26.2	2373.3	19.3	2373.3	19.3
G76	248	446	0.3872	0.0046	8.0550	0.1378	0.1540	0.0015	2109.7	42.5	2237.2	27.7	2390.5	22.6	2390.5	22.6
G29	179	297	0.4503	0.0053	9.6780	0.1624	0.1550	0.0013	2396.7	47.3	2404.6	26.6	2402.1	20.0	2402.1	20.0
G3	182	357	0.4592	0.0054	9.9951	0.1486	0.1577	0.0012	2435.9	47.7	2434.3	25.7	2430.8	18.5	2430.8	18.5
G69	297	709	0.4156	0.0049	9.0499	0.1396	0.1584	0.0014	2240.5	44.2	2343.1	27.0	2438.5	21.3	2438.5	21.3
G36	363	739	0.4633	0.0054	10.3518	0.1639	0.1591	0.0013	2454.0	47.9	2466.8	26.4	2446.3	19.8	2446.3	19.8
G106	44	83	0.4477	0.0027	9.6369	0.0583	0.1597	0.0013	2385.1	24.3	2400.7	18.3	2452.9	19.1	2452.9	19.1
G13	46	77	0.4601	0.0059	10.7850	0.3011	0.1606	0.0018	2439.8	51.7	2504.8	31.4	2462.2	25.5	2462.2	25.5
G125	67	115	0.4690	0.0007	10.1266	0.0100	0.1617	0.0011	2479.2	6.2	2446.4	12.9	2473.1	17.3	2473.1	17.3
G133	228	337	0.4666	0.0058	10.3557	0.2067	0.1620	0.0021	2468.7	51.1	2467.1	33.6	2476.7	29.0	2476.7	29.0
G103	344	574	0.4656	0.0008	10.3107	0.0096	0.1621	0.0008	2464.4	7.3	2463.1	9.3	2477.7	13.4	2477.7	13.4
G107	83	148	0.4710	0.0004	10.4066	0.0045	0.1632	0.0011	2487.9	3.1	2471.6	12.1	2488.6	16.7	2488.6	16.7

APPENDIX E (continued). U-Pb ZIRCON AGES OF SONG GIANH SEDIMENTS

Grain No.	Pb (ppm)	U (ppm)	Ratios						Ages (Ma)						Best Age (Ma)	± 2σ
			²⁰⁶ Pb/ ²³⁸ U	± 1 σ	²⁰⁷ Pb/ ²³⁵ U	± s.e.	²⁰⁷ Pb/ ²⁰⁶ Pb	± s.e.	²⁰⁶ Pb/ ²³⁸ U	± 2σ	²⁰⁷ Pb/ ²³⁵ U	± 2σ	²⁰⁷ Pb/ ²⁰⁶ Pb	± 2σ		
G87	28	44	0.4713	0.0063	10.3851	0.3511	0.1644	0.0024	2489.2	54.9	2469.7	36.4	2501.5	31.4	2501.5	31.4
G15	48	82	0.4910	0.0061	11.3532	0.2737	0.1693	0.0017	2575.0	52.7	2552.6	29.8	2550.9	23.4	2550.9	23.4
G84	711	1444	0.4816	0.0056	11.5347	0.1733	0.1735	0.0016	2534.1	48.7	2567.4	27.9	2591.8	22.3	2591.8	22.3
G131	406	700	0.4953	0.0007	12.0336	0.0115	0.1758	0.0018	2593.5	5.9	2607.0	19.4	2613.4	23.9	2613.4	23.9
G35	252	497	0.4660	0.0055	11.6162	0.1839	0.1820	0.0015	2465.8	48.2	2574.0	26.7	2671.3	19.9	2671.3	19.9
Sample A36612061807 River Mouth																
G46	14	478	0.0289	0.0004	0.2164	0.0045	0.0538	0.0009	183.5	4.5	198.9	7.6	361.0	12.8	183.5	4.5
G4	8	210	0.0361	0.0005	0.2939	0.0079	0.0570	0.0013	228.4	6.1	261.6	12.1	490.4	20.5	228.4	6.1
G7	36	979	0.0374	0.0005	0.2735	0.0043	0.0530	0.0006	236.8	5.6	245.5	7.0	327.5	8.4	236.8	5.6
G74	16	397	0.0377	0.0005	0.2865	0.0061	0.0545	0.0010	238.6	6.0	255.8	9.7	392.2	13.8	238.6	6.0
G11	12	300	0.0380	0.0005	0.2789	0.0058	0.0519	0.0009	240.7	6.0	249.8	9.3	281.4	10.8	240.7	6.0
G29	16	429	0.0382	0.0005	0.2943	0.0057	0.0556	0.0009	241.5	6.0	262.0	9.2	434.4	13.3	241.5	6.0
G64	19	500	0.0383	0.0005	0.2818	0.0058	0.0523	0.0009	242.4	6.0	252.1	9.2	299.0	11.1	242.4	6.0
G90	49	1100	0.0385	0.0017	0.2931	0.0209	0.0549	0.0007	243.7	20.9	261.0	20.7	407.3	10.3	243.7	20.9
G105	36	764	0.0390	0.0005	0.2960	0.0043	0.0547	0.0005	246.3	6.0	263.2	7.0	398.3	8.3	246.3	6.0
G77	26	561	0.0391	0.0005	0.3143	0.0053	0.0576	0.0007	247.3	5.8	277.5	8.4	512.7	12.6	247.3	5.8
G40	19	450	0.0392	0.0005	0.2889	0.0047	0.0531	0.0006	247.7	5.8	257.7	7.6	330.9	9.1	247.7	5.8
G75	20	481	0.0394	0.0005	0.3152	0.0055	0.0574	0.0008	248.9	6.0	278.2	8.7	506.6	12.9	248.9	6.0
G52	15	367	0.0395	0.0005	0.2905	0.0060	0.0525	0.0009	250.0	6.2	258.9	9.5	308.5	11.3	250.0	6.2
G69	14	358	0.0396	0.0005	0.2874	0.0055	0.0520	0.0008	250.2	6.1	256.5	8.8	285.8	9.9	250.2	6.1
G51	13	338	0.0396	0.0005	0.3036	0.0063	0.0561	0.0010	250.5	6.2	269.2	10.1	454.3	14.8	250.5	6.2
G15	12	311	0.0397	0.0005	0.3145	0.0062	0.0562	0.0009	251.2	6.2	277.6	9.6	460.3	13.9	251.2	6.2
G87	16	381	0.0398	0.0005	0.2865	0.0059	0.0527	0.0009	251.8	6.2	255.8	9.6	315.5	11.5	251.8	6.2
G2	25	581	0.0399	0.0005	0.2844	0.0044	0.0519	0.0006	252.2	6.0	254.1	7.3	282.8	7.7	252.2	6.0
G26	26	639	0.0401	0.0005	0.3116	0.0052	0.0566	0.0007	253.3	6.0	275.4	8.2	476.0	11.5	253.3	6.0
G57	15	267	0.0401	0.0005	0.2999	0.0060	0.0535	0.0009	253.6	6.2	266.3	9.4	350.9	11.9	253.6	6.2
G14	13	295	0.0402	0.0005	0.3049	0.0066	0.0532	0.0010	253.8	6.3	270.2	10.1	335.6	12.6	253.8	6.3
G79	16	360	0.0402	0.0005	0.3143	0.0061	0.0560	0.0009	253.8	6.2	277.5	9.5	452.8	13.6	253.8	6.2
G73	29	736	0.0403	0.0005	0.2896	0.0044	0.0519	0.0006	254.4	5.9	258.3	7.2	281.9	7.6	254.4	5.9

APPENDIX E (continued). U-Pb ZIRCON AGES OF SONG GIANH SEDIMENTS

Grain No.	Pb (ppm)	U (ppm)	Ratios						Ages (Ma)						Best Age (Ma)	± 2σ
			²⁰⁶ Pb/ ²³⁸ U	± 1 σ	²⁰⁷ Pb/ ²³⁵ U	± s.e.	²⁰⁷ Pb/ ²⁰⁶ Pb	± s.e.	²⁰⁶ Pb/ ²³⁸ U	± 2σ	²⁰⁷ Pb/ ²³⁵ U	± 2σ	²⁰⁷ Pb/ ²⁰⁶ Pb	± 2σ		
G62	18	413	0.0405	0.0005	0.2956	0.0061	0.0520	0.0009	256.2	6.3	262.9	9.6	283.2	10.6	256.2	6.3
G103	76	1764	0.0409	0.0041	0.3041	0.0957	0.0541	0.0011	258.2	51.3	269.6	49.0	373.1	15.0	258.2	51.3
G81	204	3415	0.0412	0.0005	0.3177	0.0043	0.0559	0.0005	260.1	5.9	280.1	6.9	449.6	8.2	260.1	5.9
G30	20	492	0.0414	0.0005	0.2927	0.0050	0.0507	0.0006	261.2	6.2	260.7	7.9	227.7	7.4	261.2	6.2
G10	15	354	0.0414	0.0005	0.3004	0.0058	0.0522	0.0008	261.3	6.3	266.7	9.2	295.1	10.2	261.3	6.3
G5	16	370	0.0415	0.0005	0.3473	0.0066	0.0586	0.0009	262.2	6.4	302.7	9.8	553.8	14.9	262.2	6.4
G36	13	325	0.0415	0.0005	0.3511	0.0061	0.0617	0.0008	262.2	6.3	305.6	9.5	663.7	15.0	262.2	6.3
G82	22	527	0.0415	0.0005	0.3032	0.0054	0.0516	0.0007	262.3	6.3	268.9	8.5	269.5	8.8	262.3	6.3
G42	23	485	0.0416	0.0005	0.3012	0.0055	0.0512	0.0007	262.5	6.3	267.3	8.6	251.2	8.6	262.5	6.3
G83	17	409	0.0419	0.0005	0.3356	0.0067	0.0573	0.0009	264.7	6.6	293.9	10.3	503.1	15.0	264.7	6.6
G107	15	357	0.0421	0.0009	0.3270	0.0139	0.0565	0.0011	266.0	11.6	287.2	14.7	472.5	16.8	266.0	11.6
G78	12	278	0.0426	0.0005	0.3330	0.0065	0.0562	0.0009	268.9	6.6	291.9	10.0	461.1	13.8	268.9	6.6
G100	17	389	0.0429	0.0009	0.3526	0.0112	0.0593	0.0009	270.6	10.6	306.7	13.2	577.8	15.6	270.6	10.6
G84	28	664	0.0433	0.0005	0.3420	0.0058	0.0574	0.0007	273.2	6.5	298.7	9.1	505.4	12.5	273.2	6.5
G50	33	744	0.0437	0.0005	0.3039	0.0046	0.0509	0.0005	275.7	6.4	269.4	7.5	235.9	6.7	275.7	6.4
G67	11	239	0.0439	0.0005	0.3172	0.0062	0.0525	0.0008	277.0	6.7	279.8	9.7	308.1	10.6	277.0	6.7
G22	34	740	0.0451	0.0005	0.3382	0.0050	0.0542	0.0005	284.6	6.5	295.8	7.8	378.5	8.4	284.6	6.5
G93	26	497	0.0539	0.0007	0.4097	0.0337	0.0555	0.0034	338.5	8.2	348.6	37.1	432.8	45.5	338.5	8.2
G66	19	323	0.0566	0.0007	0.4194	0.0081	0.0542	0.0008	354.8	8.5	355.6	11.6	377.7	11.7	354.8	8.5
G28	14	215	0.0627	0.0008	0.4863	0.0104	0.0559	0.0009	392.0	9.6	402.4	13.8	448.8	14.4	392.0	9.6
G8	38	504	0.0677	0.0008	0.5400	0.0087	0.0574	0.0006	422.0	9.8	438.4	11.4	507.7	11.0	422.0	9.8
G86	34	434	0.0678	0.0008	0.5533	0.0100	0.0597	0.0008	422.7	10.0	447.2	13.1	592.7	14.2	422.7	10.0
G39	29	379	0.0689	0.0008	0.6199	0.0103	0.0637	0.0007	429.3	10.0	489.8	12.6	731.7	14.1	429.3	10.0
G99	17	226	0.0693	0.0056	0.5732	0.1499	0.0601	0.0012	431.8	66.9	460.1	61.2	607.5	21.1	431.8	66.9
G61	108	1566	0.0713	0.0008	0.5550	0.0077	0.0569	0.0005	443.7	10.1	448.2	10.6	488.8	8.9	443.7	10.1
G16	26	343	0.0716	0.0009	0.6498	0.0116	0.0642	0.0008	446.0	10.5	508.3	13.7	747.9	15.6	446.0	10.5
G27	28	329	0.0718	0.0009	0.6321	0.0114	0.0622	0.0008	446.7	10.6	497.4	13.7	682.4	15.1	446.7	10.6
G80	43	543	0.0727	0.0009	0.5674	0.0087	0.0563	0.0006	452.2	10.3	456.3	11.4	465.8	9.9	452.2	10.3
G106	14	165	0.0730	0.0039	0.6171	0.0741	0.0618	0.0009	454.3	47.1	488.0	43.4	668.6	16.8	454.3	47.1
G18	11	125	0.0767	0.0010	0.6655	0.0137	0.0627	0.0010	476.3	11.5	518.0	16.0	698.8	17.8	476.3	11.5

APPENDIX E (continued). U-Pb ZIRCON AGES OF SONG GIANH SEDIMENTS

Grain No.	Pb (ppm)	U (ppm)	Ratios						Ages (Ma)						Best Age (Ma)	± 2σ
			²⁰⁶ Pb/ ²³⁸ U	± 1 σ	²⁰⁷ Pb/ ²³⁵ U	± s.e.	²⁰⁷ Pb/ ²⁰⁶ Pb	± s.e.	²⁰⁶ Pb/ ²³⁸ U	± 2σ	²⁰⁷ Pb/ ²³⁵ U	± 2σ	²⁰⁷ Pb/ ²⁰⁶ Pb	± 2σ		
G1	27	341	0.0793	0.0010	0.7433	0.0117	0.0659	0.0007	491.8	11.3	564.3	13.3	803.2	11.1	491.8	11.3
G47	118	1072	0.0807	0.0009	0.6474	0.0088	0.0579	0.0005	500.0	11.2	506.9	11.2	527.1	8.9	500.0	11.2
G31	43	483	0.0868	0.0010	0.7953	0.0127	0.0656	0.0007	536.4	12.3	594.2	14.2	794.6	13.8	536.4	12.3
G102	46	519	0.0926	0.0006	0.9261	0.0074	0.0714	0.0009	570.7	6.5	665.6	13.9	969.7	18.6	570.7	6.5
G9	55	510	0.0987	0.0012	0.9467	0.0142	0.0695	0.0006	606.8	13.7	676.4	14.7	912.1	13.3	606.8	13.7
G32	36	334	0.1028	0.0013	0.9584	0.0168	0.0673	0.0008	630.9	14.6	682.5	16.7	847.4	15.7	630.9	14.6
G12	22	200	0.1063	0.0013	1.0576	0.0221	0.0692	0.0010	650.9	15.5	732.6	19.5	905.9	19.7	650.9	15.5
G24	30	238	0.1071	0.0013	0.9326	0.0170	0.0621	0.0008	655.9	15.1	669.0	16.7	678.2	14.5	655.9	15.1
G55	55	489	0.1113	0.0013	1.0117	0.0143	0.0653	0.0005	680.0	15.2	709.7	14.6	782.7	11.4	680.0	15.2
G89	47	416	0.1178	0.0035	1.0971	0.0941	0.0661	0.0012	717.9	40.0	751.9	36.5	808.3	22.8	717.9	40.0
G34	104	821	0.1212	0.0014	1.1835	0.0168	0.0705	0.0006	737.4	16.3	793.0	15.6	941.8	12.3	737.4	16.3
G6	39	252	0.1325	0.0016	1.2368	0.0209	0.0673	0.0007	802.3	18.1	817.4	17.8	847.4	14.3	802.3	18.1
G72	76	476	0.1349	0.0016	1.2444	0.0182	0.0667	0.0006	815.6	18.1	820.9	16.5	826.9	12.2	815.6	18.1
G94	30	180	0.1350	0.0018	1.4083	0.0211	0.0736	0.0006	816.4	20.6	892.5	18.3	1031.3	12.7	816.4	20.6
G17	49	305	0.1380	0.0016	1.2683	0.0193	0.0658	0.0006	833.6	18.5	831.6	16.6	799.4	12.1	833.6	18.5
G88	88	642	0.1423	0.0005	1.4041	0.0059	0.0723	0.0009	857.4	5.6	890.6	15.2	994.4	18.0	857.4	5.6
G60	113	801	0.1444	0.0017	1.4711	0.0212	0.0742	0.0006	869.6	19.2	918.6	17.4	1045.6	13.1	869.6	19.2
G49	79	520	0.1446	0.0017	1.4490	0.0224	0.0729	0.0007	870.7	19.4	909.5	18.0	1010.9	14.0	870.7	19.4
G71	95	609	0.1621	0.0019	1.5374	0.0216	0.0695	0.0006	968.7	21.1	945.5	17.6	912.1	12.1	912.1	12.1
G92	126	857	0.1542	0.0030	1.4932	0.0811	0.0709	0.0013	924.2	33.2	927.6	32.0	953.4	24.3	953.4	24.3
G37	102	632	0.1557	0.0018	1.5137	0.0211	0.0710	0.0006	932.6	20.3	935.9	17.2	956.5	12.0	956.5	12.0
G35	55	309	0.1584	0.0019	1.5798	0.0245	0.0712	0.0006	948.0	20.9	962.3	18.4	961.7	13.5	961.7	13.5
G41	58	287	0.1621	0.0019	1.6191	0.0246	0.0716	0.0006	968.5	21.3	977.6	18.4	973.7	13.4	973.7	13.4
G43	111	701	0.1664	0.0019	1.6636	0.0220	0.0719	0.0005	992.1	21.4	994.7	17.2	984.2	11.1	984.2	11.1
G68	22	106	0.1518	0.0019	1.5235	0.0317	0.0725	0.0010	911.0	21.2	939.9	22.5	1001.1	19.6	1001.1	19.6
G98	142	878	0.1625	0.0019	1.6113	0.0319	0.0730	0.0010	970.7	21.1	974.6	22.3	1015.1	19.4	1015.1	19.4
G63	56	325	0.1666	0.0020	1.7057	0.0263	0.0731	0.0007	993.5	21.8	1010.7	18.9	1016.7	14.0	1016.7	14.0
G44	69	362	0.1768	0.0021	1.8127	0.0274	0.0746	0.0006	1049.7	22.9	1050.1	19.1	1056.4	13.6	1056.4	13.6
G96	22	133	0.1535	0.0016	1.5877	0.0250	0.0747	0.0008	920.7	18.3	965.4	19.3	1061.2	17.2	1061.2	17.2
G45	192	1096	0.1755	0.0020	1.8680	0.0244	0.0768	0.0005	1042.6	22.4	1069.8	17.8	1115.0	11.7	1115.0	11.7

APPENDIX E (continued). U-Pb ZIRCON AGES OF SONG GIANH SEDIMENTS

Grain No.	Pb (ppm)	U (ppm)	Ratios						Ages (Ma)						Best Age (Ma)	$\pm 2\sigma$
			$^{206}\text{Pb}/^{238}\text{U}$	$\pm 1\sigma$	$^{207}\text{Pb}/^{235}\text{U}$	$\pm \text{s.e.}$	$^{207}\text{Pb}/^{206}\text{Pb}$	$\pm \text{s.e.}$	$^{206}\text{Pb}/^{238}\text{U}$	$\pm 2\sigma$	$^{207}\text{Pb}/^{235}\text{U}$	$\pm 2\sigma$	$^{207}\text{Pb}/^{206}\text{Pb}$	$\pm 2\sigma$		
G58	169	762	0.1886	0.0022	2.0015	0.0272	0.0769	0.0006	1113.8	23.9	1116.0	18.7	1118.6	12.4	1118.6	12.4
G85	85	435	0.1987	0.0023	2.1605	0.0302	0.0791	0.0006	1168.4	25.1	1168.4	19.7	1175.1	13.4	1175.1	13.4
G33	159	798	0.1857	0.0022	2.0667	0.0288	0.0799	0.0006	1098.3	23.7	1137.8	18.9	1194.0	12.7	1194.0	12.7
G108	71	348	0.1806	0.0020	1.9957	0.0478	0.0801	0.0012	1070.3	21.8	1114.0	25.2	1199.2	23.4	1199.2	23.4
G3	36	152	0.1923	0.0023	2.2006	0.0368	0.0809	0.0008	1134.0	24.9	1181.2	21.0	1219.3	15.5	1219.3	15.5
G48	86	462	0.1958	0.0023	2.3063	0.0348	0.0836	0.0007	1152.6	24.9	1214.2	20.3	1282.3	14.4	1282.3	14.4
G21	131	535	0.2343	0.0027	2.7977	0.0372	0.0854	0.0006	1357.2	28.5	1354.9	20.0	1325.5	12.2	1325.5	12.2
G13	22	78	0.2429	0.0030	3.0321	0.0663	0.0877	0.0011	1401.7	31.2	1415.7	26.1	1374.8	20.4	1374.8	20.4
G54	90	346	0.2319	0.0027	3.1385	0.0469	0.0960	0.0008	1344.2	28.6	1442.2	21.7	1548.6	14.9	1548.6	14.9
G95	75	238	0.2758	0.0007	3.6922	0.0071	0.0984	0.0007	1570.3	6.6	1569.7	12.2	1593.1	14.0	1593.1	14.0
G111	176	478	0.2987	0.0054	4.2748	0.1399	0.1054	0.0013	1685.0	53.4	1688.5	35.7	1720.8	22.2	1720.8	22.2
G65	138	484	0.2793	0.0033	4.0706	0.0550	0.1054	0.0008	1587.8	32.9	1648.4	22.3	1721.8	14.2	1721.8	14.2
G53	210	728	0.2849	0.0033	4.4170	0.0578	0.1123	0.0008	1616.1	33.3	1715.5	22.2	1837.6	13.7	1837.6	13.7
G56	82	208	0.3325	0.0039	5.2158	0.0786	0.1128	0.0009	1850.6	37.8	1855.2	23.8	1845.0	15.2	1845.0	15.2
G104	157	443	0.3337	0.0011	5.2176	0.0150	0.1129	0.0008	1856.4	10.7	1855.5	12.9	1846.9	14.0	1846.9	14.0
G70	130	357	0.3474	0.0041	5.6408	0.0796	0.1165	0.0009	1922.0	38.9	1922.4	23.8	1902.4	14.9	1902.4	14.9
G110	307	768	0.3607	0.0022	6.3038	0.0320	0.1287	0.0008	1985.7	20.4	2019.0	15.0	2079.6	13.2	2079.6	13.2
G19	51	122	0.3799	0.0045	6.7401	0.1110	0.1294	0.0010	2075.8	42.0	2077.9	25.0	2089.8	15.9	2089.8	15.9
G101	105	279	0.3520	0.0034	6.4326	0.0845	0.1333	0.0012	1944.2	32.8	2036.7	23.3	2141.5	18.3	2141.5	18.3
G59	99	248	0.3873	0.0046	7.1539	0.1114	0.1345	0.0010	2110.1	42.5	2130.8	25.0	2156.9	15.9	2156.9	15.9
G25	168	350	0.4106	0.0048	7.8631	0.1092	0.1362	0.0009	2217.7	43.8	2215.5	24.1	2178.9	14.2	2178.9	14.2
G20	253	515	0.4118	0.0048	7.9111	0.1031	0.1382	0.0009	2223.1	43.7	2220.9	23.8	2205.1	13.6	2205.1	13.6
G109	313	619	0.4595	0.0005	9.9962	0.0069	0.1593	0.0010	2437.5	4.8	2434.4	11.6	2447.9	13.7	2447.9	13.7
G38	83	137	0.4761	0.0056	10.8531	0.1762	0.1642	0.0012	2510.4	49.1	2510.6	25.7	2499.7	15.7	2499.7	15.7
G97	357	627	0.4756	0.0033	11.0497	0.0546	0.1653	0.0008	2508.2	28.4	2527.3	15.6	2510.2	11.5	2510.2	11.5
G23	98	178	0.4730	0.0056	11.1118	0.1786	0.1655	0.0012	2496.8	48.8	2532.5	25.6	2513.0	15.5	2513.0	15.5
G76	239	484	0.4406	0.0052	10.2452	0.1468	0.1672	0.0012	2353.1	46.2	2457.2	25.4	2529.8	15.7	2529.8	15.7
G91	174	243	0.6420	0.0005	22.5163	0.0046	0.2536	0.0006	3197.0	3.6	3206.3	5.0	3207.3	7.1	3207.3	7.1

Sample A50212061712 Rao Tro

APPENDIX E (continued). U-Pb ZIRCON AGES OF SONG GIANH SEDIMENTS

Grain No.	Pb (ppm)	U (ppm)	Ratios						Ages (Ma)						Best Age (Ma)	$\pm 2\sigma$
			$^{206}\text{Pb}/^{238}\text{U}$	$\pm 1\sigma$	$^{207}\text{Pb}/^{235}\text{U}$	$\pm \text{s.e.}$	$^{207}\text{Pb}/^{206}\text{Pb}$	$\pm \text{s.e.}$	$^{206}\text{Pb}/^{238}\text{U}$	$\pm 2\sigma$	$^{207}\text{Pb}/^{235}\text{U}$	$\pm 2\sigma$	$^{207}\text{Pb}/^{206}\text{Pb}$	$\pm 2\sigma$		
G44	25.7	668.3	0.0351	0.0005	0.2496	0.0071	0.0524	0.0014	222.1	5.7	226.2	11.9	300.7	16.9	222.1	5.73
G122	58.1	1706.1	0.0355	0.0005	0.2535	0.0050	0.0518	0.0009	225.0	5.6	229.4	8.9	274.4	11.9	225.0	5.60
G106	29.6	738.4	0.0358	0.0005	0.2543	0.0058	0.0512	0.0011	226.5	5.7	230.0	10.0	251.6	12.6	226.5	5.73
G98	7.3	179.4	0.0368	0.0005	0.2614	0.0107	0.0520	0.0020	233.2	6.7	235.8	17.2	284.1	22.1	233.2	6.71
G17	22.7	598.2	0.0372	0.0005	0.2786	0.0079	0.0539	0.0014	235.3	6.0	249.6	12.8	367.7	19.4	235.3	5.97
G49	12.0	326.6	0.0372	0.0005	0.2559	0.0108	0.0520	0.0020	235.7	6.7	231.4	17.7	283.2	22.6	235.7	6.71
G96	18.9	522.4	0.0373	0.0005	0.2655	0.0076	0.0521	0.0014	236.0	6.1	239.1	12.5	288.9	16.5	236.0	6.09
G66	10.3	263.4	0.0373	0.0005	0.2501	0.0092	0.0503	0.0017	236.1	6.5	226.7	15.3	210.3	16.2	236.1	6.46
G10	12.3	328.5	0.0374	0.0005	0.2407	0.0095	0.0508	0.0019	236.5	6.6	219.0	16.5	233.1	18.6	236.5	6.59
G129	22.0	590.0	0.0377	0.0005	0.2653	0.0067	0.0517	0.0012	238.7	6.1	238.9	11.2	272.2	14.1	238.7	6.09
G2	15.5	418.2	0.0378	0.0006	0.2714	0.0115	0.0538	0.0021	239.1	6.8	243.8	18.5	361.8	27.2	239.1	6.83
G90	50.0	1151.5	0.0379	0.0005	0.2703	0.0059	0.0510	0.0010	239.7	6.0	242.9	10.0	240.4	11.8	239.7	5.96
G73	28.6	728.3	0.0379	0.0005	0.2658	0.0062	0.0505	0.0011	239.9	6.0	239.3	10.4	219.4	11.7	239.9	5.96
G110	10.2	252.0	0.0379	0.0005	0.2557	0.0081	0.0512	0.0015	239.9	6.3	231.2	13.7	250.7	16.2	239.9	6.34
G118	38.5	875.5	0.0383	0.0005	0.2705	0.0065	0.0510	0.0011	242.2	6.1	243.1	10.7	242.6	12.6	242.2	6.08
G3	18.6	485.8	0.0387	0.0005	0.2688	0.0082	0.0508	0.0014	244.8	6.3	241.7	13.4	231.3	15.0	244.8	6.33
G35	17.6	444.7	0.0387	0.0005	0.2710	0.0098	0.0517	0.0017	244.9	6.6	243.5	15.8	271.7	19.3	244.9	6.58
G88	13.6	354.4	0.0389	0.0005	0.2627	0.0082	0.0507	0.0014	245.7	6.5	236.8	13.6	227.2	15.0	245.7	6.45
G94	11.5	297.5	0.0389	0.0005	0.2735	0.0080	0.0525	0.0014	246.3	6.5	245.5	13.2	305.1	17.4	246.3	6.45
G12	24.9	659.5	0.0390	0.0005	0.2732	0.0082	0.0514	0.0014	246.3	6.3	245.2	13.3	259.3	15.9	246.3	6.33
G77	60.0	1244.4	0.0390	0.0005	0.2785	0.0055	0.0524	0.0009	246.7	6.0	249.4	9.6	303.3	12.6	246.7	5.96
G79	10.1	264.0	0.0391	0.0005	0.2584	0.0083	0.0504	0.0015	247.3	6.6	233.4	14.0	212.6	14.6	247.3	6.58
G102	18.6	463.6	0.0391	0.0005	0.2648	0.0072	0.0509	0.0013	247.4	6.3	238.5	12.2	234.5	13.8	247.4	6.33
G1	38.5	863.5	0.0392	0.0005	0.2899	0.0061	0.0538	0.0010	247.6	6.0	258.5	10.4	362.3	15.1	247.6	5.96
G119	12.0	291.8	0.0392	0.0005	0.2643	0.0079	0.0509	0.0014	247.6	6.5	238.1	13.2	234.0	14.7	247.6	6.45
G116	11.1	283.6	0.0392	0.0005	0.2697	0.0082	0.0520	0.0014	248.1	6.6	242.4	13.7	286.7	17.2	248.1	6.58
G81	11.7	293.1	0.0394	0.0005	0.2743	0.0078	0.0520	0.0014	248.8	6.5	246.1	13.0	286.7	16.4	248.8	6.45
G95	13.8	348.7	0.0394	0.0005	0.2633	0.0078	0.0500	0.0014	248.9	6.5	237.3	13.0	195.9	13.0	248.9	6.45
G5	12.5	306.4	0.0395	0.0005	0.2702	0.0098	0.0504	0.0017	249.4	6.7	242.9	15.7	213.0	16.1	249.4	6.70

APPENDIX E (continued). U-Pb ZIRCON AGES OF SONG GIANH SEDIMENTS

Grain No.	Pb (ppm)	U (ppm)	Ratios						Ages (Ma)						Best Age (Ma)	± 2σ
			²⁰⁶ Pb/ ²³⁸ U	± 1 σ	²⁰⁷ Pb/ ²³⁵ U	± s.e.	²⁰⁷ Pb/ ²⁰⁶ Pb	± s.e.	²⁰⁶ Pb/ ²³⁸ U	± 2σ	²⁰⁷ Pb/ ²³⁵ U	± 2σ	²⁰⁷ Pb/ ²⁰⁶ Pb	± 2σ		
G33	12.9	325.9	0.0396	0.0005	0.2829	0.0084	0.0529	0.0014	250.1	6.4	252.9	13.7	322.4	18.3	250.1	6.45
G58	18.6	432.7	0.0396	0.0005	0.2799	0.0074	0.0524	0.0013	250.4	6.3	250.6	12.3	300.7	15.9	250.4	6.32
G62	20.2	509.8	0.0396	0.0005	0.2776	0.0070	0.0518	0.0012	250.4	6.3	248.7	11.8	277.0	14.5	250.4	6.32
G113	11.8	298.1	0.0397	0.0005	0.2742	0.0080	0.0519	0.0014	250.7	6.6	246.1	13.3	278.8	16.3	250.7	6.57
G74	10.9	274.1	0.0398	0.0005	0.2724	0.0082	0.0518	0.0014	251.8	6.6	244.6	13.7	274.8	16.6	251.8	6.57
G127	55.0	1168.6	0.0399	0.0005	0.2816	0.0062	0.0512	0.0010	252.0	6.3	251.9	10.4	248.5	12.0	252.0	6.32
G64	37.1	974.7	0.0399	0.0005	0.2804	0.0060	0.0509	0.0010	252.2	6.2	251.0	10.1	237.7	11.5	252.2	6.20
G128	22.3	581.1	0.0401	0.0005	0.2859	0.0070	0.0522	0.0011	253.1	6.4	255.3	11.5	294.2	14.6	253.1	6.45
G100	13.5	343.0	0.0401	0.0006	0.2725	0.0116	0.0514	0.0020	253.5	7.3	244.7	18.7	260.1	21.2	253.5	7.31
G34	13.3	312.7	0.0401	0.0005	0.2885	0.0083	0.0538	0.0014	253.7	6.4	257.3	13.6	361.0	19.3	253.7	6.45
G126	14.0	352.5	0.0402	0.0005	0.2749	0.0078	0.0513	0.0013	254.1	6.6	246.6	13.0	254.3	15.0	254.1	6.57
G7	15.3	386.6	0.0402	0.0005	0.2838	0.0078	0.0521	0.0013	254.3	6.4	253.6	12.8	289.4	16.0	254.3	6.44
G32	12.8	308.3	0.0404	0.0005	0.2821	0.0080	0.0528	0.0014	255.1	6.4	252.3	13.3	321.1	17.6	255.1	6.44
G63	23.1	575.5	0.0404	0.0005	0.2838	0.0069	0.0511	0.0011	255.1	6.3	253.7	11.3	244.9	12.9	255.1	6.32
G123	12.7	309.5	0.0405	0.0005	0.2704	0.0077	0.0509	0.0013	255.7	6.7	243.0	13.0	234.0	14.2	255.7	6.69
G39	14.9	332.9	0.0406	0.0005	0.2835	0.0085	0.0524	0.0014	256.6	6.6	253.4	13.9	304.6	17.8	256.6	6.57
G76	12.3	299.4	0.0406	0.0005	0.2678	0.0083	0.0502	0.0014	256.7	6.7	240.9	13.9	202.4	13.8	256.7	6.69
G69	12.4	305.7	0.0407	0.0006	0.2717	0.0103	0.0510	0.0018	256.9	7.1	244.0	16.8	239.0	18.1	256.9	7.06
G108	14.3	352.5	0.0408	0.0005	0.2805	0.0078	0.0519	0.0013	257.8	6.7	251.1	13.0	280.1	15.7	257.8	6.69
G87	17.2	416.3	0.0408	0.0005	0.2718	0.0074	0.0505	0.0013	257.9	6.6	244.1	12.6	219.9	13.2	257.9	6.57
G82	12.8	320.3	0.0409	0.0005	0.2879	0.0084	0.0531	0.0014	258.3	6.7	256.9	13.9	330.9	18.4	258.3	6.69
G46	16.4	410.0	0.0410	0.0005	0.2911	0.0076	0.0527	0.0012	258.8	6.6	259.4	12.5	316.3	16.2	258.8	6.56
G4	13.6	329.1	0.0410	0.0005	0.2848	0.0086	0.0514	0.0014	259.2	6.6	254.4	13.9	257.9	15.9	259.2	6.56
G15	9.2	212.2	0.0411	0.0006	0.2767	0.0143	0.0497	0.0024	259.3	7.9	248.0	22.3	181.5	19.2	259.3	7.93
G84	19.4	484.5	0.0411	0.0006	0.3017	0.0095	0.0543	0.0015	259.7	6.8	267.7	15.0	385.2	21.6	259.7	6.81
G31	11.7	279.2	0.0412	0.0005	0.2977	0.0087	0.0546	0.0014	260.0	6.7	264.6	14.1	395.9	20.7	260.0	6.69
G83	8.4	191.4	0.0412	0.0006	0.2919	0.0096	0.0532	0.0016	260.0	6.9	260.0	15.5	335.6	20.5	260.0	6.93
G47	10.6	243.8	0.0413	0.0006	0.2872	0.0097	0.0518	0.0016	260.9	6.9	256.3	15.6	274.4	18.3	260.9	6.93
G89	21.5	546.4	0.0413	0.0005	0.2880	0.0069	0.0521	0.0011	261.1	6.6	257.0	11.6	290.2	14.3	261.1	6.56
G45	15.6	347.4	0.0413	0.0006	0.3013	0.0109	0.0539	0.0018	261.1	7.1	267.4	17.1	368.1	23.8	261.1	7.06

APPENDIX E (continued). U-Pb ZIRCON AGES OF SONG GIANH SEDIMENTS

Grain No.	Pb (ppm)	U (ppm)	Ratios						Ages (Ma)						Best Age (Ma)	$\pm 2\sigma$
			$^{206}\text{Pb}/^{238}\text{U}$	$\pm 1\sigma$	$^{207}\text{Pb}/^{235}\text{U}$	$\pm \text{s.e.}$	$^{207}\text{Pb}/^{206}\text{Pb}$	$\pm \text{s.e.}$	$^{206}\text{Pb}/^{238}\text{U}$	$\pm 2\sigma$	$^{207}\text{Pb}/^{235}\text{U}$	$\pm 2\sigma$	$^{207}\text{Pb}/^{206}\text{Pb}$	$\pm 2\sigma$		
G40	16.2	398.6	0.0414	0.0006	0.3094	0.0100	0.0567	0.0017	261.3	6.9	273.7	16.1	481.1	26.0	261.3	6.93
G60	12.5	303.2	0.0414	0.0006	0.2817	0.0086	0.0521	0.0015	261.4	6.8	252.0	14.4	290.2	17.4	261.4	6.81
G9	11.3	267.2	0.0415	0.0006	0.3098	0.0098	0.0545	0.0016	262.2	6.8	274.0	15.2	392.2	22.0	262.2	6.81
G43	14.2	341.1	0.0416	0.0006	0.2829	0.0085	0.0514	0.0014	262.5	6.8	252.9	14.0	260.6	15.9	262.5	6.81
G28	23.4	547.0	0.0416	0.0005	0.3544	0.0100	0.0620	0.0016	262.7	6.7	308.0	15.2	675.1	28.4	262.7	6.68
G25	16.3	389.1	0.0417	0.0005	0.2983	0.0081	0.0534	0.0013	263.4	6.7	265.0	13.2	346.3	17.8	263.4	6.68
G18	14.2	334.8	0.0419	0.0005	0.2971	0.0084	0.0528	0.0014	264.4	6.7	264.1	13.7	318.5	17.5	264.4	6.68
G101	14.2	332.9	0.0421	0.0006	0.2886	0.0088	0.0514	0.0014	265.7	6.9	257.4	14.2	258.4	15.9	265.7	6.93
G14	15.1	355.0	0.0421	0.0005	0.2934	0.0084	0.0516	0.0013	266.0	6.7	261.2	13.6	266.8	15.6	266.0	6.68
G70	11.0	245.1	0.0422	0.0006	0.2746	0.0110	0.0507	0.0019	266.7	7.4	246.3	18.2	226.3	18.3	266.7	7.42
G42	18.2	441.5	0.0423	0.0005	0.2842	0.0076	0.0502	0.0012	266.9	6.7	254.0	12.5	203.8	12.3	266.9	6.68
G29	10.9	259.0	0.0424	0.0006	0.3302	0.0122	0.0577	0.0019	267.7	7.3	289.7	18.5	519.1	30.4	267.7	7.30
G125	10.8	251.4	0.0426	0.0006	0.3192	0.0125	0.0582	0.0021	268.8	7.7	281.3	19.8	536.2	32.9	268.8	7.67
G36	14.3	337.3	0.0426	0.0006	0.2968	0.0084	0.0524	0.0014	269.2	6.8	263.9	13.8	302.0	16.9	269.2	6.80
G6	16.2	373.9	0.0430	0.0006	0.2971	0.0098	0.0511	0.0015	271.2	7.0	264.2	15.5	244.9	16.5	271.2	7.05
G105	13.4	307.6	0.0430	0.0006	0.3122	0.0122	0.0559	0.0020	271.5	7.7	275.9	19.3	449.6	29.0	271.5	7.66
G67	56.4	1401.0	0.0432	0.0005	0.3007	0.0056	0.0504	0.0008	272.4	6.6	266.9	9.6	212.6	9.7	272.4	6.55
G20	19.0	442.8	0.0435	0.0006	0.3030	0.0110	0.0521	0.0017	274.4	7.4	268.7	17.2	287.6	19.9	274.4	7.41
G38	14.1	319.6	0.0438	0.0006	0.3455	0.0128	0.0587	0.0020	276.5	7.7	301.3	19.2	557.1	31.9	276.5	7.66
G50	12.5	283.0	0.0443	0.0006	0.3312	0.0133	0.0544	0.0020	279.1	7.9	290.5	19.8	388.5	26.9	279.1	7.90
G68	16.1	312.7	0.0445	0.0006	0.3616	0.0127	0.0611	0.0019	280.5	7.7	313.4	19.0	643.1	33.3	280.5	7.65
G53	13.0	310.8	0.0446	0.0006	0.3767	0.0108	0.0640	0.0016	281.4	7.3	324.6	16.5	742.3	30.4	281.4	7.28
G41	28.3	626.6	0.0452	0.0006	0.3148	0.0094	0.0512	0.0014	284.7	7.3	277.9	14.8	251.2	15.5	284.7	7.28
G22	13.5	292.5	0.0466	0.0006	0.3773	0.0131	0.0599	0.0019	293.5	7.9	325.1	19.1	599.6	31.4	293.5	7.88
G23	13.7	289.3	0.0466	0.0006	0.3436	0.0117	0.0544	0.0017	293.6	7.8	299.9	17.6	386.4	23.0	293.6	7.76
G71	46.5	1016.4	0.0469	0.0006	0.4020	0.0093	0.0626	0.0013	295.2	7.4	343.1	14.0	694.7	23.8	295.2	7.39
G93	12.7	251.4	0.0493	0.0007	0.3488	0.0108	0.0540	0.0015	310.0	8.1	303.8	16.8	371.5	20.7	310.0	8.11
G55	14.5	271.6	0.0531	0.0007	0.4181	0.0130	0.0581	0.0016	333.6	8.7	354.7	18.5	531.6	26.1	333.6	8.69
G13	29.4	495.9	0.0535	0.0007	0.3845	0.0087	0.0533	0.0011	335.7	8.1	330.3	13.5	340.3	15.0	335.7	8.08
G115	18.4	333.5	0.0539	0.0007	0.3908	0.0116	0.0558	0.0015	338.2	8.8	334.9	17.5	443.2	22.2	338.2	8.81

APPENDIX E (continued). U-Pb ZIRCON AGES OF SONG GIANH SEDIMENTS

Grain No.	Pb (ppm)	U (ppm)	Ratios						Ages (Ma)						Best Age (Ma)	$\pm 2\sigma$
			$^{206}\text{Pb}/^{238}\text{U}$	$\pm 1\sigma$	$^{207}\text{Pb}/^{235}\text{U}$	$\pm \text{s.e.}$	$^{207}\text{Pb}/^{206}\text{Pb}$	$\pm \text{s.e.}$	$^{206}\text{Pb}/^{238}\text{U}$	$\pm 2\sigma$	$^{207}\text{Pb}/^{235}\text{U}$	$\pm 2\sigma$	$^{207}\text{Pb}/^{206}\text{Pb}$	$\pm 2\sigma$		
G92	17.6	332.3	0.0542	0.0007	0.4234	0.0133	0.0587	0.0016	340.4	8.9	358.5	19.0	557.1	27.1	340.4	8.93
G117	44.6	739.7	0.0566	0.0007	0.4169	0.0089	0.0534	0.0010	354.7	8.8	353.8	13.5	346.3	14.4	354.7	8.79
G72	73.9	1213.4	0.0588	0.0007	0.4527	0.0100	0.0549	0.0011	368.1	9.0	379.2	14.4	409.4	16.4	368.1	9.01
G86	9.9	140.2	0.0623	0.0009	0.4596	0.0217	0.0544	0.0022	389.5	11.4	384.0	28.2	388.5	29.9	389.5	11.41
G103	33.0	450.4	0.0696	0.0009	0.5394	0.0126	0.0561	0.0011	433.7	10.7	438.0	17.0	455.1	18.2	433.7	10.73
G11	51.6	553.3	0.0731	0.0009	0.5732	0.0116	0.0568	0.0010	454.5	10.7	460.1	15.6	483.8	16.7	454.5	10.69
G56	20.5	232.5	0.0746	0.0010	0.5514	0.0158	0.0574	0.0014	463.8	11.6	445.9	20.8	505.0	22.8	463.8	11.64
G124	23.7	214.1	0.0795	0.0011	0.5911	0.0179	0.0567	0.0015	492.9	12.7	471.6	22.4	479.5	22.9	492.9	12.66
G75	11.9	132.0	0.0797	0.0012	0.5897	0.0246	0.0575	0.0020	494.0	13.7	470.7	29.9	509.6	31.6	494.0	13.73
G97	20.1	236.2	0.0805	0.0010	0.6786	0.0174	0.0656	0.0014	499.1	12.4	525.9	21.6	793.0	27.2	499.1	12.41
G109	78.3	621.6	0.0814	0.0010	0.6406	0.0131	0.0575	0.0010	504.4	12.2	502.7	17.2	511.1	17.5	504.4	12.16
G30	65.7	648.7	0.0851	0.0011	0.7797	0.0172	0.0663	0.0012	526.2	12.6	585.3	19.6	814.3	23.9	526.2	12.60
G114	37.2	408.7	0.0912	0.0012	0.7708	0.0204	0.0665	0.0015	562.7	14.1	580.2	23.6	821.2	28.1	562.7	14.06
G48	116.7	1234.9	0.1006	0.0012	0.9261	0.0181	0.0665	0.0011	618.1	14.5	665.6	19.9	822.8	21.7	618.1	14.53
G99	18.3	145.9	0.1089	0.0015	0.9525	0.0364	0.0653	0.0020	666.5	17.8	679.4	33.3	784.3	36.2	666.5	17.79
G121	46.3	410.0	0.1129	0.0015	1.0675	0.0272	0.0719	0.0015	689.8	17.0	737.5	26.0	982.8	29.1	689.8	17.03
G65	54.3	500.9	0.1130	0.0014	1.0624	0.0251	0.0703	0.0013	690.2	16.6	735.0	24.2	937.7	26.6	690.2	16.56
G80	129.7	1090.3	0.1173	0.0015	1.2099	0.0223	0.0743	0.0011	714.8	16.7	805.1	21.7	1049.1	23.3	714.8	16.73
G51	41.6	341.1	0.1194	0.0015	1.0701	0.0262	0.0680	0.0013	727.0	17.4	738.8	24.7	867.9	25.9	727.0	17.39
G54	39.2	253.3	0.1285	0.0017	1.2317	0.0384	0.0709	0.0017	779.4	19.3	815.1	30.5	954.8	32.5	779.4	19.31
G85	37.2	267.8	0.1298	0.0017	1.1432	0.0316	0.0657	0.0014	786.6	19.2	774.0	27.5	795.2	27.1	786.6	19.17
G112	86.7	694.8	0.1306	0.0017	1.2171	0.0270	0.0686	0.0012	791.3	18.8	808.5	24.6	887.0	24.6	791.3	18.82
G104	57.6	379.6	0.1367	0.0018	1.2147	0.0297	0.0665	0.0013	825.7	19.8	807.4	26.1	820.9	25.1	825.7	19.85
G120	86.1	644.9	0.1373	0.0017	1.3682	0.0265	0.0725	0.0012	829.2	19.5	875.4	24.0	1000.8	23.9	829.2	19.50
G19	169.3	1238.1	0.1412	0.0017	1.3738	0.0227	0.0712	0.0010	851.6	19.1	877.8	21.4	962.9	20.3	851.6	19.09
G61	213.5	1476.2	0.1533	0.0019	1.4744	0.0239	0.0692	0.0009	919.5	20.8	919.9	22.0	903.2	19.7	903.2	19.66
G78	14.0	85.9	0.1535	0.0020	1.4266	0.0430	0.0709	0.0016	920.6	22.5	900.1	31.5	955.1	31.0	955.1	30.98
G59	104.7	572.9	0.1623	0.0020	1.5780	0.0294	0.0712	0.0011	969.7	22.1	961.6	24.1	962.0	21.9	962.0	21.92
G16	128.0	763.1	0.1523	0.0018	1.5033	0.0266	0.0714	0.0010	914.0	20.5	931.7	22.7	968.9	21.2	968.9	21.24
G107	50.7	327.8	0.1569	0.0020	1.5034	0.0319	0.0720	0.0012	939.7	22.0	931.8	26.1	986.8	24.8	986.8	24.78

APPENDIX E (continued). U-Pb ZIRCON AGES OF SONG GIANH SEDIMENTS

Grain No.	Pb (ppm)	U (ppm)	Ratios						Ages (Ma)						Best Age (Ma)	± 2σ
			²⁰⁶ Pb/ ²³⁸ U	± 1 σ	²⁰⁷ Pb/ ²³⁵ U	± s.e.	²⁰⁷ Pb/ ²⁰⁶ Pb	± s.e.	²⁰⁶ Pb/ ²³⁸ U	± 2σ	²⁰⁷ Pb/ ²³⁵ U	± 2σ	²⁰⁷ Pb/ ²⁰⁶ Pb	± 2σ		
G8	65.7	328.5	0.1781	0.0022	1.7612	0.0446	0.0743	0.0014	1056.5	24.3	1031.3	29.0	1050.4	27.4	1050.4	27.35
G91	156.4	935.5	0.1579	0.0020	1.6517	0.0343	0.0758	0.0012	945.3	21.9	990.2	26.0	1088.7	25.3	1088.7	25.26
G111	179.7	1006.9	0.1714	0.0022	1.7733	0.0372	0.0766	0.0013	1019.7	23.8	1035.7	27.2	1109.5	25.8	1109.5	25.79
G37	247.9	668.9	0.3360	0.0041	5.3614	0.0942	0.1159	0.0015	1867.3	39.2	1878.7	30.5	1893.1	25.9	1893.1	25.91
G27	242.4	583.0	0.3869	0.0047	8.2790	0.1537	0.1585	0.0020	2108.2	43.4	2262.0	32.0	2439.5	27.2	2439.5	27.17
G57	25.0	38.5	0.4622	0.0067	10.1142	0.5421	0.1675	0.0037	2449.4	58.7	2445.3	48.5	2533.0	44.0	2533.0	43.99
G21	1455.1	2587.3	0.5117	0.0061	12.8844	0.1871	0.1793	0.0022	2663.7	51.9	2671.2	31.8	2646.4	26.0	2646.4	25.95
G52	488.0	790.2	0.5184	0.0063	14.0648	0.2253	0.1951	0.0025	2692.6	53.2	2754.1	33.2	2785.8	27.5	2785.8	27.55
G26	75.4	113.7	0.5371	0.0069	14.5178	0.5419	0.1975	0.0031	2771.3	58.2	2784.2	38.8	2805.7	33.5	2805.7	33.45
G24	49.6	78.3	0.6043	0.0076	19.9798	0.6606	0.2411	0.0034	3047.0	61.3	3090.4	36.9	3127.4	31.0	3127.4	31.04
Sample 14052705 Song Trac																
G68	66.8	2613.8	0.0236	0.0003	0.1620	0.0031	0.0498	0.0009	150.4	3.7	152.5	6.3	185.7	6.3	150.4	3.7
G11	8.3	328.5	0.0240	0.0003	0.1655	0.0056	0.0499	0.0017	153.1	4.0	155.5	10.5	192.2	11.9	153.1	4.0
G31	8.7	347.4	0.0248	0.0003	0.1676	0.0061	0.0491	0.0018	157.8	4.3	157.3	11.4	150.2	10.2	157.8	4.3
G57	8.1	274.1	0.0292	0.0004	0.2289	0.0099	0.0568	0.0025	185.7	5.5	209.3	17.5	484.6	33.8	185.7	5.5
G121	10.8	274.8	0.0356	0.0005	0.2558	0.0100	0.0522	0.0021	225.3	6.5	231.2	17.3	292.9	20.0	225.3	6.5
G14	11.9	304.5	0.0358	0.0005	0.2577	0.0076	0.0523	0.0015	226.6	5.7	232.8	13.4	297.7	15.2	226.6	5.7
G51	56.3	1308.2	0.0362	0.0005	0.2864	0.0063	0.0574	0.0012	229.3	5.6	255.7	11.3	506.2	17.2	229.3	5.6
G119	15.4	272.2	0.0364	0.0006	0.2548	0.0112	0.0507	0.0023	230.7	7.0	230.5	19.4	228.1	18.1	230.7	7.0
G55	21.8	507.2	0.0367	0.0005	0.2539	0.0069	0.0502	0.0013	232.5	5.8	229.7	12.2	202.4	9.8	232.5	5.8
G112	22.6	530.0	0.0382	0.0005	0.2739	0.0076	0.0520	0.0014	241.7	6.3	245.8	13.3	285.4	13.6	241.7	6.3
G102	18.8	406.8	0.0383	0.0005	0.2734	0.0083	0.0518	0.0016	242.2	6.5	245.4	14.4	277.5	14.6	242.2	6.5
G50	9.9	200.2	0.0390	0.0006	0.2749	0.0102	0.0512	0.0019	246.6	6.8	246.6	17.6	247.6	16.5	246.6	6.8
G58	20.1	420.1	0.0398	0.0005	0.2831	0.0077	0.0517	0.0014	251.3	6.3	253.1	13.4	271.3	12.9	251.3	6.3
G60	26.9	575.5	0.0401	0.0005	0.2866	0.0070	0.0519	0.0013	253.1	6.3	255.9	12.4	281.9	11.9	253.1	6.3
G98	6.8	151.0	0.0402	0.0006	0.3001	0.0123	0.0542	0.0022	253.9	7.4	266.5	20.6	379.0	26.1	253.9	7.4
G7	32.0	656.9	0.0421	0.0005	0.3218	0.0082	0.0555	0.0014	265.8	6.6	283.3	14.0	430.8	17.7	265.8	6.6
G3	16.8	334.8	0.0436	0.0005	0.3230	0.0081	0.0538	0.0014	275.0	6.7	284.2	13.9	361.4	15.3	275.0	6.7
G84	2.7	54.3	0.0436	0.0009	0.3610	0.0275	0.0601	0.0047	275.0	11.4	312.9	43.3	606.8	70.9	275.0	11.4

APPENDIX E (continued). U-Pb ZIRCON AGES OF SONG GIANH SEDIMENTS

Grain No.	Pb (ppm)	U (ppm)	Ratios						Ages (Ma)						Best Age (Ma)	$\pm 2\sigma$
			$^{206}\text{Pb}/^{238}\text{U}$	$\pm 1\sigma$	$^{207}\text{Pb}/^{235}\text{U}$	$\pm \text{s.e.}$	$^{207}\text{Pb}/^{206}\text{Pb}$	$\pm \text{s.e.}$	$^{206}\text{Pb}/^{238}\text{U}$	$\pm 2\sigma$	$^{207}\text{Pb}/^{235}\text{U}$	$\pm 2\sigma$	$^{207}\text{Pb}/^{206}\text{Pb}$	$\pm 2\sigma$		
G118	11.7	212.2	0.0477	0.0008	0.3445	0.0161	0.0524	0.0025	300.3	9.2	300.6	25.9	303.8	24.7	300.3	9.2
G106	23.2	445.3	0.0485	0.0006	0.3565	0.0096	0.0533	0.0014	305.3	7.9	309.6	15.9	342.9	15.5	305.3	7.9
G115	2.4	37.9	0.0487	0.0013	0.3595	0.0385	0.0536	0.0058	306.2	15.4	311.8	60.1	354.7	65.2	306.2	15.4
G123	12.4	202.8	0.0498	0.0008	0.3860	0.0161	0.0562	0.0024	313.5	9.3	331.5	25.2	460.7	31.0	313.5	9.3
G107	21.4	393.5	0.0517	0.0007	0.3911	0.0105	0.0548	0.0015	325.2	8.3	335.2	16.9	405.7	17.7	325.2	8.3
G99	47.1	879.3	0.0571	0.0007	0.4339	0.0091	0.0551	0.0011	357.9	8.8	365.9	14.6	417.5	13.8	357.9	8.8
G35	49.4	778.2	0.0614	0.0007	0.4741	0.0090	0.0560	0.0010	384.2	9.0	394.0	14.4	452.8	13.4	384.2	9.0
G13	43.5	668.9	0.0626	0.0008	0.4770	0.0088	0.0553	0.0010	391.2	9.1	396.0	14.1	424.8	12.4	391.2	9.1
G43	75.5	1142.7	0.0639	0.0008	0.4888	0.0088	0.0555	0.0010	399.5	9.3	404.1	14.0	431.2	12.0	399.5	9.3
G30	43.8	610.8	0.0645	0.0008	0.4949	0.0098	0.0557	0.0011	402.8	9.4	408.2	15.4	439.6	13.8	402.8	9.4
G69	12.1	329.1	0.0647	0.0008	0.4994	0.0122	0.0560	0.0013	404.4	10.1	411.3	18.4	450.8	17.4	404.4	10.1
G38	58.3	708.7	0.0656	0.0008	0.5017	0.0096	0.0555	0.0010	409.7	9.6	412.9	15.0	431.6	13.1	409.7	9.6
G79	44.2	578.6	0.0657	0.0008	0.5050	0.0110	0.0558	0.0012	410.0	9.9	415.1	16.7	444.0	15.2	410.0	9.9
G53	55.9	826.2	0.0661	0.0008	0.5060	0.0120	0.0556	0.0013	412.3	10.0	415.8	18.1	435.6	16.6	412.3	10.0
G104	27.3	339.2	0.0661	0.0009	0.5125	0.0151	0.0563	0.0016	412.6	10.8	420.1	22.1	462.6	21.7	412.6	10.8
G86	49.1	698.0	0.0663	0.0008	0.5066	0.0108	0.0554	0.0011	413.8	10.0	416.1	16.4	429.6	14.4	413.8	10.0
G96	73.6	1074.5	0.0670	0.0008	0.5009	0.0101	0.0542	0.0010	418.3	10.1	412.3	15.5	379.4	12.1	418.3	10.1
G81	40.9	546.4	0.0675	0.0009	0.6053	0.0142	0.0651	0.0015	421.1	10.5	480.6	20.2	776.3	25.0	421.1	10.5
G117	33.5	416.3	0.0679	0.0009	0.5306	0.0162	0.0567	0.0017	423.2	11.2	432.2	23.3	481.1	23.1	423.2	11.2
G100	40.4	560.9	0.0685	0.0009	0.5289	0.0128	0.0560	0.0013	426.9	10.6	431.1	18.9	454.0	17.2	426.9	10.6
G92	22.6	299.4	0.0685	0.0009	0.5269	0.0137	0.0558	0.0014	427.1	10.7	429.7	20.0	444.4	18.3	427.1	10.7
G54	35.5	398.0	0.0693	0.0009	0.5184	0.0119	0.0543	0.0012	431.6	10.5	424.1	18.0	383.9	14.5	431.6	10.5
G77	11.0	137.1	0.0695	0.0010	0.5372	0.0179	0.0561	0.0019	433.3	11.6	436.6	25.6	454.7	24.5	433.3	11.6
G21	16.4	195.2	0.0701	0.0009	0.5330	0.0144	0.0552	0.0015	436.8	10.8	433.8	21.0	418.7	18.4	436.8	10.8
G124	40.5	483.2	0.0702	0.0010	0.5495	0.0166	0.0568	0.0017	437.1	11.6	444.7	23.6	484.9	22.9	437.1	11.6
G87	45.1	520.5	0.0728	0.0010	0.6280	0.0158	0.0626	0.0016	453.1	11.4	494.9	21.9	693.6	24.9	453.1	11.4
G65	22.2	300.0	0.0735	0.0009	0.5800	0.0143	0.0573	0.0014	457.1	11.3	464.5	20.5	501.9	19.2	457.1	11.3
G63	82.1	1039.1	0.0785	0.0010	0.6245	0.0113	0.0577	0.0010	487.0	11.4	492.7	16.4	519.9	14.0	487.0	11.4
G48	48.3	538.2	0.0787	0.0010	0.6143	0.0121	0.0566	0.0011	488.2	11.5	486.3	17.5	477.5	14.5	488.2	11.5
G46	11.8	137.7	0.0788	0.0011	0.6224	0.0192	0.0573	0.0018	488.8	12.7	491.4	26.2	503.9	24.5	488.8	12.7

APPENDIX E (continued). U-Pb ZIRCON AGES OF SONG GIANH SEDIMENTS

Grain No.	Pb (ppm)	U (ppm)	Ratios						Ages (Ma)						Best Age (Ma)	$\pm 2\sigma$
			$^{206}\text{Pb}/^{238}\text{U}$	$\pm 1\sigma$	$^{207}\text{Pb}/^{235}\text{U}$	$\pm \text{s.e.}$	$^{207}\text{Pb}/^{206}\text{Pb}$	$\pm \text{s.e.}$	$^{206}\text{Pb}/^{238}\text{U}$	$\pm 2\sigma$	$^{207}\text{Pb}/^{235}\text{U}$	$\pm 2\sigma$	$^{207}\text{Pb}/^{206}\text{Pb}$	$\pm 2\sigma$		
G23	24.8	229.3	0.0816	0.0010	0.6504	0.0158	0.0578	0.0014	505.8	12.3	508.7	21.7	522.6	19.6	505.8	12.3
G18	35.5	445.3	0.0850	0.0011	0.6919	0.0190	0.0591	0.0016	525.9	13.2	534.0	25.2	569.3	23.9	525.9	13.2
G12	43.7	413.1	0.0880	0.0011	0.7215	0.0138	0.0595	0.0011	543.9	12.6	551.6	18.9	584.0	16.6	543.9	12.6
G116	35.5	313.9	0.0894	0.0012	0.7374	0.0219	0.0598	0.0018	552.1	14.6	560.9	28.0	597.4	26.6	552.1	14.6
G25	65.7	708.7	0.0978	0.0012	0.8590	0.0176	0.0637	0.0013	601.3	14.1	629.6	22.1	733.0	21.0	601.3	14.1
G93	37.5	251.4	0.1194	0.0015	1.0511	0.0239	0.0639	0.0014	726.9	17.6	729.4	26.6	738.0	23.2	726.9	17.6
G70	23.4	159.8	0.1200	0.0016	1.1217	0.0293	0.0678	0.0018	730.7	18.3	763.8	31.3	862.4	30.2	730.7	18.3
G111	35.1	277.3	0.1208	0.0016	1.0569	0.0254	0.0635	0.0015	735.1	17.9	732.3	27.8	724.4	24.1	735.1	17.9
G28	72.4	533.8	0.1228	0.0015	1.1052	0.0188	0.0653	0.0011	746.8	16.9	755.9	21.5	783.4	17.7	746.8	16.9
G71	19.7	157.9	0.1236	0.0017	1.2937	0.0357	0.0760	0.0021	751.1	19.4	842.9	35.2	1093.8	36.9	751.1	19.4
G122	19.1	125.7	0.1242	0.0018	1.1064	0.0378	0.0647	0.0022	754.5	20.8	756.4	39.5	763.0	36.5	754.5	20.8
G66	67.3	343.0	0.1243	0.0016	1.1078	0.0240	0.0647	0.0014	755.4	18.0	757.1	26.2	763.0	22.6	755.4	18.0
G114	20.9	134.5	0.1279	0.0018	1.1675	0.0370	0.0662	0.0021	775.7	20.7	785.5	37.8	814.0	35.3	775.7	20.7
G59	58.2	399.8	0.1282	0.0016	1.1498	0.0218	0.0651	0.0012	777.8	17.9	777.1	23.8	776.0	19.7	777.8	17.9
G5	42.3	328.5	0.1329	0.0016	1.2644	0.0241	0.0690	0.0013	804.4	18.3	829.9	25.3	899.3	22.3	804.4	18.3
G125	25.9	158.5	0.1341	0.0020	1.1914	0.0440	0.0645	0.0024	810.9	23.0	796.6	44.0	757.4	39.4	810.9	23.0
G36	102.3	737.8	0.1358	0.0016	1.2980	0.0210	0.0694	0.0011	820.6	18.3	844.9	22.2	909.8	18.4	820.6	18.3
G91	52.8	264.0	0.1396	0.0020	1.2373	0.0385	0.0643	0.0020	842.6	22.2	817.7	38.3	751.2	33.0	842.6	22.2
G73	60.0	362.6	0.1409	0.0017	1.3360	0.0254	0.0688	0.0013	849.7	19.7	861.5	25.5	892.4	21.6	849.7	19.7
G8	85.2	534.4	0.1419	0.0017	1.3865	0.0243	0.0709	0.0012	855.6	19.1	883.2	24.4	954.0	20.9	855.6	19.1
G19	96.4	528.1	0.1446	0.0017	1.4607	0.0259	0.0733	0.0013	870.6	19.6	914.3	25.2	1022.3	22.0	870.6	19.6
G56	174.5	1271.5	0.1461	0.0018	1.4540	0.0253	0.0722	0.0012	879.0	19.9	911.5	24.7	991.9	21.0	879.0	19.9
G47	65.5	439.0	0.1478	0.0019	1.5507	0.0339	0.0761	0.0016	888.4	21.1	950.8	30.9	1098.8	28.9	888.4	21.1
G16	107.5	741.6	0.1479	0.0017	1.3996	0.0216	0.0687	0.0010	889.2	19.5	888.8	22.2	888.5	17.2	889.2	19.5
G34	55.2	314.6	0.1485	0.0019	1.4272	0.0327	0.0697	0.0016	892.7	21.2	900.4	31.0	919.8	27.4	892.7	21.2
G1	84.6	529.3	0.1498	0.0018	1.4734	0.0229	0.0714	0.0011	899.6	19.6	919.5	22.9	968.3	18.5	899.6	19.6
G113	147.6	1020.8	0.1498	0.0019	1.4492	0.0292	0.0702	0.0013	899.6	21.2	909.5	27.5	934.2	23.3	899.6	21.2
G101	45.7	256.5	0.1608	0.0021	1.5372	0.0333	0.0693	0.0015	961.4	22.8	945.4	30.1	908.9	25.1	908.9	25.1
G4	34.6	190.1	0.1571	0.0020	1.5207	0.0344	0.0702	0.0016	940.9	22.1	938.8	31.6	934.5	27.5	934.5	27.5
G6	33.5	193.9	0.1546	0.0020	1.5122	0.0346	0.0710	0.0016	926.7	21.8	935.3	31.7	956.5	28.1	956.5	28.1

APPENDIX E (continued). U-Pb ZIRCON AGES OF SONG GIANH SEDIMENTS

Grain No.	Pb (ppm)	U (ppm)	Ratios						Ages (Ma)						Best Age (Ma)	± 2σ
			²⁰⁶ Pb/ ²³⁸ U	± 1 σ	²⁰⁷ Pb/ ²³⁵ U	± s.e.	²⁰⁷ Pb/ ²⁰⁶ Pb	± s.e.	²⁰⁶ Pb/ ²³⁸ U	± 2σ	²⁰⁷ Pb/ ²³⁵ U	± 2σ	²⁰⁷ Pb/ ²⁰⁶ Pb	± 2σ		
G120	67.4	468.7	0.1535	0.0020	1.5021	0.0352	0.0710	0.0016	920.6	22.5	931.3	31.8	957.4	27.9	957.4	27.9
G52	44.2	241.3	0.1645	0.0020	1.6107	0.0313	0.0710	0.0013	981.6	22.5	974.4	28.1	958.6	23.2	958.6	23.2
G90	96.6	581.1	0.1592	0.0020	1.5653	0.0305	0.0713	0.0013	952.2	22.1	956.6	27.8	967.2	23.3	967.2	23.3
G85	27.4	138.3	0.1611	0.0021	1.6127	0.0382	0.0726	0.0017	963.0	23.3	975.2	33.3	1003.4	29.5	1003.4	29.5
G49	14.3	70.7	0.1718	0.0026	1.7597	0.0640	0.0743	0.0027	1021.7	28.7	1030.7	51.6	1050.4	48.3	1050.4	48.3
G33	195.8	891.3	0.1708	0.0021	1.7749	0.0299	0.0754	0.0012	1016.7	22.6	1036.3	26.0	1078.4	21.3	1078.4	21.3
G108	47.4	257.1	0.1726	0.0022	1.8343	0.0388	0.0771	0.0016	1026.2	24.2	1057.8	31.6	1124.3	27.7	1124.3	27.7
G82	92.3	445.3	0.1817	0.0023	1.9363	0.0394	0.0773	0.0015	1076.4	25.0	1093.7	31.3	1128.9	26.8	1128.9	26.8
G110	41.3	224.9	0.1689	0.0022	1.8344	0.0399	0.0788	0.0017	1006.3	23.9	1057.8	32.3	1166.6	29.1	1166.6	29.1
G105	86.3	411.2	0.1818	0.0023	2.0005	0.0396	0.0798	0.0015	1076.9	25.0	1115.7	30.6	1192.8	26.4	1192.8	26.4
G61	197.8	935.5	0.1969	0.0024	2.1938	0.0354	0.0808	0.0012	1158.5	25.4	1179.1	26.9	1217.6	21.4	1217.6	21.4
G9	82.4	442.8	0.1854	0.0022	2.0916	0.0366	0.0819	0.0014	1096.2	24.3	1146.1	28.6	1242.4	24.3	1242.4	24.3
G62	81.2	282.4	0.2329	0.0030	2.7114	0.0561	0.0845	0.0017	1349.8	30.8	1331.6	35.3	1302.9	29.6	1302.9	29.6
G17	19.8	61.9	0.2372	0.0031	2.9256	0.0651	0.0895	0.0020	1372.3	31.9	1388.6	38.8	1414.2	33.8	1414.2	33.8
G89	396.4	1399.8	0.2325	0.0029	2.9163	0.0505	0.0910	0.0015	1347.7	29.8	1386.2	30.7	1446.4	24.9	1446.4	24.9
G20	36.0	135.2	0.2395	0.0031	3.1196	0.0674	0.0945	0.0020	1384.3	32.0	1437.5	38.4	1517.7	33.7	1517.7	33.7
G24	267.0	1094.1	0.2571	0.0030	3.6097	0.0542	0.1019	0.0014	1475.1	31.1	1551.7	29.3	1658.3	23.1	1658.3	23.1
G76	31.9	98.5	0.2909	0.0040	4.1971	0.1001	0.1047	0.0025	1645.9	39.5	1673.5	44.7	1708.7	39.0	1708.7	39.0
G95	27.7	87.8	0.2946	0.0038	4.2830	0.0904	0.1055	0.0022	1664.2	38.1	1690.1	39.8	1722.9	33.8	1722.9	33.8
G45	14.4	43.0	0.2872	0.0039	4.2132	0.1013	0.1064	0.0026	1627.5	39.2	1676.6	45.2	1739.3	39.9	1739.3	39.9
G39	18.8	53.7	0.2736	0.0039	4.1530	0.1130	0.1101	0.0030	1558.9	39.9	1664.8	50.7	1801.7	46.2	1801.7	46.2
G26	160.7	451.6	0.3275	0.0039	5.0671	0.0797	0.1122	0.0017	1826.3	38.1	1830.6	32.4	1836.0	25.3	1836.0	25.3
G75	264.3	802.2	0.2982	0.0036	4.6669	0.0781	0.1135	0.0018	1682.4	36.1	1761.3	33.2	1856.8	26.7	1856.8	26.7
G42	130.1	341.7	0.3290	0.0040	5.1501	0.0841	0.1136	0.0018	1833.6	38.6	1844.4	33.4	1857.3	26.4	1857.3	26.4
G97	251.8	825.6	0.3162	0.0039	4.9694	0.0909	0.1140	0.0020	1771.1	38.6	1814.1	35.9	1864.5	29.3	1864.5	29.3
G41	260.2	761.2	0.3113	0.0037	4.8975	0.0757	0.1141	0.0017	1747.2	36.6	1801.8	31.6	1866.2	24.7	1866.2	24.7
G83	232.5	675.9	0.3227	0.0039	5.0779	0.0855	0.1142	0.0018	1803.0	38.3	1832.4	33.7	1866.7	26.8	1866.7	26.8
G32	280.6	750.4	0.3121	0.0037	4.9166	0.0740	0.1143	0.0016	1750.9	36.4	1805.1	31.1	1868.9	24.1	1868.9	24.1
G94	67.8	172.4	0.3044	0.0039	4.8036	0.0980	0.1145	0.0023	1712.9	38.8	1785.5	39.5	1872.0	33.6	1872.0	33.6
G29	124.9	357.5	0.3298	0.0040	5.2103	0.0832	0.1146	0.0017	1837.2	38.4	1854.3	33.0	1874.1	26.0	1874.1	26.0

APPENDIX E (continued). U-Pb ZIRCON AGES OF SONG GIANH SEDIMENTS

Grain No.	Pb (ppm)	U (ppm)	Ratios						Ages (Ma)						Best Age (Ma)	± 2σ
			²⁰⁶ Pb/ ²³⁸ U	± 1 σ	²⁰⁷ Pb/ ²³⁵ U	± s.e.	²⁰⁷ Pb/ ²⁰⁶ Pb	± s.e.	²⁰⁶ Pb/ ²³⁸ U	± 2σ	²⁰⁷ Pb/ ²³⁵ U	± 2σ	²⁰⁷ Pb/ ²⁰⁶ Pb	± 2σ		
G27	86.4	245.1	0.3307	0.0040	5.2437	0.0884	0.1151	0.0019	1841.7	39.0	1859.7	34.5	1880.7	27.7	1880.7	27.7
G88	127.5	350.6	0.3405	0.0042	5.5299	0.0963	0.1178	0.0019	1889.1	40.3	1905.2	35.1	1923.4	28.1	1923.4	28.1
G74	132.0	326.6	0.3515	0.0044	6.6105	0.1164	0.1364	0.0023	1941.8	41.7	2060.8	36.7	2182.5	30.0	2182.5	30.0
G37	42.1	85.9	0.3814	0.0051	7.9631	0.1640	0.1515	0.0031	2083.0	47.5	2226.9	43.9	2362.6	37.3	2362.6	37.3
G103	231.6	447.2	0.4533	0.0056	9.8865	0.1758	0.1582	0.0026	2410.0	49.8	2424.3	38.1	2436.8	30.6	2436.8	30.6
G109	129.3	219.2	0.4576	0.0057	10.2183	0.1889	0.1620	0.0028	2428.9	50.8	2454.7	39.5	2476.9	32.0	2476.9	32.0
G40	133.1	252.0	0.4634	0.0055	10.4233	0.1560	0.1632	0.0023	2454.7	48.6	2473.1	33.9	2488.9	25.8	2488.9	25.8
G67	81.9	186.3	0.4087	0.0053	9.2510	0.1718	0.1642	0.0029	2209.1	48.0	2363.2	40.4	2499.5	33.3	2499.5	33.3
G72	86.9	180.7	0.4339	0.0053	9.8587	0.1645	0.1649	0.0026	2323.1	47.8	2421.7	36.7	2506.0	29.1	2506.0	29.1
G80	116.6	230.6	0.4280	0.0053	9.7711	0.1651	0.1656	0.0026	2296.9	47.5	2413.4	36.9	2513.8	29.4	2513.8	29.4
G2	112.9	181.9	0.4608	0.0054	10.5946	0.1525	0.1668	0.0023	2442.9	47.7	2488.2	33.3	2526.0	25.2	2526.0	25.2
G44	152.0	349.3	0.4103	0.0049	9.4762	0.1430	0.1676	0.0024	2216.1	44.8	2385.2	33.8	2533.6	26.1	2533.6	26.1
G22	187.5	317.7	0.4785	0.0056	11.0734	0.1588	0.1679	0.0022	2520.6	49.1	2529.3	33.1	2536.8	24.9	2536.8	24.9
G64	216.4	380.3	0.4863	0.0059	11.3799	0.1840	0.1698	0.0026	2554.7	51.4	2554.8	36.2	2555.4	28.2	2555.4	28.2
G10	44.0	104.2	0.4173	0.0050	9.7687	0.1505	0.1698	0.0025	2248.2	45.7	2413.2	34.9	2556.1	27.4	2556.1	27.4
G78	44.0	81.5	0.4292	0.0059	10.2591	0.2180	0.1734	0.0036	2302.0	53.1	2458.4	46.1	2591.0	39.0	2591.0	39.0
G15	283.7	560.9	0.4425	0.0052	10.9587	0.1571	0.1797	0.0024	2361.7	46.6	2519.6	33.2	2650.0	25.2	2650.0	25.2
Sample 14052801 Song Nan																
G100	12.0	297.3	0.0395	0.0005	0.2772	0.0076	0.0509	0.0014	249.8	6.3	248.5	13.3	236.8	11.5	249.8	6.33
G34	92.4	1521.6	0.0498	0.0006	0.3726	0.0078	0.0543	0.0011	313.0	7.5	321.6	13.2	384.3	13.2	313.0	7.49
G55	45.0	723.2	0.0582	0.0007	0.4579	0.0107	0.0571	0.0013	364.4	8.9	382.8	16.9	496.2	18.3	364.4	8.89
G24	99.5	1263.0	0.0633	0.0008	0.4782	0.0078	0.0548	0.0009	395.5	9.1	396.8	12.9	404.9	10.5	395.5	9.09
G69	50.3	784.6	0.0651	0.0008	0.4969	0.0091	0.0554	0.0010	406.3	9.4	409.6	14.5	428.4	12.5	406.3	9.44
G87	72.3	959.9	0.0657	0.0008	0.5085	0.0095	0.0562	0.0010	410.1	9.6	417.4	14.8	458.7	13.3	410.1	9.56
G39	48.7	524.7	0.0661	0.0008	0.5052	0.0097	0.0555	0.0010	412.5	9.7	415.2	15.2	430.8	13.2	412.5	9.67
G68	33.3	376.1	0.0665	0.0008	0.5018	0.0106	0.0547	0.0011	415.1	9.9	412.9	16.4	401.2	13.8	415.1	9.91
G61	20.6	249.2	0.0675	0.0008	0.5153	0.0120	0.0554	0.0013	420.8	10.1	422.0	18.0	428.8	16.0	420.8	10.15
G38	18.0	246.1	0.0675	0.0009	0.5072	0.0120	0.0545	0.0013	421.3	10.3	416.6	18.1	390.9	15.1	421.3	10.27
G64	29.9	349.4	0.0679	0.0009	0.5285	0.0135	0.0565	0.0014	423.6	10.5	430.8	20.0	470.5	19.2	423.6	10.50

APPENDIX E (continued). U-Pb ZIRCON AGES OF SONG GIANH SEDIMENTS

Grain No.	Pb (ppm)	U (ppm)	Ratios						Ages (Ma)						Best Age (Ma)	$\pm 2\sigma$
			$^{206}\text{Pb}/^{238}\text{U}$	$\pm 1\sigma$	$^{207}\text{Pb}/^{235}\text{U}$	$\pm \text{s.e.}$	$^{207}\text{Pb}/^{206}\text{Pb}$	$\pm \text{s.e.}$	$^{206}\text{Pb}/^{238}\text{U}$	$\pm 2\sigma$	$^{207}\text{Pb}/^{235}\text{U}$	$\pm 2\sigma$	$^{207}\text{Pb}/^{206}\text{Pb}$	$\pm 2\sigma$		
G20	39.5	529.6	0.0688	0.0008	0.5123	0.0097	0.0540	0.0010	428.7	10.0	420.0	15.2	372.7	11.5	428.7	10.01
G33	22.8	284.8	0.0696	0.0009	0.5354	0.0117	0.0558	0.0012	433.6	10.4	435.4	17.6	445.2	15.5	433.6	10.37
G22	12.1	145.5	0.0697	0.0009	0.5219	0.0153	0.0543	0.0016	434.4	11.1	426.4	22.5	383.9	18.8	434.4	11.09
G12	24.5	320.4	0.0701	0.0009	0.5335	0.0113	0.0552	0.0012	436.9	10.4	434.1	17.1	419.5	14.3	436.9	10.36
G89	22.8	260.8	0.0702	0.0009	0.5425	0.0157	0.0561	0.0016	437.2	11.2	440.1	22.7	455.9	21.2	437.2	11.20
G16	23.4	331.1	0.0703	0.0009	0.5436	0.0115	0.0561	0.0012	438.1	10.5	440.8	17.2	455.1	15.2	438.1	10.48
G90	45.0	559.4	0.0704	0.0009	0.5414	0.0109	0.0558	0.0011	438.5	10.4	439.4	16.4	444.8	14.1	438.5	10.36
G79	32.9	418.3	0.0708	0.0009	0.5438	0.0113	0.0558	0.0011	440.7	10.5	440.9	17.1	442.8	14.7	440.7	10.48
G125	32.3	388.1	0.0711	0.0009	0.5530	0.0125	0.0564	0.0013	442.7	10.6	447.0	18.4	469.7	16.7	442.7	10.59
G99	11.0	142.9	0.0713	0.0009	0.5382	0.0154	0.0547	0.0016	444.2	11.3	437.2	22.4	401.2	19.0	444.2	11.31
G77	36.7	404.1	0.0716	0.0009	0.5550	0.0116	0.0563	0.0012	445.5	10.6	448.3	17.3	463.0	15.2	445.5	10.59
G123	37.4	453.0	0.0720	0.0009	0.5484	0.0120	0.0553	0.0012	448.0	10.7	443.9	17.9	423.6	14.9	448.0	10.70
G119	10.3	117.0	0.0723	0.0010	0.6248	0.0188	0.0627	0.0019	449.9	11.7	492.8	25.9	698.4	30.6	449.9	11.66
G37	15.0	178.9	0.0723	0.0009	0.5584	0.0141	0.0560	0.0014	450.2	11.1	450.5	20.4	452.0	18.2	450.2	11.06
G122	10.6	108.6	0.0727	0.0010	0.5756	0.0176	0.0575	0.0018	452.2	11.7	461.6	24.9	509.6	24.7	452.2	11.66
G105	30.9	374.7	0.0728	0.0009	0.5525	0.0122	0.0550	0.0012	453.2	10.8	446.6	18.0	413.4	14.7	453.2	10.82
G81	30.2	368.5	0.0730	0.0009	0.5820	0.0124	0.0578	0.0012	454.1	10.8	465.7	18.1	523.7	17.1	454.1	10.81
G83	18.5	225.2	0.0730	0.0009	0.5729	0.0137	0.0569	0.0014	454.1	11.1	459.9	19.9	489.2	18.4	454.1	11.05
G130	18.8	230.5	0.0730	0.0010	0.5806	0.0161	0.0577	0.0016	454.4	11.4	464.8	22.9	517.6	22.5	454.4	11.41
G05	54.5	582.6	0.0744	0.0009	0.5699	0.0104	0.0556	0.0010	462.7	10.8	458.0	15.8	434.8	12.5	462.7	10.80
G120	16.2	206.5	0.0746	0.0010	0.6117	0.0172	0.0595	0.0017	463.5	11.8	484.6	24.0	586.9	25.2	463.5	11.76
G128	10.7	118.4	0.0772	0.0011	0.6050	0.0215	0.0569	0.0021	479.3	13.0	480.4	29.6	486.5	27.9	479.3	13.05
G109	14.7	158.4	0.0783	0.0010	0.5994	0.0159	0.0555	0.0015	486.1	12.1	476.9	22.4	433.6	18.7	486.1	12.08
G106	43.8	523.4	0.0791	0.0010	0.6330	0.0128	0.0580	0.0012	490.9	11.6	498.0	18.3	531.3	16.4	490.9	11.59
G53	37.3	335.6	0.0833	0.0010	0.6524	0.0131	0.0568	0.0011	515.8	12.1	510.0	18.6	484.2	15.2	515.8	12.14
G02	22.2	212.7	0.0851	0.0011	0.6522	0.0158	0.0556	0.0013	526.3	12.8	509.8	21.8	436.8	17.1	526.3	12.83
G85	16.1	89.0	0.0936	0.0013	0.7919	0.0230	0.0614	0.0018	576.7	14.7	592.2	28.8	652.6	28.1	576.7	14.74
G41	31.2	317.8	0.1013	0.0012	0.8479	0.0161	0.0607	0.0011	622.0	14.4	623.5	20.6	629.3	17.3	622.0	14.40
G49	6.5	60.5	0.1054	0.0014	0.8694	0.0274	0.0599	0.0019	645.9	16.8	635.2	32.6	598.2	28.7	645.9	16.80
G95	45.9	373.4	0.1066	0.0013	0.8984	0.0196	0.0612	0.0013	652.8	15.4	650.9	23.8	645.2	20.5	652.8	15.38

APPENDIX E (continued). U-Pb ZIRCON AGES OF SONG GIANH SEDIMENTS

Grain No.	Pb (ppm)	U (ppm)	Ratios						Ages (Ma)						Best Age (Ma)	$\pm 2\sigma$
			$^{206}\text{Pb}/^{238}\text{U}$	$\pm 1\sigma$	$^{207}\text{Pb}/^{235}\text{U}$	$\pm \text{s.e.}$	$^{207}\text{Pb}/^{206}\text{Pb}$	$\pm \text{s.e.}$	$^{206}\text{Pb}/^{238}\text{U}$	$\pm 2\sigma$	$^{207}\text{Pb}/^{235}\text{U}$	$\pm 2\sigma$	$^{207}\text{Pb}/^{206}\text{Pb}$	$\pm 2\sigma$		
G15	128.1	1235.9	0.1072	0.0013	1.0132	0.0154	0.0685	0.0010	656.6	14.8	710.5	19.0	884.9	16.9	656.6	14.79
G57	29.4	230.1	0.1111	0.0015	1.1674	0.0291	0.0762	0.0019	679.1	16.8	785.4	30.8	1100.9	33.5	679.1	16.83
G92	10.0	73.9	0.1145	0.0016	0.9974	0.0311	0.0632	0.0020	699.0	18.2	702.5	34.7	714.3	32.1	699.0	18.16
G46	50.8	453.5	0.1165	0.0014	1.0293	0.0179	0.0641	0.0011	710.4	16.2	718.6	21.2	744.6	17.6	710.4	16.17
G65	25.8	209.6	0.1199	0.0015	1.0828	0.0243	0.0655	0.0015	730.1	17.4	745.0	26.9	790.4	24.3	730.1	17.38
G35	20.6	156.7	0.1235	0.0015	1.0936	0.0232	0.0642	0.0013	750.7	17.7	750.3	25.8	749.5	22.1	750.7	17.67
G124	12.9	87.2	0.1235	0.0016	1.0981	0.0294	0.0645	0.0017	750.8	18.6	752.4	31.7	757.7	28.6	750.8	18.59
G14	11.9	76.5	0.1245	0.0018	1.2084	0.0403	0.0704	0.0024	756.2	20.5	804.5	40.8	940.9	41.5	756.2	20.52
G48	12.2	77.0	0.1269	0.0017	1.1591	0.0295	0.0662	0.0017	770.4	18.9	781.5	31.1	814.0	28.4	770.4	18.88
G102	25.0	129.5	0.1271	0.0016	1.1370	0.0268	0.0649	0.0015	771.5	18.4	771.1	28.8	770.4	25.3	771.5	18.42
G19	34.7	217.6	0.1275	0.0016	1.1619	0.0224	0.0661	0.0012	773.6	17.8	782.8	24.4	809.5	20.9	773.6	17.84
G30	26.7	177.1	0.1292	0.0016	1.1901	0.0240	0.0668	0.0013	783.4	18.2	796.0	25.7	831.5	22.4	783.4	18.15
G62	5.4	36.5	0.1311	0.0021	1.3057	0.0548	0.0723	0.0031	793.9	24.1	848.2	52.5	993.8	54.2	793.9	24.05
G129	10.2	96.6	0.1312	0.0017	1.1879	0.0303	0.0657	0.0017	794.9	19.4	795.0	31.5	796.2	28.1	794.9	19.38
G107	24.5	147.8	0.1330	0.0017	1.2036	0.0273	0.0657	0.0015	804.9	19.0	802.3	28.5	795.6	24.7	804.9	19.00
G56	21.8	113.5	0.1334	0.0018	1.2212	0.0331	0.0664	0.0018	807.5	20.1	810.3	33.7	818.7	30.5	807.5	20.13
G60	114.7	757.9	0.1365	0.0016	1.2996	0.0212	0.0691	0.0011	825.0	18.4	845.5	22.5	900.2	18.7	825.0	18.38
G131	26.2	172.7	0.1389	0.0017	1.4004	0.0313	0.0732	0.0016	838.2	19.7	889.1	30.1	1018.9	28.5	838.2	19.70
G11	64.3	398.3	0.1423	0.0018	1.3163	0.0259	0.0671	0.0013	857.4	19.8	852.9	26.3	841.2	22.0	857.4	19.75
G132	21.9	122.8	0.1473	0.0019	1.4304	0.0338	0.0705	0.0017	885.7	21.0	901.7	31.8	942.1	28.7	885.7	21.01
G01	125.2	757.0	0.1569	0.0019	1.5051	0.0230	0.0696	0.0010	939.2	20.6	932.5	22.7	916.6	17.3	916.6	17.35
G10	12.2	69.9	0.1635	0.0021	1.5787	0.0386	0.0701	0.0017	975.9	23.5	961.9	34.2	930.1	29.6	930.1	29.56
G58	55.8	320.4	0.1556	0.0019	1.5040	0.0266	0.0701	0.0012	932.4	21.0	932.0	25.6	931.3	20.9	931.3	20.87
G25	99.9	567.0	0.1589	0.0019	1.5411	0.0243	0.0703	0.0011	950.8	21.0	946.9	23.5	938.3	18.3	938.3	18.28
G21	43.6	259.9	0.1501	0.0018	1.4570	0.0260	0.0704	0.0012	901.5	20.4	912.8	25.5	940.3	21.2	940.3	21.25
G32	24.8	138.9	0.1664	0.0021	1.6168	0.0323	0.0705	0.0014	992.4	22.8	976.8	29.1	942.1	24.0	942.1	24.04
G71	49.3	244.3	0.1683	0.0020	1.6343	0.0303	0.0705	0.0013	1002.5	22.5	983.5	27.4	942.1	22.1	942.1	22.13
G17	105.4	551.0	0.1514	0.0018	1.4735	0.0233	0.0706	0.0011	908.8	20.2	919.6	23.2	945.9	18.5	945.9	18.48
G50	60.4	318.6	0.1695	0.0020	1.6512	0.0284	0.0707	0.0012	1009.6	22.5	990.0	25.9	947.3	20.4	947.3	20.40
G70	58.0	369.8	0.1565	0.0019	1.5357	0.0305	0.0712	0.0014	937.0	21.5	944.8	28.3	963.4	24.1	963.4	24.12

APPENDIX E (continued). U-Pb ZIRCON AGES OF SONG GIANH SEDIMENTS

Grain No.	Pb (ppm)	U (ppm)	Ratios						Ages (Ma)						Best Age (Ma)	± 2σ
			²⁰⁶ Pb/ ²³⁸ U	± 1 σ	²⁰⁷ Pb/ ²³⁵ U	± s.e.	²⁰⁷ Pb/ ²⁰⁶ Pb	± s.e.	²⁰⁶ Pb/ ²³⁸ U	± 2σ	²⁰⁷ Pb/ ²³⁵ U	± 2σ	²⁰⁷ Pb/ ²⁰⁶ Pb	± 2σ		
G28	78.2	445.0	0.1547	0.0018	1.5230	0.0246	0.0714	0.0011	927.0	20.5	939.7	23.9	969.7	19.2	969.7	19.24
G111	108.9	573.7	0.1626	0.0020	1.6045	0.0298	0.0716	0.0013	971.1	21.7	971.9	27.1	974.6	22.6	974.6	22.58
G43	38.8	213.6	0.1526	0.0019	1.5101	0.0308	0.0718	0.0014	915.5	21.3	934.5	28.8	980.0	25.2	980.0	25.22
G23	31.5	161.1	0.1623	0.0020	1.6074	0.0308	0.0719	0.0013	969.4	22.1	973.1	27.9	981.7	23.5	981.7	23.47
G134	35.2	206.9	0.1643	0.0020	1.6294	0.0348	0.0720	0.0015	980.7	22.6	981.6	30.7	984.5	26.5	984.5	26.46
G101	13.7	67.6	0.1736	0.0023	1.7413	0.0441	0.0728	0.0018	1031.6	24.9	1024.0	36.7	1008.4	32.3	1008.4	32.31
G47	67.5	397.4	0.1656	0.0020	1.6625	0.0300	0.0728	0.0013	987.9	22.2	994.3	26.9	1008.9	22.3	1008.9	22.31
G117	68.6	381.4	0.1654	0.0020	1.6606	0.0321	0.0728	0.0014	986.9	22.2	993.6	28.4	1009.2	24.1	1009.2	24.06
G06	19.5	94.3	0.1599	0.0020	1.6066	0.0363	0.0729	0.0016	956.1	22.7	972.8	32.2	1010.9	28.6	1010.9	28.63
G84	49.9	240.3	0.1712	0.0021	1.7240	0.0367	0.0730	0.0015	1018.9	23.6	1017.5	31.4	1015.1	26.9	1015.1	26.89
G94	78.3	473.1	0.1727	0.0021	1.7458	0.0328	0.0734	0.0013	1026.9	23.1	1025.6	28.3	1023.6	23.6	1023.6	23.56
G74	27.6	135.3	0.1791	0.0022	1.8193	0.0366	0.0737	0.0015	1062.2	24.3	1052.4	30.5	1032.7	25.5	1032.7	25.51
G113	62.4	309.3	0.1611	0.0021	1.6456	0.0390	0.0741	0.0017	962.7	22.9	987.9	33.8	1044.7	30.6	1044.7	30.63
G98	46.9	203.4	0.1862	0.0023	1.9175	0.0385	0.0747	0.0015	1100.8	24.9	1087.2	31.0	1060.7	25.9	1060.7	25.90
G121	84.0	441.5	0.1788	0.0022	1.8441	0.0355	0.0748	0.0014	1060.3	23.7	1061.3	29.4	1064.2	24.7	1064.2	24.67
G135	70.6	360.5	0.1819	0.0023	1.8813	0.0394	0.0750	0.0015	1077.5	24.5	1074.5	31.8	1069.6	27.1	1069.6	27.14
G72	72.5	341.3	0.1863	0.0022	1.9283	0.0335	0.0751	0.0013	1101.1	24.3	1091.0	27.6	1071.4	22.2	1071.4	22.21
G67	88.1	482.9	0.1762	0.0021	1.8368	0.0314	0.0756	0.0012	1046.0	23.1	1058.7	26.7	1085.6	21.9	1085.6	21.86
G108	113.1	652.4	0.1791	0.0022	1.8725	0.0340	0.0759	0.0013	1061.8	23.6	1071.4	28.2	1091.6	23.5	1091.6	23.45
G29	24.0	116.6	0.1664	0.0022	1.7474	0.0450	0.0762	0.0020	992.4	24.5	1026.2	37.4	1099.3	34.6	1099.3	34.56
G86	24.0	104.1	0.1991	0.0026	2.0920	0.0540	0.0762	0.0020	1170.3	28.4	1146.2	39.9	1101.4	34.7	1101.4	34.74
G97	174.4	851.8	0.1767	0.0021	1.8580	0.0331	0.0763	0.0013	1049.1	23.2	1066.3	27.7	1102.2	23.1	1102.2	23.10
G114	9.3	51.2	0.1767	0.0024	1.8737	0.0536	0.0769	0.0022	1048.8	26.5	1071.8	42.1	1119.6	39.0	1119.6	38.97
G66	30.7	123.7	0.1912	0.0024	2.0453	0.0401	0.0776	0.0015	1128.1	25.5	1130.7	31.1	1136.4	26.3	1136.4	26.26
G51	48.7	183.8	0.1912	0.0023	2.0492	0.0372	0.0778	0.0014	1127.8	25.2	1132.0	29.2	1140.5	24.1	1140.5	24.15
G54	79.6	362.7	0.1918	0.0023	2.0651	0.0344	0.0781	0.0012	1130.8	24.8	1137.3	27.2	1150.2	21.8	1150.2	21.85
G137	66.2	271.5	0.1873	0.0023	2.0189	0.0413	0.0782	0.0016	1106.6	25.0	1121.9	32.0	1152.5	27.7	1152.5	27.66
G91	52.3	221.2	0.2003	0.0024	2.1884	0.0413	0.0793	0.0015	1176.7	26.2	1177.4	30.6	1179.1	25.5	1179.1	25.51
G96	103.9	352.5	0.2054	0.0025	2.2852	0.0413	0.0807	0.0014	1204.0	26.5	1207.7	30.0	1215.1	24.7	1215.1	24.75
G52	121.7	549.6	0.2074	0.0025	2.3430	0.0372	0.0820	0.0012	1215.0	26.3	1225.4	27.2	1244.3	21.5	1244.3	21.53

APPENDIX E (continued). U-Pb ZIRCON AGES OF SONG GIANH SEDIMENTS

Grain No.	Pb (ppm)	U (ppm)	Ratios						Ages (Ma)						Best Age (Ma)	± 2σ
			²⁰⁶ Pb/ ²³⁸ U	± 1 σ	²⁰⁷ Pb/ ²³⁵ U	± s.e.	²⁰⁷ Pb/ ²⁰⁶ Pb	± s.e.	²⁰⁶ Pb/ ²³⁸ U	± 2σ	²⁰⁷ Pb/ ²³⁵ U	± 2σ	²⁰⁷ Pb/ ²⁰⁶ Pb	± 2σ		
G136	43.1	178.0	0.2188	0.0027	2.5771	0.0536	0.0855	0.0017	1275.7	28.7	1294.2	34.9	1325.8	30.1	1325.8	30.15
G126	24.1	85.9	0.2533	0.0032	3.2175	0.0703	0.0922	0.0020	1455.5	32.9	1461.4	38.8	1470.7	33.5	1470.7	33.55
G78	87.6	289.3	0.2678	0.0032	3.5651	0.0605	0.0966	0.0016	1529.8	32.7	1541.8	32.1	1558.7	25.9	1558.7	25.91
G26	115.5	402.8	0.2722	0.0032	3.6380	0.0549	0.0970	0.0014	1551.8	32.6	1557.9	29.5	1566.4	22.7	1566.4	22.72
G115	149.1	606.1	0.2538	0.0031	3.3998	0.0616	0.0972	0.0017	1457.9	31.5	1504.3	33.3	1571.1	28.0	1571.1	27.96
G31	61.7	186.5	0.2796	0.0034	3.7603	0.0612	0.0976	0.0015	1589.2	33.9	1584.3	31.4	1578.0	24.8	1578.0	24.79
G75	48.9	128.6	0.2812	0.0034	3.8342	0.0695	0.0989	0.0017	1597.3	34.6	1600.0	34.5	1604.0	28.4	1604.0	28.36
G93	53.5	163.8	0.2924	0.0036	4.1279	0.0793	0.1024	0.0019	1653.7	36.1	1659.8	36.7	1668.3	30.7	1668.3	30.71
G40	88.6	247.4	0.2881	0.0034	4.0741	0.0644	0.1026	0.0015	1632.2	34.4	1649.1	31.3	1671.0	24.6	1671.0	24.61
G104	75.9	210.1	0.3032	0.0037	4.3412	0.0795	0.1039	0.0018	1707.1	36.4	1701.2	35.4	1694.6	29.2	1694.6	29.19
G07	66.3	189.6	0.3034	0.0036	4.3550	0.0691	0.1041	0.0016	1708.0	36.0	1703.8	31.8	1698.8	24.9	1698.8	24.87
G08	70.0	197.2	0.3218	0.0039	4.7377	0.0747	0.1068	0.0016	1798.5	37.6	1773.9	32.2	1745.3	25.0	1745.3	24.97
G44	23.8	61.4	0.3054	0.0038	4.5681	0.0873	0.1085	0.0020	1718.1	37.9	1743.5	37.6	1774.4	31.4	1774.4	31.38
G09	240.6	700.0	0.3192	0.0038	4.7827	0.0692	0.1087	0.0015	1785.7	36.7	1781.9	30.1	1777.4	22.7	1777.4	22.70
G03	82.5	252.3	0.2792	0.0034	4.1836	0.0704	0.1087	0.0018	1587.2	34.3	1670.8	33.2	1777.6	27.2	1777.6	27.17
G36	40.0	128.6	0.2935	0.0037	4.4876	0.0850	0.1109	0.0021	1659.0	36.8	1728.7	37.1	1814.4	31.2	1814.4	31.25
G82	91.6	236.8	0.3332	0.0040	5.2275	0.0889	0.1138	0.0019	1853.9	38.8	1857.1	34.6	1861.3	27.9	1861.3	27.88
G112	57.8	116.6	0.4027	0.0049	7.2287	0.1356	0.1302	0.0024	2181.6	45.4	2140.1	39.2	2101.1	32.3	2101.1	32.29
G116	56.6	119.3	0.3920	0.0048	7.2177	0.1366	0.1336	0.0025	2132.1	44.6	2138.7	39.5	2145.7	32.9	2145.7	32.88
G45	54.4	93.9	0.4554	0.0055	10.0920	0.1624	0.1607	0.0025	2419.3	49.0	2443.2	36.2	2463.5	28.4	2463.5	28.45
G18	76.8	107.7	0.4394	0.0054	9.7428	0.1575	0.1608	0.0025	2348.0	48.3	2410.8	36.4	2464.4	28.7	2464.4	28.66
G42	388.3	906.1	0.4249	0.0050	9.4211	0.1383	0.1608	0.0022	2282.6	45.2	2379.9	33.2	2464.5	25.4	2464.5	25.44
G63	102.9	190.9	0.4444	0.0054	9.8621	0.1597	0.1610	0.0025	2370.5	47.8	2422.0	36.1	2465.9	28.5	2465.9	28.53
G103	145.2	192.3	0.4609	0.0056	10.2327	0.1805	0.1611	0.0027	2443.5	49.2	2456.0	38.6	2467.0	31.5	2467.0	31.50
G80	81.7	135.7	0.4592	0.0056	10.2717	0.1735	0.1623	0.0026	2435.9	49.1	2459.6	37.4	2479.7	30.0	2479.7	30.05
G04	226.1	440.1	0.4663	0.0055	10.4786	0.1500	0.1630	0.0022	2467.4	48.4	2478.0	33.0	2486.9	24.7	2486.9	24.70
G59	233.5	415.7	0.4457	0.0053	10.0405	0.1543	0.1634	0.0024	2376.1	47.2	2438.5	34.6	2491.4	26.9	2491.4	26.92
G118	134.0	231.4	0.4777	0.0058	10.7900	0.1972	0.1639	0.0029	2517.2	50.4	2505.2	39.7	2496.2	32.7	2496.2	32.75
G133	59.0	96.6	0.4553	0.0058	10.4010	0.2135	0.1658	0.0033	2418.7	51.1	2471.1	44.1	2515.3	37.5	2515.3	37.48
G73	109.3	177.6	0.5041	0.0061	11.6851	0.1895	0.1682	0.0026	2631.5	51.9	2579.5	36.6	2539.3	28.8	2539.3	28.83

APPENDIX E (continued). U-Pb ZIRCON AGES OF SONG GIANH SEDIMENTS

Grain No.	Pb (ppm)	U (ppm)	Ratios						Ages (Ma)						Best Age (Ma)	± 2σ
			²⁰⁶ Pb/ ²³⁸ U	± 1 σ	²⁰⁷ Pb/ ²³⁵ U	± s.e.	²⁰⁷ Pb/ ²⁰⁶ Pb	± s.e.	²⁰⁶ Pb/ ²³⁸ U	± 2σ	²⁰⁷ Pb/ ²³⁵ U	± 2σ	²⁰⁷ Pb/ ²⁰⁶ Pb	± 2σ		
G27	370.8	646.6	0.4700	0.0056	11.3018	0.1653	0.1744	0.0024	2483.6	48.8	2548.4	33.8	2600.5	25.7	2600.5	25.68
G127	48.2	88.1	0.4760	0.0061	11.8463	0.2400	0.1806	0.0036	2510.0	52.8	2592.3	44.2	2658.0	37.4	2658.0	37.43
G88	72.0	110.4	0.5241	0.0064	13.1822	0.2278	0.1825	0.0030	2716.7	54.1	2692.8	38.9	2675.4	31.3	2675.4	31.30
G76	128.4	193.6	0.5345	0.0065	16.9115	0.2761	0.2296	0.0036	2760.2	54.2	2929.8	37.7	3049.0	30.0	3049.0	30.01
G110	146.5	232.3	0.5878	0.0071	18.8884	0.3332	0.2331	0.0040	2980.5	57.6	3036.1	40.2	3073.7	32.8	3073.7	32.82
G13	150.1	212.7	0.6346	0.0075	23.6373	0.3397	0.2702	0.0036	3167.9	59.3	3253.6	34.9	3307.0	26.2	3307.0	26.16
Sample 12061801 Song Trac																
G92	81	1789	0.0377	0.0005	0.2774	0.0043	0.0524	0.0006	238.8	5.6	248.6	7.0	304.2	12.1	238.8	5.6
G58	21	477	0.0385	0.0005	0.2681	0.0052	0.0510	0.0008	243.2	6.0	241.2	8.5	239.0	12.9	243.2	6.0
G6	16	414	0.0390	0.0005	0.2809	0.0063	0.0514	0.0010	246.4	6.1	251.3	10.0	260.6	10.2	246.4	6.1
G27	24	610	0.0410	0.0005	0.3186	0.0063	0.0552	0.0009	259.2	6.4	280.8	9.8	418.7	17.2	259.2	6.4
G75	6	111	0.0413	0.0006	0.3201	0.0116	0.0558	0.0018	260.9	7.9	282.0	17.6	445.6	29.8	260.9	7.9
G81	14	312	0.0432	0.0006	0.3373	0.0070	0.0567	0.0009	272.3	6.8	295.1	10.7	479.1	19.1	272.3	6.8
G31	24	447	0.0529	0.0007	0.4340	0.0084	0.0595	0.0009	332.5	8.1	366.0	12.0	586.5	19.7	332.5	8.1
G54	42	826	0.0535	0.0006	0.3958	0.0062	0.0534	0.0006	335.7	7.8	338.6	9.3	347.1	12.8	335.7	7.8
G85	18	329	0.0554	0.0007	0.4100	0.0094	0.0551	0.0010	347.4	8.8	348.9	13.6	414.7	19.0	347.4	8.8
G116	94	1543	0.0561	0.0039	0.4844	0.1039	0.0605	0.0011	352.0	47.6	401.1	46.4	622.9	22.5	352.0	47.6
G56	22	355	0.0611	0.0008	0.4551	0.0086	0.0552	0.0008	382.3	9.2	380.9	12.1	418.7	16.1	382.3	9.2
G28	24	398	0.0615	0.0008	0.5036	0.0090	0.0593	0.0008	384.8	9.2	414.1	12.2	576.7	17.8	384.8	9.2
G36	55	744	0.0632	0.0008	0.4882	0.0087	0.0559	0.0007	395.0	9.3	403.7	11.8	448.8	15.7	395.0	9.3
G32	109	1275	0.0646	0.0008	0.5011	0.0077	0.0563	0.0006	403.4	9.3	412.5	10.7	465.4	14.1	403.4	9.3
G62	37	582	0.0654	0.0008	0.5587	0.0091	0.0615	0.0007	408.3	9.6	450.7	11.9	658.2	17.1	408.3	9.6
G115	79	1129	0.0655	0.0010	0.5147	0.0122	0.0566	0.0007	408.7	12.3	421.6	13.9	474.0	16.2	408.7	12.3
G34	43	537	0.0655	0.0008	0.5627	0.0100	0.0631	0.0008	409.1	9.8	453.3	13.1	712.3	19.5	409.1	9.8
G63	31	420	0.0659	0.0008	0.5180	0.0106	0.0556	0.0009	411.4	10.0	423.8	13.7	435.2	17.5	411.4	10.0
G46	27	379	0.0659	0.0008	0.5111	0.0102	0.0563	0.0009	411.5	9.9	419.2	13.4	465.8	17.7	411.5	9.9
G64	16	229	0.0661	0.0008	0.4936	0.0109	0.0546	0.0009	412.8	10.2	407.3	14.4	395.9	17.7	412.8	10.2
G11	79	1239	0.0667	0.0008	0.5137	0.0088	0.0554	0.0007	416.2	9.5	421.0	12.0	427.6	10.4	416.2	9.5
G80	31	459	0.0678	0.0009	0.5419	0.0116	0.0586	0.0010	422.6	10.4	439.7	14.9	551.5	20.3	422.6	10.4

APPENDIX E (continued). U-Pb ZIRCON AGES OF SONG GIANH SEDIMENTS

Grain No.	Pb (ppm)	U (ppm)	Ratios						Ages (Ma)						Best Age (Ma)	± 2σ
			²⁰⁶ Pb/ ²³⁸ U	± 1 σ	²⁰⁷ Pb/ ²³⁵ U	± s.e.	²⁰⁷ Pb/ ²⁰⁶ Pb	± s.e.	²⁰⁶ Pb/ ²³⁸ U	± 2σ	²⁰⁷ Pb/ ²³⁵ U	± 2σ	²⁰⁷ Pb/ ²⁰⁶ Pb	± 2σ		
G104	89	1323	0.0686	0.0018	0.5695	0.0201	0.0594	0.0005	427.6	21.4	457.7	19.8	581.4	13.8	427.6	21.4
G91	68	1036	0.0688	0.0008	0.5895	0.0095	0.0611	0.0007	429.1	10.0	470.5	12.1	643.8	16.8	429.1	10.0
G61	44	504	0.0696	0.0009	0.5431	0.0094	0.0557	0.0007	433.4	10.2	440.5	12.2	440.4	15.1	433.4	10.2
G14	36	493	0.0711	0.0009	0.5462	0.0101	0.0562	0.0008	442.5	10.2	442.5	13.3	461.1	11.8	442.5	10.2
G39	30	381	0.0715	0.0009	0.5488	0.0097	0.0555	0.0007	445.4	10.5	444.2	12.6	430.8	15.3	445.4	10.5
G1	23	256	0.0722	0.0009	0.5508	0.0118	0.0549	0.0009	449.6	10.8	445.5	15.0	408.2	12.7	449.6	10.8
G99	25	335	0.0724	0.0009	0.5714	0.0115	0.0567	0.0009	450.4	10.9	458.9	14.4	479.9	17.9	450.4	10.9
G108	16	211	0.0724	0.0020	0.5673	0.0266	0.0561	0.0006	450.6	23.4	456.3	21.2	456.3	14.5	450.6	23.4
G10	18	247	0.0725	0.0009	0.5562	0.0124	0.0557	0.0010	450.9	10.8	449.0	15.7	440.8	14.1	450.9	10.8
G18	31	420	0.0728	0.0009	0.5574	0.0109	0.0558	0.0009	452.8	10.6	449.8	14.2	443.2	12.4	452.8	10.6
G70	182	2280	0.0730	0.0009	0.6202	0.0087	0.0602	0.0005	454.3	10.3	490.0	11.0	610.1	14.0	454.3	10.3
G2	30	435	0.0730	0.0009	0.6333	0.0124	0.0630	0.0009	454.4	10.7	498.1	15.1	706.5	16.4	454.4	10.7
G78	36	483	0.0736	0.0009	0.5617	0.0095	0.0556	0.0007	457.7	10.7	452.6	12.4	434.8	14.8	457.7	10.7
G66	27	349	0.0739	0.0009	0.6090	0.0108	0.0599	0.0008	459.5	10.9	482.9	13.5	601.4	17.7	459.5	10.9
G97	21	256	0.0747	0.0009	0.5770	0.0122	0.0560	0.0009	464.4	11.3	462.6	15.2	450.8	18.1	464.4	11.3
G109	33	362	0.0757	0.0015	0.5911	0.0174	0.0554	0.0007	470.5	17.5	471.6	16.8	427.2	14.6	470.5	17.5
G26	189	2173	0.0761	0.0009	0.7193	0.0095	0.0685	0.0005	473.0	10.8	550.2	11.8	884.3	15.0	473.0	10.8
G29	44	546	0.0778	0.0010	0.6573	0.0126	0.0608	0.0008	482.8	11.6	512.9	14.9	631.5	19.4	482.8	11.6
G107	19	232	0.0796	0.0009	0.6205	0.0122	0.0558	0.0008	493.4	10.5	490.2	14.3	444.0	17.1	493.4	10.5
G24	13	116	0.0817	0.0011	0.6558	0.0194	0.0598	0.0014	506.3	13.6	512.0	22.4	596.0	27.7	506.3	13.6
G114	60	701	0.0836	0.0067	0.6886	0.3706	0.0593	0.0020	517.8	79.1	532.0	70.9	577.0	35.4	517.8	79.1
G69	28	217	0.0851	0.0011	0.6946	0.0154	0.0590	0.0010	526.3	13.0	535.6	17.4	568.6	20.8	526.3	13.0
G19	66	761	0.0857	0.0010	0.6927	0.0130	0.0597	0.0009	529.8	12.2	534.4	15.8	593.1	14.3	529.8	12.2
G20	47	234	0.0884	0.0011	0.7392	0.0164	0.0607	0.0011	545.9	13.0	561.9	18.4	628.6	17.6	545.9	13.0
G8	118	1388	0.0922	0.0011	0.7819	0.0129	0.0603	0.0007	568.7	12.7	586.6	14.6	615.8	12.3	568.7	12.7
G98	46	502	0.0975	0.0012	0.8069	0.0137	0.0599	0.0007	599.6	13.9	600.7	15.0	598.9	16.7	599.6	13.9
G42	26	189	0.1005	0.0013	0.8876	0.0181	0.0623	0.0009	617.2	14.8	645.1	17.9	685.1	20.6	617.2	14.8
G93	146	1308	0.1011	0.0012	0.8625	0.0132	0.0613	0.0006	621.0	14.2	631.5	14.3	648.0	15.5	621.0	14.2
G57	157	1199	0.1038	0.0012	0.9200	0.0138	0.0648	0.0006	636.5	14.5	662.4	14.7	768.2	16.2	636.5	14.5
G9	48	431	0.1048	0.0013	0.9407	0.0177	0.0652	0.0009	642.3	14.7	673.2	17.9	779.5	16.3	642.3	14.7

APPENDIX E (continued). U-Pb ZIRCON AGES OF SONG GIANH SEDIMENTS

Grain No.	Pb (ppm)	U (ppm)	Ratios						Ages (Ma)						Best Age (Ma)	$\pm 2\sigma$
			$^{206}\text{Pb}/^{238}\text{U}$	$\pm 1\sigma$	$^{207}\text{Pb}/^{235}\text{U}$	$\pm \text{s.e.}$	$^{207}\text{Pb}/^{206}\text{Pb}$	$\pm \text{s.e.}$	$^{206}\text{Pb}/^{238}\text{U}$	$\pm 2\sigma$	$^{207}\text{Pb}/^{235}\text{U}$	$\pm 2\sigma$	$^{207}\text{Pb}/^{206}\text{Pb}$	$\pm 2\sigma$		
G43	43	312	0.1098	0.0014	0.9928	0.0197	0.0671	0.0009	671.3	15.9	700.2	18.9	842.1	21.9	671.3	15.9
G33	242	1903	0.1104	0.0013	1.0295	0.0141	0.0674	0.0005	675.1	15.1	718.7	14.4	848.6	15.1	675.1	15.1
G37	76	529	0.1122	0.0014	1.0067	0.0173	0.0643	0.0007	685.5	15.8	707.2	16.6	749.9	18.1	685.5	15.8
G110	104	982	0.1134	0.0010	1.0415	0.0161	0.0665	0.0013	692.3	11.5	724.6	22.0	821.8	28.3	692.3	11.5
G13	151	1234	0.1165	0.0014	1.1216	0.0185	0.0689	0.0008	710.6	15.8	763.7	17.8	895.7	15.6	710.6	15.8
G51	210	1751	0.1183	0.0014	1.2166	0.0157	0.0730	0.0005	720.7	16.0	808.2	14.9	1012.6	15.0	720.7	16.0
G50	58	492	0.1188	0.0014	1.2012	0.0199	0.0728	0.0008	723.8	16.6	801.1	17.6	1008.4	19.6	723.8	16.6
G101	26	170	0.1227	0.0017	1.1283	0.0312	0.0694	0.0014	745.9	19.1	766.9	26.2	909.5	30.1	745.9	19.1
G86	27	169	0.1250	0.0016	1.1528	0.0272	0.0648	0.0011	759.3	18.5	778.6	22.3	768.8	24.0	759.3	18.5
G21	444	3362	0.1276	0.0015	1.2680	0.0159	0.0720	0.0005	774.3	17.0	831.5	15.0	985.1	14.3	774.3	17.0
G44	107	822	0.1298	0.0015	1.2559	0.0181	0.0696	0.0006	786.8	17.6	826.0	16.2	915.4	16.3	786.8	17.6
G47	46	220	0.1326	0.0016	1.2192	0.0236	0.0672	0.0009	802.6	18.7	809.4	19.8	844.9	20.9	802.6	18.7
G77	62	401	0.1341	0.0016	1.2180	0.0199	0.0659	0.0007	811.2	18.3	808.9	17.4	802.9	17.5	811.2	18.3
G49	214	1323	0.1351	0.0016	1.3198	0.0187	0.0710	0.0006	816.9	18.2	854.4	16.5	956.8	16.2	816.9	18.2
G30	216	1542	0.1352	0.0016	1.4090	0.0183	0.0750	0.0005	817.3	18.1	892.7	16.0	1067.4	15.2	817.3	18.1
G105	131	955	0.1352	0.0022	1.3121	0.0446	0.0712	0.0010	817.5	24.8	851.0	24.3	963.7	23.2	817.5	24.8
G53	183	1273	0.1394	0.0017	1.4940	0.0208	0.0768	0.0006	841.5	18.7	927.9	17.0	1115.2	16.6	841.5	18.7
G89	292	1741	0.1433	0.0017	1.4405	0.0188	0.0723	0.0005	863.4	18.9	905.9	16.2	993.6	15.0	863.4	18.9
G41	162	1043	0.1463	0.0017	1.5468	0.0221	0.0758	0.0006	880.2	19.5	949.2	17.5	1090.6	17.0	880.2	19.5
G38	185	1156	0.1464	0.0017	1.4673	0.0207	0.0714	0.0006	881.0	19.5	917.0	16.9	970.0	16.0	881.0	19.5
G94	60	377	0.1467	0.0018	1.4601	0.0284	0.0708	0.0009	882.2	20.4	914.0	20.8	952.2	21.6	882.2	20.4
G95	200	1286	0.1477	0.0018	1.4747	0.0209	0.0708	0.0006	888.3	19.7	920.0	17.0	951.6	16.0	888.3	19.7
G84	108	714	0.1500	0.0018	1.4607	0.0222	0.0701	0.0006	901.2	20.1	914.3	17.7	929.8	17.0	929.8	17.0
G87	194	1264	0.1549	0.0018	1.4889	0.0210	0.0702	0.0005	928.4	20.4	925.9	17.2	934.2	15.8	934.2	15.8
G5	114	699	0.1594	0.0019	1.5390	0.0241	0.0708	0.0007	953.5	20.7	946.1	19.4	950.5	14.3	950.5	14.3
G17	97	634	0.1555	0.0018	1.5001	0.0259	0.0709	0.0009	931.7	20.4	930.4	21.1	953.7	16.9	953.7	16.9
G102	73	396	0.1561	0.0026	1.5083	0.0621	0.0710	0.0010	934.9	29.4	933.8	27.0	958.3	23.9	958.3	23.9
G45	94	578	0.1601	0.0019	1.5739	0.0255	0.0712	0.0007	957.1	21.3	960.0	19.0	961.7	18.3	961.7	18.3
G103	304	1958	0.1504	0.0017	1.5057	0.0312	0.0713	0.0014	903.0	18.6	932.7	26.8	966.6	30.3	966.6	30.3
G48	91	435	0.1655	0.0020	1.6278	0.0243	0.0714	0.0006	987.0	21.8	981.0	18.3	968.3	16.9	968.3	16.9

APPENDIX E (continued). U-Pb ZIRCON AGES OF SONG GIANH SEDIMENTS

Grain No.	Pb (ppm)	U (ppm)	Ratios						Ages (Ma)						Best Age (Ma)	± 2σ
			²⁰⁶ Pb/ ²³⁸ U	± 1 σ	²⁰⁷ Pb/ ²³⁵ U	± s.e.	²⁰⁷ Pb/ ²⁰⁶ Pb	± s.e.	²⁰⁶ Pb/ ²³⁸ U	± 2σ	²⁰⁷ Pb/ ²³⁵ U	± 2σ	²⁰⁷ Pb/ ²⁰⁶ Pb	± 2σ		
G74	65	379	0.1530	0.0019	1.5487	0.0269	0.0721	0.0008	917.5	20.7	950.0	19.5	987.6	19.5	987.6	19.5
G25	146	697	0.1594	0.0019	1.5972	0.0227	0.0724	0.0006	953.5	21.0	969.1	17.7	996.1	16.2	996.1	16.2
G100	37	146	0.1672	0.0021	1.6809	0.0376	0.0724	0.0010	996.6	23.3	1001.3	24.0	996.9	24.3	996.9	24.3
G68	42	232	0.1696	0.0021	1.6689	0.0289	0.0724	0.0007	1010.1	22.6	996.8	20.2	998.3	19.4	998.3	19.4
G72	41	237	0.1622	0.0020	1.6825	0.0340	0.0725	0.0009	968.8	22.3	1001.9	22.2	999.4	22.4	999.4	22.4
G7	101	1202	0.1555	0.0018	1.6197	0.0252	0.0753	0.0008	931.9	20.2	977.9	19.7	1076.3	15.3	1076.3	15.3
G40	93	502	0.1771	0.0021	1.8628	0.0321	0.0755	0.0008	1051.3	23.4	1068.0	20.7	1081.3	19.8	1081.3	19.8
G23	107	531	0.1878	0.0023	1.9837	0.0332	0.0760	0.0007	1109.4	24.5	1110.0	20.6	1094.0	19.1	1094.0	19.1
G55	143	718	0.1871	0.0022	1.9789	0.0291	0.0763	0.0006	1105.6	24.1	1108.3	19.3	1101.9	17.1	1101.9	17.1
G96	163	886	0.1855	0.0022	1.9596	0.0275	0.0765	0.0006	1096.9	23.8	1101.8	18.8	1106.9	16.4	1106.9	16.4
G35	263	1358	0.1764	0.0021	1.8713	0.0257	0.0767	0.0006	1047.4	22.8	1071.0	18.2	1113.4	16.1	1113.4	16.1
G65	290	1444	0.1881	0.0022	2.0468	0.0268	0.0775	0.0005	1111.2	24.0	1131.2	18.3	1133.8	15.4	1133.8	15.4
G67	173	1003	0.1752	0.0021	1.8895	0.0260	0.0779	0.0006	1040.7	22.7	1077.4	18.3	1143.0	16.3	1143.0	16.3
G79	89	455	0.1896	0.0023	2.0360	0.0302	0.0781	0.0006	1119.1	24.4	1127.6	19.6	1148.1	17.5	1148.1	17.5
G90	128	675	0.1765	0.0021	2.0078	0.0304	0.0807	0.0007	1047.7	23.0	1118.1	19.5	1214.9	18.1	1214.9	18.1
G106	113	480	0.2058	0.0016	2.2312	0.0187	0.0808	0.0006	1206.4	17.1	1190.9	14.8	1217.6	16.4	1217.6	16.4
G73	163	885	0.1929	0.0023	2.1831	0.0304	0.0822	0.0006	1136.8	24.6	1175.7	19.4	1249.1	16.9	1249.1	16.9
G60	104	448	0.2191	0.0026	2.6659	0.0444	0.0874	0.0008	1277.3	27.8	1319.1	22.0	1370.2	19.8	1370.2	19.8
G15	123	424	0.2465	0.0029	3.0544	0.0532	0.0904	0.0011	1420.3	30.0	1421.3	25.8	1433.1	19.9	1433.1	19.9
G22	76	224	0.2631	0.0032	3.4694	0.0631	0.0977	0.0009	1505.5	32.6	1520.3	24.3	1580.5	21.5	1580.5	21.5
G52	355	1043	0.2762	0.0033	3.8261	0.0535	0.0983	0.0007	1572.0	32.8	1598.3	21.9	1592.1	17.5	1592.1	17.5
G16	46	159	0.2429	0.0030	3.2517	0.0704	0.0994	0.0014	1401.5	30.8	1469.6	29.3	1612.3	24.3	1612.3	24.3
G12	148	481	0.2885	0.0034	4.0153	0.0664	0.1021	0.0012	1633.9	33.8	1637.3	26.5	1662.3	19.8	1662.3	19.8
G76	320	934	0.2879	0.0034	4.1761	0.0615	0.1055	0.0008	1631.1	34.1	1669.3	22.7	1723.2	18.3	1723.2	18.3
G59	272	885	0.2887	0.0034	4.3521	0.0598	0.1076	0.0007	1635.1	34.0	1703.3	22.3	1759.5	17.6	1759.5	17.6
G88	127	413	0.2935	0.0035	4.4562	0.0726	0.1085	0.0009	1659.0	35.0	1722.9	23.7	1773.9	19.7	1773.9	19.7
G71	186	494	0.3374	0.0040	6.0664	0.0897	0.1306	0.0009	1874.0	38.5	1985.4	23.9	2105.9	18.8	2105.9	18.8
G111	213	593	0.3361	0.0009	6.1323	0.0117	0.1336	0.0008	1867.6	9.1	1994.9	11.7	2146.1	17.2	2146.1	17.2
G3	28	48	0.4125	0.0052	7.9377	0.2054	0.1464	0.0018	2226.3	47.0	2224.0	31.8	2304.4	23.8	2304.4	23.8
G82	76	123	0.4736	0.0058	10.3344	0.2163	0.1623	0.0014	2499.3	50.7	2465.2	27.6	2480.1	22.2	2480.1	22.2

APPENDIX E (continued). U-Pb ZIRCON AGES OF SONG GIANH SEDIMENTS

Grain No.	Pb (ppm)	U (ppm)	Ratios						Ages (Ma)						Best Age (Ma)	$\pm 2\sigma$
			$^{206}\text{Pb}/^{238}\text{U}$	$\pm 1\sigma$	$^{207}\text{Pb}/^{235}\text{U}$	$\pm \text{s.e.}$	$^{207}\text{Pb}/^{206}\text{Pb}$	$\pm \text{s.e.}$	$^{206}\text{Pb}/^{238}\text{U}$	$\pm 2\sigma$	$^{207}\text{Pb}/^{235}\text{U}$	$\pm 2\sigma$	$^{207}\text{Pb}/^{206}\text{Pb}$	$\pm 2\sigma$		
G83	703	1156	0.5043	0.0059	12.5393	0.1689	0.1793	0.0011	2632.3	50.7	2645.7	24.9	2646.7	17.9	2646.7	17.9
G4	169	277	0.4983	0.0058	11.9822	0.1971	0.1794	0.0017	2606.3	49.9	2603.0	28.4	2647.1	19.5	2647.1	19.5
G112	64	103	0.5231	0.0014	13.8736	0.0164	0.1998	0.0007	2712.1	11.5	2741.1	7.9	2824.6	12.6	2824.6	12.6
G113	1054	1779	0.5974	0.0040	25.4057	0.0931	0.3012	0.0010	3019.2	32.2	3323.9	14.4	3476.3	12.6	3476.3	12.6

APPENDIX F. APATITE FISSION TRACK AGES OF SONG GIANH SEDIMENTS

Details		Summary							
Sample No.	14052705	Central age	54.5 ± 3.6 Ma						
Irrad. No.	GAR 60	Age dispersion	22.7 %						
Position	0								
Date	22/04/15	Pooled age	54.4 ± 2.6 Ma						
		Mean age	57.5 ± 2.1 Ma						
zeta (CN5)	338								
zeta error	5	Chi squared	53.7 with 61 df						
No. of grains	31	P(chi-sq)	73.6 %						
Total Ni	2907 tr								
Total Nd	4640 tr								
rho-d (CN5)	1.674E+06 tr/cm ²								
mean rho-s	8.375E+05 tr/cm ²								
mean rho-i	4.091E+06 tr/cm ²								
mean U	30.6 ppm								
Crystal	Ng	Ns	rho-s	Ni	rho-i	Ns/Ni	U (ppm)	Age (Ma)	Error
1	16	20	9.019E+05	116	5.231E+06	0.1724	39.1	48.6	11.8
2	15	61	2.934E+06	261	1.255E+07	0.2337	93.7	65.8	9.4
3	10	15	1.082E+06	121	8.730E+06	0.1240	65.2	35.0	9.6
4	12	40	2.405E+06	107	6.433E+06	0.3738	48.0	104.9	19.5
5	18	9	3.608E+05	21	8.418E+05	0.4286	6.3	120.1	47.9
6	12	41	2.465E+06	158	9.500E+06	0.2595	70.9	73.0	12.8
7	18	29	1.162E+06	158	6.333E+06	0.1835	47.3	51.7	10.5
8	10	26	1.876E+06	97	6.999E+06	0.2680	52.3	75.4	16.7
9	21	5	1.718E+05	28	9.620E+05	0.1786	7.2	50.3	24.4
10	20	11	3.968E+05	83	2.994E+06	0.1325	22.4	37.4	12.0
11	9	12	9.620E+05	49	3.928E+06	0.2449	29.3	68.9	22.2
12	12	1	6.013E+04	11	6.614E+05	0.0909	4.9	25.7	26.8
13	30	44	1.058E+06	237	5.700E+06	0.1857	42.6	52.3	8.6
14	18	13	5.211E+05	86	3.447E+06	0.1512	25.7	42.6	12.7
15	20	16	5.772E+05	89	3.211E+06	0.1798	24.0	50.7	13.8
16	25	17	4.906E+05	110	3.175E+06	0.1545	23.7	43.6	11.4
17	14	30	1.546E+06	156	8.040E+06	0.1923	60.0	54.2	10.8
18	21	22	7.559E+05	92	3.161E+06	0.2391	23.6	67.3	16.0
19	36	4	8.017E+04	19	3.808E+05	0.2105	2.8	59.3	32.6
20	20	8	2.886E+05	28	1.010E+06	0.2857	7.5	80.3	32.2
21	8	21	1.894E+06	64	5.772E+06	0.3281	43.1	92.2	23.2
22	16	11	4.960E+05	82	3.698E+06	0.1341	27.6	37.8	12.2
23	18	10	4.008E+05	57	2.285E+06	0.1754	17.1	49.4	17.0
24	18	28	1.122E+06	226	9.059E+06	0.1239	67.6	35.0	7.0
25	30	13	3.127E+05	92	2.213E+06	0.1413	16.5	39.9	11.8
26	40	4	7.215E+04	11	1.984E+05	0.3636	1.5	102.1	59.6
27	40	10	1.804E+05	116	2.092E+06	0.0862	15.6	24.3	8.0
28	32	9	2.029E+05	58	1.308E+06	0.1552	9.8	43.8	15.7
29	25	15	4.329E+05	73	2.107E+06	0.2055	15.7	57.9	16.4
30	12	11	6.614E+05	71	4.269E+06	0.1549	31.9	43.7	14.2
31	40	5	9.019E+04	30	5.411E+05	0.1667	4.0	47.0	22.7

VITA

Tara N. Jonell was born on the glaciated Appalachian Plateau of Ohio and spent most of her childhood growing up on the remains of an old Christmas tree farm. After completing high school, she entered Kent State University as a geology major and received a Bachelor of Science degree with Distinction in Geology in May 2010. For the next two years Tara pursued volcanology at New Mexico State University for her Master of Science in Geological Sciences. After graduating in 2012, she entered Louisiana State University to pursue her doctoral degree focused in sediment provenance and geomorphology until completion in May 2017.